Advanced Global Optimisation Tools for Mission Analysis and Design

Authors: Pierluigi Di Lizia, Gianmarco Radice
Contractor: Department of Aerospace Engineering, University of Glasgow.

Technical officer: Dario Izzo, Advanced Concepts Team (ESTEC)

Contacts:

Gianmarco Radice
Tel: +44-(0)141-3304068
Fax: +44-(0)141-3305560
e-mail: gradice@aero.gla.ac.uk

Dario Izzo
Tel: +31 (0)71-5653511
Fax: +31 (0)71-5658018
e-mail: act@esa.int

Ariadna id: 03/4101
Study length: 6 months.
Contract Number: 18139/04/NL/MV

Available on the ACT net (www.esa.int/act)

TABLE OF CONTENTS

EXECUTIVE SUMMARY

A study of global optimisation methods in the field of interplanetary trajectory has been performed. The idea was to understand why and how a particular approach is more suited than others in optimising the trajectory for a certain type of interplanetary transfer. From the No Free Lunch Theorem (NFLT) it is impossible that an algorithm outperforms all others in all the possible applications, therefore the aim of this work was two fold: to identify a suitable global optimisation algorithm that outperforms all others in a particular transfer typology; to identify a suitable global optimisation algorithm family that outperforms all others in all mission analysis transfer problems.

At first a characterisation of the different transfer families, depending on propulsion system (impulsive and low thrust) and number of planetary bodies (planet-to-planet, multiple gravity assist, weak stability boundary) was conducted. The model characterisation was performed within the search space to describe the morphological features of the objective function, and within the objective function to identify to evaluate continuity and convexity. Box-constrained optimisation problems have been taken into account by defining proper upper and lower bounds for each design variable, while possible inequality constraints have been treated using the classical approach of defining the objective function as a suitable weighted sum of several terms, including the constraints violation.

Once the optimisation problem has been fully defined, an exhaustive and systematic analysis of the resulting objective function structure has been performed in order to identify typical features which would mostly affect the global search; discontinuity as well as non-differentiability regions have been identified over the search space and particular care has been taken to characterize the objective function in the neighbourhood of the best known solution, as this constitutes a remarkable feature strongly affecting the effectiveness of some global optimisation algorithms at identifying it. The use of a multi-start search using local optimisation processes starting from initial

guesses randomly distributed over the search space assisted the systematic analysis and allowed the identification of big valley structures. Such structures turned out to be mainly related to the periodicity of all the investigated objective functions with respect to particular design variables

Global optimisation algorithms can be classified into three main classes: stochastic, deterministic and metmodels. A particular type of stochastic approach, evolutionary algorithms can be further divided into genetic algorithms, evolutionary programming and evolutionary strategies. In total eleven algorithms, taken from the three main classes mentioned above, were tested and their performances in identifying global optimal solutions evaluated. The previously described optimisation problems corresponding to the four different mission analysis classes were submitted to the whole set of global optimisation tools and an extensive study carried out in order to recognize suitable problem-method relations corresponding to the identification of the best performing algorithms for each mission analysis problem.

1. INTRODUCTION

In the last two decades, global optimisation approaches have been extensively used towards the solution of complex interplanetary trajectory transfers. As operational costs have been increasingly reduced, space systems engineers have been facing the challenging task of maximising the payload-launch mass ratio while still achieving the primary mission goals. Methods ranging from genetic algorithms [Hughes and McInnes, 2001] to neurocontrollers [Dachwald, 2004], from shooting methods [Wirthman et al., 1995] to collocation methods [Betts and Erb, 2003] have been used with varying effectiveness. Unfortunately the efficiency, both computational and performance-wise, of these approaches are strongly linked to the type of problem that has to be solved. It would therefore be hugely beneficial if mission designers could rely on a limited number of global optimisation methods depending on the type of trajectory design, which has to be accomplished.

To achieve this ambitious goal, initially, a thorough identification and modelling of the main types of orbital transfers has to be performed. The orbital transfer typologies will be identified both on the basis of the propulsive system (impulsive or low thrust) and on the number of planetary bodies contributing to the dynamics of the system. The aim therefore is to achieve the characterisation of interplanetary transfers based upon:

- 2-Impulse Transfers
- Multiple Gravity Assist Transfers
- Weak Stability Boundary Transfers
- Low Thrust Spiral Transfers

This classification, ranging from simple two body transfers to more complex interplanetary trajectories, encompasses the current and future requirements of mission analysis and design problems.

The models identified previously will then have to be characterised, in order to hopefully identify some common features. Also, considering the future requirement of this study for trajectory optimisation, the characterisation performed will be two-fold:

- Within the search space, by means of a topological analysis aiming to identify variables which are useful in the description of the morphological structure of the objective function.
- Within the objective function aiming to identify its structure and evaluating its continuity and convexity characteristics.

The characterisation will be performed using systematic and/or probabilistic methodologies. The aim is to identify different transfer families within the same transfer typology as a function of the parameters of the problem: mass parameters of the planets in an MGA transfer, parameters of the low thrust propulsion system, etc.

The attempt here is to assess if commonly encountered problems in mission analysis are solvable in polynomial time or, if a solution is available, if the global optimality of this solution can be verified in polynomial time.

We try to asses if, for a given global optimisation problem in mission analysis *Π*:

- An algorithm A_Π exists such that in polynomial time, given a domain *D* and a function *f*: $f(x): x \in D \subseteq \Re^n \to \Re^m$ a solution x^* can be computed.
- An algorithm B_Π that, given *D*, *f* and x^* is able to compute in polynomial time f^*;
- An algorithm C_Π, that given *D, f* and x^*, either produces a new solution $x \in D$ with $f(x) < f(x^*)$ (assuming a minimization problem) or else concludes that no such solution exists and x^* is a global optimum.

To do this we first proceed by analysing the main characteristics of common trajectory design problems in mission analysis. From this analysis, we will try to infer if the aforementioned algorithm exists or can be derived from problem characteristics. In doing this we make use of two simple and basic algorithms:

- A random start search with SQP local optimisation
- A grid search with regular sampling of *f*

The inferred complexity of the problem under study will be done by similarity with NP-hard problems or associating the solution of the problem Π to the solution of an equivalent reduced problem Π_r. This analysis will contain the seed for the development of the appropriate solution algorithm since the complexity of the problem is intrinsically associated to the solving algorithm.

In the following sections we will look at:

- Two impulse direct planet-to-planet transfer
- Multiple gravity assist planet-to-planet transfer
- Low-thrust direct planet-to-planet transfer
- Weak Stability Boundary Transfer

Note that we see the planet-to-planet transfer problem as a generalisation of the orbit-to-orbit transfer problem since in the former case the phase of the departure and arrival point must also be considered.

2. 2-IMPULSE DIRECT PLANET-TO-PLANET TRANSFER

As an example of a 2-impulse transfer, let us consider a direct transfer from Earth to Mars. We have taken the Mars Express mission as our reference mission.

2.1 Problem Formulation

Let us suppose the objective function as the overall impulsive ΔV; the sum of the magnitudes of the relative velocities at the beginning, ΔV_I, and the end, ΔV_F, of the interplanetary transfer phase:

$$f = \Delta V = \Delta V_I + \Delta V_F \qquad [1]$$

In order to evaluate the previous objective function, the following mathematical models and methods have been used:

- Restricted 2-body dynamical model (C^2 in the whole solution space except in the origin)
- Three dimensional motion
- Analytical ephemeris model (generated by time polynomial series of the orbital elements)
- Impulsive manoeuvres (i.e. instantaneous variations in velocity)
- Lambert's problem formulation (Battin's algorithm for the problem solution)

As a consequence of the mathematical models and methods used for the objective function assessment, the search space is characterized by two design variables:

- Date of departure from Earth, t_0
- Transfer time from Earth to Mars, tt

Both the previous design variables continuously vary above the set of real numbers.

$$x = [t_0, tt] \in D$$
$$D \subseteq \Re^2$$
$$f(x) : x \in D \subseteq \Re^2 \rightarrow \Re \qquad [2]$$
$$f \in \Re$$

T-periodicity: $f(t_0 + T) \cong f(t_0)$

Upper and lower bounds on the design variables are considered. As the date of departure from Earth coincides with the lower bound, the interval of variation has been imposed in order to include the date of departure of Mars Express mission (2 June 2003) and seven synodic period of the Earth-Mars system (780 days). The resulting intervals of variation are:

$$\left[t_0^{LB}, t_0^{UB}\right] = \left[01/01/2003, 31/12/2017\right] \qquad [3]$$
$$\left[t_{tt}^{LB}, t_{tt}^{UB}\right] = \left[100, 600\right] \ days \qquad [4]$$

Note that, when describing the date of departure by means of the Julian date in days, the dimension of the search space with respect to this design variable is 8 times wider than the other.

2.2 Objective Function Structure Analysis

As the search space has only two dimensions, a visual representation of the objective function over the whole search space is possible, as illustrated in Figure 1 and Figure 2.

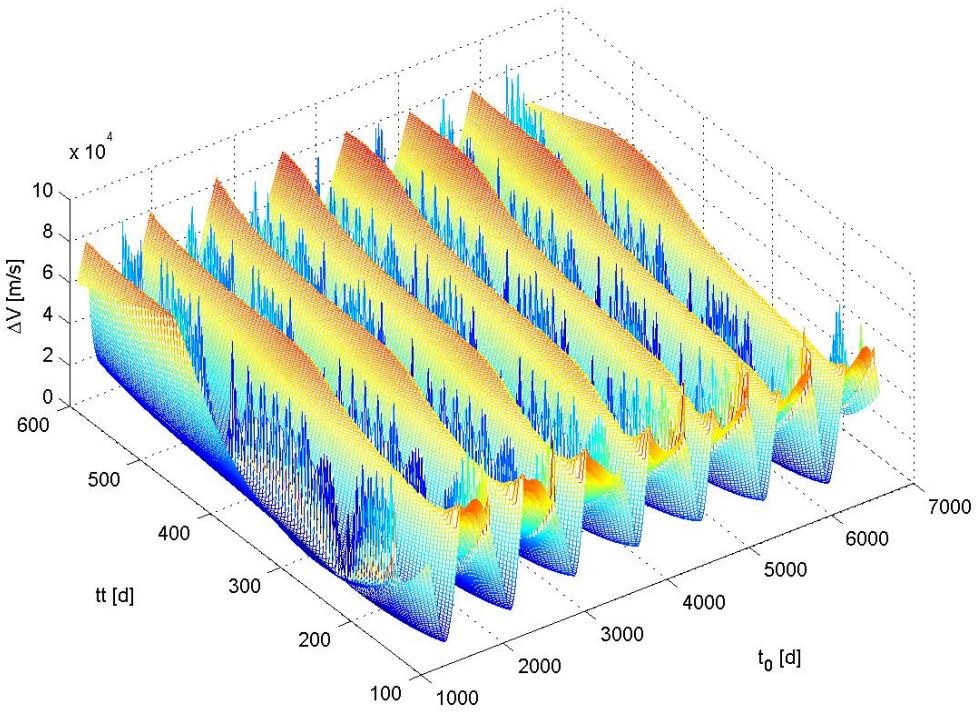

Figure 1: Total ΔV for a direct impulsive Earth-Mars transfer as a function of the date of departure and the transfer time

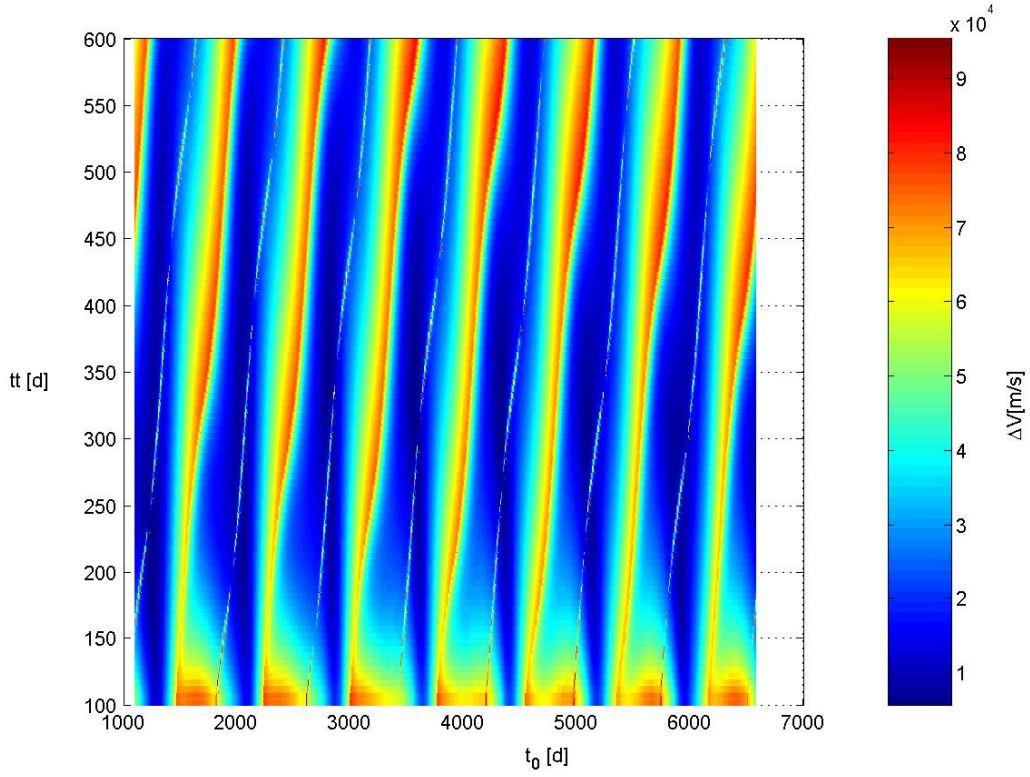

Figure 2: Total ΔV for a direct impulsive Earth-Mars transfer as a function of the date of departure and the transfer time (projection on t_0-tt plane)

Note that the date of departure in Figure 1 has been indicated as the modified Julian date, starting from 1st January 2000. As can be seen from Figure 1, the objective function is a non-convex function over the considered search space, mainly due to its quasi-periodical feature on the date of departure values. This result is illustrated in Figure 3, which shows the variation of the objective function with respect to the date of departure corresponding to a 200 days interplanetary transfer phase: from Figure 3 a period of approximately 780 days can be identified, which obviously corresponds to the synodic period of the Earth-Mars system. This suggests the possibility of exploiting the quasi-periodicity information of the objective function, and consequently the synodic period values, in the global optimisation process. The global optimisation algorithms can use such information in several ways such as:

- Typical step sizes for global search in the direction of the date of departure values can be assessed in order to evaluate the goodness of the various basins of attraction, effectively escaping from convergence to local optima.

- Smart dimensions of subintervals in case of Branch & Bound algorithms and global optimisation algorithms using interval analysis can be evaluated. Note that, in case of using interval analysis, the problem of programmability must be considered: e.g. the ephemeris model, due to the use of polynomial time series, can be effectively applied for the interval evaluation of planetary orbital elements, while the conversion in Cartesian coordinates must be accurately analysed.

- Smart clustering techniques can be developed in multi-start search algorithm.

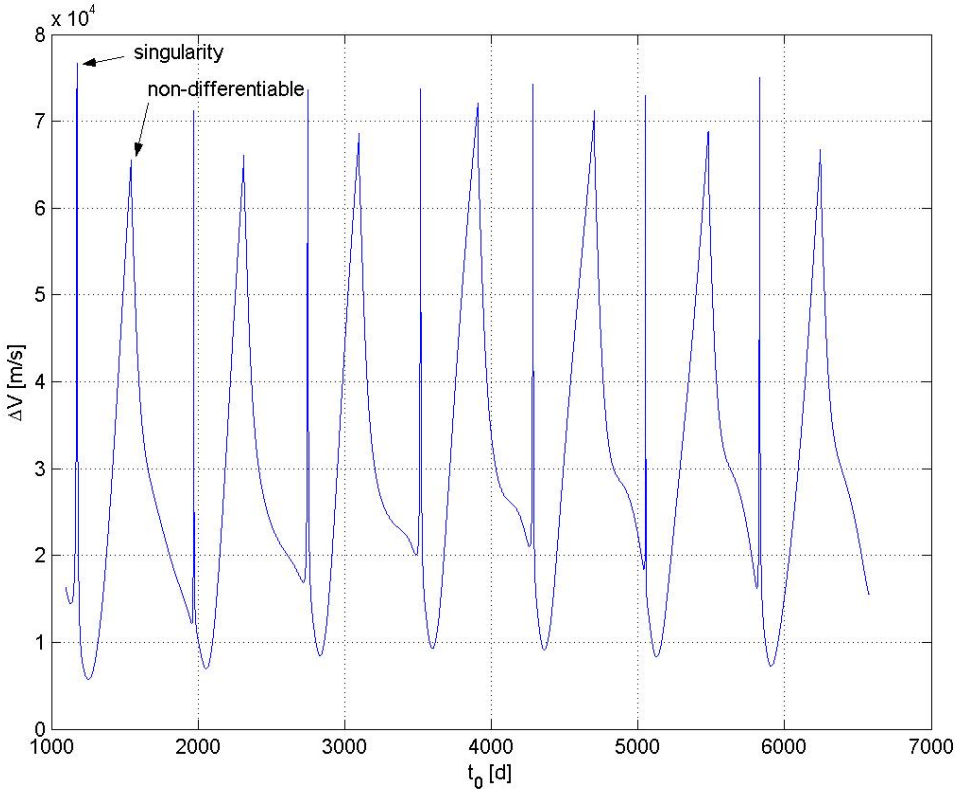

Figure 3: Periodicity of the objective function with respect to the date of departure for a 200 days long interplanetary transfer phase

In order to further analyse the structure of the objective function, the distribution of the local minima over the whole search domain has been studied. Reeves and Yamada [Reeves and Yamada, 1998] proposed to assess the objective function structure in a flow-shop scheduling environment by firstly identifying as many local minima as possible and then by computing for each local optimum its average distance from all the other local optima, since the global optima for the problem are *a priori* unknown. Not only does this allow us to identify the best solutions, but also:

- to evaluate the closeness of the local optima to each other
- to analyse the structure of the objective function near the global optima, by assessing the density and goodness of the nearby local optima
- to identify the presence and features of similar local optima

Due to these attractive features and the important results it led to in the Flow-Shop Scheduling environment, this objective function structure analysis methodology has been applied in this work to space mission design. In order to generate the local minima, 100 randomly distributed points on the overall search space have been used as starting points for a local search, based on a Sequential Quadratic Programming algorithm. Figure 4 shows the resulting local minima distribution over the search domain (black dots plus the red one), where level curves of the objective function are also illustrated.

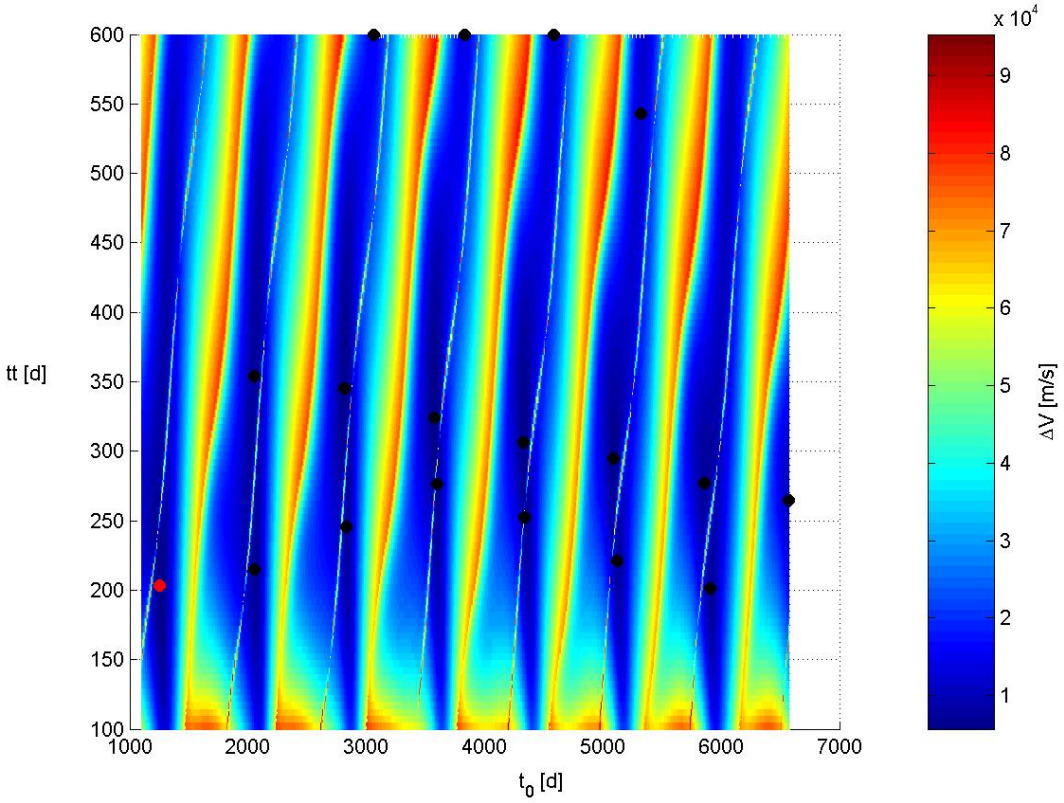

Figure 4: Distribution of the generated local minima.

Figure 4 also highlight the best identified local minimum (red dot), whose main features are presented in the following pages; Table 1 and Table 2 report the values of the design variables and of the objective function terms respectively, while Figure 5 reports the corresponding transfer trajectory.

Search space	
Design variable	**Best identified solution**
Date of departure [*d*]:	1253.510
Transfer time [*d*]:	203.541

Table 1: Best identified solution: search space

Objective function space	
Term	**Best identified solution**
ΔV [*m/s*]:	5678.904
ΔV_I [*m/s*]:	2999.464
ΔV_F [*m/s*]:	2679.439

Table 2: Best identified solution: objective function space

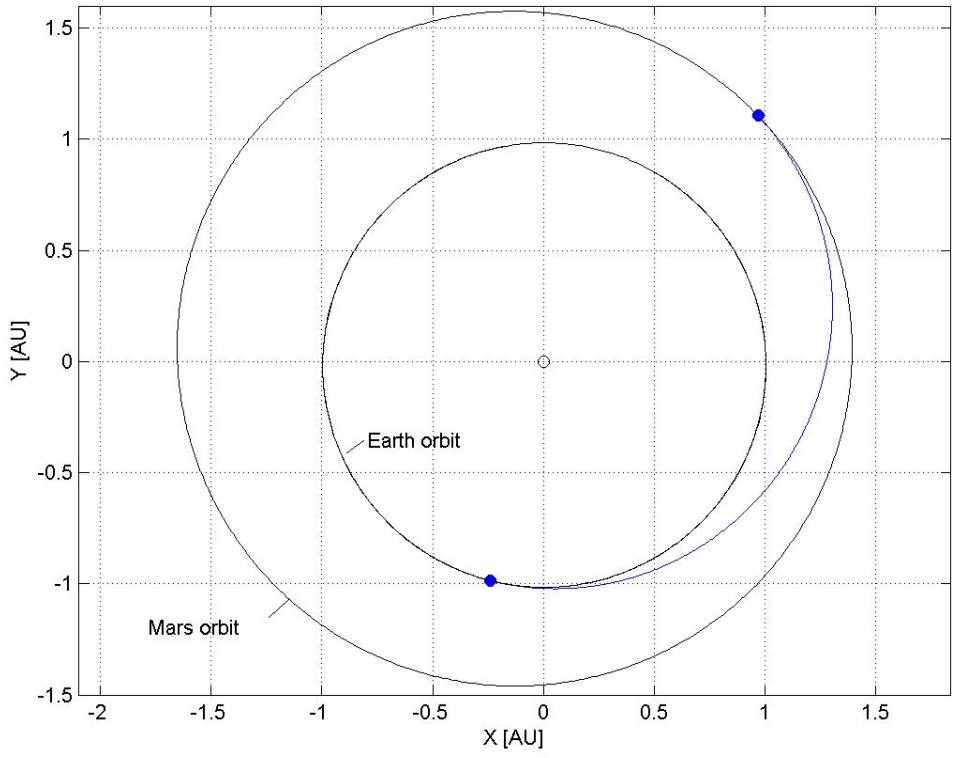

Figure 5: Best identified solution: transfer trajectory.

Note that in the case of the real Mars Express mission, the interplanetary transfer solution corresponds exactly to the solution here identified: in particular, besides the dates of departure and arrival and the transfer time, the best identified solution has a velocity, relative to the Earth, at the beginning of the transfer phase, ΔV_I, equal to 2679.439 *m/s*. This corresponds to a $C3$ performance for the launcher of about 7.179 km^2/s^2; referring to the launcher adopted in the real mission (Soyuz-Fregat), the performance curve is illustrated in Figure 6.

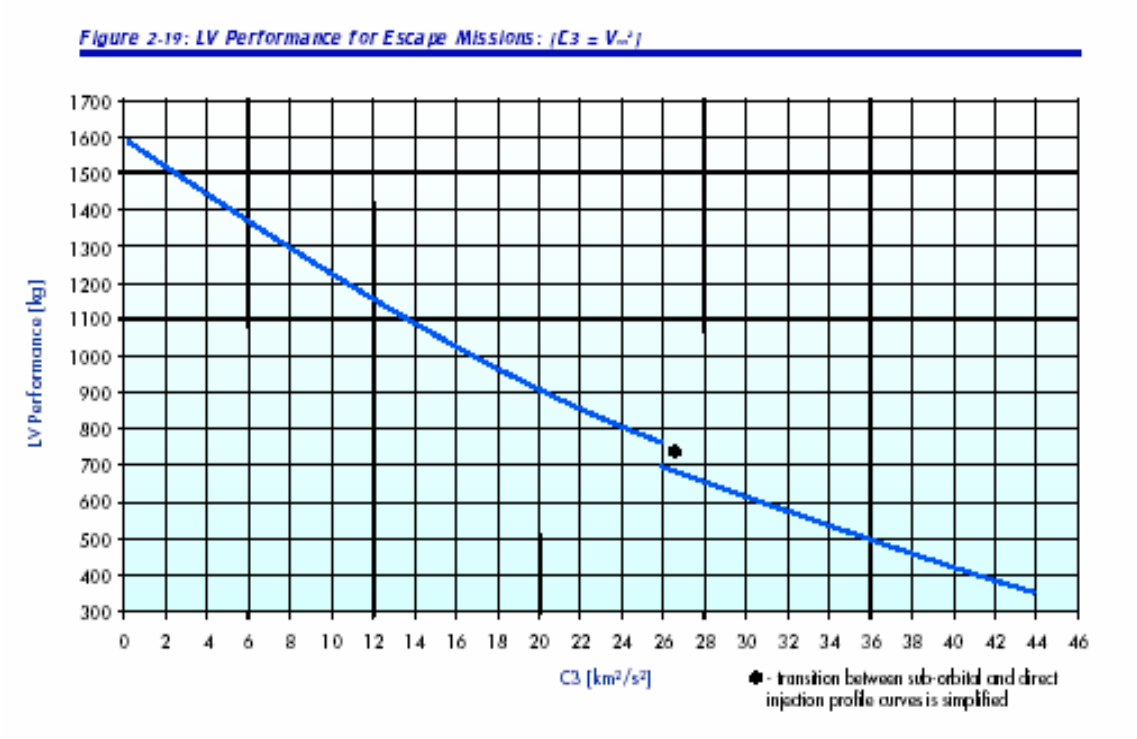

Figure 6: Soyuz-Fregat launcher: performance for Escape Missions.

The maximum launch mass for the spacecraft can then be evaluated from Figure 6, that is about 1350 *kg* (the launch mass of Mars Express was equal to 1120 *kg*). This result can be seen as a confirmation of the validity of the used mathematical models and methods. Another important feature can be highlighted on the objective function structure by means of the identified minima, concerning the comparability of the various local minima. Figure reports the identified local minima gathered in three subgroups, corresponding to different level of the objective function value, as described in Table 3.

Level of the Objective Function Value [*m/s*]	Dots Colour
$\Delta V < 6000$	red
$6000 \leq \Delta V \leq 7000$	green
$\Delta V > 7000$	black

Table 3 – Objective function levels and corresponding colours in Figure .

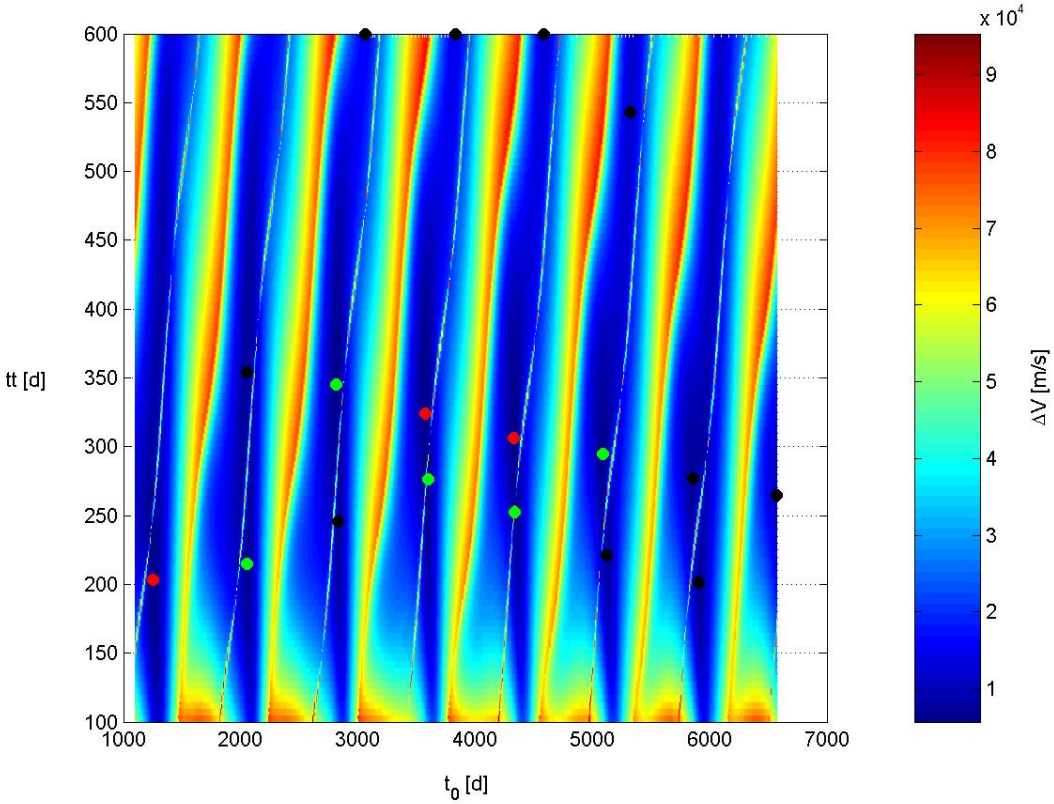

Figure 7: Local minima comparability in terms of objective function value.

Figure 7 shows that local minima exist which can be considered quite comparable. In particular, by analysing the red dotted and the green dotted local minima, the corresponding objective function value are characterized by a mean value of 5952.538 *m/s* and a standard deviation of 328.778 *m/s*. Such features make the 2-impulse direct planet-to-planet transfer problem over the considered intervals of date of departures an interesting means for evaluating the effectiveness and robustness of a global solver. Once generated the local minima, it is possible to analyze the structure of the objective function by using the Reeves and Yamada methodology. The mean distances of the distinct local

optima from each other have been evaluated: for a clearer interpretation, the mean distances have been normalized to the length of the iper-diagonal of the search space. Figure 8 shows the resulting structure: the x-axis reports the mean distances of each local optima, while the corresponding objective function values are indicated along the y-axis.

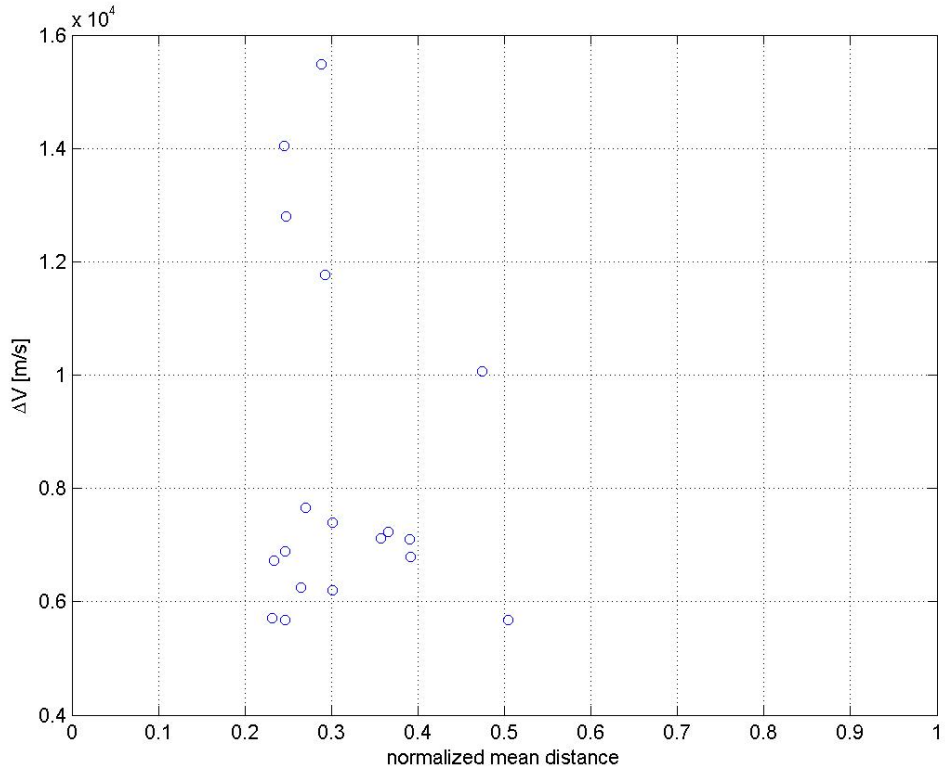

Figure 8: Objective function structure analysis for a direct 2-impulse Earth-Mars transfer.

Figure 8 shows that the mean distance of most local minima from the others is bounded in the interval [0.2, 0.4] times the typical dimension of the search space. As a consequence, the distribution of the local minima turns out to be quite uniform, as Figure 8 fairly illustrates. Table 4 summarizes the problem characteristics for a direct two-impulse transfer.

Problem Dimension	Constraints	Search Space	Objective function	T-periodicity
2	Box constraints	$D \in \Re^2$	$f \in \Re$ almost everywhere C^2, locally discontinuous in a countable number limited sets	Yes

Table 4: Summary of problem characteristics.

3. MULTIPLE GRAVITY ASSIST TRANSFERS

As an example of a multiple gravity assist (MGA) interplanetary mission, let us consider a transfer from Earth to Saturn, taking Cassini as the reference mission.

3.1 Problem Formulation

Let us suppose the objective function as the overall impulsive ΔV_{TOT}. In order to evaluate it, the following mathematical models and methods have been used:

- Restricted 2-body dynamic model
- Three dimensional motion
- Analytical ephemeris model
- Linked-conic approximation for gravity assist manoeuvres
- Impulsive manoeuvres, i.e. instantaneous variations in velocity
- Lambert's problem formulation (Battin's algorithm for the problem solution)

The objective function is assumed to be the sum of several terms:

- The magnitude of the velocity, relative to Earth, at the beginning of the interplanetary transfer phase, ΔV_I.
- The magnitude of the velocity variation required to the reach the insertion orbit at Saturn, ΔV_F.
- The magnitudes of the minimum corrective ΔV at each gravity assist manoeuvre, $\Delta V_{GA,P}$ (where the subscript "*P*" will be substituted with the initial letter of the name of the planet that contributes to the gravity assist manoeuvre), which is necessary to link two consecutive interplanetary transfer arcs resulting from the formulation of Lambert's problem.

For the evaluation of $\Delta V_{GA,P}$, given the input relative velocity vector v_I and the output relative velocity vector v_O, an hyperbolic orbit around the planet is considered as lying on the plane identified by the two vectors v_I and v_O. The pericentre of the hyperbole is selected in order to have the minimum misalignment between the final asymptotic velocity and v_O, always imposing the minimum radius necessary to avoid interferences with the planet. For the evaluation of ΔV_F, the insertion orbit has been taken from the Cassini-Huygens mission, with the following features:

Pericentre radius:	$1.0895 \cdot 10^8$ *m*
Eccentricity:	0.98

Table 5: Saturn insertion orbit parameters.

The ΔV_F manoeuvre is applied at the pericentre of the hyperbolic entrance orbit, tangentially to the velocity vector.

As a consequence of the mathematical models and methods used for the objective function assessment, the search space is characterized by the following design variables:

- Date of departure from the Earth, t_0
- Sequence of planets, $\vec{P} = \{P_1, P_2, ..., P_n\}$ (where P_1 is the departure planet – in our case the Earth – and P_n is the arrival planet). Note that a planet P_i can appear more than once in the sequence.
- *n-1* transfer times (that is the transfer times of the linking arcs)

Note that the number of design variables is not *a priori* fixable in this case and depends on the dimension of the vector $\vec{P}$. To evaluate the value of the objective function, one has to analyse the discrete variable $\vec{P}$ at first, looking for its dimension and the sequence of planets it leads to. Supposing an *n*-

dimensional $\vec{P}$ vector, then the number of linking arcs (and the associated transfer times) is *n-1*. By indicating with *dim* the operator which evaluates the dimension of a vector, then the dimension of the whole search space, *DIM*, is calculated as follows:

$$DIM = dim\left(\vec{P}\right) \quad [5]$$

The more $dim\left(\vec{P}\right)$ is large, the more the design variables there are and the more the complex the global search is. In this case the vector $\vec{P}$ is defined in the natural numbers set, that is the sequence of planets, while the others are continuous. No Deep Space Manoeuvre (DSM) is considered in the previous search space. Should *m* Deep Space Manoeuvres be performed, the following design variables would then have to be considered:

- The allocation of the *m* Deep Space Manoeuvres over the sequence of planets.
- The *m* additional transfer times that are related to the *m* additional linking arcs.

While the transfer times have a continuous characterization, the allocation of the *m* DSMs is a discrete variable and affects the dimension of the search space in a similar way as the previous vector $\vec{P}$.

Upper and lower bounds on the design variables are considered. As the date of departure from Earth coincides with the lower bound, the interval of variation has been imposed in order to include a period of 5 years centred around 1st January 1999. This includes the date of departure of Cassini-Huygens mission, 15th October 1997. The upper and lower bounds for the transfer times will be specified for each case in the objective function structure analysis.

3.2 Objective function structure analysis

In order to analyse the structure of the objective function over the search space, a distinction between discrete and continuous variables has been considered: a fixed number of sequence of planets has been chosen for the evaluation of the effects of the discrete variable on the local minima distribution and consequently on the objective function structure.

Considering the interplanetary transfer from Earth to Saturn and referring to the Cassini-Huygens mission, the following sequences of planets have been probed:

1. Earth – Jupiter – Saturn (EJS)
2. Earth – Mars – Jupiter – Saturn (EMJS)
3. Earth – Venus – Earth – Jupiter – Saturn (EVEJS)
4. Earth – Venus – Venus – Earth – Jupiter – Saturn (EVVEJS)

As for the case of the 2-impulse transfer, the objective function structure analysis for a multiple gravity assist has been based on the Reeves and Yamada methodology: for each of the previous sequences of planets, 1000 local minima have been found with a random start search (with uniformly distributed random start points) followed by an SQP optimisation process; the mean distances of each solution from each other is then assessed and compared to the corresponding goodness.

For the sake of a clearer analysis, the case of no deep space manoeuvres is considered at first. The effects of such manoeuvres on the objective function structure will be assessed later.

3.3 Earth – Jupiter – Saturn (EJS)

Once fixed the value of the discrete variable "sequence of planets" to EJS, the number of continuous variables which complete the search space is three: the date of departure from Earth, t_0, and the transfer times Earth – Jupiter and Jupiter – Saturn, tt_{EJ} and tt_{JS} respectively. The upper and lower bounds for the transfer time associated to the two linking arcs E-J and J-S have been posed equal to 0.1 and 2 times the associated Homann transfer time respectively. The resulting intervals are:

$$\left[tt_{EJ}^{L}, tt_{EJ}^{U}\right] = \left[99.65,\ 1993.1\right] d \qquad [6]$$

$$\left[tt_{JS}^{L}, tt_{JS}^{U}\right] = \left[365.02, 7300.4\right] d \qquad [7]$$

Figure 9 compares the widths of the interval of variation associated to the three design variables: Earth departure, Earth-Jupiter transfer time and Jupiter-Saturn transfer time.

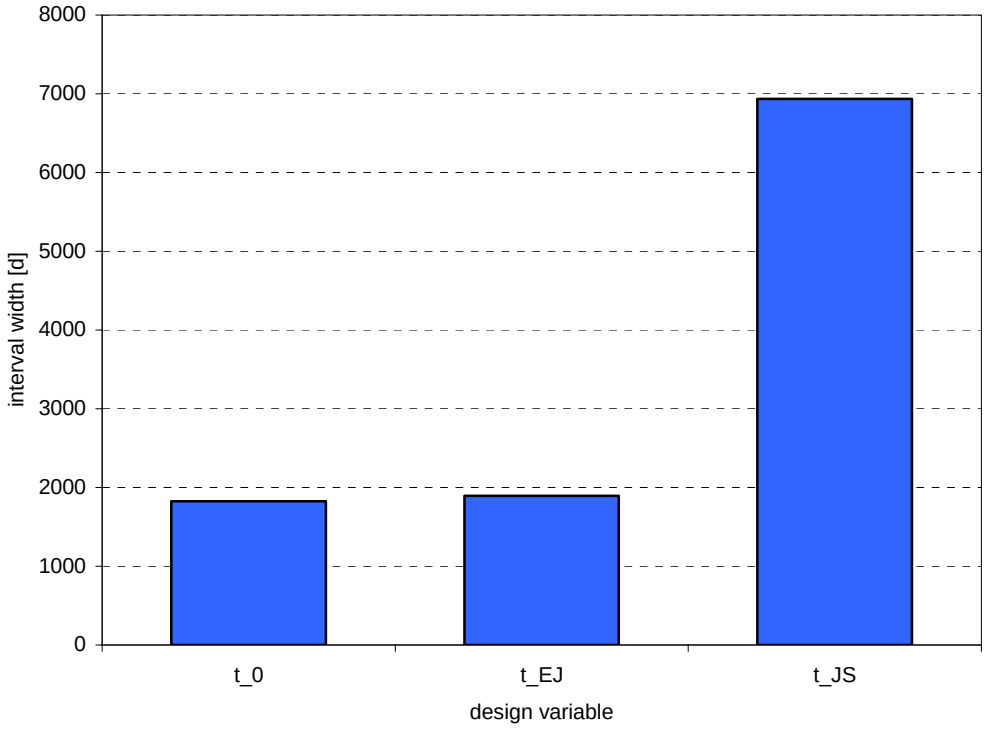

Figure 9: Comparison between the widths of the intervals of variation in the search space.

After generating the 1000 local minima, the mean distances of each solution to the others have been evaluated. By using the Reeves and Yamada's methodology, Figure 10 shows the resulting structure of the objective function: the x-axis reports the normalized mean distance of each local optima (for the definition of the normalized mean distance see the 2-impulse transfer case), while the corresponding objective function values are indicated along the y-axis.

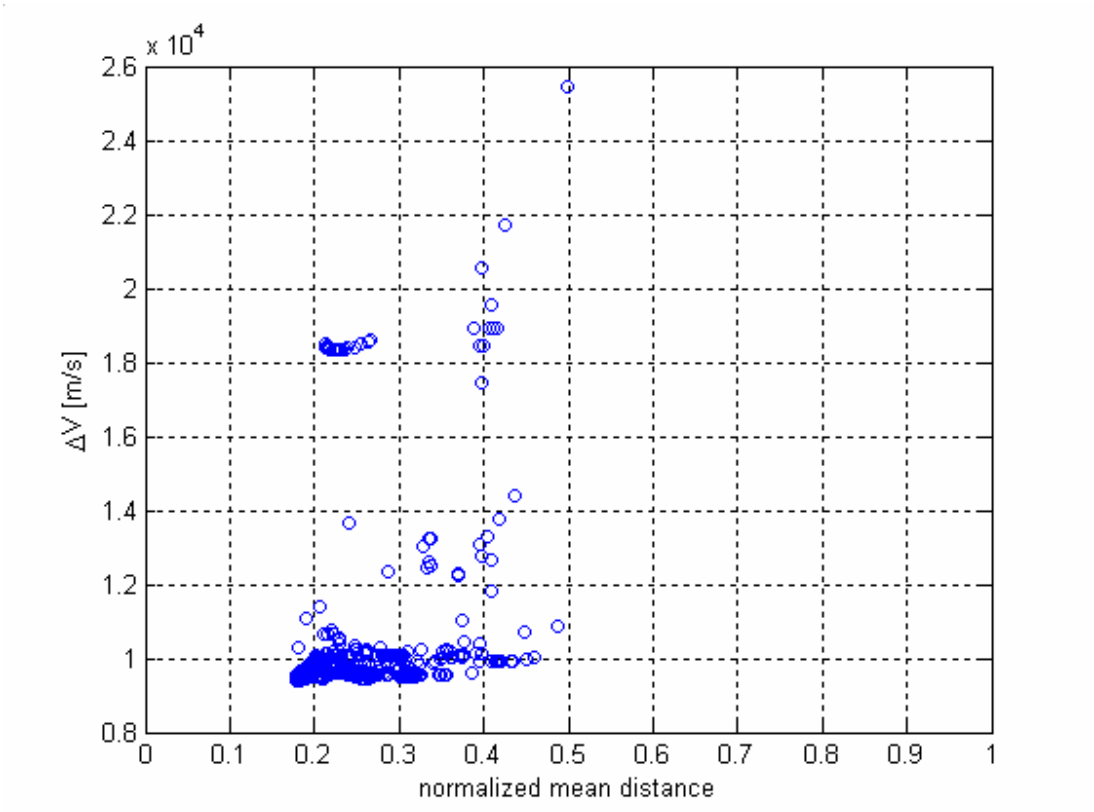

Figure 10: Objective function structure analysis for an EJS transfer.

An important observation can be made by analysing Figure 10: the objective function for an EJS transfer display a *big-valley* problem structure. A *big-valley* structure has the following features:

1. Local optima tend to be relatively close to other local optima
2. Better local optima tend to be closer to global optima
3. Local optima near one another have similar evaluations

As a consequence, the global optima tend to have good local optima as neighbourhoods. The mean closeness of most local optima tends to range between 0.18 and 0.3 times the hyper-diagonal magnitude, that is between 1350 *d* and 2250 *d*. In order to analyse the distribution of the local minima and verify the existence of a *big valley* structure, the search space is probed further. Figure 11 shows the dates of departure (*x*-axis) and the objective function values (*y*-axis) corresponding to the identified local optima.

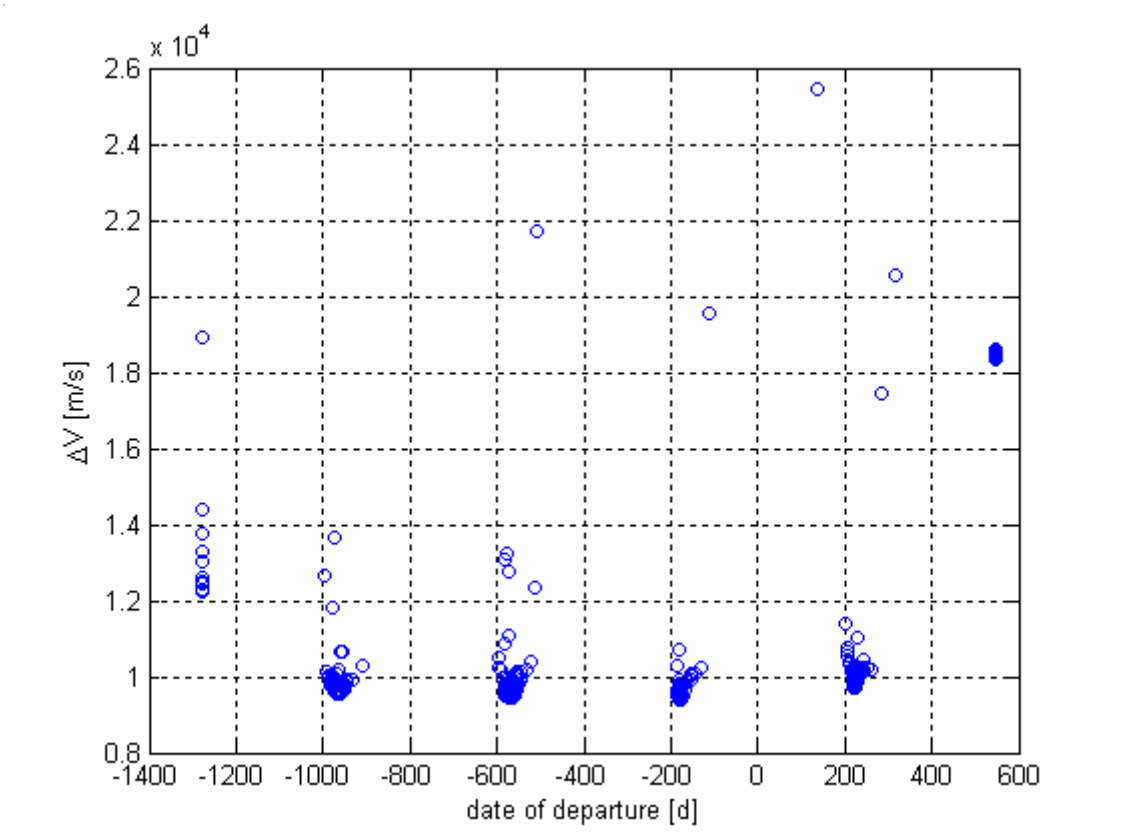

Figure 11: Local optima distribution over the date of departure design variable.

The local optima tend to gather in groups near fixed date of departure values. The interval between two of these fixed dates is almost constant and equal to approximately 400 days. This result can be intuitively explaneed by means of the quasi-periodicity of the objective function with respect to the date of departure; that is caused by the synodic periods of the planetary systems. The synodic period of the Earth-Jupiter system is equal to 398 days associable to the intervals identified in Figure 11. The synodic period of the Jupiter–Saturn

system is equal to 7254 days, and is not included in the considered interval of variation due to being one order of magnitude larger.

The local optima corresponding to a fixed date tend to have similar objective function evaluations. Let us consider now the remaining design variables. The *x*-axis of Figure 12 shows the Earth-Jupiter local minima transfer times, while the Jupiter-Saturn local minima transfer times are reported on the *y*-axis.

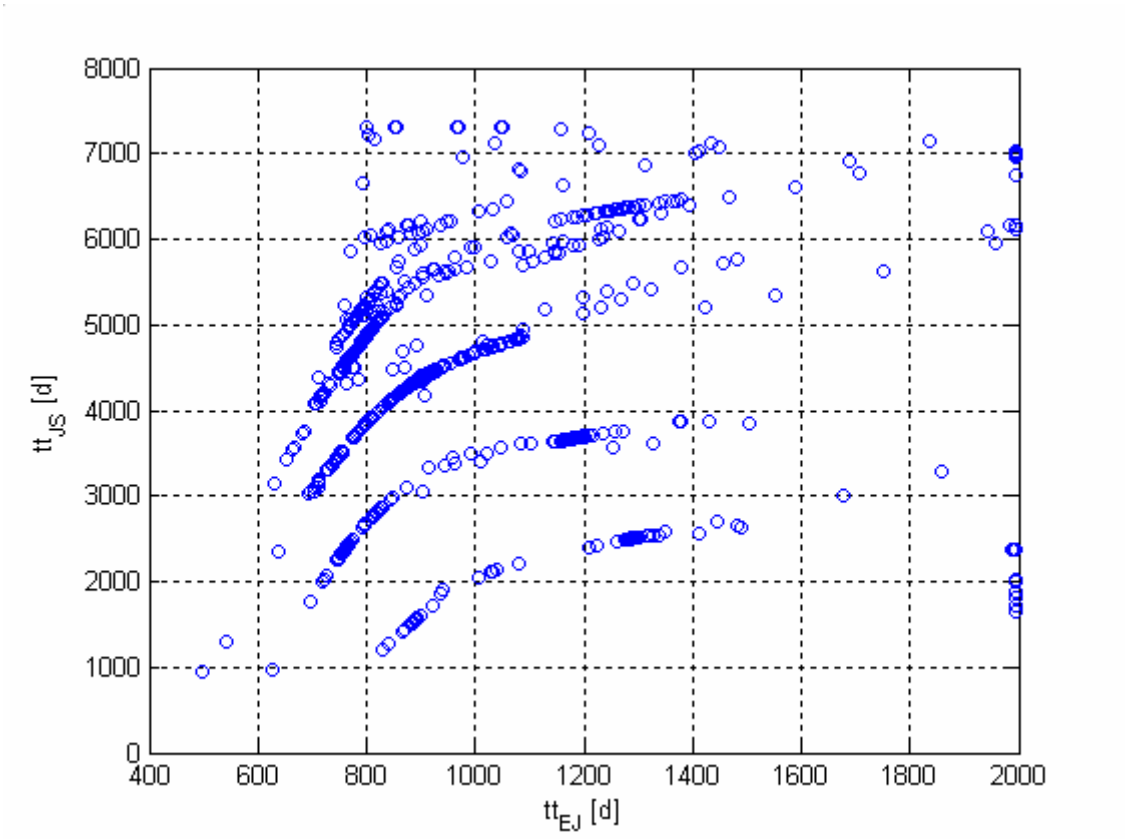

Figure 12: Local minima distribution over transfer times design variables.

The local minima tend to distribute themselves in clearly identifiable structures over the transfer times subspace: these structures look like curves on this subspace. A more important consequence can be highlighted by noting that each identified structure is in fact associable to a well defined date of departure: consider, for example, the subgroup of local minima associated with values of the dates of departure close to -200 *d*; the corresponding transfer times values are shown in red in Figure 13, together with the remaining local minima.

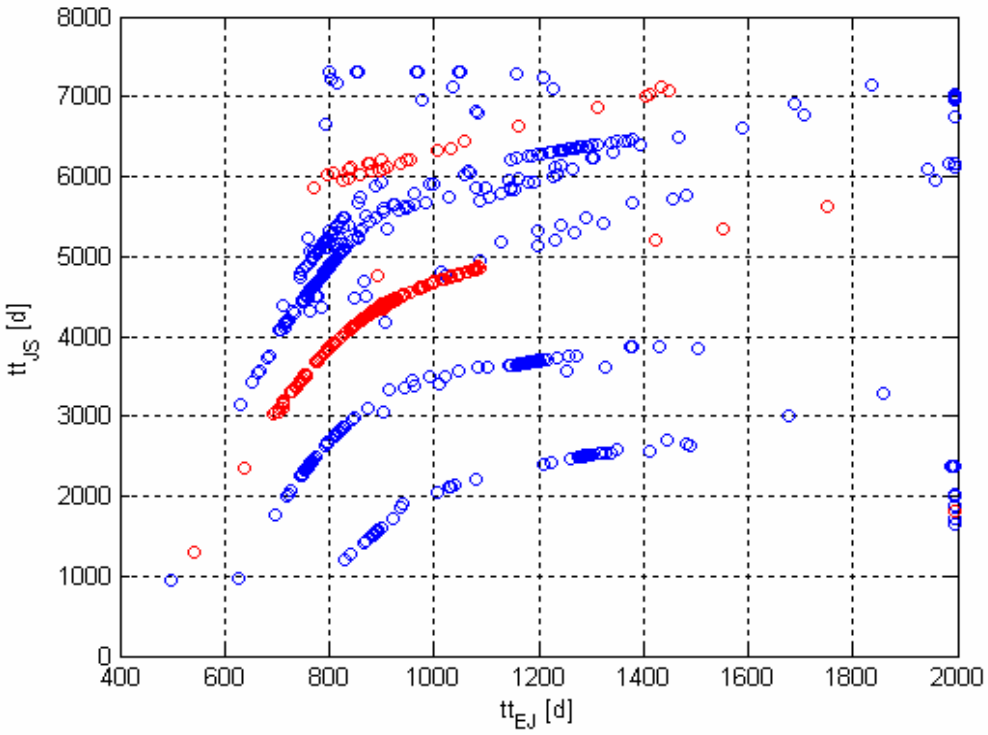

Figure 13: The structures associated to the subgroup of local minima corresponding to dates of departure values close to -200 *d*.

The previous results show the existence of structures where local optima tend to be relatively close to other local optima and local optima near one another have similar evaluations: these are in fact *big valley* structures in the $tt_{EJ} - tt_{JS}$ subspace. A three dimensional illustration of the local minima in the search space is showed in Figure 14.

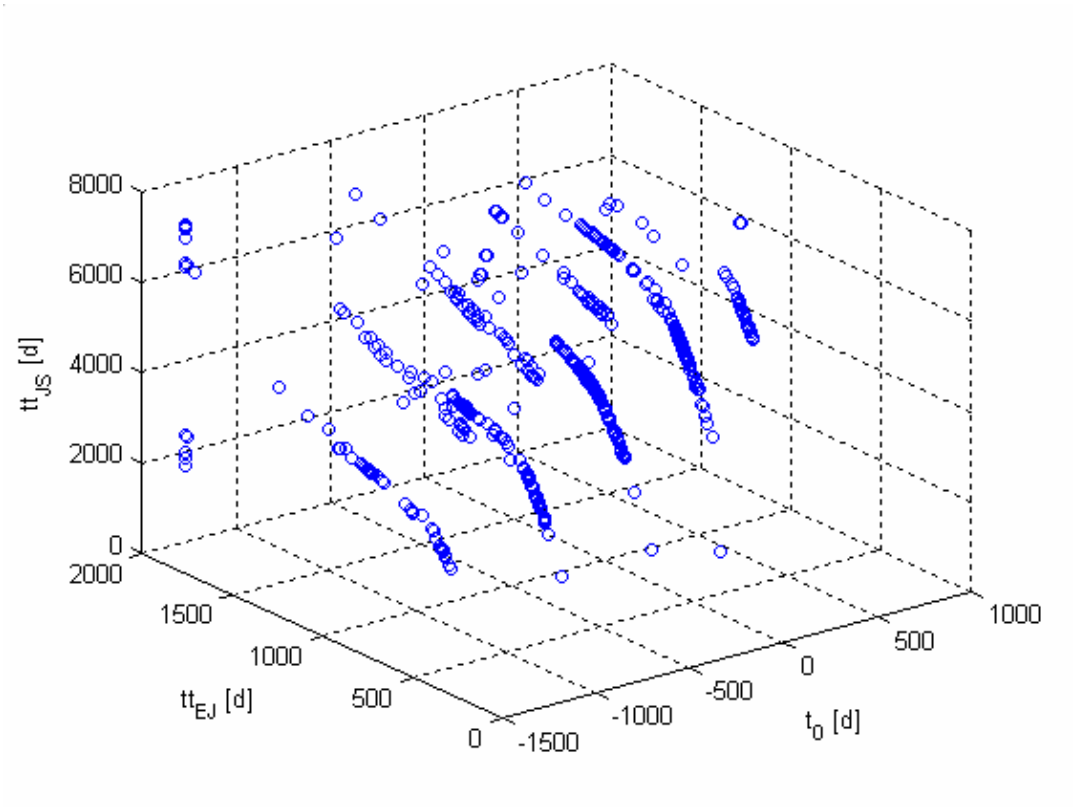

Figure 14: Three dimensional illustration of the local minima in the search space.

Figure 14 shows that, besides the presence of the previously identified big-valley structure in the $tt_{EJ} - tt_{JS}$ subspace, a similar structure can be also identified in $t_0 - tt_{EJ}$ and $t_0 - tt_{JS}$ subspaces. These results have been observed in all mission analysis classes analysed so far and can be associated to the date of departure design variable and its quasi-periodicity features due to the planetary geometry. To better understand the reasons for the presence of the big-valley structures in the $tt_{EJ} - tt_{JS}$ space, a thorough analysis is performed by fixing the value of the date of departure and plotting the objective function with respect to the other design variables. The date of departure is set to -180 *d* and the analysis to the intervals on the Earth-Jupiter transfer time is restricted to $[600, 1000]d$ and on the Jupiter-Saturn transfer time to $[1000, 7300]$ *d*. The resulting objective function values are showed in Figure 15.

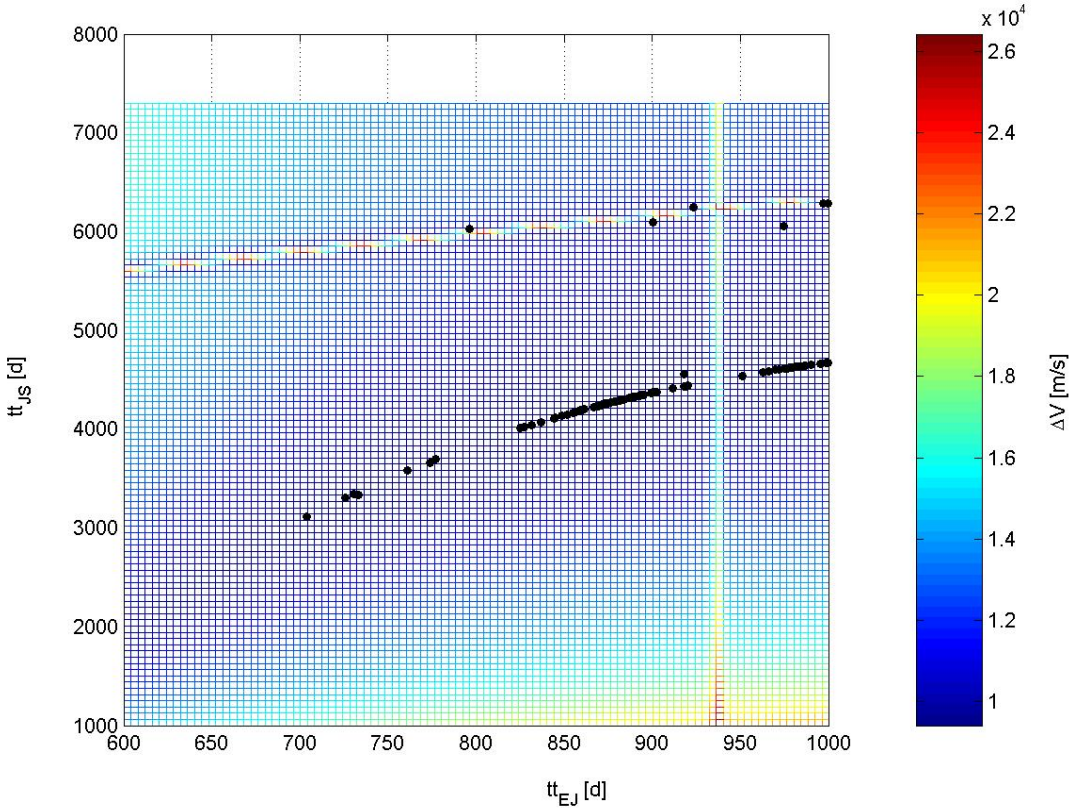

Figure 15: The ΔV as a function of the transfer times at a fixed date of departure (-180 *d*).

Figure 15 also shows 100 local minima generated with a random start search and a consequent local optimisation process by a SQP algorithm: there is evidence of the existence of a structure that is associable to a *big valley*. For the sake of completeness, note that the two lines of discontinuity, easily identifiable in Figure 15, correspond to the case when the Earth-Jupiter and Jupiter-Saturn transfer angles are at 180 degrees. In this case the orbital plane is ambiguous (an infinite number of transfer orbits exist) and Battin's algorithm here is singular. An important observation can be made by considering the trend of each term in the objective function, that is ΔV_I at Earth, ΔV_F at Saturn and the corrective $\Delta V_{GA,J}$ at Jupiter. Figure 16 and Figure 17 respectively show the $(\Delta V_I + \Delta V_F)$ and $\Delta V_{GA,J}$ as functions of the Earth-Jupiter and Jupiter-Saturn transfer times.

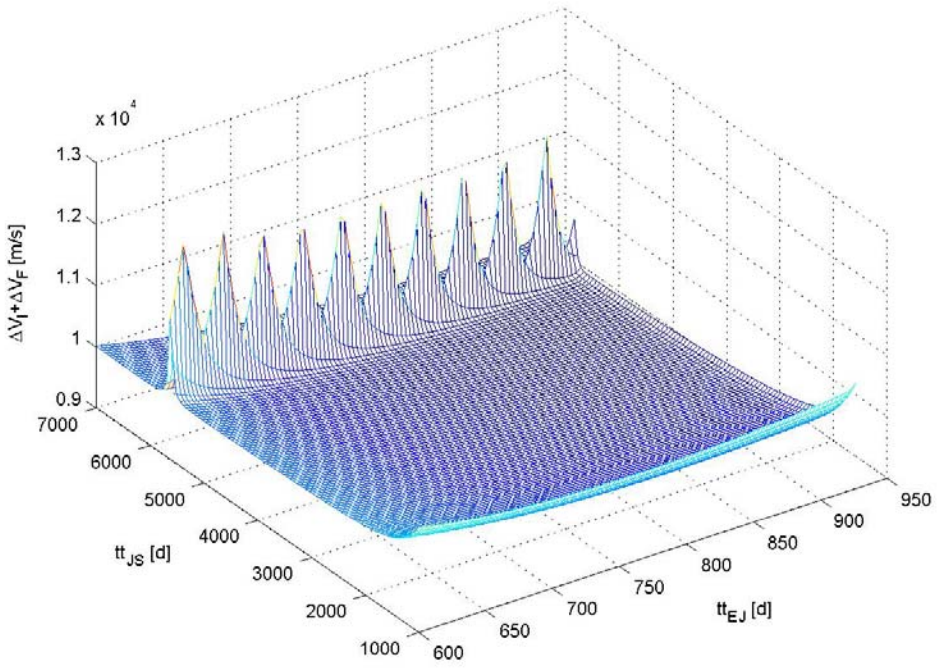

Figure 16: $\Delta V_I + \Delta V_F$ as a function of the transfer times at a fixed date of departure (-180 *d*).

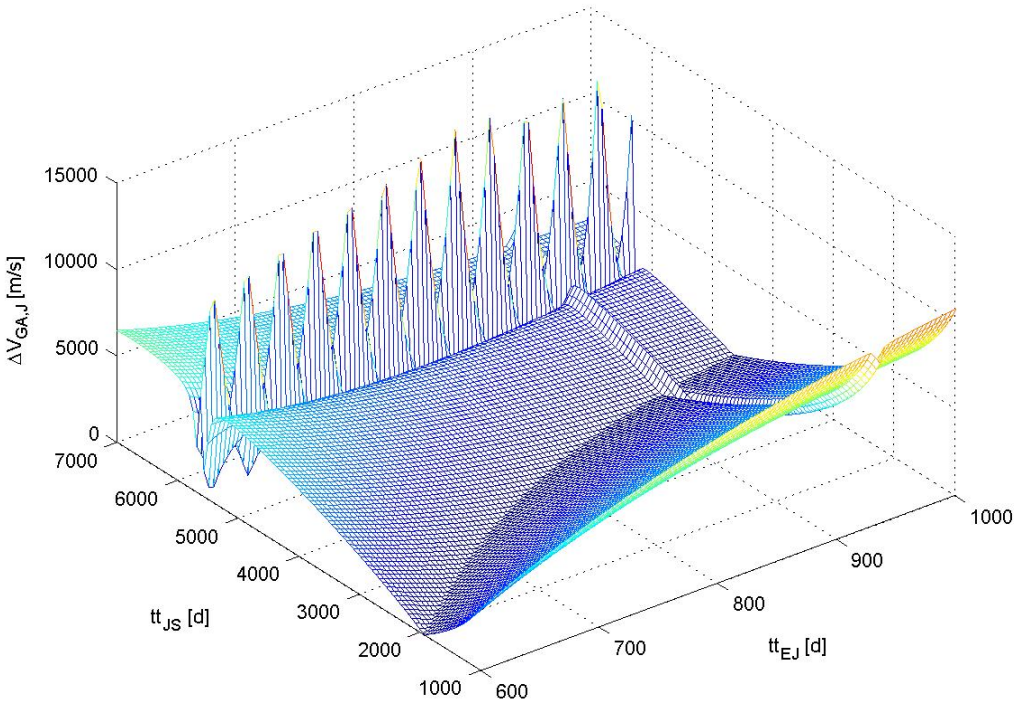

Figure 17: $\Delta V_{GA,J}$ as a function of the transfer times at a fixed date of departure (-180 *d*).

Figure 16 and Figure 17 show that, while the sum $\Delta V_I + \Delta V_F$ has a monotonic trend with respect to the transfer times in the considered search space by fixing the date of departure, the $\Delta V_{GA,J}$ can be considered as the principal reason of existence of the big-valley structures above identified in the $tt_{EJ} - tt_{JS}$ subspace. As a confirmation of this observation let us concentrate on the values of each objective function term along the big-valley structure, highlighted in red in Figure 18.

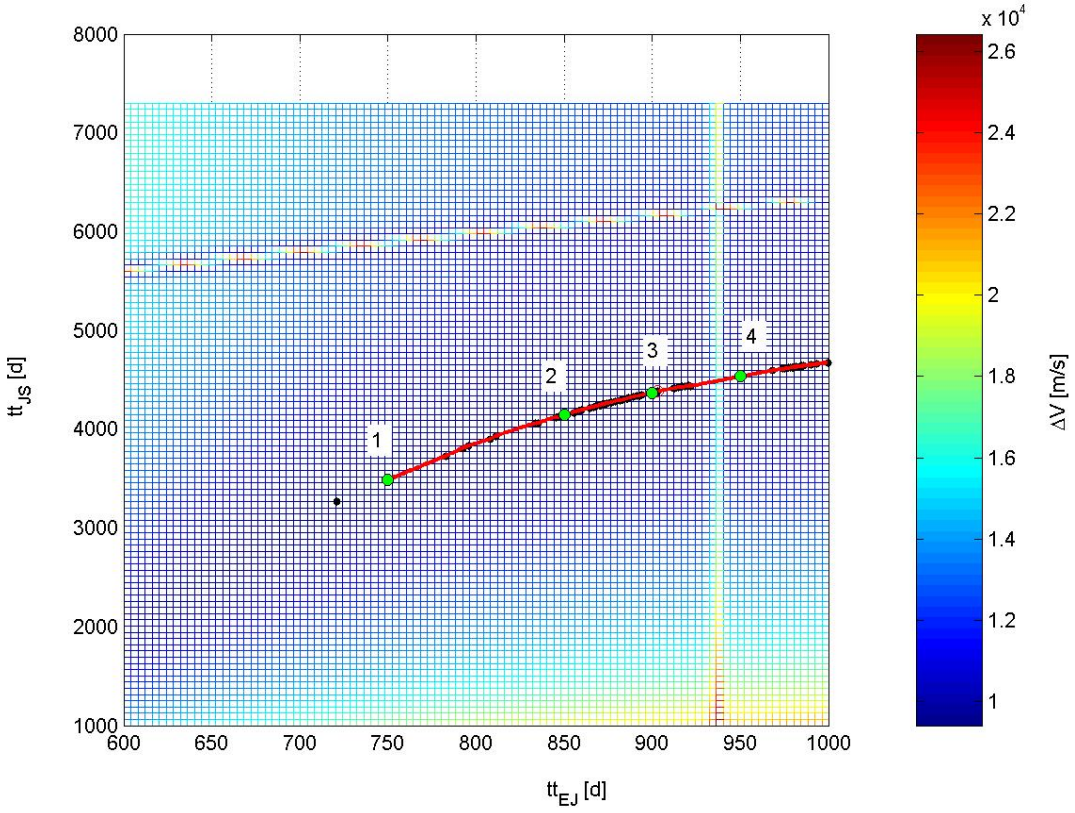

Figure 18: Big-valley structure analysis.

Figure 19 shows the transfer trajectories for solutions 1, 2, 3 and 4 highlighted in Figure 18, along the big-valley structure, while Table 6 shows the corresponding values of the objective function terms.

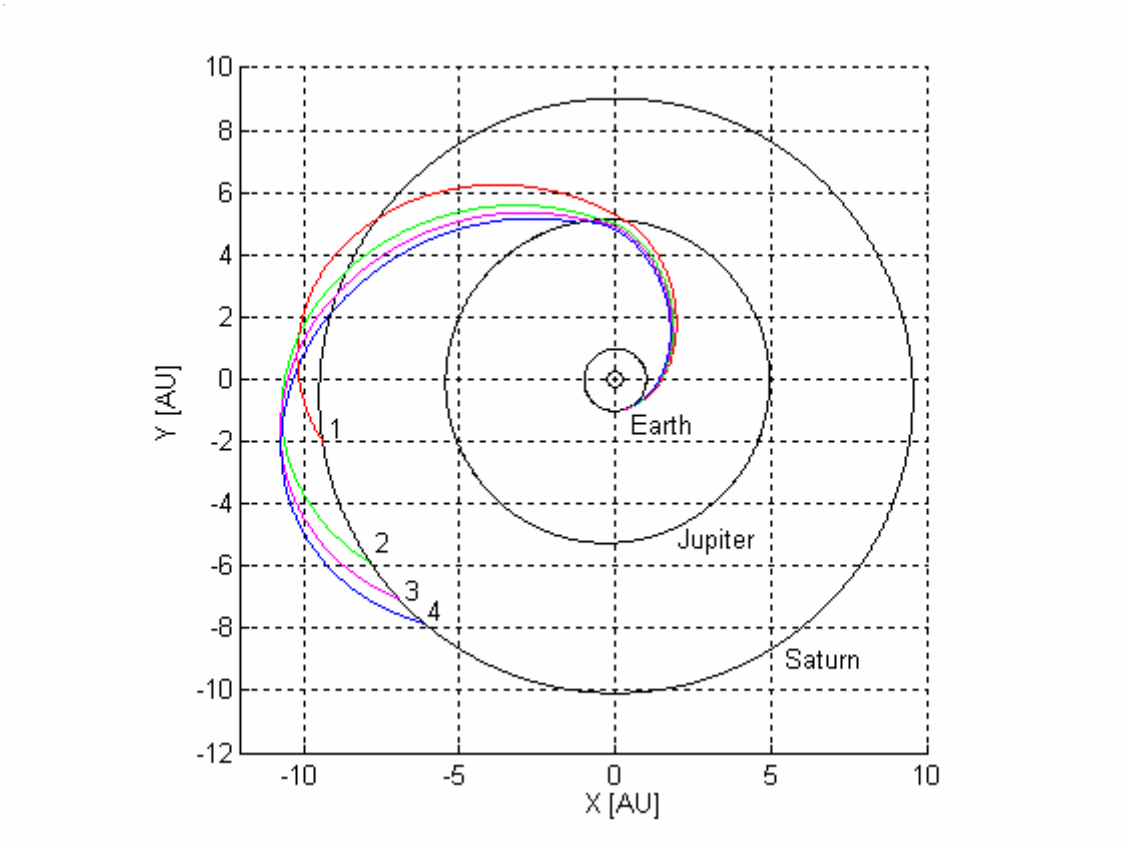

Figure 19: Transfer trajectories for solutions 1, 2, 3 and 4.

Solution	ΔV_I [*m/s*]	$\Delta V_{GA,J}$ [*m/s*]	ΔV_F [*m/s*]
Solution 1:	9131.2	14.28	437.31
Solution 2:	9001.3	4.84	430.63
Solution 3:	8977.4	0.0057	431.33
Solution 4:	9214.3	6.68	434.85

Table 6: Values of the objective function terms for solutions 1, 2, 3 and 4.

Table 6 shows that the big-valley structure corresponds to low values of the corrective $\Delta V_{GA,J}$. Moreover, similar structures can be identified even in case of simpler mathematical models: as an example a circular and coplanar planetary orbital model has been investigated. After assuming medium values for planetary orbital parameters and imposing Earth, Jupiter and Saturn positions at the date of departure as the projections on the ecliptic plane of their real position vector in a three dimensional analytical ephemeris model at the

previously fixed date of departure (-180 *d*), the trend of the corresponding objective function has been analysed.

Figure 20 shows the objective function values with respect to the transfer times, while Figure 21 compares the objective function structure with respect to the three dimensional case, by showing the differences in the position of the big-valley structure.

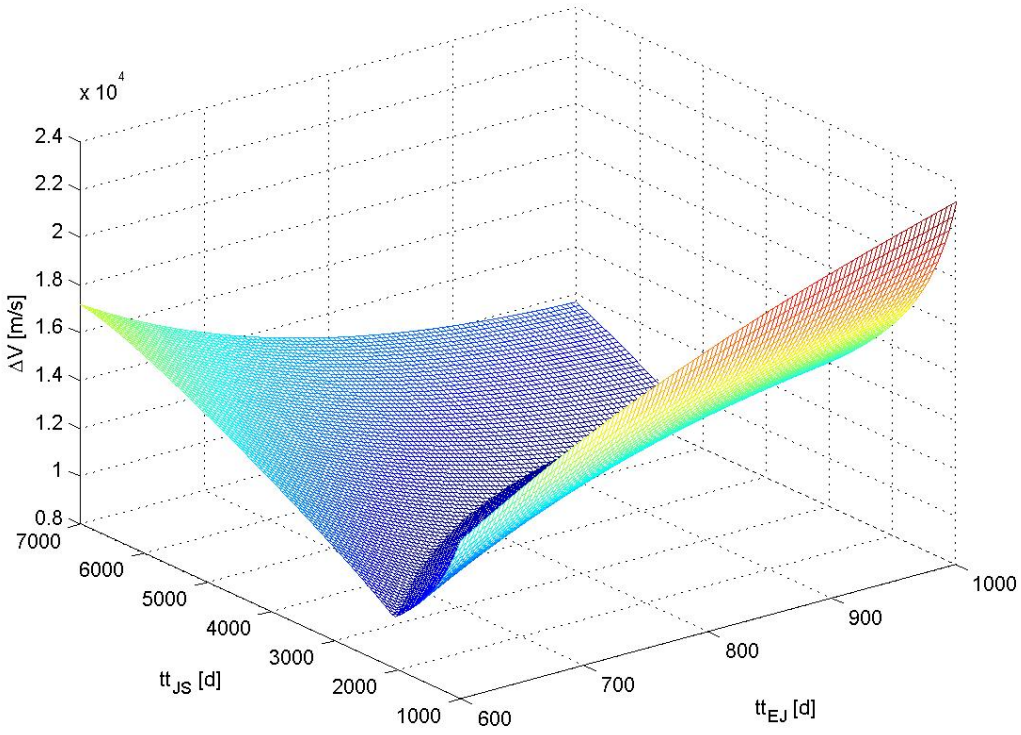

Figure 20: Objective function values with respect to the transfer times in a circular and coplanar planetary mathematical model.

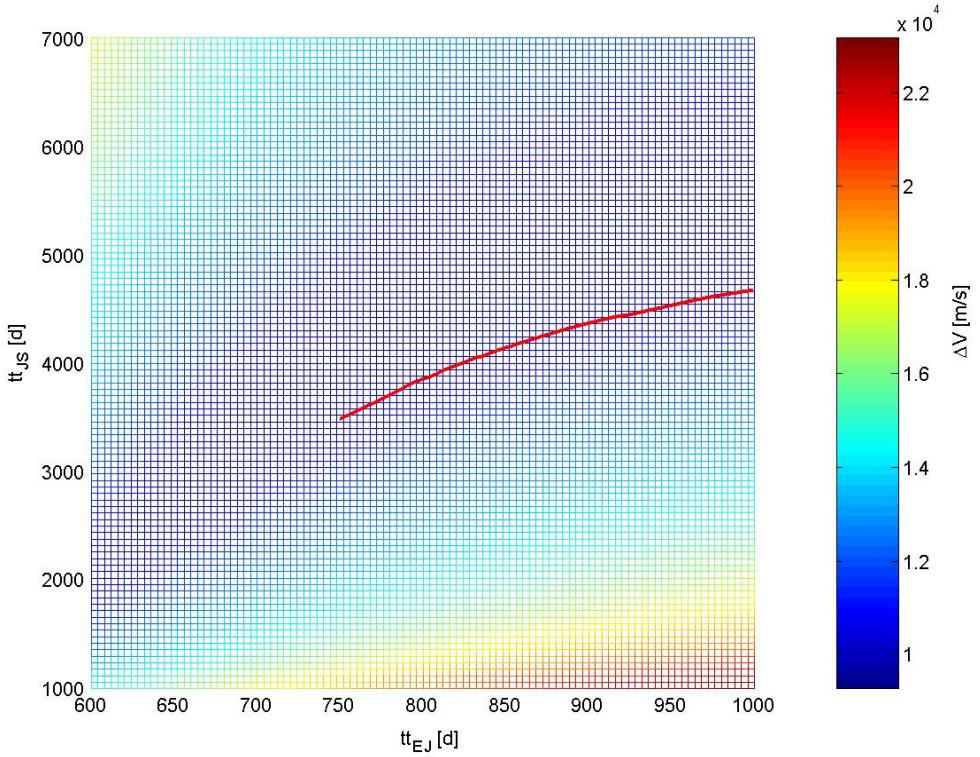

Figure 21: The objective function structure in the circular and coplanar planetary orbital model. Comparison with respect to the three dimensional case (big valley structure is shown in red).

A big-valley structure can be easily identified also in the coplanar and circular case and the position of such a structure is quite different with respect to the three dimensional case, especially in the Jupiter-Saturn transfer time.

Note that, in case of interest in solutions corresponding to the big-valley structure, the objective function structures are quite similar in the two dimensional and three dimensional case. Using as a first guess solution for a deterministic local optimisation process in the three dimensional model an optimal solution of the two dimensional model, we can easily converge to the optima of the corresponding structure in the three dimensional case. This suggests the possibility of firstly executing a global optimisation process in the two dimensional model, which is far simpler and faster due to the lower computational costs, and then searching for the global optimum in the three dimensional case using a local optimisation process, which could be run in the convex big-valley structure and then solved with a polynomial time algorithm.

Moreover, note that the principal reason of the presence of the big-valley structure in the $tt_{EJ} - tt_{JS}$ subspace is again the $\Delta V_{GA,J}$. Figure 22 and Figure 23 respectively show the $\Delta V_I + \Delta V_F$ and the $\Delta V_{GA,J}$ trend over the transfer times search space in the two dimensional case.

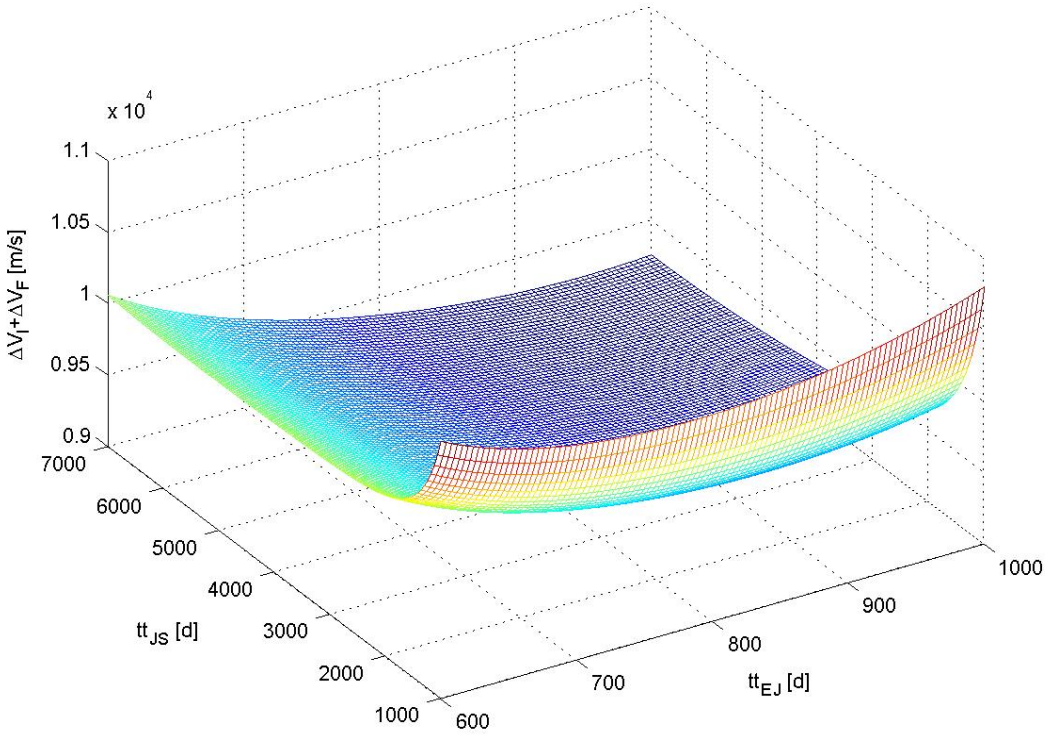

Figure 22: ($\Delta V_I + \Delta V_F$) values over the transfer times search space in two dimensional case.

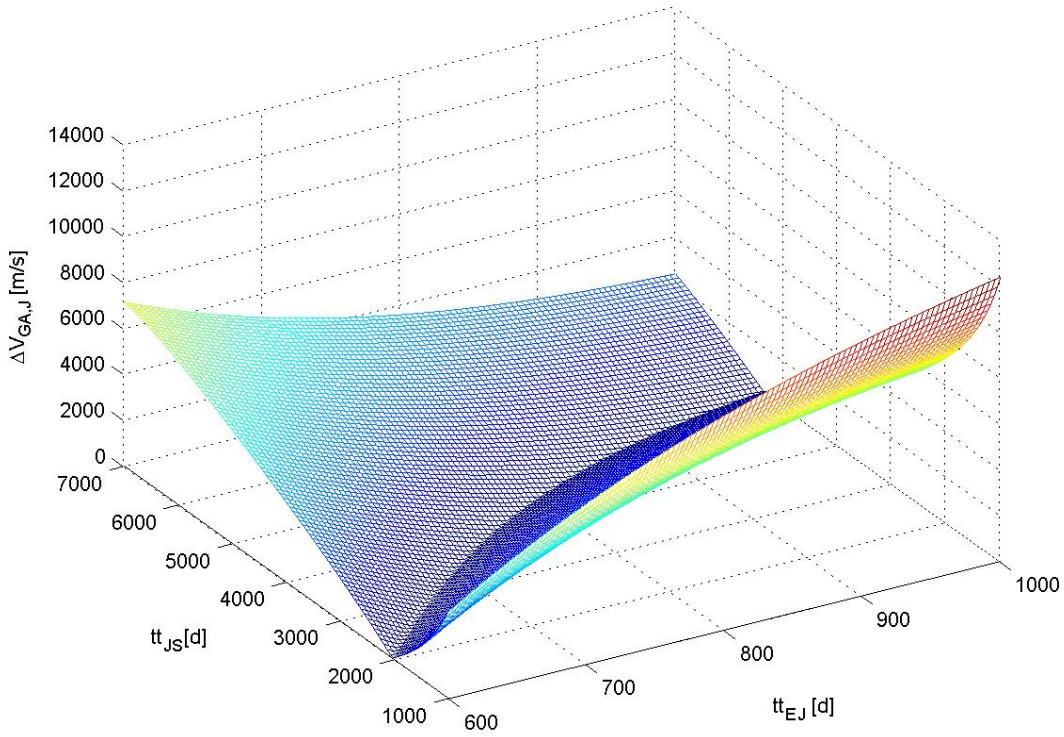

Figure 23: $\Delta V_{GA,J}$ values over the transfer times search space in the two dimensional case.

The big valley structure corresponds again to low values of the $\Delta V_{GA,J}$ term. This leads to the intuition that other mathematical models for multiple gravity assist interplanetary missions which don't make use of $\Delta V_{GA,J}$ corrective terms will show a different objective function structure. In order to analyse this important aspect, the consequence of using deep space manoeuvres instead of $\Delta V_{GA,J}$ corrective terms will be addressed at the end of this section. Finally, the transfer trajectory and the ΔV features corresponding to the best solution identified are now presented in Tables 7-8 and Figure 24.

Date of departure:	06/07/1999
Earth–Jupiter transfer time:	910.11 *d*
Jupiter–Saturn transfer time:	4416.7 *d*

Table 7: search space parameters.

Overall ΔV :	9391.2 *m/s*
ΔV_I :	8959.3 *m/s*
$\Delta V_{GA,J}$:	$4.83 \cdot 10^{-4}$ *m/s*
ΔV_F :	431.94 *m/s*

Table 8: Objective space parameters.

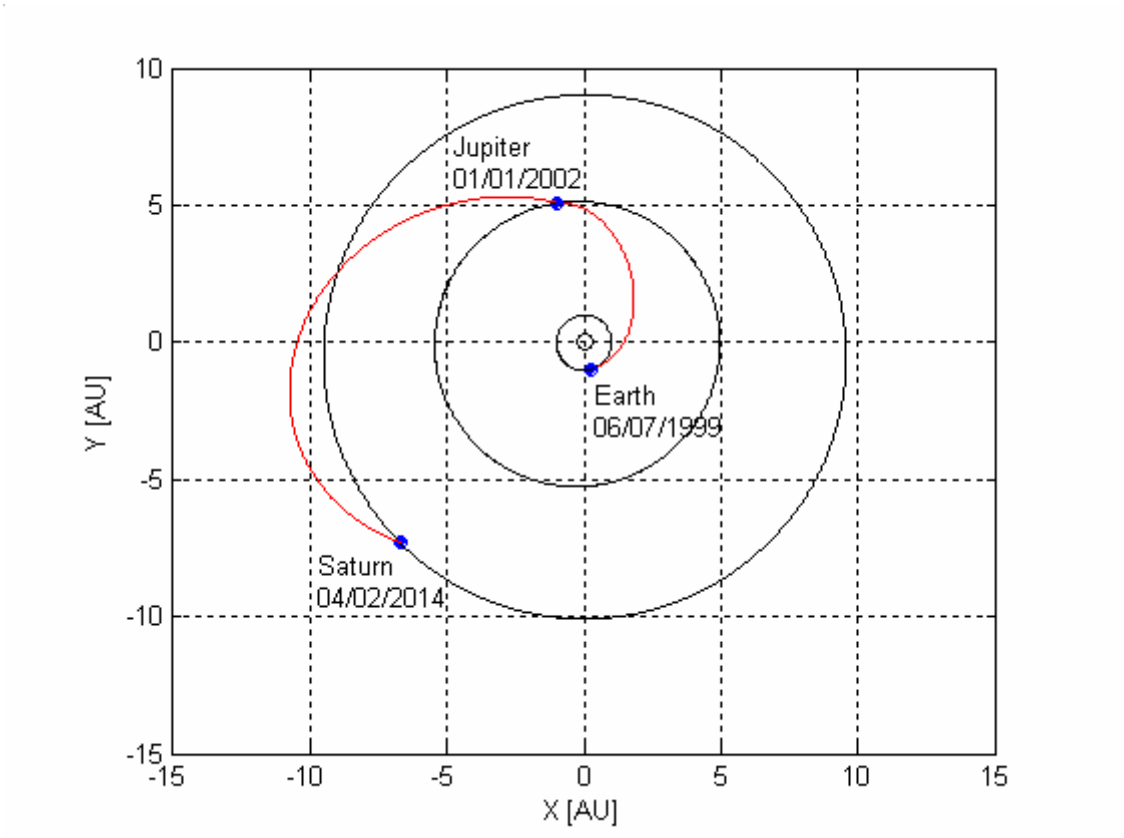

Figure 24: Transfer trajectory corresponding to the best solution found

3.4 Earth – Mars – Jupiter – Saturn (EMJS)

Once fixed the value of the discrete variable “sequence of planets” to EMJS, the number of continuous variables which complete the search space is four: the date of departure from Earth, t_0, and the transfer times Earth–Mars, Mars–Jupiter and Jupiter–Saturn, tt_{EM}, tt_{MJ} and tt_{JS} respectively. The upper and lower bounds for the transfer time associated to the three linking arcs E-M, M-J and J-S have been posed equal to 0.1 and 2 times the associated Homann transfer time respectively. The resulting intervals are:

$$\left[tt_{EM}^{L}, tt_{EM}^{U}\right] = \left[25.86,\ 517.17\right] d \quad [8]$$

$$\left[tt_{MJ}^{L}, tt_{MJ}^{U}\right] = \left[112.54,\ 2250.7\right] d \quad [9]$$

$$\left[tt_{JS}^{L}, tt_{JS}^{U}\right] = \left[365.02, 7300.4\right] d \quad [10]$$

Figure 25 compares the widths of the interval of variation associated to the design variables.

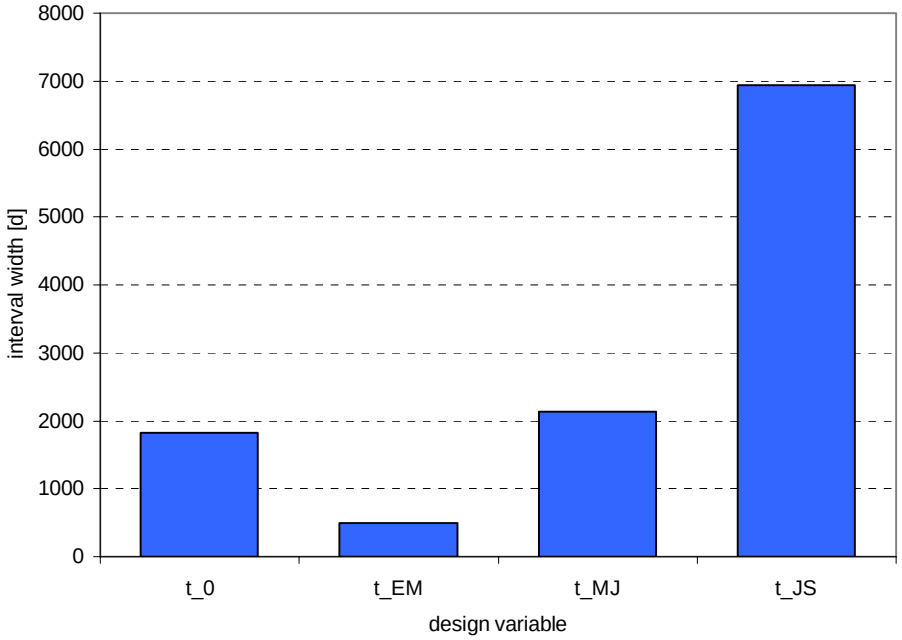

Figure 25: Comparison between the widths of the intervals of variation in the search space.

After generating the 1000 local minima, the mean distances of each solution to the others have been evaluated. By using the Reeves and Yamada methodology, Figure 26 shows the resulting structure of the objective function: the x-axis reports the normalized mean distance of each local optima, while the corresponding objective function values are indicated along the y-axis.

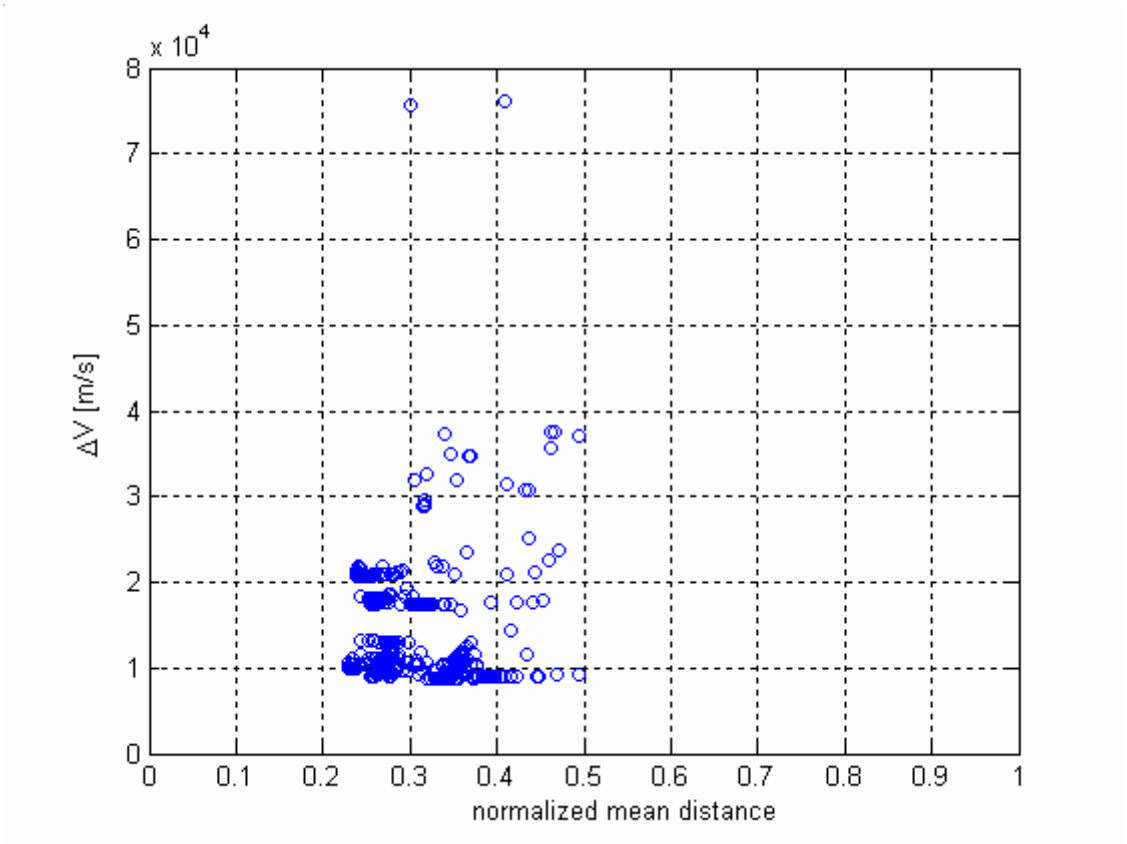

Figure 26: Objective function structure analysis for an EMJS transfer

By analysing Figure 26, a *big-valley* structure of the objective function for an EMJS transfer can once again be identified. The mean closeness of most local optima tends to range between 0.2 and 0.4 times the hyper-diagonal magnitude, corresponding to an interval between 1500 *d* and 2250 *d*. In order to analyse the distribution of the local minima and verify the existence of a *big valley* structure, the search space is probed in the following. Figure 27 shows the dates of departure (*x*-axis) and the objective function values (*y*-axis) corresponding to the identified local optima.

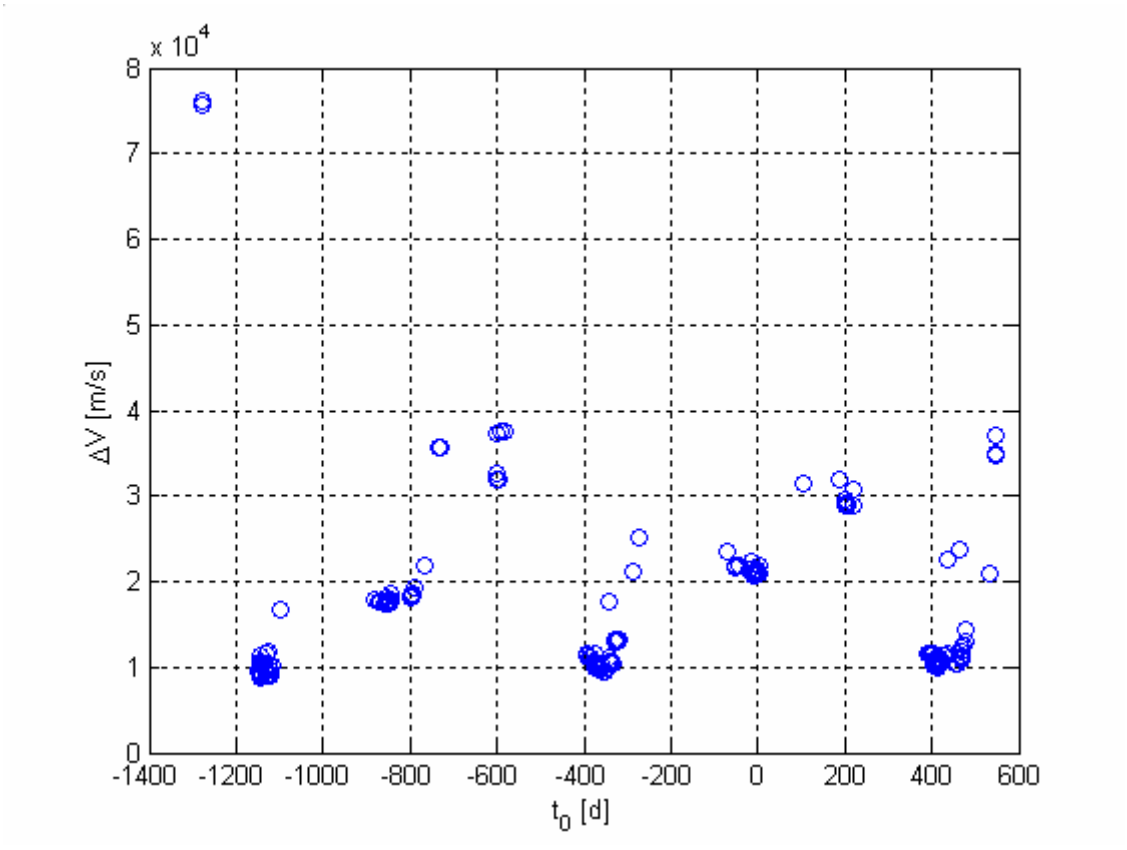

Figure 27: Local optima distribution over the date of departure design variable.

Even in the EMJS case, the local optima tend to gather in groups near fixed date of departure values; however, compared to the previous case, the interval between two of this fixed dates is not constant. This result can be intuitively explaneed by means of the synodic periods of the planetary systems: in fact, note that the synodic period of the Earth-Mars system is equal to 780 days and that of the Mars-Jupiter system is equal to 815 days; this leads to two comparable frequencies on the quasi-periodicity of the objective function with respect to the design variables that interact with each other (note that the synodic period of the Jupiter – Saturn system is equal to 7254 days, corresponding to a frequency that is one order of magnitude bigger). Moreover, the local optima corresponding to a fixed date tend to have similar objective function evaluations. Consider now the remaining design variables. Figure 28 shows the local minima distribution over the three dimensional transfer times subspace, while Figure 29, Figure 30 and Figure 31 plot the projection along the three *z*, *y* and *x* axis respectively.

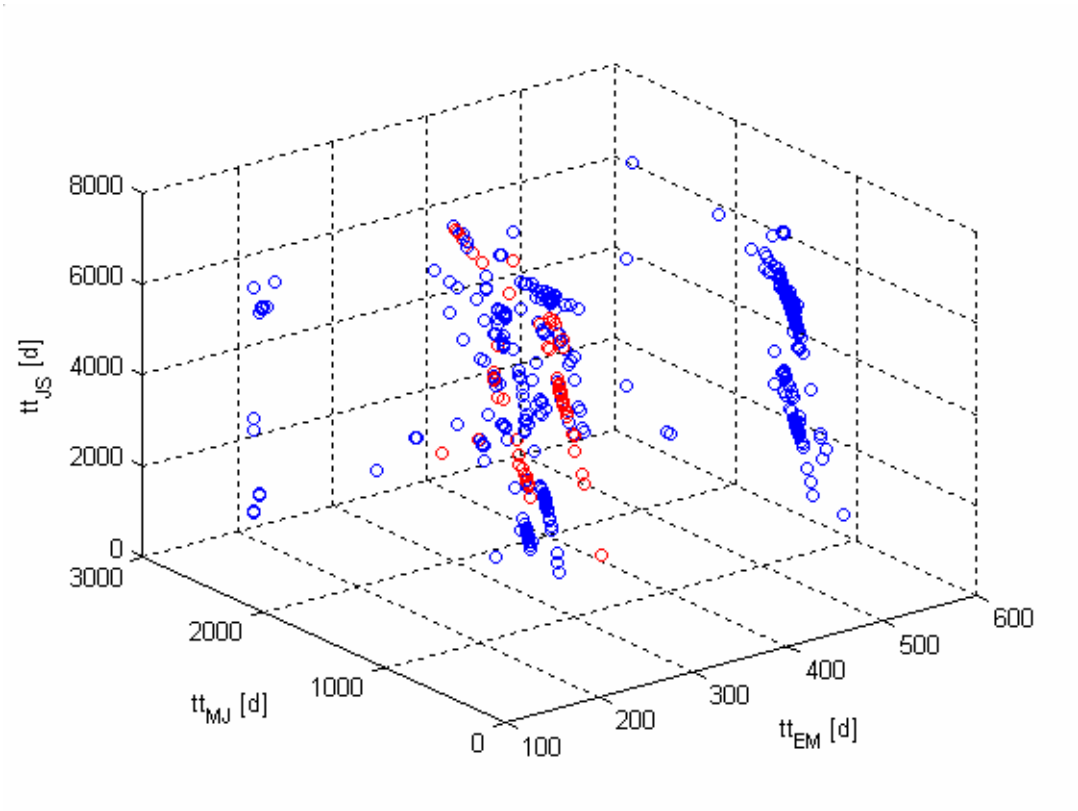

Figure 28: Three dimensional illustration of the local minima in the transfer times subspace.

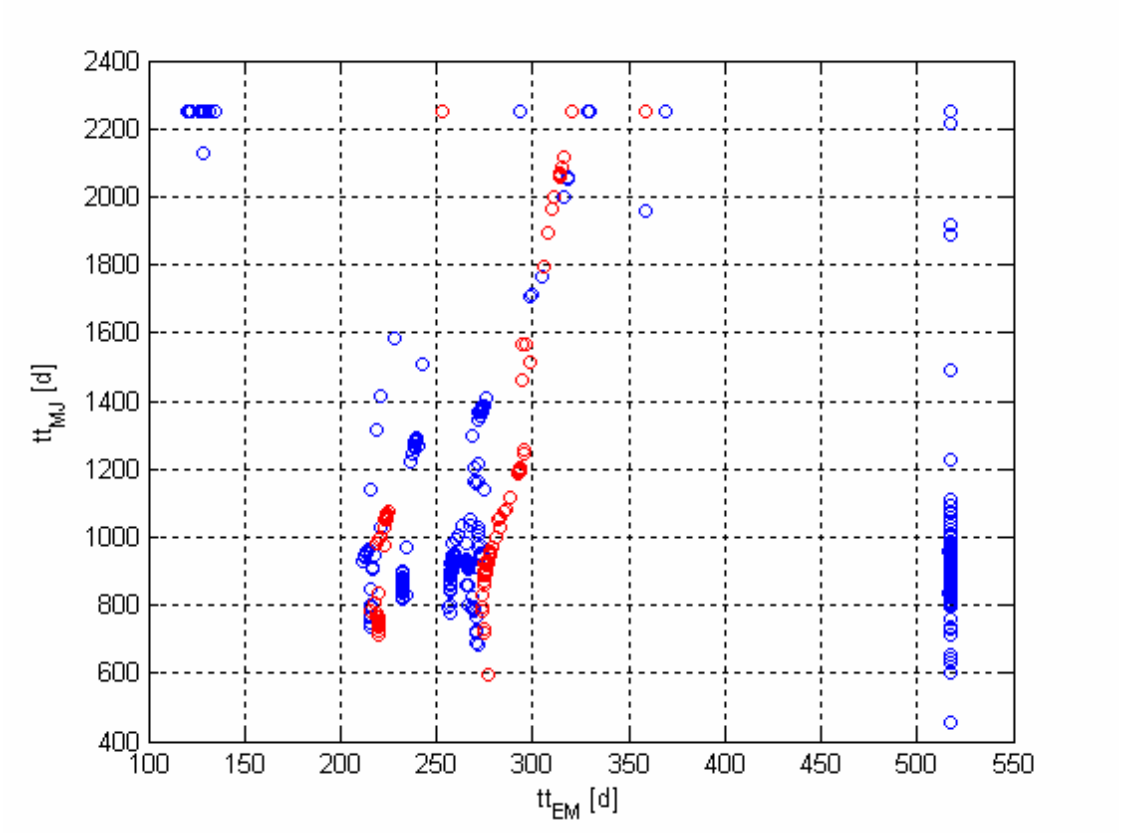

Figure 29: Local minima distribution in the tt_{EM} - tt_{MJ} subspace.

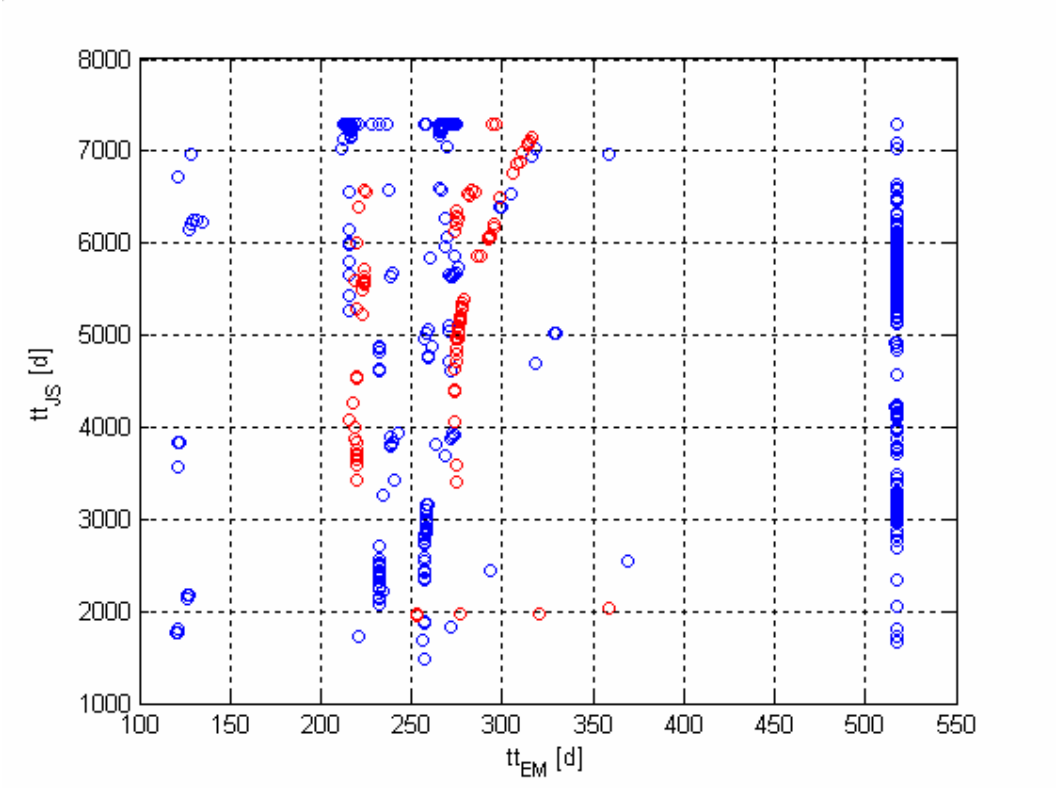

Figure 30: Local minima distribution in the tt_{EM} - tt_{JS} subspace.

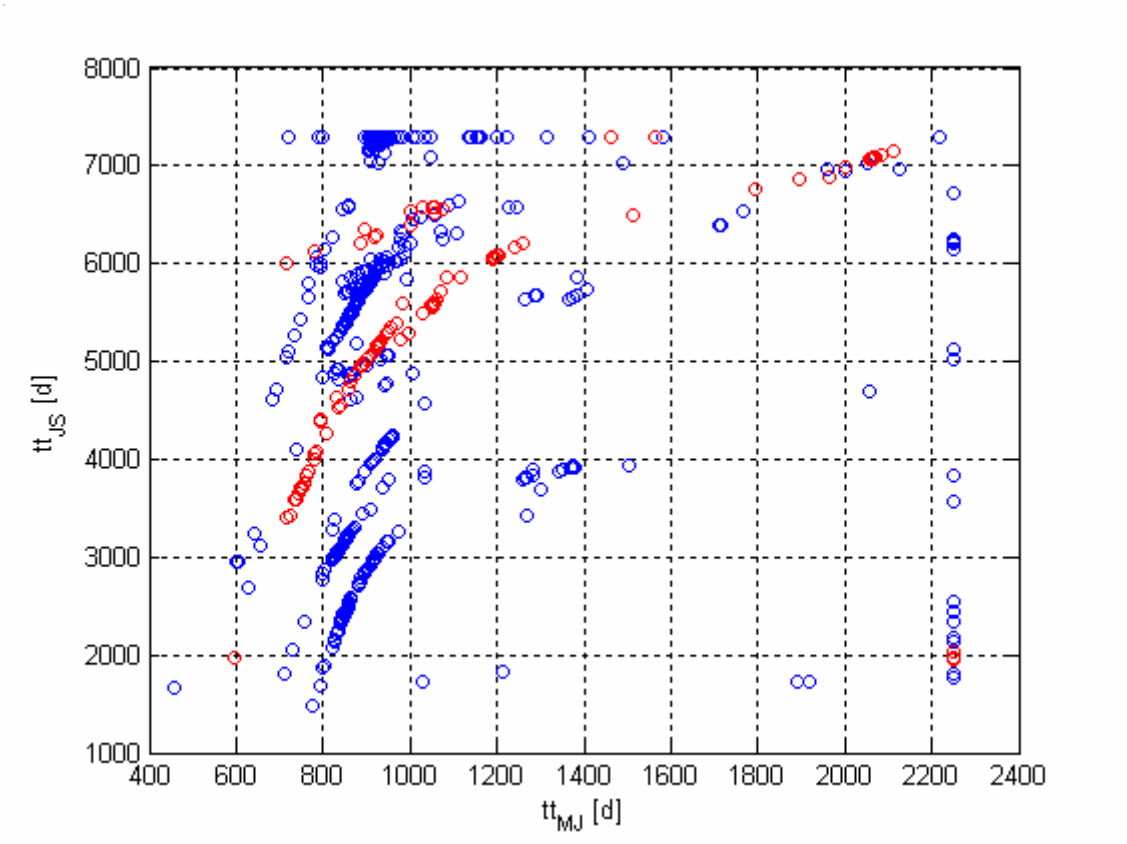

Figure 31: Local minima distribution in the tt_{MJ} - tt_{JS} subspace.

One again *big valley* structures are easily identifiable. The previous figures also show (in red) the local optima corresponding to date of departure values close to -400 *d*: these local optima tend to distribute themselves over three dimensional curves on the transfer times subspace with similar objective function evaluation. Finally, the transfer trajectory and the ΔV features corresponding to the best solution found are now presented.

Date of departure:	11/11/1996
Earth–Mars transfer time:	257.87 *d*
Mars-Jupiter transfer time:	906.93 *d*
Jupiter-Saturn transfer time:	2918.8 *d*

Table 9: Search space parameters.

Overall ΔV :	8866.5 *m/s*
ΔV_I :	3282.5 *m/s*
$\Delta V_{GA,M}$:	5309.6 *m/s*
$\Delta V_{GA,J}$	0.0043 *m/s*
ΔV_F :	274.41 *m/s*

Table 10: Objective space parameters.

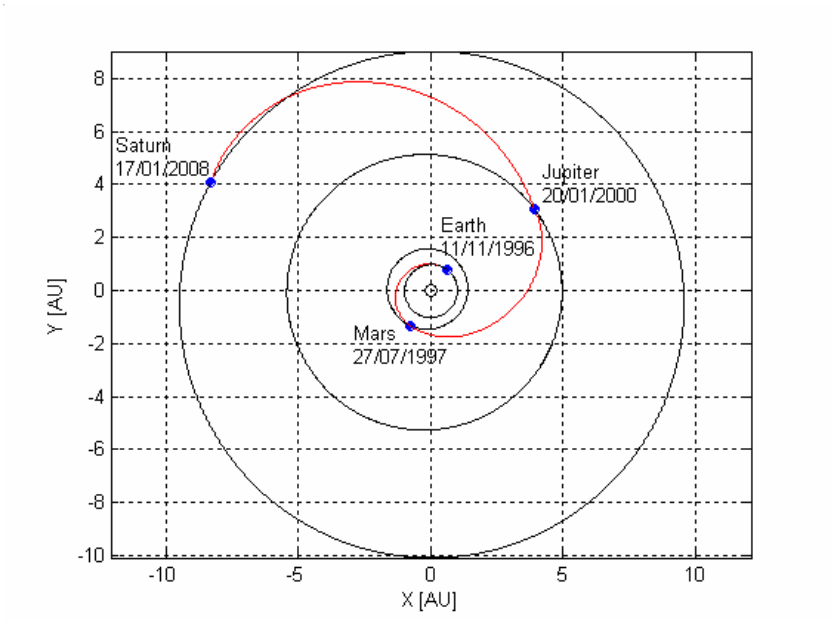

Figure 32: Transfer trajectory corresponding to the best solution found.

3.5 Earth – Venus – Earth – Jupiter – Saturn (EVEJS)

Once fixed the value of the discrete variable “sequence of planets” to EVEJS, the number of continuous variables which complete the search space is five: the date of departure from Earth, t_0, and the transfer times Earth–Venus, Venus– Earth, Earth–Jupiter and Jupiter–Saturn ($tt_{EV}, tt_{VE}, tt_{EJ}$ and tt_{JS} respectively). The upper and lower bounds for the transfer time associated to the four linking arcs E-V, V-E, E-J and J-S have been set equal to 0.1 and 2 times the associated Homann transfer time respectively. The resulting intervals are:

$$\left[tt_{EV}^{L}, tt_{EV}^{U}\right] = [14.59, 291.83]\,d \quad [11]$$

$$\left[tt_{VE}^{L}, tt_{VE}^{U}\right] = \left[tt_{EV}^{L}, tt_{EV}^{U}\right]d \quad [12]$$

$$\left[tt_{EJ}^{L}, tt_{EJ}^{U}\right] = [99.65, 1993.1]\,d \quad [13]$$

$$\left[tt_{JS}^{L}, tt_{JS}^{U}\right] = [365.02, 7300.4]\,d \quad [14]$$

Figure 33 compares the widths of the interval of variation associated with the five design variables.

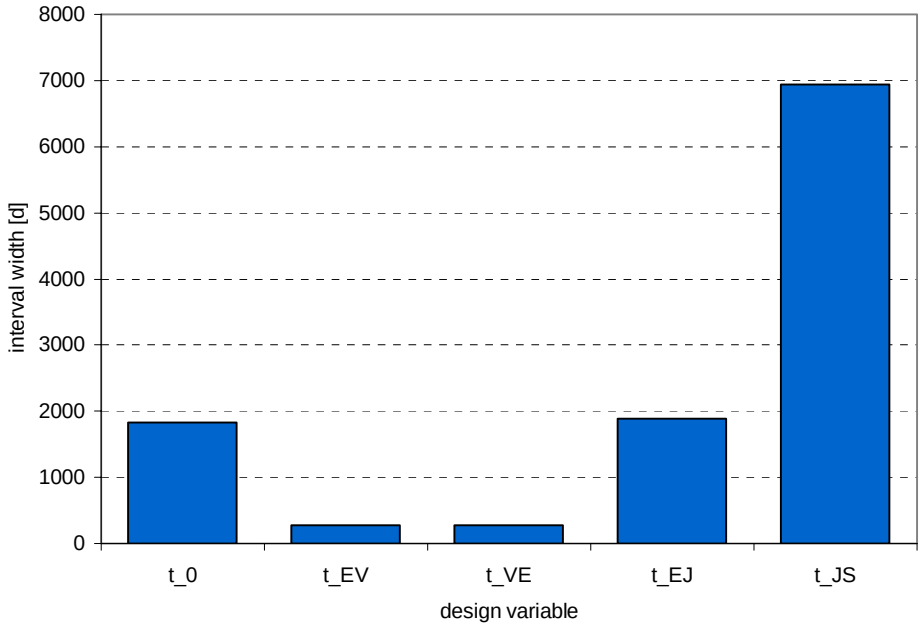

Figure 33: Comparison between the widths of the intervals of variation in the search space.

After generating the 1000 local minima, the mean distances of each solution to the others have been evaluated. By using the Reeves and Yamada methodology, Figure 34 shows the resulting structure of the objective function: the *x*-axis reports the normalized mean distance of each local optima, while the corresponding objective function values are indicated along the *y*-axis.

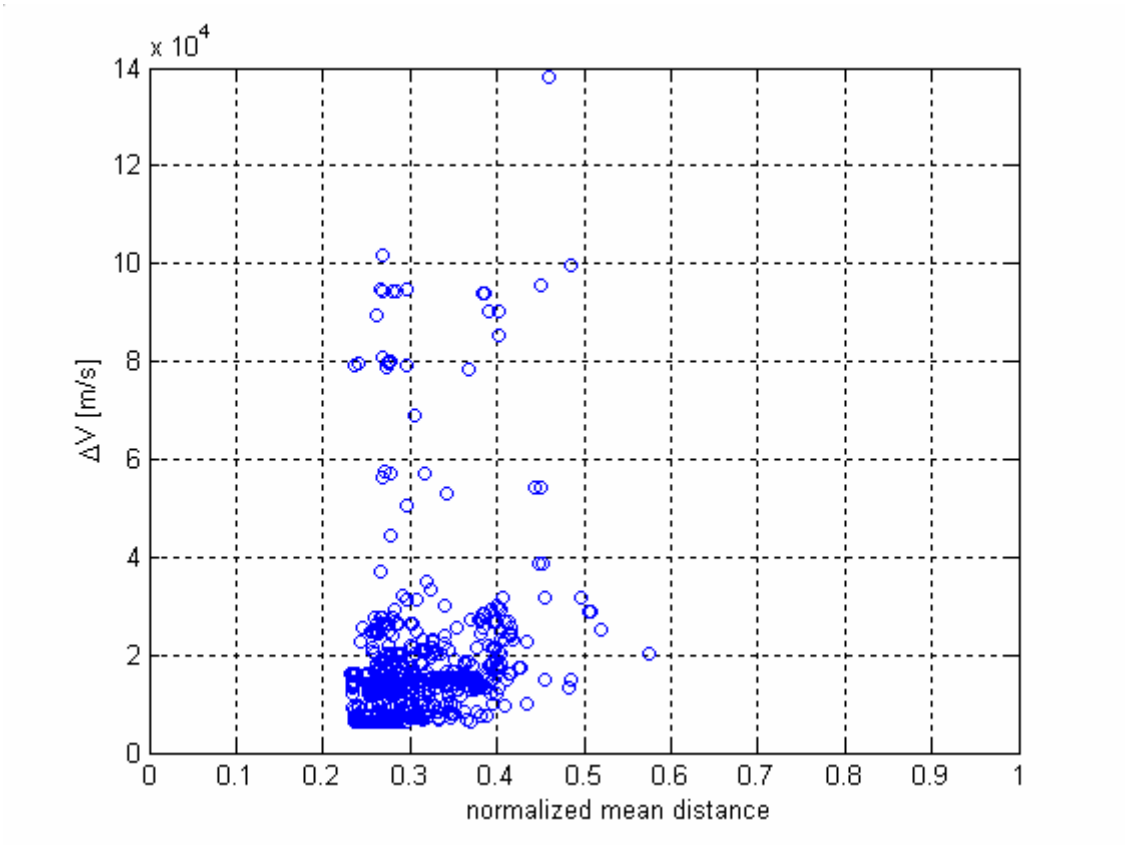

Figure 34: Objective function structure analysis for an EVEJS transfer.

By analysing Figure 34, the objective function for an EVEJS transfer presents a *big-valley* structure. The mean closeness of most local optima tends to range between 0.22 and 0.4 times the hyper-diagonal magnitude that is between 1634.1 *d* and 2971 *d*. In order to analyse the distribution of the local minima and verify the existence of a *big valley* structure, the search space is probed in more detail. Figure 35 shows the dates of departure (*x*-axis) and the objective function values (*y*-axis) corresponding to the identified local optima.

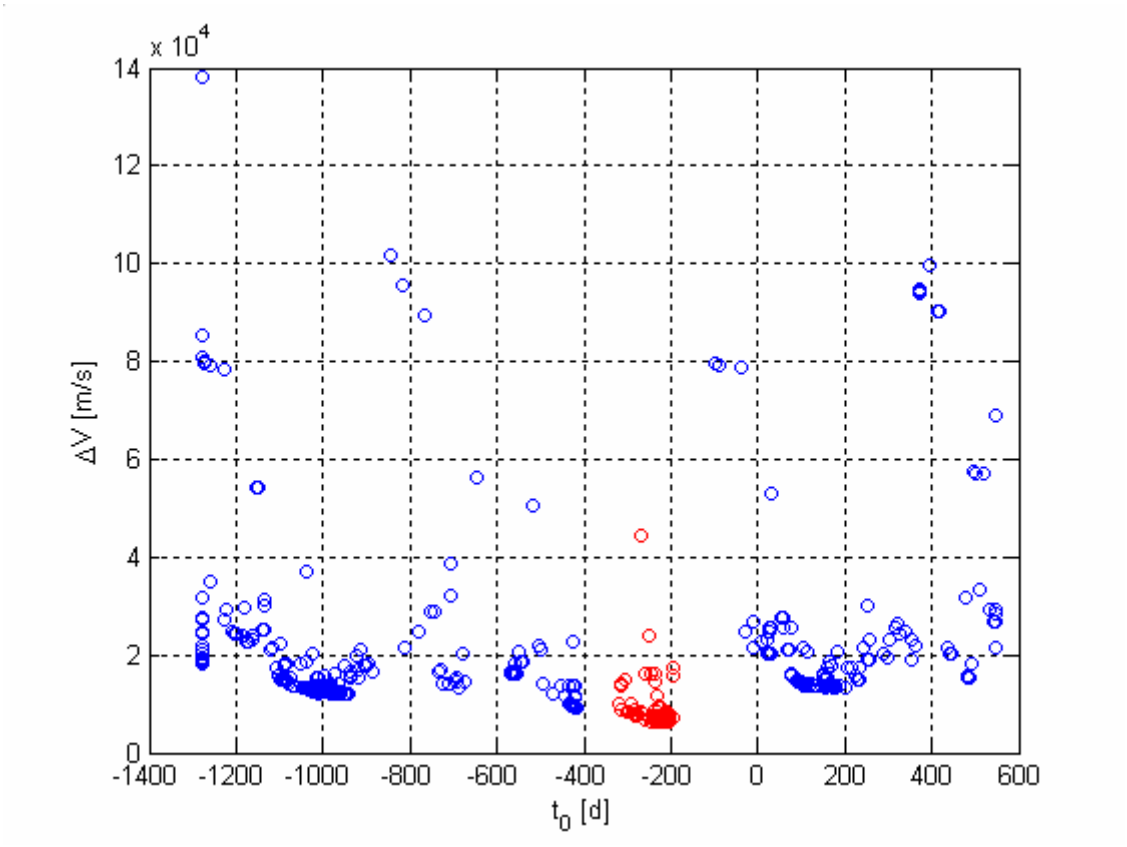

Figure 35: Local optima distribution over the date of departure design variable.

In the EVEJS case, the tendency of local optima to gather in groups near fixed date of departure values is less recognizable. By analysing the synodic periods of the planetary systems, one can note that the synodic period of the Earth-Venus system (583 days) and that of the Earth-Jupiter system (398 days) are comparable, leading to frequencies on the quasi-periodicity of the objective function with respect to the design variables that interact with each other (note that in this case there are two transfer phase that involve the Earth-Venus system). However, the local optima near a fixed date tend to have similar objective function evaluations. Consider now the remaining design variables. Figures 36-39 show the local minima distribution over the four dimensional transfer times subspace, by mean of the four projections along the four axes.

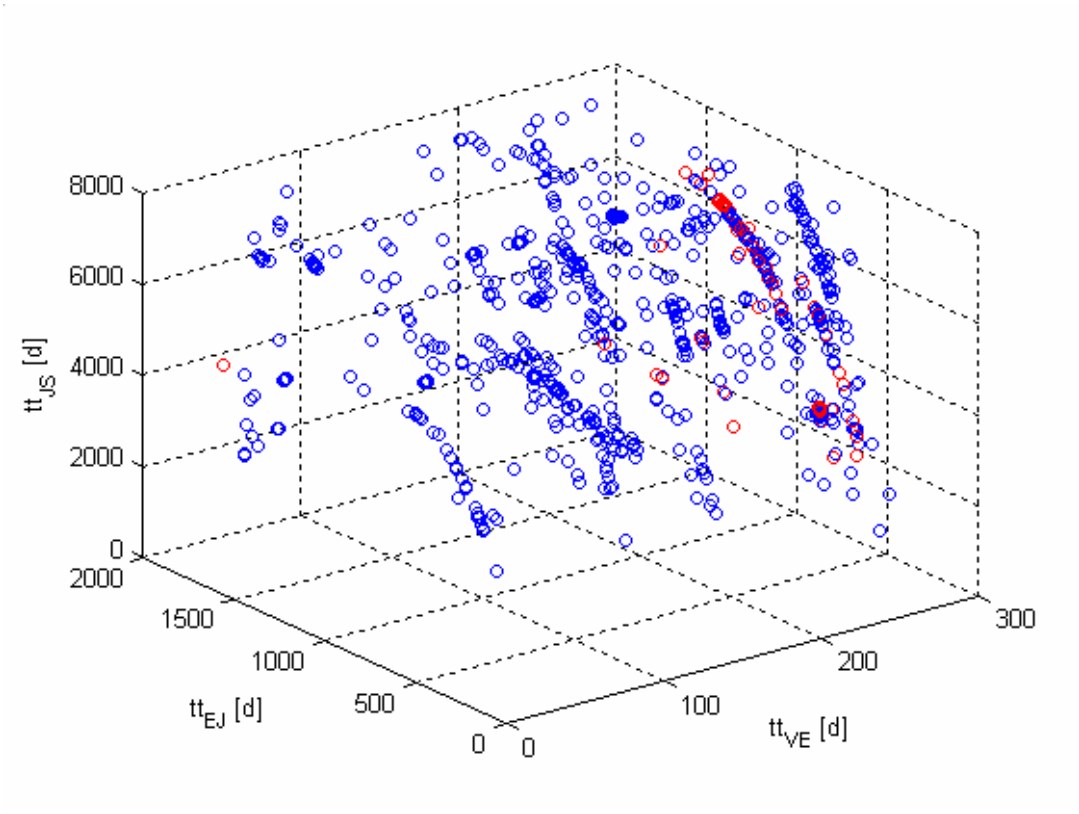

Figure 36: Local minima distribution in the tt_{VE} - tt_{EJ} - tt_{JS} subspace.

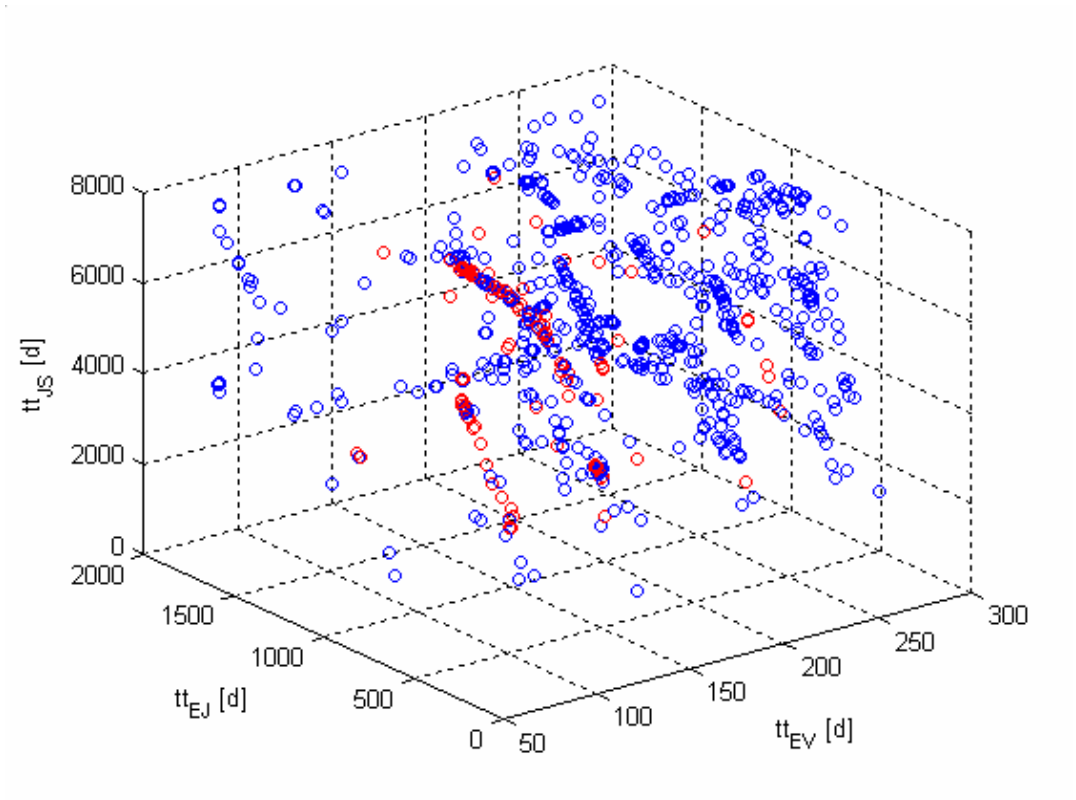

Figure 37: Local minima distribution in the tt_{EV} - tt_{EJ} - tt_{JS} subspace.

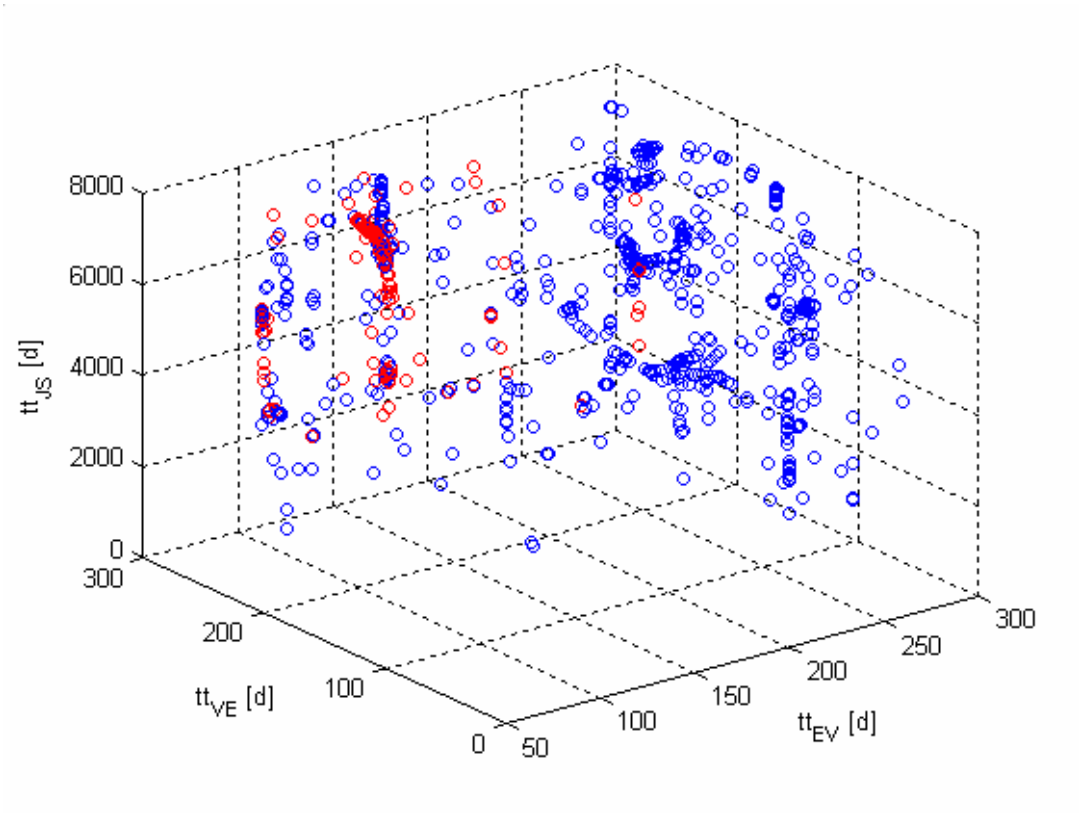

Figure 38: Local minima distribution in the tt_{EV} - tt_{VE} - tt_{JS} subspace.

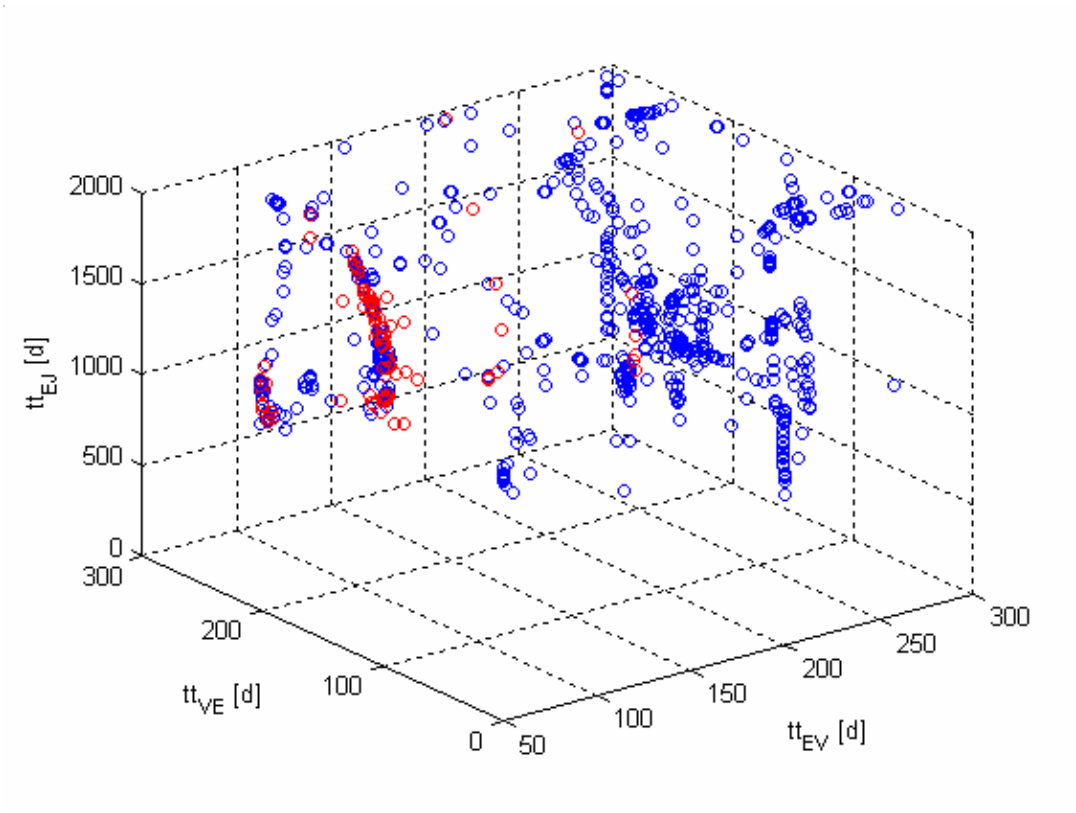

Figure 39: Local minima distribution in the tt_{EV} - tt_{VE} - tt_{EJ} subspace.

Big valley structures are again identifiable: the local optima corresponding to date of departure values near -200 *d* are shown (in red) in the previous figures; they tend to distribute themselves over three dimensional curves with similar objective function evaluations. The transfer trajectory and the ΔV features corresponding to the best solution found are now shown.

Date of departure:	12/06/1999
Earth–Venus transfer time:	160.07 *d*
Venus-Earth transfer time:	278.59 *d*
Earth-Jupiter transfer time:	1071.4 *d*
Jupiter-Saturn transfer time:	5999.7 *d*

Table 11: Search space parameters.

Overall ΔV :	6245.2 *m/s*
ΔV_I :	3069.7 *m/s*
$\Delta V_{GA,V}$:	0.0208 *m/s*
$\Delta V_{GA,E}$:	2708.4 *m/s*
$\Delta V_{GA,J}$:	0.0398 *m/s*
ΔV_F :	467.00 *m/s*

Table 12: Objective space parameters.

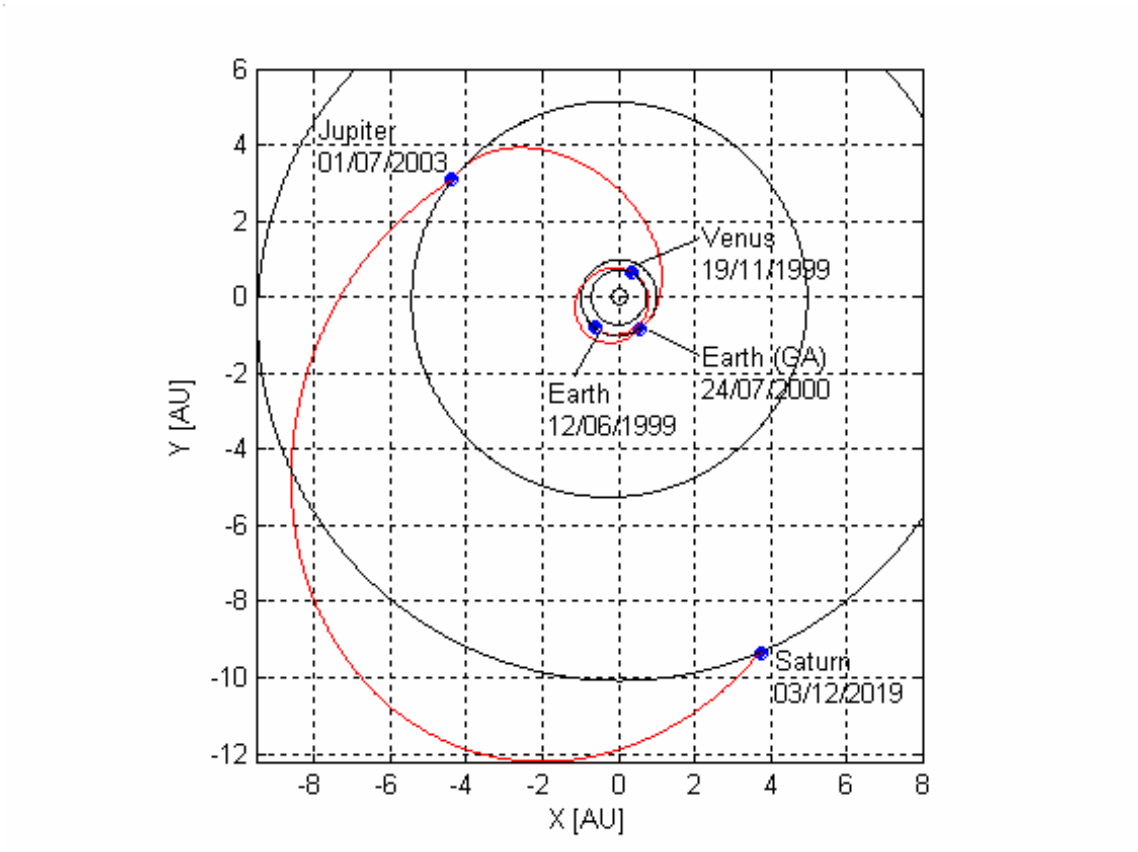

Figure 40: Transfer trajectory corresponding to the best solution found.

Figure 40 shows the best solution, by measuring the goodness with respect to the objective function, corresponding to the overall ΔV. In fact this could lead to the identification of a long transfer time solution as in this case (approximately 19 years travel). A careful analysis of the identified solutions however demonstrates that some of the local minima correspond to solutions with present shorter transfer times but more expensive energy requirements. For a better description and understanding of this phenomenon and its consequences, the next transfer case is presented.

3.6 Earth – Venus – Venus – Earth – Jupiter – Saturn (EVVEJS)

Once fixed the value of the discrete variable “sequence of planets” to EVVEJS, the number of continuous variables which complete the search space is six: the date of departure from Earth, t_0, and the transfer times Earth–Venus, Venus–Venus, Venus–Earth, Earth–Jupiter and Jupiter–Saturn (tt_{EV}, tt_{VV}, tt_{VE}, tt_{EJ} and tt_{JS} respectively). By indicating H as the Homann transfer time corresponding to the four linking arcs E-V, V-E, E-J and J-S and as T the period of Venus’ orbit, the upper and lower bounds for the transfer times variables have been set to:

$$\left[tt_{EV}^{L}, tt_{EV}^{U}\right] = [0.1, 2]H = [14.59, 291.83]\,d \quad [15]$$

$$\left[tt_{VV}^{L}, tt_{VV}^{U}\right] = [0.1, 2]T = [11.23, 448.92]\,d \quad [16]$$

$$\left[tt_{VE}^{L}, tt_{VE}^{U}\right] = [0.1, 1]H = [14.592, 145.92]\,d \quad [17]$$

$$\left[tt_{EJ}^{L}, tt_{EJ}^{U}\right] = [0.1, 1]H = [99.65, 996.54]\,d \quad [18]$$

$$\left[tt_{JS}^{L}, tt_{JS}^{U}\right] = [0.1, 1]H = [365.02, 3650.2]\,d \quad [19]$$

Figure 41 compares the widths of the interval of variation associated to the six design variables.

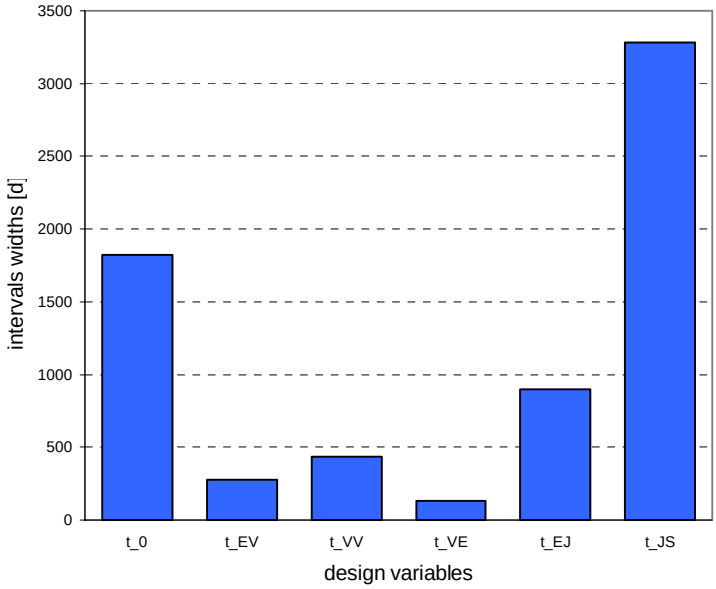

Figure 41: Comparison between the widths of the intervals of variation in the search space.

After generating the 1000 local minima, the mean distances of each solution to the others have been evaluated. By using the Reeves and Yamada methodology, Figure 42 shows the resulting structure of the objective function: the *x*-axis reports the normalized mean distance of each local optima, while the corresponding objective function values are indicated along the *y*-axis.

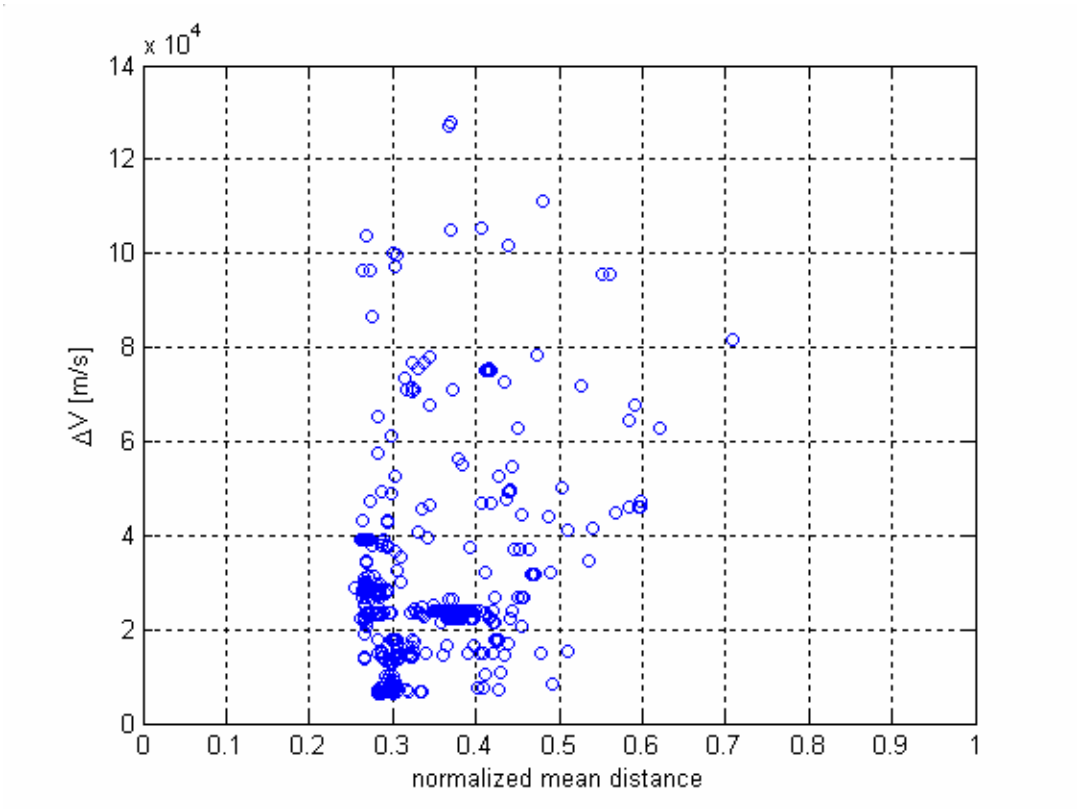

Figure 42: Objective function structure analysis for an EVVEJS transfer.

The objective function for an EVVEJS transfer holds again a *big-valley* structure. The mean closeness of most local optima tends to range between 0.25 and 0.4 times the hyper-diagonal magnitude, corresponding to a value between 975.1 *d* and 1560.2 *d*. In order to analyse the distribution of the local minima and verify the existence of a *big valley* structure, the search space is probed further. The local minima distribution over the search space is now difficult to show, due to the six dimensions and the search space homogeneity with respect to the design variables. Figure 43 shows the dates of departure (*x*-axis) and the objective function values (*y*-axis) corresponding to the identified local optima, while Figure 44-46 illustrate the local minima distribution over the transfer times subspace.

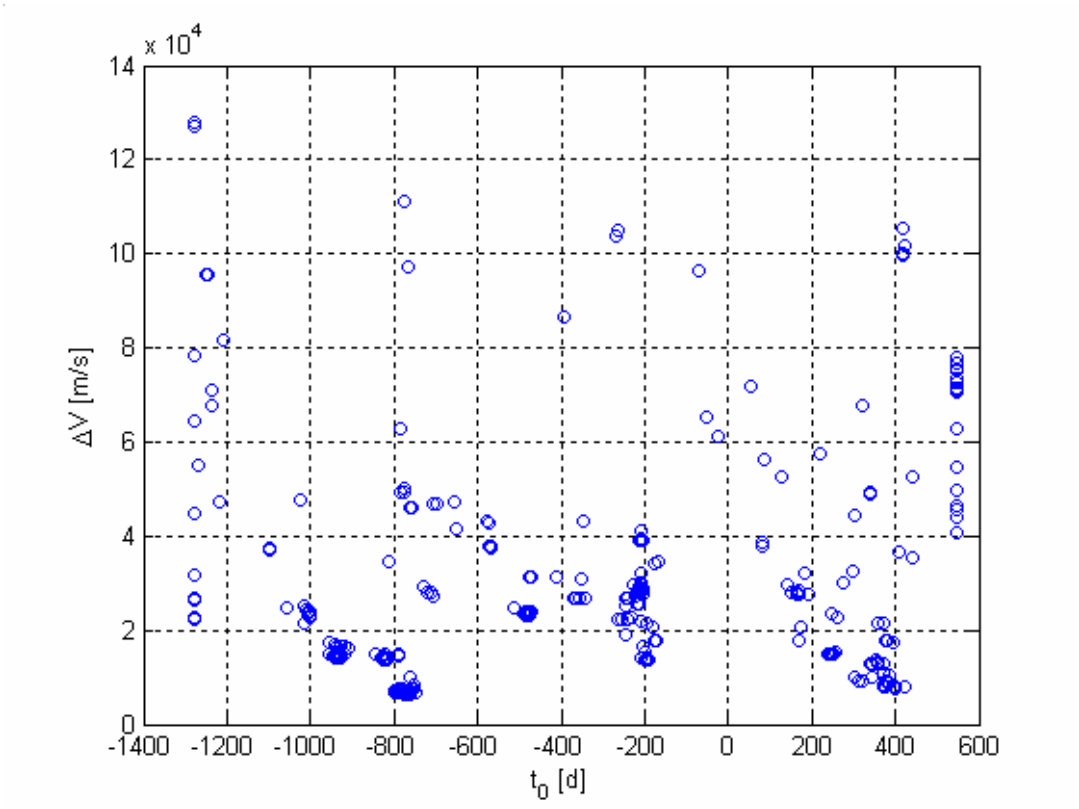

Figure 43: Local optima distribution over the date of departure design variable.

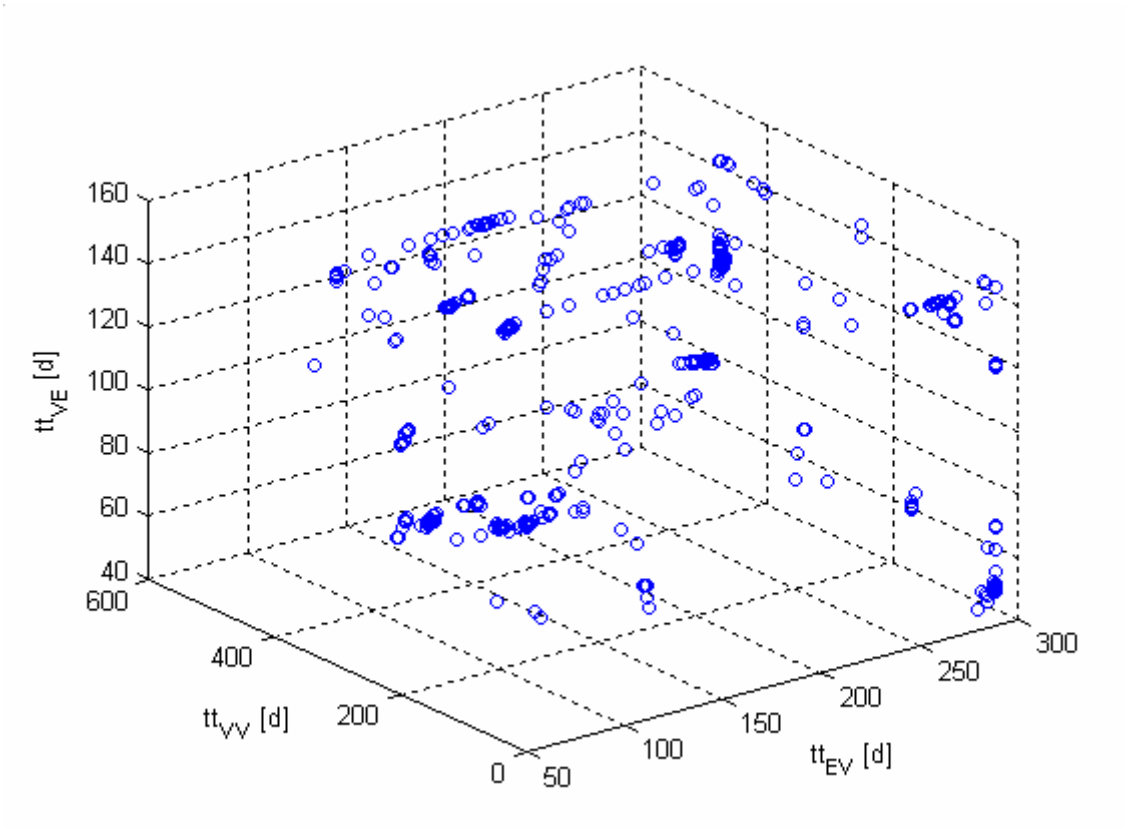

Figure 44: Local minima distribution in the tt_{EV} - tt_{VV} - tt_{VE} subspace.

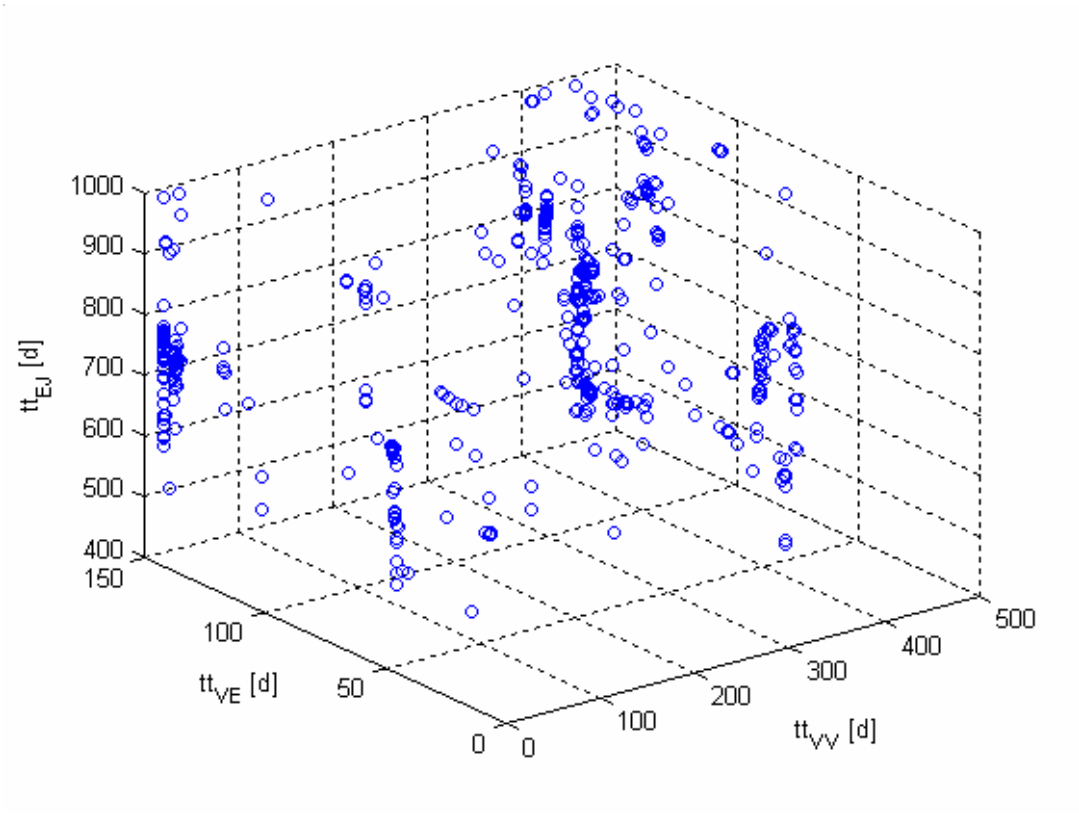

Figure 45: Local minima distribution in the tt_{VV} - tt_{VE} - tt_{EJ} subspace.

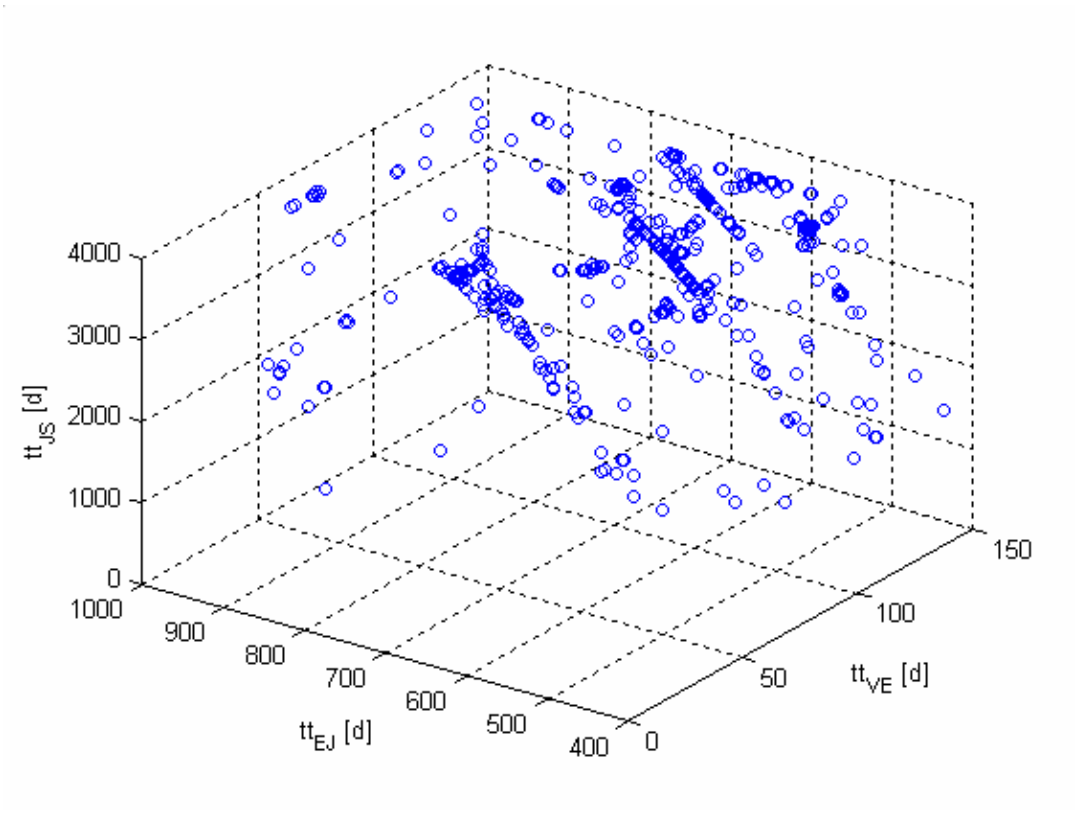

Figure 46: Local minima distribution in the tt_{VE} - tt_{EJ} - tt_{JS} subspace.

Big valley structures are now identifiable with difficulty (we hypothesize that more than 1000 local minima are necessary to find such a structure in this six dimensional case), but nonetheless exist. These structures have been found in this case particularly at the boundaries of the search space. The transfer trajectory and the ΔV features corresponding to the best solution found are presented now in Figure 47.

Best solution

Date of departure:	20/11/1997
Earth–Venus transfer time:	179.14 *d*
Venus–Venus transfer time :	406.53 *d*
Venus–Earth transfer time:	53.18 *d*
Earth–Jupiter transfer time:	758.33 *d*
Jupiter–Saturn transfer time:	3650.2 *d*

Table 13: Search space parameters.

Overall ΔV :	6368.2 *m/s*
ΔV_I :	3888.0 *m/s*
1st $\Delta V_{GA,V}$:	2032.7 *m/s*
2nd $\Delta V_{GA,V}$:	0.0327 *m/s*
$\Delta V_{GA,E}$:	0.0057 *m/s*
$\Delta V_{GA,J}$	0.0078 *m/s*
ΔV_F :	447.40 *m/s*

Table 14: Objective space parameters.

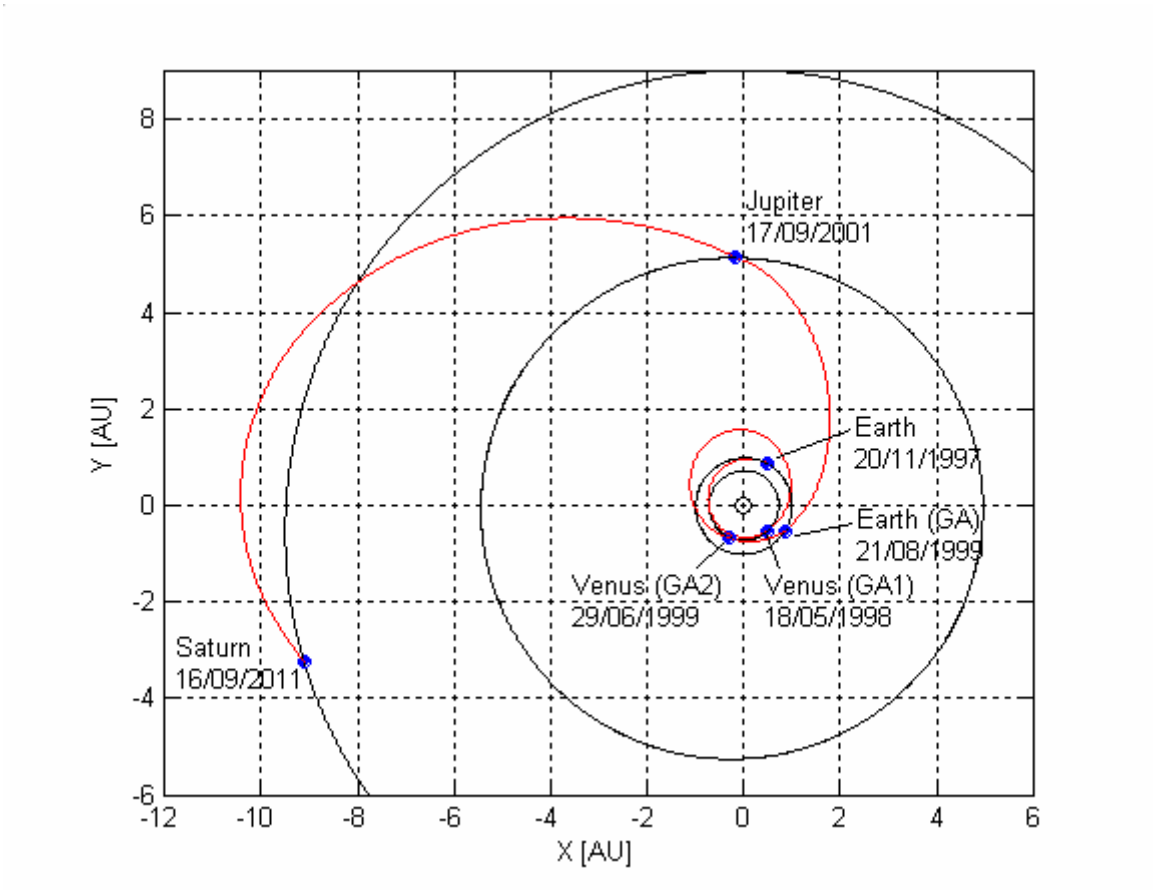

Figure 47: Transfer trajectory corresponding to the best solution found.

The best solution is obtained by measuring the goodness with respect to the objective function, the overall ΔV. In fact this could lead to the identification of long transfer time solution, as in this case. Let us consider now an alternative solution that has been found between the identified local minima.

Alternative solution

Date of departure:	25/10/1997
Earth–Venus transfer time:	206.38 *d*
Venus–Venus transfer time:	401.21 *d*
Venus–Earth transfer time:	54.52 *d*
Earth–Jupiter transfer time:	548.84 *d*
Jupiter–Saturn transfer time:	1747.90 *d*

Table 16: Solution space parameters.

Overall ΔV :	7154.6 *m/s*
ΔV_I :	5756.2 *m/s*
1st $\Delta V_{GA,V}$:	883.54 *m/s*
2nd $\Delta V_{GA,V}$:	0.0283 *m/s*
$\Delta V_{GA,E}$:	2.3098 *m/s*
$\Delta V_{GA,J}$	0.0056 *m/s*
ΔV_F :	512.52 *m/s*

Table 17: Objective space parameters.

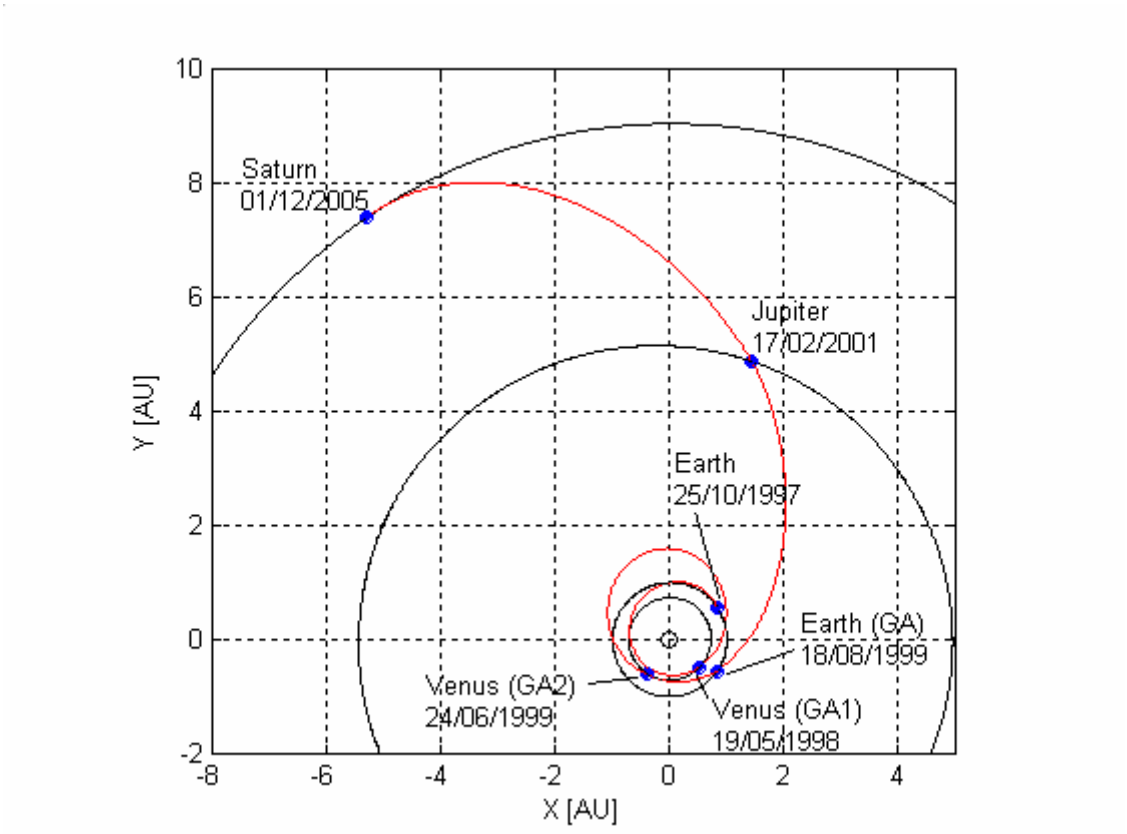

Figure 48: Transfer trajectory corresponding to the alternative solution.

A comparison of the best solution with respect to this alternative solution shows that, although there are little differences in the transfer times E-V, V-V, V-E and E-J, the J-S transfer time of the best solution is twice that of the alternative solution. This leads to an alternative solution that is just a little bit more energetically expensive than the best solution (about 800 *m/s*) but with a much shorter travel time of approximately 5.7 years, thus identifying a different

solution family. In fact, a solution similar to the alternative one has been adopted in the Cassini-Huygens mission. This is due to the fact that in real problems the overall ΔV often is not the unique criterion used for the choice of the transfer trajectory: the transfer time is, for example an important parameter. The previous consideration leads to an important observation: in order to avoid the loss of good solutions one alternatively has to:

- Use global multi-objective optimisation techniques (pareto optimality).
- Build a proper objective function mathematical model, by including as many terms as the number of the objective function to be considered.
- Use global optimisation techniques that allow maintaining subgroups of local minima solutions, each one having different characteristics and then identifying different solution families.

Note that, while in the first two cases one has to clearly know all the objective functions to be optimised before starting the optimisation process, the last case has the advantage of identifying different solution families with different features, so permitting a more flexible choice on the solution to be adopted. This constitutes an important subject for further studies. Similar results have been obtained [Gurfil and Kasdin, 2002] in case of orbits characterization in 3D elliptic restricted three-body problem.

Finally let us consider the comparison between the alternative solution and the Cassini-Huygens transfer solution. Figure 49 shows the Cassini-Huygens transfer trajectory.

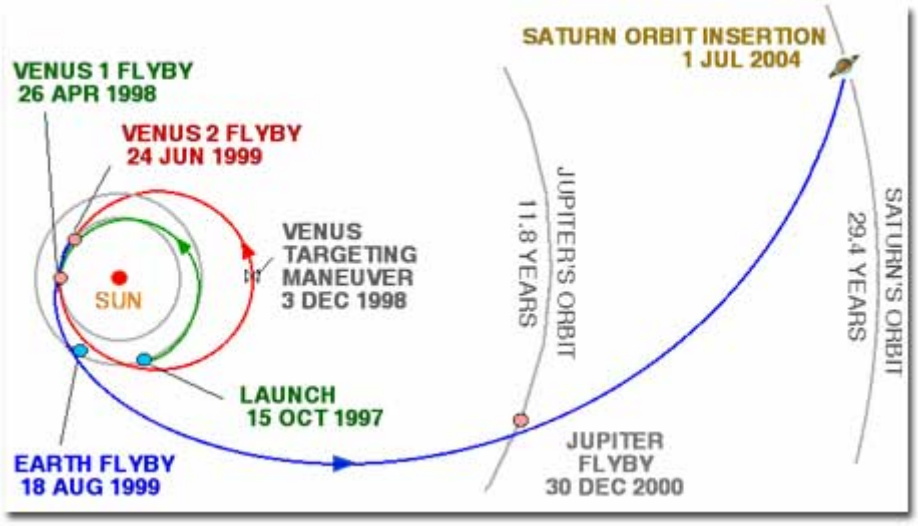

Figure 49: Cassini-Huygens transfer trajectory.

The alternative solution trajectory shown in Figure 49, can be seen to be very similar to the Cassini-Huygens trajectory. By analysing the ΔV requirements and by excluding the ΔV_I, the following table compares the two solutions.

	Alternative solution	**Cassini-Huygens**
(Overall ΔV*)* - ΔV_I	1398.4 *m/s*	*about* 2000 *m/s*

Table 18: Solution comparision.

The ΔV requirements can be seen to be quite different: the alternative solution resulting to be close to 600 *m/s* cheaper than the Cassini-Huygens mission. But one has also to compare the ΔV_I requirements. The ΔV_I requirement corresponding to the alternative solution is equal to 5756.2 *m/s*. By considering the same launcher as the Cassini-Huygens mission, Figure 0 shows the C3 performance of the Titan IV / Centaur.

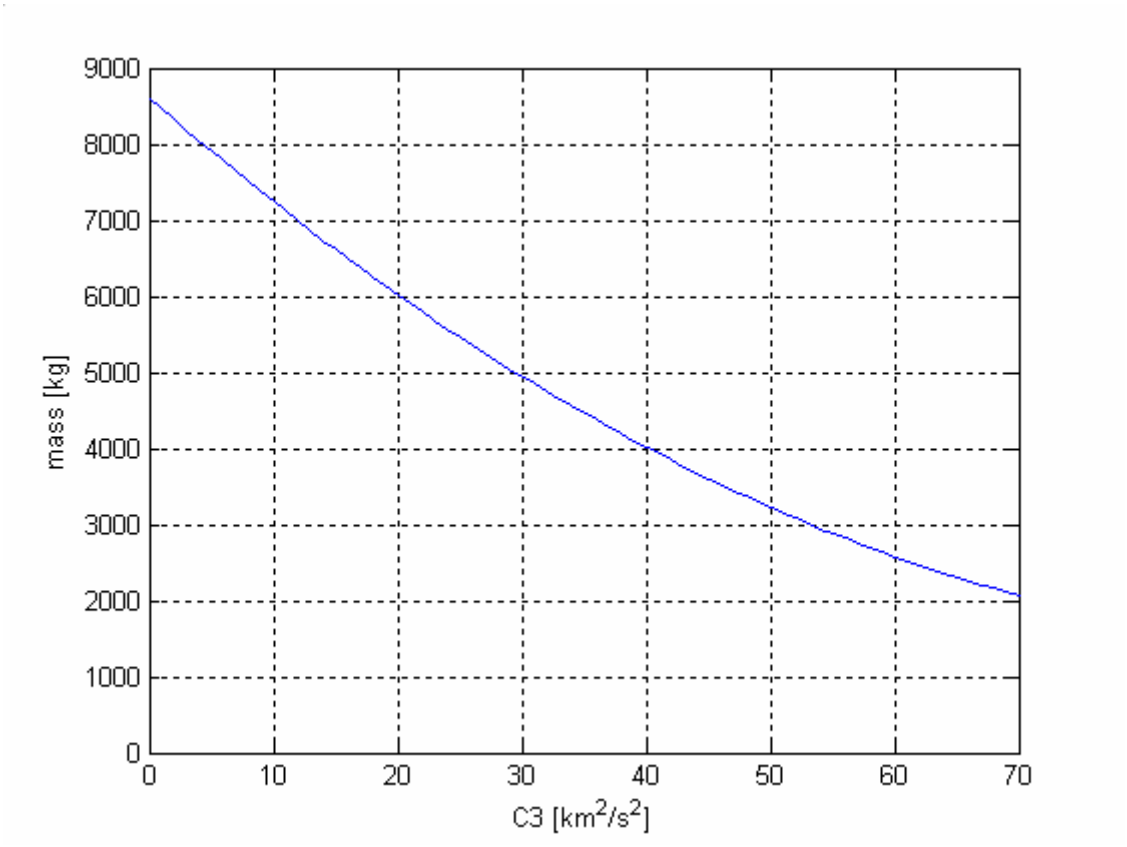

Figure 50: Titan IV-Centaur launcher: performance for Escape Missions.

The C3 requirement, corresponding to a ΔV_I of 5756.2 *m/s*, is 33.13 km^2/s^2, which leads to a maximum launch mass of about 4655 *kg*. However the Cassini-Huygens launch mass was approximately 5600 *kg*; consequently the alternative solution would not be admissible for such a spacecraft. It is also worth noting that no Deep Space Manoeuvres have been considered here, while the Cassini-Huygens mission executed a 500 *m/s* DSM Venus targeting manoeuvre on the 3rd December 1998: this could lead to a better solution than the here analysed alternative one.

Table 19 summarizes the problem characteristics for multiple gravity assist interplanetary missions.

Problem Dimension	Constraints	Search Space	Objective Function	T-periodicity
Yes	Box constraints	$D \in \Re^n$ (fixed $\vec{P}$) or $D \in \Re^n \times \aleph^n$	$f \in \Re$ almost everywhere C^2, locally discontinuous in a countable number limited sets or $f \in \Re^p$ in case of multiobjective optimisation.	

Table 19: Problem characteristics for MGA missions.

Note that analogies of multiple gravity assist interplanetary missions with either the Hamiltonian circuit problem or the Travelling Salesman problems could be stated: in fact the optimisation of MGA interplanetary missions can be associated to the search of an optimum path which links two planets by visiting a finite set of other planets where the gravity assist manoeuvres are performed. The planets could be then considered as analogous to the cities in the Travelling Salesman problem. However, the positions of the cities, or rather planets, in the case of MGA interplanetary missions are not fixed and the costs of each link will vary depending on those positions. By highlighting that both Hamiltonian circuit problem and Travelling Salesman problem have been demonstrated to be NP-Hard, this analogy could assist in demonstrating that the MGA interplanetary mission problem is also NP-Hard. This could lead to better analysis in the future following this proof.

3.7 MGA With Deep Space Manoeuvres

The consequences of using deep space manoeuvres instead of ΔV_{GA} corrective terms on the objective function structure are here analysed. For the sake of a clearer analysis, the case of an Earth-Saturn transfer trajectory with a Jupiter gravity assist manoeuvre has been considered. The ΔV_{GA} corrective term has been removed and a deep space manoeuvre inserted during the Jupiter-Saturn transfer phase. As a consequence of such a decision, the Earth-Jupiter transfer trajectory is propagated through the hyperbolic gravity assist manoeuvre into the Jupiter-Saturn transfer phase until the application of the deep space manoeuvre, which puts the spacecraft in the final Lambert's transfer trajectory to Saturn. The plane of the gravity assist manoeuvre and the pericentre of the hyperbole constitute new design variables. The resulting design variables are:

- The date of departure from Earth, t_0
- The transfer time from Earth to Jupiter, tt_{EJ}
- The plane of the hyperbole (defined by an angular variable ϑ around the input relative velocity to Jupiter)
- The pericentre of the hyperbole, r_p
- The transfer time from Jupiter to Saturn, tt_{JS}
- The percentage of tt_{JS} that is spent from Jupiter until the deep space manoeuvre, α.

Note that in the previous case the number of the design variables was three. The inclusion of a deep space manoeuvre increases the design variables to six. The interval of variation has been set equal to that of the previous cases. The upper and lower bounds for the transfer times associated to the two linking arcs E-J and J-S have set equal again to 0.1 and 2 times the associated Homann transfer time respectively. The resulting intervals being:

$$\left[tt_{EJ}^{L}, tt_{EJ}^{U}\right] = \left[99.65, 1993.1\right] d \quad [20]$$

$$\left[tt_{JS}^{L}, tt_{JS}^{U}\right] tt_{JS} = \left[365.02, 7300.4\right] d \quad [21]$$

The minimum and maximum values for the pericentre of the hyperbole have been set to 1.1 the Jupiter mean radius and the Jupiter sphere of influence radius respectively, are:

$$\left[r_p^L, r_p^U\right] = \left[7.69 \cdot 10^7, 4.82 \cdot 10^{10}\right] m \quad [22]$$

While the upper and lower bounds for the remaining design variables are:

$$\left[\vartheta^L, \vartheta^U\right] = \left[-\pi, \pi\right] rad \quad [23]$$

$$\left[\alpha^L, \alpha^U\right] = \left[0, 1\right] rad \quad [24]$$

In order to avoid the problem of high differences in the interval dimensions corresponding to each design variables, a normalization process has been implemented: the resulting upper and lower bounds are therefore $\left[0,1\right]$ for all of the design variables. After generating the 100 local minima, the mean distances of each solution from each other have been evaluated. By using the Reeves and Yamada methodology, Figure 51 shows the resulting objective function structure, while Figure 52 presents the distribution of the local optima.

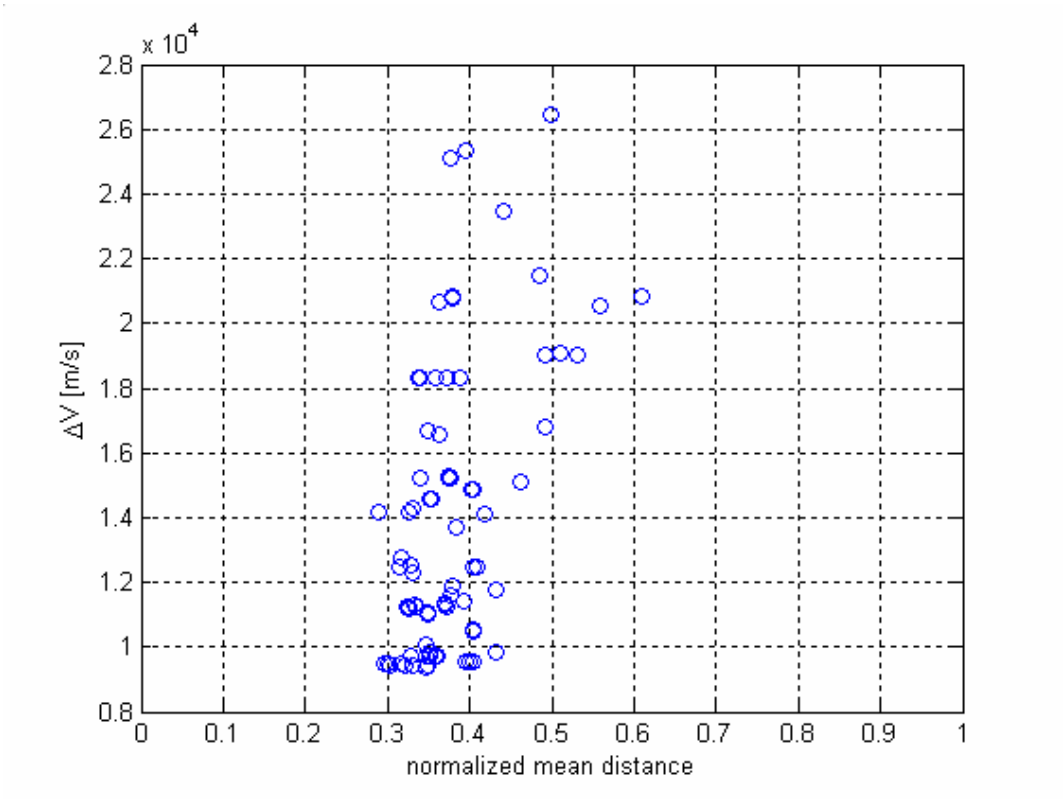

Figure 51: Objective function structure for an EJS transfer with a deep space manoeuvre.

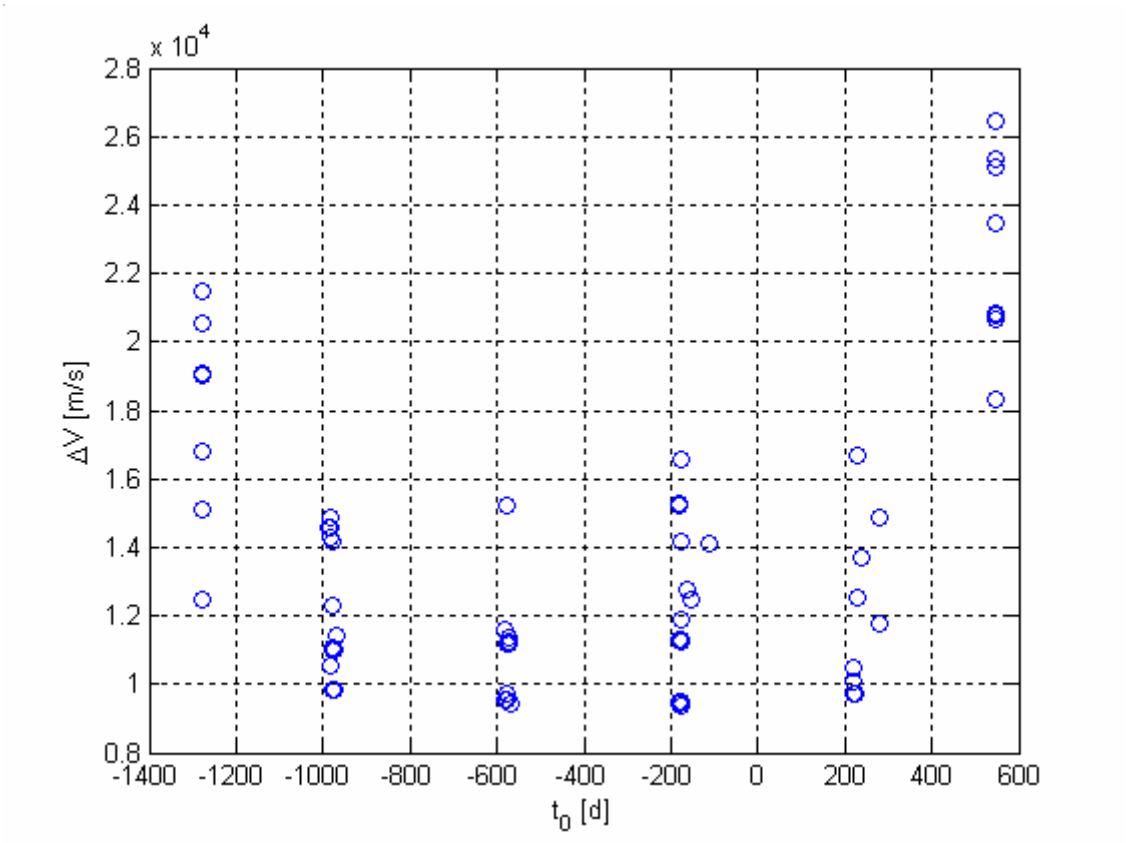

Figure 52: Local optima distribution over the date of departure design variable.

The big valley structure is here less identifiable: the most important difference with respect to the previous case can be seen in the diversification of the local minima over the objective function values. This feature is better illustrated in Figure 53, which shows that, although the local minima gather in groups near fixed values of the date of departure at regular intervals, which are again associable to the synodic period of the Earth-Jupiter planetary system, the objective function evaluations are not similar in each group. In order to analyse the reasons for such a result, let us consider the best identified solution.

Date of departure:	02/07/1999 (-181 *d* [MJD])
Earth–Jupiter transfer time:	911.65 *d*
ϑ:	0.074 *rad*
r_p:	$1.7029 \cdot 10^9$ *m*
Jupiter-Saturn transfer time:	4429.2 *d*
α:	0.36

Table 20: Search space parameters.

Overall ΔV:	9441.1 *m/s*
ΔV_I:	9009.8 *m/s*
ΔV_{DSM}:	0.888 *m/s*
ΔV_F:	430.41 *m/s*

Table 21: Objective space parameters.

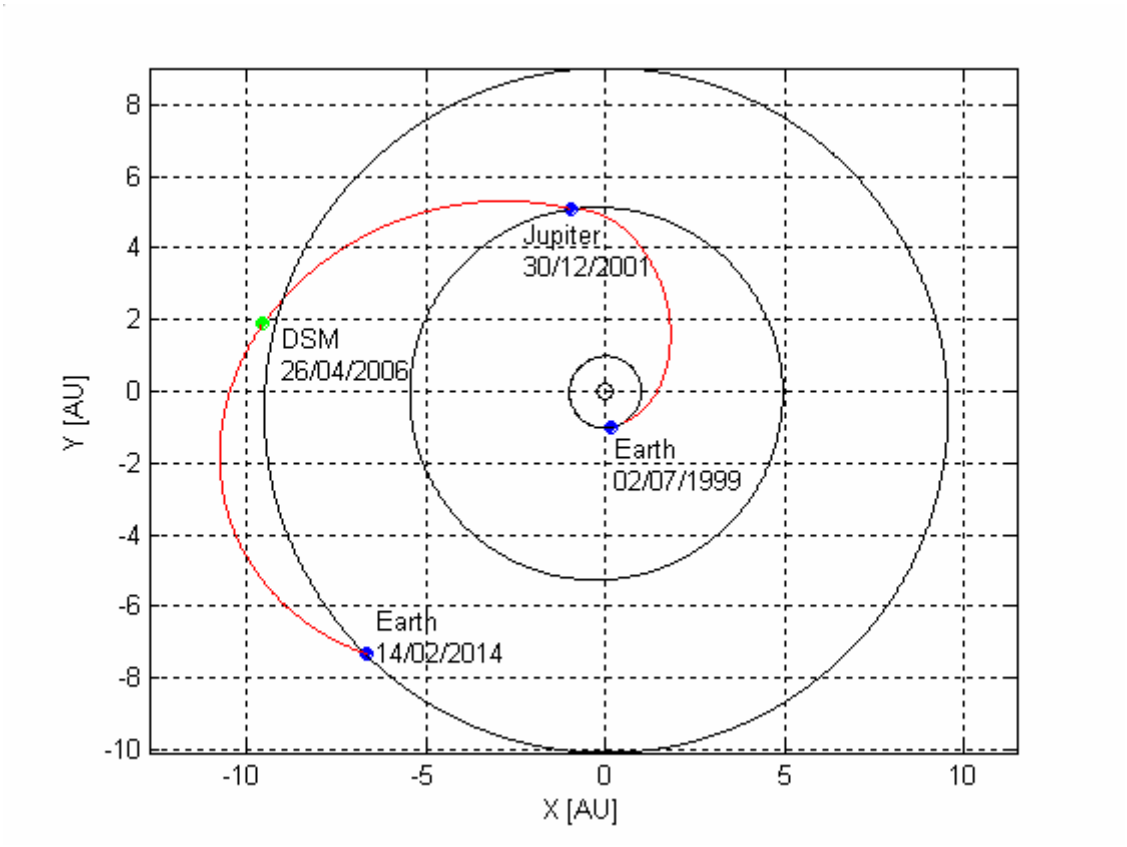

Figure 53: Transfer trajectory corresponding to the best solution found.

We now fix the value of the date of departure, as well as the values of ϑ, r_P and α, to that of the best solution. The objective function is plotted with respect to the other design variables, setting the intervals on the Earth-Jupiter transfer time equal to $[600, 1000]$ *d* and on the Jupiter-Saturn transfer time equal to $[1000, 7300]$ *d*. The resulting objective function values are showed in Figure 54.

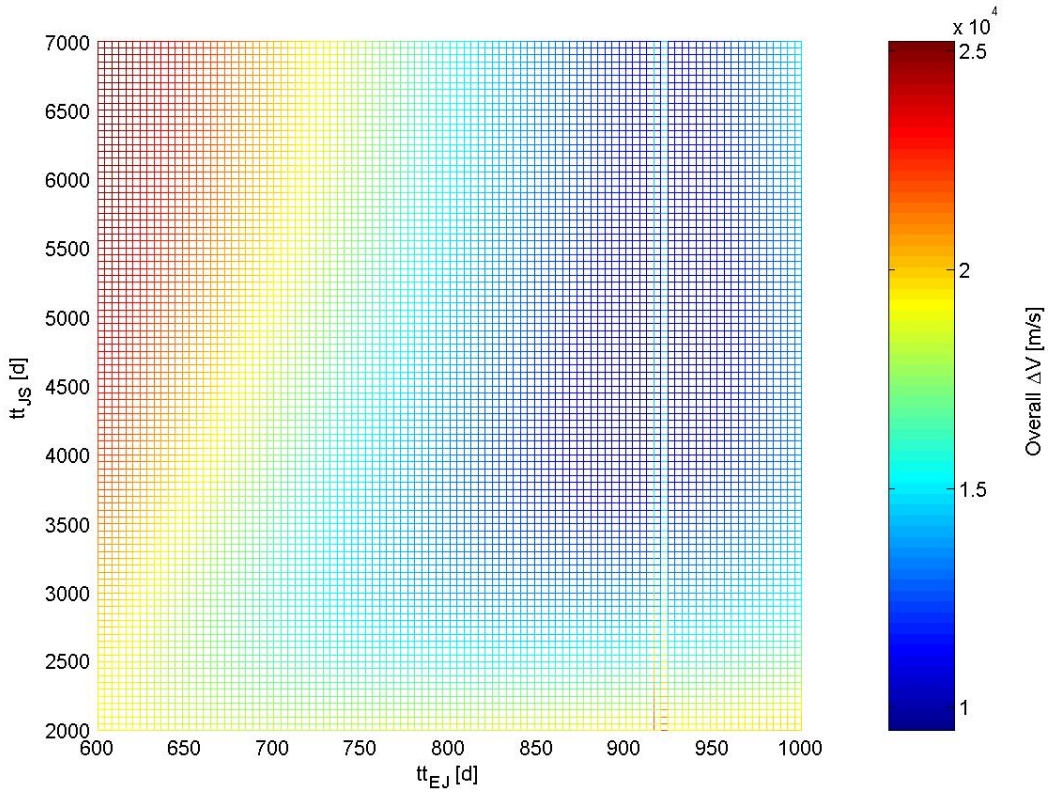

Figure 54: The overall ΔV as a function of the transfer times at a fixed date of departure.

The comparison of Figure 54 with Figure 18 shows that the big valley structure in the $tt_{EJ} - tt_{JS}$ subspace is absent in this case. This result is also illustrated in Figure 55 and Figure 56, which shows the $(\Delta V_I + \Delta V_F)$ and the ΔV_{DSM} objective function terms respectively.

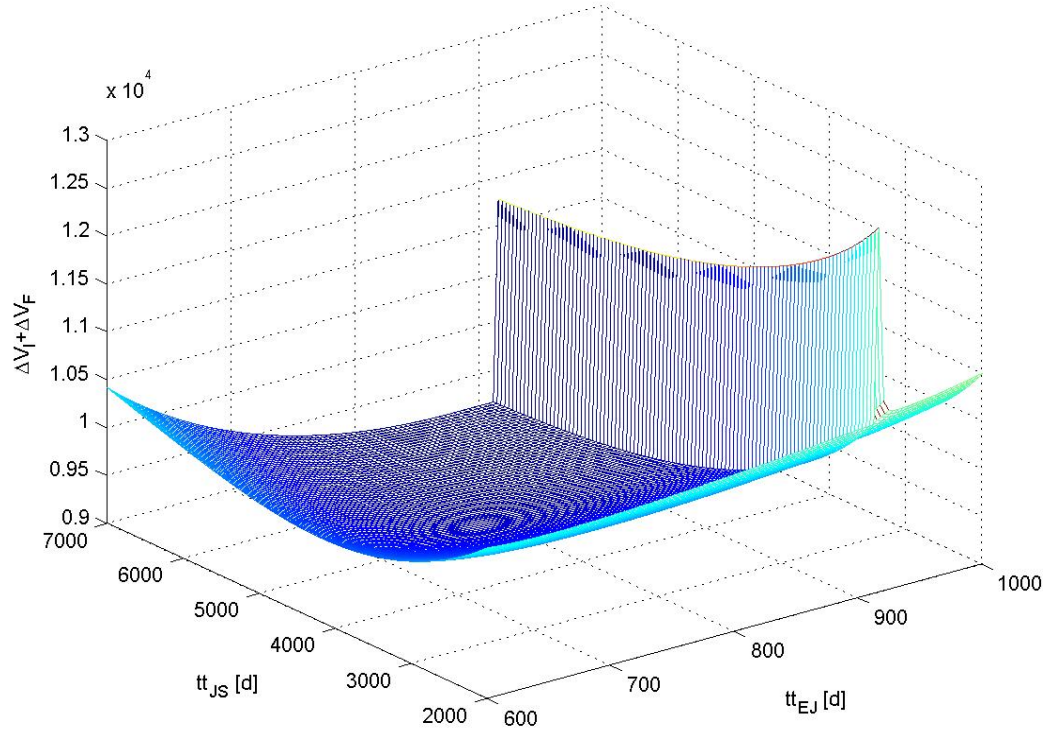

Figure 55: ($\Delta V_I + \Delta V_F$)as a function of the transfer times at a fixed date of departure.

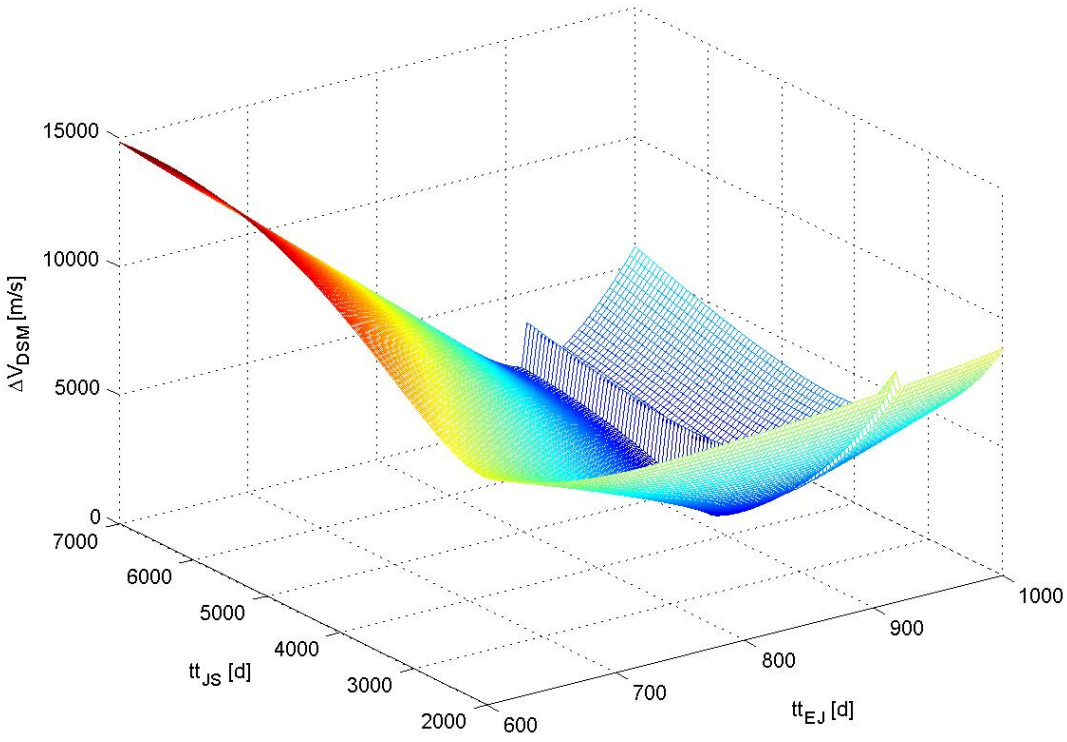

Figure 56: ΔV_{DSM} as a function of the transfer times at a fixed date of departure.

Another important observation comes from the comparison of Figure 54 with Figure 18: the application of the deep space manoeuvre in the Jupiter-Saturn transfer phase allows the mathematical model to avoid the singularities of Battin's algorithm, which is here used for the Lambert's problem solution, corresponding to 180 degrees Jupiter-Saturn transfer angles.

4. LOW THRUST TRANSFERS

As an example of a low thrust interplanetary mission, let us consider a transfer from Earth to Mars.

4.1 Problem Formulation

In order to assess the objective function, the following mathematical models and methods have been used:

- Restricted 2-bodies dynamical model
- Three dimensional motion
- Analytical ephemeris model (generated by time polynomial series of the orbital elements)
- Low thrust interplanetary transfer (constant thrust level and variable direction)
- Forward propagation of initial conditions and thrust control law

The thrust level has been supposed to be constant throughout the whole transfer and bounded in intervals corresponding to real thrusters values. The thrust direction during the transfer trajectory is however a design variable and is evaluated by means of azimuth and elevation angles defined in the local horizontal plane. To avoid singularities, the integration of motion has been processed by means of equinoctial elements. The spacecraft initial position coincides with that of the Earth at the date of departure, while the escape velocity from Earth has been imposed to have the same direction as the Earth velocity vector (its magnitude has been considered as a design variable).
The objective function is assumed to be the sum of several terms:

- The magnitude of the spacecraft relative position with respect to Mars at the end of the integration of motion, R_F: this term has been included in order to reach the planet at the end of the transfer orbit. This can be viewed as an inclusion of a constraint term in the objective function. The

planet is considered reached when the spacecraft final position lies into the sphere of influence of Mars.

- The magnitude of the spacecraft relative velocity with respect to Mars at the end of the integration of motion, v_F: this term has been included in order to reach the planet at the end of the transfer orbit with a low relative velocity and to avoid the necessity of consequent impulsive manoeuvres. Values of v_F smaller than 100 *m/s* have been considered as adequate.
- The propellant mass that is required by the thrusters for the interplanetary transfer, m_{prop}. Adequate values of m_{prop} have been considered to be smaller than 200 *kg*.

In order to evaluate the m_{prop} term, typical electric propulsion systems performances have been used. The interval of variation of the thrust level has been chosen to be $[0, 0.168]$ *N*, while the specific impulse has been fixed to 3000 *s*. The spacecraft launch mass has been set to 1000 *kg*. The resulting objective function analytical form has been taken as:

$$obj = \alpha_1 \cdot R_F + \alpha_2 \cdot v_F + \alpha_3 \cdot m_{prop} \qquad [25]$$

where the values of the weights α_1, α_2 and α_3 have been fixed in order to make the order of magnitude of obj, corresponding to good R_F, v_F and m_{prop} values, equal to 10.

Note that the use of a weighted sum of several terms for the objective function assessment has been considered in order to take into account the features of common global optimisation algorithms (which will be used in the second part of this work). As this concerns the constraints handling methodologies, most of the existing global optimisation algorithms tend to include the constraints terms in the objective function by means of penalty terms; the weighted sum can be seen as a way of defining such penalty terms.

4.2 Objective Function Structure

As a consequence of the mathematical models and methods used for the objective function assessment, the search space has been characterized by the following design variables:

- Date of departure from Earth, t_0
- Transfer time, tt
- Magnitude of the escape velocity from Earth, $v_{\infty,E}$
- Thrust level, u
- Thrust azimuth and elevation over the transfer trajectory

The thrust azimuth and elevation, respectively, az and *el*, over the transfer trajectory have been modelled by means of a linear interpolation of their values corresponding to six points on the trajectory, which are uniformly distributed in the time domain (including initial and final time). The previous choices make the number of the design variables equal to 16. All the previous design variables have a continuous characterization over the search space.

Upper and lower bounds on the design variables are considered. The interval of variation has been imposed in order to include a period of 4 years starting from 1st January 2000. The upper and lower bounds for the remaining design variables are listed in the following:

$$tt = [150, 300]\, d \quad [26]$$

$$v_{\infty,E} = [0, 3000]\, m/s \quad [27]$$

$$u = [0.1, 0.168]\, N \quad [28]$$

$$az_i = [-\pi, \pi],\ i = 1,...,6 \quad [29]$$

$$el_i = [-\pi/2, \pi/2],\ i = 1,...,6 \quad [30]$$

In order to avoid the problem of high differences in the interval dimensions corresponding to each design variables, a normalization process has been implemented: the resulting upper and lower bounds are then $[0,1]$ for all of the design variables.

As for the previous cases, the objective function structure analysis for a low thrust interplanetary transfer starts with the Reeves and Yamada methodology: 100 local minima have been found with a random start search (with uniformly distributed random start points) followed by an SQP optimisation process; the mean distances of each solution from each other is then assessed and compared to the corresponding goodness; consequently, the values of the design variables corresponding to the best local minimum has been used in order to analyse the convexity of the objective function. By using the Reeves and Yamada methodology, Figure 57 shows the resulting local minima distribution: the x-axis reports the normalized mean distance of each local optima, while the corresponding objective function values are indicated along the y-axis.

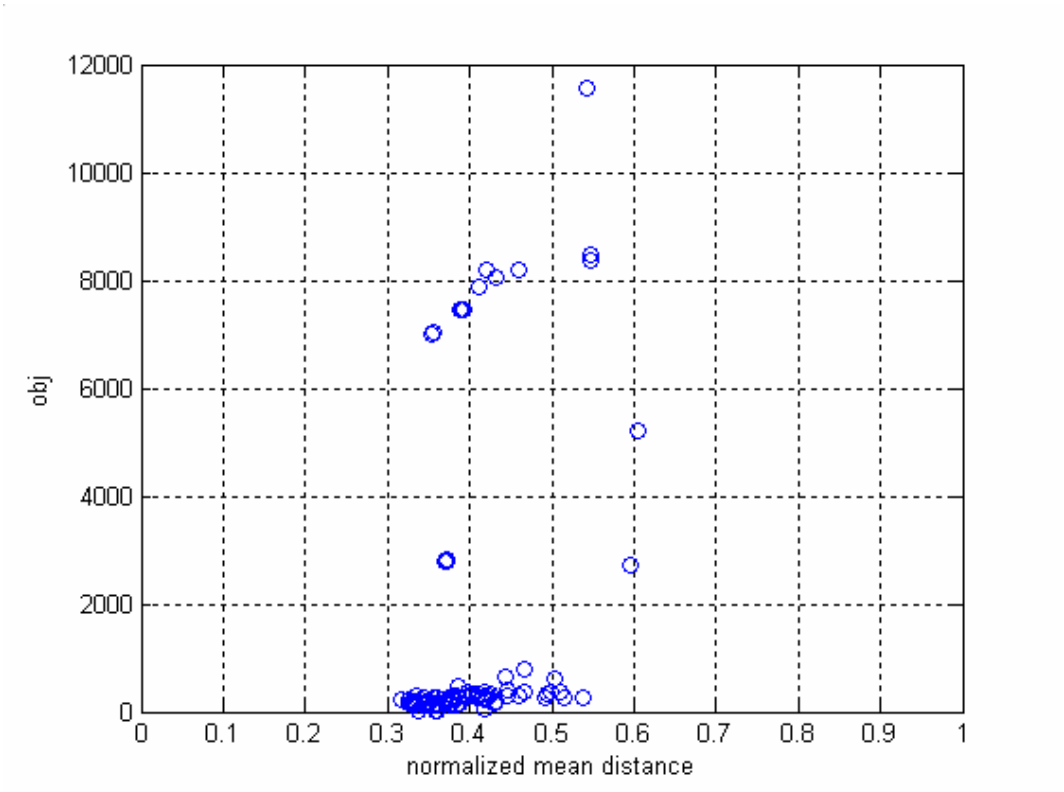

Figure 57: Objective function structure analysis for a low thrust interplanetary mission.

The objective function for a low thrust interplanetary mission shows again a *big-valley* structure. The mean closeness of most local optima tends to range between 0.3 and 0.5 times the hyper-diagonal magnitude. Before analysing the distribution of the local minima and verifying the existence of a *big valley* structure, let us consider the best local minimum found. The main features are listed below, together with the resulting transfer trajectory, Figure 58.

Best solution

Date of departure:	12/07/2001
Transfer time:	281.5 *d*
Escape velocity from Earth:	2730.5 *m/s*
Thrust level:	0.151 *N*

Table 22: Search space parameters.

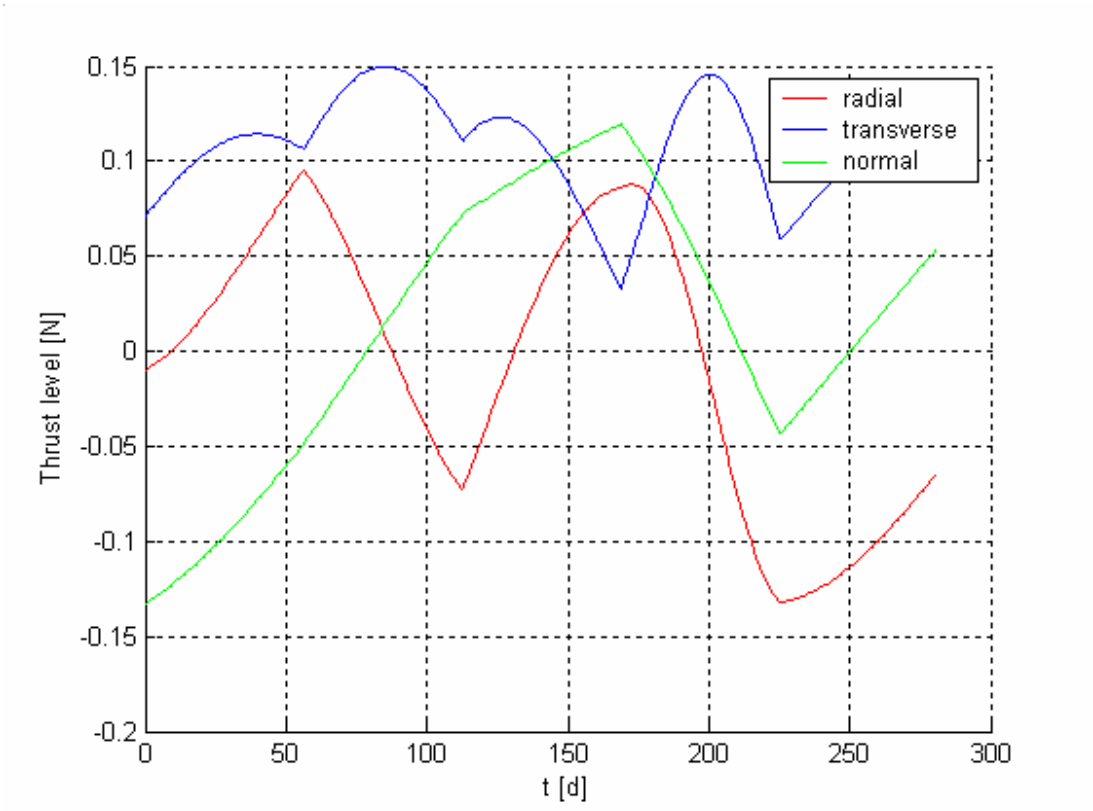

Figure 58: Thrust components in the orbital reference frame.

Objective space	
obj:	6.37
R_F :	$3.19 \cdot 10^6$ *m*
v_F :	0.88 *m/s*
m_{prop} :	124.59 *kg*

Table 23: Objective space parameters.

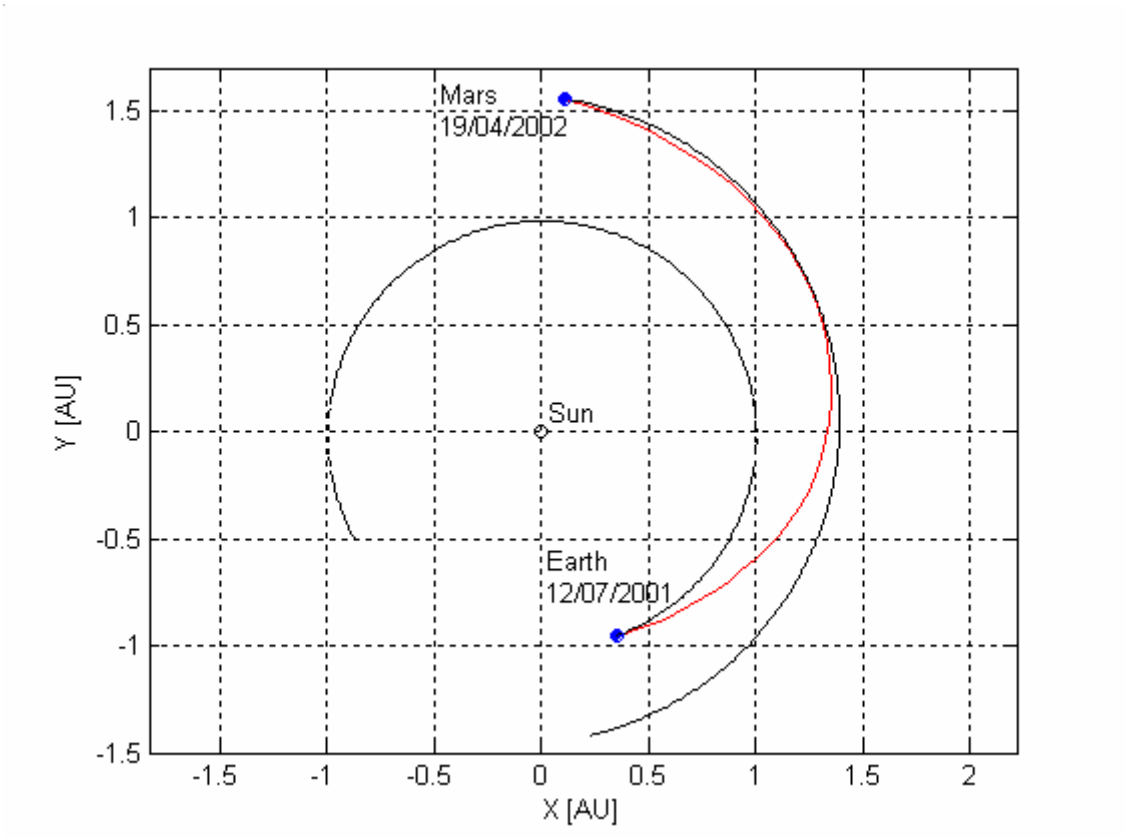

Figure 59: Transfer trajectory of the best solution in the ecliptic plane.

Let us now the shape of the objective function over the search domain, by considering two significant design variables at a time and fixing the values of the remaining design variables to those of the previous best identified solution. Figure 60 shows the resulting objective function values with respect to the date of departure and the transfer time.

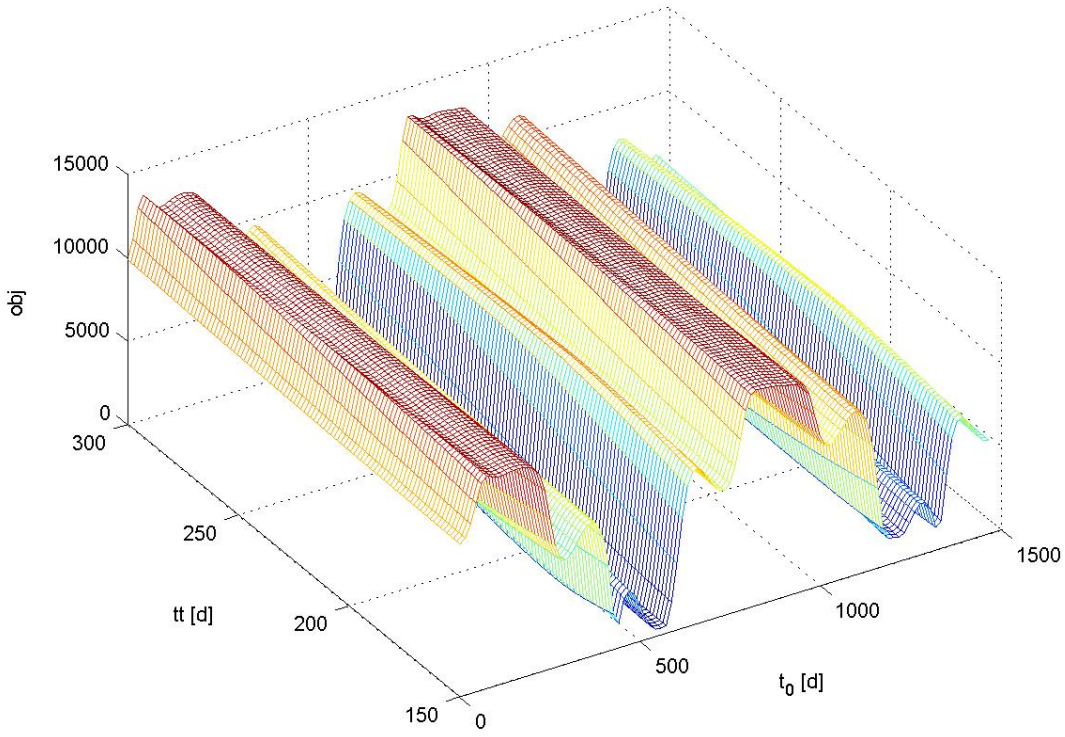

Figure 60: Objective function values with respect to the date of departure and the transfer time.

We can see that the objective function is non-convex in the considered search space. Such a feature is again mainly due to the trend of the objective function with respect to the date of departure, while convex features seems to exists with respect to the transfer time. A better illustration of this aspect can be seen in Figure 61, where the objective function is plotted with respect to the date of departure by fixing the transfer time to that of the best identified solution.

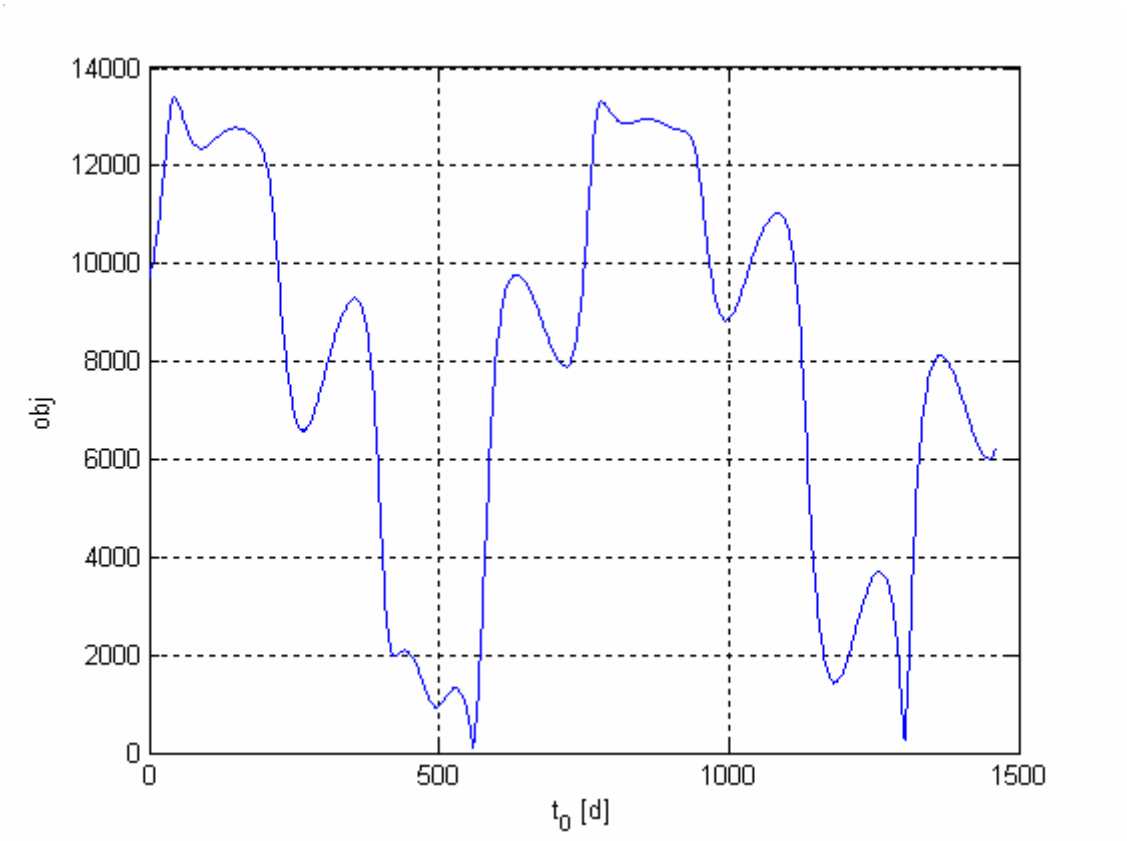

Figure 61: Objective function values with respect to the date of departure and the transfer time.

An important observation can be done by looking at the evolution of the objective function values in Figure 62. Although we have the presence of several basins of attraction, a certain regularity can be recognized: a quasi periodicity feature with a period of approximately 765 days, which is again amenable to the synodic period of the Earth-Mars transfer (780 days). Figure 60 and Figure 61 allow us to identify the existence of a big-valley structure, the existence of which is again associable to the dependence on the date of departure. One can object that this feature has been found by fixing the values of the remaining design variables, but in fact it can be also identified by analysing the distribution of the generated local minima in the $t_0 - tt$ subspace as shown in Figure 62.

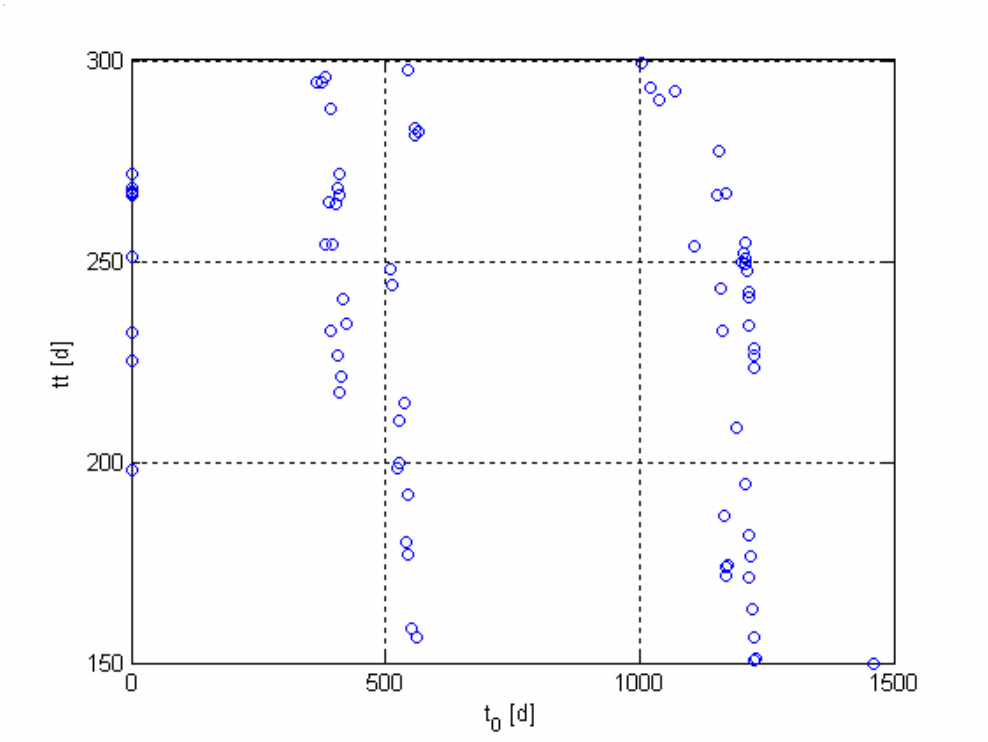

Figure 62: Distribution of the generated local minima in the $t_0 - tt$ subspace.

Let us consider now the shape of each objective function term over the same search space, as illustrated in Figure 63-65.

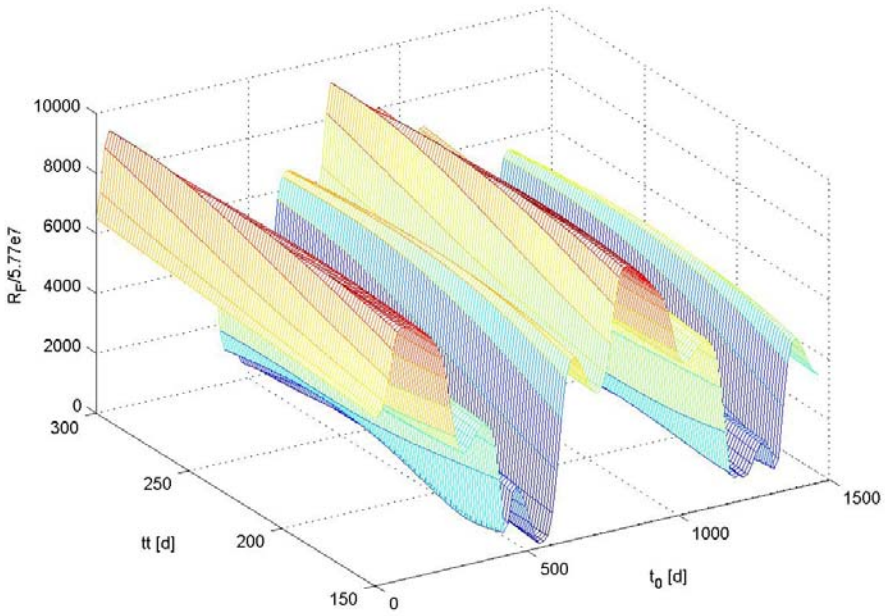

Figure 63: $R_F / 5.77e7$ values in the $t_0 - tt$ subspace.

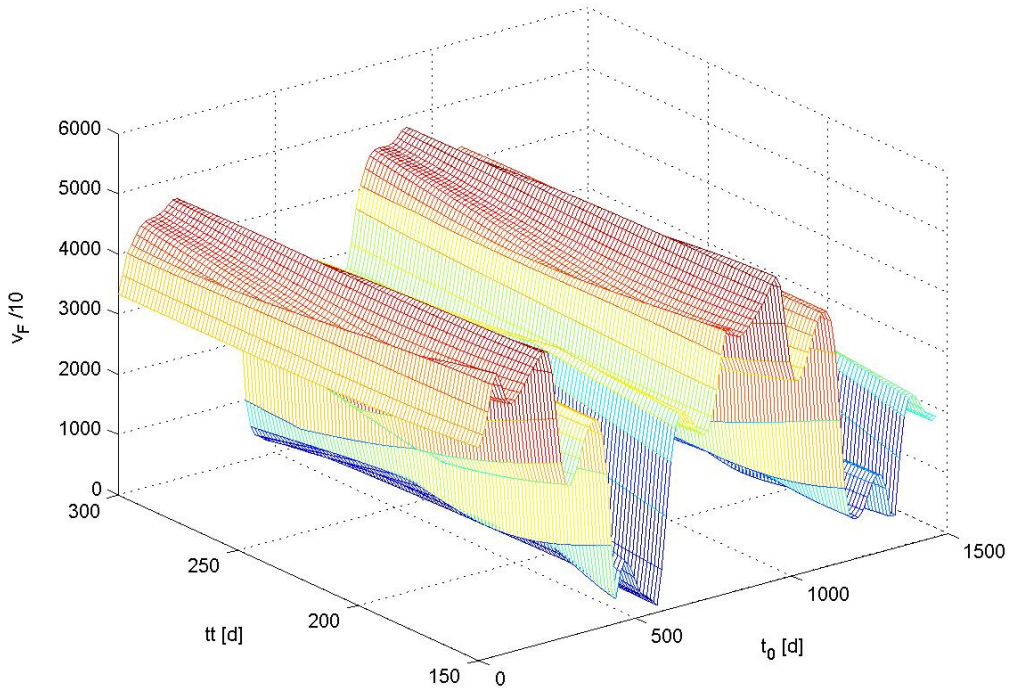

Figure 64: $v_F / 10$ values in the $t_0 - tt$ subspace.

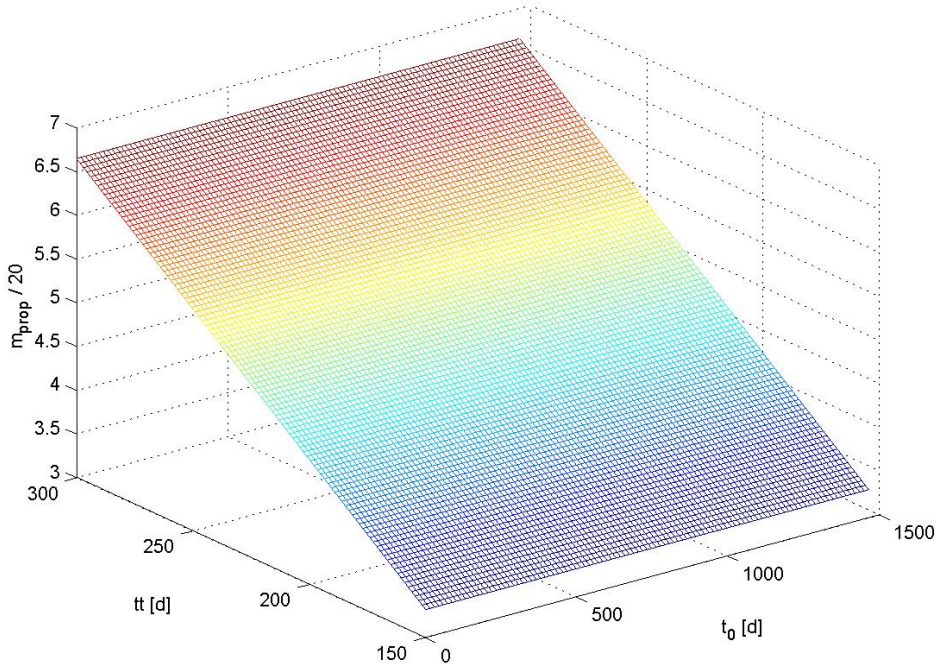

Figure 65: $m_{prop} / 20$ values in the $t_0 - tt$ subspace.

The first thing to note is that, while the first two objective function terms show similar non-convexity features as the overall objective function, the propellant mass is in fact monotone with respect the transfer time and does not depend on the t_0 values. This result can be easily justified by considering the equation of the propellant mass consumption:

$$m_{prop} = \int_0^{tt} \frac{u}{I_{sp} \cdot g_0} dt \qquad [31]$$

By noting that the integrand is a positive quantity, m_{prop} can be recognized as a monotonic function of the transfer time *tt* and the mean value of *u*. In particular, in the model we are considering, the thrust level is constant during the whole transfer phase and coincides with its mean value; the consequence of this is therefore that m_{prop} is monotonic with respect to the *u* design variable. The consequences of the previous results will be better addressed later, by analysing the structure of the objective function with respect to *tt* and *u*. Moreover, Figure 63, Figure 64 and Figure 65 show the importance of the weights of the weighted sum which constitutes the objective function: in fact parameters α_1, α_2 and α_3 deeply affect the shape of the objective function over the search domain and the consequent position of the global optimum, thus influencing the global search. Note that several global optimisation processes actually tend to have such a weighted sum in order to either handle multi-objective optimisation problems or include constraints terms in the objective function. As an example of such an influence, let us consider a propellant mass term with a weight α_3 = 1000. The resulting objective function values over the $t_0 - tt$ subspace can be seen in Figure 66.

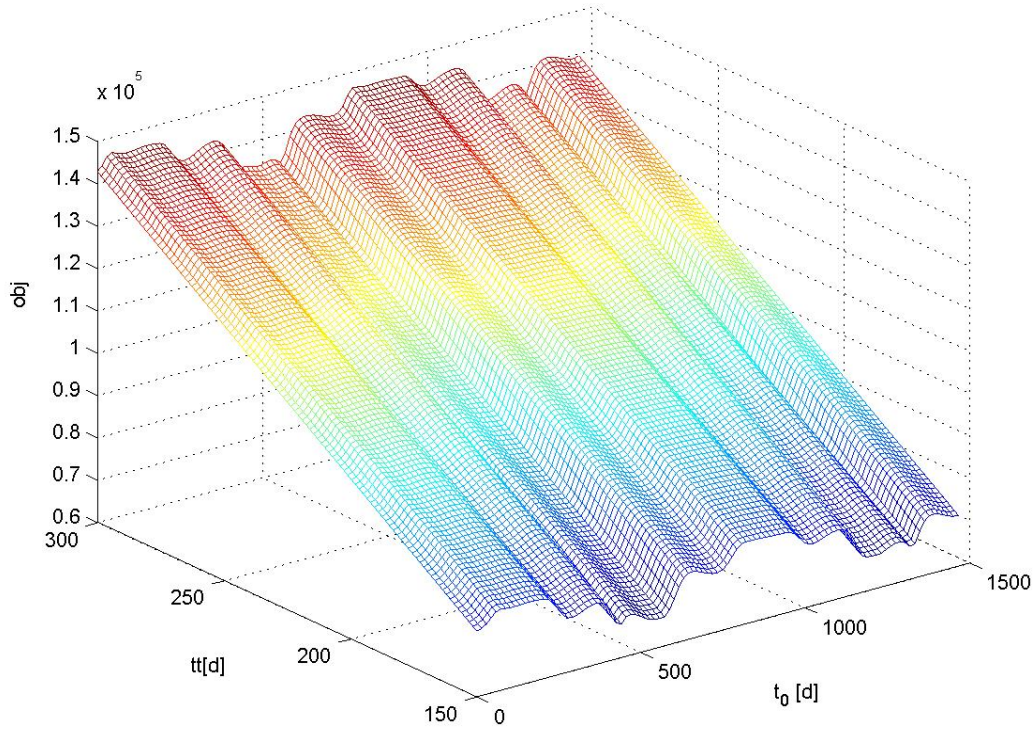

Figure 66: Objective function values with respect to the date of departure and the transfer time.

Figure 66 clearly shows that the structure of the objective function changes with respect to the weights and this has to be considered as a general result every time a weighted sum is used in the assessment of the objective function. Let us now consider the first term of the objective function as a constraint term: suppose the admissible solutions to be those where the spacecraft final position lies into the Mars sphere of influence. The resulting optimisation problem can therefore be summarised as:

$$\textit{Minimize}:\ obj = \alpha_2 \cdot v_F + \alpha_3 \cdot m_{prop}\ \ \textit{subject to}:\ R_F < 5.77 \cdot 10^8\, m$$

Figure 67 illustrates the consequent admissible region near the best solution, while Figure 68 and Figure 69 show the second and third objective function terms values.

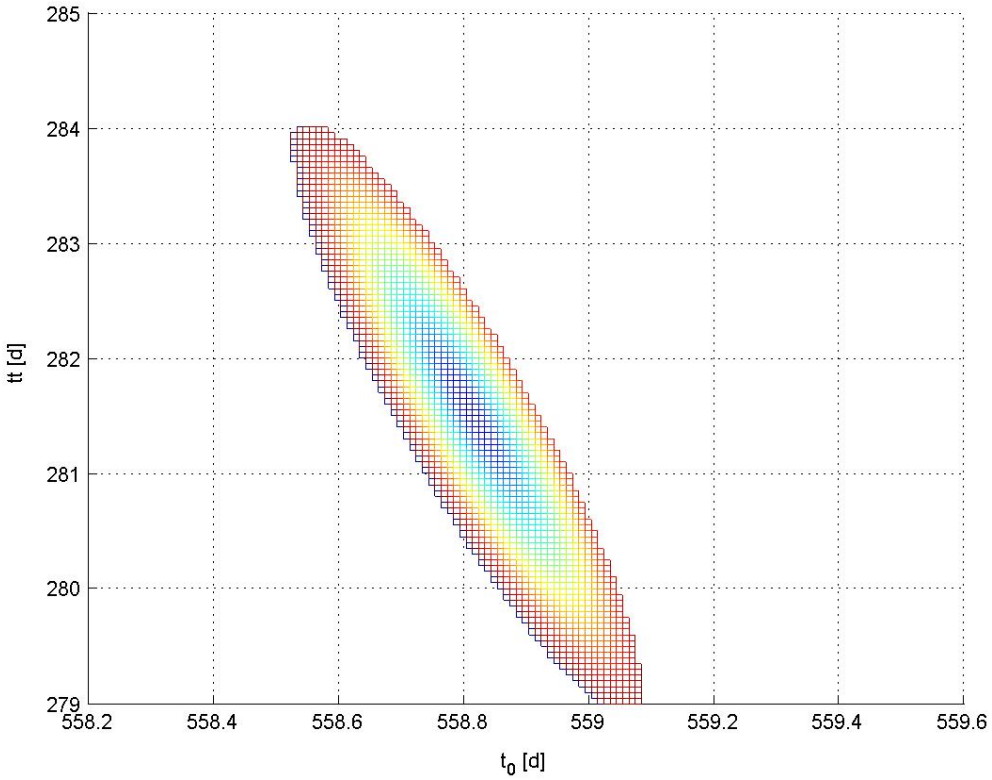

Figure 67: Admissible region near the best solution.

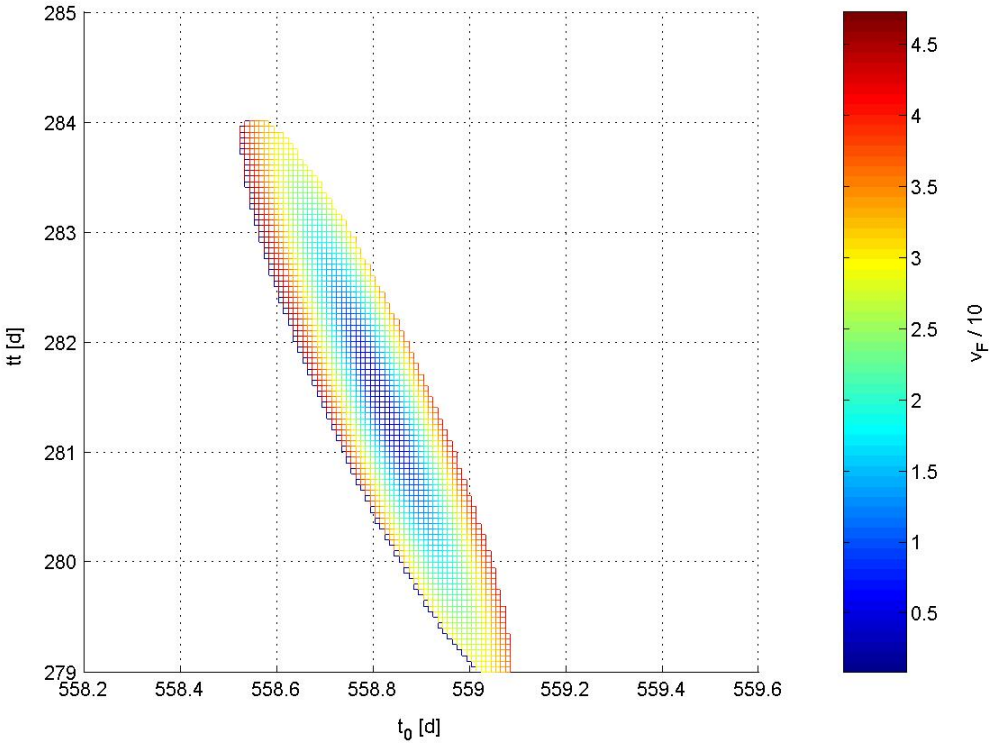

Figure 68: $v_F / 10$ values over the admissible region near the best solution.

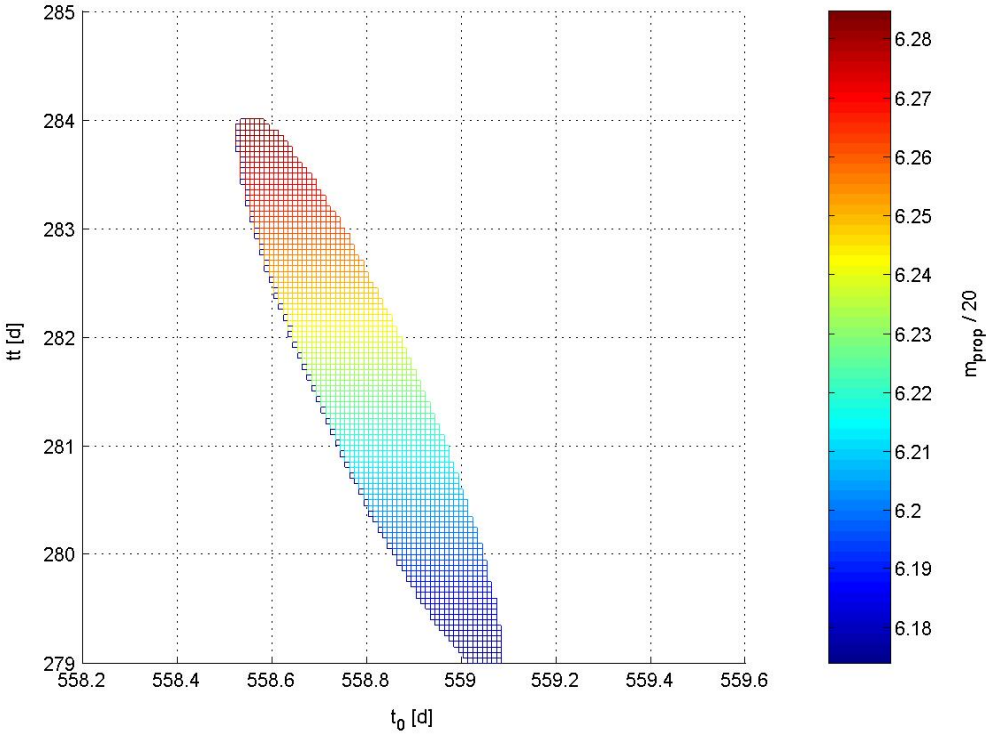

Figure 69: $m_{prop} / 20$ values over the admissible region near the best solution.

It is worth noting that the axes intervals have been strictly reduced and the admissible region near the best identified solution, by varying only t_0 and *tt*, is in fact really narrow; just one day in t_0 and five days in *tt*. In the admissible region the remaining objective function seems to show convexity features with respect to t_0 and *tt*. Several constraints handling methodologies consider the introduction of penalty terms in different ways in the case of non admissible solutions. It is important to note that such methodologies deeply affect the structure of the objective function, sometimes introducing discontinuities in either objective function values or derivatives, corresponding to the admissible region boundaries. Figure 70 shows the objective function values with respect to the thrust level, *u*, and the escape velocity from Earth, $v_{\infty,E}$, while Figure 71, Figure 72 and Figure 73 illustrate each objective function term.

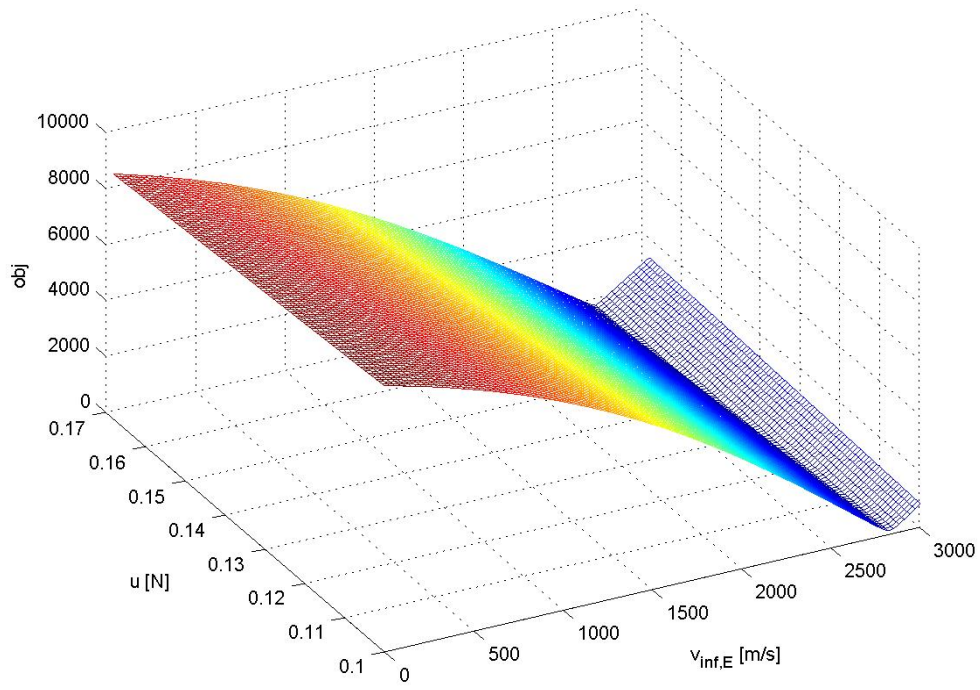

Figure 70: Objective function values with respect to the escape velocity from Earth and thrust.

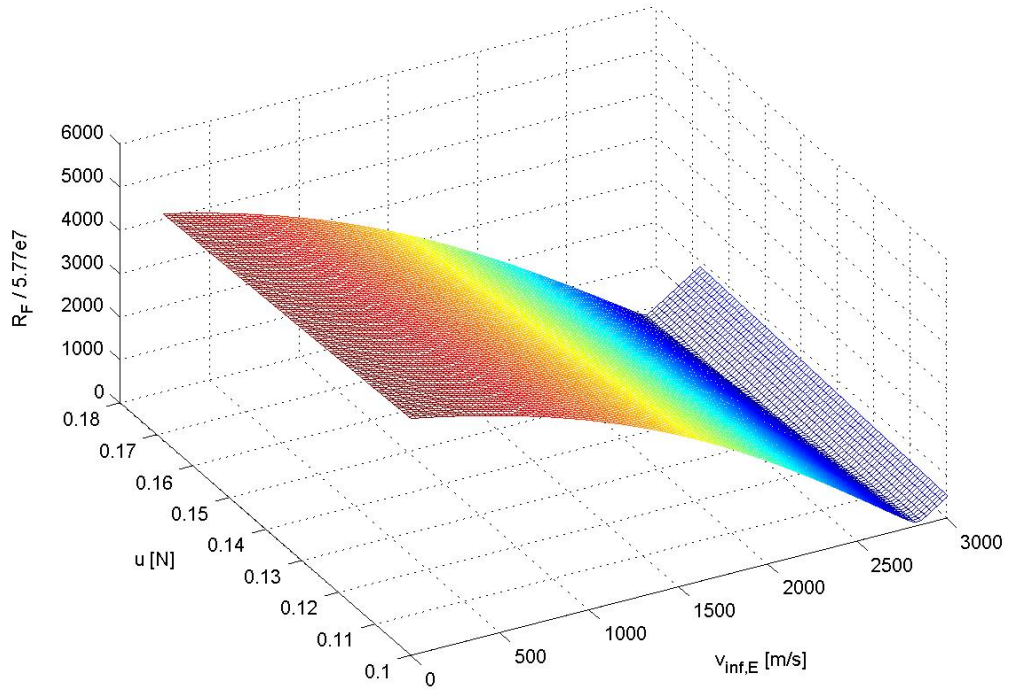

Figure 71: $R_F / 5.77e7$ values with respect to the escape velocity from Earth and the thrust .

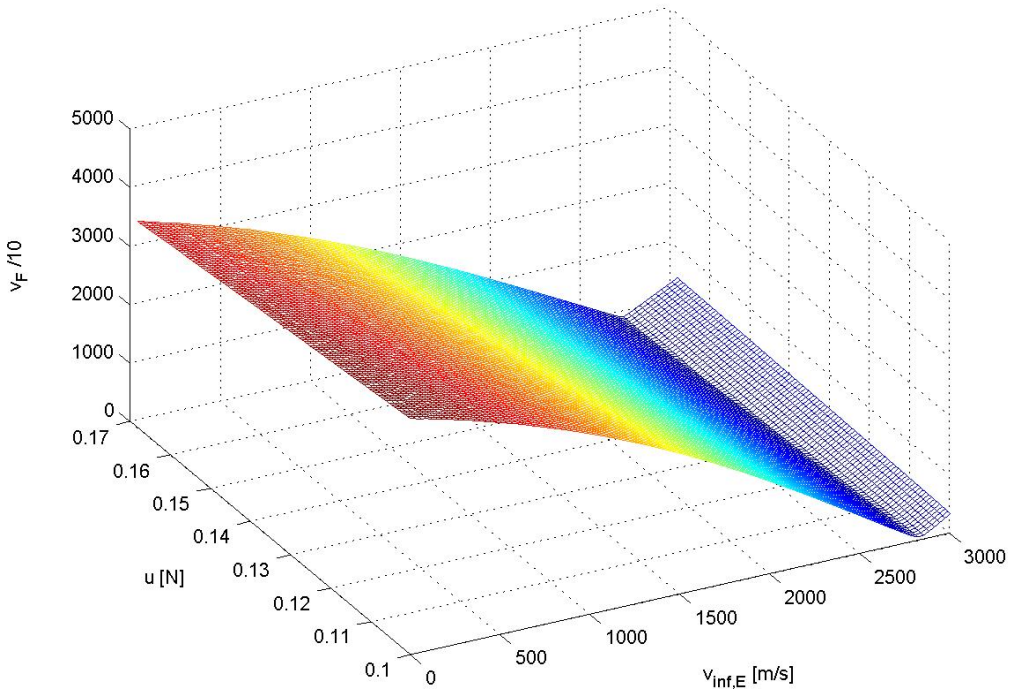

Figure 72: $v_F / 10$ values with respect to the escape velocity from Earth and the thrust.

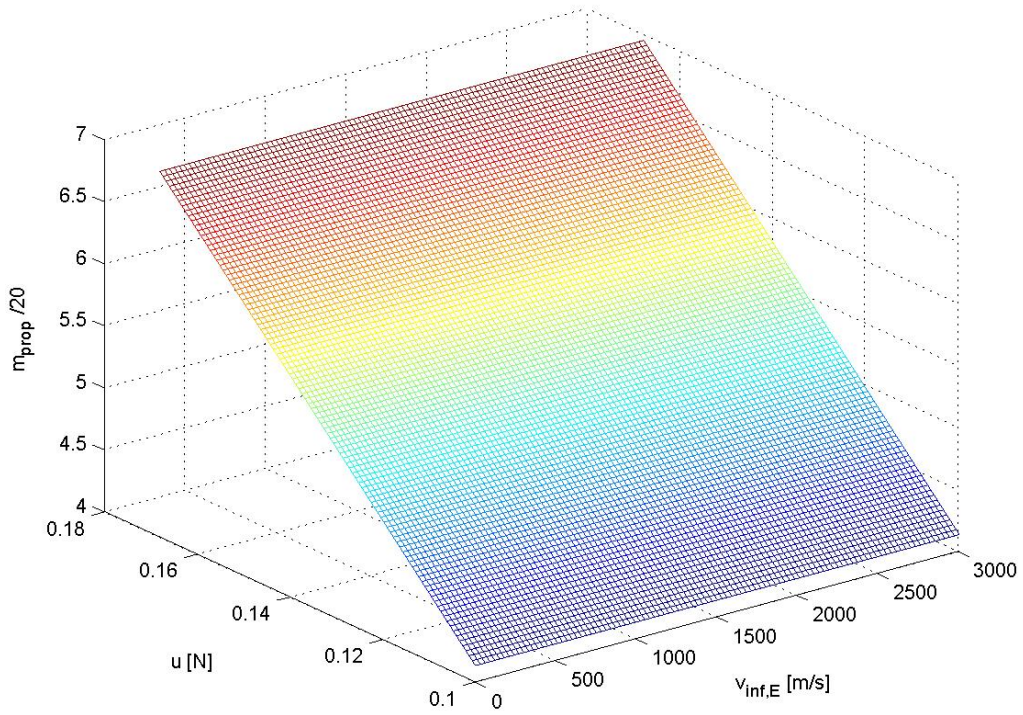

Figure 73: $m_{prop} / 20$ values with respect to the escape velocity from Earth and the thrust.

Figure 70 shows the convexity features of the objective function with respect to the escape velocity from Earth and the thrust level. In particular, monotonic features are again identifiable from Figure 73 with respect to the thrust level: the reason of such a feature is again associable to the propellant mass equation as explaneed earlier. Figure 74 illustrates the admissible region near the best solution as the only part of the search space where $R_F < 5.77 \cdot 10^8\ m$.

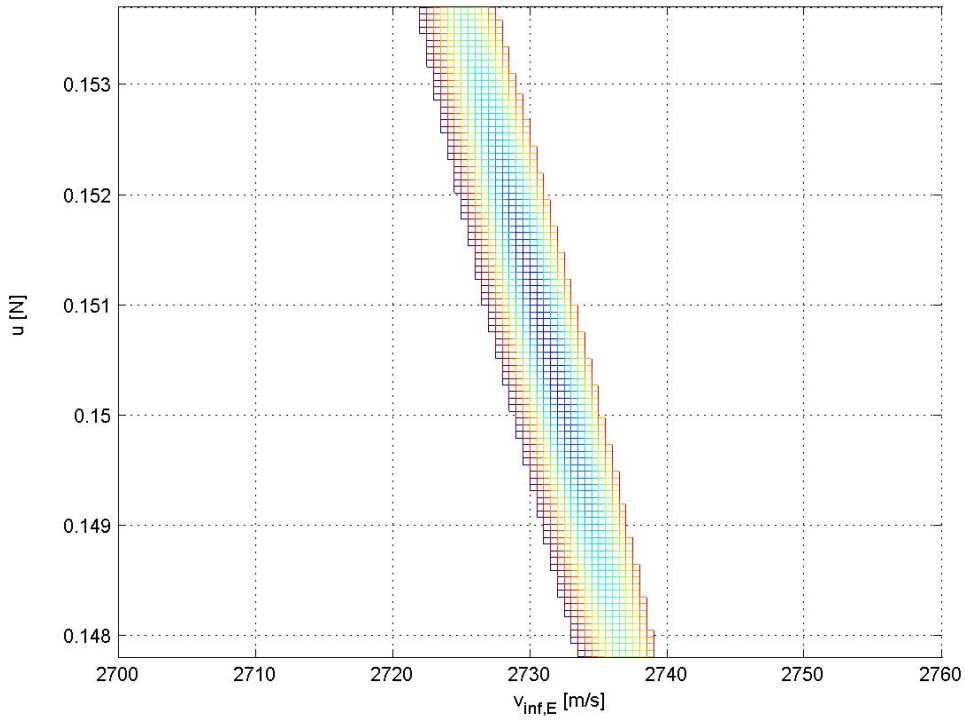

Figure 74: Admissible region near the best solution in the $v_{\inf,E} - u$ subspace.

Similar consideration as those made in the previous cases are here still valid. In particular the admissible region is again very narrow and has regular boundaries.

The objective function shape with respect to the azimuth and elevation at the first and final sample points is now analysed. The results in case of considering the remaining sample points have been shown to be similar. Figure75 shows the objective function values with respect to the azimuth and elevation at the first sample point (remember that the thrust direction along the whole transfer trajectory is given by a linear interpolation of six uniformly distributed time sample points), while Figure 76 and Figure 77 illustrate each objective function term. The propellant mass term has been omitted because only dependent on the transfer time and the thrust level and then constant in this case. Figure 78 illustrates the admissible region near the best solution as the only part of the search space where $R_F < 5.77 \cdot 10^8\ m$.

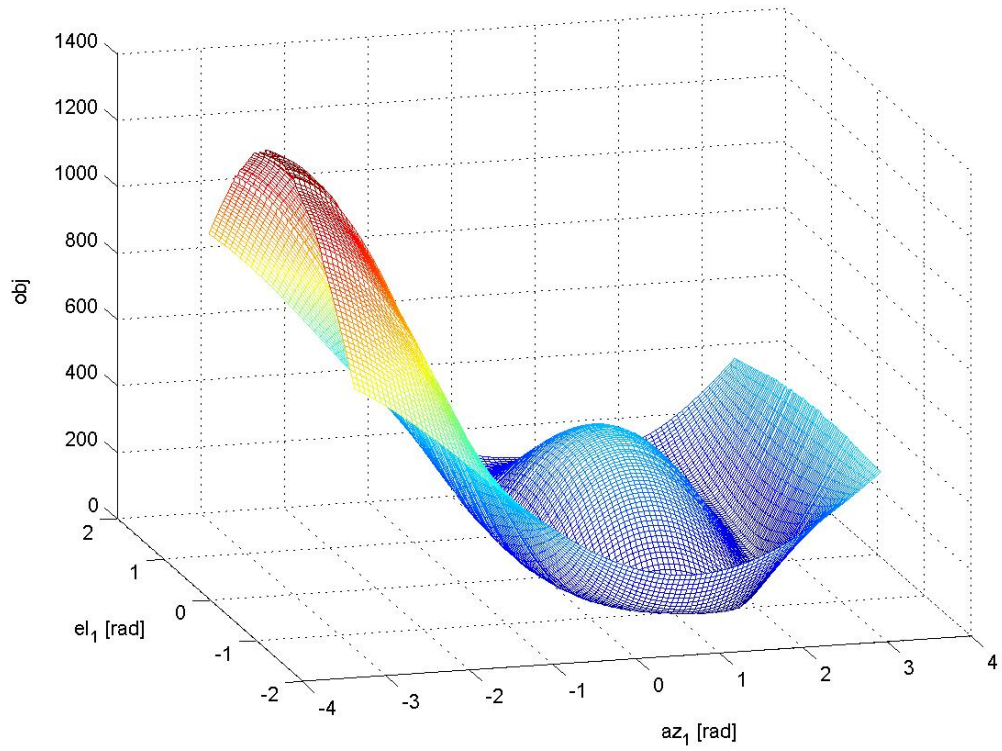

Figure 75: Objective function with respect to the azimuth and elevation at first sampled point.

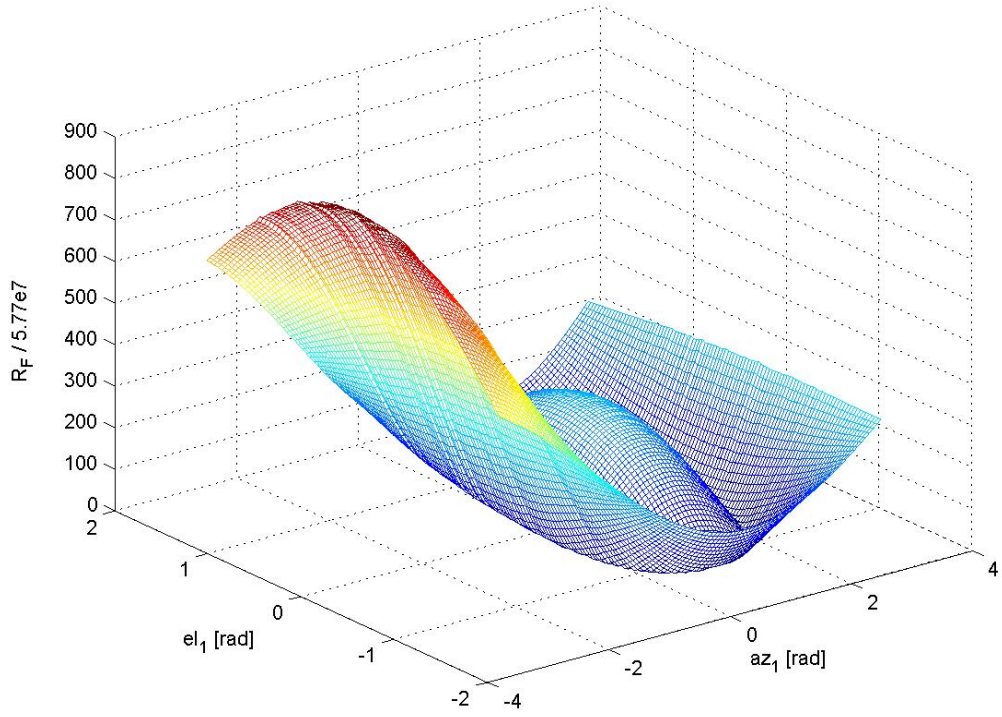

Figure 76: $R_F / 5.77e7$ values with respect to the azimuth and elevation at first sampled point.

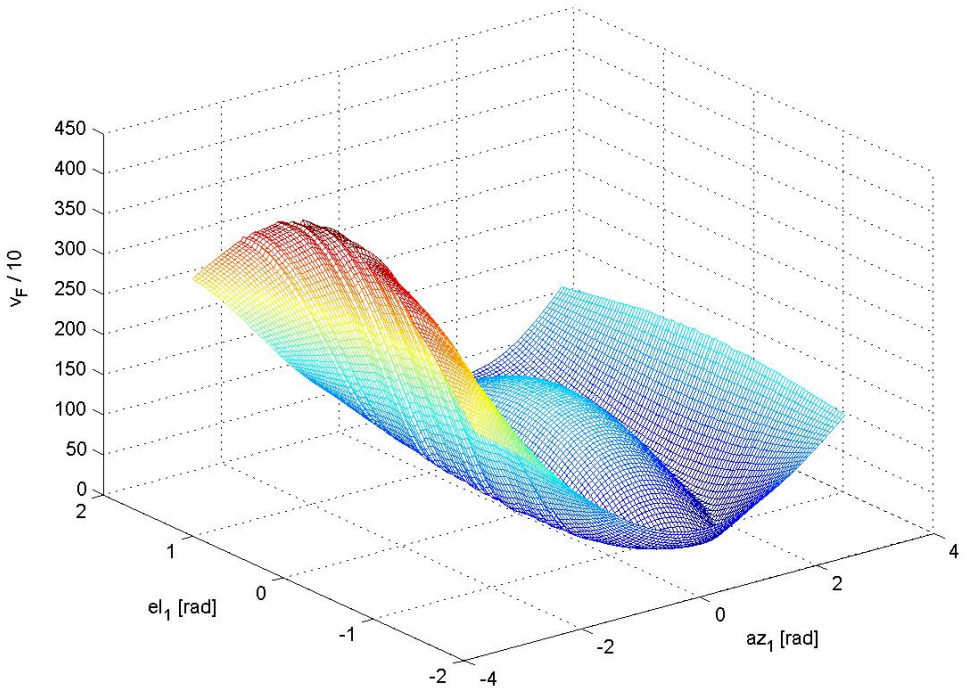

Figure 77: v_F /10 values with respect to the azimuth and elevation at first sampled point.

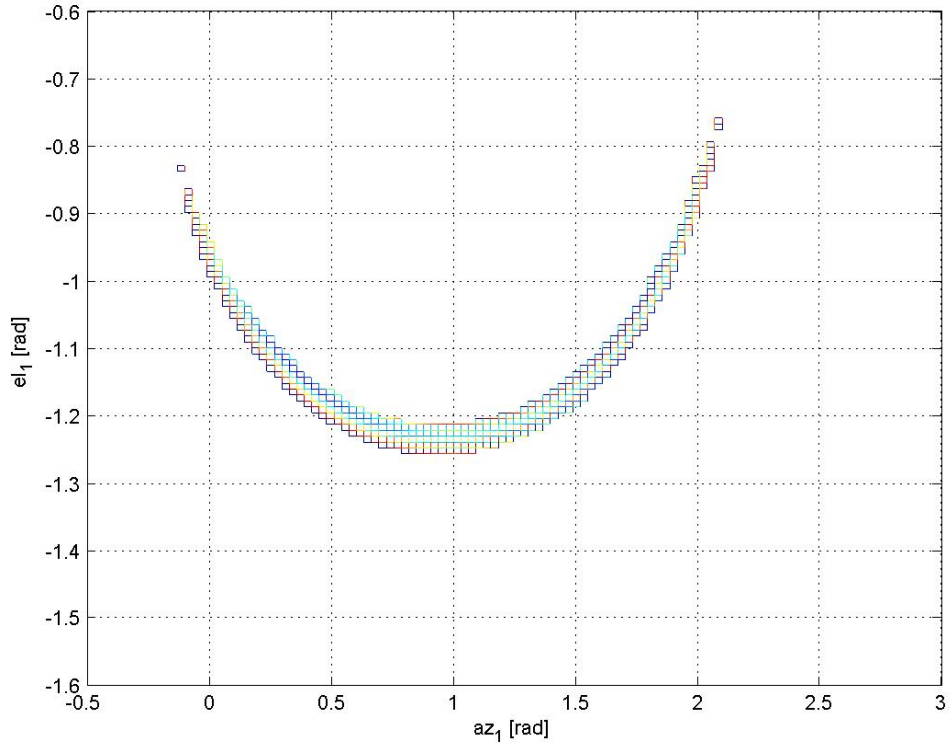

Figure 78: Admissible region near the best solution in the $az_1 - el_1$ subspace.

Figure 79 shows the objective function values with respect to the azimuth and elevation at the sixth sample point, while Figure 80 and Figure 81 illustrate each objective function term. The propellant mass term has been again omitted because only dependent on the transfer time and the thrust level and therefore constant. Figure 82 illustrates the admissible region near the best identified solution as the only part of the search space where $R_F < 5.77 \cdot 10^8\ m$.

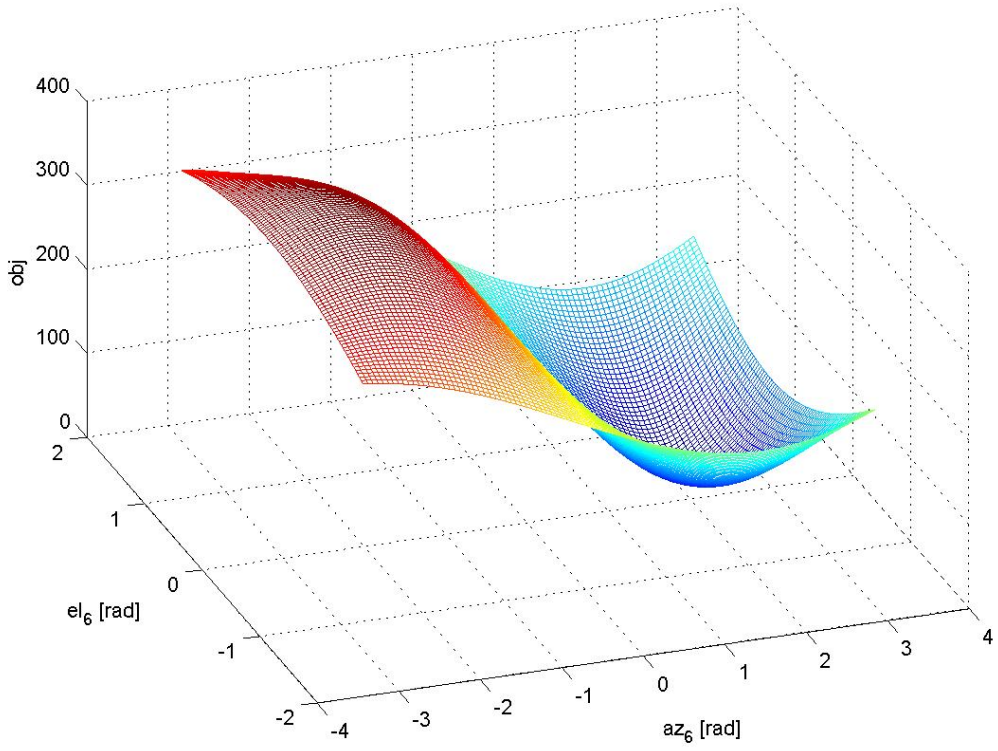

Figure 79: Objective function with respect to the azimuth and elevation at sixth sampled point.

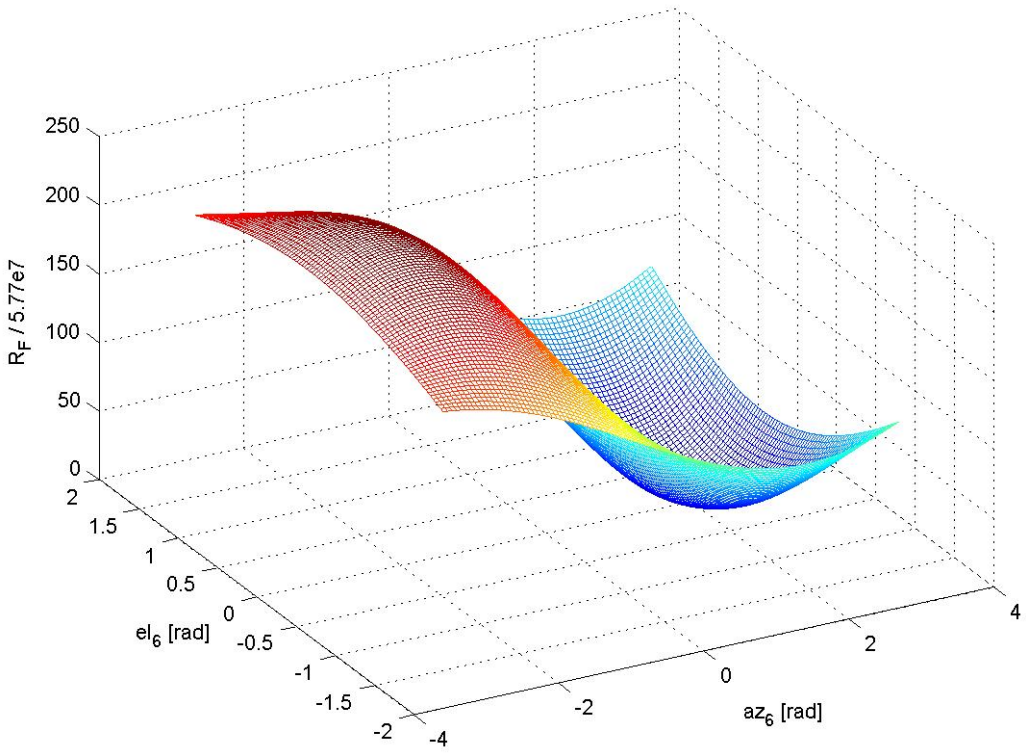

Figure 80: $R_F / 5.77e7$ values with respect to the azimuth and elevation at sixth sampled point.

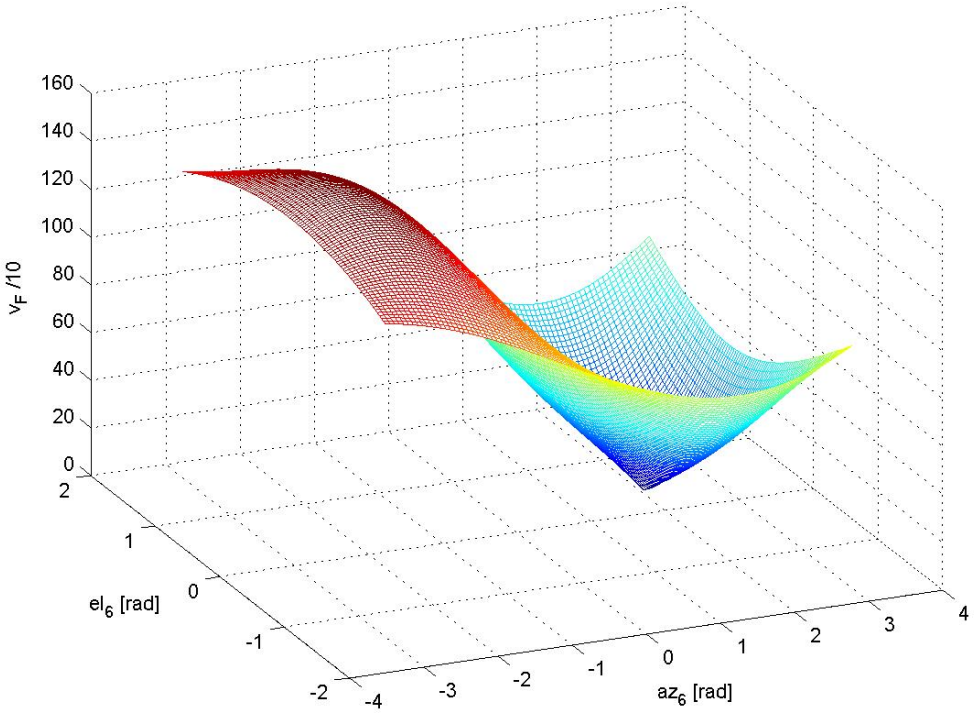

Figure 81: $v_F / 10$ values with respect to the azimuth and elevation at the sixth sampled point.

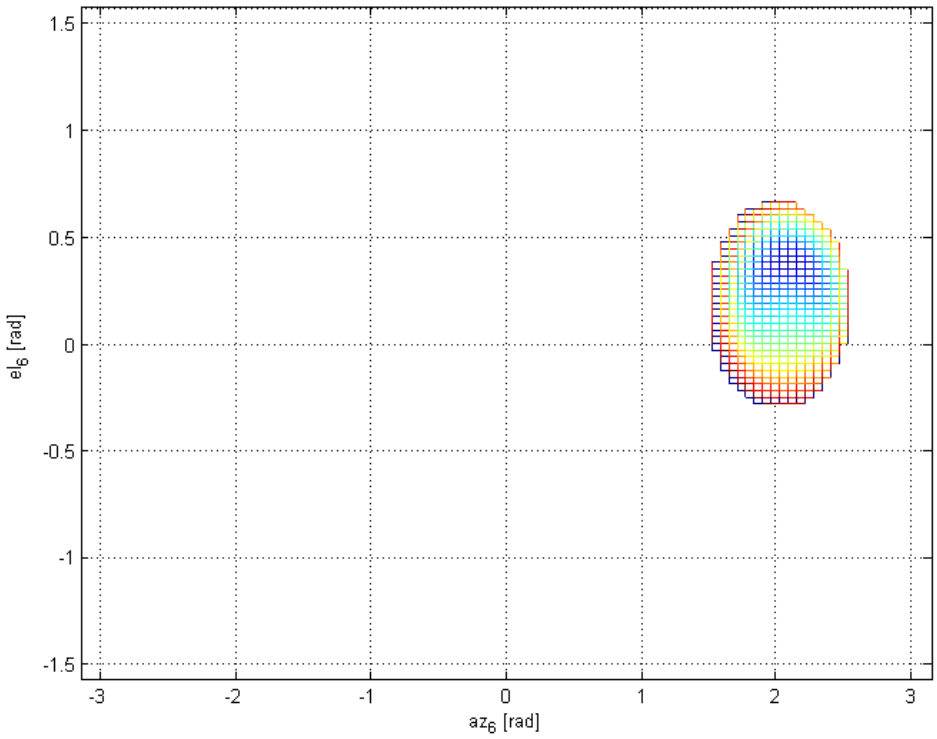

Figure 82: Admissible region near the best solution in the $az_6 - el_6$ subspace.

We now analyse in order to better understand the shape of the third term over the thrust level and the transfer time subspace; the only design variables that directly affect the propellant mass. In the case of constant thrust level, Equation 31 yields:

$$m_{prop} = \frac{u \cdot tt}{I_{sp} \cdot g_0} \qquad [32]$$

The previous equation shows that the propellant mass is monotonic with respect to the thrust level and the transfer time. This can be seen from Figure 83 where the propellant mass is plotted as a function of *u* and *tt*. Similarly to the previous cases, Figures 84 shows the shape of the overall objective function in the *u* – *tt* subspace, while Figure Figures 85-87 illustrate the values of each term.

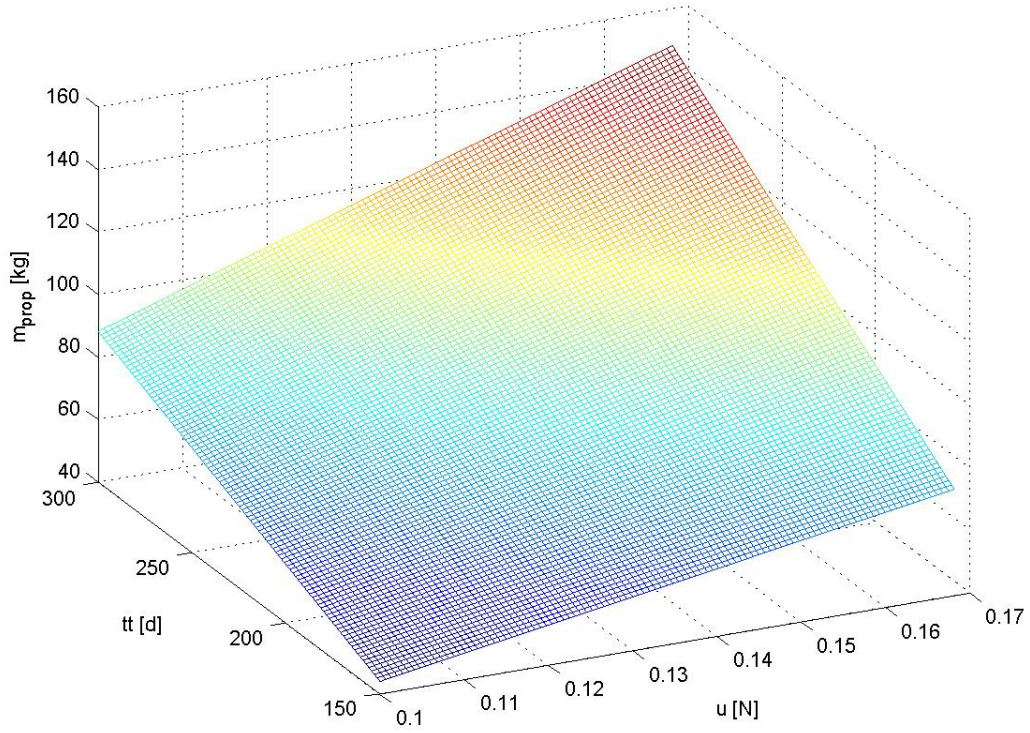

Figure 83: Propellant mass in the *u* – *tt* subspace.

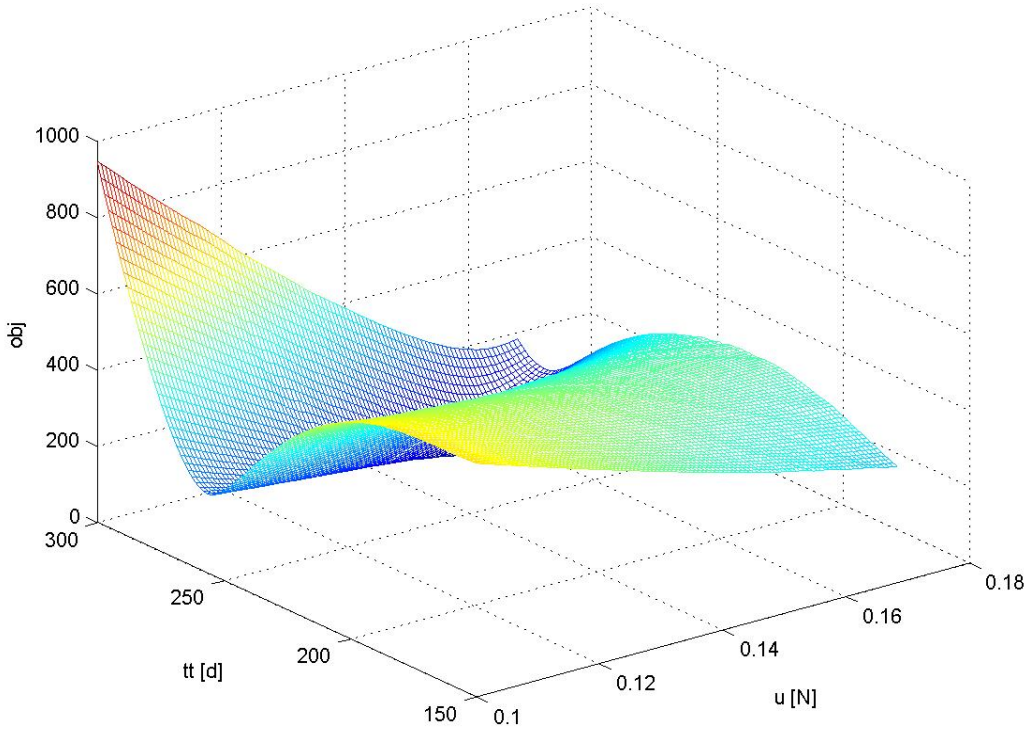

Figure 84: Objective function values with respect to the thrust level and the transfer time.

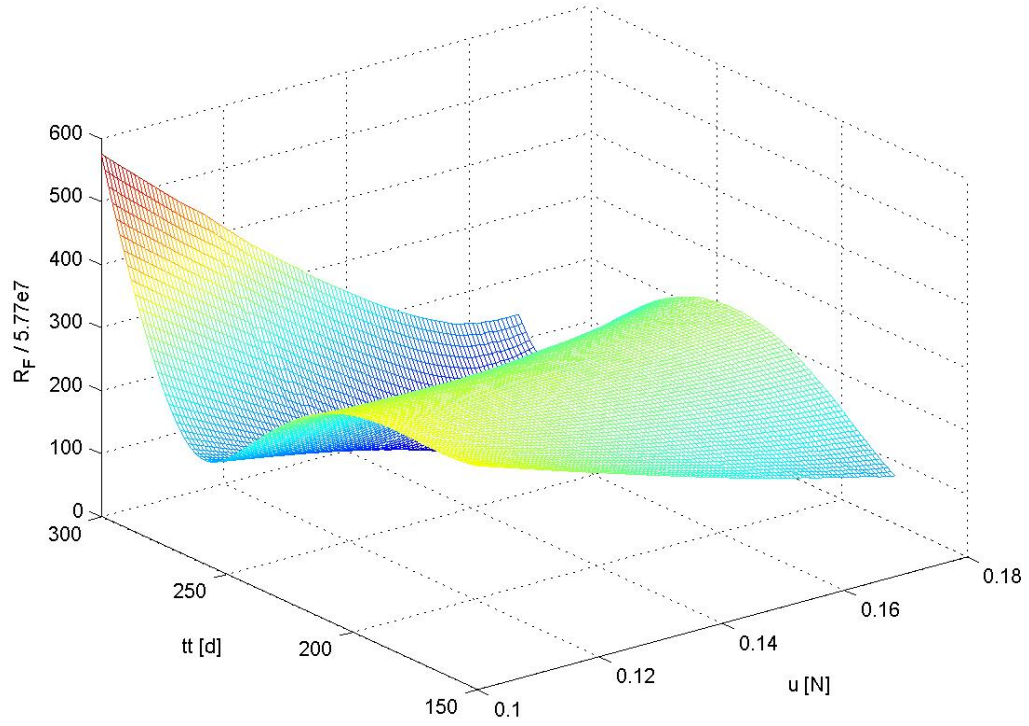

Figure 85: $R_F / 5.77e7$ values with respect to the thrust level and the transfer time.

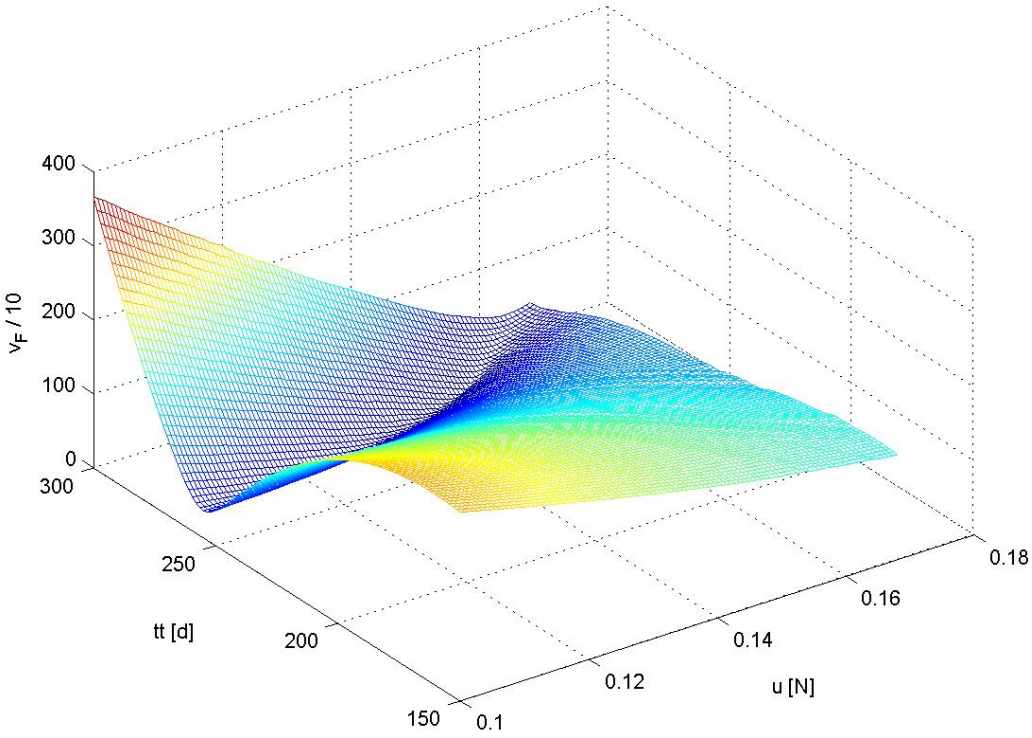

Figure 86: $v_F / 10$ values with respect to the thrust level and the transfer time.

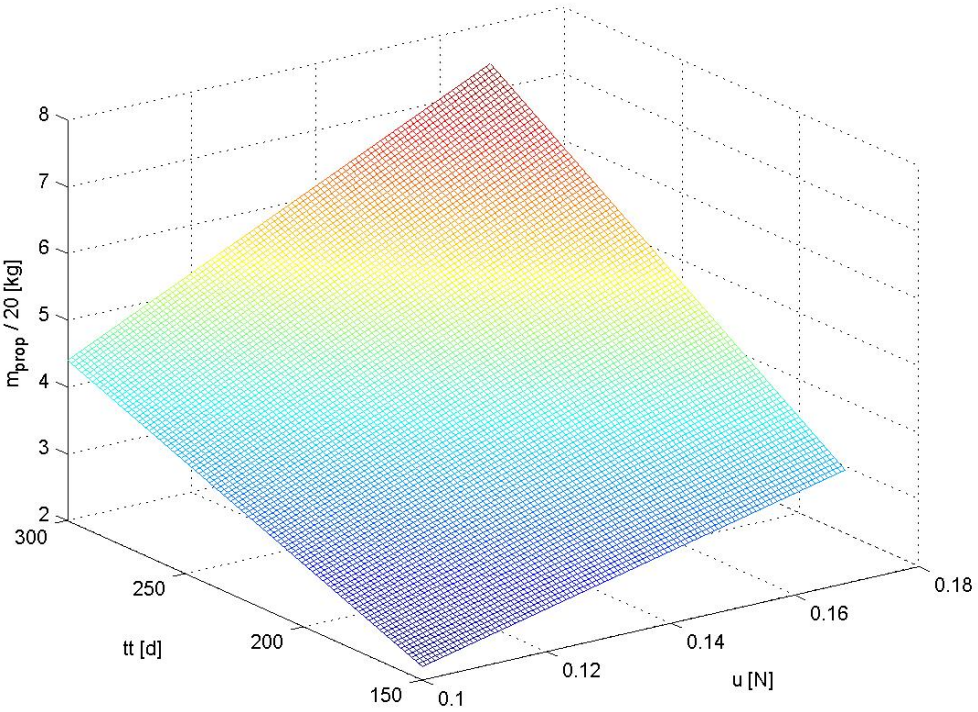

Figure 87: $m_{prop} / 20$ values with respect to the thrust level and the transfer time.

Let us now consider the final relative position with respect to Mars as a constraint. Figure 88 illustrates the admissible region near the best identified solution as the only part of the search space where $R_F < 5.77 \cdot 10^8\ m$, while Figure 89 shows the values of the remaining objective function.

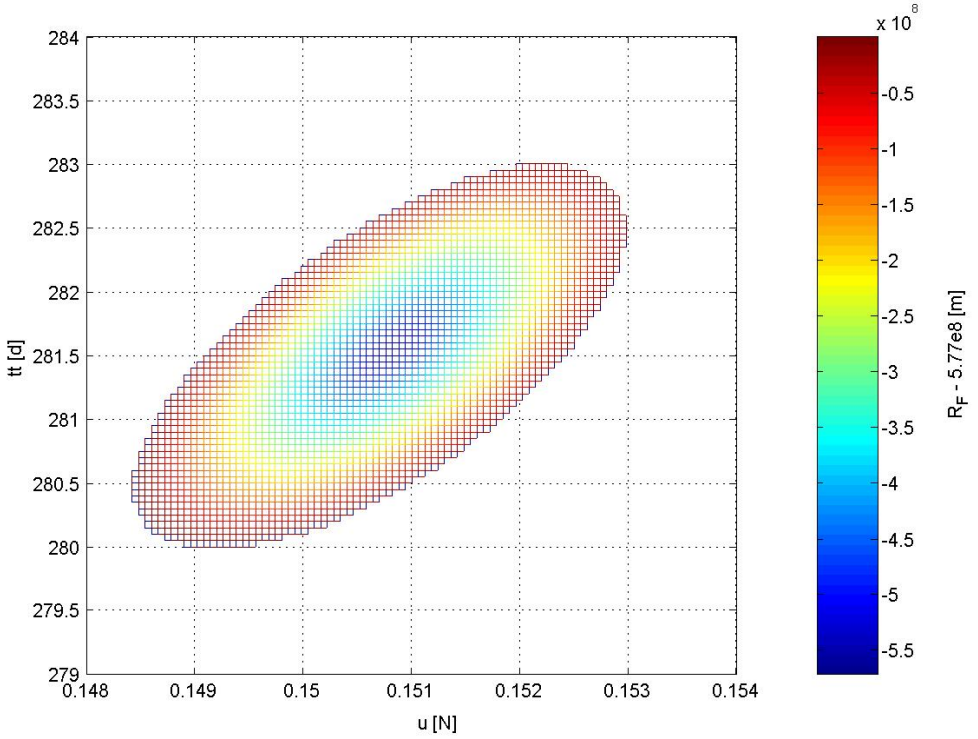

Figure 88: $R_F - 5.77 \cdot 10^8 \, m$ and the admissible region.

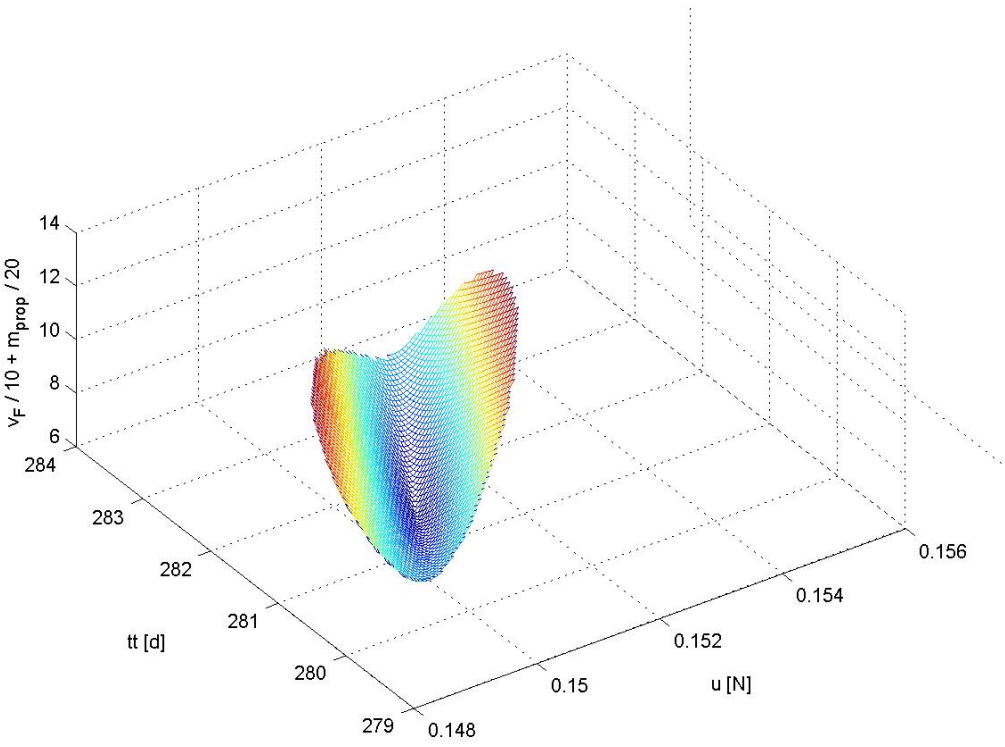

Figure 89: $v_F / 10 + m_{prop} / 20$ over the admissible region.

The remaining objective function shows convexity features over the admissible region. Now, note that this observation has a general validity as it is related to the propellant mass term. Finally let us consider the second term of the objective function as a further constraint, imposing a maximum final relative velocity with respect to Mars equal to 50 *m/s*. The resulting optimisation problem is therefore summarised as:

$$\textit{Minimize}:\ obj = m_{prop}\ \textit{subject to}:\ R_F < 5.77 \cdot 10^8 m\ \textit{and}\ v_F < 50\, m/s$$

Figure 90 consequently shows the resulting objective function values (that is the values of only the propellant mass) over the admissible search space.

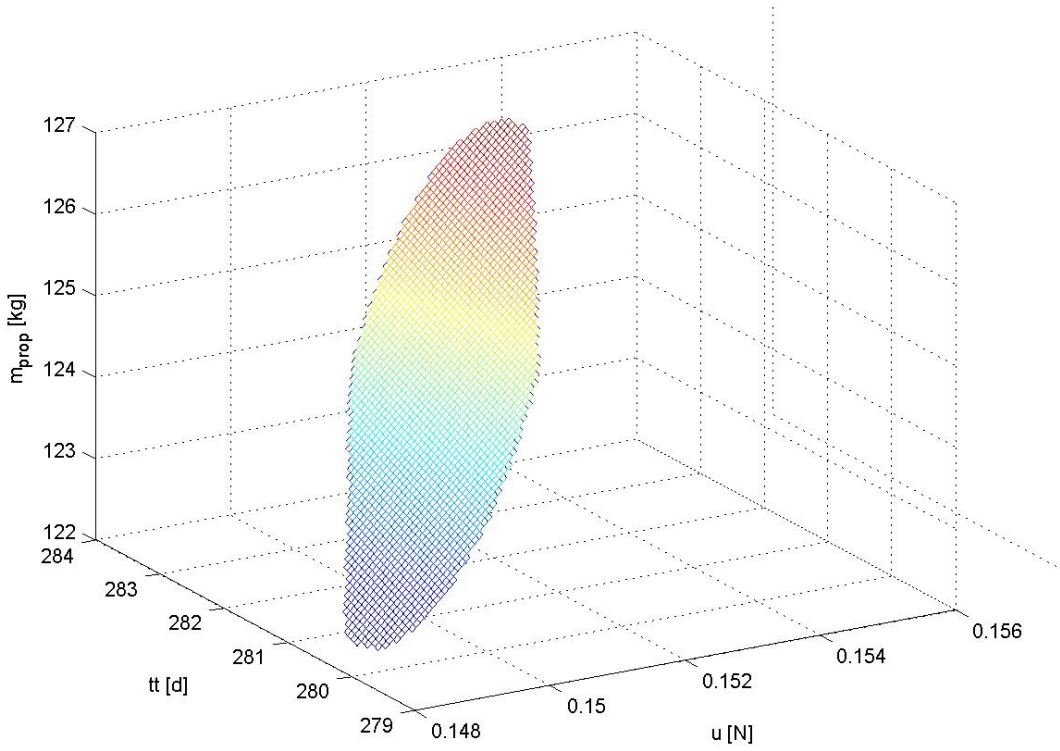

Figure 90: m_{prop} in the admissible region.

Note that by considering the first two objective function terms as constraints in the optimisation process, the only design variables that affect the values of the objective function are the thrust level, *u*, and the transfer time, *tt*, while the remaining design variables only affect the shape and position of the admissible region in the *u* – *tt* space. In this case the values of the remaining design variables have been fixed to those corresponding to the best solution, however this has not been proven to be a global optimum. By varying those values one can completely identify the whole admissible region in the *u* – *tt* subspace. Once solved the problem of characterizing the whole admissible region, which is certainly a very complex problem in itself, one can find the global optimum by analysing the boundaries of such a region, due to the monotonic features of the remaining objective function.

Problem Dimension	Constraints	Search Space	Objective function	T-periodicity
N	Box constraints	$D \in \Re^n$	$f \in \Re$ almost everywhere C^2, locally discontinuous in a countable number limited sets	Yes

Table 24: Summary of problem characteristics.

Finally, note that if we can demonstrate that the A-to-B low thrust transfer with fixed A and B is not NP-hard, meaning that the solution for the controls is unique and easy to find, then the problem is similar to the 2-impulse direct transfer and a polynomial time optimisation algorithm can be developed. This possibility will be accurately analysed in the future.

5. LUNAR WEAK STABILITY BOUNDARY TRANSFERS

The possibility of designing low energy lunar space trajectory exploiting more than one gravitational attraction is now investigated. In particular, the framework of the Restricted Three-Body Problem (R3BP) is here analysed and Lunar transfers are studied which take advantage of the dynamic of the corresponding libration points [Topputo at al., 2004].

5.1 Problem Formulation

In order to assess the objective function, the following mathematical models and methods have been used:

- Restricted three-body dynamical model
- Two dimensional motion (synodic dimensionless reference frame)
- Combination of invariant manifolds and Lambert's three-body arcs
- Impulsive manoeuvres (i.e. instantaneous variations in velocity) for linking the three-body arcs

The interior stable manifold associated to the libration point *L1* in the Earth-Moon system, W_{L1}^{S}, is propagated backward for an interval of time t_W. Corresponding to W_{L1}^{S}, the exterior unstable manifold, W_{L1}^{U}, can be evaluated. The manifolds W_{L1}^{S} and W_{L1}^{U} constitute in fact a transit orbit between the forbidden region through the corresponding thin transit region. As a consequence, if a spacecraft lies on the stable manifold W_{L1}^{S}, the natural evolution of the system will bring it from the region close to the Earth to the region close to the Moon. However, the backward integration of the manifold W_{L1}^{S} for several Moon's periods has shown that this manifold does not reach low distances from Earth: in particular, the minimum Earth distance seems to be constant and almost equal to 0.35 Earth-Moon unit distances. To solve this problem, starting from a circular orbit around the Earth, an arc resulting from

the solution of a Lambert's three-body problem is used for targeting a point on the manifold W_{L1}^{S}. It is worth noting that such an approach leads to a final unstable orbit around the Moon with mean altitude equal to 21600 *km*, which can be further stabilized with additional manoeuvres. Data corresponding to the considered initial circular orbit around the Earth are reported in Table 25.

Initial circular orbit	
Altitude:	200 *km*
Inclination:	0 *deg*

Table 25: Initial conditions.

As a consequence of the previously described formulation, a first impulsive manoeuvre, ΔV_1, is used to put the spacecraft in the Lambert's three-body arc from the initial circular orbit around the Earth. A second impulsive manoeuvre, ΔV_2, is performed to inject the spacecraft on the capture trajectory W_{L1}^{S}. The overall ΔV, which is necessary for performing the Lunar transfer and which has been considered as objective function for the optimisation processes, can be evaluated as follows: $\Delta V = \Delta V_1 + \Delta V_2$

As a consequence of the mathematical models and methods used for the objective function assessment, the search space is characterized by the following design variables:

- The angle identifying the starting point over the initial circular orbit (θ)
- The time of the backward propagation of the stable manifold W_{L1}^{S} from the libration point *L1*, whose final point identify the target of the Lambert's three-body arc (t_W)
- The transfer time corresponding to the Lambert's three-body arc from the initial circular orbit to the target point on the stable manifold W_{L1}^{S} previously identified (t_L)

The previous choices make the number of the design variables equal to 3. All the previous design variables have a continuous characterization over the search space.

Upper and lower bounds on the design variables are considered. The imposed intervals of variation are:

$$\begin{aligned} &\left[\theta^{LB},\theta^{UB}\right]=[0,360]deg \\ &\left[t_L^{LB},t_L^{UB}\right]=[0.1,3]\ d \\ &\left[t_W^{LB},t_W^{UB}\right]=[5,150]\ d \end{aligned} \qquad [33]$$

In order to avoid the problem of high differences in the interval dimensions corresponding to each design variables, a normalization process has been implemented which renders the search space a unit 3-dimensional hypercube.

5.2 Objective Function Structure Analysis

As for the previous mission analysis test cases, the objective function structure analysis for a Lunar transfer using libration points starts with the Reeves and Yamada methodology: 100 local minima have been found with a random start search (with uniformly distributed random start points) followed by an SQP optimization process; the mean distances of each solution to each other is then assessed and compared to the corresponding goodness; consequently, the values of the design variables corresponding to the best local minimum has been used in order to analyse the convexity of the objective function. By using the Reeves and Yamada's methodology, Figure 91 shows the resulting local minima distribution: the x-axis reports the normalized mean distance of each local optima, while the corresponding objective function values are indicated along the y-axis.

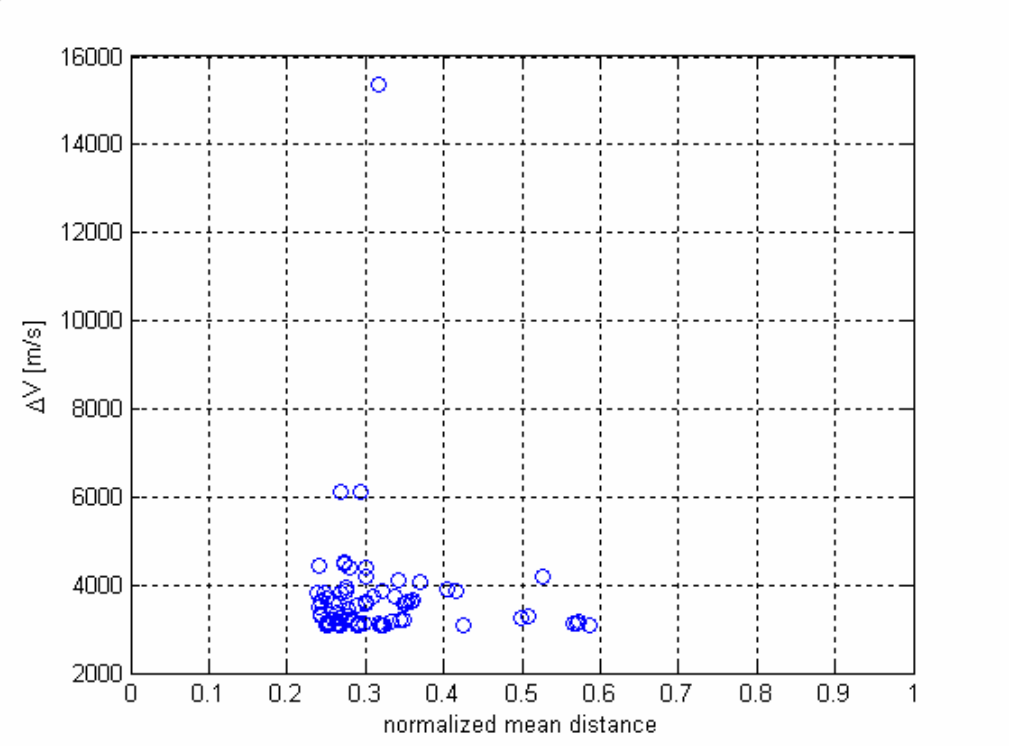

Figure 91: Objective function structure analysis for Lunar transfers using libration points.

As already noted in previous mission analysis classes, the objective function for a Lunar transfer using libration points shows a *big-valley* structure. The mean closeness of most local optima tends to range between 0.2 and 0.4 times the hyper-diagonal magnitude. The features of the best found local minimum are reported in Table 26 and Table 27, together with the illustration of the resulting transfer trajectory in a dimensionless Earth-Moon rotating frame, Figure 92.

Search space	
θ :	70.835 *deg*
t_L :	1.273 *d*
t_W :	107.670 *d*

Table 26: Best identified solution: search space.

Objective space	
ΔV :	3080.767 *m/s*
ΔV_1 :	3080.756 *m/s*
ΔV_2 :	0.011 *m/s*

Table 27: Best identified solution: objective function space.

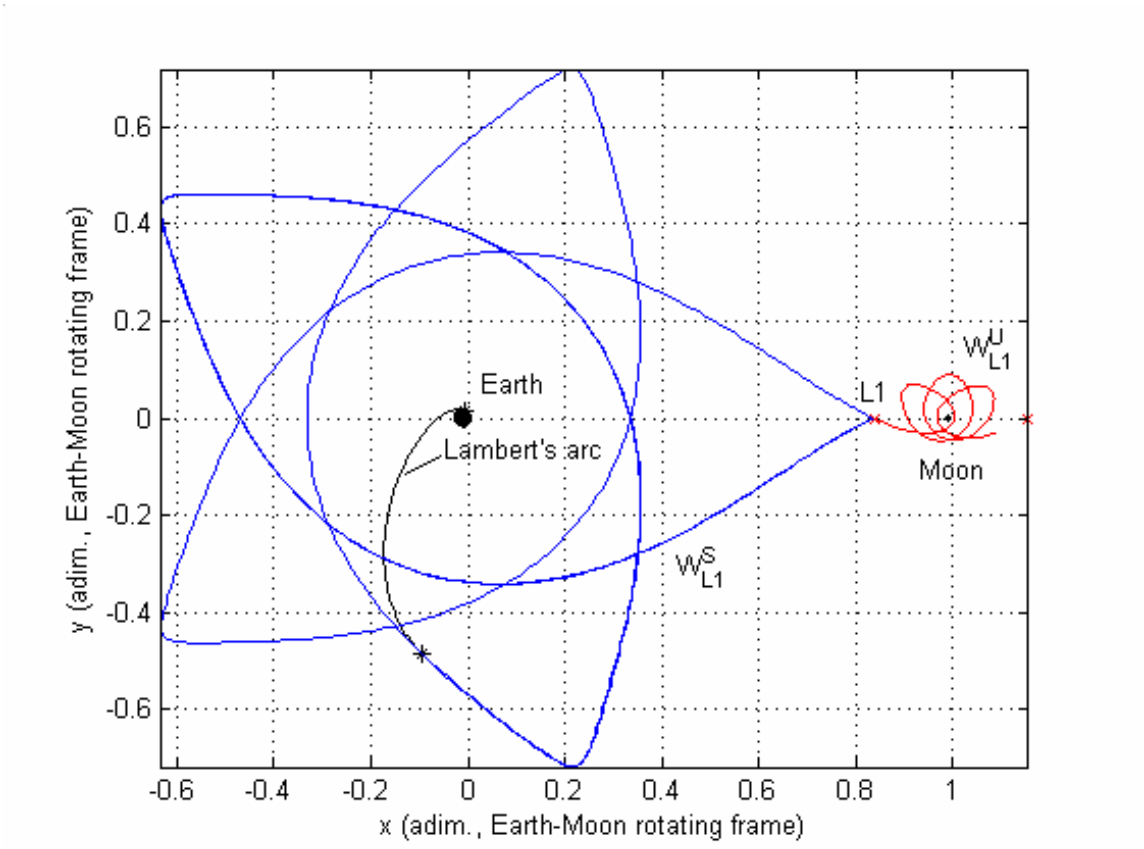

Figure 92: Best known solution: trajectory representation in the dimensionless Earth-Moon rotating frame.

Let us now analyse the shape of the objective function over the search domain, by considering two significant design variables at time and fixing the values of the remaining design variables to those of the previous best identified solution.

Starting angle (θ) – Lambert's three body arc transfer time (t_L)

Figure 93 shows the resulting objective function values with respect to angle identifying the starting point over the initial circular orbit (θ) and the transfer time corresponding to the Lambert's three-body arc from the initial circular orbit to the target point on the stable manifold W_{L1}^{S} (t_L).

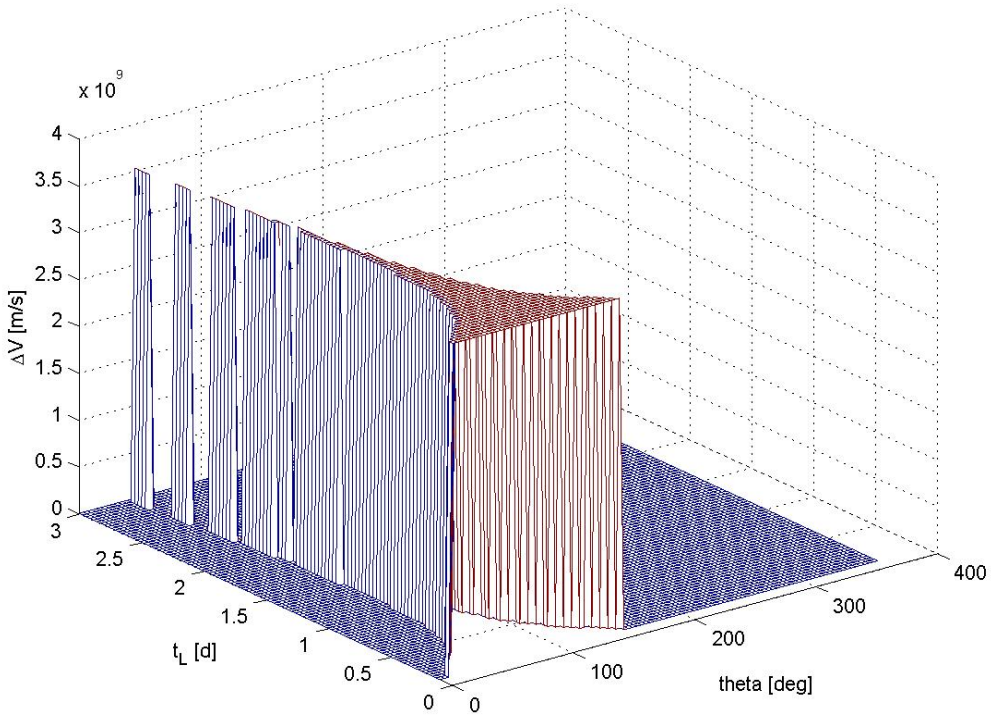

Figure 93: Objective function values with respect to θ and t_L.

The shape of the objective function illustrated in Figure 93 shows important discontinuities. The reason of such irregularity is related to the mathematical model used for the objective function evaluation. In particular, as stated above the mathematical model here analysed involves the solution of a Lambert's three body problem; the solution of such a problem is carried out by means of a shooting method which try to link the initial and final desired states with a three-body trajectory by opportunely modifying the initial conditions through several iterations until either a certain tolerance is satisfied or a maximum number of iterations is reached. In case the algorithm implementing

the shooting method does not converge to a solution within the considered tolerance before the maximum number of iterations is reached, it returns output values that fix the objective function value to a relatively high constant penalty value. This is not an efficient approach, which eliminates objective function gradients in particular regions of the search space and high discontinuities on the boundaries of such regions. Anyway, it is worth noting that it is still quite used in practical problem, although it could make ineffective the global and local search. As a consequence, the red flat region in Figure 93 corresponds in fact to such non-converging solutions. On the contrary, this situation does not hold in case of the apparently flat blue region in the same figure: Figue 94 reports a close up of the same function where non converging points have not been considered.

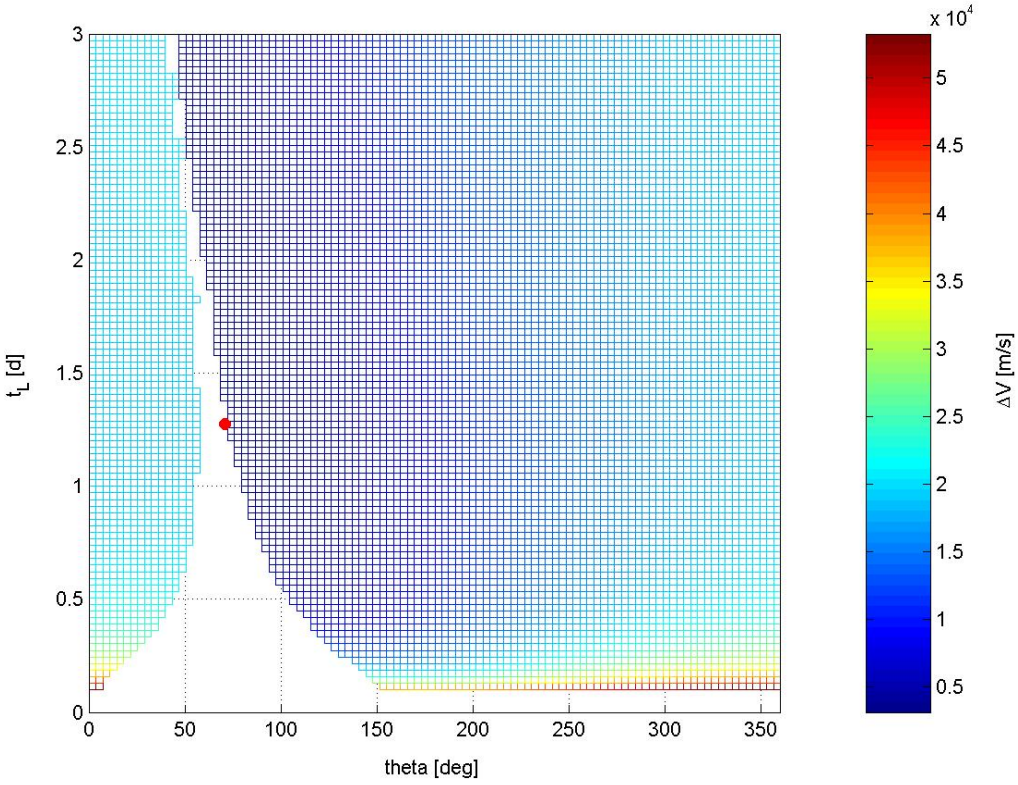

Figure 94: Objective function values with respect to θ and t_L: close up of Figure 93 (the red point is the best identified solution).

Figure 94 shows that, by omitting the non converging solutions, the objective function has quite regular structure on the θ - t_L plane, whit monotonic feature in fact. The red point in figure represents the best identified solution.

However, it is important to note that, the approach used for the objective function definition make this best solution lying on the boundaries of a discontinuity line. Such feature makes the search of the global optimum solution quite complex, because of discontinuities in the neighbourhood of the global optimum solution.

Starting angle (θ) – backward propagation on the stable manifold (t_W)

Figure 95 shows the resulting objective function values with respect to angle identifying the starting point over the initial circular orbit (θ) and the time of the backward propagation on the stable manifold W_{L1}^{S} from the libration point *L1* (t_W).

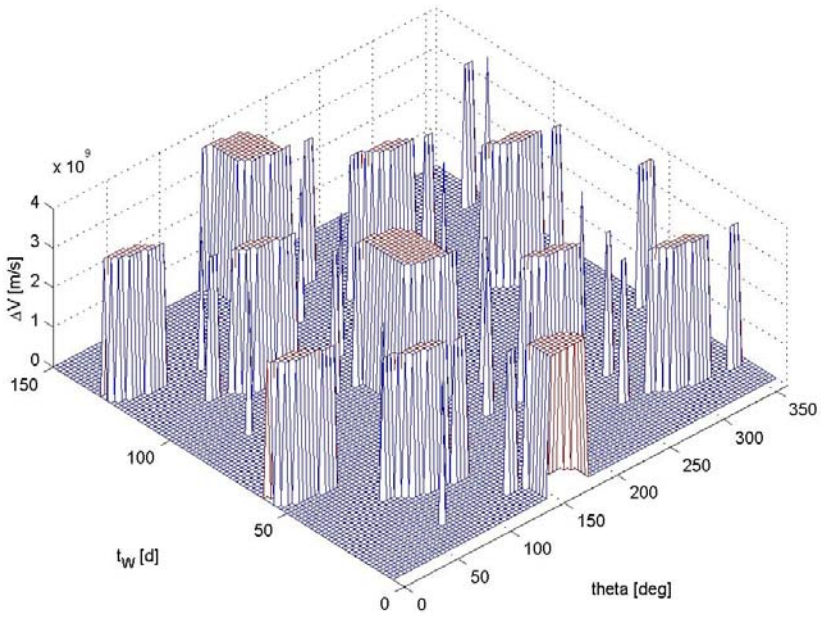

Figure 95: Objective function values with respect to θ and t_W.

Figure 95 shows again the important discontinuities related to the objective function evaluation corresponding to solutions whose associated Lambert's three-body problem solution do not converge. Important observations can be highlighted now by analysing Figures 96-97 which are a close up of Figure 95 omitting the non converging solutions.

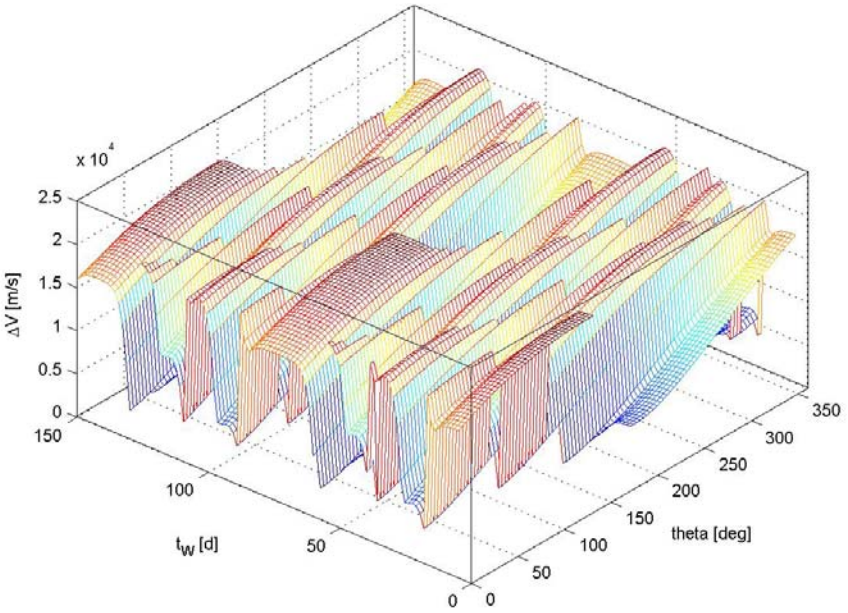

Figure 96: Objective function values with respect to θ and t_W:.

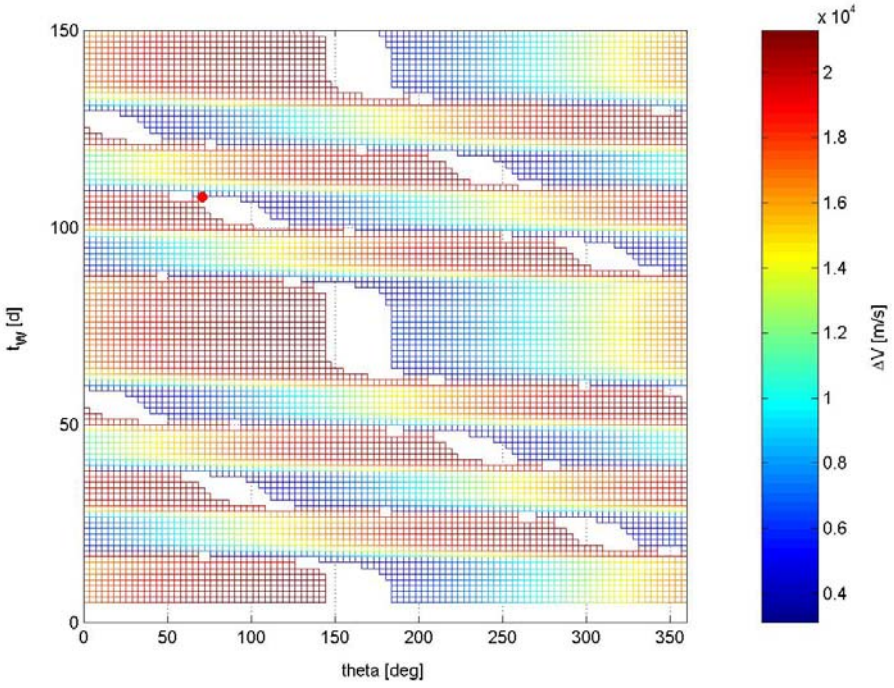

Figure 97: Objective function values with respect to θ and t_W:

Besides the previously identified discontinuities, which are in fact related to a particular management of penalty terms in case of missed convergence, the objective function shows remarkable periodicity on the time spent on the

stable manifold W_{L1}^{S}. Many comparable local minima exist which lie on different slots clearly identifiable analysing the t_W design variable and which seem to be positioned on the boundaries of the multiple discontinuity region: in particular, the best identified solution (the red dot in Figure 97), confirms such considerations. In order to better illustrate the periodic feature, Figure 98 plots the objective function values with respect to t_W by fixing the value of the starting angle θ to that characterizing the best identified solution.

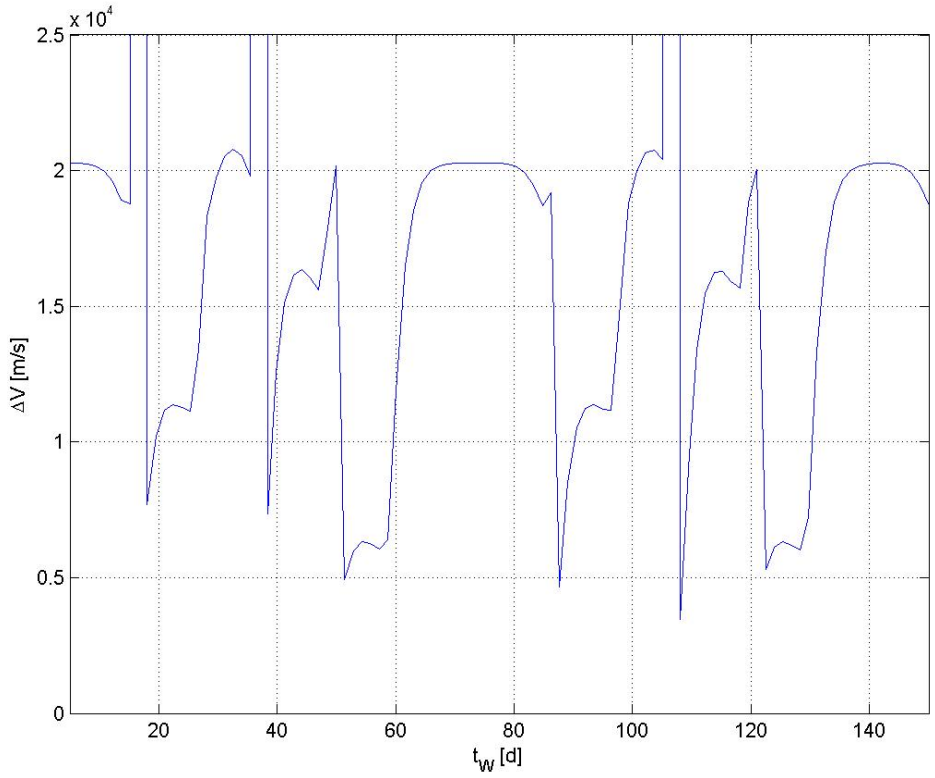

Figure 98: Objective function values with respect to t_W: values of remaining design variables fixed.

As it concerns the trend of the objective function with respect to the starting angle θ, omitting the effects of discontinuities, a non periodic objective function structure holds. Before investigating the reasons of such periodicity, let analyse the remaining combination of design variables.

Lambert's three body arc transfer time (t_L) –backward propagation time on the stable manifold (t_W)

Figure 99 shows the resulting objective function values with respect to the transfer time corresponding to the Lambert's three-body arc from the initial circular orbit to the target point on the stable manifold W_{L1}^{S} (t_L) and the time of the backward propagation on the stable manifold W_{L1}^{S} from the libration point *L1* (t_W).

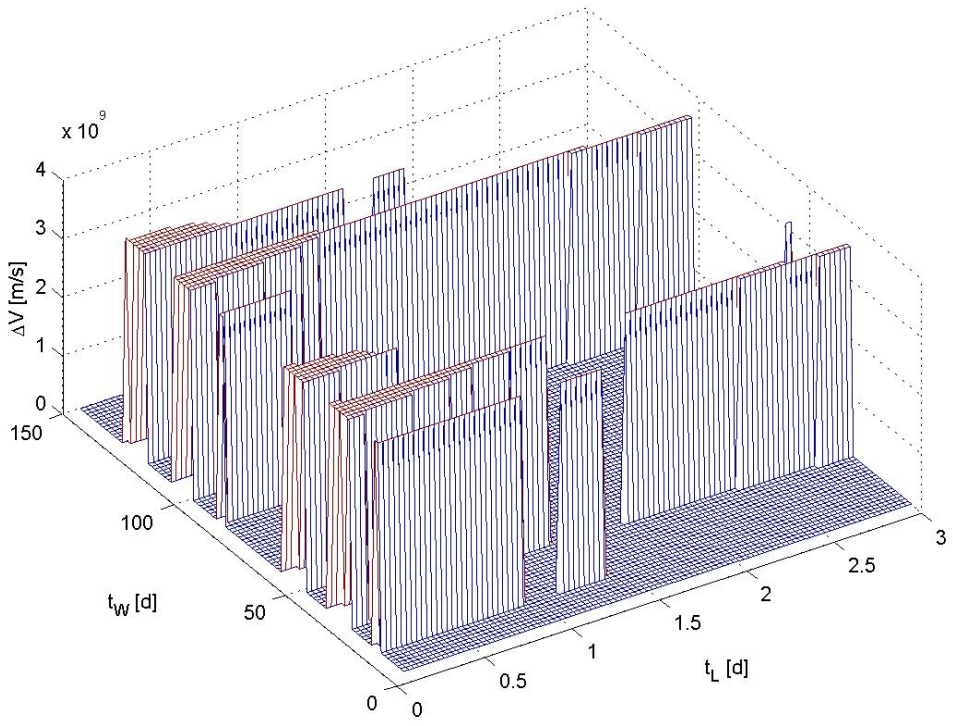

Figure 99: Objective function values with respect to t_L and t_W.

Important discontinuities related to the objective function evaluation corresponding to solutions whose associated Lambert's three-body problem solution do not converge are again identifiable in Figure 99. Let now analyse Figure 100 and Figure 101, which, similarly to the previous cases, constitute close ups of Figure 99 omitting the non converging solutions.

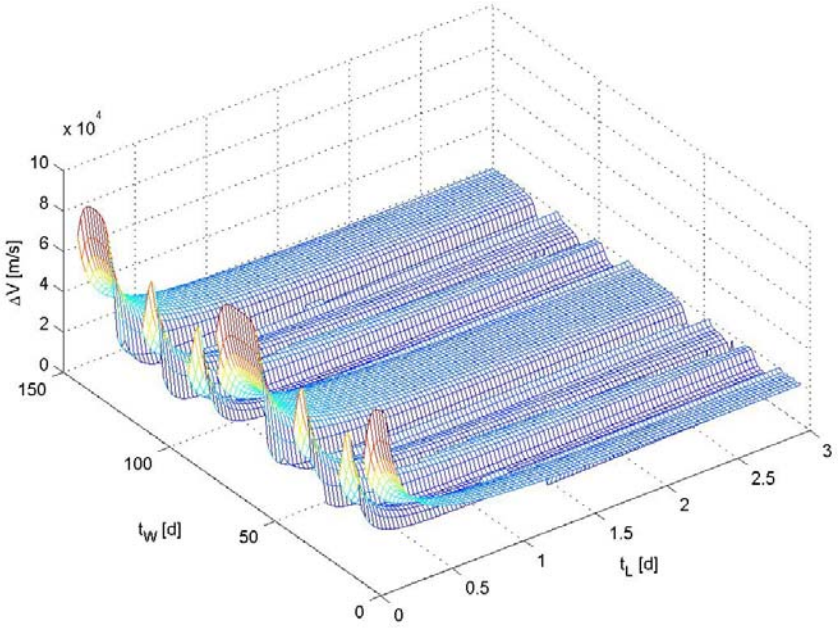

Figure 100: Objective function values with respect to t_L and t_W: close up of Figure 99.

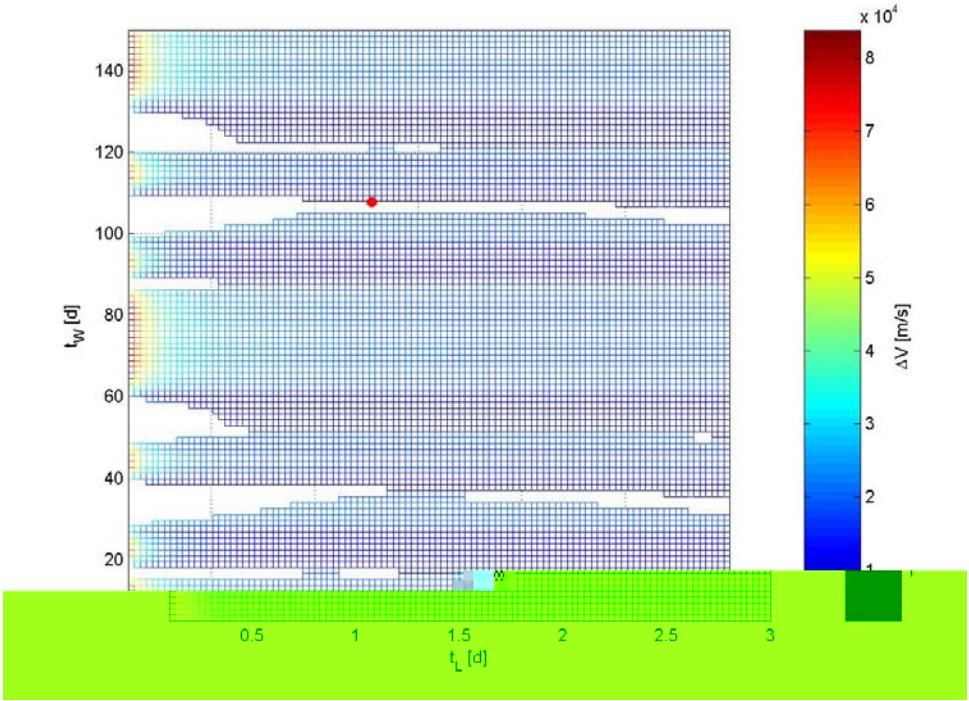

Figure 101: Objective function values with respect to t_L and t_W:

As previously highlighted, omitting the identified discontinuities, the objective function shows remarkable periodicity on the time spent on the stable manifold W_{L1}^{S}, which causes the presence of many comparable local minima

corresponding to different slots clearly identifiable on the t_W design variable. As it concerns the objective function profile with respect to the transfer time corresponding to the Lambert's three-body arc, t_L, monotonic features can be recognized. The best identified solution (the red dot in Figure 101) lies again on the boundary of the multiple discontinuity region.

Let us now investigate the possible reasons of the objective function periodicity with respect to the backward propagation time on the stable manifold W_{L1}^{S} from the libration point *L1* (t_W). Figure 102 is a 3-dimensional plot of the 100 local minima identified by the local optimization processes on the search space, while Figure 103 is a projection of Figure 102 along the three axis.

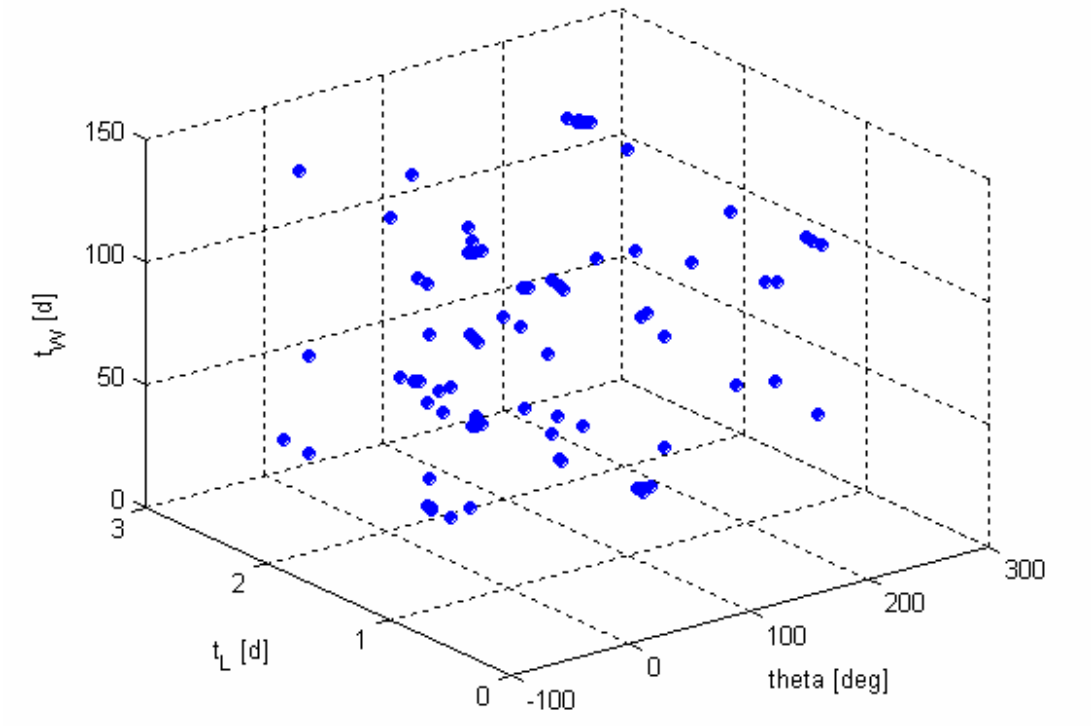

Figure 102: Local minima distribution on the 3-dimensional search space.

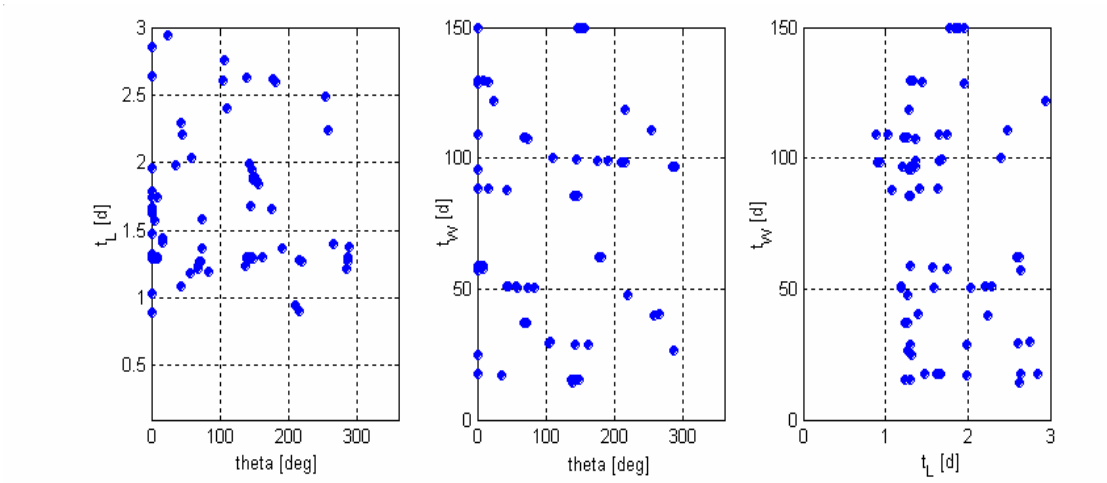

Figure 103: Local minima distribution on the search space: projections of Figure 102.

We can see that the transfer times corresponding to the Lambert's three-body arc, t_L, in case of the identified local minima tend to assume relatively high values: such an observation can be related in fact to the monotonic feature of the objective function with respect to this design variable which has been previously identified (see Figure 102). As it concern the backward propagation time on the stable manifold W_{L1}^{S}, a careful analysis of Figure 103 let us recognize the presence of several set of local minima which tend to assume similar t_W values. The presence of such subgroups can be related to the identification of the big valley structures deriving from the periodicity of the objective function described above (see Figure 97 and Figure 100). Moreover, let consider Figure 104, which simply plots the objective function values corresponding to the identified local minima which are reported in ordinal way.

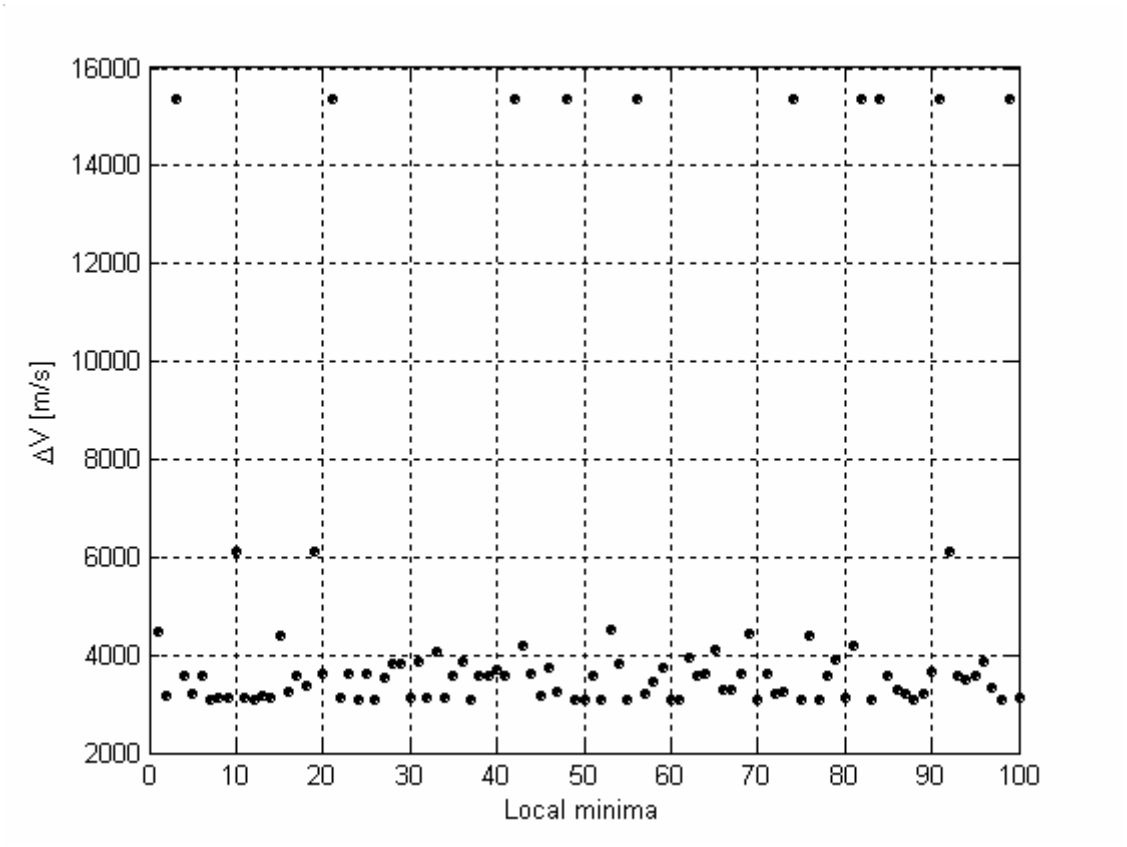

Figure 104: Objective function values corresponding to the identified local minima.

By excluding the worst local minima, Figure 105 reports the identified solutions corresponding to objective function values lower than 4000 *m/s*. Two different objective function levels seems to characterize the identified local minima, the lowest being upper bounded by a value of about 3200 *m/s*. By considering only local minima included in this interval, Figure 106 reports their distribution over the search space.

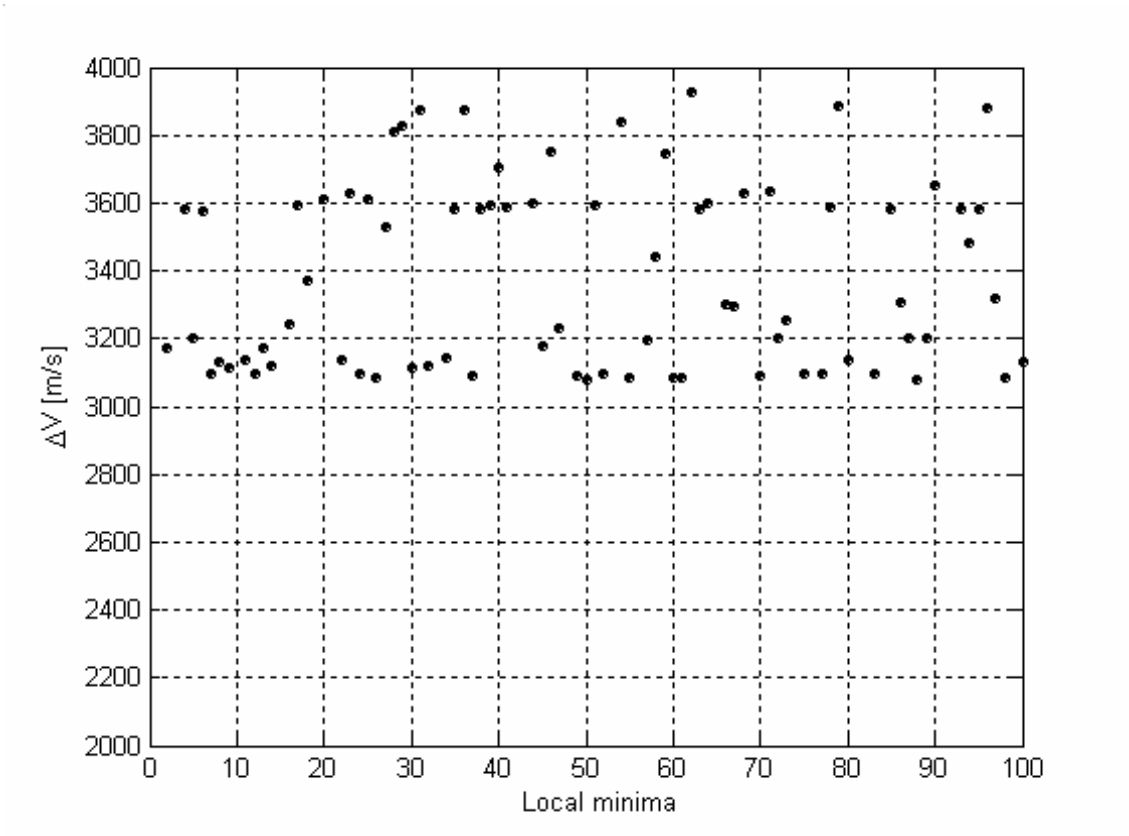

Figure 105: Objective function values corresponding to the identified local minima: close up of Figure 104.

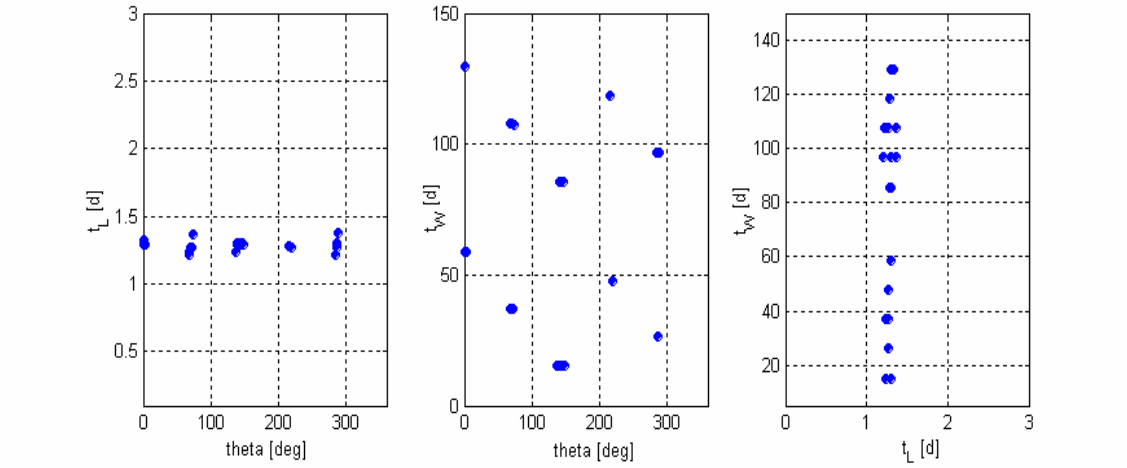

Figure 106: Local minima distribution on the search space: solutions corresponding to *objFun* < 3400 *m/s*.

It is interesting to note that the isolated local minima, which are in fact all comparable in terms of objective function values, gather into subgroups in the search space. In particular, all local minima tend to assume the same value of

transfer time corresponding to the Lambert's three-body arc, t_L, from the initial circular orbit to the target point on the stable manifold W_{L1}^{S}. As it concerns the starting angle θ, a finite set of clusters can be clearly identified (five in this case: see the left plot in Figure 106). Corresponding to each cluster on the θ design variable, by analysing the central plot in Figure 106, two different subgroups can be recognized on the t_W design variable, that is the time spent on the stable manifold W_{L1}^{S} to *L1*. As a consequence, we can state that the subgroups identifiable on the central plot in Figure 106 describe a set of different families of Lunar transfers (where the term "family" is referred to solutions lying on different niches on the search space, as defined by Gurfil and Kasdin in their work about a similar systematic characterization of geocentric orbits in the 3D elliptic restricted three-body problem [Gurfil, and Kasdin, 2002]).

Let us now analyse the details of such families. Figure 107 reports the central plot of Figure 106 where subgroups have been numerated from 1 to 10 following an increasing t_W value. Corresponding to each number in Figure 107 and randomly selecting one solution from each subgroup, Figures 108-117 illustrate the resulting Lunar transfer. Moreover, the minimum objective function value related to each subgroup is indicated in brackets in Figure 117.

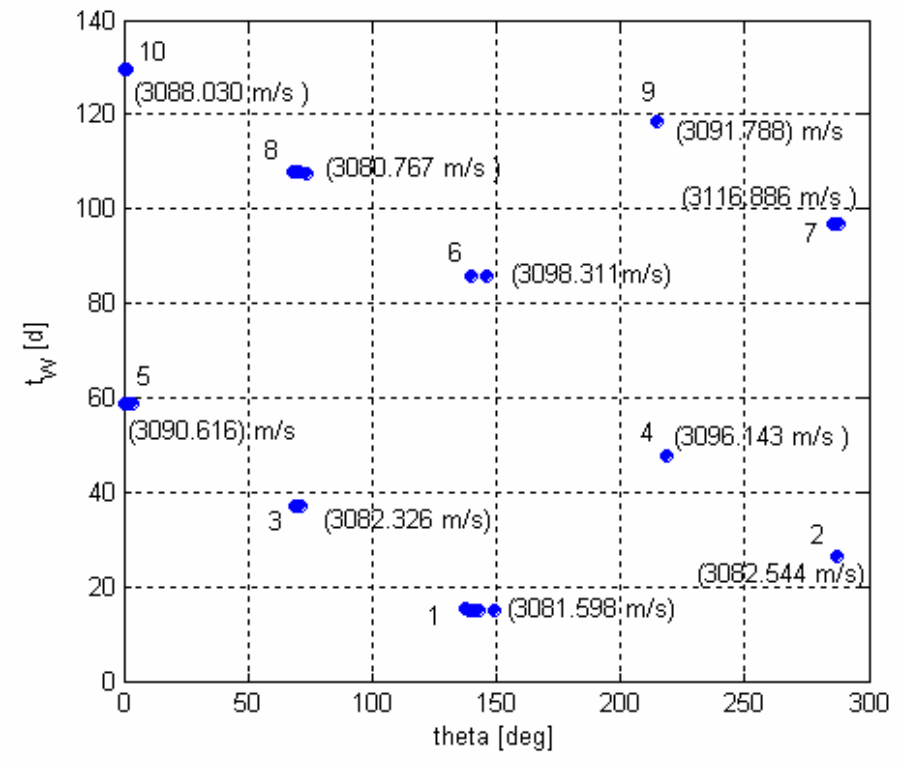

Figure 107: Local minima distribution on the search space: central plot of Figure 106 identifying the set of local minima subgroups.

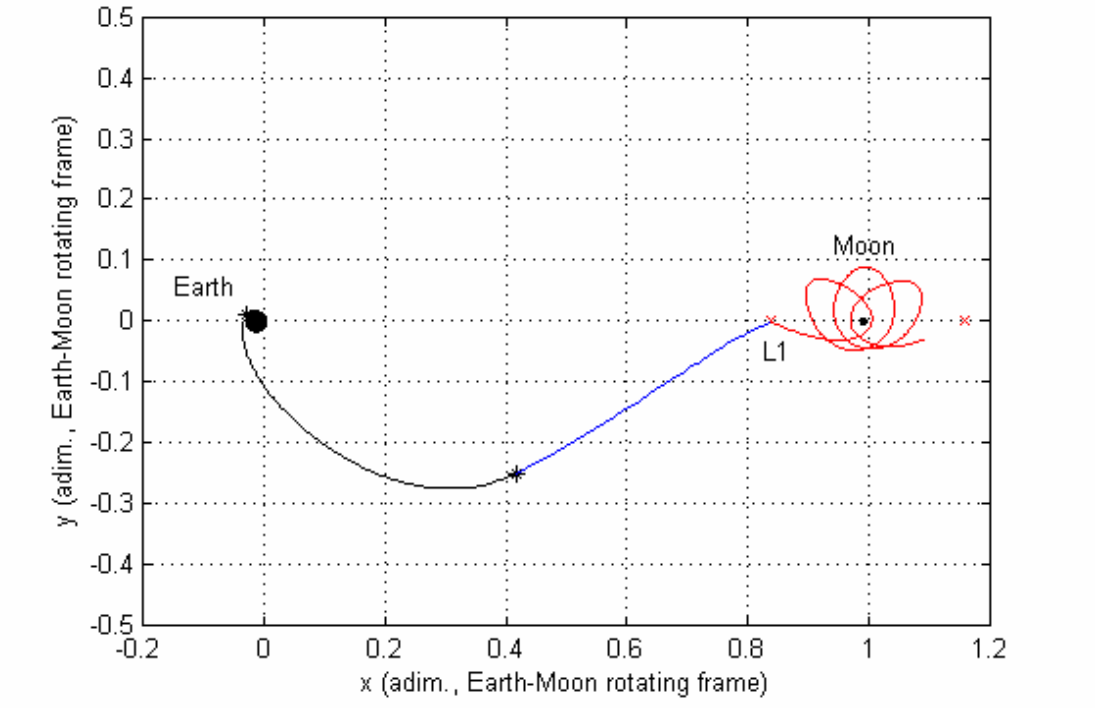

Figure 108: Local minima: subgroup 1.

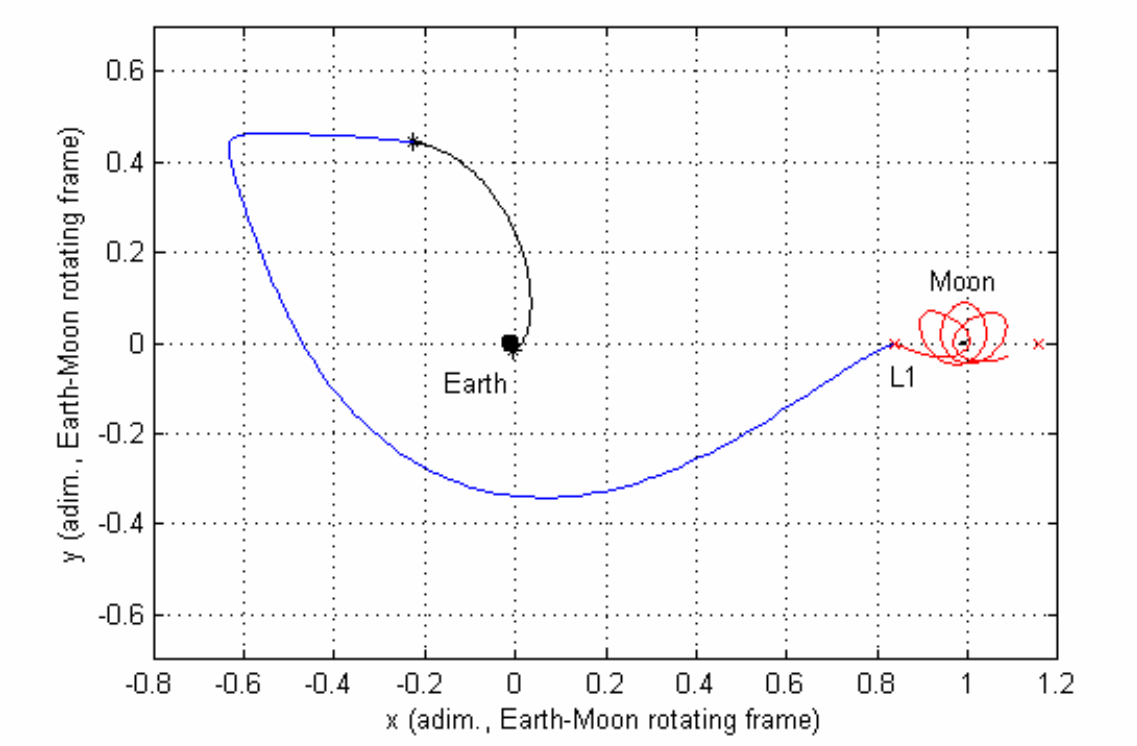

Figure 109: Local minima: subgroup 2.

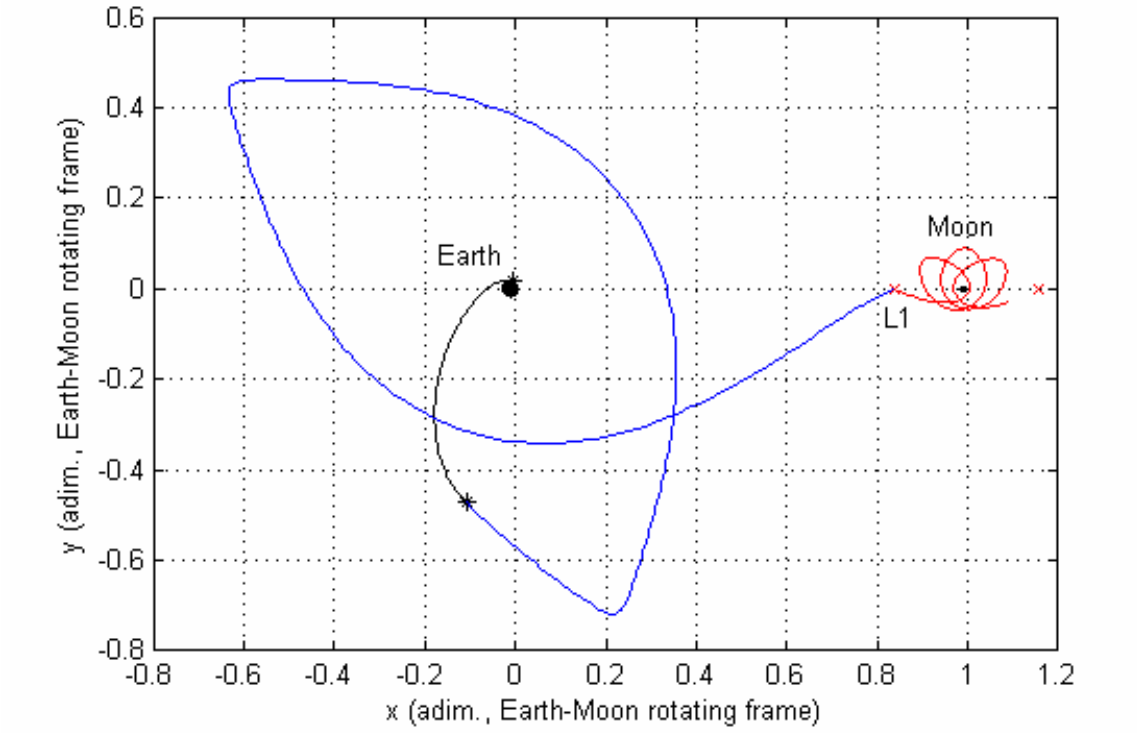

Figure 110: Local minima: subgroup 3.

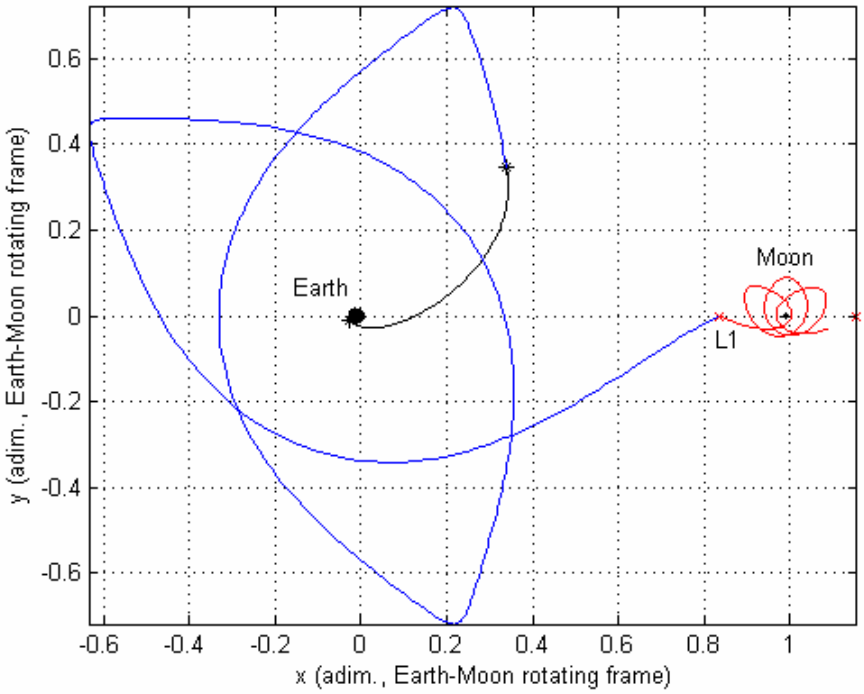

Figure 111: Local minima: subgroup 4.

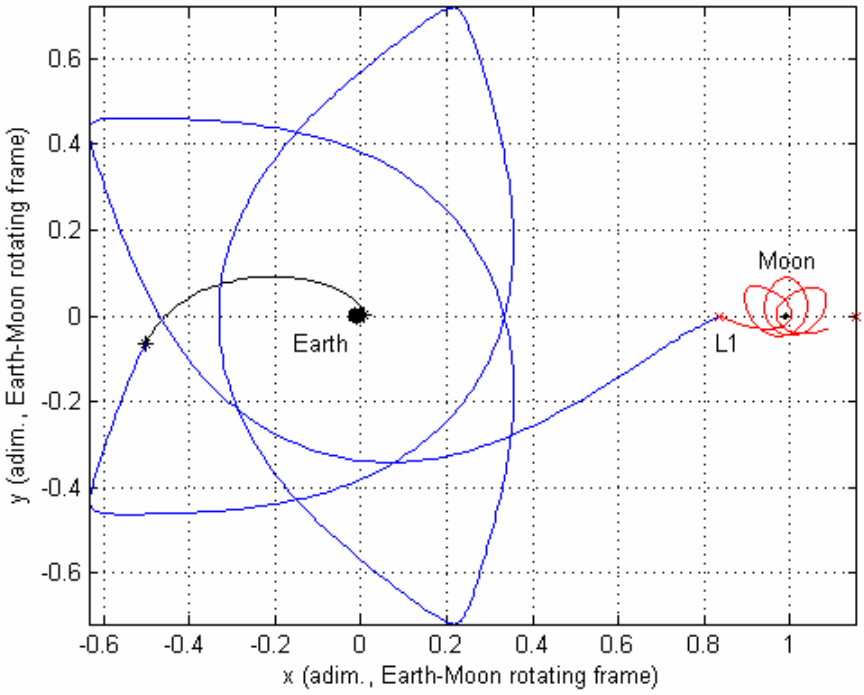

Figure 112: Local minima: subgroup 5.

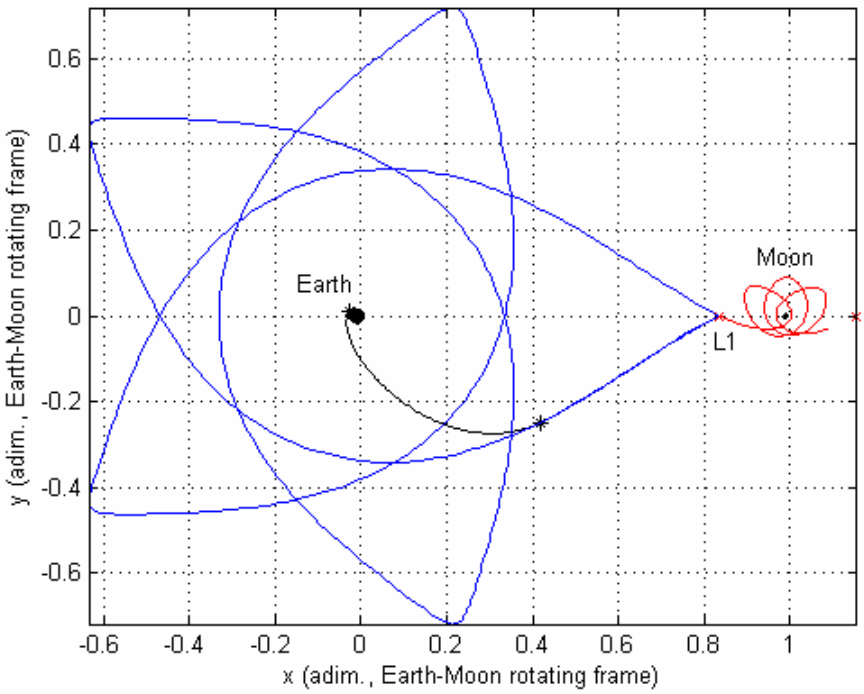

Figure 113: Local minima: subgroup 6.

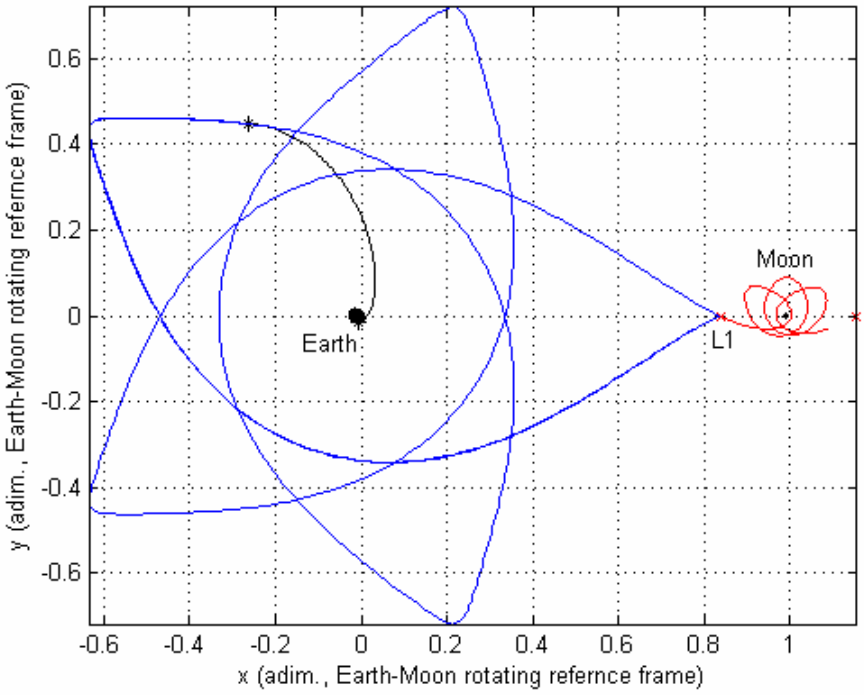

Figure 114: Local minima: subgroup 7.

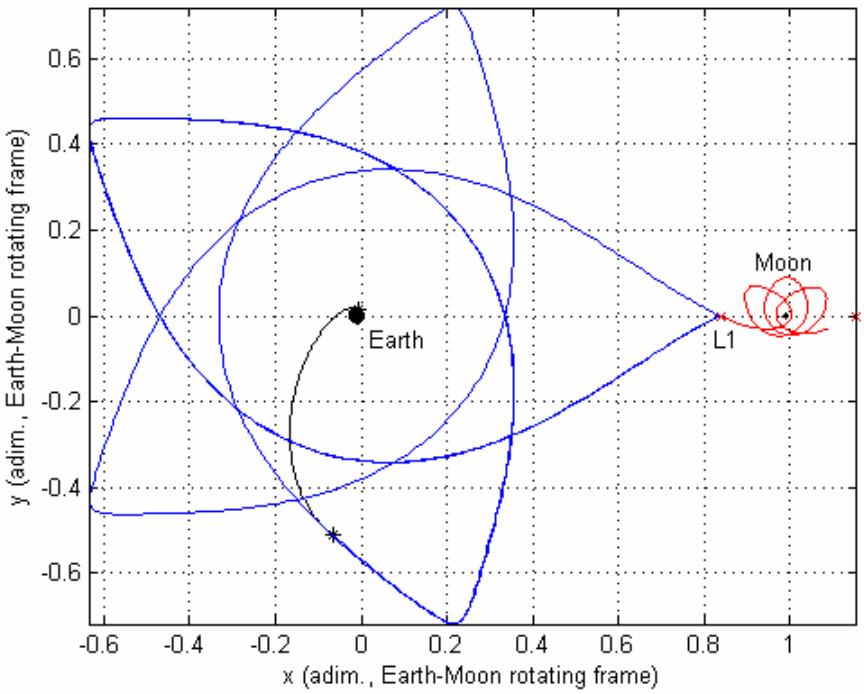

Figure 115: Local minima: subgroup 8.

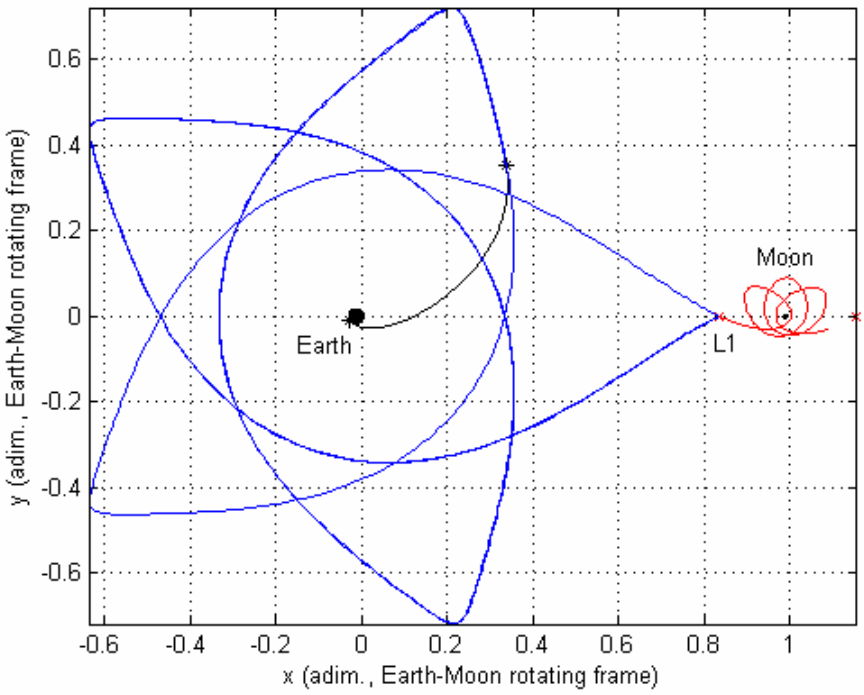

Figure 116: Local minima: subgroup 9.

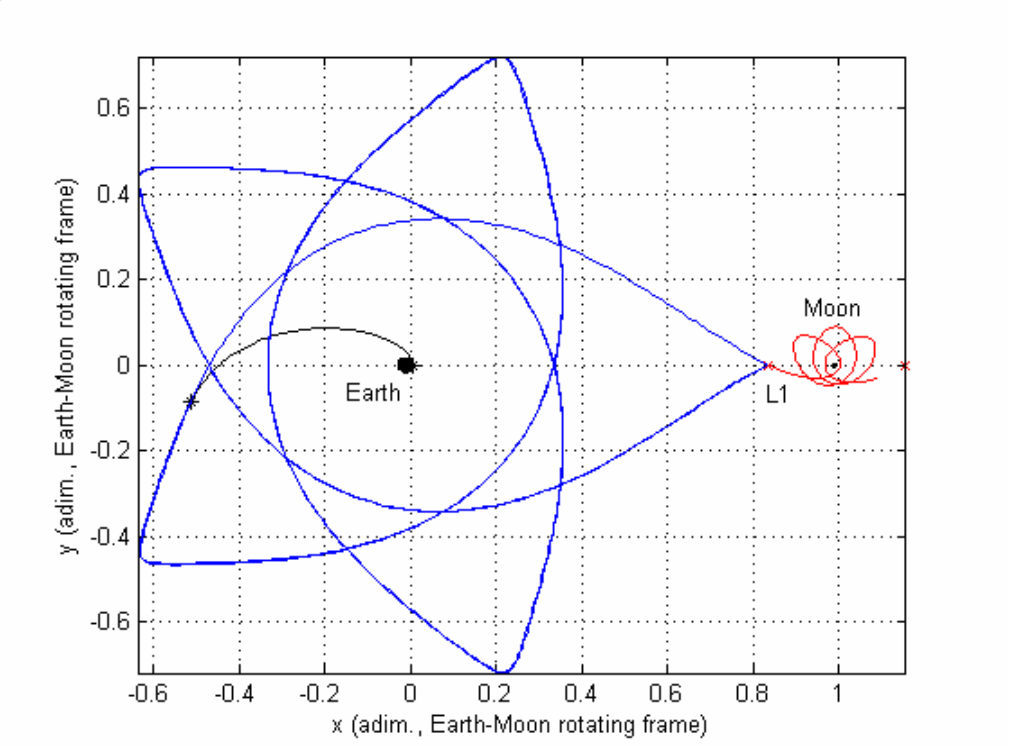

Figure 117: Local minima: subgroup 10.

Figure 117 shows that all the identified local minima are in fact comparable, with little variance on the objective function values. The best identified solution belong to subgroup 8, as can be seen by the corresponding transfer trajectory illustrated in Figure 98. By carefully analysing the transfer trajectories related to the comparable local minima, a common feature can be recognized: in all cases, the injection on the stable manifold W_{L1}^{S} from the Lambert's three body arc occurs in a point near the farthest five points clearly identifiable in the Earth-Moon rotating frame (see for example Figure 117) on the incoming line to them. Moreover, starting from Figure 108, once all the farthest five points have been described, similar solutions seem to occur again in a perturbed orbit with respect to the previous one. The trajectories in Figures 108-117 are represented in the rotating reference frame. However, if viewed in the usual Earth-centered inertial frame, the previous trajectories appears as a conic-like perturbed orbit, with the farthest points corresponding to the apogees and the closest ones to the perigees. As a consequence, in the Earth centred inertial reference frame, the previously identified injections occur in points close to the

apogee of the conic-like perturbed orbit on the incoming line to it. Note that, when the Earth-Moon line occurs near the apogee of the conic-like orbit, the Moon "pumps" up the apogee until it captures the orbit that breaks and become non-elliptic. Such a consideration let us understand that the transfer in Figure 108 corresponds in fact to the injection on the conic-like orbit in a time which corresponds to the phase between the apogee line and the Earth-Moon line directly leading to the capture by the moon, while the subsequent figures are related to injections that occur in antecedent revolutions on the same conic-like perturbed orbit. In particular, it is interesting to note that solution represented in Figure 97 corresponds to an injection on a favourable phase between the apogee line and the Earth-Moon line (where the Moon "pumps" up the apogee), but which constitute a missed Moon capture, thus confirming that the trajectory is in fact a *perturbed* conic-like orbit. The previous considerations recognize the reason of comparability of the many distinct identified local minima and the periodicity features of the objective function on the time spent on the stable manifold W_{L1}^{S}, which can be related to injections on the conic-like perturbed orbit in the Earth-centred inertial reference frame corresponding to different points of the orbit and different revolutions around the Earth. Moreover note that, although the local minima are in fact comparable (the mean value being 3111.697 *m/s* with a standard deviation of 29.129 *m/s*) high differences on the time spent to reach the libration point *L1* ($t_L + t_W$) obviously characterize them, as shown in Table 27, where features of the best member of each subgroup are reported. Each transfer family is then characterized by different features resulting from the different niches occupied by the design variables on the search space.

Subgroup #	ΔV [*m/s*]	$t_L + t_W$ [*d*]
Subgroup 1	3081.598	16.434
Subgroup 2	3082.544	27.501
Subgroup 3	3082.326	38.251
Subgroup 4	3096.143	49.002
Subgroup 5	3090.616	60.062
Subgroup 6	3098.311	87.135
Subgroup 7	3116.886	98.174
Subgroup 8	3080.767	108.943
Subgroup 9	3091.788	119.679
Subgroup 10	3088.030	130.782

Table 27: Subgroups characterization on ΔV and time spent to get *L1*.

Finally, Table 28 reports a summary of the previously performed objective function structure analysis.

Problem Dimension	Constraints	Search Space	Objective function	Periodicity
3	Box constraints	$D \in \Re^3$	$f \in \Re$ discontinuous on the boundaries of a finite set of regions over the search space; C^2 in the remaining points.	Yes, and related to the time spent on the stable manifold W_{L1}^S to *L1*.

Table 28: Summary of Problem Characteristics.

6. GLOBAL OPTIMISATION TOOLS

In this section, a brief introduction to the global optimisation tools that have been used in the present work is outlined. The main principles and features of each algorithm scheme is presented and corresponding references to dedicated literature are indicated for specific and more detailed information. Then, general considerations are finally highlighted regarding the choice of some algorithm parameters. Algorithms for global optimisation can be mainly classified in three classes (see Figure 118, where the tested global optimisation tools are presented in tree outline form):

- *Stochastic algorithms*, which involve at a suitably chosen random sample of points and subsequent manipulation of the sample to find good local minima.
- *Guaranteed algorithms*, which are deterministic algorithms which guarantee to find a global optimum with a required accuracy.
- Algorithms exploiting the construction of *metamodels*, which do not perform the global search on the real objective function, but on a metamodel of it.

Further, stochastic algorithms two main subclasses have been analysed:

- *Evolutionary Algorithms (EAs)*, which globally search the solution space by simulating the self-optimising natural process of evolution: the fittest individuals tend to reproduce and survive in the next generation, improving the fitness in successive generations; however, also individuals with a lower fitness level can survive and reproduce.
- *Simulated Annealing (SA)*, which performs the global search based on successive update steps, where the update step length is proportional to an arbitrarily set parameter which can play the role of a temperature. In analogy with the annealing of metals, the temperature is increased in the early stages of the process for faster optimisation, and then reduced for greater stability.

In particular, as stated by Yao [Yao, 1997], the general subclass of Evolutionary Algorithms (EAs) can be divided in three main branches:

- *Genetic Algorithms (GAs)*, where a wide exploration of the search space and the exploitation of promising area are ensured by means of the mutation, crossover and selection operators which are applied to the individuals in the population (for a careful description of such operators see [Michalewicz, 1994]).
- *Evolutionary Programming (EP)*, whose classical scheme makes use of the only mutation operator and, unlike GAs, they simulate the natural evolution at phenotypic level; moreover, as it concerns the selection process, it is based on a tournament selection carried out on a population including both parents and offspring.
- *Evolutionary Strategies (ESs)*, which, similarly to EP, simulate the natural evolution at a phenotypic level, but, unlike EP, make use of recombination operators.

The most important class of methods belonging to the class of guaranteed algorithms are in fact the branch and bounds methods, whose basic idea is that of splitting recursively the configuration space by branching into smaller and smaller parts; the way the branching procedure is performed depends on the bounding procedures, which aim at evaluating lower bounds of the objective function over the generated portions of the configuration space. However, glbSolve and MCS algorithms, which have been tested in this work, have been indicated by the authors as “branching without bounding” methods (see the dedicated references). Anyway, proofs of deterministic convergence to the global optimum with a desired accuracy exist; as a consequence, they have been included in the set of guaranteed algorithms. Finally, an important family of algorithms exploiting the construction of *metamodels* is that of response surface based optimisation algorithms, which use the objective function evaluations at a set of points for fitting response surfaces constituting fast surrogates of the objective function that can be used for optimisation purposes.

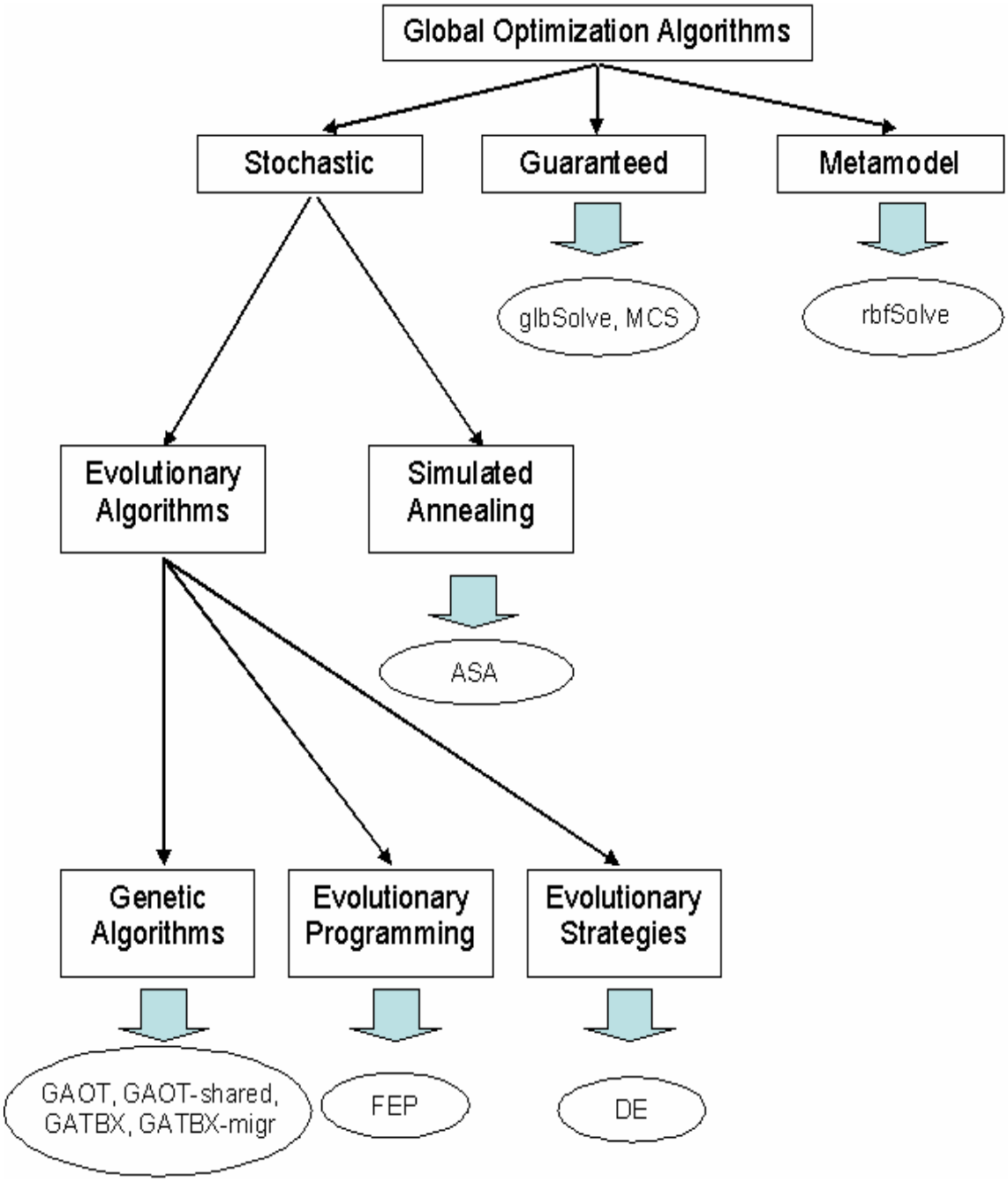

Figure 118: Tested global optimisation tools: a tree outline form.

The test phase, which will be presented in the following chapters, has been performed following the scheme reported in Figure 119.

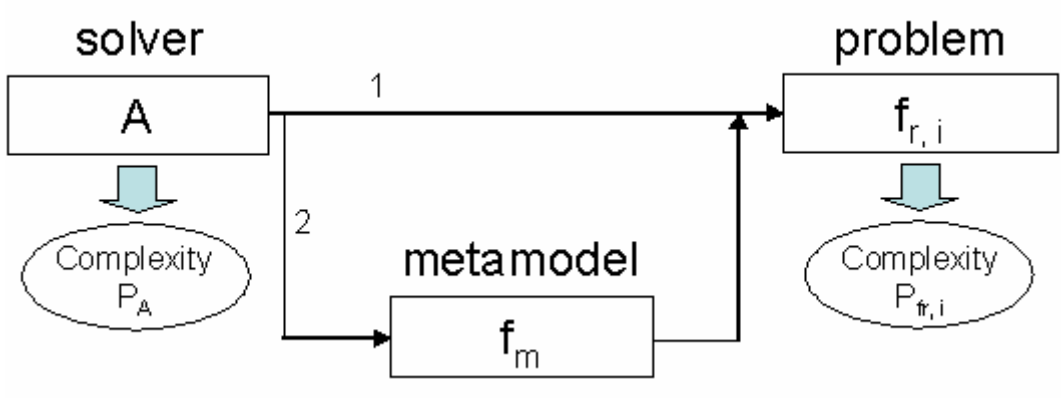

Figure 119: Test scheme.

A problem of computational complexity $P_{fr,i}$, which involves the optimisation of an objective function $f_{r,i}$, modelling the real problem is submitted to a solver A which has a complexity P_A. As stated above, the application of the solver A might shift (but not necessarily) the submission of the real objective function $f_{r,i}$ by facing a metamodel of it, f_m, which can reduce the computational complexity of the real objective function, $P_{fr,i}$ (direction 2 in Figure 119). By facing the test problems with this scheme, if a global solver A could solve an optimisation problem of complexity $P_{fr,i}$, we might state that (although no rigorous demonstrations exist) all global solvers with a computational complexity P_A should be able to solve the problem of optimising the objective function $f_{r,i}$. On the other hand, if the solver A which could solve the problem of minimizing $f_{r,i}$ turns out not to be able to solve the further problem of optimising an objective function $f_{r,j}$ (with $f_{r,j} \neq f_{r,i}$), we might state that (although no rigorous demonstrations exist) the corresponding computational complexity $P_{fr,j}$ must be higher than the complexity of the problem $f_{r,i}$ ($P_{fr,j} > P_{fr,i}$). Before starting the description of the tested tools, as it concerns the termination condition, note that, as stated by Huyer and Neumaier [Huyer and Neumaier, 1999], in practical global optimisation problems as those analysed in this work, one does not know the solution in advance and needs a criterion that tells the program when to stop searching for a better local optimum. This criterion should accomplish a trade-off between avoiding wasting too many objective function evaluations after the global minimum has been found and ensuring that the algorithm does not terminate before the global optimum has been found. Some of the global

optimisation tools which have been tested in this work have been already supplied by a suitable termination condition; for those algorithms where such a criterion was not included, a common stopping rule has been implemented, as described in the following, which, after an exhaustive practice phase, seemed to be suitable and robust.

6.1 Genetic Algorithm for Optimisation Toolbox (GAOT)

Genetic Algorithm for Optimisation Toolbox (GAOT) implements a global search based on a genetic algorithm scheme. The fundamentals issues which must be identified before using a genetic algorithm can be resumed as follows: the identification of the chromosome representation, the management of the selection function, the choice of the genetic operators for the reproduction, the termination criteria and the evaluation function. A complete description of the features and the options offered by GAOT to the user is available at reference [Houck et al., 1995]. The code is freely available at: http://www.ie.ncsu.edu/mirage/GAToolBox/gaot/. As it concerns the pre-set configurations in all tests performed in this work, default options have been maintained: in particular, the real coded version of the genetic algorithm has been used. Moreover, note that GAOT can handle upper-lower bounds constraints by itself. One modification was necessary for implementing a new termination condition. The set offered by GAOT in the standard version includes in fact two termination rules: one based on a fixed number of generations and the other based on the achievement of either a predefined optimal objective function value or a maximum number of generations. The previous rules are not suitable for applications where no a priori information are available on the global optimum, as in the cases here analysed. As a consequence a new termination condition has been implemented which stops the evolutionary process when the absolute improvement of the best objective function value corresponding to the best solution, $\Delta objFun$, over a number of successive generations equal to $5 \cdot n$, where *n* is the number of design variables, is less than 10^{-3}:

Stop when: $\Delta objFun_{[5n]} < 10^{-3}$

6.2 GAOToolbox with sharing operator (GAOT-shared)

In order to assess the theoretical advantages offered by the use of niching methods in evolutionary global searches, GAOT scheme presented in Section 6.1 has been modified by the authors for including such techniques. Traditional genetic algorithms with elitist selection usually converge to a single global optimum on the search space. As stated by Sareni and Krähenbühl [Sareni and Krähenbuhl, 1998], real optimisation problems often lead to multimodal domain, where the identification of multiple optima, either global or local, is required. Niching methods are then used to promote the formation of stable subpopulations in the neighbourhood of optimal solutions. In particular, sharing methods have been considered, which are in fact the most used among the available niching techniques. The operation of fitness sharing modify the search landscape by typically modifying the fitness f_i of an individual *i* as follows:

$$f'_i = \frac{f_i}{m_i} \qquad [34]$$

where m_i is the niche count which measure the approximate number of individuals with whom the fitness f_i is shared and f'_i is the shared fitness. The niche count is calculated by summing a sharing function over all members of the population:

$$m_i = \sum_{j=1}^{N} sh\left(d_{ij}\right) \qquad [35]$$

where *N* is the number of individuals in the population and d_{ij} is the distance between individuals *i* and *j*. The sharing function *sh* measures the similarity level between two population elements and it usually has two main feature: its value is one if the two solutions are identical and zero in case their distance is

higher than a threshold of dissimilarity. The most widely used sharing function, which has been used in the present work, is defined as follows:

$$sh(d_{ij}) = \begin{cases} 1-(d_{ij}/\sigma_S)^{\alpha}, & if\ d < \sigma_S \\ 0, & otherwise \end{cases} \quad [36]$$

where σ_S is the threshold of dissimilarity (distance cut-off of the niche radius) and α is a constant parameter which regulates the shape of the sharing function. The value of α is commonly set to one, resulting in the so-called triangular sharing function. Moreover, a phenotype similarity for defining the distance between two individuals has been considered by evaluating d_{ij} as the Euclidean distance measured on the search space. Set values for α and σ_S parameters will be indicated corresponding to the performed tests.

6.3 Genetic Algorithm Toolbox (GATBX)

Genetic Algorithm Toolbox (GATBX) implements again a global search based on a genetic algorithm scheme. The main features are then similar to those presented in case of GAOT tool, especially concerning the fundamentals issues which must be identified before using it. However, some differences can be identified: they mainly concern with the way selection, mutation and crossover operations are performed. A detailed description of the features and the options offered by GATBX to the user is included in references [Chipperfield, Fleming, and Fonseca, 1994] and [Chipperfield, and Fleming, 1995]. The whole source code is freely available at: http://www.shef.ac.uk/cgi-bin/cgiwrap/~gaipp/gatbx-download. The GATBX configuration used in all tests performed in this work makes use of default options: in particular, the real coded version of the genetic algorithm has been considered and discrete recombination operator has been used instead of crossover. GATBX can handle upper-lower bounds constraints by itself. Due to the absence of termination conditions suitable for tests performed, the termination condition described in case of GAOT tool has been implemented again, which can be resumed by the following rule:

Stop when: $\Delta objFun_{[5n]} < 10^{-3}$

6.4 Genetic Algorithm Toolbox with migration operator (GATBX-migr)

Options offered by the previously described GATBX tool have been exploited in order to assess the variation of performances in solving the global optimisation problem which are associated to the use of the migration operator. In such case the whole population is gathered into subpopulations, which independently evolve searching for the global optimum solution. The number of subpopulations can be defined by the user: its value has been suitably set in each performed test. Information can be exchanged between the various subpopulation during the optimisation process at predefined intervals of generations with a fixed migration rate: the default values of such parameters have been considered. GATBX can handle upper-lower bounds constraints by itself. As stated above, GATBX algorithm has been supplied by a suitable termination condition, which can be resumed as follows:

Stop when: $\Delta objFun_{[5n]} < 10^{-3}$

6.5 Fast Evolutionary Programming (FEP)

The mutation operator associated to classical Evolutionary Programming is based on the generation of random numbers with a normal distribution. However, Yao, Liu and Lin [Yao, Liu, and Lin, 1999] showed that the classical Evolutionary Programming suffers from low convergence rate in some single-objective multimodal optimization problems and proposed the use of a mutation operator based on Cauchy random numbers to solve this problem, developing the Fast Evolutionary Programming (FEP). FEP scheme has been implemented by the authors for solving generally constrained multiobjective optimization of space mission design [Di Lizia, Lavagna and Finzi, 2004]. By considering that, as stated by Zitzler [Zitzler, 2002], single-objective optimisation problems can be seen as particular cases of multiobjective optimisation problems (and not

vice versa), the algorithm has been easily modified for performing the single objective optimisation test presented in this work. However, note that the implemented code is not optimised and runtime performances could be quite improved in the future. In particular, the implemented FEP tool can deal with generally constrained optimisation problems thanks to the use of an efficient constraint handling methodology proposed by Deb [Deb, 2000], which makes use of suitable comparison criteria for opportunely defining the fitness function. It is worth noting that, thanks to the use of a tournament selection approach, Fast Evolutionary Programming code can be easily parallellized. As it concerns the termination condition implemented in the tests performed in this work, FEP algorithm has been supplied by the termination condition previously described:

Stop when: $\Delta objFun_{[5n]} < 10^{-3}$

6.6 Differential Evolution (DE)

Differential Evolution (DE) is a heuristic approach for solving the minimization problem of possibly nonlinear and non differentiable continuous space functions [Storn and Price, 1995]. It can be included in the set of Evolutionary Strategies based algorithms described above. The main idea driving DE search is a peculiar scheme for generating vectors of design variables: in particular, new vectors are generated by adding the weighted difference vector between two population members to a third member. The resulting scheme turns out to be easily parallelizable. A complete description of DE features is available at reference [Storn and Price, 1995]. As it concerns the code used in this work, the version “devec3” has been investigated, which is freely available at: http://www.icsi.berkeley.edu/~storn/code.html. Default DE options for the evolutionary parameters have been kept. It is worth noting that the codes available at the previous web page can’t handle upper-lower bounds constraints by itself. As a consequence, the code has been modified by introducing a constraint handling methodology proposed by Deb [Deb, 2000]. Moreover, due again to the lack of a suitable termination condition for the investigated optimisation problems, the termination condition described in case of GAOT tool

has been implemented in DE code, thus stopping the evolutionary process by analysing the improvement of the objective function value over a certain interval of generations:

Stop when: $\Delta objFun_{[5n]} < 10^{-3}$

6.7 Adaptive Simulated Annealing (ASA)

Adaptive Simulated Annealing (ASA) is a global optimisation tool based on Simulated Annealing (SA), which has been proven to outperform the simple SA scheme [Ingber, 2000]. The origin of the standard Simulated Anealing is dated back to the inclusion of a temperature schedule for efficient searching carried out by Kirkpatrick [Kirkpatrick ,1983] on the Monte Carlo integration algorithm by Metropolis [Metropolis, 1953]. However, classical implementation of the SA scheme does not consider that, in case of a *D*-dimensional search space, different design variables can have different finite ranges and different sensitivities; Adaptive Simulated Annealing takes advantage of such considerations for improving the performances of the simple SA scheme. It is worth noting that the direct parallelization of an SA algorithm has been shown to be quite difficult [Ingberg, 1993]. A complete description of the features and the options offered by ASA to the user is available at reference [Ingber, 2000]. The code is freely available at: http://www.ingber.com/#ASA-CODE. Default options have been retained in all tests performed in this work: in particular, note that limits of generated and accepted solutions have been opportunely imposed for each problem. ASA can handle upper-lower bounds constraints by itself and has a default termination condition which is useful for problems whose global optimum solutions are not known a priori.

6.8 Global Solver (glbSolve) and Multilevel Coordinate Search (MCS)

The global solver (glbSolve) and the Multilevel Coordinate Search (MCS) are algorithms based on a combination of purely heuristic methods and methods that guarantee to find a global optimum with a required accuracy. They are both

inspired by the DIRECT method for global optimisation by Jones et al. [Jones et al., 1993], of which glbSolve constitutes a more classical implementation. Moreover, as stated by Huyer and Neumaier [Huyer, and Neumaier, 1999], both methods are guaranteed to converge if the objective function is continuous in the neighbourhood of a global minimiser, without any additional smoothness properties. As it concerns the differences between MCS algorithm and the DIRECT one (which can be also related to differences between MCS and glbSolve), it is worth noting that DIRECT method partitions a normalized search space into smaller boxes, which are characterized by their midpoint. The main disadvantages of DIRECT are related to two aspects: it cannot handle infinite box bounds and it converges unnecessarily slowly if the global minimum lies on the boundary of the box, because its structure makes it unable to reach such regions.

The above described drawbacks are solved by Multilevel Coordinate Search algorithm by allowing a more irregular splitting procedure. Moreover, unlike many stochastic methods, MCS allows operating and searching at a local level also, leading to accurate quick convergence once the global part of the algorithm has found a point in the basin of attraction of a global minimizer. Complete descriptions of the features and the options offered by glbSolve and MCS to the user are available at reference [Jones et al., 1993] and [Huyer, and Meumaier, 1999] respectively. The commercial version of glbSolve code is available at: http://www.tomlab.biz/. The MCS tool is freely available at: http://www.mat.univie.ac.at/~neum/software/mcs/. Default options have been held in all tests performed in this work. However, as it concerns the termination condition, the criterion already described in GAOT case and adopted in some of the previous tools has been implemented in case of glbSolve due to the lack of presence of good stopping criteria:

Stop when: $\Delta objFun_{[5n]} < 10^{-3}$

Default termination condition has been used in case of MCS algorithm instead, which stops the optimisation process when no improvement of the objective

function value is gained after *m* consecutive sweeps, where *m* is set to be equal to 5·*n*, with *n* indicating again the number of design variables.

6.9 Radial Basis Function Solver (rbfSolve)

Radial basis function solver (rbfSolve) is a global optimisation tool based on the generation of response surfaces using radial basis functions. As stated by Jones [Jones, 2001], the main advantage of such an approach is related to the fact that, by running simulations or objective function evaluations at a set of points and fitting response surfaces based on this data, fast surrogates of the objective function are generated which can be used for optimisation purposes. However, due to the high computational time required to fit the generated data, response surface based global optimisation algorithms seem to be suitable for costly global optimisation problems, where runtime for evaluating the objective function is too high for allowing a pure stochastic search, thus promoting the use of smart techniques for exploiting information gained by previous evaluations, trying to reduce the required number of objective function evaluations. Moreover, it is worth noting that the runs used to fit the surfaces can be done in parallel, so allowing saving further time. The available approaches that use response surfaces to solve global optimisation problems can be classified by distinguishing the type of response surface and the method used to select search points. Response surfaces can be differentiated in non-interpolating and interpolating, although the interpolating ones, which are based on interpolation of data via linear combination of “basis functions”, have shown to be the most reliable. As it concerns the implemented method, rbfSolve belongs to the class of the so-called two stage methods. Such methods involve a first stage, where a response surface is fitted, and a second stage, where the generated surface is exploited to compute new promising search points. Such a scheme might present drawbacks related to the initial sampling procedure, which can leads to misleading shape of the function to be optimised. A description of the main principles used by rbfSolve tool is available at reference [Jones, 2001]. A commercial version of the tool is available at: http://www.tomlab.biz/. The rbfSolve configuration used in all tests performed in

this work makes use of default options. However, it is worth noting that no suitable termination conditions have been found on the tested code. Moreover, because rbfSolve is not a freely available code, no modifications have been performed on it. As a consequence, this forced us to stop the optimisation process when a maximum number of objective function evaluations was reached. The maximum value of such parameters has been set in each case by looking at the performances of the other optimization tools.

6.10 Evolutionary Predictive Interval Computation (EPIC)

EPIC, is based on a hybrid deterministic-stochastic approach to the solution and characterisation of constrained and unconstrained multimodal, multivariate nonlinear programming problems with mixed integer-real variables and discontinuous quantities. The EB approach is based on the following principal ideas:

- An evolutionary strategy is used to explore globally and locally the solution space *D*. Then a branching scheme, dependent on the findings of the evolutionary step, is used to partition the solution domain in subdomains. On each subdomain a new evolutionary search is performed. The process continues until a number of good minima and eventually the global one are found.
- The search is performed by a number of agents (explorers): each solution y is associated to an agent. and is represented by a string, of length *n*, containing in the first *m* components integer values and in the remaining *s* components real values. This particular encoding allows the treatment of problems with a mixed integer-real data structure. A hypercube S enclosing a region of the solution space surrounding each agent, is then associated to y. The solution space is then explored locally by acquiring information about the landscape within each region S and globally by a portion of the population, which is continuously regenerated forming a pool of potential explorers.
- Each agent can communicate its findings to the others in order to evolve the entire population towards a better status.

- During the evolutionary step a discoveries-resources balance is maintained: a level of resources is associated to each agent and is reduced or increased depending of the number of good findings of the agent.
- If many agents are intersecting their S regions and their reciprocal distance falls down below a given threshold, a repelling mechanism is activated.

This novel and very promising global optimisation algorithm is currently being developed by Dr Massimiliano Vasile of the Dipartimento di Ingegneria Aerospaziale at Politecnico di Milano, who has kindly agreed to allows us to test the performances within our dynamical models.

6.11 General Considerations

As stated in the previous sections, default values of algorithm parameters have been used. Note that, as widely known, the performance of a specific solver can be even significantly improved by opportunely tuning proper parameters. However, as already done in many comparative studies for global optimisation tools, due to the comparative purposes of this work, the tuning effects have not been investigated here. However, some algorithm parameters had to be changed based on the complexity of the faced problem: examples of such parameters are the number of individuals and the maximum number of generations for evolutionary based optimisation tools, the maximum number of solutions generated in case of ASA and MCS and the maximum number of iterations in case of glbSolve. Such parameters have been mainly set based on information that has been found in the dedicated literature, on the experience gained by the authors during previous works on this subject and, of course, on a tuning process performed after a suitable practice period. The final configuration adopted in the test phase corresponding to each problem seems to authors to constitute an effective choice. As a final remark, it is worth noting that all the tested tools work in a Matlab environment, except the Adaptive Simulated

Annealing tool, for which a MEX Matlab file has been generated for use it in the same environment.

7. 2-IMPULSE DIRECT PLANET-TO-PLANET TRANSFER

Problem class statement:

Objective function assessment	
Objective function:	$\Delta V = \Delta V_I + \Delta V_F$ where: • ΔV_I is the magnitude of the relative velocity at the beginning of the nterplanetary transfer phase. • ΔV_F is the magnitude of the relative velocity at the end of the interplanetary transfer phase.
Mathematical models:	• Restricted 2-body dynamical model (C^2 in the whole solution space except in the origin) • Three dimensional motion • Analytical ephemeris model (generated by time polynomial series of the orbital elements) • Impulsive manoeuvres (i.e. instantaneous variations in velocity) • Lambert's problem formulation (Battin's algorithm for the problem solution)

Search space characterization	
Number of design variables:	2
Design Variables:	• Date of departure from Earth, t_0 • Transfer time from Earth to Mars, tt
Topology:	Continuous variables

Constraints	
Constraints typology:	Box constraints
Box intervals:	• $\left[t_0^{LB}, t_0^{UB}\right] = \left[01/01/2003, 31/12/2017\right]$ • $tt \in \left[100, 300\right]$ *d*

General considerations	
Objective function analysis:	The objective function is almost everywhere C^2, locally discontinuous in a countable number limited set
Problem complexity:	Low

Number of global optima: A priori unknown

A systematic analysis of the objective function over the search space, followed by local optimization processes starting from 100 random first guess solutions uniformly distributed over the search space (each local search requiring a number of objective function evaluations of the order of 10^2) led to the following

best known solution, that seems to be the global one over the considered search space (although no rigorous mathematical demonstration has been provided).

Search space	
Date of departure:	06/06/2003
Transfer time:	203.541 *d*
Objective space	
ΔV :	5678.904 *m/s*
ΔV_I :	2999.464 *m/s*
ΔV_F :	2679.439 *m/s*

Number of local optima: A priori unknown.

A systematic analysis of the objective function over the search space, together with a local optimization process led to 17 solutions (see Figure 120, where the 17 local minima are represented by the black dots; the red dot indicates instead the best known solution), which seem to represent the complete set of local optima over the considered search space (although no rigorous mathematical demonstration has been provided).

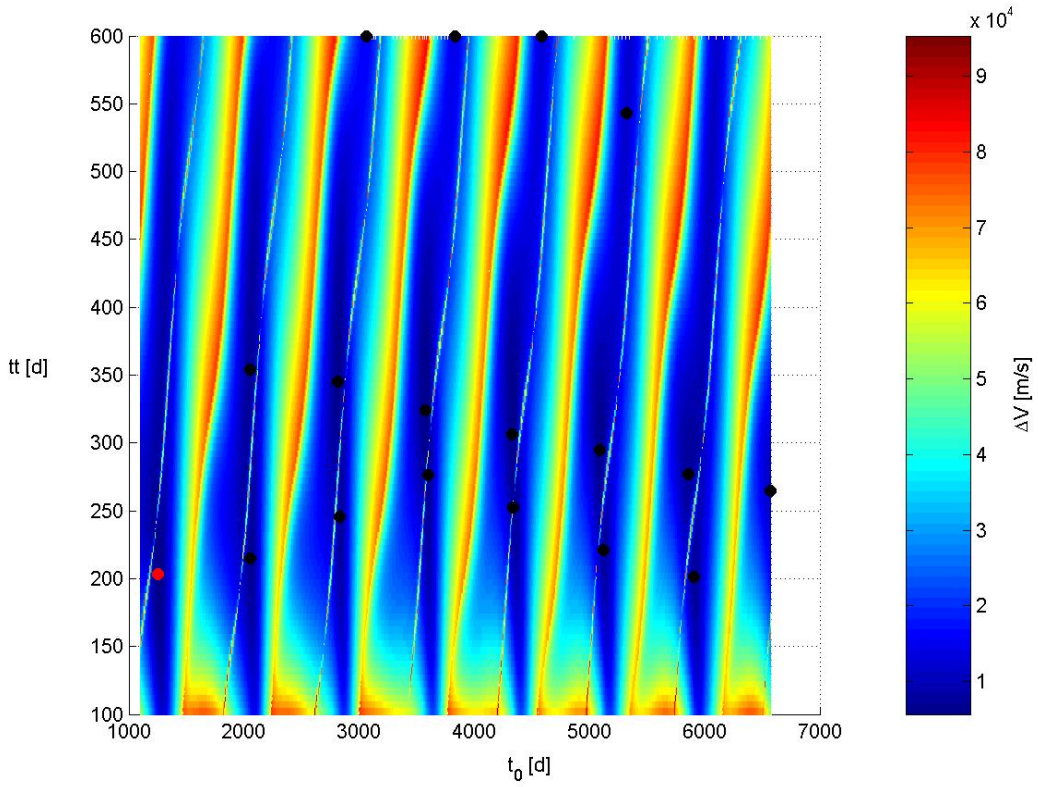

Figure 120:Distribution of the local minima.

Hardware platform:

Intel Pentium 4 – 3.06GHz laptop.

Operating system:

Microsoft Windows XP

Home edition

Version 2002

Service Pack 1

Timings:

The Standard Unit Time (see Dixon & Szegö, 1978) has been measured.

Performances:

In the following pages, the performances of each global optimization tool in solving the 2-impulse direct planet-to-planet transfer are reported. The evaluation criteria will be mainly based on the analysis of the optimal solution reached and the number of the required model function evaluations. Due to the presence of not optimized codes among the tested ones, timing will not be considered as a main evaluation criterion.

GAOT

As GAOT implements a genetic algorithm, we report the statistical characteristic, typically considered in case of randomized solution methods. Ten run have been processed in order to solve the previously defined problem. Default options suggested by the providers of the code have been used in all the runs: note that by tuning the algorithm parameters one may improve the performance of the solvers, but, due to the comparative purposes of this work, the tuning effects have not been considered. As the 2-impulse direct planet-to-planet transfer has low complexity features, we used 50 individuals evolving for a maximum number of generations equal to 100.

Algorithm parameters	
Number of individuals:	50
Maximum number of generations:	100

Tables 29-30 report the best identified solution compared with the best known solution (note that the best solution is here measured by considering the minimum objective function value reached and is different from the Pareto optimal solution described below).

Search space		
Design variable	**Best identified solution**	**Best known solution**
Date of departure [*d*]:	1253.508	1253.510
Transfer time [*d*]:	203.542	203.541

Table 29: Comparison between the best identified solution and the best known solution: search space.

Objective function space		
Term	**Best identified solution**	**Best known solution**
ΔV [*m/s*]:	5678.904	5678.904
ΔV_I [*m/s*]:	2999.463	2999.464
ΔV_F [*m/s*]:	2679.441	2679.439

Table 30: Comparison between the best identified solution and the best known solution: objective function space.

The previous tables show that the best identified solution coincides in fact with the best known one. Let us now consider the statistical characteristics of the identified solution set. Table 31 reports the mean value and the standard deviation of the performances which will be used for comparisons with the other optimization algorithms.

Evaluation criterion	**Mean value**	**Standard deviation**
ΔV [*m/s*]:	5741.524	163.525
Model function evaluations:	1270.5	345.683
Runtime [STU]:	$8.198 \cdot 10^{-3}$	$3.306 \cdot 10^{-3}$

Table 31: Statistical characteristics of the identified solutions.

Tabe 31 shows that the mean value of the optimal objective function values reached at the end of each optimization process is quite different from the best identified one and is characterized by a high standard deviation. Such a result let us suppose that no all the performed optimization processes have been able to identify the basin of attraction of the best known solution. Figure 121 reports the final solutions corresponding to each optimization run in the *nFunc-ΔV* plane (where *nFunc* is the number of objective function evaluations), while Figure 122 illustrates their distribution over the search space.

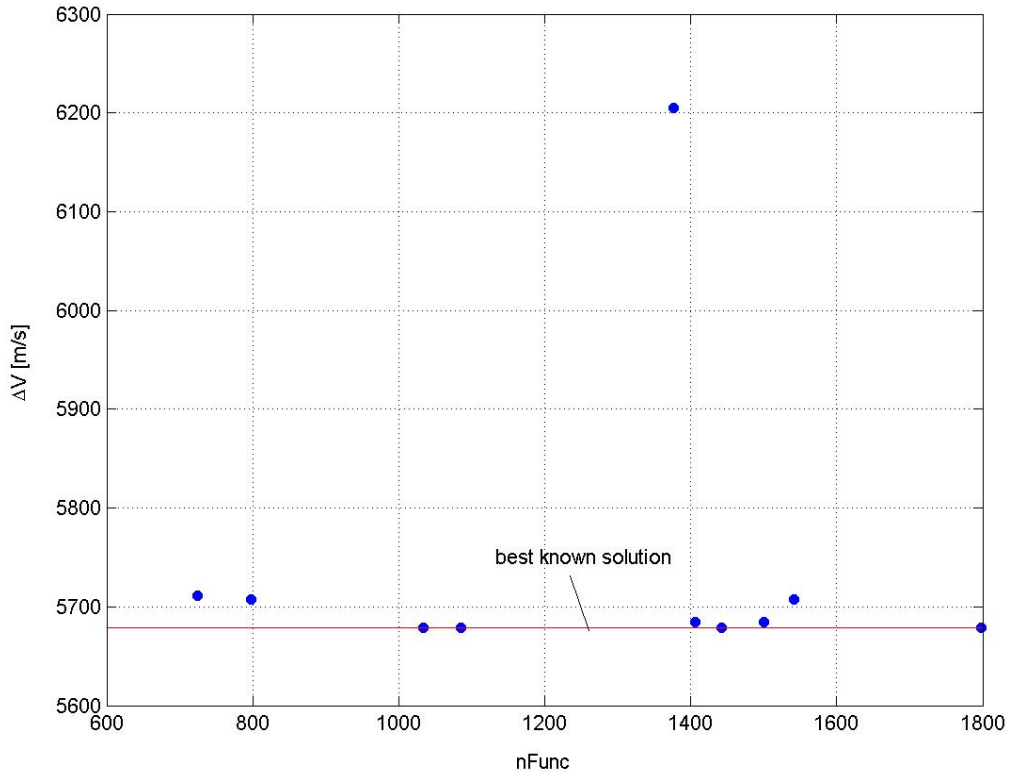

Figure 121: Distribution of the final solutions corresponding to each optimization run on the *nFunc-ΔV* plane.

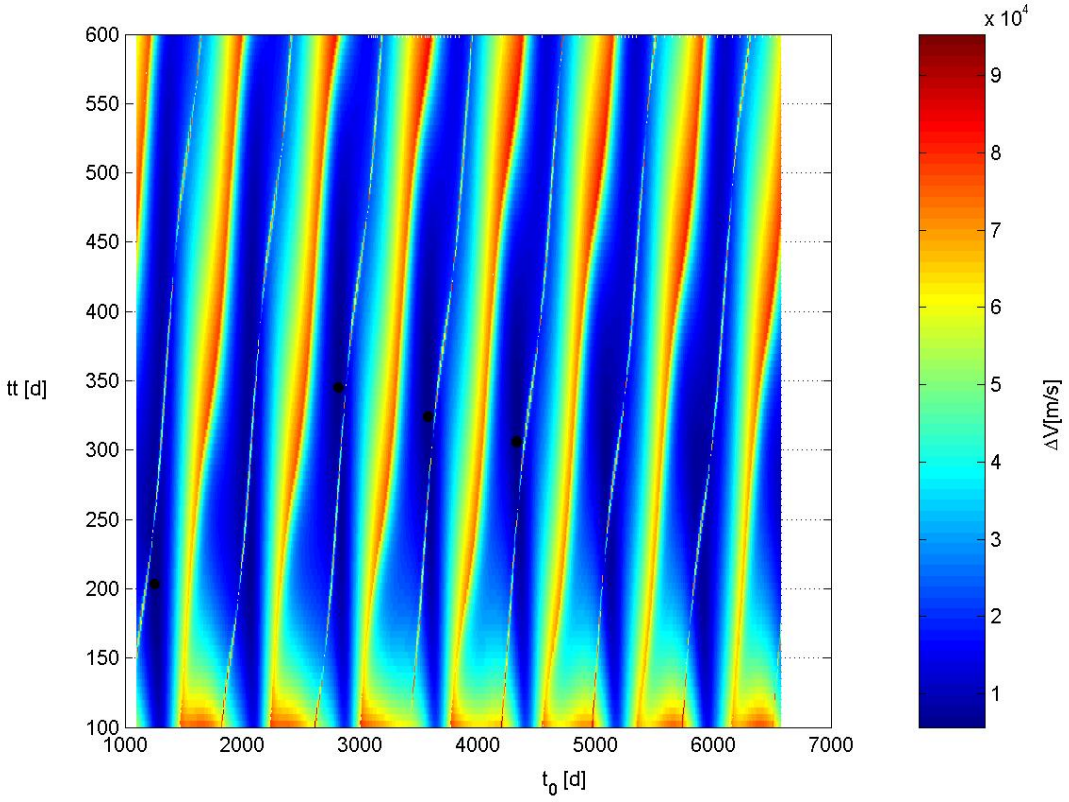

Figure 122 - Distribution of the final solutions corresponding to each optimization run on the search space.

Figure 121 and Figure 122 fairly illustrates that the presence of comparable local minima over the analysed search space hindered the effectiveness of GAOT algorithm at reaching the basin of attraction of the best known solution. In particular, by investigating the normalized search space, Table 32 reports the Euclidean distance of each final solution form the best known one.

Run	Euclidean distance
run 1	$6.334 \cdot 10^{-5}$
run 2	0.487
run 3	$1.083 \cdot 10^{-5}$
run 4	0.598
run 5	0.402

run 6	0.598
run 7	0.598
run 8	$1.425 \cdot 10^{-5}$
run 9	$2.719 \cdot 10^{-6}$
run 10	0.487

Table 32: Euclidean distance of each final solution form the best known one in the normalized search space.

By considering two solutions as identical when their Euclidean distance is less then 5% of the hyper-diagonal of the normalized search space (that is 0.071 in this case), only 4/10 GAOT runs were able to get the best known solution. Further interesting observations can be pointed out by analysing the main features of the final population: Figure 123 shows the distribution of the population over the search space at the end of the optimization process corresponding to the best identified solution.

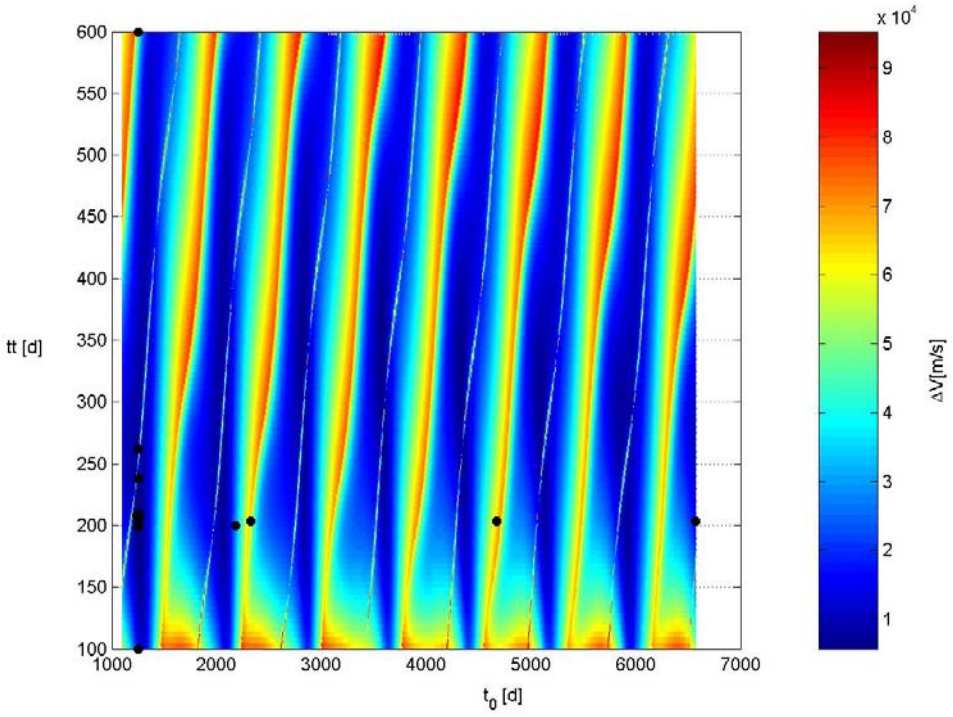

Figure 123: Distribution of the population over the search space at the end of the optimization process corresponding to the best identified solution.

The previous figures show that the individuals in the final population mainly concentrated in a narrow neighbourhood of the global optimum. This results held in all runs on average, including the cases where a non global optimum has been identified. As an example, Figure 124 shows the distribution of the final population corresponding to the worst identified solution: the final population of a typical GAOT run mainly concentrates in a neighbourhood of the identified minimum.

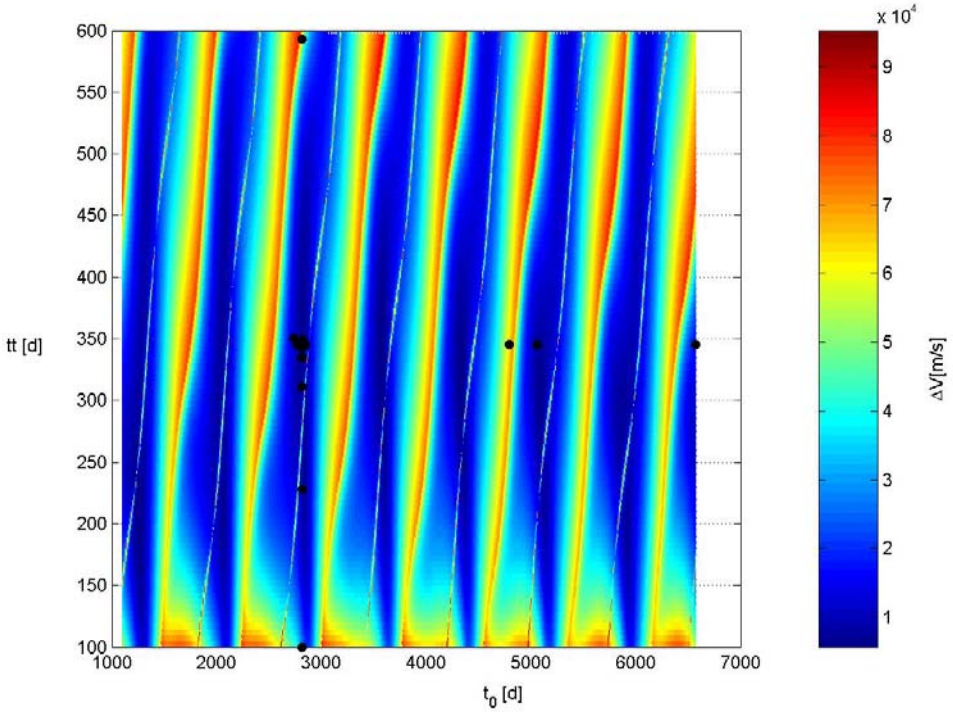

Figure 124: Distribution of the population over the search space at the end of the optimization process corresponding to the worst identified solution.

Figure 125 shows the trace of the best solution during the optimization run corresponding to the best identified solution: GAOT search process typically investigates the basin of attraction of different local minima before converging to the final solution.

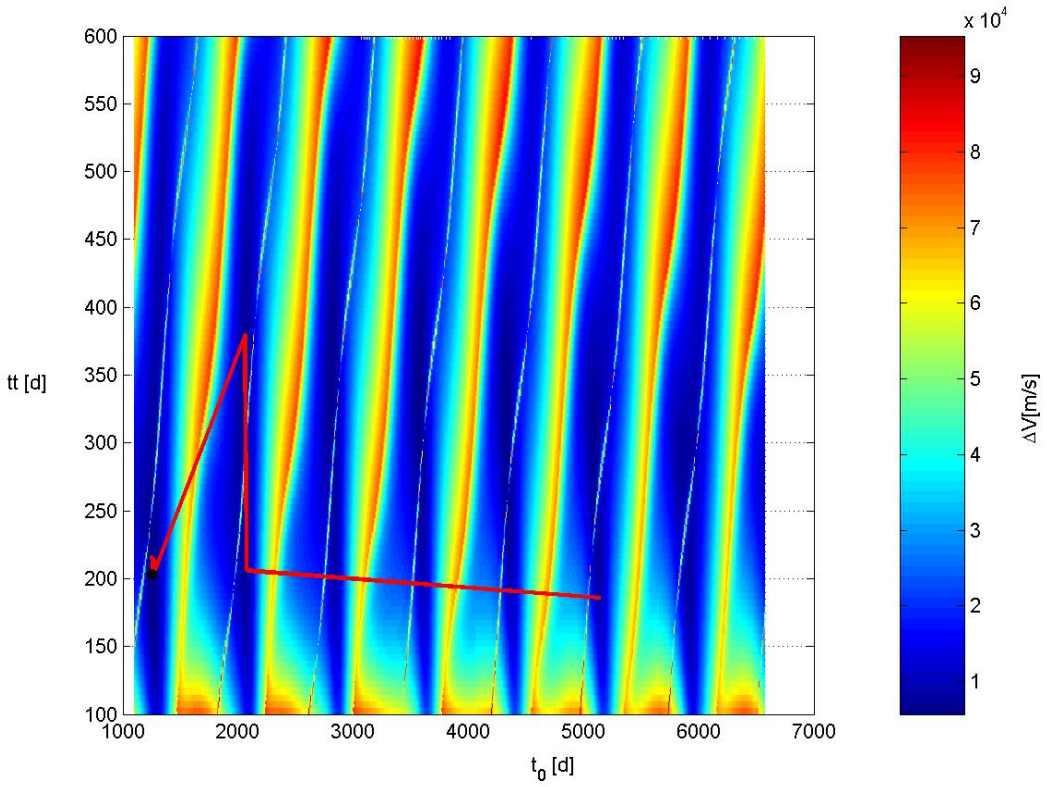

Figure 125: Trace of the best solution during the optimization run corresponding to the best identified solution.

GAOT-shared

As GAOT-shared implements a genetic algorithm including a niching technique, we report again the statistical characteristics. Ten run have been processed in order to solve the previously defined problem. Default options suggested by the providers of the code have been used in all the runs. The threshold of dissimilarity, σ_S, for the sharing method and the shape parameter of the sharing function, α, have been set respectively to:

$$\sigma_S = 0.1$$

$$\alpha = 1$$

We used again a population of 50 individuals, evolving for a maximum number of generations equal to 100.

Algorithm parameters	
Number of individuals:	50
Maximum number of generations:	100

Tables 34-35 report the best identified solution compared with the best known solution.

Search space		
Design variable	**Best identified solution**	**Best known solution**
Date of departure [*d*]:	1251.761	1253.510
Transfer time [*d*]:	212.302	203.541

Table 34: Comparison between the best identified solution and the best known solution: search space.

Objective function space		
Term	**Best identified solution**	**Best known solution**
ΔV [*m/s*]:	5720.530	5678.904
ΔV_I [*m/s*]:	3017.740	2999.464
ΔV_F [*m/s*]:	2702.790	2679.439

Table 35: Comparison between the best identified solution and the best known solution: objective function space.

The previous tables show that the best identified solution seems to lie into the basin of attraction of the best known solution, as Figure 126 fairly illustrates.

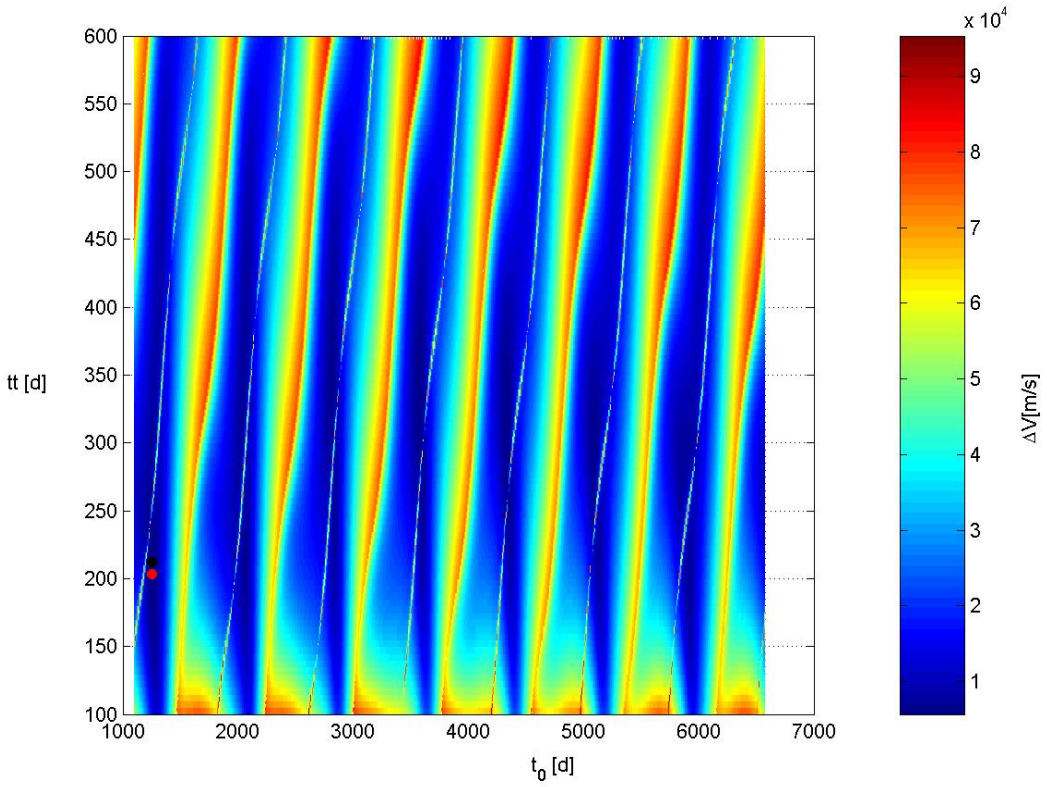

Figure 126*: GAOT-shared* best identified solution (black point) compared with the best known solution (red point).

However, as shown in Figure 126, the niching technique avoids a concentration of the individuals near the global optimum as evident as in the case of the simple GAOT algorith: as we will state later, this can decrease the accuracy in finding the global optimum solution. Let now consider the statistical characteristics of the identified solution set. Table 36 reports the mean value and the standard deviation of the performances which will be used for comparisons with the other optimization algorithms.

Evaluation criterion	Mean value	Standard deviation
ΔV [*m/s*]:	6420.207	574.220
Model function evaluations:	590.4	320.350
Runtime [STU]:	$4.907 \cdot 10^{-3}$	$2.776 \cdot 10^{-3}$

Table 36: Statistical characteristics of the identified solutions.

As already noted in case of GAOT algorithm, the mean value of the optimal objective function values and the high standard deviation reported in Table 36 let us suppose that no all the performed optimization processes have been able to identify the basin of attraction of the best known solution. Figure 127 reports the final solutions corresponding to each optimization run in the *nFunc-ΔV* plane, while Figure 128 illustrates their distribution over the search space.

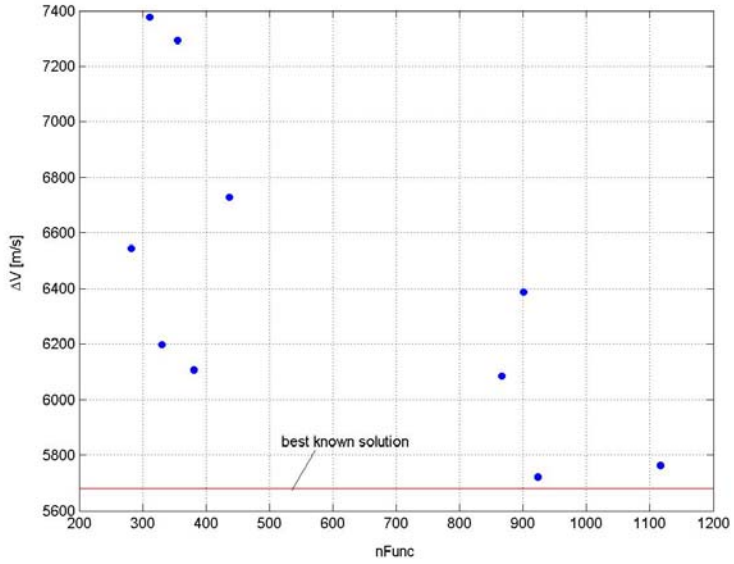

Figure 127: Distribution of the final solutions corresponding to each optimization run on the *nFunc-ΔV* plane.

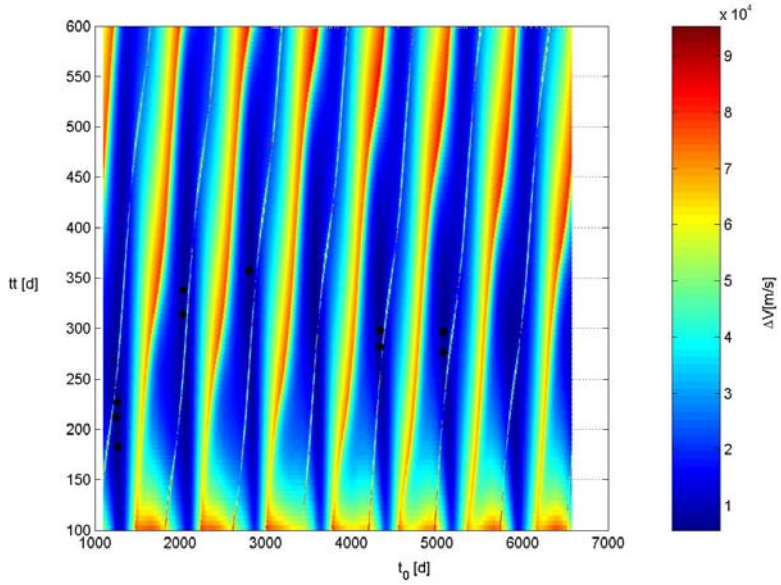

Figure 128: Distribution of the final solutions corresponding to each optimization run on the search space.

Figure 128 fairly illustrates that some GAOT-shared algorithm runs failed at reaching the basin of attraction of the best known solution. In particular, by investigating the normalized search space, Table 37 reports the Euclidean distance of each final solution form the best known one.

run	Euclidean distance
run 1	$4.756 \cdot 10^{-2}$
run 2	$5.936 \cdot 10^{-1}$
run 3	$4.101 \cdot 10^{-2}$
run 4	$7.216 \cdot 10^{-1}$
run 5	$1.752 \cdot 10^{-2}$
run 6	$2.626 \cdot 10^{-1}$
run 7	$4.188 \cdot 10^{-1}$
run 8	$5.844 \cdot 10^{-1}$
run 9	$3.043 \cdot 10^{-1}$
run 10	$7.128 \cdot 10^{-1}$

Table 37: Euclidean distance of each final solution form the best known one in the normalized search space.

By analysing Figure 128 and by considering two solutions as identical when their Euclidean distance is less then 5% of the hyper-diagonal of the normalized search space (that is 0.071 in this case), only 3/10 GAOT-shared runs were able to get the best known solution. Let us now analyse the main features of the final population: Figure 129 shows the distribution of the population over the search space at the end of the optimization process corresponding to the best identified solution.

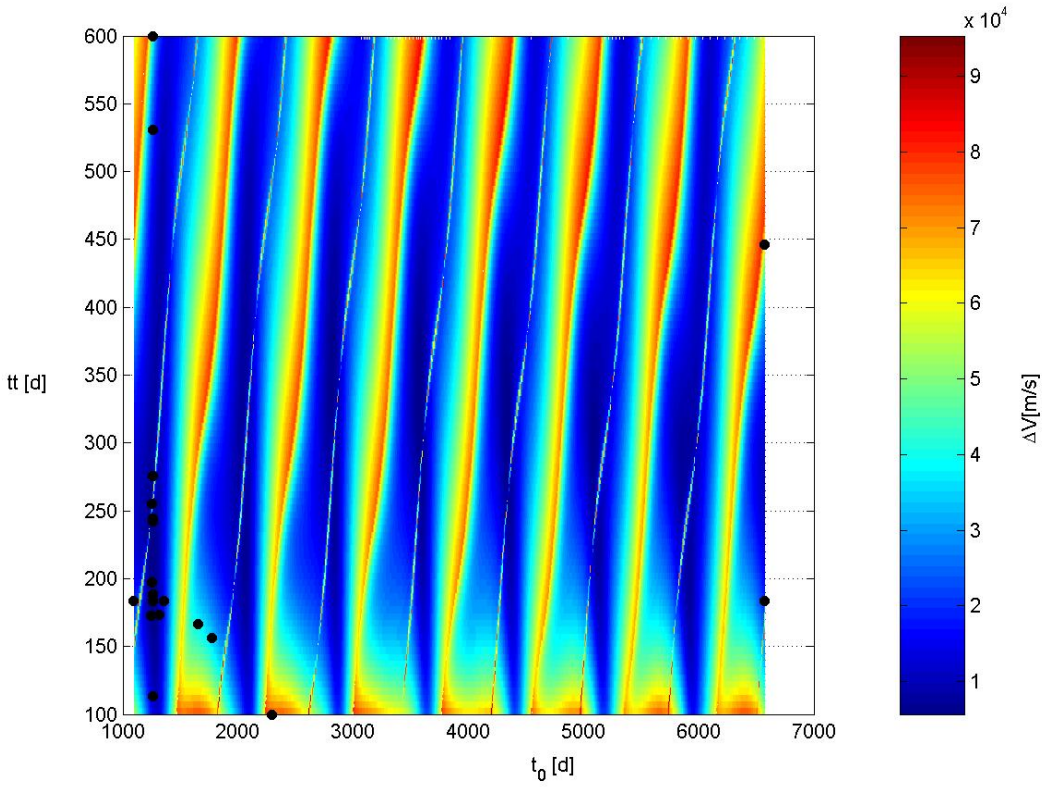

Figure 129: Distribution of the population over the search space at the end of the optimization process corresponding to the best identified solution.

Figure 129 fairly illustrates again the effects of the sharing operator on the distribution of the final population: the niching technique avoids a concentration of the individuals near the global optimum as evident as in the case of the simple GAOT algorithm (see Figu123), as will be clearly illustrated later. This results held in all runs on average, including the cases where a non global optimum has been identified. Figure 130 shows the trace of the best solution during the optimization run corresponding to the best identified solution: GAOT-shared search process immediately gained the basin of attraction of the best known solution.

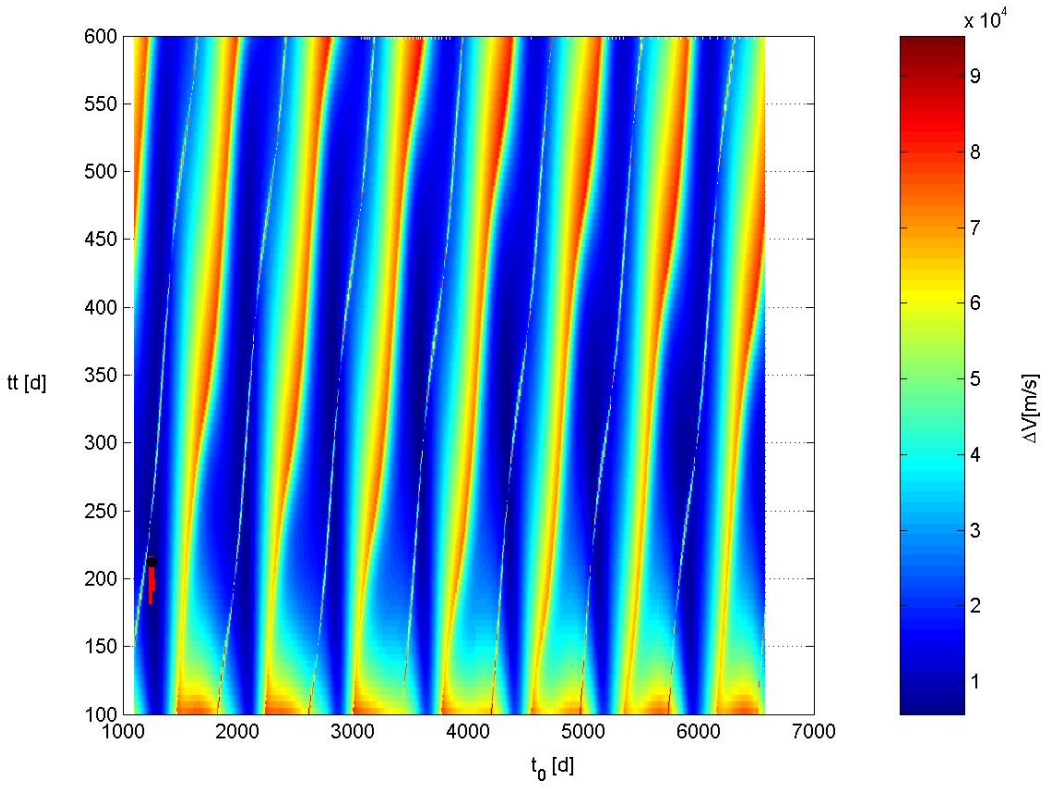

Figure 130: Trace of the best solution during the optimization run corresponding to the best identified solution.

It is interesting to analyse the effects of the sharing operator on the GAOT performances: in fact, by promoting the diversity of the individuals in the population, the GAOT – shared algorithm doesn't allow the concentration of the individuals around every point in the solution space and then also around the optimal solution. But this concentration process is typically recognizable in the convergence phase: suppose we have an individual close to the optimal solution and let it participate to the reproduction process; the presence of individuals similar to the previously identified one is promoted in the new generation and this may lead to another individual close to the optimal solution; by processing the sharing operator both the good individuals will be then penalized due to their closeness; this has two important consequences:

- The accuracy at finding the optimum solution is penalized;

- Improvements in the objective function value are more difficult as the closeness to the optimal solution increase and the stopping criteria easily become active.

These consequences can obviously be applied to the interpretation of the results in the previous figures: algorithms supplied by a sharing operator are penalized in terms of effectiveness in identifying the basin of attraction of the global optimum in case of presence of several local minima comparable with the global one, because, due to the low accuracy, little differences on the objective function values corresponding to comparable local minima can't be detected and exploited. On the other hand, it is well-known that the promotion of diversity in the population allow to maintain subpopulations and to avoid premature convergence to local optima. The previous considerations suggest the possibility of improving the performance of GAOT-shared algorithm by exploiting the advantages of the sharing operator during the first phases of the global search and by decreasing its action along the optimization process in order to gain more accuracy in describing the reached local minimum: this could lead to better results even in presence of several comparable local minima.

GATBX

As GATBX implements a genetic algorithm, we report the statistical characteristics. Ten run have been processed in order to solve the previously defined problem. Default options suggested by the providers of the code have been used in all the runs. A population of 50 individuals evolving for a maximum number of generations equal to 100 has been processed again.

Algorithm parameters	
Number of individuals:	50
Maximum number of generations:	100

Table 37 reports the best identified solution and the best known solution.

Search space		
Design variable	**Best identified solution**	**Best known solution**
Date of departure [*d*]:	1253.511	1253.510
Transfer time [*d*]:	203.536	203.541

Table 37: Comparison between the best identified solution and the best known solution: search space.

Objective function space		
Term	**Best identified solution**	**Best known solution**
ΔV [*m/s*]:	5678.904	5678.904
ΔV_I [*m/s*]:	2999.462	2999.464
ΔV_F [*m/s*]:	2679.442	2679.439

Table 38: Comparison between the best identified solution and the best known solution: objective function space.

The previous tables show that the best identified solution coincides in fact with the best known one. As it concerns the statistical characteristics of the identified solution set. Table 39 reports the mean value and the standard deviation of the performances which will be used for comparisons with the other optimization algorithms.

Evaluation criterion	**Mean value**	**Standard deviation**
ΔV [*m/s*]:	5740.887	177.082
Model function evaluations:	2322	424.075
Runtime [STU]:	$1.037 \cdot 10^{-2}$	$4.405 \cdot 10^{-3}$

Table 39: Statistical characteristics of the identified solutions.

Table 39 shows that the mean value of the optimal objective function values reached at the end of each optimization process is quite different from the best identified one and is characterized by a high standard deviation. Again, such a result let us suppose that no all the performed optimization processes have been able to identify the basin of attraction of the best known solution. Figure 131 reports the final solutions corresponding to each optimization run in the *nFunc-ΔV*, while Figure 132 illustrates their distribution over the search space.

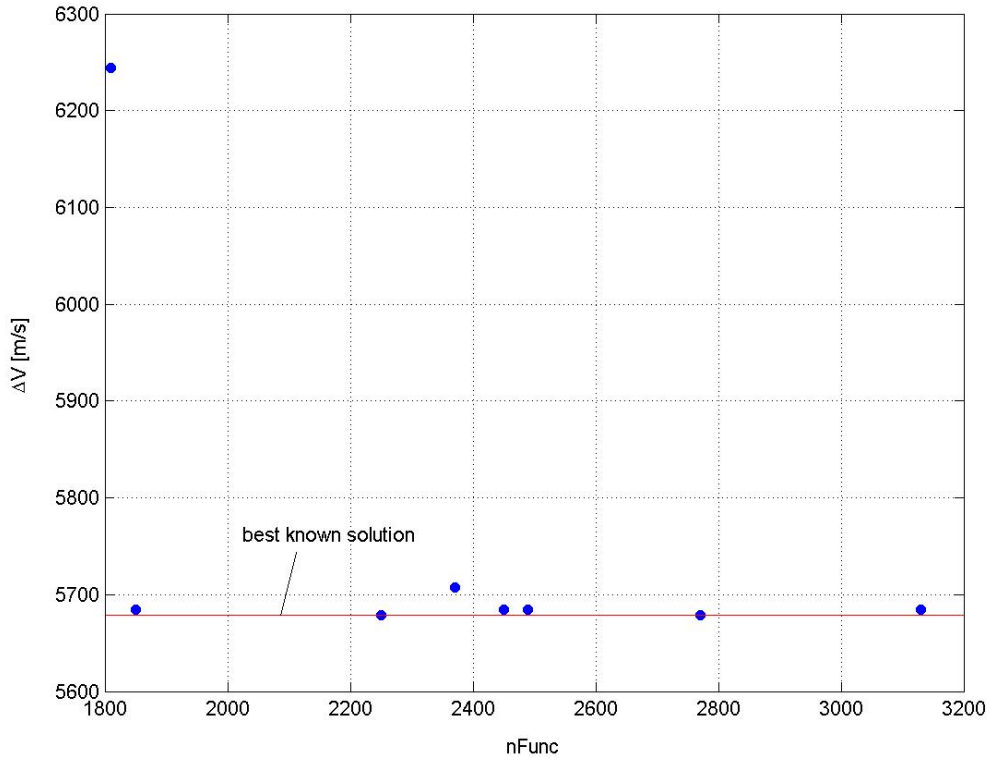

Figure 131: Distribution of the final solutions corresponding to each optimization run on the *nFunc-ΔV* plane.

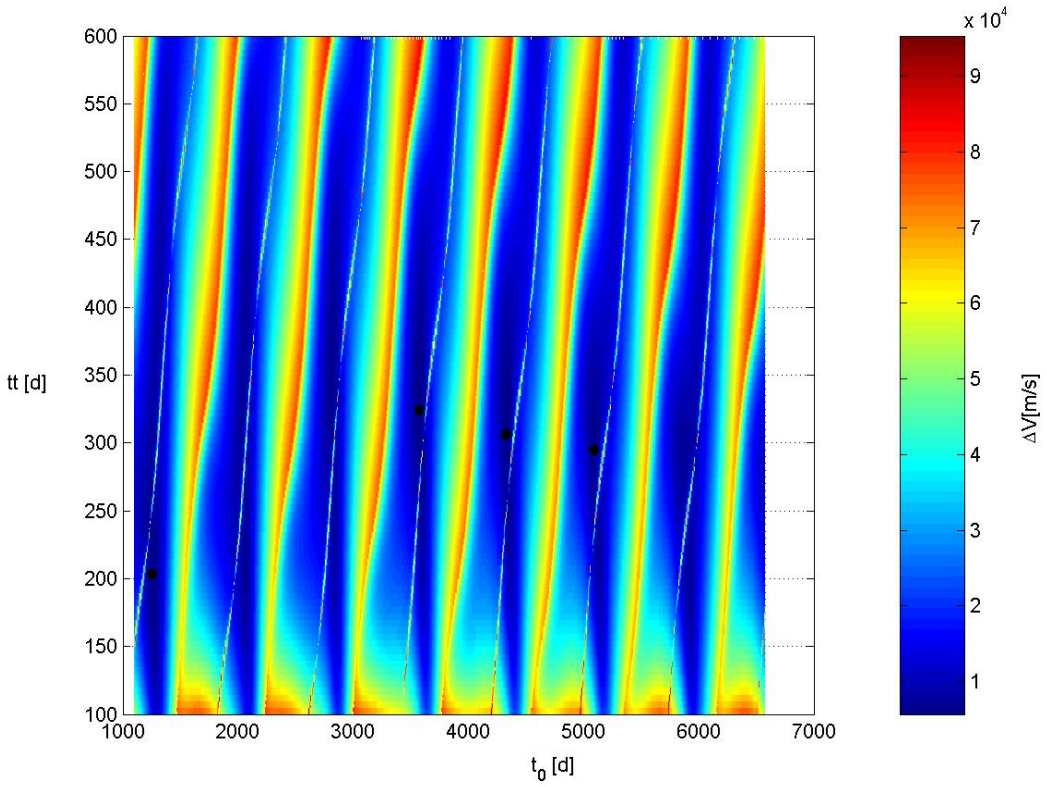

Figure 132: Distribution of the final solutions corresponding to each optimization run on the search space.

Figure 131 and Figure 132 illustrate that GATBX algorithm could not reach the basin of attraction of the best known solution corresponding to all the optimization runs. In particular, by investigating the normalized search space, Table 40 reports the Euclidean distance of each final solution form the best known one.

Run	Euclidean distance
Run 1	$4.870 \cdot 10^{-1}$
Run 2	$4.870 \cdot 10^{-1}$
Run 3	$4.871 \cdot 10^{-1}$
Run 4	$5.818 \cdot 10^{-6}$
Run 5	$5.981 \cdot 10^{-1}$
Run 6	$4.870 \cdot 10^{-1}$

Run 7	$4.870 \cdot 10^{-1}$
Run 8	$1.195 \cdot 10^{-4}$
Run 9	$1.042 \cdot 10^{-5}$
run 10	$7.234 \cdot 10^{-1}$

Table 40: Euclidean distance of each final solution form the best known one in the normalized search space.

By considering two solutions as identical when their Euclidean distance is less then 5% of the hyper-diagonal of the normalized search space (that is 0.071 in this case), only 3/10 GATBX runs were able to get the best known solution. Let now investigate the main features of the final population: Figure 133 shows the distribution of the population over the search space at the end of the optimization process corresponding to the best identified solution.

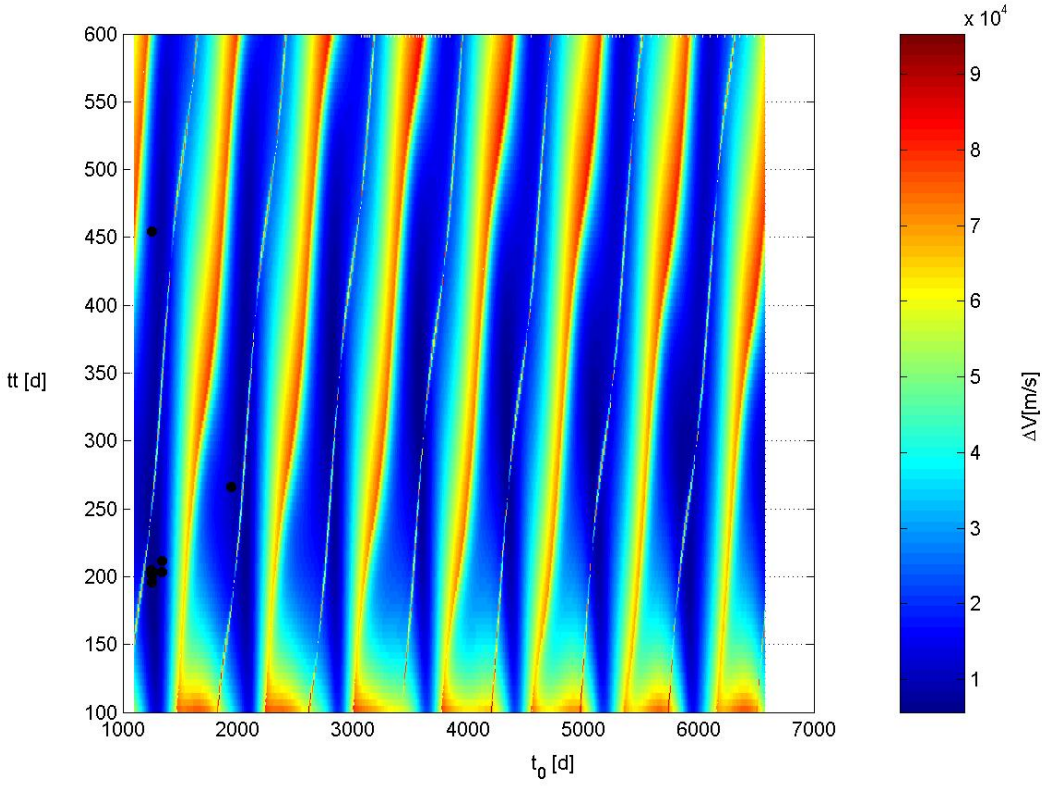

Figure 133: Distribution of the population over the search space at the end of the optimization process corresponding to the best identified solution.

Figure 133 shows that the individuals in the final population mainly concentrated in a narrow neighbourhood of the global optimum, in a more evident manner than in case of GAOT algorithm. This results held in all runs on average, including the cases where a non global optimum has been identified. Figure 134 shows the trace of the best solution during the optimization run corresponding to the best identified solution: GATBX search process typically investigates the basin of attraction of different local minima before converging to the final solution.

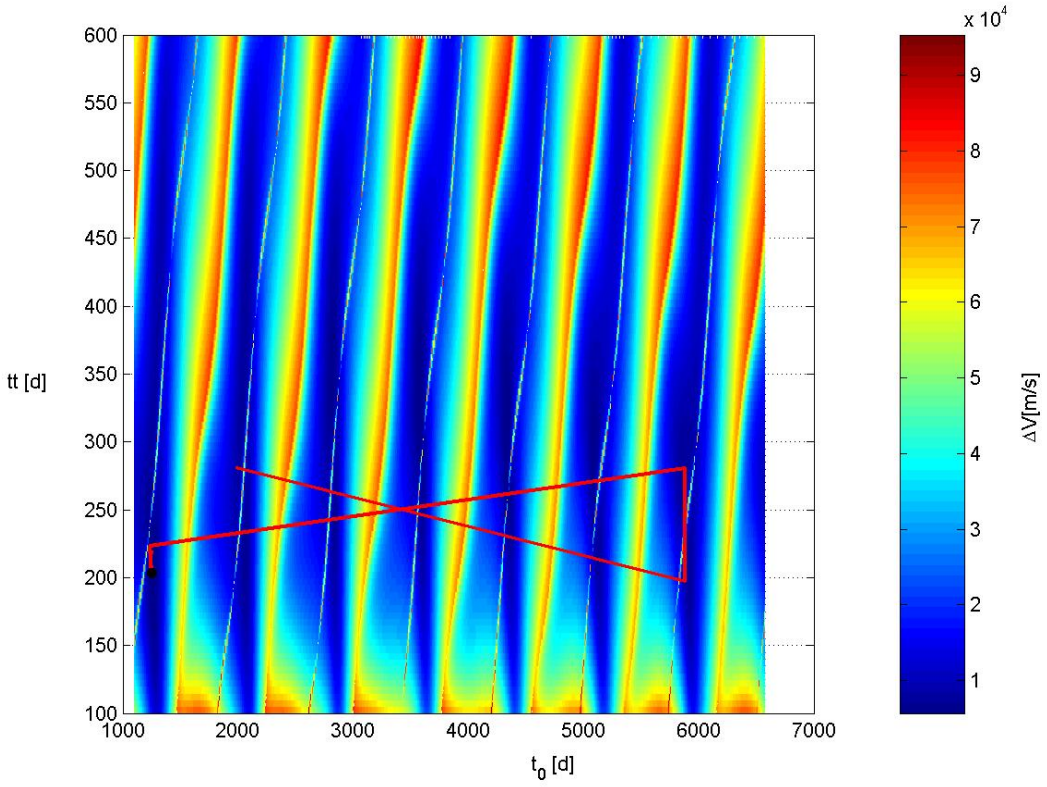

Figure 134: Trace of the best solution during the optimization run corresponding to the best identified solution.

GATBX-migr

As GATBX-migr implements a genetic algorithm including a migration operator applied among a predefined set of subpopulations, we report the statistical characteristics. Ten run have been processed in order to solve the previously defined problem. Default options suggested by the providers of the code have been used in all the runs. A population of 50 individuals evolving for a maximum

number of generations equal to 100 has been processed again. The population has been divided in 5 subpopulations, each one including 10 individuals.

Algorithm parameters	
Number of individuals:	50
Maximum number of generations:	100
Number of subpopulations:	5
Number of individuals per subpopulation:	10

Tables 41-42 report the best identified solution compared with the best known solution.

Search space		
Design variable	**Best identified solution**	**Best known solution**
Date of departure [*d*]:	1253.519	1253.510
Transfer time [*d*]:	203.537	203.541

Table 41: Comparison between the best identified solution and the best known solution: search space.

Objective function space		
Term	**Best identified solution**	**Best known solution**
ΔV [*m/s*]:	5678.904	5678.904
ΔV_I [*m/s*]:	2999.472	2999.464
ΔV_F [*m/s*]:	2679.432	2679.439

Table 42: Comparison between the best identified solution and the best known solution: objective function space.

The previous tables show that the best identified solution coincides in fact with the best known one. Let now consider the statistical characteristics of the identified solution set. Table 43 reports the mean value and the standard deviation of the performances which will be used for comparisons with the other optimization algorithms.

Evaluation criterion	Mean value	Standard deviation
ΔV [*m/s*]:	5679.957	2.191
Model function evaluations:	2650	909.799
Runtime [STU]:	$1.646 \cdot 10^{-2}$	$6.529 \cdot 10^{-3}$

Table 43: Statistical characteristics of the identified solutions.

Although the little standard deviation identified in case of GATBX-migr algorithm, the mean value of the optimal objective function values lets us suppose that no all the performed optimization processes have been able to identify the basin of attraction of the best known solution. Figure 135 reports the final solutions corresponding to each optimization run in the *nFunc-ΔV* plane, while Figure 136 illustrates their distribution over the search space.

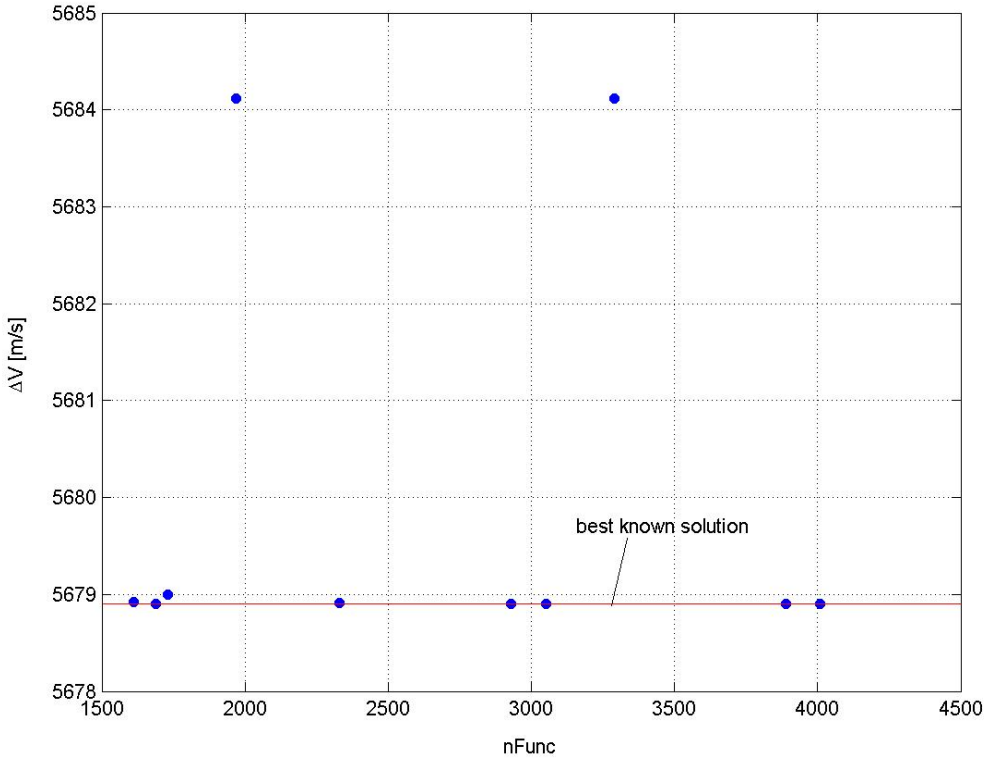

Figure 135: Distribution of the final solutions corresponding to each optimization run on the *nFunc-ΔV* plane.

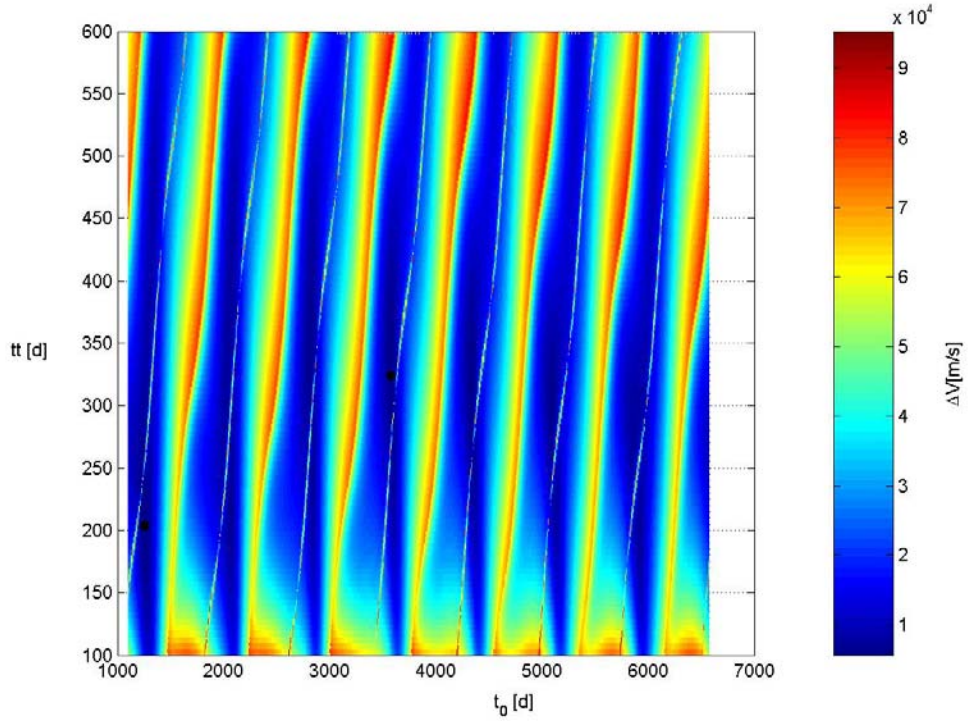

Figure 136: Distribution of the final solutions corresponding to each optimization run on the search space.

Results illustrated in Figure 135 and Figure 136 are quite impressive: most GATBX-migr runs effectively and accurately reached the best known solution. Only few runs, as showed in the following, got stuck in a different local minimum, which is in fact totally comparable with the best known one in terms of objective function value. In particular, by investigating the normalized search space, Table 44 reports the Euclidean distance of each final solution form the best known one.

Run	Euclidean distance
run 1	$2.668 \cdot 10^{-4}$
run 2	$7.691 \cdot 10^{-4}$
run 3	$8.619 \cdot 10^{-6}$
run 4	$4.822 \cdot 10^{-5}$
run 5	$2.949 \cdot 10^{-5}$
run 6	$3.793 \cdot 10^{-5}$
run 7	$2.777 \cdot 10^{-5}$
run 8	$4.871 \cdot 10^{-1}$
run 9	$3.502 \cdot 10^{-5}$
run 10	$4.871 \cdot 10^{-1}$

Table 44 - Euclidean distance of each final solution form the best known one in the normalized search space.

By considering two solutions as identical when their Euclidean distance is less then 5% of the hyper-diagonal of the normalized search space (that is 0.071 in this case), 8/10 GATBX-migr runs were able to get the best known solution. Let now analyse the main features of the final population: Figure 137 shows the distribution of the population over the search space at the end of the optimization process corresponding to the best identified solution.

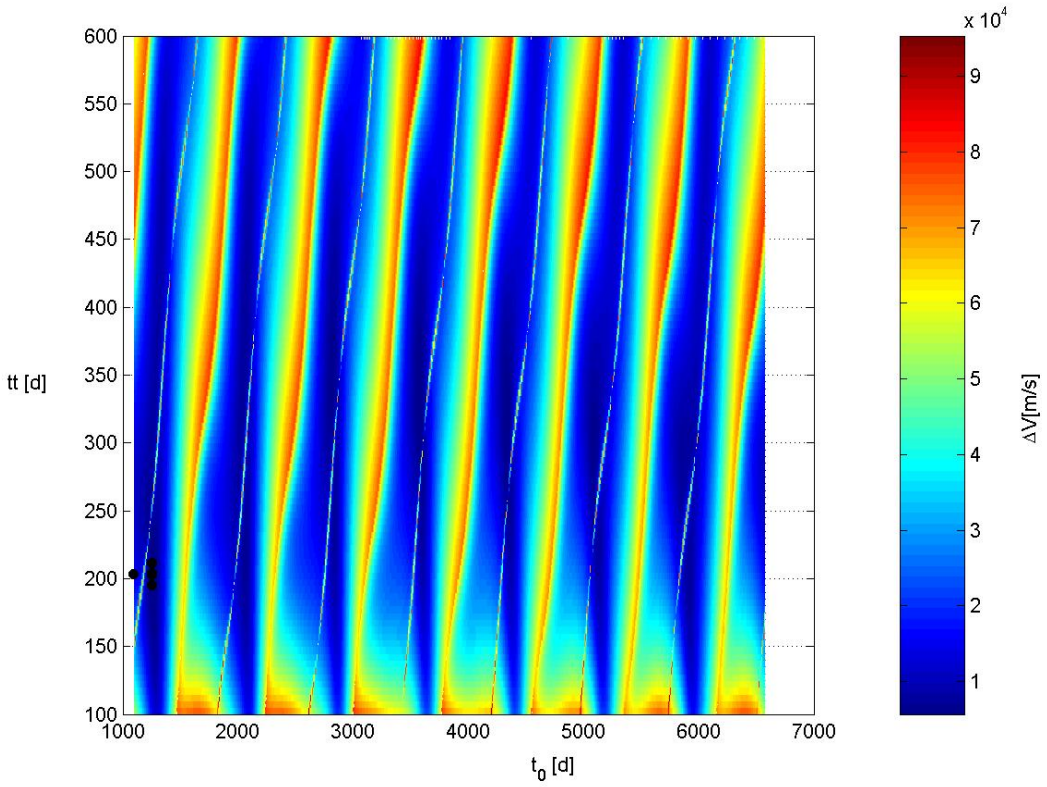

Figure 137: Distribution of the population over the search space at the end of the optimization process corresponding to the best identified solution.

Figure 137 shows that the individuals in the final population mainly concentrated in a narrow neighbourhood of the global optimum: although the GATBX-migr performs independent evolutions of subpopulation, the mutation operator finally forces the convergence to the same local optimum. However, the benefits of such evolutionary scheme are quite evident: GATBX-migr effectively avoids the premature convergence to local optima, thanks to a better coverage of the search space. This results held in all runs on average, including the cases where a non global optimum has been identified. Figure 138 shows the trace of the best solution during the optimization run corresponding to the best identified solution: after few iteration, GATBX-migr search process immediately gained the basin of attraction of the best known solution.

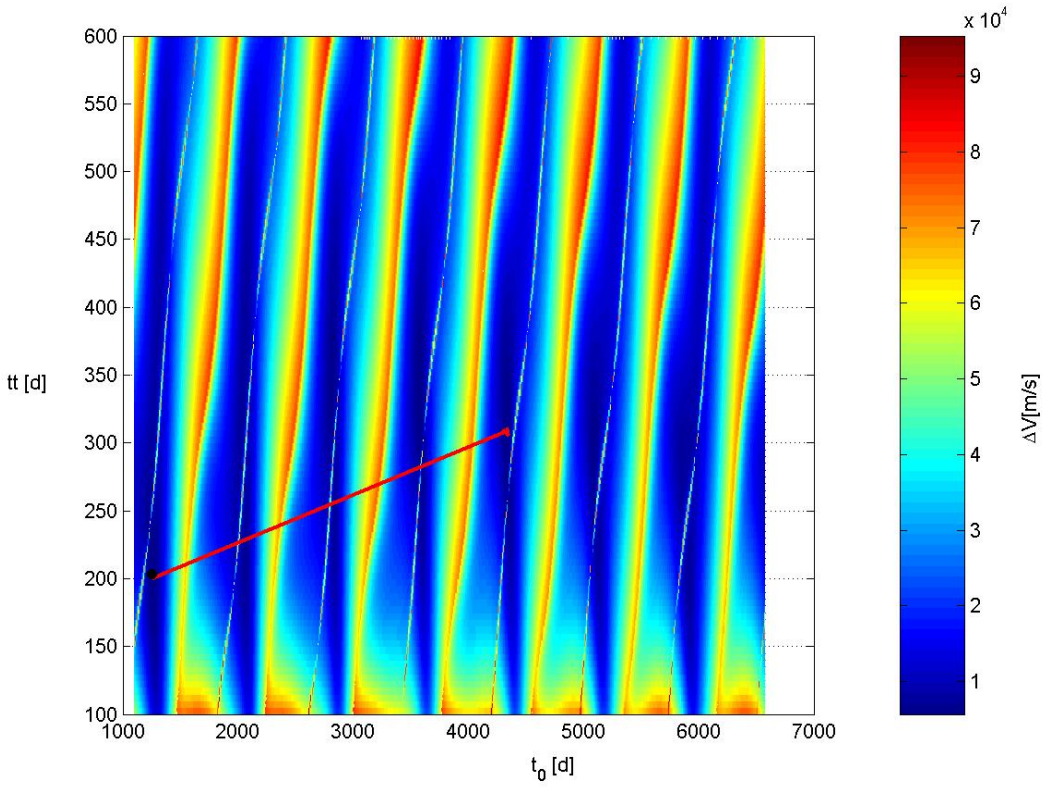

Figure 138: Trace of the best solution during the optimization run corresponding to the best identified solution.

FEP

As FEP implements an evolutionary programming algorithm, we report, as already done for genetic algorithms, the statistical characteristics. Ten run have been processed in order to solve the previously defined problem. Default options suggested by the providers of the code have been used in all the runs. As the 2-impulse direct planet-to-planet transfer has low complexity features, we used 50 individuals evolving for a maximum number of generations equal to 100.

Algorithm parameters	
Number of individuals:	50
Maximum number of generations:	100

Table 45 and Table 46 report the best identified solution compared with the best known solution.

Search space		
Design variable	**Best identified solution**	**Best known solution**
Date of departure [*d*]:	1253.509	1253.510
Transfer time [*d*]:	203.540	203.541

Table 45: Comparison between the best identified solution and the best known solution: search space.

Objective function space		
Term	**Best identified solution**	**Best known solution**
ΔV [*m/s*]:	5678.904	5678.904
ΔV_I [*m/s*]:	2999.463	2999.464
ΔV_F [*m/s*]:	2679.441	2679.439

Table 46: Comparison between the best identified solution and the best known solution: objective function space.

The previous tables show that the best identified solution coincides in fact with the best known one. As it concerns the statistical characteristics of the identified solution set, Table 47 reports the mean value and the standard deviation of the performances which will be used for comparisons with the other optimization algorithms.

Evaluation criterion	Mean value	Standard deviation
ΔV [*m/s*]:	5711.337	95.130
Model function evaluations:	2478.9	953.829
Runtime [STU]:	$2.463 \cdot 10^{-2}$	$9.004 \cdot 10^{-3}$

Table 47: Statistical characteristics of the identified solutions.

Although the presence, similarly to GATBX-migr algorithm, of a little standard deviation identified, the mean value of the optimal objective function values lets us suppose that no all the performed optimization processes have been able to identify the basin of attraction of the best known solution. Figure 139 reports the final solutions corresponding to each optimization run in the *nFunc-ΔV* plane, while Figure 140 illustrates their distribution over the search space.

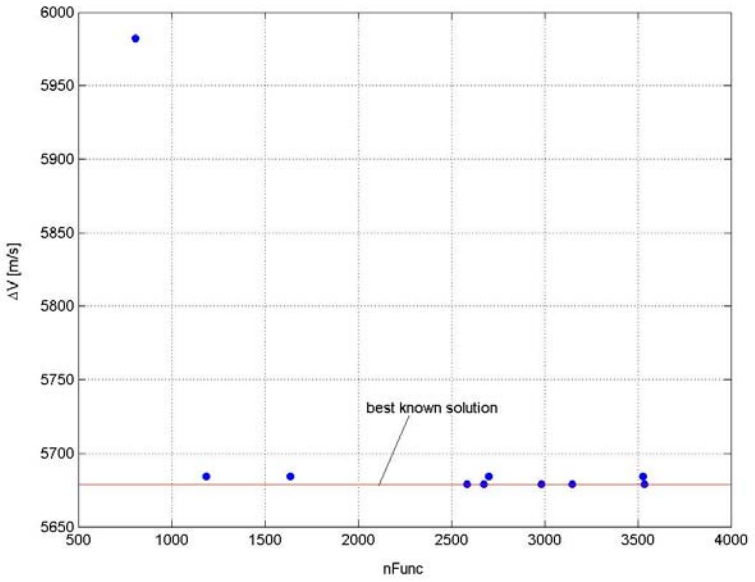

Figure 139: Distribution of the final solutions corresponding to each optimization run on the *nFunc-ΔV* plane.

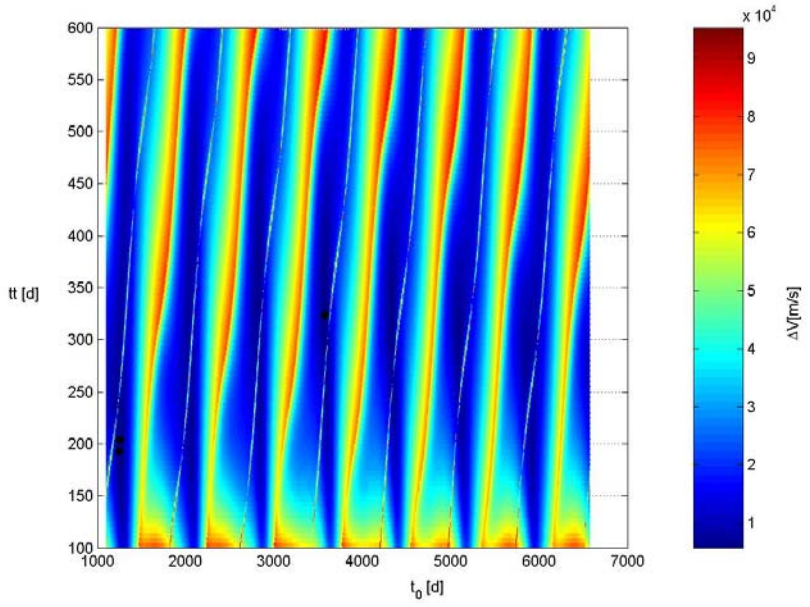

Figure 140: Distribution of the final solutions corresponding to each optimization run on the search space.

Results illustrated in Figure 139 and Figure 140 are quite similar to those gained in case of GATBX-migr algorithm: most FEP runs effectively and accurately reached the best known solution. Only few runs, as showed in the following, got stuck in a different local minimum, which is in fact totally comparable with the best known one in terms of objective function value. By investigating the normalized search space, Table 49 reports the Euclidean distance of each final solution form the best known one.

run	Euclidean distance
run 1	$9.651 \cdot 10^{-7}$
run 2	$2.471 \cdot 10^{-6}$
run 3	$3.914 \cdot 10^{-5}$
run 4	$4.871 \cdot 10^{-1}$
run 5	$5.672 \cdot 10^{-4}$
run 6	$4.864 \cdot 10^{-1}$
run 7	$2.060 \cdot 10^{-2}$
run 8	$1.441 \cdot 10^{-4}$
run 9	$3.614 \cdot 10^{-6}$
run 10	$4.871 \cdot 10^{-1}$

Table 49: Euclidean distance of each final solution form the best known one in the normalized search space.

By considering two solutions as identical when their Euclidean distance is less then 5% of the hyper-diagonal of the normalized search space (that is 0.071 in this case), 7/10 FEP runs were able to get the best known solution. Further interesting observations can be pointed out by analysing the main features of the final population: Figure 141 shows the distribution of the population over the search space at the end of the optimization process corresponding to the best identified solution.

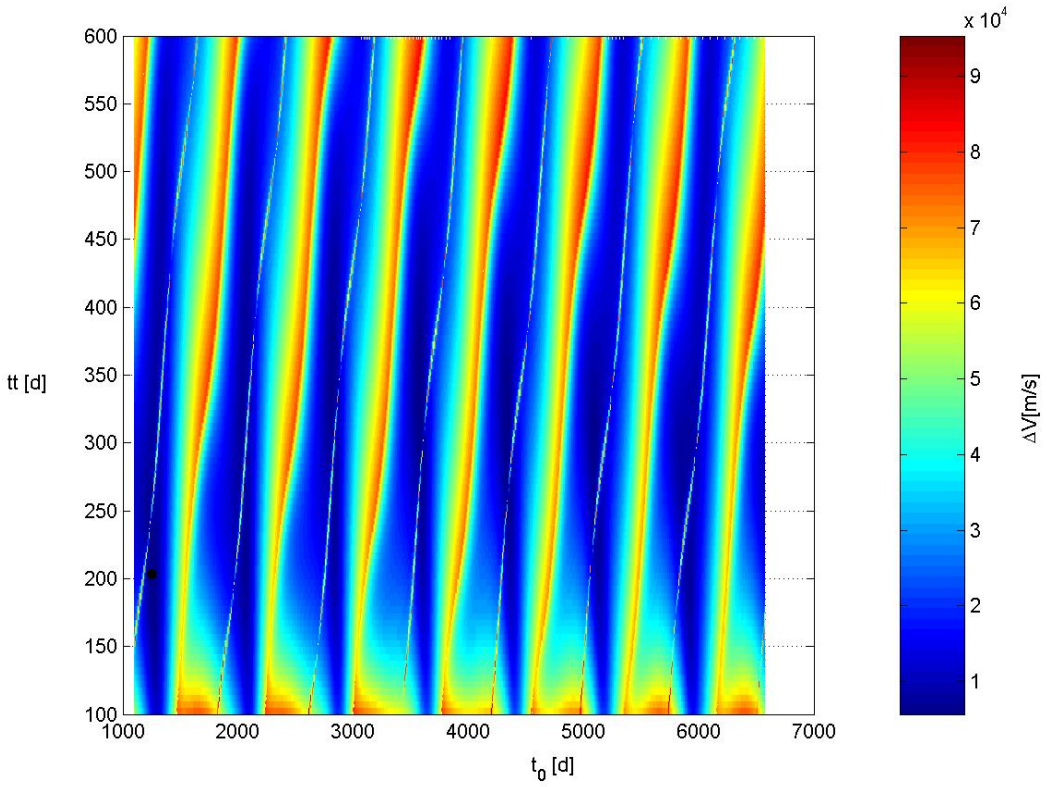

Figure 141: Distribution of the population over the search space at the end of the optimization process corresponding to the best identified solution.

The final population of the run identifying the best solution is strongly concentrated around the best known solution and is characterized by quite similar individuals. Such result could be though as negative, as diversity in the population generally promotes a better coverage of the search space; however, the use of self-adaptive evolutionary parameters based on Cauchy random numbers generation seem to tune in a proper way the search step, effectively avoiding the premature convergence to local minima. This results held in all runs on average, including the cases where a non global optimum has been identified, as shown in Figure 142.

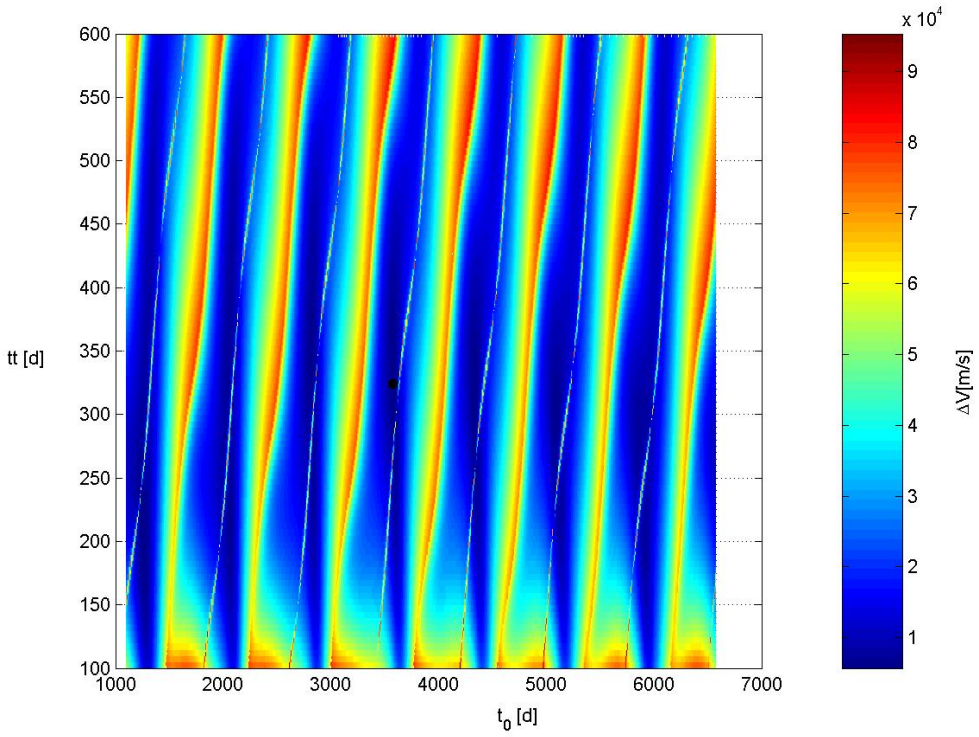

Figure 142 - Distribution of the population over the search space at the end of an optimization process corresponding to a local optimum solution.

Figure 143 shows the trace of the best solution during the optimization run corresponding to the best identified solution: FEP search process immediately converged to the basin of attraction of the best identified solution, thanks to a good trade-off between exploration and exploitation via the self-adaptivity of the evolutionary parameters tuning the search step.

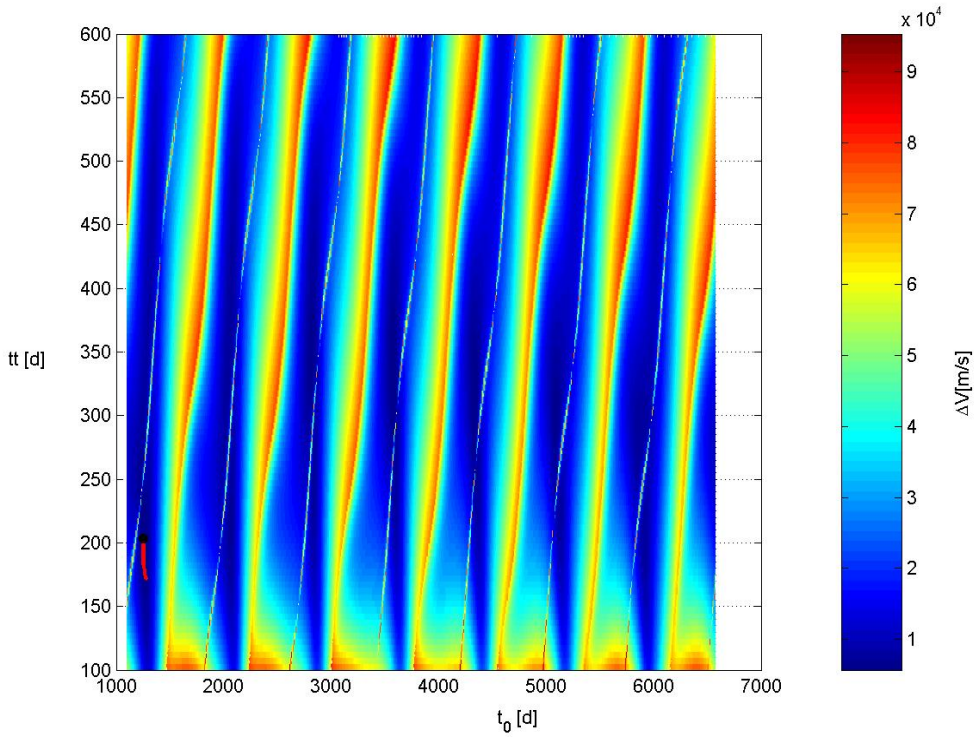

Figure 143: Trace of the best solution during the optimization run corresponding to the best identified solution.

DE

As DE implements a Differential Evolution algorithm, we report the statistical characteristics. Ten run have been processed in order to solve the previously defined problem. Default options suggested by the providers of the code have been used in all the runs. Again, due to the low complexity of the 2-impulse direct planet-to-planet transfer problem, we used 50 individuals evolving for a maximum number of iterations equal to 100.

Algorithm parameters	
Number of individuals:	50
Maximum number of generations:	100

Table 50 and Table 51 report the best identified solution compared with the best known solution.

Search space		
Design variable	**Best identified solution**	**Best known solution**
Date of departure [*d*]:	4330.221	1253.510
Transfer time [*d*]:	307.746	203.541

Table 50: Comparison between the best identified solution and the best known solution: search space.

Objective function space		
Term	**Best identified solution**	**Best known solution**
ΔV [*m/s*]:	5708.130	5678.904
ΔV_I [*m/s*]:	3029.958	2999.464
ΔV_F [*m/s*]:	2678.171	2679.439

Table 51: Comparison between the best identified solution and the best known solution: objective function space.

The previous tables show that the best identified solution doesn't coincide in fact with the best known one, as illustrated in Figure 144, where the best solution identified by DE (black dot) is compared with the best known one (red dot) on the search space.

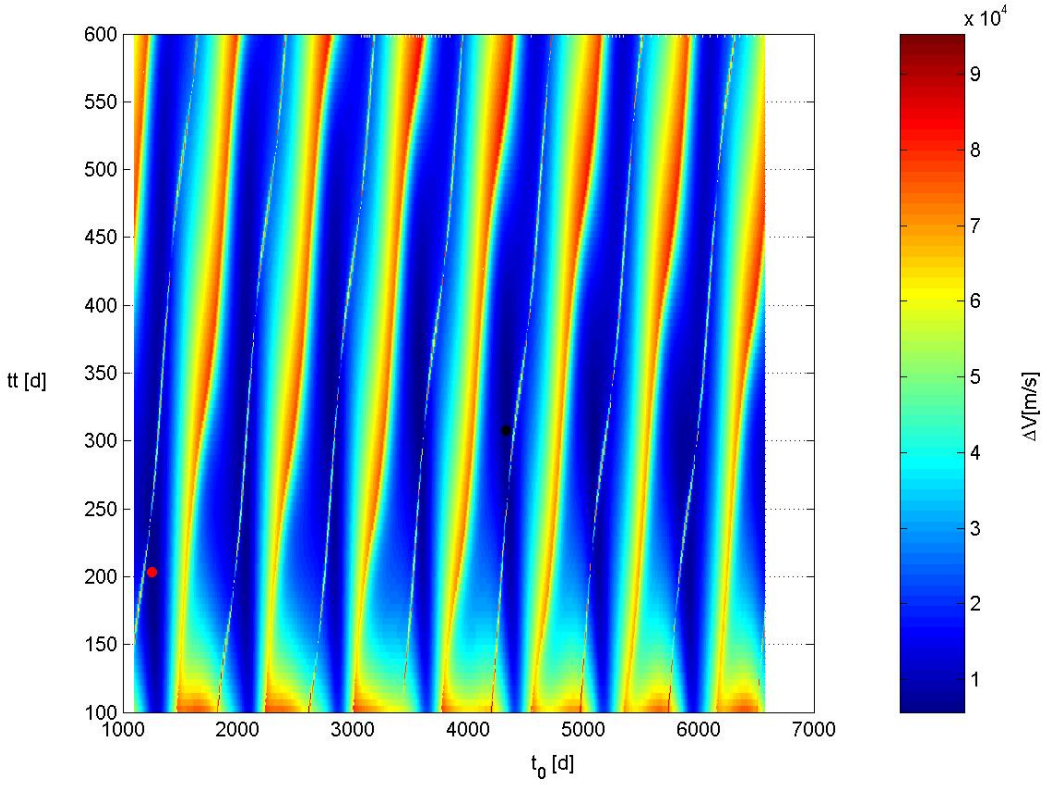

Figure 144: Comparison between the best solution identified by DE (black dot) and the best known one (red dot).

Statistical characteristics of the identified solution set are reported in Table 52: the mean value and the standard deviation of the performances which will be used for comparisons with the other optimization algorithms are highlighted.

Evaluation criterion	Mean value	Standard deviation
ΔV [*m/s*]:	5986.674	408.679
Model function evaluations:	828.3	319.692
Runtime [STU]:	$3.019 \cdot 10^{-3}$	$1.098 \cdot 10^{-3}$

Table 52: Statistical characteristics of the identified solutions.

Table 52 shows that the set of identified solutions is characterized by a high standard deviation. Such a result let us suppose that no all the performed optimization processes have been able to identify the basin of attraction of the

best known solution. Figure 145 reports the final solutions corresponding to each optimization run in the *nFunc-ΔV*, while Figure 146 illustrates their distribution over the search space.

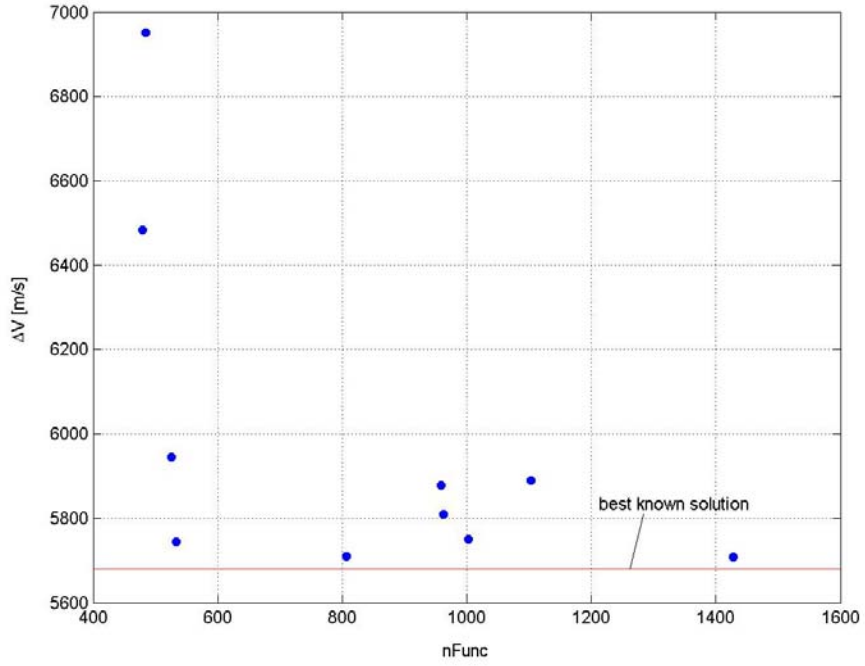

Figure 145: Distribution of the final solutions corresponding to each optimization run on the *nFunc-ΔV* plane.

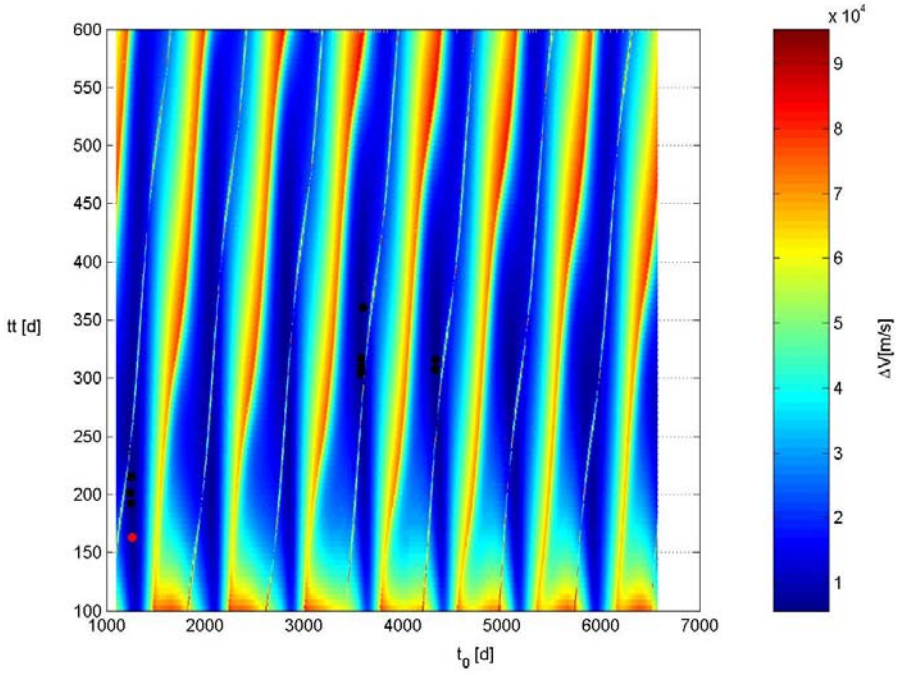

Figure 146: Distribution of the final solutions corresponding to each optimization run on the search space.

Figure 145 and Figure 146 illustrate that DE algorithm couldn't reach the basin of attraction of the best known solution corresponding to all the optimization runs. It is worth noting that, although the best identified solution doesn't lie into the basin of attraction of the best known one, other runs were able to identify it; however, the low accuracy demonstrated by DE algorithm in such cases in describing the corresponding minimum led to objective function values higher than the best identified one. As a consequence, one can state that the performances of DE algorithm are strongly affected by a low accuracy. Let now analyse the normalized search space in order to identify the number of successful runs in identifying the basin of attraction of the best known solution: Table 53 reports the Euclidean distance of each final solution form the best known one.

run	Euclidean distance
Run 1	$6.045 \cdot 10^{-1}$
Run 2	$2.218 \cdot 10^{-2}$
Run 3	$8.062 \cdot 10^{-2}$
Run 4	$4.562 \cdot 10^{-3}$
Run 5	$2.244 \cdot 10^{-2}$
Run 6	$5.307 \cdot 10^{-1}$
Run 7	$4.744 \cdot 10^{-1}$
Run 8	$5.990 \cdot 10^{-1}$
Run 9	$4.807 \cdot 10^{-1}$
run 10	$4.698 \cdot 10^{-1}$

Table 53: Euclidean distance of each final solution form the best known one in the normalized search space.

By considering two solutions as identical when their Euclidean distance is less then 5% of the hyper-diagonal of the normalized search space (that is 0.071 in this case), only 3/10 DE runs were able to get the best known solution.

However, by analysing Figure 147, we can see that solution corresponding to run 3 (the red dot in figure), although quite different from the best known one, lies in fact in the basin of attraction of the best known solution. As a consequence, we can state that 4/10 DE runs were able to get the basin attraction of the best known solution. Let now investigate the main features of the final population: Figure 147 shows the distribution of the population over the search space at the end of the optimization process corresponding to the best identified solution.

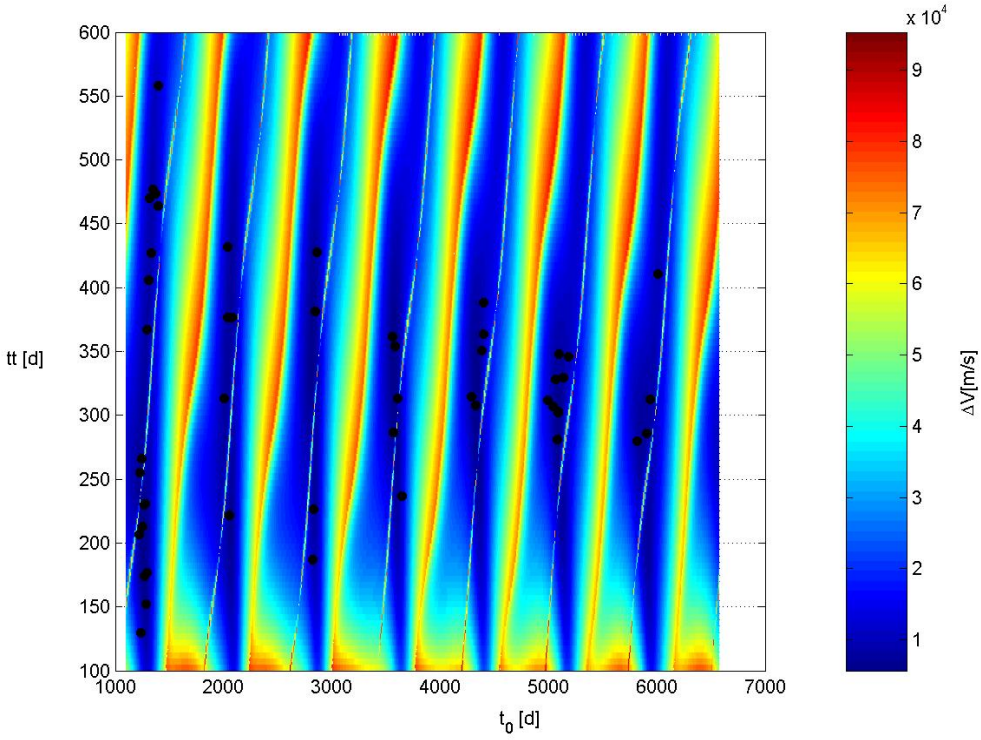

Figure 147: Distribution of the population over the search space at the end of the optimization process corresponding to the best identified solution.

Figure 147 shows that the individuals in the final population are widely distributed on the search space. This results held in all runs on average, including the cases where the basin of attraction of the global optimum has been identified, as shown in Figure 148.

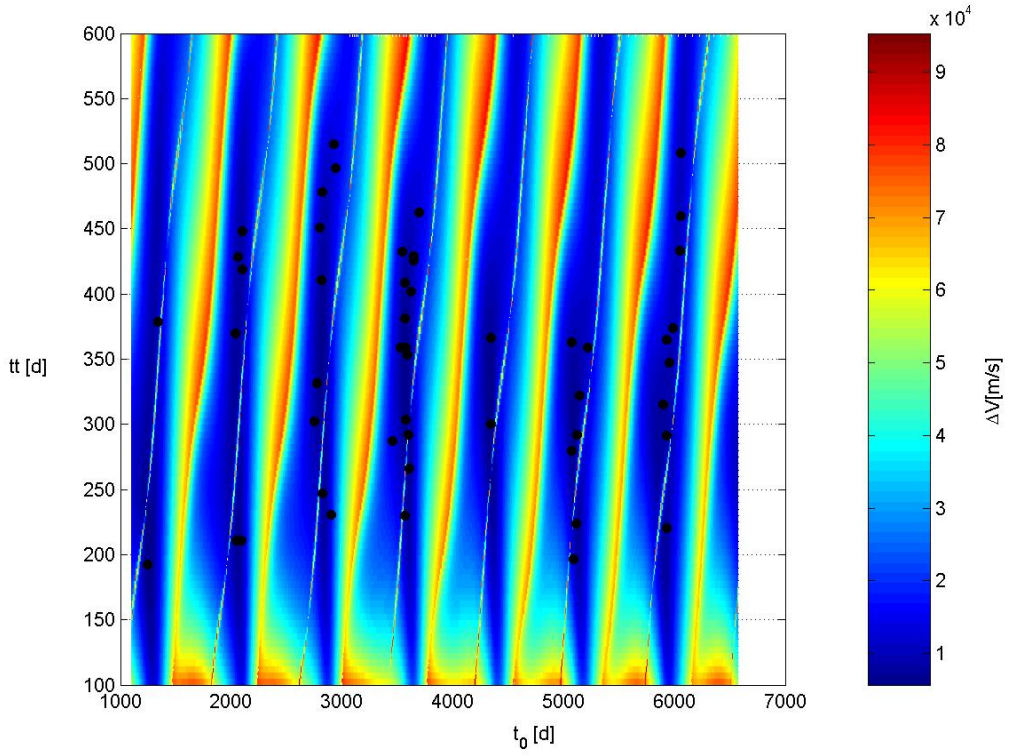

Figure 148: Distribution of the population over the search space at the end of the optimization process corresponding to an identified solution lying on the basin of attraction of the best known one.

In particular it is quite interesting observing that the basin of attraction of several local minima are kept at the end of the optimization process. Such result could be effectively used by performing local optimization processes at the end of DE run in order to accurately identify the local minimum corresponding to each basin: in this way, although the low accuracy, DE algorithm is able to recognize different space trajectory families corresponding to different basin of attraction and to keep information about them during the whole optimization process. Consequences of such DE feature are highlighted in Figures 149-150, which show the trace of the best solution during the optimization runs corresponding to the best identified solution and to an identified solution lying on the basin of attraction of the best known one respectively: DE search processes typically investigates the basin of attraction of different local minima before converging to the final solution.

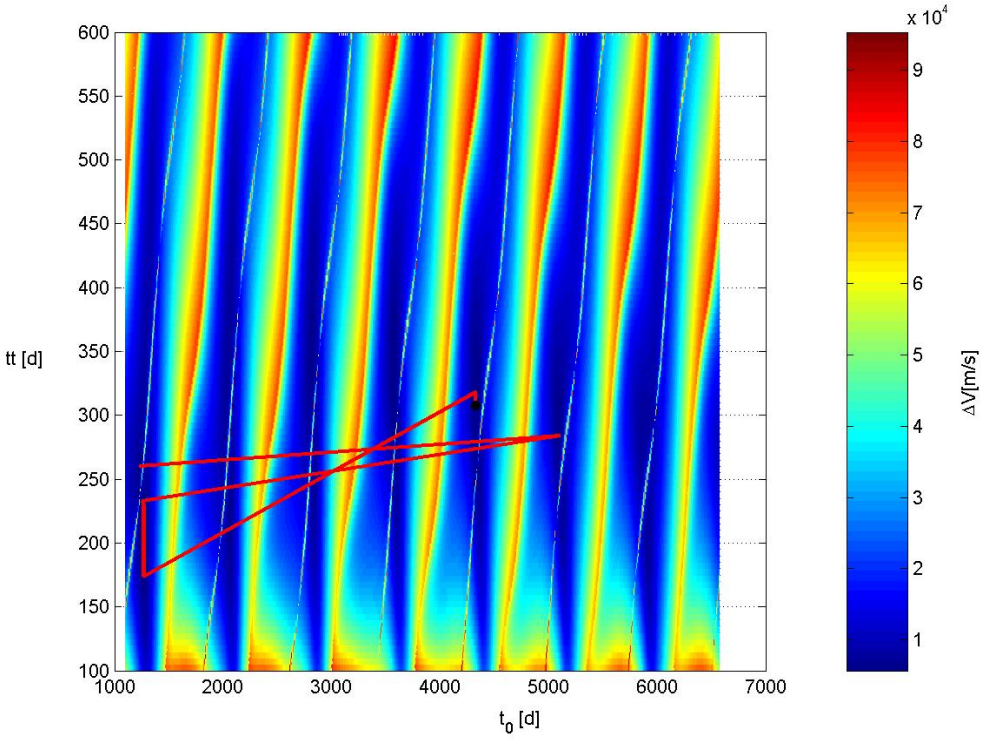

Figure 149: Trace of the best solution during the optimization run corresponding to the best identified solution.

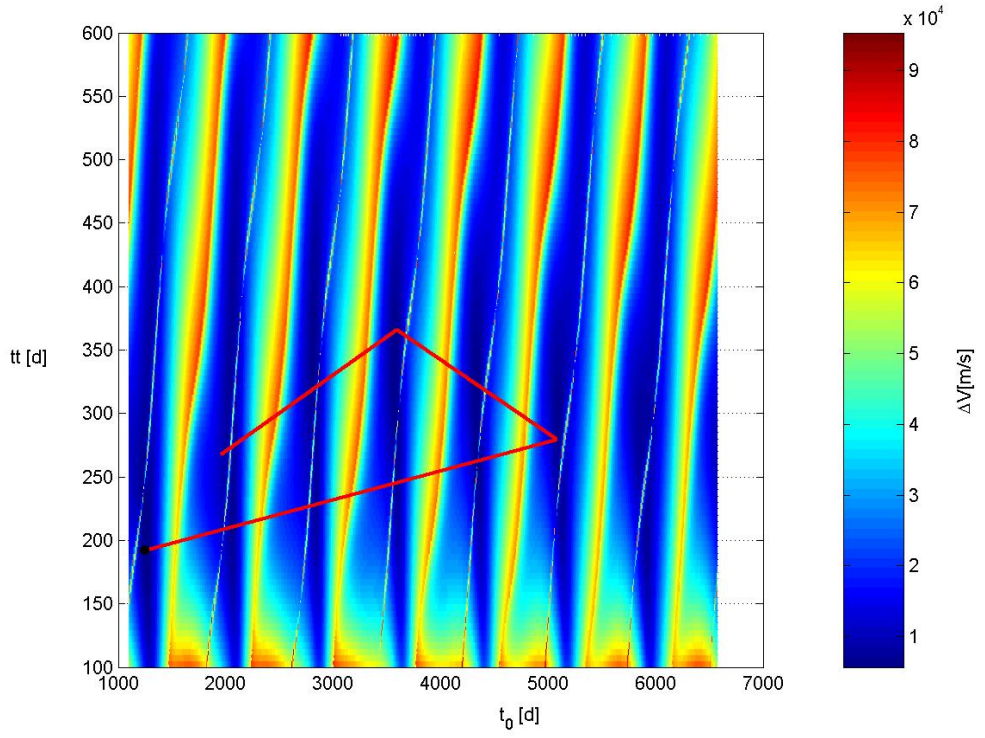

Figure 150 - Trace of the best solution during the optimization run corresponding to an identified solution lying on the basin of attraction of the best known one.

ASA

As ASA implements an Adaptive Simulated Annealing algorithm, we report the statistical performance characteristics. Ten runs have been processed in order to solve the previously defined problem. Default options suggested by the providers of the code have been used in all the runs. Note that, unlike the previous cases, the adaptive simulated annealing needs a starting solution, which strongly affects the optimal solution reached. Due to the comparative purposes of this work, we decided to use ten different random starting solutions, uniformly distributed in the search box. Table 54 and Table report the best identified solution compared with the best known solution.

Search space		
Design variable	**Best identified solution**	**Best known solution**
Date of departure [*d*]:	1253.509	1253.510
Transfer time [*d*]:	203.542	203.541

Table 54: Comparison between the best identified solution and the best known solution: search space.

Objective function space		
Term	**Best identified solution**	**Best known solution**
ΔV [*m/s*]:	5678.904	5678.904
ΔV_I [*m/s*]:	2999.464	2999.464
ΔV_F [*m/s*]:	2679.440	2679.439

Table 55: Comparison between the best identified solution and the best known solution: objective function space.

The previous tables show that the best identified solution seems to coincide with the best known one. Let now consider the statistical characteristics of the identified solution set. Table 56 reports the mean value and the standard

deviation of the performances which will be used for comparisons with the other optimization algorithms.

Evaluation criterion	Mean value	Standard deviation
ΔV [*m/s*]:	6328.291	1330.247
Model function evaluations:	1289.7	56.555
Runtime [STU]:	$3.814 \cdot 10^{-3}$	$1.555 \cdot 10^{-4}$

Table 56: Statistical characteristics of the identified solutions.

The mean value of the optimal objective function values and the high standard deviation reported in Table 56 let us suppose that no all the performed optimization processes have been able to identify the basin of attraction of the best known solution. Figure 151 reports the final solutions corresponding to each optimization run in the *nFunc-ΔV* plane, while Figure 152 illustrates their distribution over the search space.

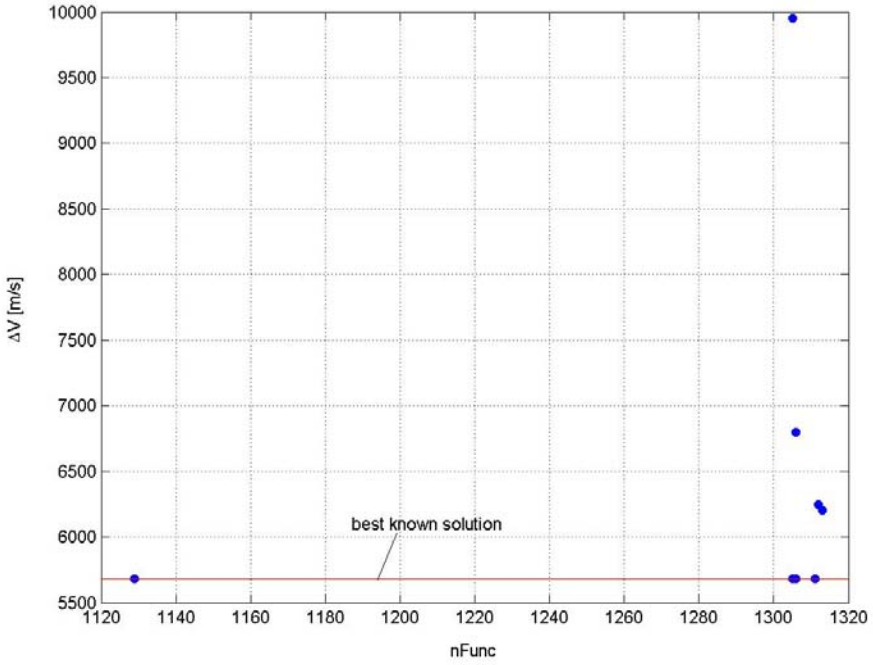

Figure151: Distribution of the final solutions corresponding to each optimization run on the *nFunc-ΔV* plane.

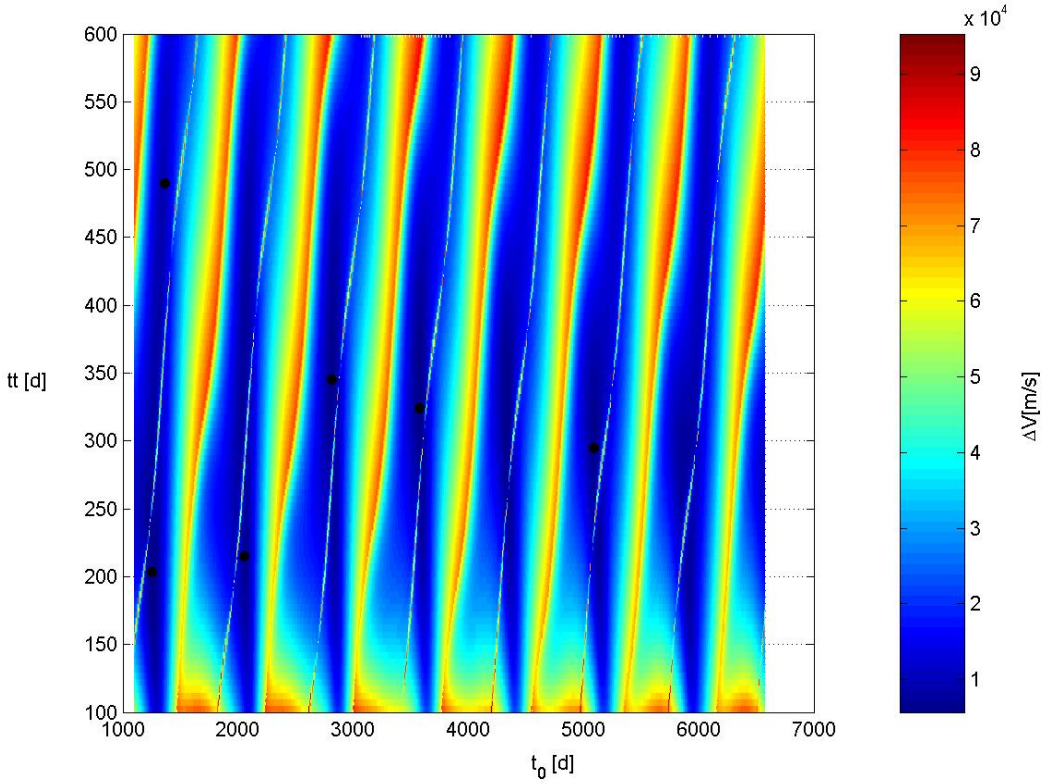

Figure 152: Distribution of the final solutions corresponding to each optimization run on the search space.

Figure 151 and Figure 152 fairly illustrates that some ASA algorithm runs failed at reaching the basin of attraction of the best known solution: in particular, ASA got stuck in a set of local minima which is wider than in the previous cases, even if they are comparable in terms of objective function values (except in one case). By investigating the normalized search space, Table 57 reports the Euclidean distance of each final solution form the best known one.

run	Euclidean distance
run 1	$1.485 \cdot 10^{-1}$
run 2	$3.856 \cdot 10^{-6}$
run 3	$5.731 \cdot 10^{-1}$
run 4	$1.965 \cdot 10^{-6}$

run 5	$7.234 \cdot 10^{-1}$
run 6	$4.871 \cdot 10^{-1}$
run 7	$4.014 \cdot 10^{-1}$
run 8	$2.584 \cdot 10^{-6}$
run 9	$3.243 \cdot 10^{-6}$
run 10	$2.188 \cdot 10^{-6}$

Table 57: Euclidean distance of each final solution form the best known one in the normalized search space.

By considering two solutions as identical when their Euclidean distance is less then 5% of the hyper-diagonal of the normalized search space (that is 0.071 in this case), 5/10 ASA runs were able to get the best known solution. Moreover, it is worth noting that in such successful runs, the accuracy shown by ASA is higher than all the previous algorithms, thanks to the local component of the global optimization process, as the distances corresponding to runs 2, 4, 8, 9 and 10 have an order of magnitude equal to 10^{-6}. Figure shows the history of the solution during the optimization run corresponding to the best identified solution. Note that, simulated annealing doesn't use a population based approach, but try to explore the search space using a unique solution: then Figure 153 fairly illustrates the global component of the search process characterizing a simulating annealing algorithm.

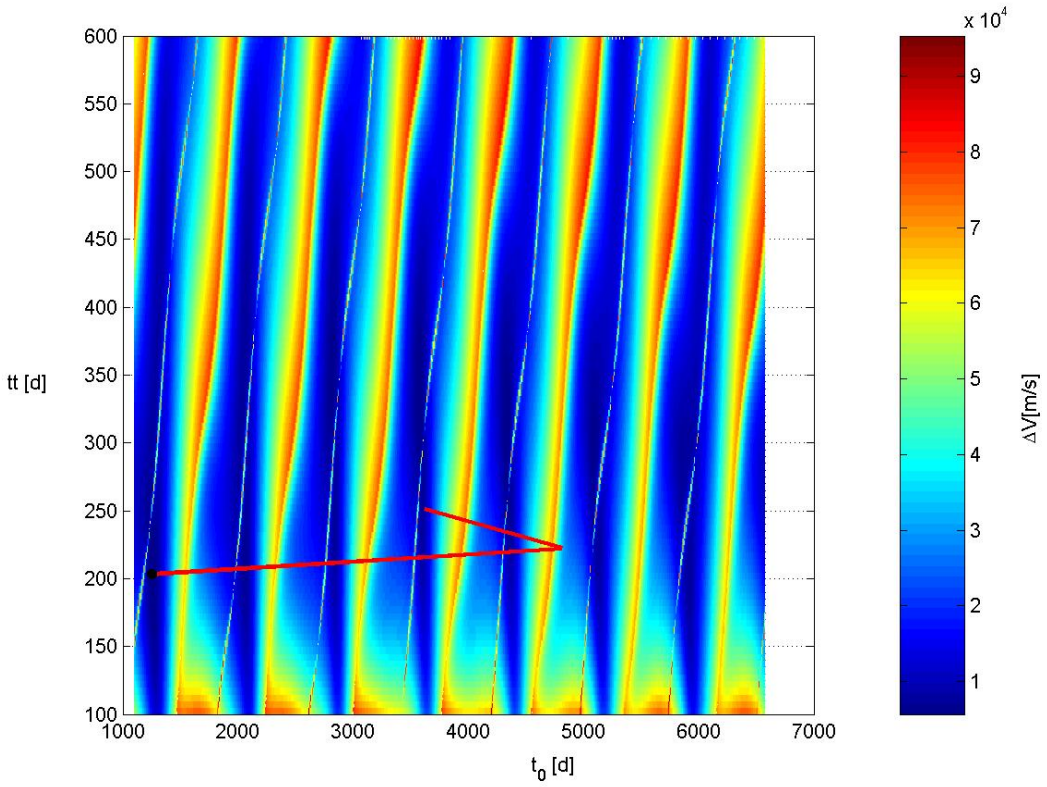

Figure 153: History of the solution during the optimization run corresponding to the best identified solution.

glbSolve

As glbSolve algorithm implements a deterministic optimization approach, statistical characteristics are not needed in this case. Only one run have been processed in order to solve the previously defined problem. Default options suggested by the providers of the code have been used. As the 2-impulse direct planet-to-planet transfer has low complexity features, we used a maximum number of iterations equal to 100.

Algorithm parameters	
Maximum number of iterations:	100

Table 58 and Table 59 report the identified solution compared with the best known solution.

Search space		
Design variable	**Identified solution**	**Best known solution**
Date of departure [*d*]:	5087.669	1253.510
Transfer time [*d*]:	309.881	203.541

Table 58: Comparison between the identified solution and the best known solution: search space.

Objective function space		
Term	**Identified solution**	**Best known solution**
ΔV [*m/s*]:	6406.750	5678.904
ΔV_I [*m/s*]:	3101.076	2999.464
ΔV_F [*m/s*]:	3305.674	2679.439

Table 59: Comparison between the identified solution and the best known solution: objective function space.

The previous tables show that the identified solution doesn't coincide in fact with the best known one, as Figure 154 fairly illustrates.

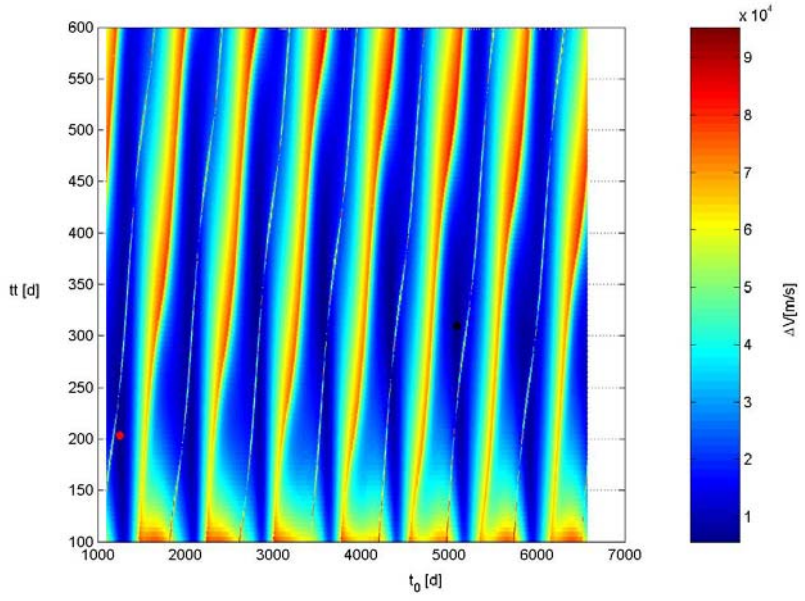

Figure 154: Comparison between the solution identified by *glbSolve* (black dot) and the best known one (red dot).

Table 60 reports the characteristics of the identified solution, which will be used for comparisons with the other optimization algorithms.

Evaluation criterion	Criterion value
ΔV [*m/s*]:	6406.750
Model function evaluations:	565
Runtime [STU]:	$3.845 \cdot 10^{-3}$

Table 60: Characteristics of the identified solutions.

One of the output of glbSolve is the matrix of all rectangle center points sampled during the whole optimization run. By means of this matrix one can analyse the ability of glbSolve in exploring the whole search space: Figure 155 shows the distribution of the sampled points over the search space.

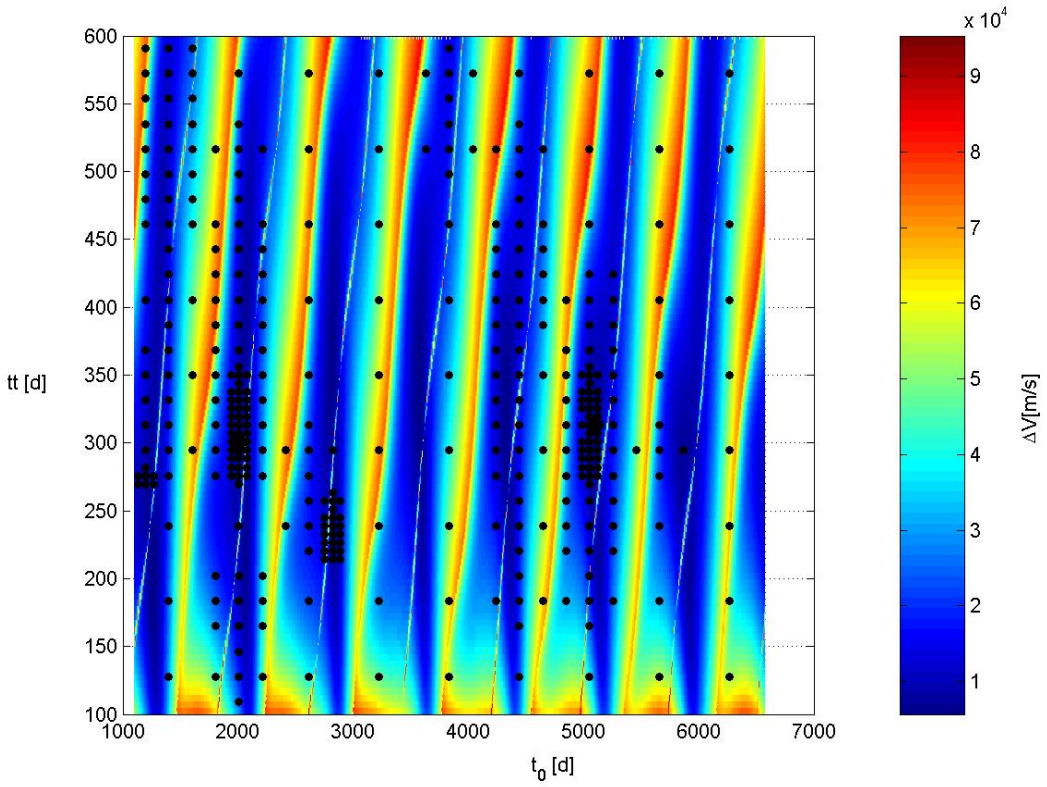

Figure 155: Distribution of all rectangle center points sampled during the whole optimization run.

Figure 155 shows that, even if glbSolve algorithm explored the neighbourhood of different local minima, it wasn't able to identify and explore the basin of attraction of the best known solution. The exploration of the basin of attraction of different local minima is fairly illustrated in Figure 156, where the objective function values corresponding to each rectangle center point are reported: the 565 sampled points are ordered along the x-axis from the first rectangle center point sampled during the optimization process to the final one.

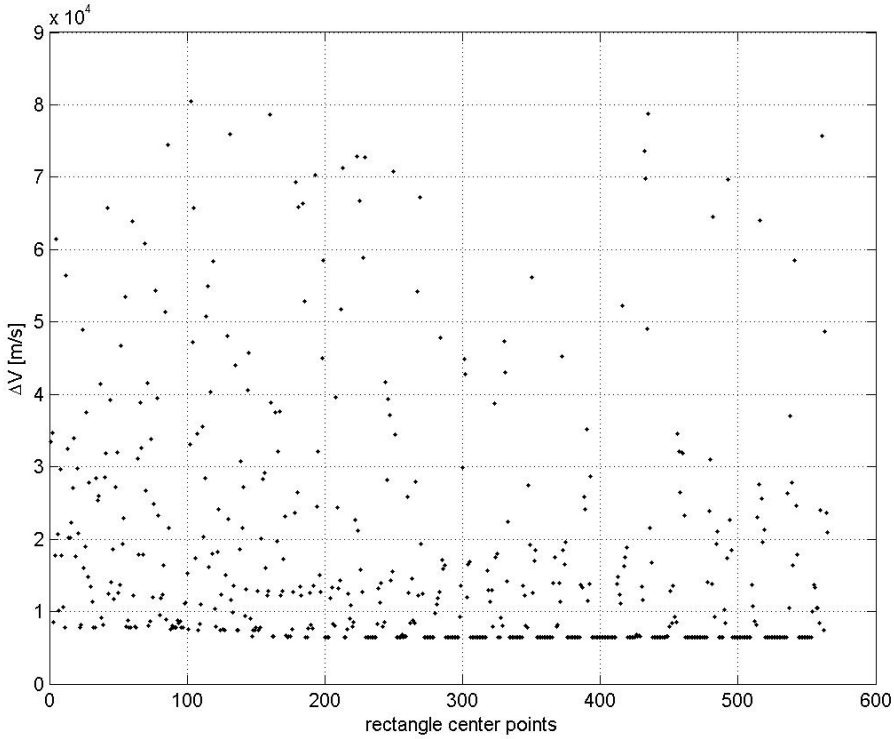

Figure 156: Objective function values corresponding to each rectangle center point.

Figure 156 confirms that at the beginning of the optimization process glbSolve algorithm could get worse local optima solution (see also Figure 157 which reports the first 140 sampled points and Figure 158 which reports the last 425 ones).

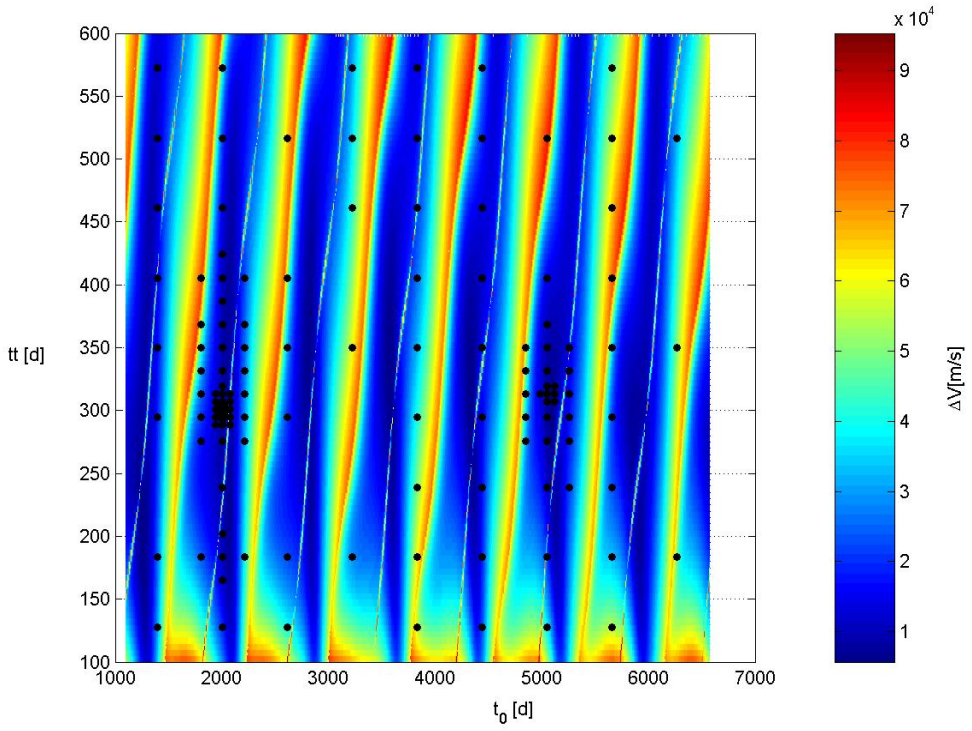

Figure 157: Distribution of the first 140 rectangle center points sampled during the whole optimization run.

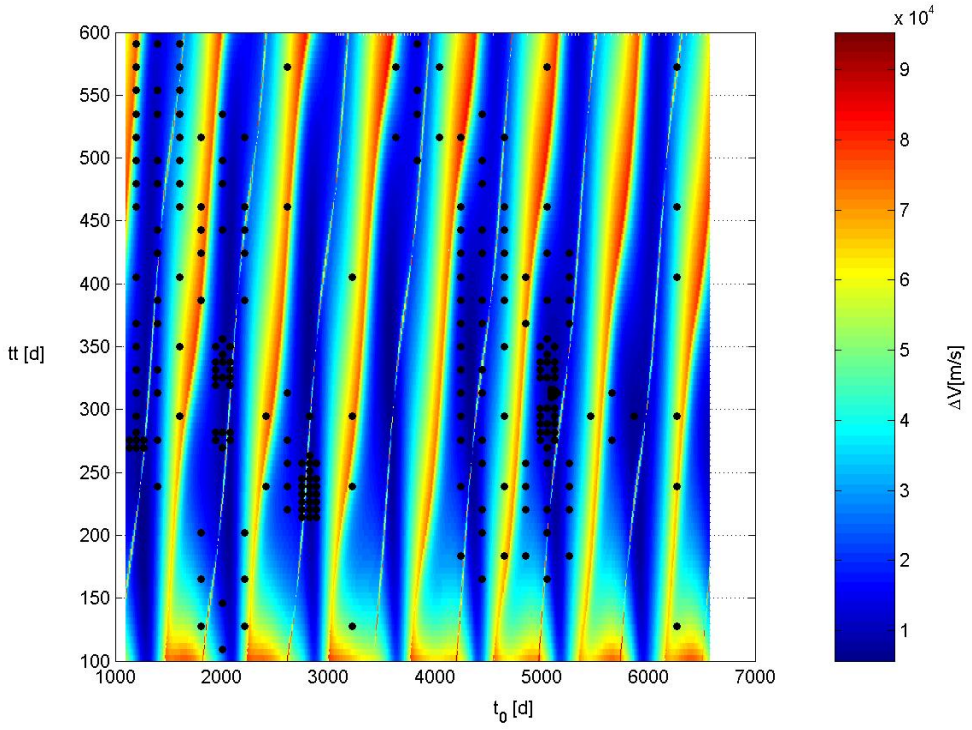

Figure 158: Distribution of the last 425 rectangle center points sampled during the whole optimization run.

MCS

As MCS algorithm implements a deterministic optimization approach, only one run have been processed in order to solve the previously defined problem. Default options suggested by the providers of the code have been used. We used a maximum number of objective function evaluation equal to 5000.

Algorithm parameters	
Maximum number of objective function evaluations:	5000

Table 61 and Table 62 report the identified solution compared with the best known solution.

Search space		
Design variable	**Identified solution**	**Best known solution**
Date of departure [*d*]:	1253.509	1253.510
Transfer time [*d*]:	203.542	203.541

Table 61: Comparison between the identified solution and the best known solution: search space.

Objective function space		
Term	**Identified solution**	**Best known solution**
ΔV [*m/s*]:	5678.903	5678.904
ΔV_I [*m/s*]:	2999.464	2999.464
ΔV_F [*m/s*]:	2679.440	2679.439

Table 62: Comparison between the identified solution and the best known solution: objective function space.

The previous tables show that the identified solution coincides with the best known one.

Table 63 reports the characteristics of the identified solution, which will be used for comparisons with the other optimization algorithms.

Evaluation criterion	Criterion value
ΔV [*m/s*]:	5678.903
Model function evaluations:	640
Runtime [STU]:	$1.019 \cdot 10^{-2}$

Table 63: Characteristics of the identified solutions.

Although MCS algorithm is a global optimization algorithm, it has the important feature of keeping, in a so called “shopping basket”, good points reached during the optimization process. Figure 159 illustrates the whole shopping basket kept by MCS in the simple case of the two impulse direct planet-to-planet transfer problem.

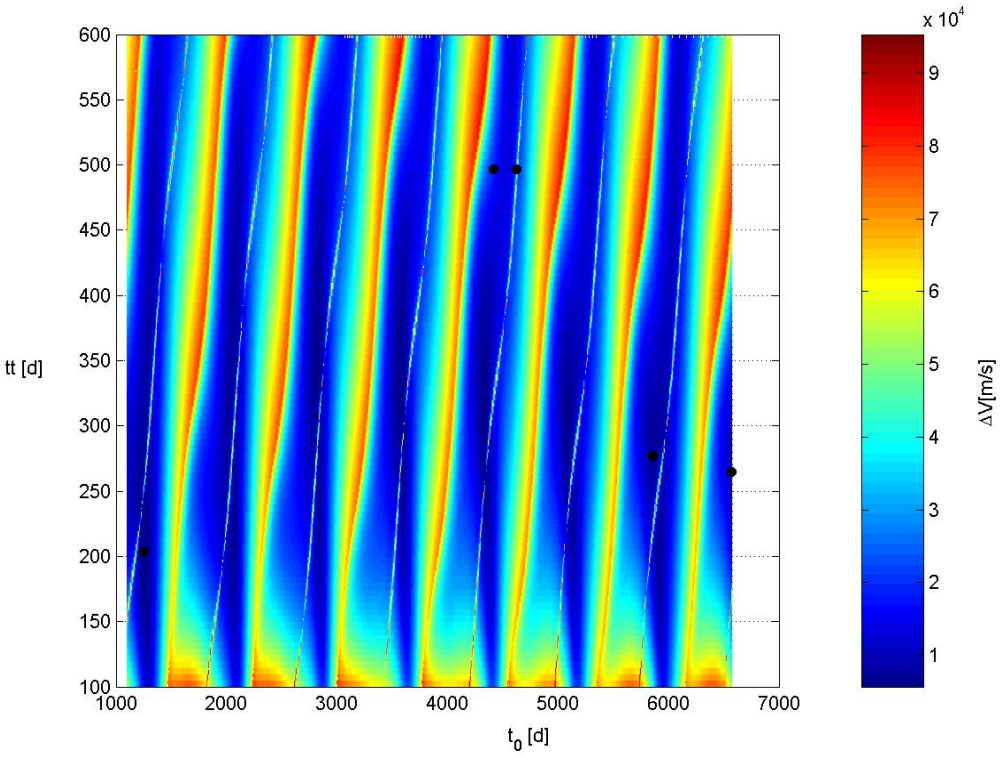

Figure 159: Shopping basket at the end of the optimization process.

Besides the global optimum, which has been get with good performances (see Table 63), the shopping basket contain information about the basin of attraction of some local optima.

rbfSolve

As rbfSolve algorithm implements a deterministic optimization approach, based on objective function response surfaces assessment and analysis suitable for costly objective function problems, statistical features analysis do not hold here. Only one run has been processed in order to solve the previously defined problem. Default options suggested by the providers of the code have been used. It is worth noting that, as already stated in the description of this optimization tool, the termination conditions available in TOMLAB version of rbfSolve tool (which is not freely available) do not include suitable rules for practical problems with not a priori information about the global optimum solution. As a consequence, a maximum number of objective function evaluations has been fixed for terminating the optimization process; the maximum value has been set based on the order of magnitude of the objective function evaluations resulting from the application of the previously analysed tools. In particular, in case of the 2-impulse direct planet-to-planet interplanetary transfer, a maximum value of 2500 objective function evaluations has been imposed.

Algorithm parameters	
Maximum number of objective function evaluations:	2500

However, a particular exit condition terminated the optimization process, which typically happens when the approximating surface generated by the algorithm can not improve due to the generation of successive identical solutions for improving the interpolation surface; the maximum number of successive identical solutions is automatically set by rbfSolve algorithm once used the default options.

Anyway, Table 64 and Table 65 report the identified solution compared with the best known solution.

Search space		
Design variable	**Identified solution**	**Best known solution**
Date of departure [*d*]:	3573.380	1253.510
Transfer time [*d*]:	324.312	203.541

Table 64: Comparison between the identified solution and the best known solution: search space.

Objective function space		
Term	**Identified solution**	**Best known solution**
ΔV [*m/s*]:	5684.196	5678.904
ΔV_I [*m/s*]:	3244.820	2999.464
ΔV_F [*m/s*]:	2439.377	2679.439

Table 65: Comparison between the identified solution and the best known solution: objective function space.

The previous tables show that the identified solution does not coincide with the best known one, as Figure 160 fairly illustrates: rbfSolve could not identify the basin of attraction of the best known solution.

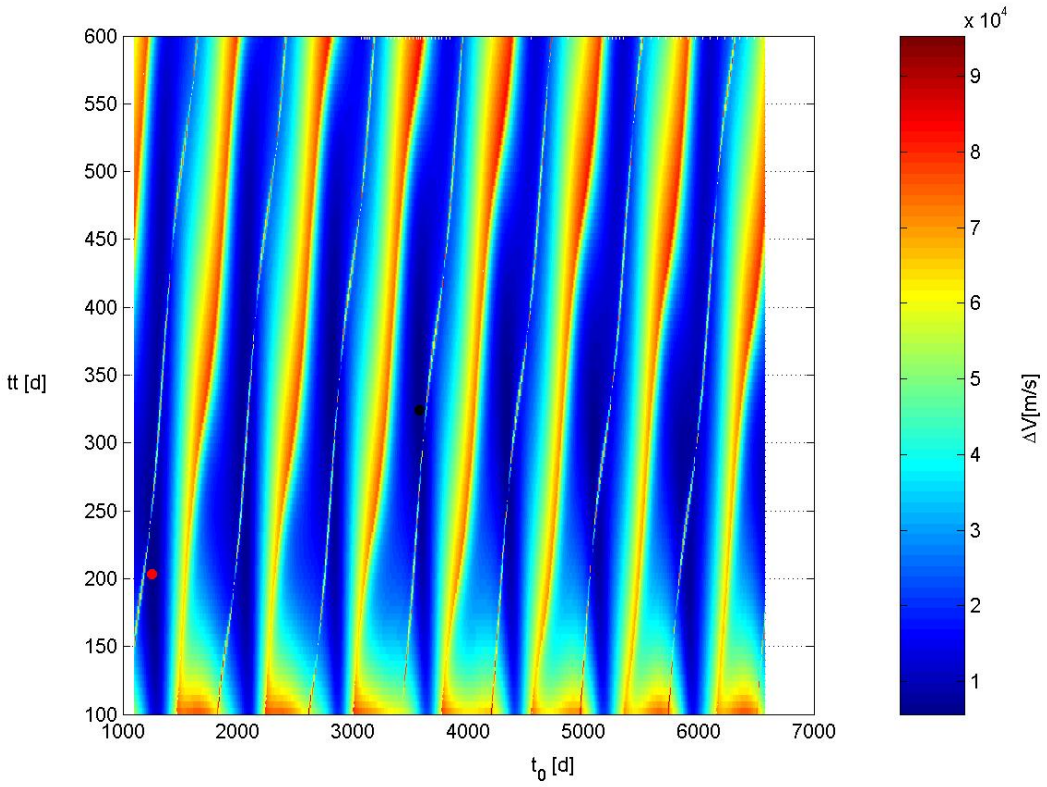

Figure 160: Comparison between the solution identified by *rbfSolve* (black dot) and the best known one (red dot).

Table 66 reports the characteristics of the identified solution, which will be used for comparisons with the other optimization algorithms.

Evaluation criterion	Criterion value
ΔV [*m/s*]:	5684.196
Model function evaluations:	953
Runtime [STU]:	30.878

Table 66: Characteristics of the identified solutions.

One of the output of the optimization process is the matrix of all sampled points in the search space, which are shown in Figure 161

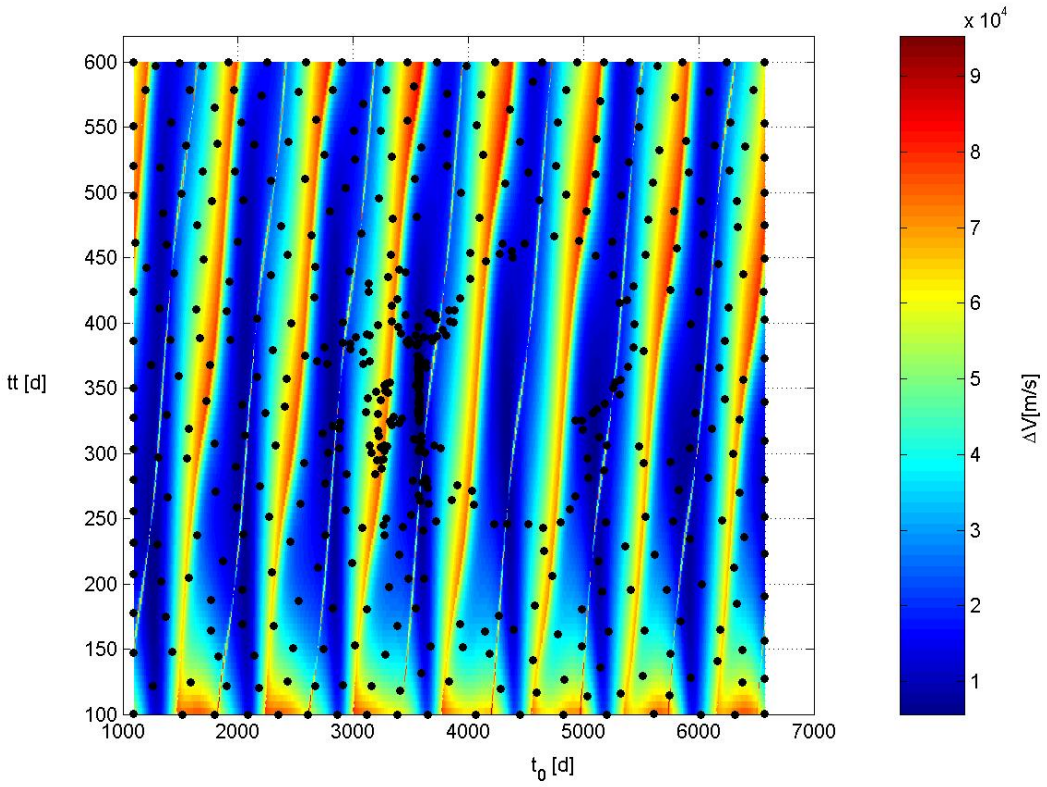

Figure 161: Distribution of all sampled points during the optimization process.

The algorithm do not accurately sample the region of the search space near the global optimum solution. Note that the objective function model has discontinuities in the search space: the global optimization algorithms based on response surface methodologies have well-known difficulties in handling such objective function structure, as confirmed in this simple test: the sampled points made the algorithm converging to a good approximation of the objective function structure in the neighbourhood of the identified local minimum.

Summary of results:

Table 67 reports the summary of results for the two impulse direct planet-to-planet transfer problem in a tabular form.

Algorithm	ΔV [*m/s*]	Fun. evaluations	Runtime [STU]
GAOT	5741.524 (σ = 163.525)	1270.5 (σ = 345.683)	$8.198 \cdot 10^{-3}$ ($\sigma = 3.306 \cdot 10^{-3}$)
GAOT-shared	6420.207 (σ = 574.22)	590.4 (σ = 320.35)	$4.907 \cdot 10^{-3}$ ($\sigma = 2.776 \cdot 10^{-3}$)
GATBX	5740.887 (σ = 177.082)	2322 (σ = 424.075)	$1.037 \cdot 10^{-2}$ ($\sigma = 4.405 \cdot 10^{-3}$)
GATBX-migr	5679.957 (σ = 2.191)	2650 (σ = 909.799)	$1.646 \cdot 10^{-2}$ ($\sigma = 6.529 \cdot 10^{-3}$)
FEP	5711.337 (σ = 95.13)	2478.9 (σ = 953.829)	$2.463 \cdot 10^{-2}$ ($\sigma = 9.004 \cdot 10^{-3}$)
DE	5986.674 (σ = 408.679)	828.3 (σ = 319.692)	$3.019 \cdot 10^{-3}$ ($\sigma = 1.098 \cdot 10^{-3}$)
ASA	6328.291 (σ = 1330.247)	1289.7 (σ = 56.555)	$3.814 \cdot 10^{-3}$ ($\sigma = 1.555 \cdot 10^{-4}$)
GlbSolve	6406.75	565	$3.845 \cdot 10^{-3}$
MCS	5678.903	640	$1.019 \cdot 10^{-2}$
RbfSolve	5684.196	953	30.878
EPIC *(1)	6000.190 (σ = 456.57)	315 (σ = 8.4)	-
EPIC *(2)	5679.1 (σ = 0.579)	2040 (σ = 21)	-

Table 67: Summary of results for the two impulse direct planet-to-planet transfer problem.

Notes:

*(1) : test performed with a 10 individuals population, of which 5 converging within 300 cycles
*(2) : test performed with a 20 individuals population, of which 10 converging within 300 cycles

Note that the performance criteria we have measured are in fact partially conflicting: the most evident example is the trade off between the global optimum solution reached at the end of the optimization process and the number of the objective function evaluations or the runtime needed to reach it.

As proposed in earlier works [Pintér, 1995], concepts and techniques typically adopted in multiobjective optimization problems (such as the concept of the Pareto dominance) can be here used in order to gain valuable insights regarding the comparative strengths and weaknesses of optimization algorithms. As stated above, due to the presence of not optimized codes among the tested ones and to the necessity of creating a MEX file for ASA algorithm (which slightly affects the runtime performances), the main evaluation criteria to be considered have been taken as the best objective function value reached, ΔV, and the number of model function evaluations needed, *nFunc*. Figure162 reports such performances in a ΔV - *nFunc* plane in order to identify the Pareto optimal solution (the red line in figure representing the best known solution).

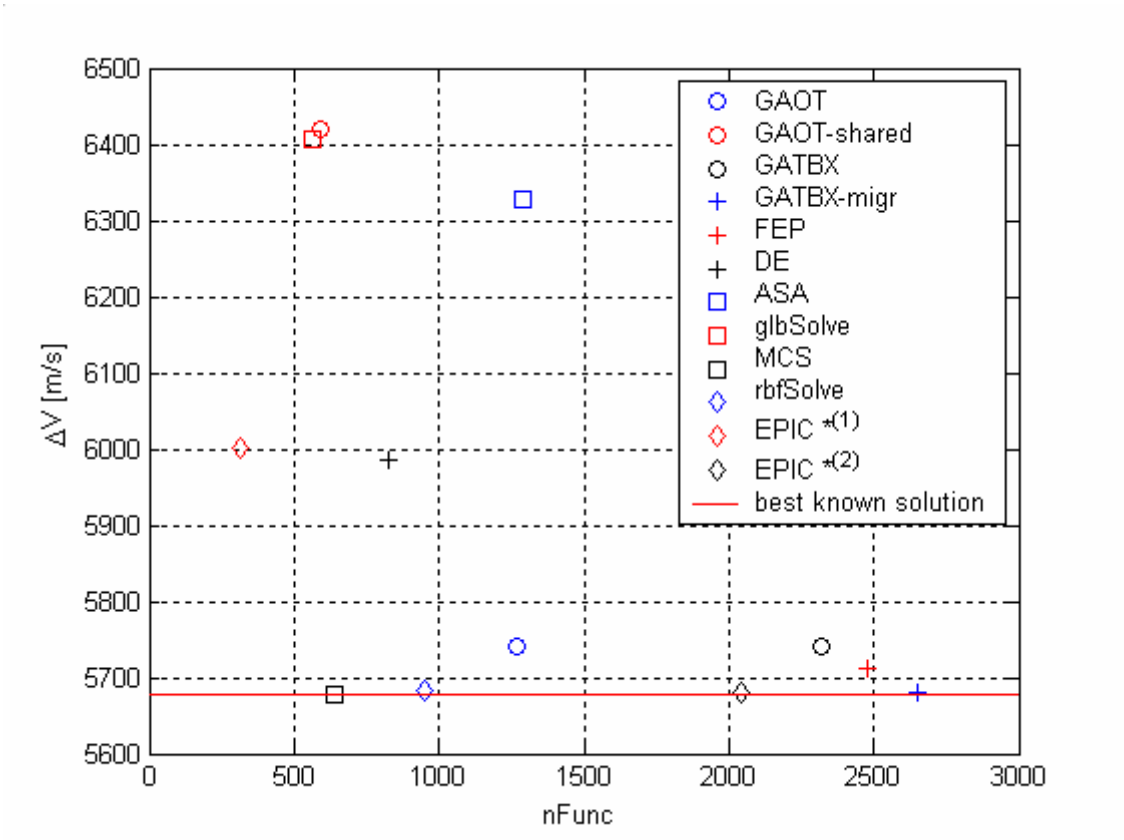

Figure 162: Algorithms performances in the ΔV - *nFunc* plane.

Note that Figure 162 reports the performances listed in Table 67, which contains statistical performances in case of randomized optimization algorithms. By applying the concepts of Pareto dominance, Table 68 reports for each

algorithm, the number of algorithms which dominated (and then outperformed) it.

Algorithm	# of dominating algorithms
GAOT	2
GAOT-shared	1
GATBX	2
GATBX-migr	1
FEP	2
DE	1
ASA	4
glbSolve	0
MCS	0
rbfSolve	1
EPIC $*^{(1)}$	0
EPIC $*^{(2)}$	1

Table 68: Number of dominating algorithms.

Table 68 shows that the set of Pareto optimal solutions includes in fact two solutions: the algorithms which best solved the 2-impulse direct planet-to-planet transfer problem (in a Pareto optimal sense) are EPIC$^{*(1)}$ and MCS, the performances of which are highlighted in Figure 163.

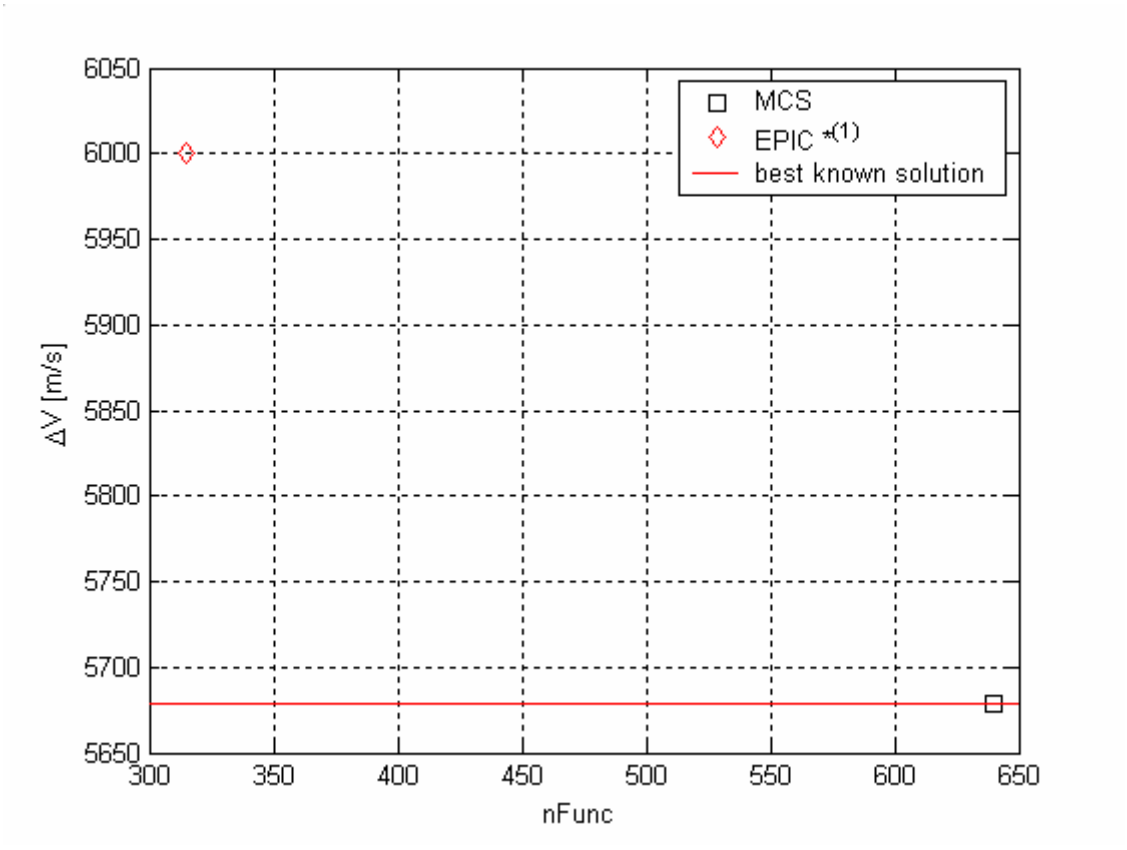

Figure 163: Pareto optimal algorithms.

However, we must take care of the fact that EPIC$^{*(1)}$ could not reach in fact the global optimum solution, but a local one in 50% of the cases. Moreover, it is interesting to observe the improvement gained by MCS algorithm compared with the performances of the more classic globSolve tool: MCS and globSolve algorithms have been both inspired by DIRECT method for global optimization [Jones et al., 1993]; however, unlike the globSolve algorithm, MCS uses a branching method which allow for a more irregular splitting procedure. As can be noted from Figure 162, the MCS approach led to evident improvements in the effectiveness at identifying the basin of attraction of the best known solution in the 2-impulse direct planet-to-planet transfer problem, making the algorithm performances less dependent on the upper lower bounds, especially referring to design variables associate to objective function periodicities. Moreover, it is interesting to highlight again the effects of the sharing operator on the GAOT performances: indeed, as stated above, by promoting the diversity of the individuals in the population, the GAOT – shared algorithm hinders the

concentration of the individuals around the optimal solutions. This can lead to low accuracy at describing the optimum solutions and to a premature optimization process arrest because the stopping criteria easily become active. These consequences can obviously be applied to the interpretation of the results in Figure 162, where GAOT-shared performances correspond to higher mean objective function value reached at the end of the optimization process but lower number of objective function evaluations, although both algorithms could find the basin of attraction of the best known solution in a comparable number of runs (4/10 for GAOT compared with 3/10 for GAOT-shared). It is worth noting that all the achieved results are strictly affected by the stopping criterion used: as an example, letting GAOT – shared evolving for a number of objective function evaluations greater than the value obtained with the here considered stopping criterion may lead to more effectiveness in finding the global optimum. However, the effects of the stopping criteria on the algorithm performances are not addressed here, where the algorithms are used as black-box tools. Finally the performances of all algorithms in identifying the basin of attraction of the best known solution are reported in Table 69 (note that for randomized algorithms the number of successful runs over the total number of performed runs is reported).

Algorithm	Success
GAOT	4/10
GAOT-shared	3/10
GATBX	3/10
GATBX-migr	8/10
FEP	7/10
DE	3/10
ASA	5/10
glbSolve	No
MCS	Yes

rbfSolve	No
EPIC *(1)	5/10
EPIC *(2)	10/10

Table 69: Algorithms performance in identifying the basin of attraction of the best known solution.

Table 69 shows that, unlike a relatively high mean number of objective function evaluations necessary to the global optimization process, GATBX-migr turned out to have the highest rate of success in reaching the basin of attraction of the best known solution if compared with other randomized optimization algorithms in case of the 2-impulse direct planet-to-planet transfer problem, thus showing a relatively robustness in performing a global search. Similar performances have been obtained by FEP tool, where 7/10 runs were successful and a slightly lower mean number of objective function evaluations with respect to GATBX-migr was required. However, note that MCS algorithm, which is based on a deterministic approach, identified the global optimum (and non a local one, as in glbSolve case) in a deterministic way (which corresponds to a probability of success equal to 100%) in a lower number of objective function evaluations with respect the other algorithms. We can then conclude that, in the simple case of 2-impulse direct planet-to-planet transfer problem, the MCS algorithm have shown to be the best performing one.

8. MULTIPLE GRAVITY ASSIST INTERPLANETARY TRANSFER

Problem class statement:

Interplanetary transfer description	
Multiple gravity assist interplanetary transfer from Earth to Saturn via Venus-Venus-Earth-Jupiter gravity assist manoeuvres (referred to Cassini-Huygens space trajectory)	
Objective function assessment	
Objective function:	$\Delta V = \Delta V_I + \Delta V_{GA,P}s + \Delta V_F$ where: • ΔV_I is the magnitude of the relative velocity at the beginning of the interplanetary transfer phase. • $\Delta V_{GA,P}s$ are the magnitudes of the minimum corrective ΔVs at each gravity assist manoeuvre corresponding to planet *P*, $\Delta V_{GA,P}$, which is necessary to link two consecutive interplanetary transfer arcs resulting from the Lambert's problem formulation. • ΔV_F is the magnitude of the velocity variation necessary to reach the insertion orbit at Saturn, ΔV_F.

Mathematical models:	• Restricted 2-body dynamical model (C^2 in the whole solution space except in the origin) • Three dimensional motion • Analytical ephemeris model (generated by time polynomial series of the orbital elements) • Linked-conic approximation for gravity assist manoeuvres • Impulsive corrective manoeuvres for matching input and output velocity conditions at each gravity assist • Impulsive manoeuvres (i.e. instantaneous variations in velocity) • Lambert's problem formulation (Battin's algorithm for the problem solution: singular for π and 2 π transfer angles)

Search space, *D*, characterization

Number of design variables:	6
Design Variables:	• Date of departure from Earth, t_0 • Transfer time from Earth to Venus, tt_{E-V} • Transfer time from Venus to Venus, tt_{V-V} • Transfer time from Venus to Earth, tt_{V-E} • Transfer time from Earth to Jupiter, tt_{E-J} • Transfer time from Jupiter to Saturn, tt_{J-S}
Topology:	Continuous variables $\Rightarrow D \subset \Re^6$

Constraints

Constraints typology:	Box constraints
Box intervals:	• t_0 included in a 5 years period centred in the 1st January 1999 (including the date of departure of Cassini-Huygens mission, 15th October 1997). • $tt_{E-V} \in [0.1,2] \cdot H_{E-V} = [14.59, 291.83] d$, where H_{E-V} is the Homann transfer time corresponding to the linking arc Earth-Venus. • $tt_{V-V} \in [0.1,2] \cdot T_V = [11.23,448.92] d$, where T_V is the period of Venus orbit. • $tt_{V-E} \in [0.1,1] \cdot H_{V-E} = [14.592,145.92] d$, where H_{V-E} is the Homann transfer time corresponding to the linking arc Venus-Earth. • $tt_{E-J} \in [0.1,1] \cdot H_{E-J} = [99.65, 996.54] d$, where H_{E-J} is the Homann transfer time corresponding to the linking arc Earth-Jupiter. • $tt_{J-S} = [0.1,1] \cdot H_{J-S} = [365.02, 3650.2] d$, where H_{J-S} is the Homann transfer time corresponding to the linking arc Jupiter-Saturn.

General considerations	
Objective function analysis:	The objective function is almost everywhere C^2, locally discontinuous in a countable number limited set
Problem complexity:	High
Search space normalization:	The search space is normalized by means of the upper-lower bounds in order to be an unit hypercube $\Rightarrow D \equiv [0,1]^6$

Number of global optima: A priori unknown.

The following best known solution has been gained by means of a multi-start search, which implement a local search process via SQP algorithm starting from 1000 random first guess solutions uniformly distributed over the search space (each one requiring a number of objective function evaluations of the order of 10^3).

Search space	
Date of departure:	20/11/1997
Earth-Venus transfer time:	179.14 *d*
Venus-Venus transfer time:	406.53 *d*
Venus-Earth transfer time:	53.18 *d*
Earth-Jupiter transfer time:	758.33 *d*
Jupiter-Saturn transfer time:	3650.2 *d*

Objective space	
ΔV :	6368.2 *m/s*
ΔV_I :	3888.0 *m/s*
1st $\Delta V_{GA,V}$	2032.7 *m/s*
2nd $\Delta V_{GA,V}$:	0.0327 *m/s*
$\Delta V_{GA,E}$:	0.0057 *m/s*
$\Delta V_{GA,J}$:	0.0078 *m/s*
ΔV_F :	447.400 *m/s*

It is worth pointing out that a family of alternative solutions have been found which, although possessing little bit higher overall ΔV values, require considerable shorter transfer times. A representative solution of this family is described in the following table.

Search space	
Date of departure:	25/10/1997
Earth-Venus transfer time:	206.38 *d*
Venus-Venus transfer time:	401.21 *d*
Venus-Earth transfer time:	54.52 *d*

Earth-Jupiter transfer time:	548.84 *d*
Jupiter-Saturn transfer time:	1747.90 *d*

Objective space	
ΔV :	7154.6 *m/s*
ΔV_I :	5756.2 *m/s*
1st $\Delta V_{GA,V}$	883.54 *m/s*
2nd $\Delta V_{GA,V}$:	0.0283 *m/s*
$\Delta V_{GA,E}$:	2.3098 *m/s*
$\Delta V_{GA,J}$:	0.0056 *m/s*
ΔV_F :	512.52 *m/s*

Number of local optima: A priori unknown.

Hardware platform:

Intel Pentium 4 – 3.06GHz laptop.

Operating system:

Microsoft Windows XP

Home edition

Version 2002

Service Pack 1

Timings:

The Standard Unit Time (see Dixon & Szegö, 1978) has been measured.

Performances:

In the following pages, the performances of each global optimization tool in solving the Multiple Gravity Assist interplanetary transfer from Earth to Saturn via Venus-Venus-Earth-Jupiter gravity assist manoeuvres are reported. The evaluation criteria will be mainly based on the analysis of the optimal solution reached and the number of the required model function evaluations. Due to the presence of not optimized codes among the tested ones, timing will not be considered as a main evaluation criterion.

GAOT

As GAOT implements a genetic algorithm, we report the statistical characteristic, typically considered in case of randomized solution methods. Ten run have been processed in order to solve the previously defined problem. Default options suggested by the providers of the code have been used in all the runs: note that by tuning the algorithm parameters one may improve the performance of the solvers, but, due to the comparative purposes of this work, the tuning effects have not been considered. As the Multiple Gravity Assist interplanetary transfer shows high complexity features, we used 100 individuals evolving for a maximum number of generations equal to 1000.

Algorithm parameters	
Number of individuals:	100
Maximum number of generations:	1000

Table 70 reports the best identified solution compared with the best known solution in terms of the values of the design variables and of the objective

function terms, while Figure 164 plots the resulting interplanetary transfer trajectories.

	Best identified solution	**Best known solution**
t_0 :	-791.277 *d*	-770.686 *d*
tt_{E-V} :	191.670 *d*	179.524 *d*
tt_{V-V} :	408.6 *d*	406.528 *d*
tt_{V-E} :	57.888 *d*	53.181 *d*
tt_{E-J} :	753.46 *d*	758.334 *d*
tt_{J-S} :	3625.9 *d*	3650.218 *d*
ΔV :	6706.599 *m/s*	6367.990 *m/s*
ΔV_I :	4291.287 *m/s*	3901.332 *m/s*
1st $\Delta V_{GA,V}$:	1712.691 *m/s*	2019.210 *m/s*
2nd $\Delta V_{GA,V}$:	250.044*m/s*	0.018 *m/s*
$\Delta V_{GA,E}$	0.425 *m/s*	0.005 *m/s*
$\Delta V_{GA,J}$	4.611 *m/s*	0.022 *m/s*
ΔV_F :	447.541 *m/s*	447.402 *m/s*

Table 70: Comparison between the best identified solution and the best known solution.

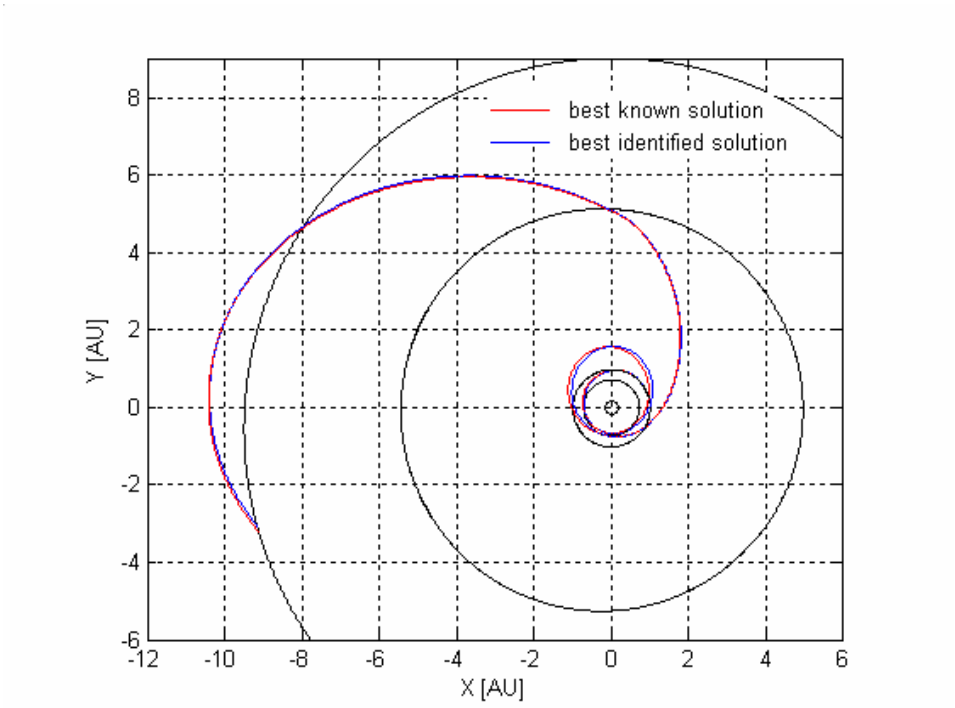

Figure 164*: GAOT:* Comparison between the best identified solution and the best known solution.

Table 70 and Figure 164 show that the best solution identified by GAOT algorithm is close to the best known one: differences in the values of the design variables are of the order of 10 days. This can be better illustrated as shown in the following: as stated above, the search space has been normalized to a unit six-dimensional hypercube for the global search process; Table reports the best identified solution and the best known solution in the normalized search space.

	t_0	tt_{E-V}	tt_{V-V}	tt_{V-E}	tt_{E-J}	tt_{J-S}
Best identified solution	0.266	0.639	0.908	0.330	0.729	0.993
Best known solution	0.278	0.594	0.903	0.294	0.734	1.000

Table 71*:GAOT*: Comparison between the best identified solution and the best known solution in the normalized search space.

Differences in the values of the design variables in the normalized search space have a maximum value of 10^{-2}. The Euclidean distance between the two solutions in the normalized search space is equal to $5.970 \cdot 10^{-2}$, showing their relative closeness. Note that, although these relative little differences in the search space, the objective function values are quite different, especially if each single terms are compared: this highlights the high sensitivity of the objective function with respect to the values of the design variables. The closeness of the two solutions corresponding to the low Euclidean distance, and, in particular, the low difference in the value of the date of departure, let us suppose that, although GAOT algorithm couldn't be able to reach the best known solution accurately, it could get its basin of attraction: actually, genetic algorithms are known as an effective tool for fast reaching the basin of attraction of good solutions, while showing poor converge performances in locally searching and accurately describing the corresponding local minimum; this is the reason why local search processes via gradient based search algorithms are often performed after the genetic algorithm based global search phase. In fact, given the best solution identified by GAOT (reported in Tabe 70) and considering it as the starting point for a local search process performed by an SQP algorithm, an improved best identified solution is identified which almost coincide with the best known solution, as shown in Table 72.

	Best identified solution + SQP	**Best known solution**
t_0:	-770.67 *d*	-770.686 *d*
tt_{E-V}:	179.5 *d*	179.524 *d*
tt_{V-V}:	406.56 *d*	406.528 *d*
tt_{V-E}:	53.175 *d*	53.181 *d*
tt_{E-J}:	758.35 *d*	758.334 *d*
tt_{J-S}:	3650.2 *d*	3650.218 *d*
ΔV:	6373.258 *m/s*	6367.990 *m/s*
ΔV_I:	3900.226 *m/s*	3901.332 *m/s*

1^{st} $\Delta V_{GA,V}$:	2016.687 *m/s*	2019.210 *m/s*
2^{nd} $\Delta V_{GA,V}$:	0.723 *m/s*	0.018 *m/s*
$\Delta V_{GA,E}$	8.203 *m/s*	0.005 *m/s*
$\Delta V_{GA,J}$	0.004 *m/s*	0.022 *m/s*
ΔV_F :	447.415 *m/s*	447.402 *m/s*

Table 72: Comparison between the best solution identified by GAOT improved by a SQP based local optimization process and the best known solution (number of function evaluations required by the local optimization process equal to 410).

Then, Table 72 shows that GAOT algorithm was able to reach the basin of attraction of the best known solution in one optimization run at least. Let now analyse the statistical values of GAOT performances. Figure 165 shows the distribution of the solutions resulting from each optimization run over the plane of the objective function, ΔV, and the number of function evaluations, *nFunc.*, while Table 73 reports the statistical characteristics, which will be used for comparisons with the other optimization algorithms, as well as the performances corresponding to the best identified solution.

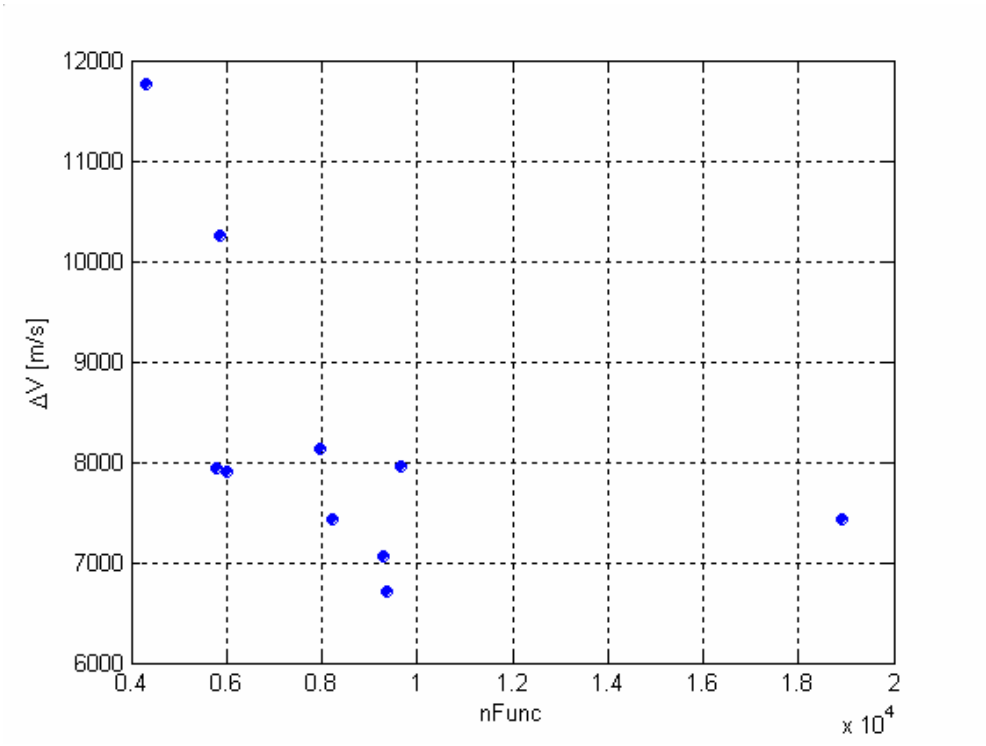

Figure 165: Distribution of the solutions resulting from each GAOT optimization run over the $nFunc - \Delta V$ plane.

Evaluation criterion	Mean value	Standard deviation	Best identified solution
ΔV :	8256.416 *m/s*	1555.107 *m/s*	6702.724 *m/s*
nFunc.:	8543.400	4075.382	9380
Runtime [STU]:	$1.883 \cdot 10^{-1}$	$9.683 \cdot 10^{-2}$	$1.986 \cdot 10^{-1}$

Table 73: Statistical characteristics of the identified solutions.

Figure 165 and Table 73 show that the resulting optimum ΔV values corresponding to the ten runs are distributed over the objective function space with a standard deviation that is in fact of the same order of magnitude of the mean value of the distribution itself. Such result can be due to the identification of different local minima; but it can turn out even if the optimal solutions lie in the basin of attraction of the same local minimum, due to the high objective function sensitivity with respect to the design variables. As a consequence, estimating the number and features of the distinct local minima reached by means of the ten runs would be particularly interesting. Moreover, it is worth noting that such an analysis will allow the estimation of the number of runs which have been able to reach the basin of attraction of the global optimum, which in fact can be considered as a success index in performing the optimization process. To attain such a task, the optimal solutions corresponding to all ten runs have been used as starting solutions for ten local optimization processes in order to accurately estimate the local minimum corresponding to the basin of attraction each optimal solution belong to. The consequences of the local optimization processes in the *nFunc* - ΔV plane are shown in Figure 166 where each improved solution is linked to the corresponding starting one by means of a straight line.

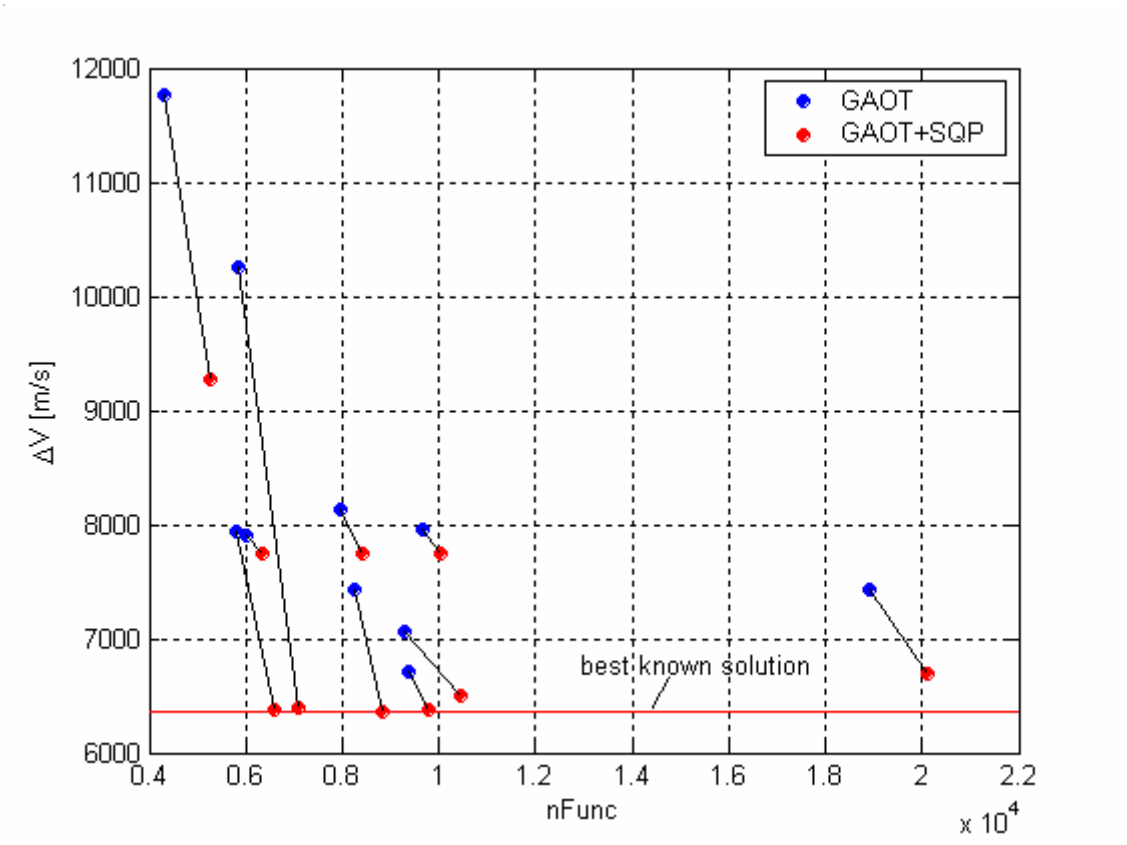

Figure 166: Comparison between solutions resulting from GAOT runs and their improvements by means of a further local optimization process via SQP algorithm over the $nFunc - \Delta V$ plane.

Figure 166 shows that different local minima corresponds to GAOT runs. In order to estimate the number of identified solutions which lie in the basin of attraction of the best known solutions, let investigate the solutions in the normalized search space. Table 74 reports, corresponding to each GAOT+SQP run, the reached objective function value and the distance (in Euclidean metric) with respect to the best known solution.

Mean value	ΔV [m/s]	Distance
run 1	6504.259	0.107
run 2	6396.589	0.021
run 3	6376.165	0.013
run 4	6698.965	0.160
run 5	6368.162	0.002
run 6	9271.339	0.670
run 7	7752.866	0.690
run 8	7753.058	0.690
run 9	7752.866	0.690
run 10	6369.524	0.001

Table 74: GAOT+SQP optimization runs: objective function values and Euclidean distance in the normalized search space with respect to the best known solution.

An empirical analysis suggest to define two solutions as identical when the Euclidean distance is less than 1% of the hyper diagonal of the normalized search space, that is 0.024. The consequence of such definition is that only runs 2, 3, 5 and 10 were able to get the best known solution, that is only 4/10 GAOT runs successfully identified the basin of attraction of the best known solution.

GAOT-shared

As GAOT-shared implements a genetic algorithm including a niching technique, we report again the statistical characteristics. Ten run have been processed in order to solve the previously defined problem. Default options suggested by the providers of the code have been used in all the runs. The threshold of dissimilarity, σ_S, for the sharing method and the shape parameter of the sharing function, α, have been set respectively to:

$\sigma_S = 0.1$

$\alpha = 1$

We used again a population of 100 individuals, evolving for a maximum number of generations equal to 1000.

Algorithm parameters	
Number of individuals:	100
Maximum number of generations:	1000

Tabke 75 reports the best identified solution compared with the best known solution in terms of the values of the design variables and of the objective function terms, while Figure 166 plots the resulting interplanetary transfer trajectories.

	Best identified solution	**Best known solution**
t_0:	-816.015 *d*	-770.686 *d*
tt_{E-V}:	186.627 *d*	179.524 *d*
tt_{V-V}:	432.194 *d*	406.528 *d*
tt_{V-E}:	73.904 *d*	53.181 *d*
tt_{E-J}:	805.177 *d*	758.334 *d*
tt_{J-S}:	2194.281 *d*	3650.218 *d*
ΔV:	14683.328 *m/s*	6367.990 *m/s*
ΔV_I:	3537.910 *m/s*	3901.332 *m/s*
1st $\Delta V_{GA,V}$:	1419.803 *m/s*	2019.210 *m/s*
2nd $\Delta V_{GA,V}$:	198.546 *m/s*	0.018 *m/s*
$\Delta V_{GA,E}$	5405.861 *m/s*	0.005 *m/s*
$\Delta V_{GA,J}$	3489.323 *m/s*	0.022 *m/s*
ΔV_F:	631.885 *m/s*	447.402 *m/s*

Table 75: Comparison between the best identified solution and the best known solution.

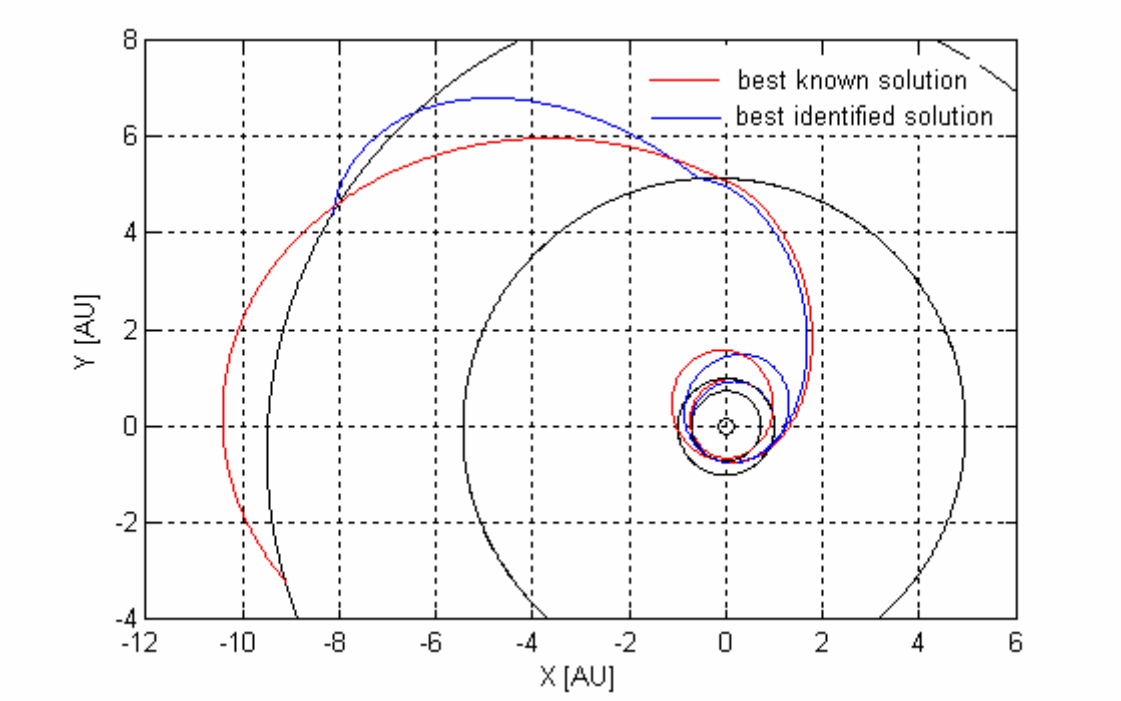

Figure 166*: GAOT-shared*: Comparison between the best identified solution and the best known solution.

By analysing Table 75 and Figure 166 differences in the values of the design variables of the order of 10 days can be recognized, except for the Jupiter-Saturn transfer time. A better evaluation of the closeness of the two solutions can be gained again by analysing them in the normalized search space, as shown in Table 76.

	t_0	tt_{E-V}	tt_{V-V}	tt_{V-E}	tt_{E-J}	tt_{J-S}
Best identified solution	0.253	0.621	0.962	0.452	0.787	0.557
Best known solution	0.278	0.594	0.903	0.294	0.734	1.000

Table 76*: GAOT-shared*: comparison between the best identified solution and the best known solution in the normalized search space.

Differences in the values of the design variables in the normalized search space are quite evident, as they assume a maximum value of 10^{-1}. The Euclidean distance between the two solutions in the normalized search space is equal to

4.783·10^{-1}. In analogy with the GAOT performance analysis, a local optimization process by means of a SQP algorithm is now performed. Given the best solution identified by GAOT-shared (reported in Table 75) and considering it as the starting point for the local search process, the improved best identified solution reported in Table 77 is identified.

	Best identified solution + SQP	**Best known solution**
t_0:	-771.089 *d*	-770.686 *d*
tt_{E-V}:	179.926 *d*	179.524 *d*
tt_{V-V}:	406.532 *d*	406.528 *d*
tt_{V-E}:	53.178 *d*	53.181 *d*
tt_{E-J}:	758.338 *d*	758.334 *d*
tt_{J-S}:	3650.218 *d*	3650.218 *d*
ΔV:	6368.116 *m/s*	6367.990 *m/s*
ΔV_I:	3915.716 *m/s*	3901.332 *m/s*
1st $\Delta V_{GA,V}$:	2004.478 *m/s*	2019.210 *m/s*
2nd $\Delta V_{GA,V}$:	0.496 *m/s*	0.018 *m/s*
$\Delta V_{GA,E}$	0.007 *m/s*	0.005 *m/s*
$\Delta V_{GA,J}$	0.015 *m/s*	0.022 *m/s*
ΔV_F:	447.404 *m/s*	447.402 *m/s*

Table 77: Comparison between the best solution identified by *GAOT-shared* improved by a SQP based local optimization process and the best known solution (number of function evaluations required by the local optimization process equal to 606).

Table 77 shows that GAOT-shared algorithm was able to reach the basin of attraction of the best known solution in the optimization run corresponding to the best identified solution. However, it is worth pointing out that very low accuracy characterizes the results achievable by *GAOT-shared*, as demonstrated by the high number of function evaluations required to the SQP optimization process to converge (606 objective function evaluations). This is due to the effects of

niching techniques: indeed, niching techniques promote diversity in the population and support the exploration of the search space; but, they avoid the concentration of the population around any local optimum which typically arises during the last phases of the optimization runs, when, once gained the basin of attraction, population evolves in order to only accurately describe the local minimum. Let now analyse the statistical values of GAOT-shared performances. Figure 167 shows the distribution of the solutions resulting from each optimization run over the plane of the objective function, ΔV, and the number of function evaluations, *nFunc*, while Table 78 reports the statistical characteristics, which will be used for comparisons with the other optimization algorithms, as well as the performances corresponding to the best identified solution. Note that, as one can expect, the low accuracy of GAOT-shared corresponds to a low number of function evaluations required for that the stopping condition becomes active.

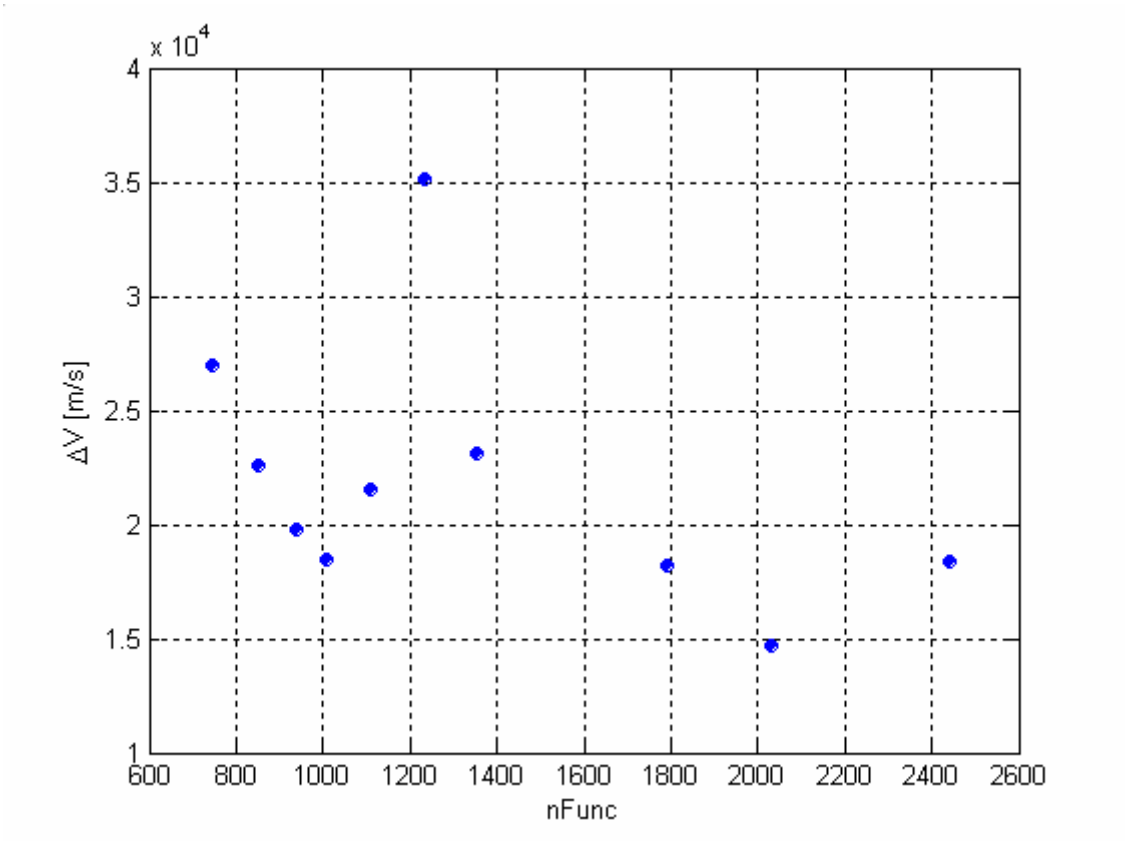

Figure 167: Distribution of the solutions resulting from each GAOT-shared optimization run over the $nFunc - \Delta V$ plane.

Evaluation criterion	Mean value	Standard deviation	Best identified solution
ΔV :	21874.731 *m/s*	5741.406 *m/s*	14681.217 *m/s*
nFunc.:	1350.400	559.057	2029
Runtime [STU]:	$2.700 \cdot 10^{-2}$	$1.192 \cdot 10^{-2}$	$4.345 \cdot 10^{-2}$

Table 78: Statistical characteristics of the identified solutions.

By proceeding in analogy with the GAOT case, the optimal solutions corresponding to all ten runs have been used as starting solutions for ten local optimization processes in order to accurately estimate the local minimum corresponding to the basin of attraction each optimal solution belong to. Figure 168 illustrates the consequences of the local optimization processes in the *nFunc* - ΔV plane.

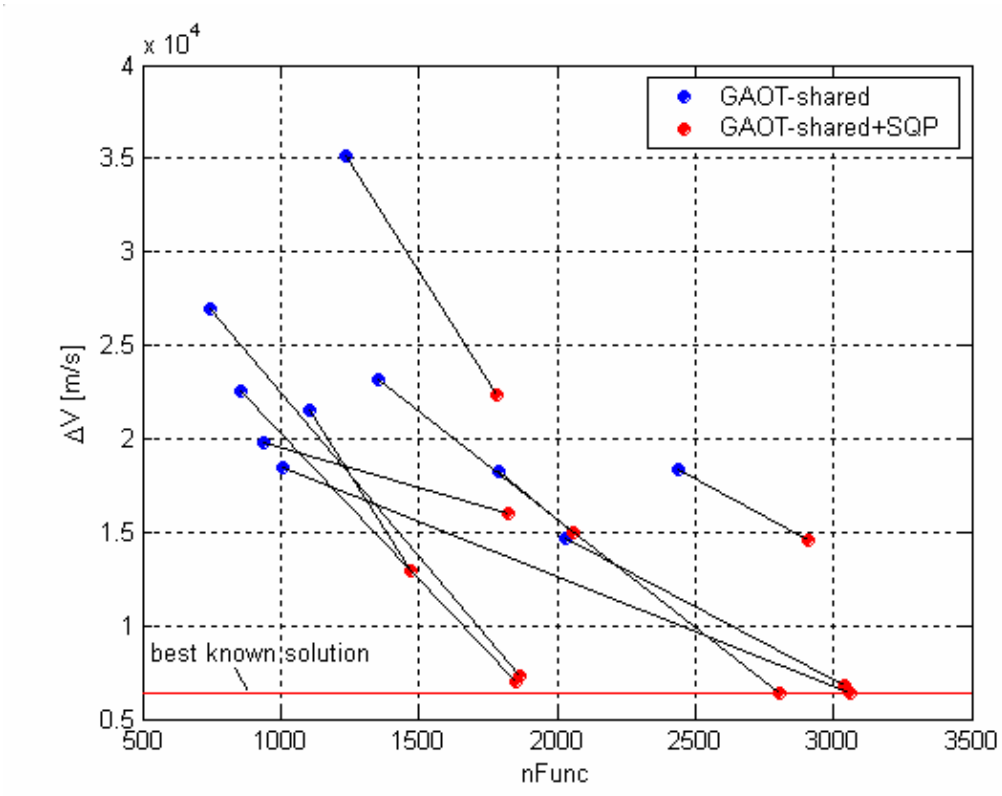

Figure 168: Comparison between solutions resulting from GAOT-shared runs and their improvements by means of a further local optimization process via SQP algorithm over the $nFunc - \Delta V$ plane.

Figure 168 shows again that different local minima corresponds to GAOT-shared runs. In order to estimate the number of identified solutions which lie in the basin of attraction of the best known solutions, solutions are now investigated in the normalized search space. Table 79 reports, corresponding to each GAOT-shared+SQP run, the reached objective function value and the distance (in Euclidean metric) with respect to the best known solution.

Mean value	ΔV [m/s]	Distance
run 1	12968.384	0.913
run 2	6824.030	0.456
run 3	7348.905	0.206
run 4	14607.801	0.582
run 5	6946.553	0.576
run 6	6372.395	0.002
run 7	15984.312	0.549
run 8	22394.289	0.833
run 9	14987.571	0.610
run 10	6368.116	0.002

Table 79: GAOT-shared+SQP optimization runs: objective function values and Euclidean distance in the normalized search space with respect to the best known solution.

As stated above, two solutions are considered as identical when the Euclidean distance is less than 0.024. As a consequence only runs 6 and 10 were able to get the best known solution, that is only 2/10 GAOT-shared runs successfully identified the basin of attraction of the best known solution.

GATBX

As GATBX implements a genetic algorithm, we report the statistical characteristics. Ten run have been processed in order to solve the previously defined problem. Default options suggested by the providers of the code have been used in all the runs. A population of 100 individuals evolving for a maximum number of generations equal to 1000 has been processed again.

Algorithm parameters	
Number of individuals:	100
Maximum number of generations:	1000

Table 80 reports the best identified solution compared with the best known solution in terms of the values of the design variables and of the objective function terms, while Figue 169 plots the resulting interplanetary transfer trajectories.

	Best identified solution	**Best known solution**
t_0:	-763.599 *d*	-770.686 *d*
tt_{E-V}:	132.419 *d*	179.524 *d*
tt_{V-V}:	434.250 *d*	406.528 *d*
tt_{V-E}:	62.334 *d*	53.181 *d*
tt_{E-J}:	756.626 *d*	758.334 *d*
tt_{J-S}:	3650.218 *d*	3650.218 *d*
ΔV:	7122.878 *m/s*	6367.990 *m/s*
ΔV_I:	4259.877 *m/s*	3901.332 *m/s*
1st $\Delta V_{GA,V}$:	0.099 *m/s*	2019.210 *m/s*
2nd $\Delta V_{GA,V}$:	2411.222 *m/s*	0.018 *m/s*
$\Delta V_{GA,E}$	0.468 *m/s*	0.005 *m/s*

$\Delta V_{GA,J}$	4.593 *m/s*	0.022 *m/s*
ΔV_F :	446.619 *m/s*	447.402 *m/s*

Table 80: Comparison between the best identified solution and the best known solution.

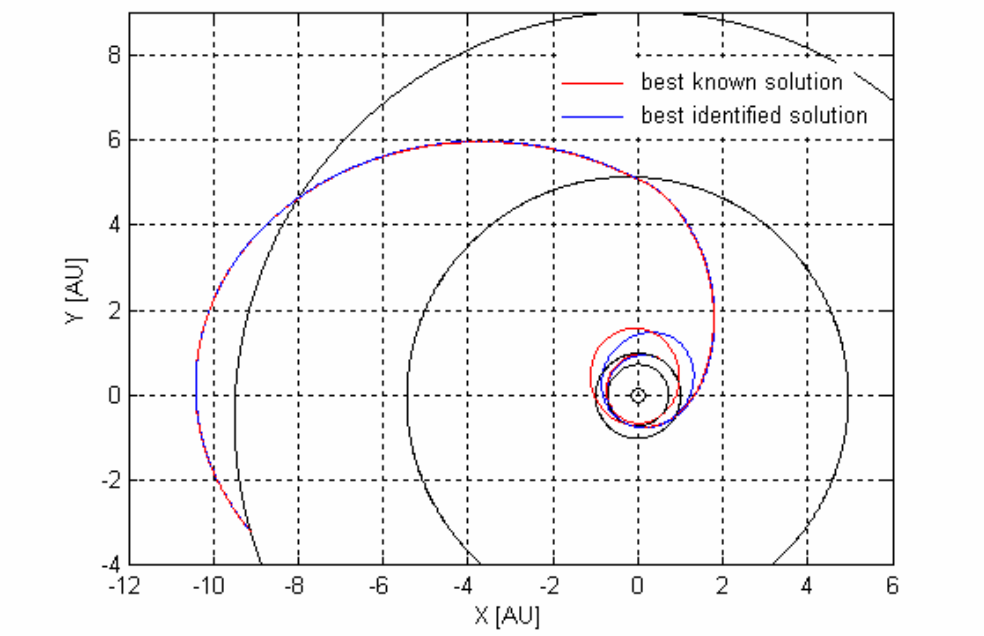

Figure 169*: GATBX*: Comparison between the best identified solution and the best known solution.

By analysing Table 80 and Figure 169, differences in the values of the design variables are mainly focused in the first phases of the interplanetary transfer. This can be better understood by analysing the two solutions in the normalized search space, as shown in Table 81.

	t_0	tt_{E-V}	tt_{V-V}	tt_{V-E}	tt_{E-J}	tt_{J-S}
Best identified solution	0.282	0.425	0.966	0.364	0.733	1.000
Best known solution	0.278	0.594	0.903	0.294	0.734	1.000

Table 81*: GATBX*: comparison between the best identified solution and the best known solution in the normalized search space.

As stated above, large differences can be noticed in the tt_{E-V}, tt_{V-V}, tt_{V-E} design variables, reaching a maximum value of the order of 10^{-1} in case of tt_{E-V}. The Euclidean distance between the two solutions is equal to $1.931 \cdot 10^{-1}$.

By performing a local optimization process by means of a SQP algorithm in order to evaluate if the best identified solution lies in the basin of attraction of the best known one, given the best solution identified by GATBX (reported in Table 81) and considering it as the starting point for the local search process, the improved best identified solution reported in Table 82 is gained.

	Best identified solution + SQP	**Best known solution**
t_0:	-782.353 *d*	-770.686 *d*
tt_{E-V}:	144.379 *d*	179.524 *d*
tt_{V-V}:	448.916 *d*	406.528 *d*
tt_{V-E}:	56.517 *d*	53.181 *d*
tt_{E-J}:	757.676 *d*	758.334 *d*
tt_{J-S}:	3650.218 *d*	3650.218 *d*
ΔV:	6743.989 *m/s*	6367.990 *m/s*
ΔV_I:	3561.103 *m/s*	3901.332 *m/s*
1st $\Delta V_{GA,V}$:	142.324 *m/s*	2019.210 *m/s*
2nd $\Delta V_{GA,V}$:	2574.414 *m/s*	0.018 *m/s*
$\Delta V_{GA,E}$	19.360 *m/s*	0.005 *m/s*
$\Delta V_{GA,J}$	0 *m/s*	0.022 *m/s*
ΔV_F:	446.788 *m/s*	447.402 *m/s*

Table 82: Comparison between the best solution identified by *GATBX* improved by a SQP based local optimization process and the best known solution (number of function evaluations required by the local optimization process equal to 626).

Table 82 shows that the local optimization process led to the identification of a local minimum which is different from and worse than the best known one. The best solution identified by GATBX algorithm doesn't lie in the basin of attraction

of the best known solution and in fact it identifies a different and more costly transfer (see Figure 170).

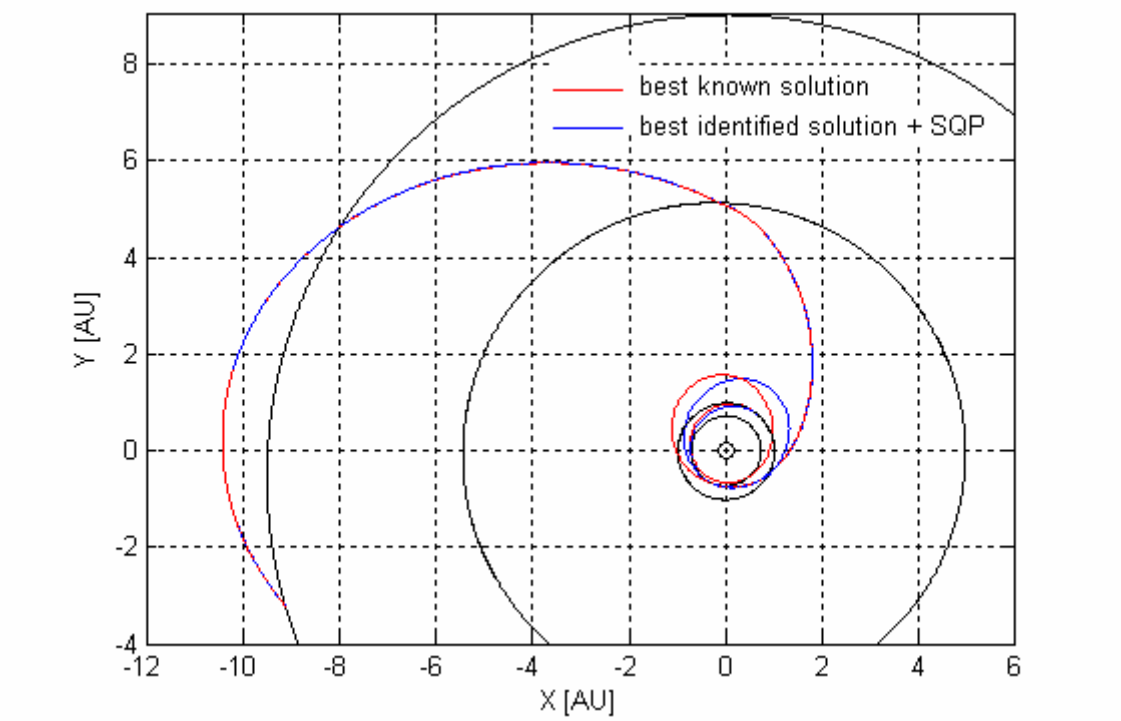

Figure 170*: GATBX*: Comparison between the improved best identified solution and the best known solution.

Let now analyse the statistical values of GATBX performances. Figure 171 shows the distribution of the solutions resulting from each optimization run over the plane of the objective function, ΔV, and the number of function evaluations, *nFunc*, while Table 83 reports the statistical characteristics, which will be used for comparisons with the other optimization algorithms, as well as the performances corresponding to the best identified solution.

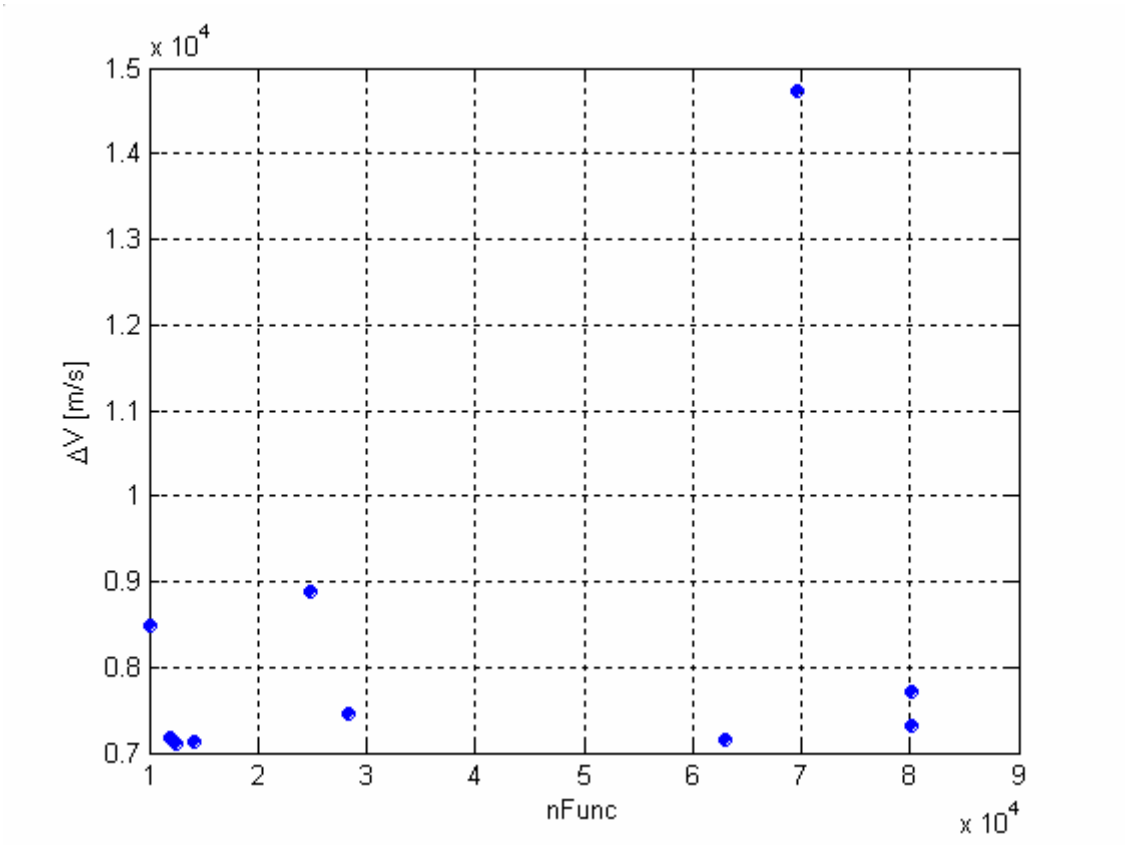

Figure 171: Distribution of the solutions resulting from each GATBX optimization run over the $nFunc - \Delta V$ plane.

Evaluation criterion	Mean value	Standard deviation	Best identified solution
ΔV :	8317.450 *m/s*	2339.832 *m/s*	7114.584 *m/s*
nFunc.:	39468.000	29981.5990	12580
Runtime [STU]:	0.748	0.584	0.239

Table 83: Statistical characteristics of the identified solutions.

The optimal solutions corresponding to all ten runs are now used again as starting solutions for ten local optimization processes in order to accurately estimate the local minimum corresponding to the basin of attraction each optimal solution belong to and to evaluate the number of GAOT-shared successful runs.

Figure 172 illustrates the consequences of the local optimization processes in the *nFunc* - ΔV plane.

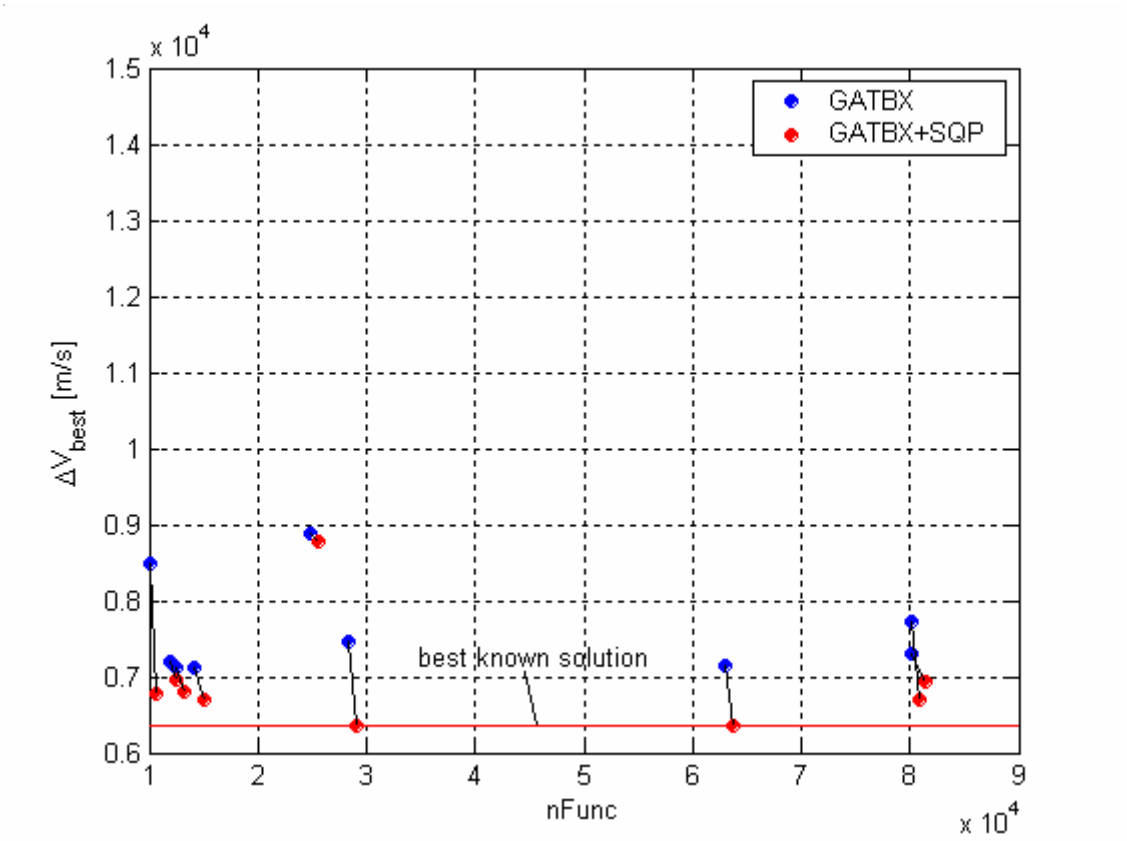

Figure 172: Comparison between solutions resulting from GATBX runs and their improvements by means of a further local optimization process via SQP algorithm over the $nFunc - \Delta V$ plane.

Different local minima corresponds to GATBX runs. In order to estimate the number of identified solutions which lie in the basin of attraction of the best known solutions, solutions are now investigated in the normalized search space. Table 84 reports, corresponding to each GATBX+SQP run, the reached objective function value and the distance (in Euclidean metric) with respect to the best known solution.

Mean value	ΔV [m/s]	Distance
run 1	8766.932	0.745
run 2	6368.134	0.001
run 3	6944.435	0.257
run 4	14171.978	0.626
run 5	6743.989	0.165
run 6	6948.181	0.170
run 7	6697.723	0.165
run 8	6368.128	0.001
run 9	6686.387	0.165
run 10	6784.485	0.370

Table 84: GATBX+SQP optimization runs: objective function values and Euclidean distance in the normalized search space with respect to the best known solution.

By considering two solutions as identical when the Euclidean distance is less than 0.024, only runs 2 and 8 were able to get the best known solution, that is only 2/10 GATBX runs successfully identified the basin of attraction of the best known solution.

GATBX-migr

As GATBX-migr implements a genetic algorithm including a migration operator applied among a predefined set of subpopulations, we report the statistical characteristics. Ten run have been processed in order to solve the previously defined problem. Default options suggested by the providers of the code have been used in all the runs. A population of 100 individuals evolving for a maximum number of generations equal to 1000 has been processed. The population has been divided in 5 subpopulations, each one including 20 individuals.

Algorithm parameters	
Number of individuals:	100
Maximum number of generations:	1000
Number of subpopulations:	5
Number of individuals per subpopulation:	20

Table 85 reports the best identified solution compared with the best known solution in terms of the values of the design variables and of the objective function terms, while Figure 173 plots the resulting interplanetary transfer trajectories.

	Best identified solution	Best known solution
t_0:	-770.714 *d*	-770.686 *d*
tt_{E-V}:	162.659 *d*	179.524 *d*
tt_{V-V}:	410.900 *d*	406.528 *d*
tt_{V-E}:	62.501 *d*	53.181 *d*
tt_{E-J}:	756.597 *d*	758.334 *d*
tt_{J-S}:	3650.215 *d*	3650.218 *d*
ΔV:	7219.480 *m/s*	6367.990 *m/s*
ΔV_I:	3254.960 *m/s*	3901.332 *m/s*
1st $\Delta V_{GA,V}$:	2880.101 *m/s*	2019.210 *m/s*
2nd $\Delta V_{GA,V}$:	632.632 *m/s*	0.018 *m/s*
$\Delta V_{GA,E}$	0.625 *m/s*	0.005 *m/s*
$\Delta V_{GA,J}$	4.573 *m/s*	0.022 *m/s*
ΔV_F:	446.588 *m/s*	447.402 *m/s*

Table 85: Comparison between the best identified solution and the best known solution.

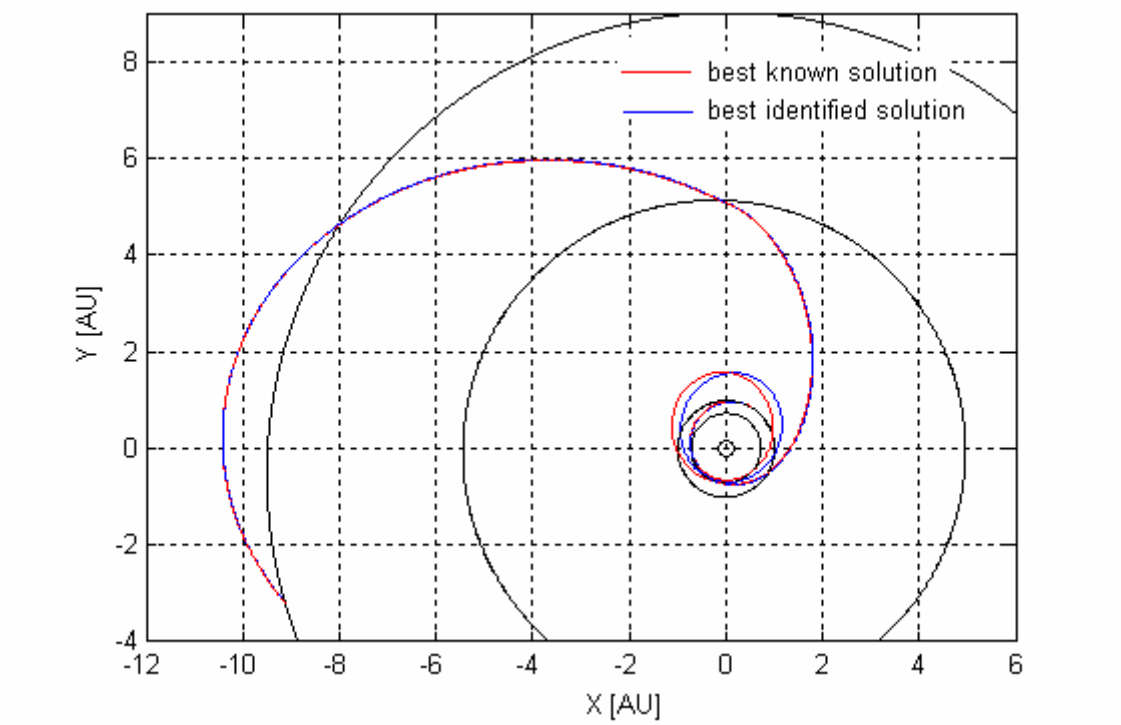

Figure 173*: GATBX-migr*: Comparison between the best identified solution and the best known solution.

In order to better analyse the differences between the two solutions, Table 86 reports again the values of their design variables in the normalized search space.

	t_0	tt_{E-V}	tt_{V-V}	tt_{V-E}	tt_{E-J}	tt_{J-S}
Best identified solution	0.278	0.534	0.913	0.365	0.732	1.000
Best known solution	0.278	0.594	0.903	0.294	0.734	1.000

Table 86*: GATBX-migr*: comparison between the best identified solution and the best known solution in the normalized search space.

Little difference exists in the values of the design variables, whose order of magnitude is equal to 10^{-2}. The Euclidean distance between the two solutions is equal to $9.312 \cdot 10^{-2}$. Given the best solution identified by GATBX-migr (reported in Table 85) and considering it as the starting point, a local optimization process

by means of a SQP algorithm is now performed, which leads to the improved best identified solution reported in Table 87.

	Best identified solution + SQP	**Best known solution**
t_0 :	-770.850 *d*	-770.686 *d*
tt_{E-V} :	179.689 *d*	179.524 *d*
tt_{V-V} :	406.521 *d*	406.528 *d*
tt_{V-E} :	53.181 *d*	53.181 *d*
tt_{E-J} :	757.902 *d*	758.334 *d*
tt_{J-S} :	3650.218 *d*	3650.218 *d*
ΔV :	6368.087 *m/s*	6367.990 *m/s*
ΔV_I :	3905.863 *m/s*	3901.332 *m/s*
1st $\Delta V_{GA,V}$:	2014.042 *m/s*	2019.210 *m/s*
2nd $\Delta V_{GA,V}$:	0.002 *m/s*	0.018 *m/s*
$\Delta V_{GA,E}$	0 *m/s*	0.005 *m/s*
$\Delta V_{GA,J}$	0 *m/s*	0.022 *m/s*
ΔV_F :	448.179 *m/s*	447.402 *m/s*

Table 87: Comparison between the best solution identified by *GATBX-migr* improved by a SQP based local optimization process and the best known solution (number of function evaluations required by the local optimization process equal to 366).

Table 87 shows that GATBX-migr algorithm was able to reach the basin of attraction of the best known solution in the optimization run corresponding to the best identified solution. Let now analyse the statistical values of GATBX-migr performances. Figure 174 shows the distribution of the solutions resulting from each optimization run over the plane of the objective function, ΔV, and the number of function evaluations, *nFunc*, while Table 88 reports the statistical characteristics, which will be used for comparisons with the other optimization algorithms, as well as the performances corresponding to the best identified solution.

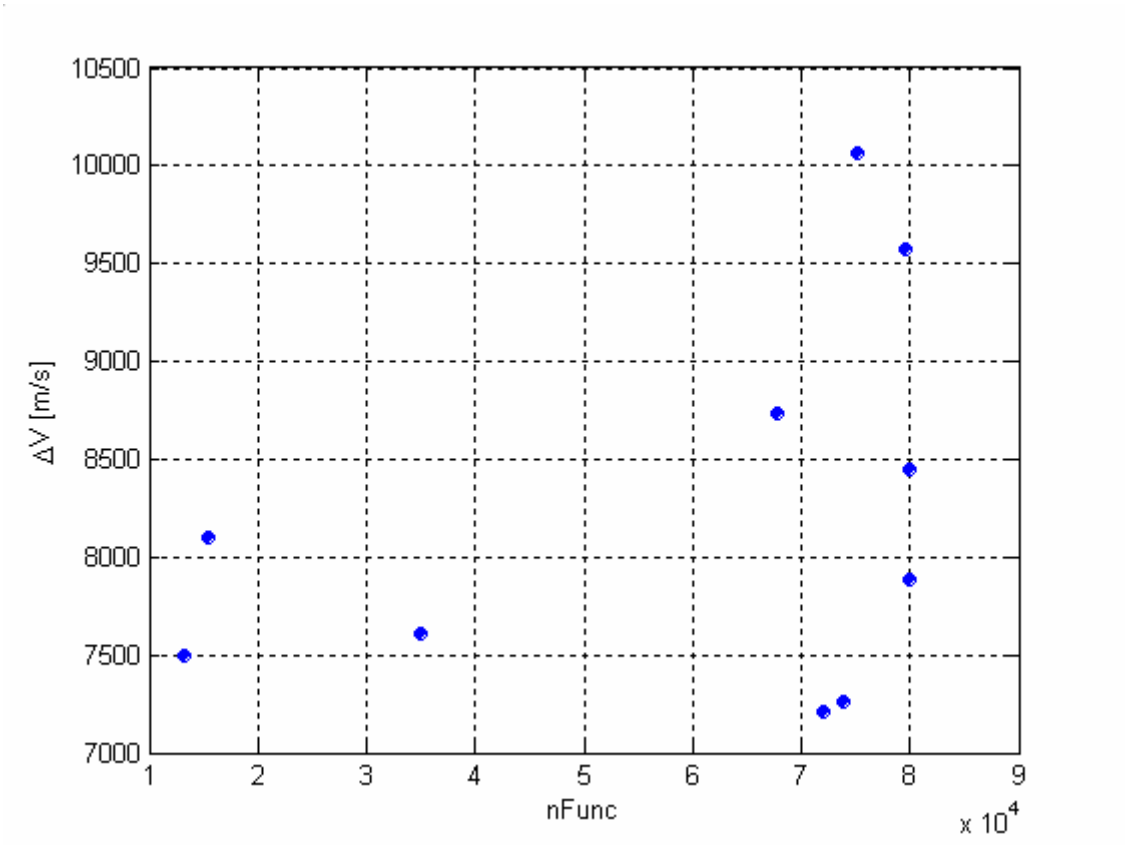

Figure 174: Distribution of the solutions resulting from each GATBX-migr optimization run over the $nFunc - \Delta V$ plane.

Evaluation criterion	Mean value	Standard deviation	Best identified solution
ΔV :	8237.810 *m/s*	972.517 *m/s*	7213.020 *m/s*
nFunc.:	59220	27105.666	72020
Runtime [STU]:	1.272	0.722	1.196

Table 88: Statistical characteristics of the identified solutions.

In order to evaluate the number of GATBX-migr successful runs, the optimal solutions corresponding to all ten runs are now used as starting solutions for ten local optimization processes. Figure 175 illustrates the consequences of the local optimization processes in the *nFunc* - ΔV plane

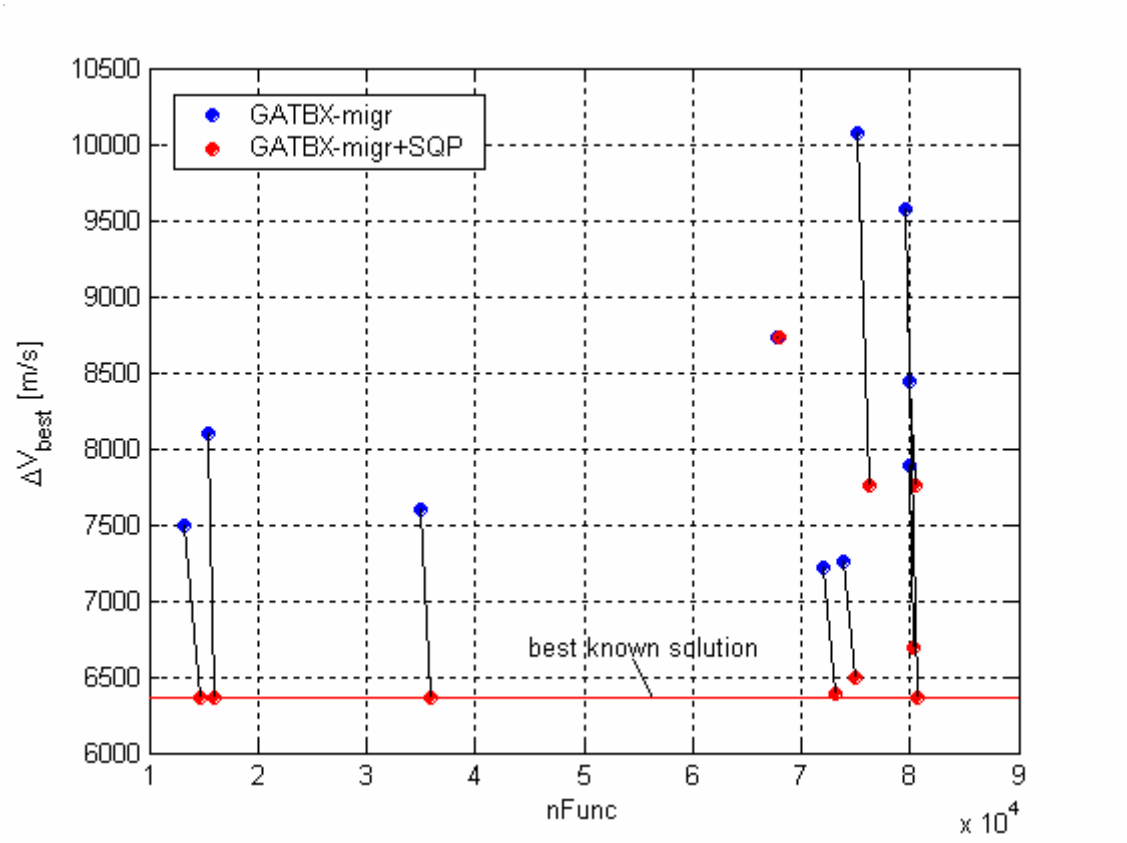

Figure 175: Comparison between solutions resulting from GATBX-migr runs and their improvements by means of a further local optimization process via SQP algorithm over the $nFunc - \Delta V$ plane.

Different local minima corresponds to GATBX-migr runs. Solutions are now investigated in the normalized search space. Table 89 reports, corresponding to each GATBX-migr+SQP run, the reached objective function value and the distance (in Euclidean metric) with respect to the best known solution.

Mean value	ΔV [m/s]	Distance
run 1	7752.872	0.690
run 2	6368.087	0.001
run 3	6692.992	0.162
run 4	6498.430	0.107
run 5	6388.254	0.022
run 6	6368.262	0.001
run 7	8734.077	0.744
run 8	6368.116	0.001
run 9	7753.498	0.690
run 10	6368.104	0.001

Table 89: GATBX-migr+SQP optimization runs: objective function values and Euclidean distance in the normalized search space with respect to the best known solution.

By considering two solutions as identical when the Euclidean distance is less than 0.024, runs 2, 5, 6, 8 and 10 were able to get the best known solution, that is 5/10 GATBX-migr runs successfully identified the basin of attraction of the best known solution.

FEP

As FEP implements an evolutionary programming algorithm, we report, as already done for genetic algorithms, the statistical characteristics. Ten runs have been processed in order to solve the previously defined problem. Default options suggested by the providers of the code have been used in all the runs. As the Multiple Gravity Assist transfer has high complexity features, we used 100 individuals evolving for a maximum number of generations equal to 1000.

Algorithm parameters	
Number of individuals:	100
Maximum number of generations:	1000

Table 90 reports the best identified solution compared with the best known solution in terms of the values of the design variables and of the objective function terms, while Figure 176 plots the resulting interplanetary transfer trajectories.

	Best identified solution	Best known solution
t_0 :	-767.492 *d*	-770.686 *d*
tt_{E-V} :	162.957 *d*	179.524 *d*
tt_{V-V} :	407.819 *d*	406.528 *d*
tt_{V-E} :	62.167 *d*	53.181 *d*
tt_{E-J} :	750.432 *d*	758.334 *d*
tt_{J-S} :	3618.752 *d*	3650.218 *d*
ΔV :	7164.248 *m/s*	6367.990 *m/s*
ΔV_I :	3365.720 *m/s*	3901.332 *m/s*
1st $\Delta V_{GA,V}$:	3006.822 *m/s*	2019.210 *m/s*
2nd $\Delta V_{GA,V}$:	298.001 *m/s*	0.018 *m/s*
$\Delta V_{GA,E}$	38.029 *m/s*	0.005 *m/s*
$\Delta V_{GA,J}$	9.275 *m/s*	0.022 *m/s*
ΔV_F :	446.402 *m/s*	447.402 *m/s*

Table 90: Comparison between the best identified solution and the best known solution.

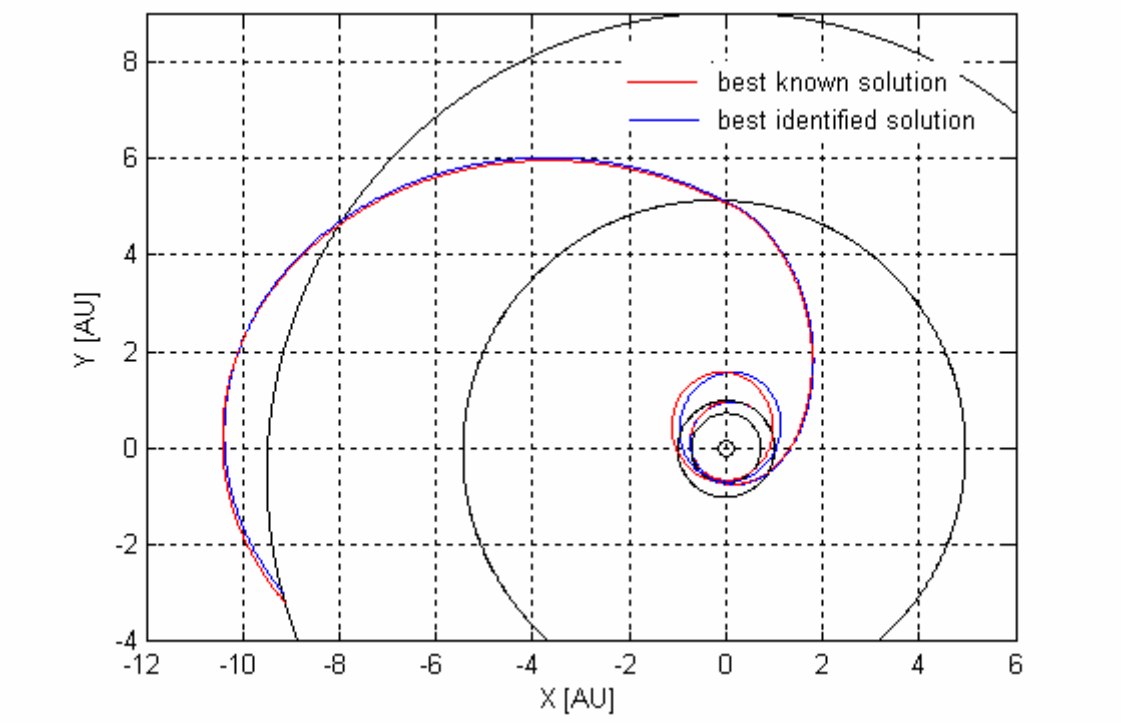

Figure 175*: FEP*: Comparison between the best identified solution and the best known solution.

Table 91 reports the values of their design variables in the normalized search space.

	t_0	tt_{E-V}	tt_{V-V}	tt_{V-E}	tt_{E-J}	tt_{J-S}
Best identified solution	0.279	0.535	0.906	0.362	0.726	0.990
Best known solution	0.278	0.594	0.903	0.294	0.734	1.000

Table 91: *FEP*: comparison between the best identified solution and the best known solution in the normalized search space.

Although the different objective function values, the values of the design variables in the normalized search space corresponding to the two solutions are close to each other, showing a maximum value of the order of 10^{-2} and an Euclidean distance equal to $9.092 \cdot 10^{-2}$; moreover, by analysing Figure 175, the two corresponding transfer trajectories seems to show similar structures. This suggest the possibility that the best identified solution lies in the basin of

attraction of the best known solution. Given the best solution identified by FEP and considering it as the starting, a local optimization process by means of a SQP algorithm leads in fact to the improved best identified solution reported in Table 91.

	Best identified solution + SQP	**Best known solution**
t_0 :	-770.924 *d*	-770.686 *d*
tt_{E-V} :	179.763 *d*	179.524 *d*
tt_{V-V} :	406.523 *d*	406.528 *d*
tt_{V-E} :	53.179 *d*	53.181 *d*
tt_{E-J} :	757.903 *d*	758.334 *d*
tt_{J-S} :	3650.218 *d*	3650.218 *d*
ΔV :	6368.128 *m/s*	6367.990 *m/s*
ΔV_I :	3908.484 *m/s*	3901.332 *m/s*
1st $\Delta V_{GA,V}$:	2011.217 *m/s*	2019.210 *m/s*
2nd $\Delta V_{GA,V}$:	0.248 *m/s*	0.018 *m/s*
$\Delta V_{GA,E}$	0 *m/s*	0.005 *m/s*
$\Delta V_{GA,J}$	0 *m/s*	0.022 *m/s*
ΔV_F :	448.179 *m/s*	447.402 *m/s*

Table 91 : Comparison between the best solution identified by *FEP* improved by a SQP based local optimization process and the best known solution (number of function evaluations required by the local optimization process equal to 473).

The little differences between the two solutions reported in Table 91 show, in fact, that the best solution identified by FEP lie in the basin of attraction of the best known solution. Let now analyse the statistical values of FEP performances. Figure 176 shows the distribution of the solutions resulting from each optimization run over the plane of the objective function, ΔV, and the number of function evaluations, *nFunc*, while Table 94 reports the statistical characteristics, which will be used for comparisons with the other optimization

algorithms, as well as the performances corresponding to the best identified solution.

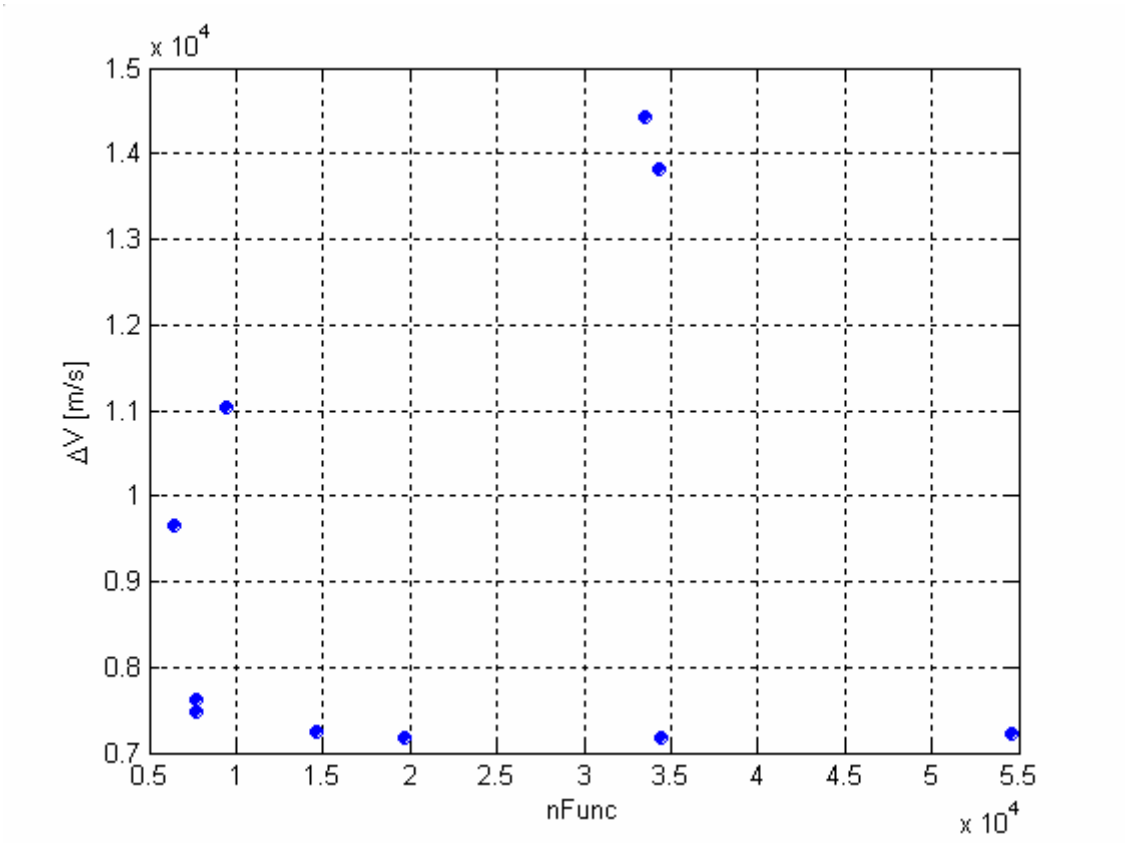

Figure 176: Distribution of the solutions resulting from each FEP optimization run over the $nFunc - \Delta V$ plane.

Evaluation criterion	Mean value	Standard deviation	Best identified solution
ΔV :	9287.112 *m/s*	2860.194 *m/s*	7168.115 *m/s*
nFunc.:	22238.300	16233.713	19642
Runtime [STU]:	0.629	0.458	0.542

Table 94: Statistical characteristics of the identified solutions.

By proceeding in analogy with the previous algorithm analyses, the optimal solutions corresponding to all ten runs have been used as starting solutions for ten local optimization processes in order to accurately estimate the local

minimum corresponding to the basin of attraction each optimal solution belong to. Figure 177 illustrates the consequences of the local optimization processes in the *nFunc* - ΔV plane.

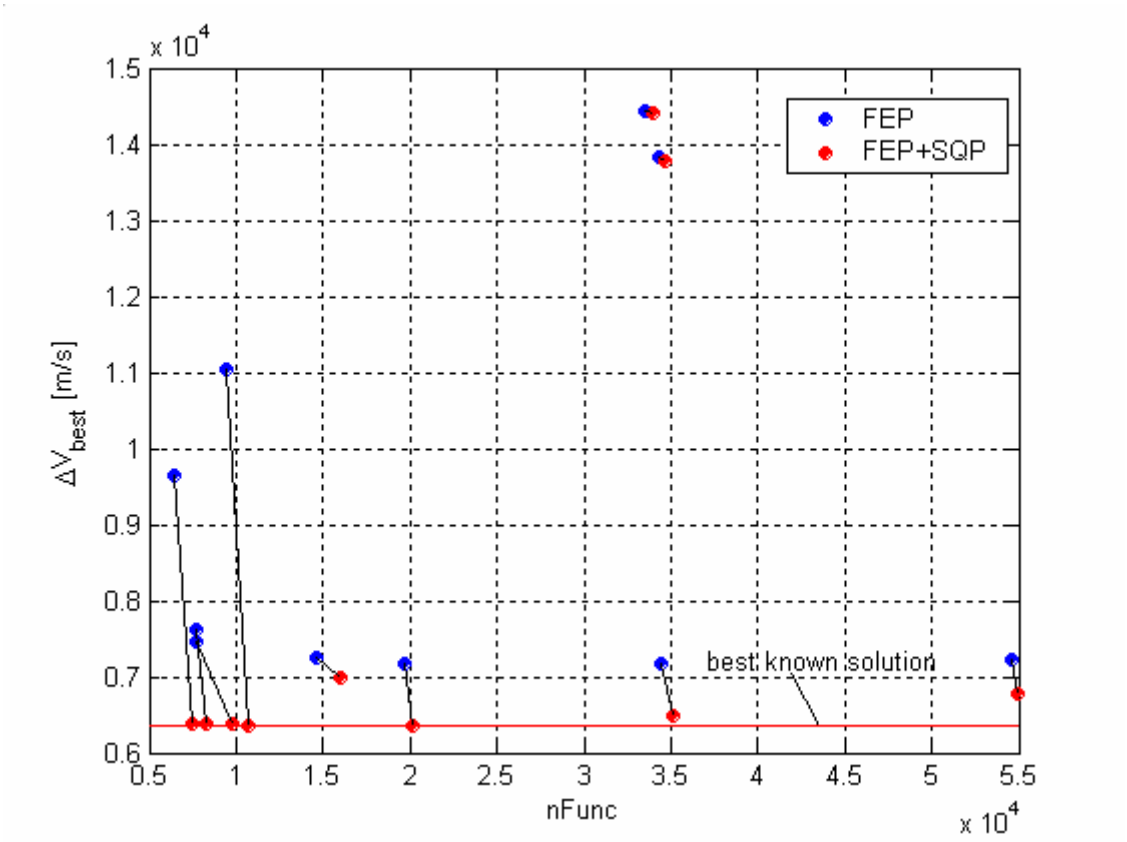

Figure 177: Cmparison between solutions resulting from FEP runs and their improvements by means of a further local optimization process via SQP algorithm over the $nFunc - \Delta V$ plane.

Different local minima corresponds to FEP runs.Solutions are now investigated in the normalized search space. Table 94 reports, corresponding to each FEP+SQP run, the reached objective function value and the distance (in Euclidean metric) with respect to the best known solution.

Mean value	ΔV [m/s]	Distance
Run 1	6381.341	0.014
Run 2	6977.111	0.496
Run 3	6370.082	0.001
run 4	6783.654	0.297
run 5	6368.128	0.001
run 6	14415.505	0.670
run 7	13774.873	0.791
run 8	6369.203	0.006
run 9	6368.001	0.001
run 10	6496.798	0.107

Table 94: FEP+SQP optimization runs: objective function values and Euclidean distance in the normalized search space with respect to the best known solution.

By considering two solutions as identical when the Euclidean distance is less than 0.024, runs 1, 3, 5, 8 and 9 were able to get the best known solution, that is 5/10 FEP runs successfully identified the basin of attraction of the best known solution.

DE

As DE implements a Differential Evolution algorithm, we report the statistical characteristics. Ten run have been processed in order to solve the previously defined problem. Default options suggested by the providers of the code have been used in all the runs. Again, due to the high complexity of the Multiple Gravity Assist interplanetary transfer problem, we used 100 individuals evolving for a maximum number of iterations equal to 1000.

Algorithm parameters	
Number of individuals:	100
Maximum number of generations:	1000

Table 95 reports the best identified solution compared with the best known solution in terms of the values of the design variables and of the objective function terms, while Figure 178 plots the resulting interplanetary transfer trajectories.

	Best identified solution	Best known solution
t_0 :	-772.497 *d*	-770.686 *d*
tt_{E-V} :	167.745 *d*	179.524 *d*
tt_{V-V} :	421.400 *d*	406.528 *d*
tt_{V-E} :	50.758 *d*	53.181 *d*
tt_{E-J} :	620.257 *d*	758.334 *d*
tt_{J-S} :	2471.348 *d*	3650.218 *d*
ΔV :	7513.354 *m/s*	6367.990 *m/s*
ΔV_I :	3332.276 *m/s*	3901.332 *m/s*
1st $\Delta V_{GA,V}$:	1667.957 *m/s*	2019.210 *m/s*
2nd $\Delta V_{GA,V}$:	1855.955 *m/s*	0.018 *m/s*
$\Delta V_{GA,E}$	46.634 *m/s*	0.005 *m/s*
$\Delta V_{GA,J}$	144.470 *m/s*	0.022 *m/s*
ΔV_F :	466.061 *m/s*	447.402 *m/s*

Table 95:Comparison between the best identified solution and the best known solution.

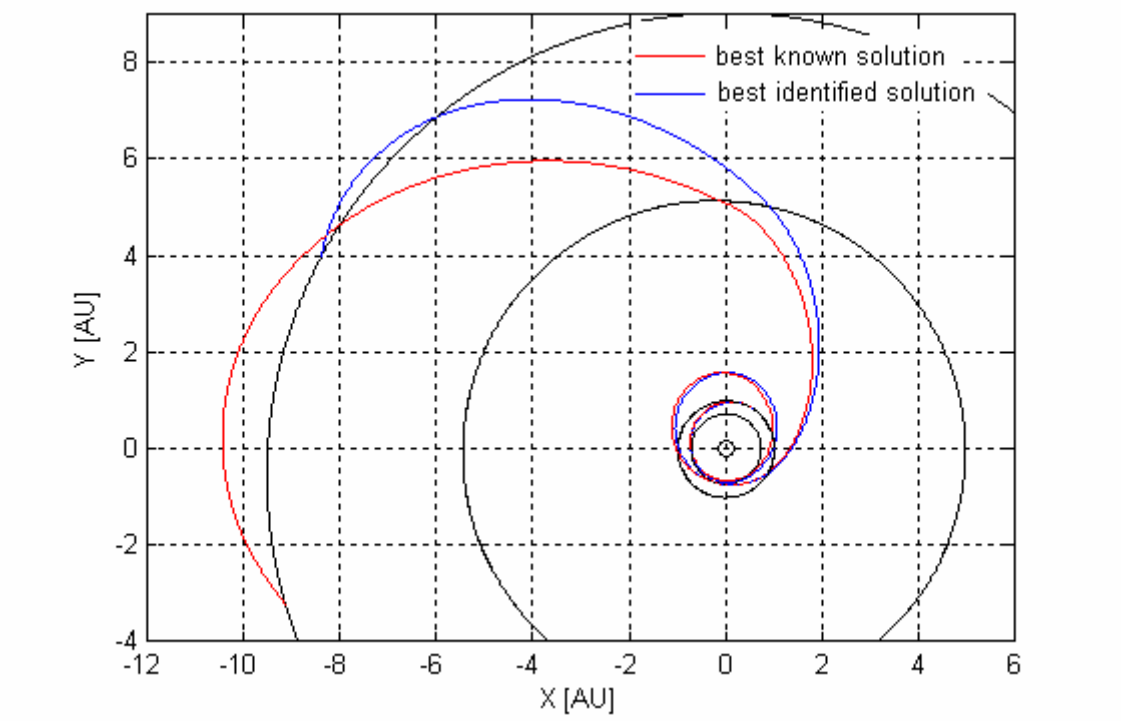

Figure 178: Comparison between the best identified solution and the best known solution.

Table 95 and Figure 178 show that, while the values of the first four design variables are quite close to each other, important differences exist in the tt_{E-J} and tt_{J-S} values, which lead to evidently dissimilar last phases of the interplanetary transfer. This can be highlighted by analysing Table 96 which reports the two solutions in the normalized search space.

	t_0	tt_{E-V}	tt_{V-V}	tt_{V-E}	tt_{E-J}	tt_{J-S}
Best identified solution	0.277	0.552	0.937	0.275	0.580	0.641
Best known solution	0.278	0.594	0.903	0.294	0.734	1.000

Table 96*: DE*: comparison between the best identified solution and the best known solution in the normalized search space.

Differences between the values of the design variables in the normalized search space attain a maximum value of 0.359 corresponding to tt_{J-S} and the

Euclidean distance between the solutions is equal to $3.945 \cdot 10^{-1}$, which is higher than the corresponding value in case of the previous algorithm. In analogy with the previous algorithm performance analysis, a local optimization process by means of a SQP algorithm is performed by considering the best solution identified by DE (reported in Table 96) as the starting point. The resulting improvement of the best identified solution is reported in Table 97.

	Best identified solution + SQP	**Best known solution**
t_0:	-772.470 *d*	-770.686 *d*
tt_{E-V}:	182.001 *d*	179.524 *d*
tt_{V-V}:	403.715 *d*	406.528 *d*
tt_{V-E}:	53.518 *d*	53.181 *d*
tt_{E-J}:	649.305 *d*	758.334 *d*
tt_{J-S}:	2819.777 *d*	3650.218 *d*
ΔV:	6672.195 *m/s*	6367.990 *m/s*
ΔV_I:	4013.102 *m/s*	3901.332 *m/s*
1st $\Delta V_{GA,V}$:	2200.297 *m/s*	2019.210 *m/s*
2nd $\Delta V_{GA,V}$:	3.121 *m/s*	0.018 *m/s*
$\Delta V_{GA,E}$	0.003 *m/s*	0.005 *m/s*
$\Delta V_{GA,J}$	0.015 *m/s*	0.022 *m/s*
ΔV_F:	455.657 *m/s*	447.402 *m/s*

Table 97: Comparison between the best solution identified by *DE* improved by a SQP based local optimization process and the best known solution (number of function evaluations required by the local optimization process equal to 1140).

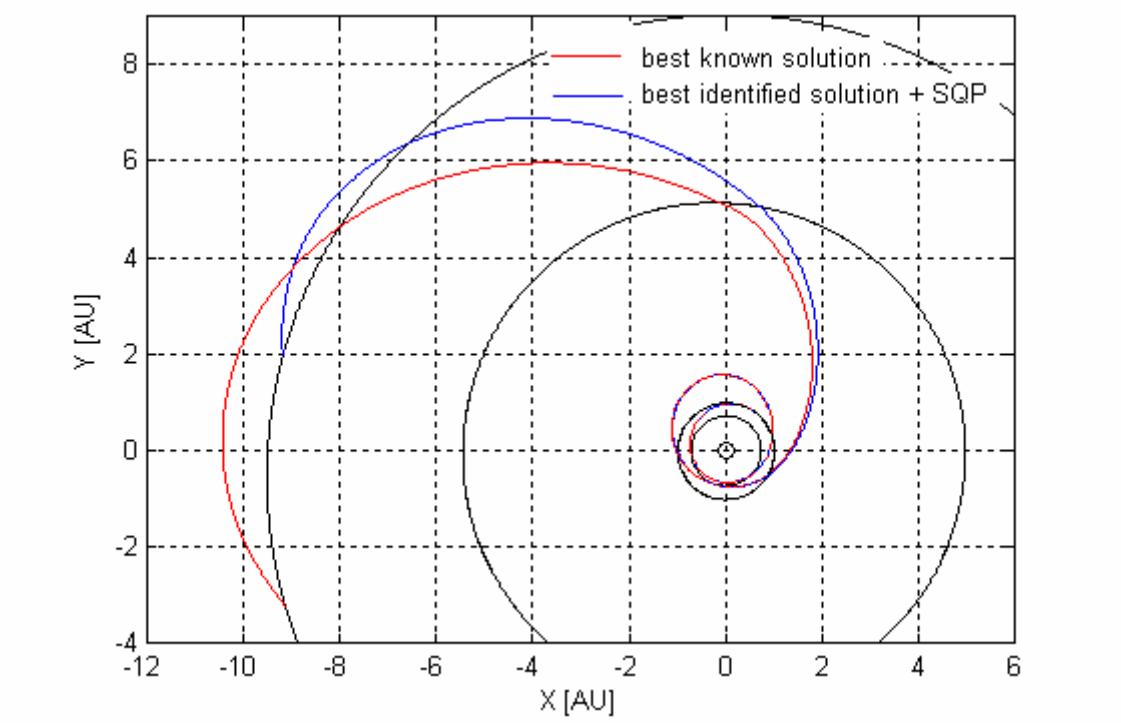

Figure 179*: DE*: comparison between the improved best identified solution and the best known solution.

As already happened in case of GATBX algorithm, the best solution identified by DE doesn't lie in the basin of attraction of the best known solution: the results of the local optimization process, reported in Table 97 and Figure 179 led to the identification of a local minimum which is different from and worse than the best known one; this solution corresponds to shorter values of the tt_{E-J} and tt_{J-S} design variables, then identifying a different family of solutions for the interplanetary transfer. Let now analyse the statistical values of DE performances. Figure 180 shows the distribution of the solutions resulting from each optimization run over the plane of the objective function, ΔV, and the number of function evaluations, *nFunc*, while Table reports the statistical characteristics, which will be used for comparisons with the other optimization algorithms, as well as the performances corresponding to the best identified solution.

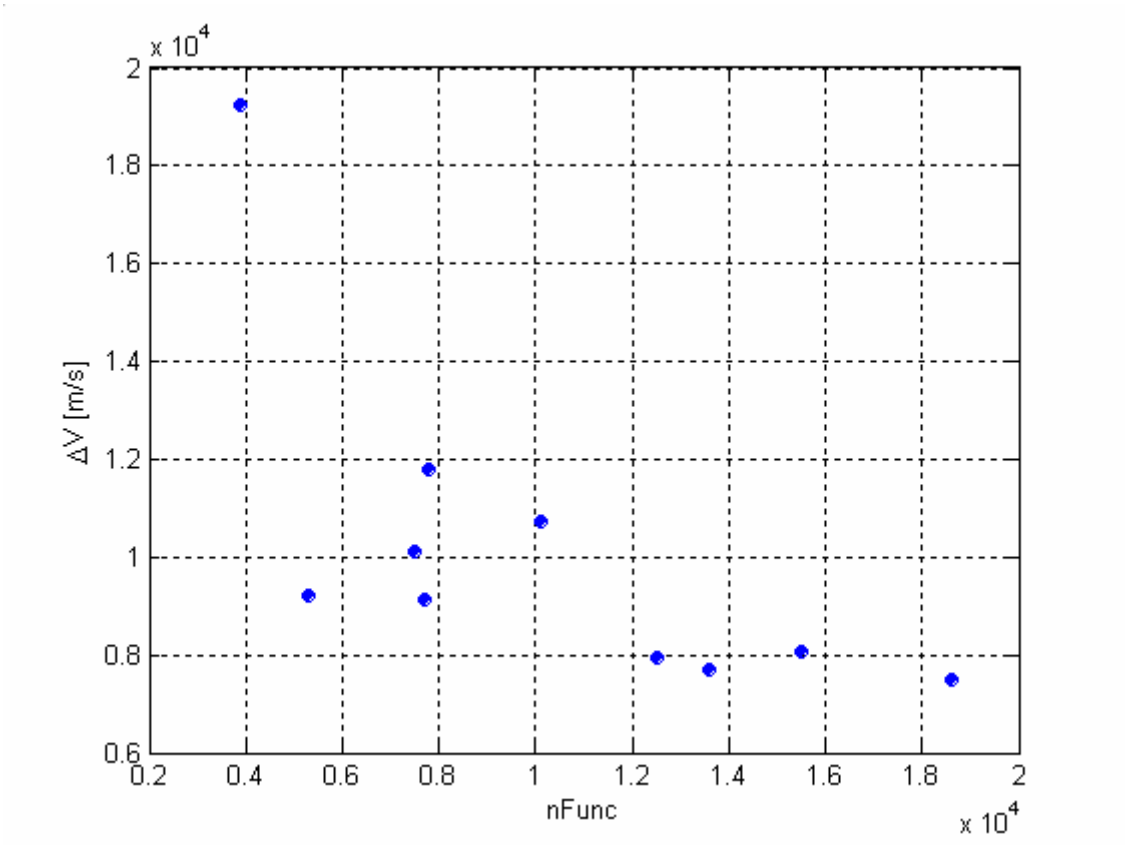

Figure 180: Distribution of the solutions resulting from each DE optimization run over the $nFunc - \Delta V$ plane.

Evaluation criterion	Mean value	Standard deviation	Best identified solution
ΔV :	10145.388 *m/s*	3494.605 *m/s*	7510.975 *m/s*
nFunc.:	10250	4696.157	18600
Runtime [STU]:	0.201	0.094	0.369

Table 98: Statistical characteristics of the identified solutions.

The optimal solutions corresponding to all ten runs are now considered as starting solutions for ten local optimization processes in order to accurately estimate the local minimum corresponding to the basin of attraction each optimal solution belong to. Figure 181 illustrates the consequences of the local optimization processes in the *nFunc* - ΔV plane.

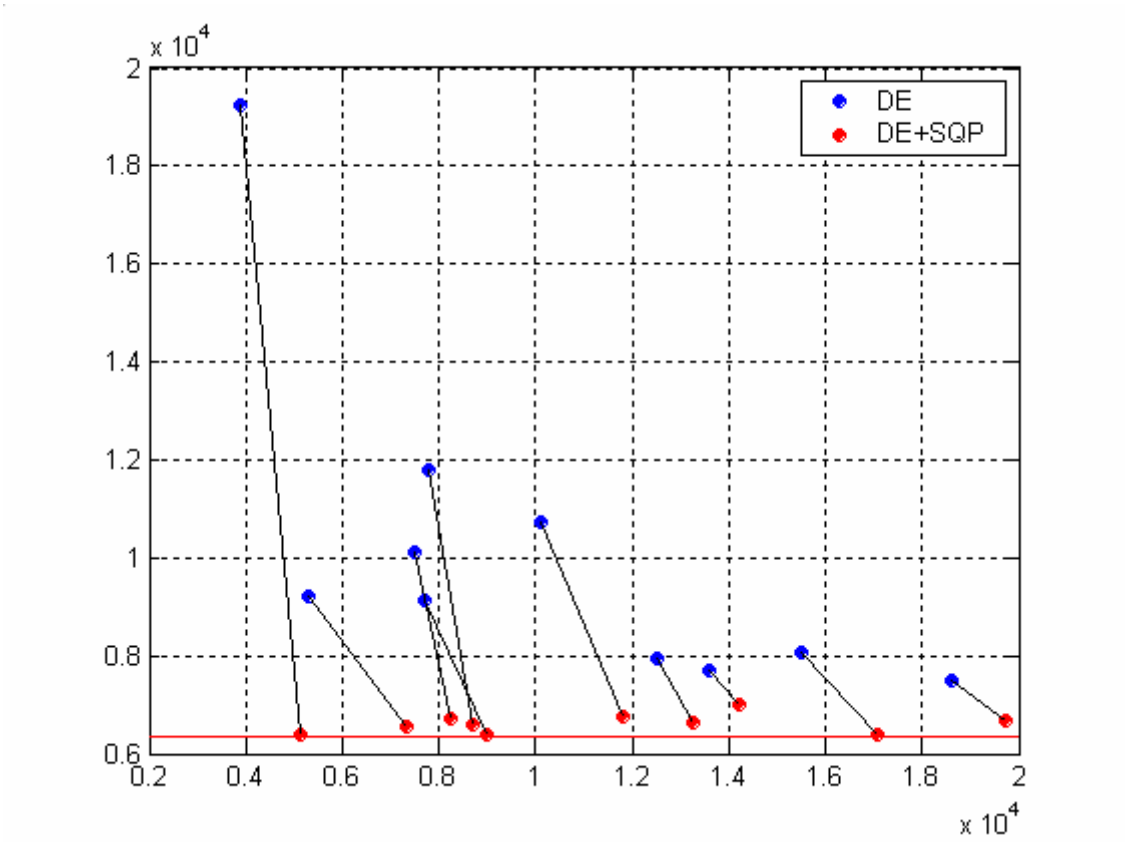

Figure 181: Comparison between solutions resulting from DE runs and their improvements by means of a further local optimization process via SQP algorithm over the $nFunc - \Delta V$ plane.

Different local minima corresponds to DE runs. In order to estimate the number of identified solutions which lie in the basin of attraction of the best known solutions, let investigate the solutions in the normalized search space. Table 99 reports, corresponding to each DE+SQP run, the reached objective function value and the distance (in Euclidean metric) with respect to the best known solution.

Mean value	ΔV [m/s]	Distance
run 1	6372.443	0.002
run 2	6740.310	0.159
run 3	6535.352	0.111
run 4	6369.829	0.002
run 5	6994.426	0.254
run 6	6672.195	0.281
run 7	6731.933	0.350
run 8	6372.292	0.009
run 9	6582.506	0.186
run 10	6652.766	0.202

Table 99: DE+SQP optimization runs: objective function values and Euclidean distance in the normalized search space with respect to the best known solution.

By considering two solutions as identical when the Euclidean distance is less than 0.024, runs 1, 4 and 8 were able to get the best known solution, that is 3/10 DE runs successfully identified the basin of attraction of the best known solution.

ASA

As ASA implements an Adaptive Simulated Annealing algorithm, we report the statistical performance characteristics. Ten run have been processed in order to solve the previously defined problem. Default options suggested by the providers of the code have been used in all the runs. Note that, unlike the previous cases, the adaptive simulated annealing needs a starting solution, which strongly affects the optimal solution reached. Due to the comparative purposes of this work, we decided to use ten different random starting solutions, uniformly distributed in the search box. Table 100 reports the best identified solution compared with the best known solution in terms of the values of the

design variables and of the objective function terms, while Figure 82 plots the resulting interplanetary transfer trajectories.

	Best identified solution	**Best known solution**
t_0:	-807.854 *d*	-770.686 *d*
tt_{E-V}:	212.421 *d*	179.524 *d*
tt_{V-V}:	406.480 *d*	406.528 *d*
tt_{V-E}:	56.343 *d*	53.181 *d*
tt_{E-J}:	752.539 *d*	758.334 *d*
tt_{J-S}:	3618.545 *d*	3650.218 *d*
ΔV:	6622.699 *m/s*	6367.990 *m/s*
ΔV_I:	6164.421 *m/s*	3901.332 *m/s*
1st $\Delta V_{GA,V}$:	5.166 *m/s*	2019.210 *m/s*
2nd $\Delta V_{GA,V}$:	0.204 *m/s*	0.018 *m/s*
$\Delta V_{GA,E}$	0.417 *m/s*	0.005 *m/s*
$\Delta V_{GA,J}$	4.630 *m/s*	0.022 *m/s*
ΔV_F:	447.860 *m/s*	447.402 *m/s*

Table 100: Comparison between the best identified solution and the best known solution.

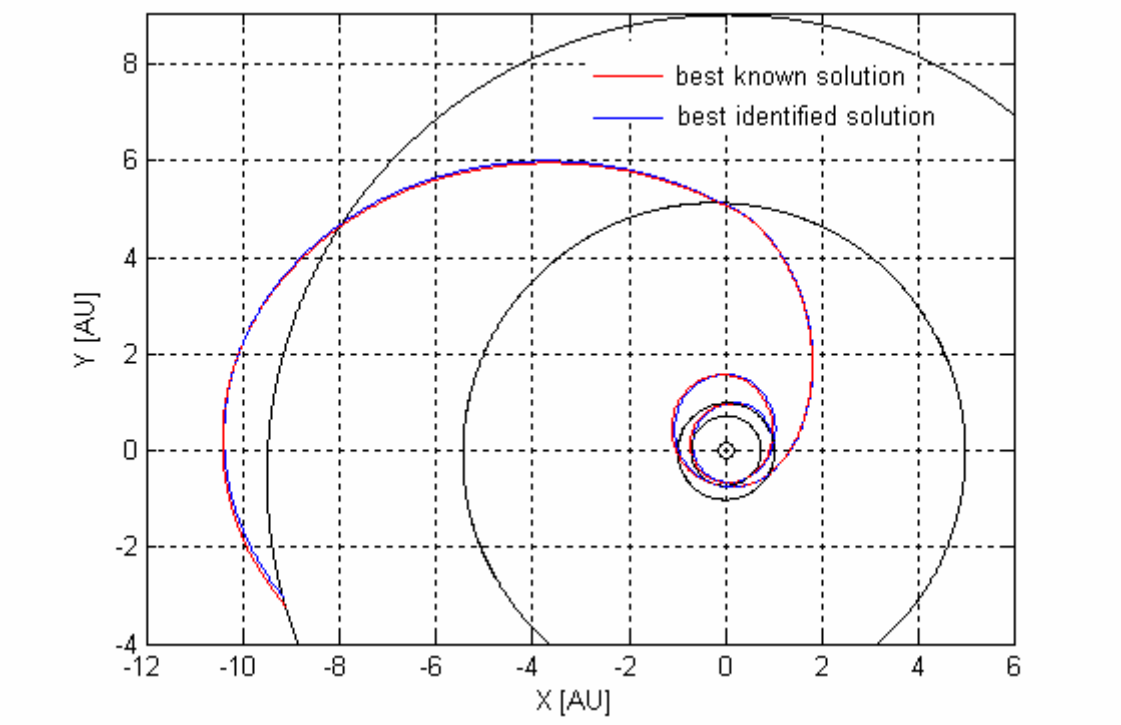

Figure 182: Comparison between the best identified solution and the best known solution.

Let now consider the two solutions in the normalized search space. Table 101 reports the values of the design variables.

	t_0	tt_{E-V}	tt_{V-V}	tt_{V-E}	tt_{E-J}	tt_{J-S}
Best identified solution	0.257	0.714	0.903	0.318	0.728	0.990
Best known solution	0.278	0.594	0.903	0.294	0.734	1.000

Table 101*: ASA*: comparison between the best identified solution and the best known solution in the normalized search space.

The differences on the values of the design variables in the normalized search space mainly involve the value of the Earth-Venus transfer time, where they assume a value of the order of 10^{-1}. The Euclidean distance between the two solutions is $1.247 \cdot 10^{-1}$. It is worth noting that, although differences on the design variables are similar to those encountered using the previous algorithms, the difference on the Earth-Venus transfer make the structures of the

interplanetary quite different, especially if we analyse the values of each objective function terms: indeed, by considering Table 100, one can note that the best solution identified by ASA has very little values of the minimum corrective ΔVs corresponding to each gravity assist manoeuvre, $\Delta V_{GA,P}$, while concentrating the major contribution to the objective function value on ΔV_I, that is the relative velocity with respect to Earth at the beginning of the interplanetary transfer. The difference in the structure of the interplanetary transfer is concentrated in the first phase of the interplanetary transfer, as highlighted in Figure 182.

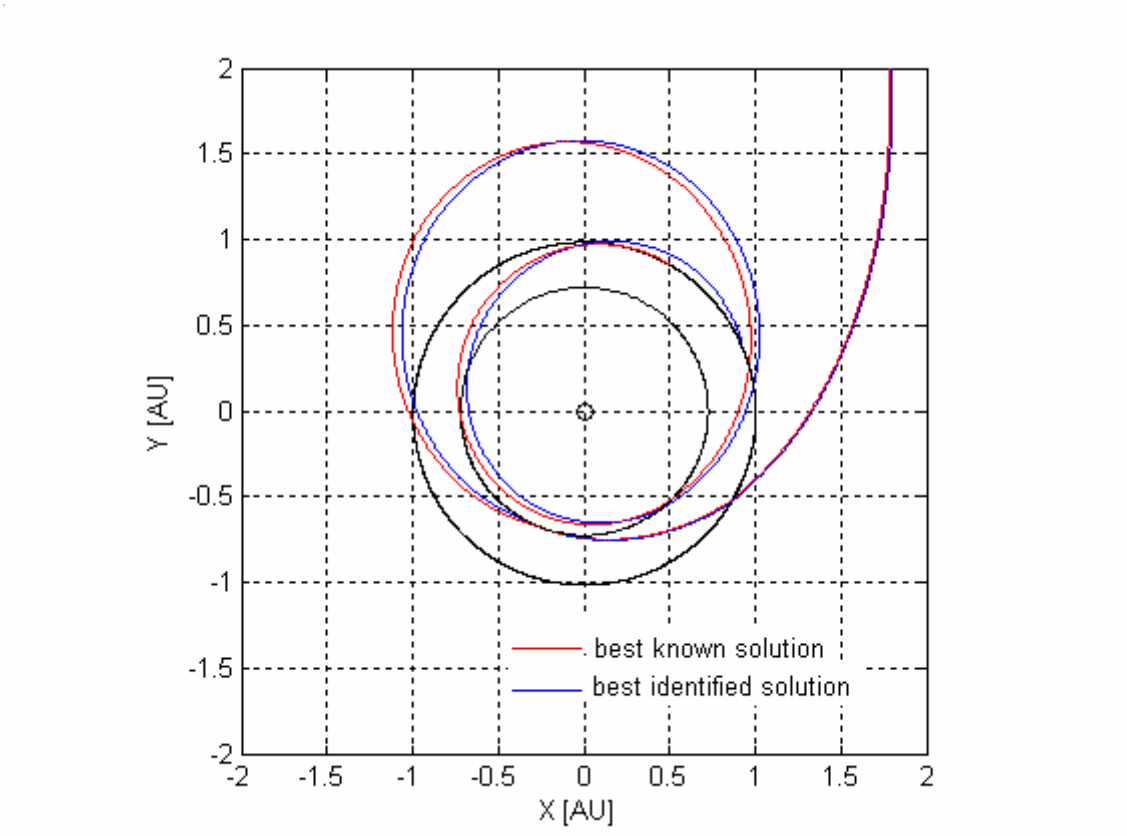

Figure 183: Comparison between the best identified solution and the best known solution: close up of the first phases of the interplanetary transfer reported in Figure 182.

In order to understand if the identified solution is in fact representative of a new family of transfer trajectories corresponding to a local minimum different from the best known one, a local optimization process by means of a SQP algorithm is performed by considering the solution identified by ASA as the starting point. The resulting improvement of the best identified solution is reported in Table

102, while Figure 184 illustrates the first phases of the resulting interplanetary transfer.

	Best identified solution + SQP	Best known solution
t_0 :	-800.089 *d*	-770.686 *d*
tt_{E-V} :	208.892 *d*	179.524 *d*
tt_{V-V} :	406.734 *d*	406.528 *d*
tt_{V-E} :	53.050 *d*	53.181 *d*
tt_{E-J} :	757.953 *d*	758.334 *d*
tt_{J-S} :	3650.218 *d*	3650.218 *d*
ΔV :	6500.786 *m/s*	6367.990 *m/s*
ΔV_I :	5987.912 *m/s*	3901.332 *m/s*
1st $\Delta V_{GA,V}$:	38.345 *m/s*	2019.210 *m/s*
2nd $\Delta V_{GA,V}$:	25.552 *m/s*	0.018 *m/s*
$\Delta V_{GA,E}$	0.537 *m/s*	0.005 *m/s*
$\Delta V_{GA,J}$	0.226 *m/s*	0.022 *m/s*
ΔV_F :	448.213 *m/s*	447.402 *m/s*

Table 184: Comparison between the best solution identified by *ASA* improved by a SQP based local optimization process and the best known solution (number of function evaluations required by the local optimization process equal to 925).

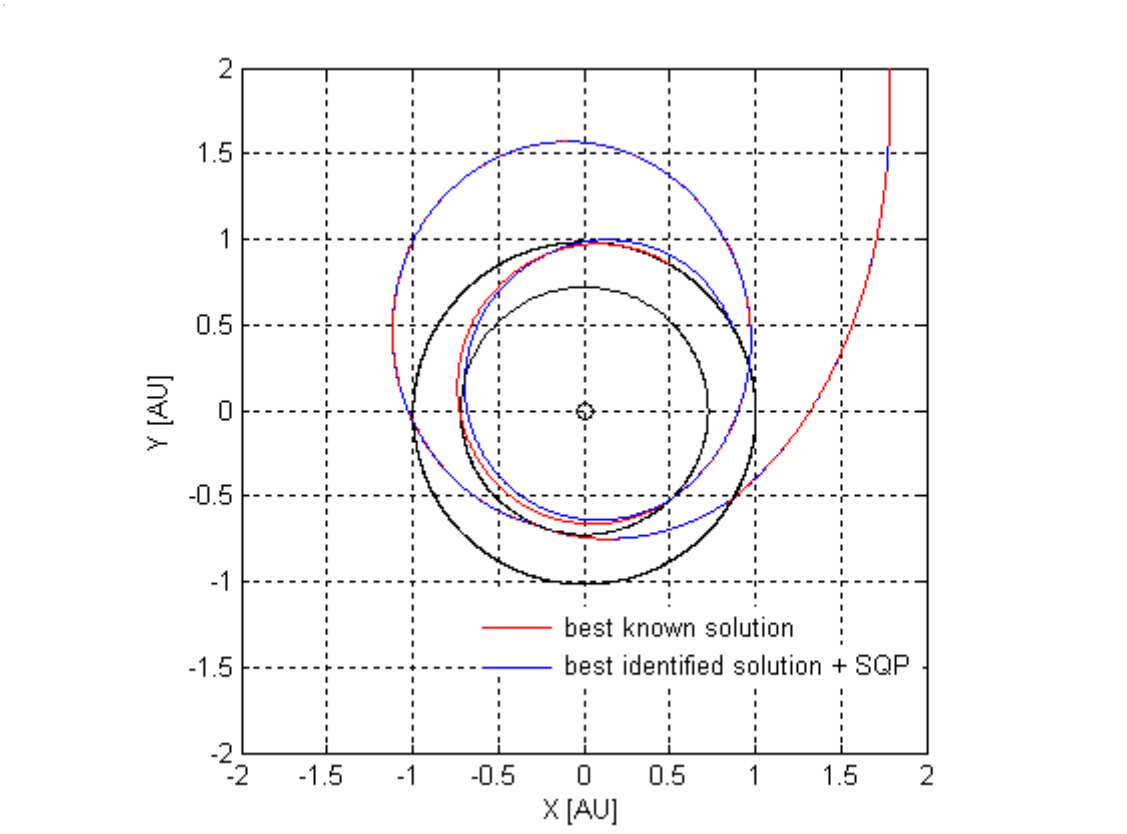

Figure 184*: ASA*: comparison between the improved best identified solution and the best known solution: close up of the first phases of the interplanetary transfer.

Table 102 shows that the best solution identified by ASA doesn't lie in the basin of attraction of the best known solution and it identifies in fact a new local optimum solution which is worse than the best known one in terms of the objective function value, but displays different and interesting features: indeed, most of the overall ΔV concentrates on ΔV_I, which is usually given by the launcher; in this way the spacecraft must provide the corrective $\Delta Vs_{GA,P}$ and the final ΔV_F, which are in fact lower than in case of the previously identified solutions; however, the high ΔV_I which can be given by the launcher limits the allowed maximum spacecraft launch mass (e.g. in case of using Titan IV-Centaur launcher, the allowed launch mass is equal to 4500 *kg*, which is about 1000 *kg* smaller than the Cassini-Huygens launch mass). It is interesting to note that the objective function value corresponding to the best solution identified by ASA is only 132.796 *m/s* higher than in case of the best known solution: this constitutes a further proof of the existence of many comparable local minima

close to each other, which increases the possibility of converging to no global optima. Let now analyse the statistical values of ASA performances. Figure shows the distribution of the solutions resulting from each optimization run over the plane of the objective function, ΔV, and the number of function evaluations, *nFunc*, while Table 102 reports the statistical characteristics, which will be used for comparisons with the other optimization algorithms, as well as the performances corresponding to the best identified solution.

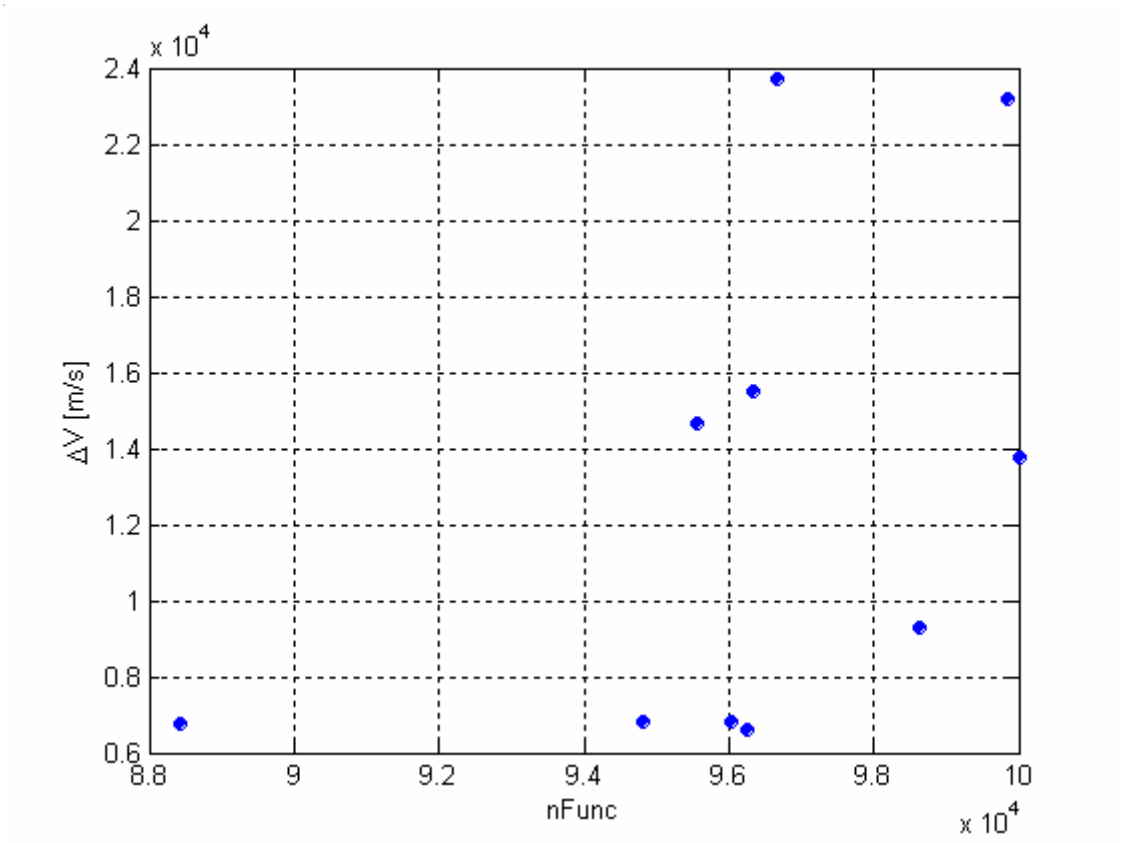

Figure 185: Distribution of the solutions resulting from each ASA optimization run over the $nFunc - \Delta V$ plane.

Evaluation criterion	Mean value	Standard deviation	Best identified solution
ΔV :	12712.987 *m/s*	6646.187 *m/s*	6618.027 *m/s*
nFunc.:	96255.800	3281.118	96250
Runtime [STU]:	1.626	0.273	1.883

Table 102: Statistical characteristics of the identified solutions.

The optimal solutions corresponding to all ten runs are now considered as starting solutions for ten local optimization processes in order to accurately estimate the local minimum corresponding to the basin of attraction each optimal solution belong to. Figure 186 illustrates the consequences of the local optimization processes in the *nFunc* - ΔV plane.

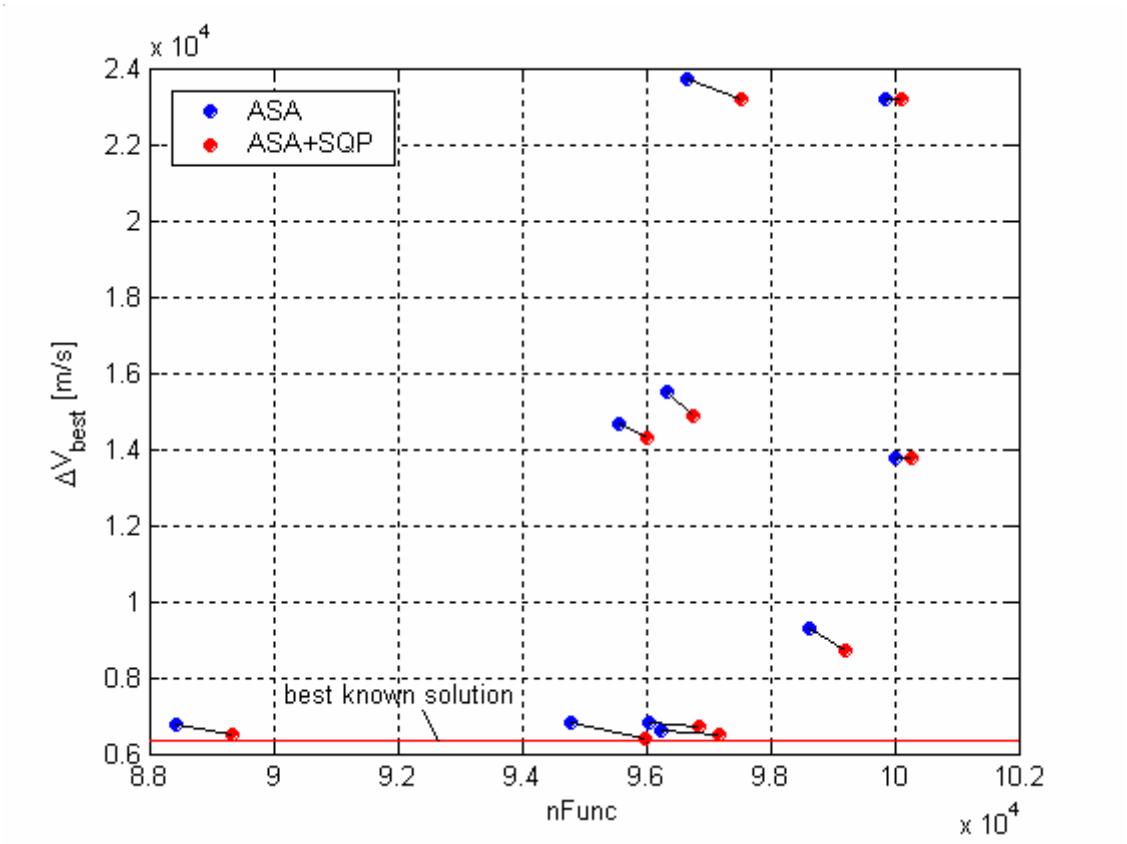

Figure 186: Comparison between solutions resulting from ASA runs and their improvements by means of a further local optimization process via SQP algorithm over the $nFunc - \Delta V$ plane.

Different local minima correspond to ASA runs. In order to estimate the number of identified solutions which lie in the basin of attraction of the best known solutions, let investigate the solutions in the normalized search space. --- reports, corresponding to each ASA+SQP run, the reached objective function value and the distance (in Euclidean metric) with respect to the best known solution.

Mean value	ΔV [m/s]	Distance
run 1	14887.689	0.883
run 2	13774.208	0.791
run 3	14286.834	0.638
run 4	6500.786	0.107
run 5	8731.842	0.744
run 6	6507.752	0.108
run 7	23174.526	1.001
run 8	6368.634	0.001
run 9	23174.528	1.001
run 10	6694.102	0.162

Table 104: ASA+SQP optimization runs: objective function values and Euclidean distance in the normalized search space with respect to the best known solution.

By considering two solutions as identical when the Euclidean distance is less than 0.024, only run 8 was able to get the best known solution, that is 1/10 ASA runs successfully identified the basin of attraction of the best known solution.

glbSolve

As glbSolve algorithm implements a deterministic optimization approach, statistical characteristics are not needed in this case. Only one run has been processed in order to solve the previously defined problem. Default options suggested by the providers of the code have been used. As the Multiple Gravity Assist interplanetary transfer has high complexity features, we used a maximum number of iterations equal to 1000.

Algorithm parameters	
Maximum number of generations:	1000

Table 105 reports the identified solution compared with the best known solution in terms of the values of the design variables and of the objective function terms, while Figure 187 plots the resulting interplanetary transfer trajectories.

	Identified solution	**Best known solution**
t_0:	244.168 *d*	-770.686 *d*
tt_{E-V}:	250.755 *d*	179.524 *d*
tt_{V-V}:	418.907 *d*	406.528 *d*
tt_{V-E}:	129.888 *d*	53.181 *d*
tt_{E-J}:	536.614 *d*	758.334 *d*
tt_{J-S}:	3605.070 *d*	3650.218 *d*
ΔV:	15354.532 *m/s*	6367.990 *m/s*
ΔV_I:	7068.211 *m/s*	3901.332 *m/s*
1st $\Delta V_{GA,V}$:	920.974 *m/s*	2019.210 *m/s*
2nd $\Delta V_{GA,V}$:	222.217 *m/s*	0.018 *m/s*
$\Delta V_{GA,E}$	6201.130 *m/s*	0.005 *m/s*
$\Delta V_{GA,J}$	0.484 *m/s*	0.022 *m/s*
ΔV_F:	941.515 *m/s*	447.402 *m/s*

Table 105: Comparison between the best identified solution and the best known solution.

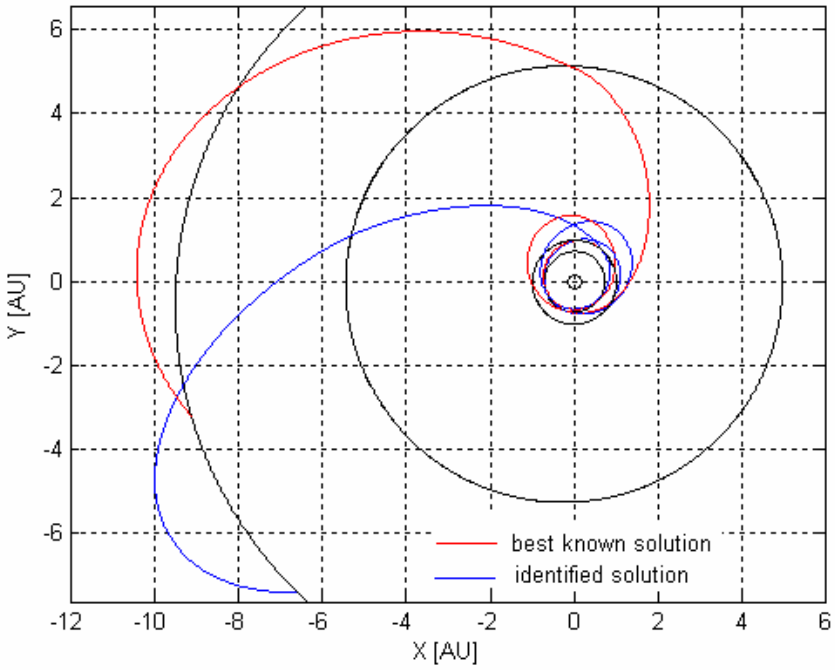

Figure 187: Comparison between the identified solution and the best known solution.

Table 105 and Figure 187 show that the two solutions are evidently different. The two solutions in the normalized search space are reported in Table 106.

	t_0	tt_{E-V}	tt_{V-V}	tt_{V-E}	tt_{E-J}	tt_{J-S}
Identified solution	0.834	0.852	0.931	0.878	0.487	0.986
Best known solution	0.278	0.594	0.903	0.294	0.734	1.000

Table 106: *glbSolve*: comparison between the identified solution and the best known solution in the normalized search space.

The differences on the values of the design variables in the normalized search space assume a maximum value of $5.841 \cdot 10^{-1}$ corresponding to the Venus-Earth transfer time. The Euclidean distance between the two solutions is $8.826 \cdot 10^{-1}$. In order to accurately identify the local minimum reached by *glbSolve* algorithm, a local optimization process by means of a SQP algorithm is now performed. Given the solution identified by *glbSolve* (reported in Table 106)

and considering it as the starting point for the local search process, the improved identified solution reported in Table 107 is identified.

	Identified solution + SQP	Best known solution
t_0 :	242.654 *d*	-770.686 *d*
tt_{E-V} :	258.873 *d*	179.524 *d*
tt_{V-V} :	412.968 *d*	406.528 *d*
tt_{V-E} :	127.574 *d*	53.181 *d*
tt_{E-J} :	540.798 *d*	758.334 *d*
tt_{J-S} :	3650.218 *d*	3650.218 *d*
ΔV :	14763.770 *m/s*	6367.990 *m/s*
ΔV_I :	7927.631 *m/s*	3901.332 *m/s*
1st $\Delta V_{GA,V}$:	0.056 *m/s*	2019.210 *m/s*
2nd $\Delta V_{GA,V}$:	0.020 *m/s*	0.018 *m/s*
$\Delta V_{GA,E}$	5905.166 *m/s*	0.005 *m/s*
$\Delta V_{GA,J}$	0 *m/s*	0.022 *m/s*
ΔV_F :	930.896 *m/s*	447.402 *m/s*

Table 107: Comparison between the solution identified by *ASA* improved by a SQP based local optimization process and the best known solution (number of function evaluations required by the local optimization process equal to 566).

Table 108 reports the characteristics of the identified solution, which will be used for comparisons with the other optimization algorithms.

Evaluation criterion	Identified solution
ΔV :	15347.899 *m/s*
nFunc.:	4345
Runtime [STU]:	0.093

Table 108: Characteristics of the identified solutions.

MCS

As MCS algorithm implements a deterministic optimization approach, only one run have been processed in order to solve the previously defined problem. Default options suggested by the providers of the code have been used. Table 109 reports the identified solution compared with the best known solution in terms of the values of the design variables and of the objective function terms, while Figure 188 plots the resulting interplanetary transfer trajectories.

	Best identified solution	**Best known solution**
t_0:	-783.935 *d*	-770.686 *d*
tt_{E-V}:	107.476 *d*	179.524 *d*
tt_{V-V}:	448.916 *d*	406.528 *d*
tt_{V-E}:	82.520 *d*	53.181 *d*
tt_{E-J}:	731.592 *d*	758.334 *d*
tt_{J-S}:	3620.137 *d*	3650.218 *d*
ΔV:	13782.954 *m/s*	6367.990 *m/s*
ΔV_I:	3717.562 *m/s*	3901.332 *m/s*
1st $\Delta V_{GA,V}$:	1764.630 *m/s*	2019.210 *m/s*
2nd $\Delta V_{GA,V}$:	4413.551*m/s*	0.018 *m/s*
$\Delta V_{GA,E}$	3221.307 *m/s*	0.005 *m/s*
$\Delta V_{GA,J}$	229.904 *m/s*	0.022 *m/s*
ΔV_F:	436.000 *m/s*	447.402 *m/s*

Table 109 - Comparison between the identified solution and the best known solution.

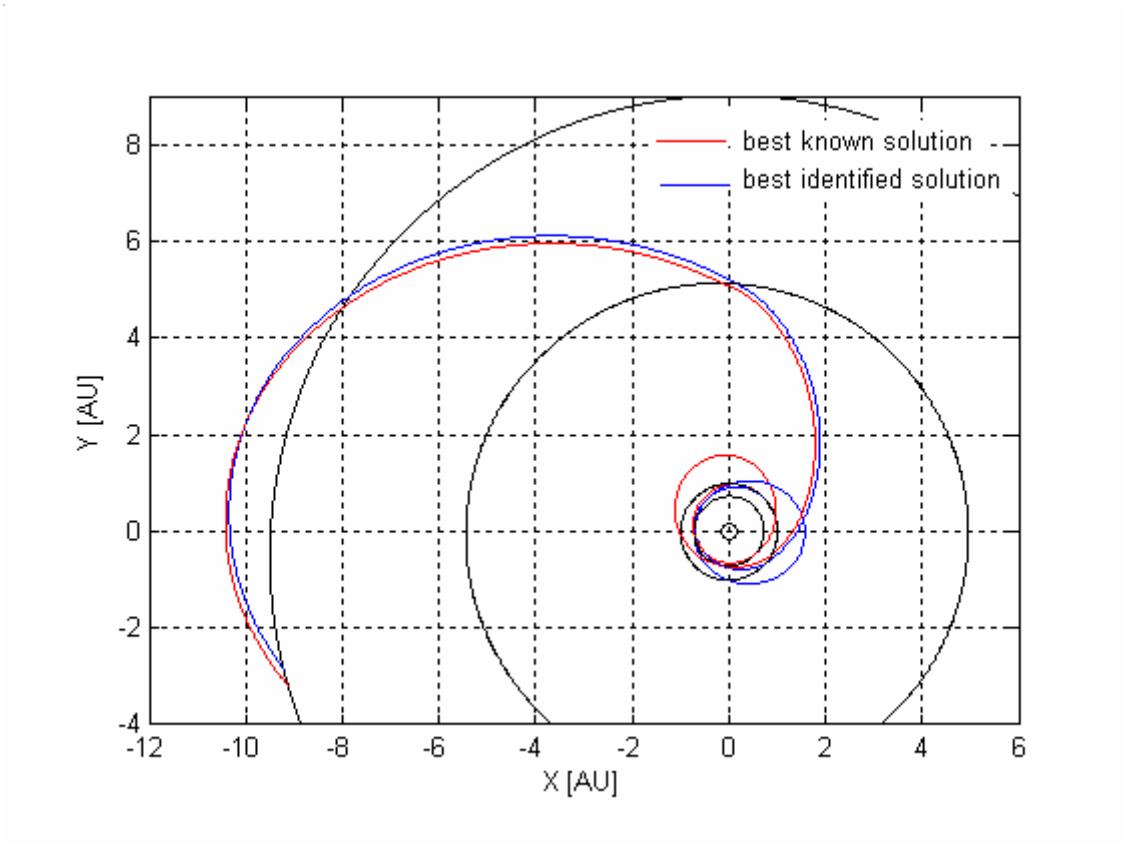

Figure 188 - Comparison between the identified solution and the best known solution.

Table 110 reports the two solutions in the normalized search space.

	t_0	tt_{E-V}	tt_{V-V}	tt_{V-E}	tt_{E-J}	tt_{J-S}
Identified solution	0.270	0.335	1.000	0.517	0.705	0.991
Best known solution	0.278	0.594	0.903	0.294	0.734	1.000

Table 110*: MCS*: comparison between the identified solution and the best known solution in the normalized search space.

The Euclidean distance between the two solutions is $3.576 \cdot 10^{-1}$. It is worth noting that the differences in the design variables mainly concentrates in the tt_{E-V} and tt_{V-E} values. In fact the solution identified by MCS can be recognized to be alternative to the best known one in terms of these two design variables: indeed, the solution identified by MCS is characterized by a lower Earth-Venus

transfer time, while having a higher value of the Venus-Earth transfer time (see Figure 189).

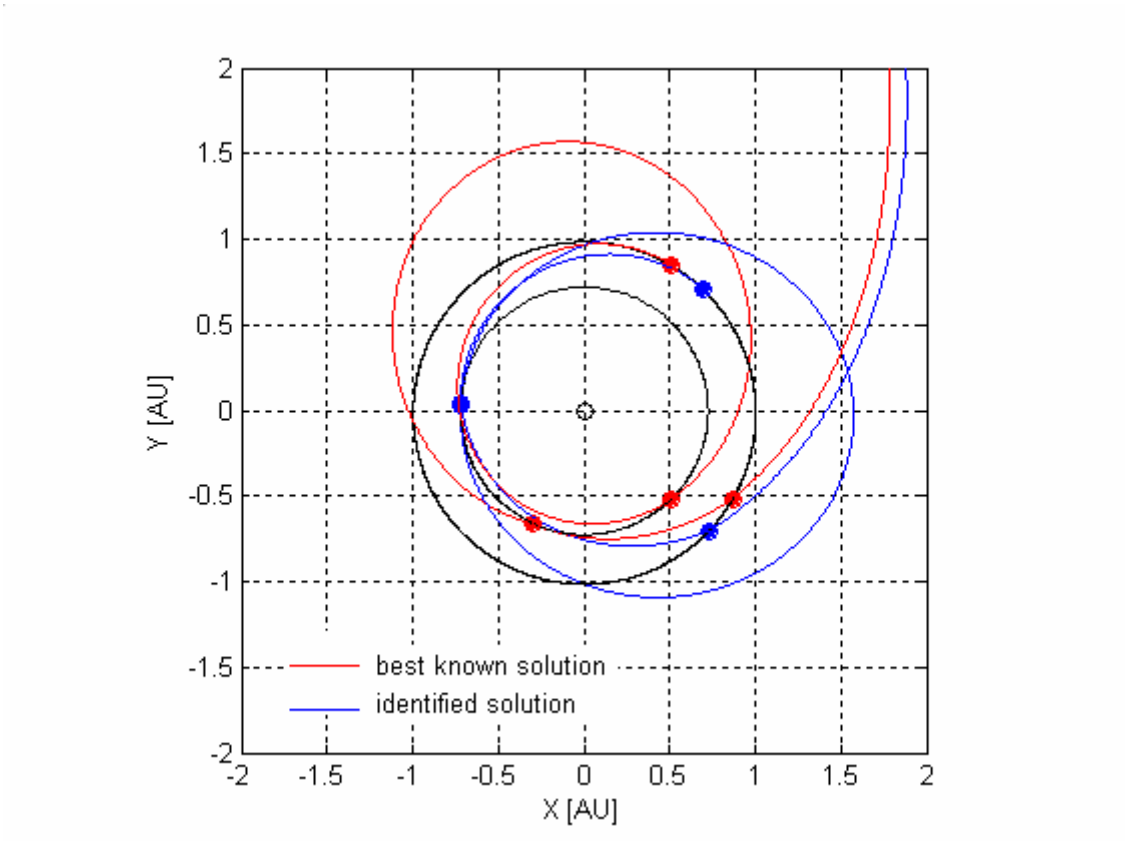

Figure 189: Close up of th initial phase from Figure 188.

The previous results let us suppose that MCS wasn't able to reach the basin of attraction of the best known solution. Such result can be confirmed by means of a local optimization process performed using a SQP algorithm. Given the solution identified by MCS and considering it as the starting point for the local search process, the improved best identified solution reported in Table 111 is identified.

	Identified solution + SQP	Best known solution
t_0:	-783.390 *d*	-770.686 *d*
tt_{E-V}:	144.713 *d*	179.524 *d*
tt_{V-V}:	448.916 *d*	406.528 *d*
tt_{V-E}:	57.004 *d*	53.181 *d*
tt_{E-J}:	757.130 *d*	758.334 *d*
tt_{J-S}:	3650.218 *d*	3650.218 *d*
ΔV:	6696.023 *m/s*	6367.990 *m/s*
ΔV_I:	3648.442 *m/s*	3901.332 *m/s*
1st $\Delta V_{GA,V}$:	8.554 *m/s*	2019.210 *m/s*
2nd $\Delta V_{GA,V}$:	2591.553 *m/s*	0.018 *m/s*
$\Delta V_{GA,E}$	0 *m/s*	0.005 *m/s*
$\Delta V_{GA,J}$	0.027 *m/s*	0.022 *m/s*
ΔV_F:	447.446 *m/s*	447.402 *m/s*

Table 111: Comparison between the solution identified by *MCS* improved by a SQP based local optimization process and the best known solution (number of function evaluations required by the local optimization process equal to 812).

Table 111 shows that MCS algorithm wasn't able to get the basin of attraction of the best known solution. Table 112 reports the characteristics of the identified solution, which will be used for comparisons with the other optimization algorithms.

Evaluation criterion	Best identified solution
ΔV:	13782.954 *m/s*
nFunc.:	46601
Runtime [STU]:	1.020

Table 112: Characteristics of the identified solutions.

rbfSolve

As rbfSolve algorithm implements a deterministic optimization approach, based on objective function response surfaces assessment and analysis suitable for costly objective function problems, statistical features analysis don't hold here. Only one run has been processed in order to solve the previously defined problem. Default options suggested by the providers of the code have been used. As already stated in the description of this optimization tool, the termination conditions available in TOMLAB version of rbfSolve tool (which is not freely available) do not include suitable rules for practical problems with not a priori information about the global optimum solution. As a consequence, a maximum number of objective function evaluations has been fixed for terminating the optimization process. The maximum value in case of the 2-impulse direct Planet-to-Planet transfer problem has been set based on the order of magnitude of the objective function evaluations resulting from the application of the previously analysed tools to that problem. By revising the previous analysis, in case of Multiple Gravity Assist the number of objective function evaluations was quite high: as an example, ASA required about 10^5 objective function evaluations. However, rbfSolve is tailored for costly optimization processes and can not dealing with so high number of objective function evaluations due to the high required memory for handling the interpolation process. As a consequence, such limitations forced us to fix a maximum number of objective function evaluations of the order of 10^3. Anyway, the achieved results can be considered as indicative of the performance of such a tool in solving the previously defined problem: response surface based global optimization algorithms use objective function evaluations for interpolating and then approximating the objective function shape; the generated response surface is then investigated to identify promising regions for the global search. The number of objective function evaluations which are usually performed using response surface based optimization algorithms are in fact low if compared with other global optimization tools, due to the aim of solving costly optimization problems. As a consequence, if the response surface algorithm is not able to identify and accurately approximate the basin of attraction of the global optimum in a low number of objective function evaluations, it is likely the case the

algorithm has not converged to the global optimum solution. Hence, the fixed number of objective function evaluations has been set to 1000.

Algorithm parameters	
Maximum number of objective function evaluations:	1000

Table 113 reports the identified solution compared with the best known solution in terms of the values of the design variables and of the objective function terms, while Figure 190 plots the resulting interplanetary transfer trajectories.

	Identified solution	Best known solution
t_0:	358.328 *d*	-770.686 *d*
tt_{E-V}:	123.810 *d*	179.524 *d*
tt_{V-V}:	418.089 *d*	406.528 *d*
tt_{V-E}:	145.917 *d*	53.181 *d*
tt_{E-J}:	461.924 *d*	758.334 *d*
tt_{J-S}:	2390.057 *d*	3650.218 *d*
ΔV:	16970.001 *m/s*	6367.990 *m/s*
ΔV_I:	3338.781 *m/s*	3901.332 *m/s*
1st $\Delta V_{GA,V}$:	3644.557 *m/s*	2019.210 *m/s*
2nd $\Delta V_{GA,V}$:	25.226 *m/s*	0.018 *m/s*
$\Delta V_{GA,E}$	8498.370 *m/s*	0.005 *m/s*
$\Delta V_{GA,J}$	109.569 *m/s*	0.022 *m/s*
ΔV_F:	1353.497 *m/s*	447.402 *m/s*

Table 113: Comparison between the identified solution and the best known solution.

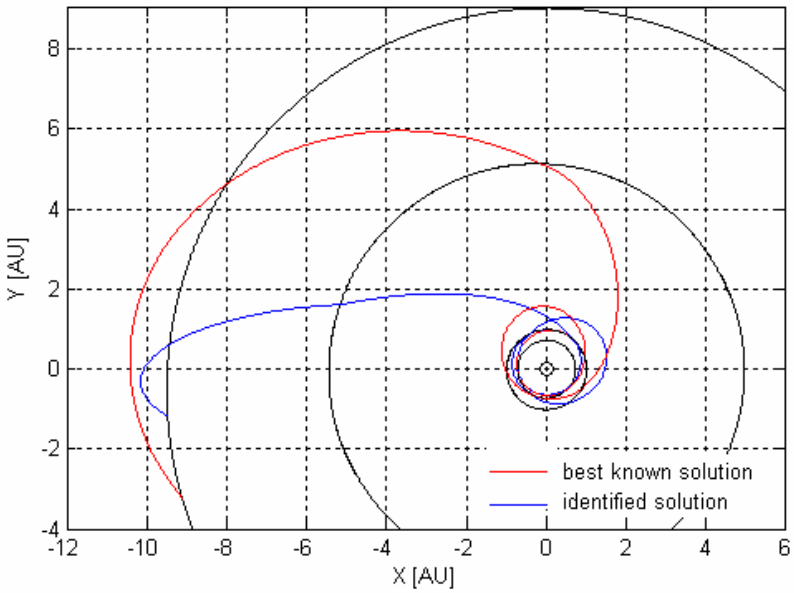

Figure 190: Comparison between the identified solution and the best known solution.

The two solutions seem to belong to basin of attraction of different local minima, especially analysing the first phase of the interplanetary transfer. Such idea is supported by Table 113, which reports the two solutions in the normalized search space.

	t_0	tt_{E-V}	tt_{V-V}	tt_{V-E}	tt_{E-J}	tt_{J-S}
Identified solution	0.896	0.394	0.930	1	0.404	0.616
Best known solution	0.278	0.594	0.903	0.294	0.734	1.000

Table 113*: rbfSolve*: comparison between the identified solution and the best known solution in the normalized search space.

The Euclidean distance between the two solutions is 1.085. In order to better investigated whether rbfSolve was able to reach the basin of attraction of the best known solution, a local optimization process is performed using a SQP algorithm. Given the solution identified by rbfSolve and considering it as the starting point for the local search process, the improved best identified solution reported in Table 116 is identified.

	Identified solution + SQP	Best known solution
t_0 :	371.436	-770.686 *d*
tt_{E-V} :	115.158	179.524 *d*
tt_{V-V} :	430.791	406.528 *d*
tt_{V-E} :	127.931	53.181 *d*
tt_{E-J} :	538.053	758.334 *d*
tt_{J-S} :	3650.218	3650.218 *d*
ΔV :	12968.322	6367.990 *m/s*
ΔV_I :	2995.515	3901.332 *m/s*
1st $\Delta V_{GA,V}$:	1715.141	2019.210 *m/s*
2nd $\Delta V_{GA,V}$:	1116.794	0.018 *m/s*
$\Delta V_{GA,E}$	6209.642	0.005 *m/s*
$\Delta V_{GA,J}$	0	0.022 *m/s*
ΔV_F :	931.231	447.402 *m/s*

Table 115: Comparison between the solution identified by *rbfSolve* improved by a SQP based local optimization process and the best known solution (number of function evaluations required by the local optimization process equal to 377).

Table 115 shows that rbfSolve algorithm wasn't able to get the basin of attraction of the best known solution. Table 116 reports the characteristics of the identified solution, which will be used for comparisons with the other optimization algorithms.

Evaluation criterion	Best identified solution
ΔV :	16970.001 *m/s*
nFunc.:	1000
Runtime [STU]:	49.350

Table 116: Characteristics of the identified solutions.

Summary of Results:

Table 117 reports the summary of results for the MGA transfer problem.

Algorithm	ΔV [*m/s*]	Fun. evaluations	Runtime [STU]
GAOT	8256.416 (σ =1555.107)	8543.4 (σ =4075.382)	0.1883 (σ =0.09683)
GAOT-shared	21874.731 (σ =5741.406)	1350.4 (σ =559.057)	0.027 (σ =0.01192)
GATBX	8317.45 (σ =2339.832)	39468 (σ =29981.599)	0.748 (σ =0.584)
GATBX-migr	8237.81 (σ =972.517)	59220 (σ =27105.666)	1.272 (σ =0.722)
FEP	9287.112 (σ =2860.194)	22238.3 (σ =16233.713)	0.629 (σ =0.458)
DE	10145.388 (σ =3494.605)	10250 (σ =4696.157)	0.201 (σ =0.094)
ASA	12712.987 (σ =6646.187)	96255.8 (σ =3281.118)	1.626 (σ =0.273)
GlbSolve	15347.899	4345	0.093
MCS	13782.954	46601	1.02
RbfSolve	16970.001	1000	49.350
EPIC*	7133.900 (σ = 431.79)	10127 (σ =115.9)	-

Table 117: Summary of results for the Multiple Gravity Assist interplanetary transfer problem (* courtesy of Dr. Massimiliano Vasile).

Note that Table 117 also reports the performances of EPIC algorithm, which have been supplied by Dr. Massimiliano Vasile. Unfortunately, the analysis of EPIC results on the search space could not be accomplished and the runtime performances were not available. As stated in the 2-impulse direct planet-to-planet transfer algorithms test phase, the performance criteria we have measured are in fact partially conflicting. As proposed in earlier works [Pintér, 1995], concepts and techniques typically adopted in multiobjective optimization problems (such as the concept of the Pareto dominance) can be here used. As stated above, due to the presence of not optimized codes among the tested ones and to the necessity of creating a MEX file for ASA algorithm (which

slightly affects the runtime performances), the main evaluation criteria to be considered have been taken as the objective function value reached, ΔV, and the number of model function evaluations needed, *nFunc*. Figure 191 reports such performances in a ΔV - *nFunc* plane in order to identify the Pareto optimal solution.

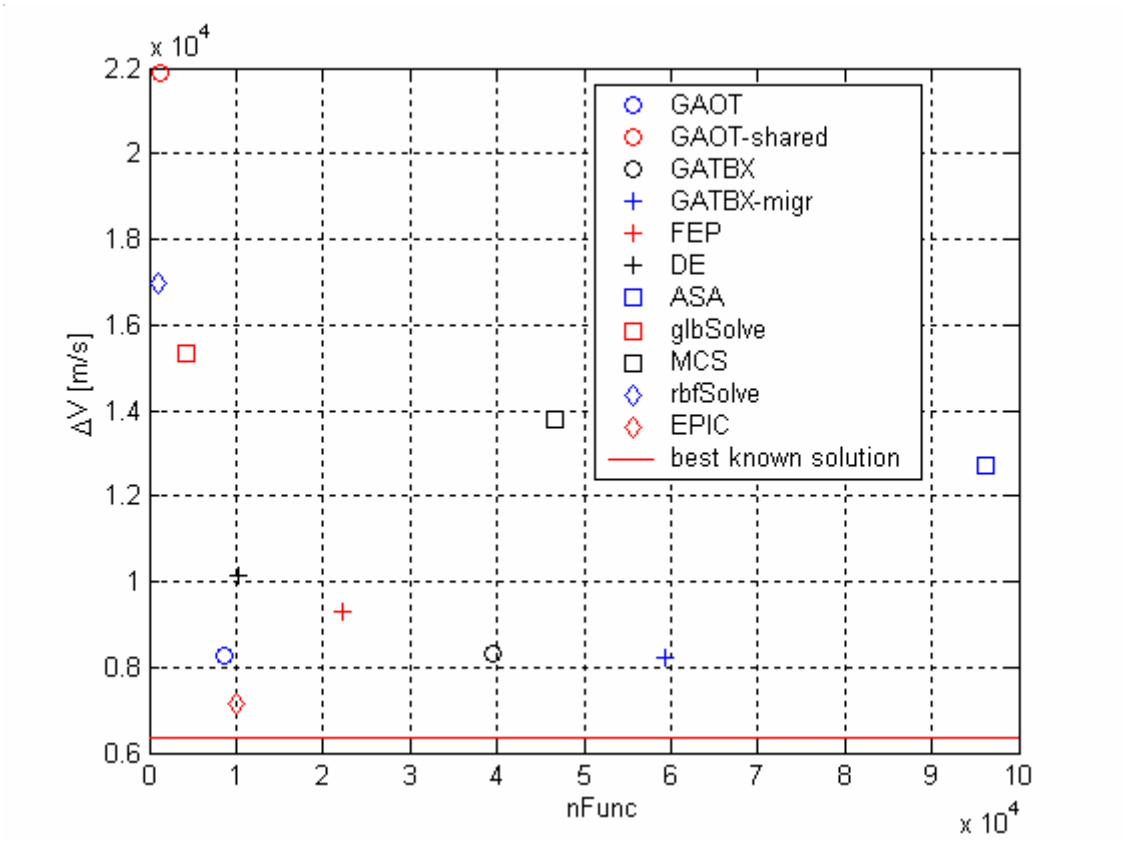

Figure 191: Algorithms performances in the ΔV - *nFunc* plane.

Note that Figure 191 reports the performances listed in Table 117, which contains statistical performances in case of randomized optimization algorithms. By applying the concepts of Pareto dominance, Table 118 reports for each algorithm, the number of algorithms which dominated (and then outperformed) it.

Algorithm	# of dominating algorithms
GAOT	0
GAOT-shared	1
GATBX	2
GATBX-migr	1
FEP	2
DE	2
ASA	6
glbSolve	0
MCS	5
rbfSolve	0
EPIC	0

Table 118: Number of dominating algorithms.

Table 118 shows that the set of Pareto optimal solutions includes in fact four solutions: the algorithms which best solved the Multiple Gravity Assist interplanetary transfer in a Pareto optimal sense are GAOT, glbSolve, rbfSolve and EPIC whose performances are shown in Figure 192.

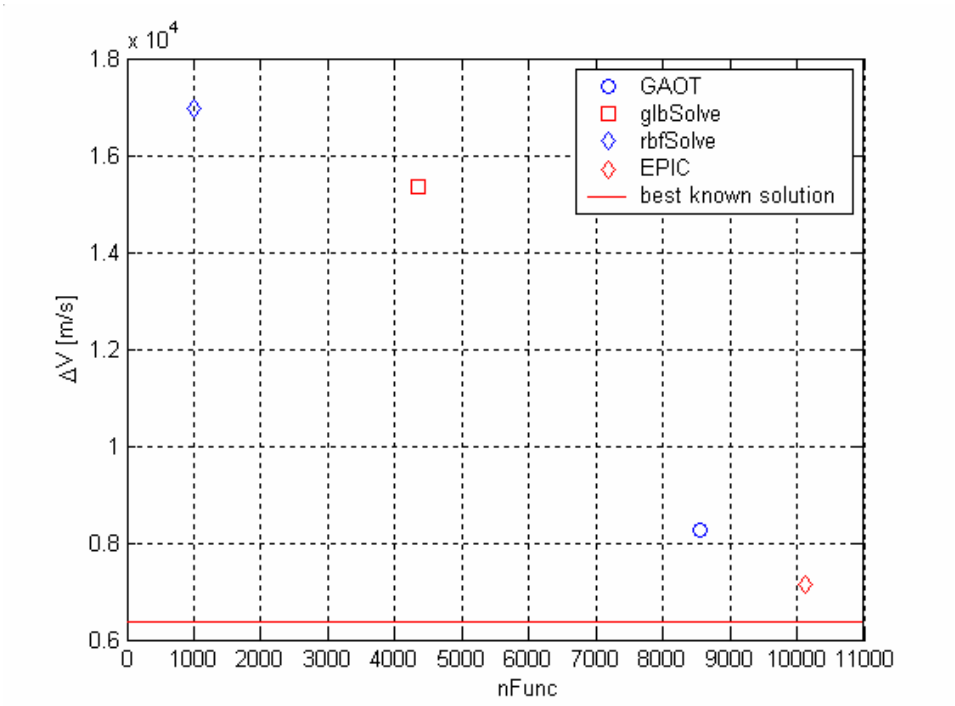

Figure 192: Pareto optimal algorithms.

It is worth noting that, the concept of Pareto optimality in multicriteria decision problems define the optimal solution by simultaneously investigating its performances on all considered criteria. This is the reason why, while EPIC is a Pareto optimal solution thanks to the identification of the mean best solution in terms of the objective function value, rbfSolve algorithm is Pareto optimal thanks to its low number of required objective function evaluations, although, as resulting from its previous analysis, it was not able to reach the basin of attraction of the best known solution. Note that these results are strictly affected by the stopping criterion used. However, the effects of the stopping criteria on the algorithm performances are not addressed here, where the algorithms are used as black-box tools. Let consider now the runtime performances: keeping in mind the previously stated considerations about the reasons of choosing ΔV and *nFunc* as main performance criteria, we want to analyze the consequences of including the runtime performance on the identification of the Pareto optimal algorithm. We have now three performance criteria. Figure 193 and Figure 194 report the algorithms performances in the ΔV -*nFunc* plane and in the *nFunc* - *runtime* plane respectively, which have not been considered so far. Note that

EPIC performances couldn't be reported in the following analysis, due to the lack on required runtime information.

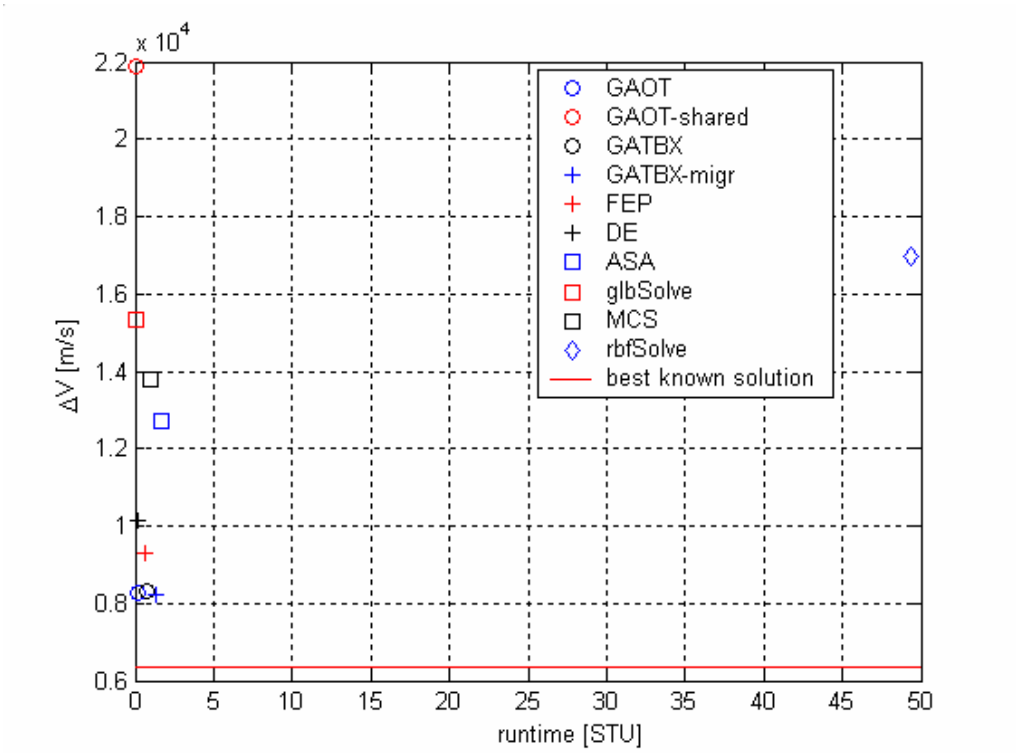

Figure 193: Algorithms performances in the ΔV - *runtime* plane.

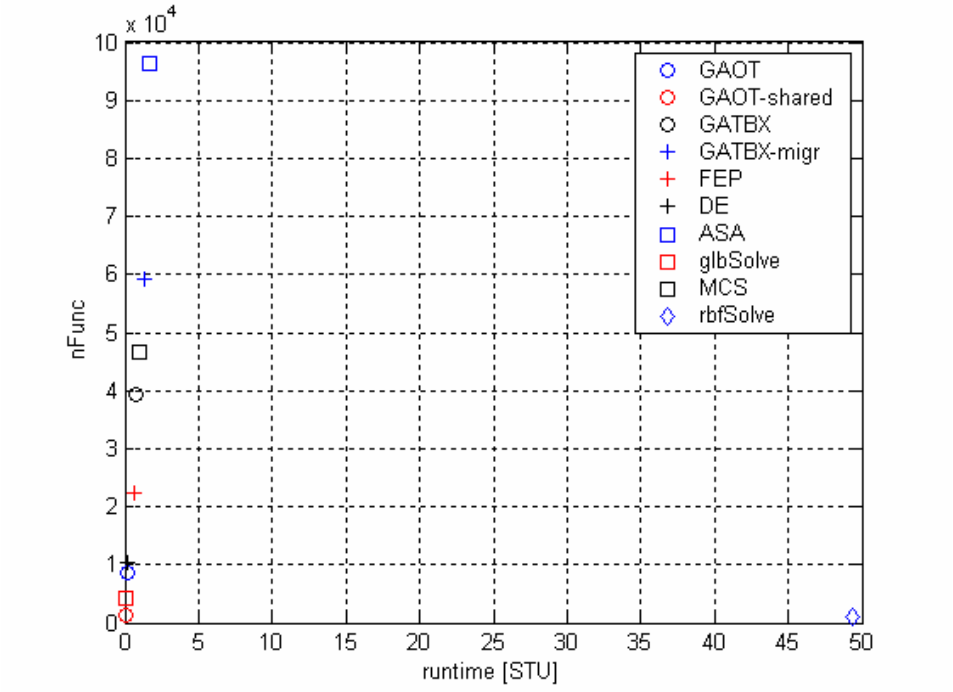

Figure 194: Algorithms performances in the *nFunc* - *runtime* plane.

As already noted in case of the 2-impulse direct planet-to-planet transfer problem, the runtime corresponding to rbfSolve is quite high if compared to the other optimization algorithms (for a better visualization of all algorithms performances excluding rbfSolve see Figure 195 and Figure 196) due to the time spent in interpolating the response surface.

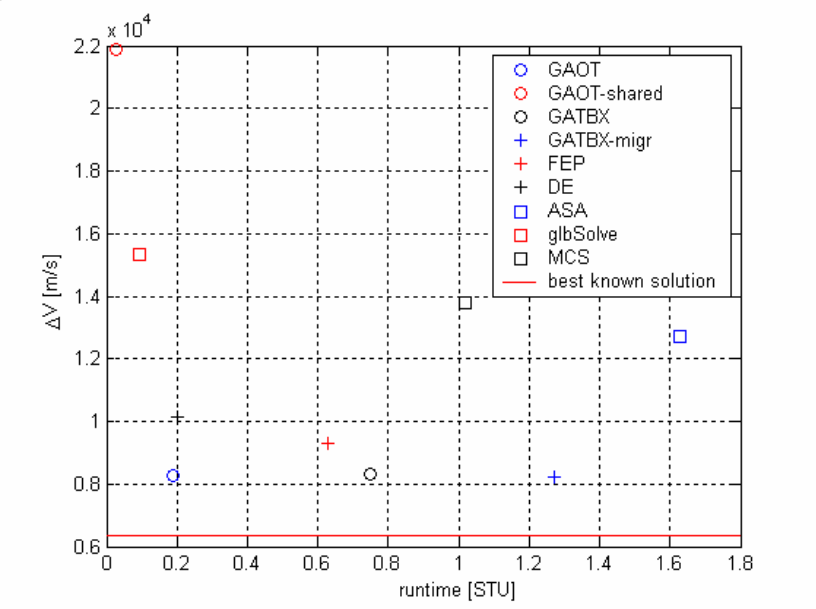

Figure 195: Algorithms performances in the ΔV - *runtime* plane (excluding rbfSolve).

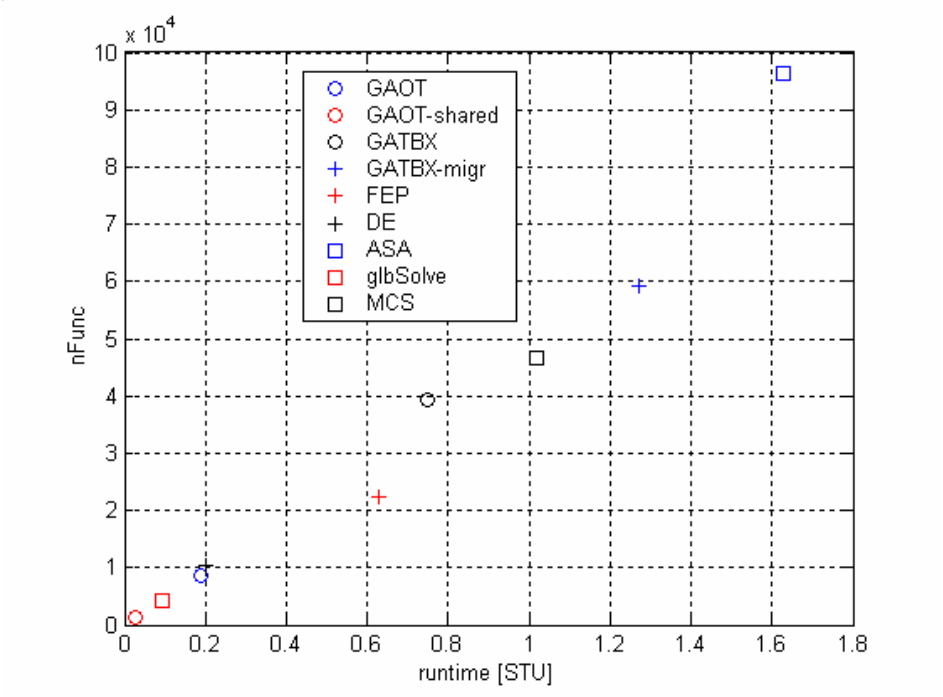

Figure 196: Algorithms performances in the *nFunc* - *runtime* plane (excluding rbfSolve).

By applying the concepts of Pareto dominance in this three-criteria case, Table 119 reports for each algorithm, the number of algorithms which dominated it.

Algorithm	# of dominating algorithms
GAOT	0
GAOT-shared	0
GATBX	1
GATBX-migr	0
FEP	1
DE	1
ASA	5
glbSolve	0
MCS	4
rbfSolve	0

Table 119: Number of dominating algorithms in the three criteria case.

Table 119 shows that GAOT-shared and GATBX-migr joined the set of Pareto optimal solutions. No changes occurred in the remaining algorithms performance. Finally the performance of all algorithms in identifying the basin of attraction of the best known solution are reported in Table 120, as resulting from the local optimization processes performed at the end of each algorithm run (note that for randomized algorithms the number of successful runs over the total number of performed runs is reported).

Algorithm	Success
GAOT	4/10
GAOT-shared	2/10
GATBX	2/10
GATBX-migr	5/10
FEP	5/10
DE	3/10
ASA	1/10
GlbSolve	No
MCS	No
RbfSolve	No

Table 120: Algorithms performance in identifying the basin of attraction of the best known solution.

Table 120 shows that GATBX-migr and FEP algorithms turned out to have the highest rate of success in reaching the basin of attraction of the best known solution in case of Multiple Gravity Assist interplanetary transfers problem. However, as reported in Table 118, they do not belong to the set of Pareto optimal algorithm in the ΔV – *nFunc* two criteria case: indeed, EPIC tool dominates them in terms of both mean objective function value reached and mean objective function evaluations required (see Figure 196). Unfortunately, no information are available to the authors regarding the success rate of EPIC. As a consequence we can state that:

- In case of interest on only the mean objective function value reached and mean number of objective function evaluations required as evaluation criteria, GAOT and EPIC tools turned out to be the best performing ones. However, due to the relatively low difference in the mean number of objective function evaluations (1583.6 over about 10000 objective function evaluations required by the two tools for performing the

optimization processes) corresponding to a relatively high difference in the mean objective function value reached (about 1000 *m/s*), EPIC tool seems to be the most suitable one for practical use in a mission analysis optimization environment.

- In case of interest on effectiveness at identifying the basin of attraction of the global optimum solution, due to the lack of information about EPIC success rate, GAOT, GATBX-migr and FEP can be considered the best performing ones. However, due to the little difference on success rate between GAOT (4/10), and GATBX-migr and FEP (5/10) corresponding to relatively high difference in the mean number of objective function evaluations (about 8543.4 for GAOT compared with 22238.3 for FEP and even 59220 for GATBX-migr), GAOT tool seems to be the most advisable one for practical use.

Note that low values of mean objective function value reached do not necessarily correspond to high success rate in identifying the basin of attraction of the best known solution. An evident example is GATBX tool: although the resulting good mean objective function value reached (which is comparable with GAOT and GATBX-migr performances), the corresponding success rate is quite low (2/10). This result can be related to the presence of several comparable local minima over the search space: indeed, most GATBX runs got trapped in local minima which are in fact comparable with the best known one in term of objective function value.

9. LOW THRUST DIRECT PLANET-TO-PLANET TRANSFER

Problem class statement:

Interplanetary transfer description
Low thrust direct planet-to-planet transfer from Earth to Mars

Objective function assessment	
Objective function:	$ObjFun = \alpha_1 \cdot R_F + \alpha_2 \cdot v_F + \alpha_3 \cdot m_{prop}$ where: • R_F is the magnitude of the spacecraft relative position with respect to Mars at the end of the integration of motion (good values: Mars sphere of influence radius, $5.77 \cdot 10^8$ *m*). • v_F is the magnitude of the spacecraft relative velocity with respect to Mars at the end of the integration of motion (good values: 100 *m/s*). • m_{prop} is the propellant mass that is required by the thrusters for the interplanetary transfer (good values: 200 *kg*). • α_1, α_2 and α_3 are weights which have been fixed in order to make the order of magnitude of $ObjFun$ equal to 10, corresponding to good R_F, v_F and m_{prop} values.

Mathematical models:	• Restricted 2-body dynamical model (C^2 in the whole solution space except in the origin) • Three dimensional motion • Analytical ephemeris model (generated by time polynomial series of the orbital elements) • Low thrust interplanetary transfer (constant thrust level and variable direction) • Parameterization of the control law on thrust azimuth and elevation in six points of interpolation over the transfer time • Forward propagation of initial conditions and thrust control law in equinoctial elements

Search space, *D*, characterization

Number of design variables:	16
Design Variables:	• Date of departure from Earth, t_0 • Transfer time, tt • Thrust level, u • Magnitude of the escape velocity from Earth, $v_{\infty,E}$ (tangential to Earth absolute velocity) • Thrust azimuth and elevation over the transfer trajectory corresponding to the six parameterization points, az_i and el_i, $i = 1,...,6$
Topology:	Continuous variables $\Rightarrow$ $D \subset \Re^{16}$

Constraints

Constraints typology:	Box constraints
Box intervals:	• t_0 included in a 4 years period starting from the 1st January 2000 • $tt \in [150,300]$ *d* • $u \in [0.1,0.168]$ *N* • $v_{\infty,E} \in [0,3000]$ *m/s*

- $az_i \in [-\pi, \pi]$ *rad*, $i = 1,...,6$
- $el_i \in [-\pi/2, \pi/2]$ *rad*, $i = 1,...,6$

General considerations	
Objective function analysis:	The objective function is almost everywhere C^2, locally discontinuous in a countable number limited set
Problem complexity:	High
Search space normalization:	The search space is normalized by means of the upper-lower bounds in order to be an unit hypercube $\Rightarrow D \equiv [0,1]^{16}$

Number of global optima: A priori unknown.

The following best known solution has been gained by means of a multi-start search, which implement a local search process via SQP algorithm starting from 100 random first guess solutions uniformly distributed over the search space (each one requiring a number of objective function evaluations of the order of 10^3).

Search space	
Date of departure:	553.253 *d*
Transfer time:	299.462 *d*
Thrust level:	0.130 *N*
Escape velocity from Earth:	2676.327 *m/s*

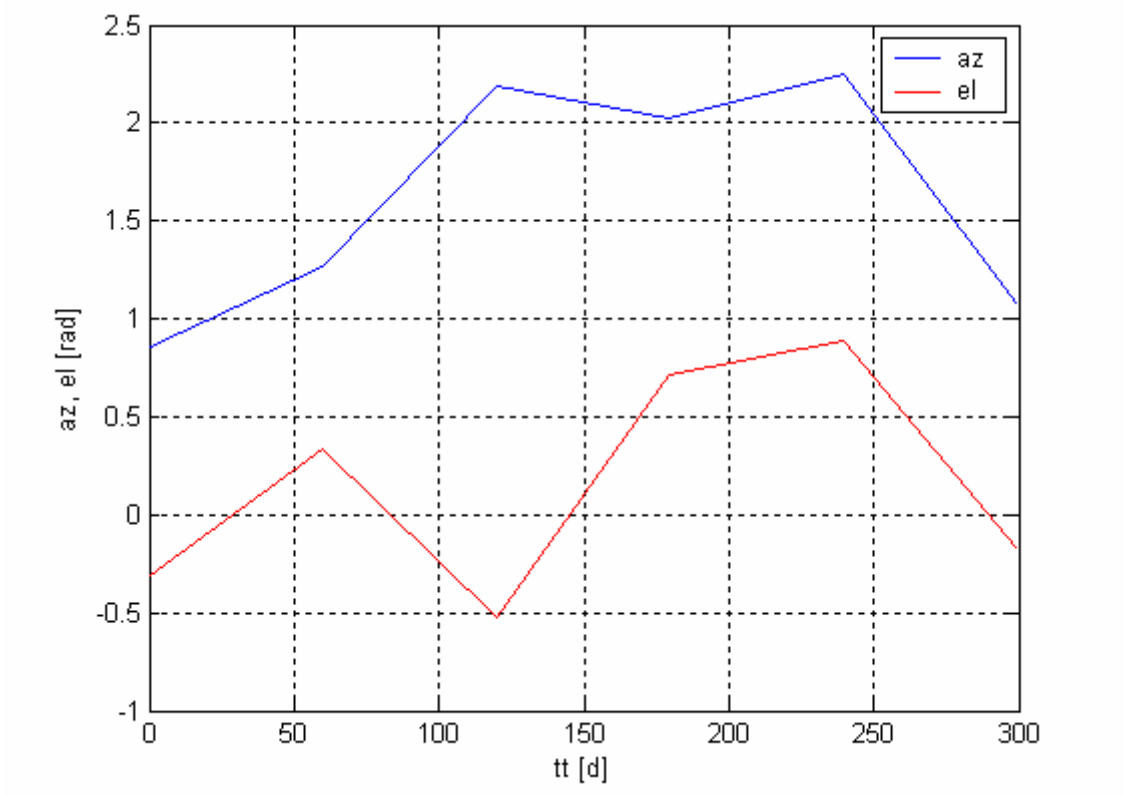

Figure 197: Thrust azimuth and elevation over the transfer trajectory corresponding to the best known solution.

Objective space	
$ObjFun$:	5.750
$R_F / R_{SoI,Mars}$:	0.002
v_F :	0.086 *m/s*
m_{prop} :	114.433 *kg*

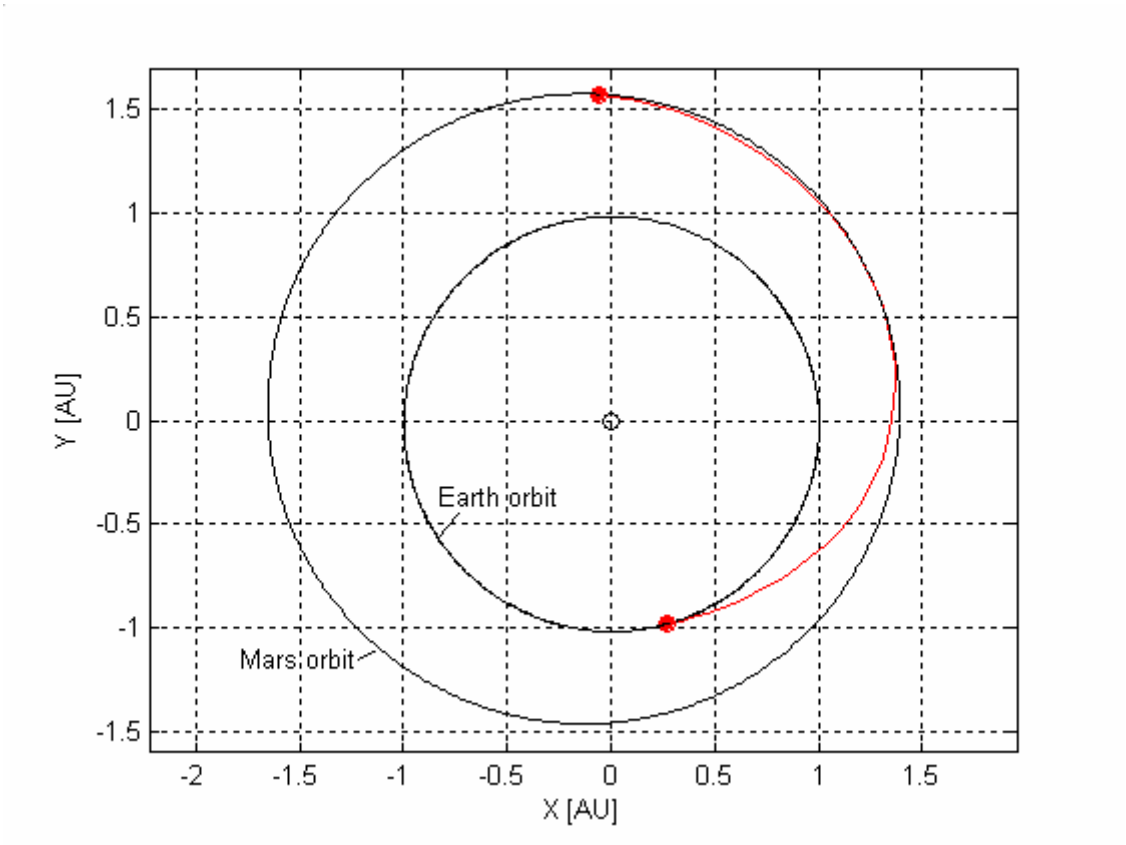

Figure 198: Low-thrust transfer trajectory corresponding to the best known solution.

Number of local optima: A priori unknown.

Hardware platform:

Intel Pentium 4 – 3.06GHz laptop.

Operating system:

Microsoft Windows XP

Home edition

Version 2002

Service Pack 1

Timings:

The Standard Unit Time (see Dixon & Szegö, 1978) has been measured.

Performances:

In the following, the performances of each global optimization tool in solving the low-thrust direct planet-to-planet transfer are reported. The evaluation criteria will be mainly based on the analysis of the optimal solution reached and the number of the required model function evaluations. Due to the presence of not optimized codes among the tested ones, timing will not be considered as a main evaluation criterion

GAOT

As GAOT implements a genetic algorithm, we report the statistical characteristic, typically considered in case of randomized solution methods. Ten runs have been processed in order to solve the previously defined problem. Default options suggested by the providers of the code have been used in all the runs: note that by tuning the algorithm parameters one may improve the performance of the solvers, but, due to the comparative purposes of this work, the tuning effects have not been considered. As the low thrust direct planet-to-planet transfer is characterized by high complexity features and a high number of design variables, we used 100 individuals evolving for a maximum number of generations equal to 10000.

Algorithm parameters	
Number of individuals:	100
Maximum number of generations:	10000

Table 121, Table 122 and Figure 199 report the best identified solution compared with the best known solution in terms of the values of the design variables and of the objective function terms, while Figure plots the resulting interplanetary transfer trajectories.

Search space		
Design variable	**Best identified solution**	**Best know solution**
Date of departure [*d*]:	1207.858	553.253
Transfer time [*d*]:	257.886	299.462
Thrust level [*N*]:	0.168	0.130
Escape velocity from Earth [*m/s*]:	2097.126	2676.327

Table 121: Comparison between the best identified solution and the best known solution: search space.

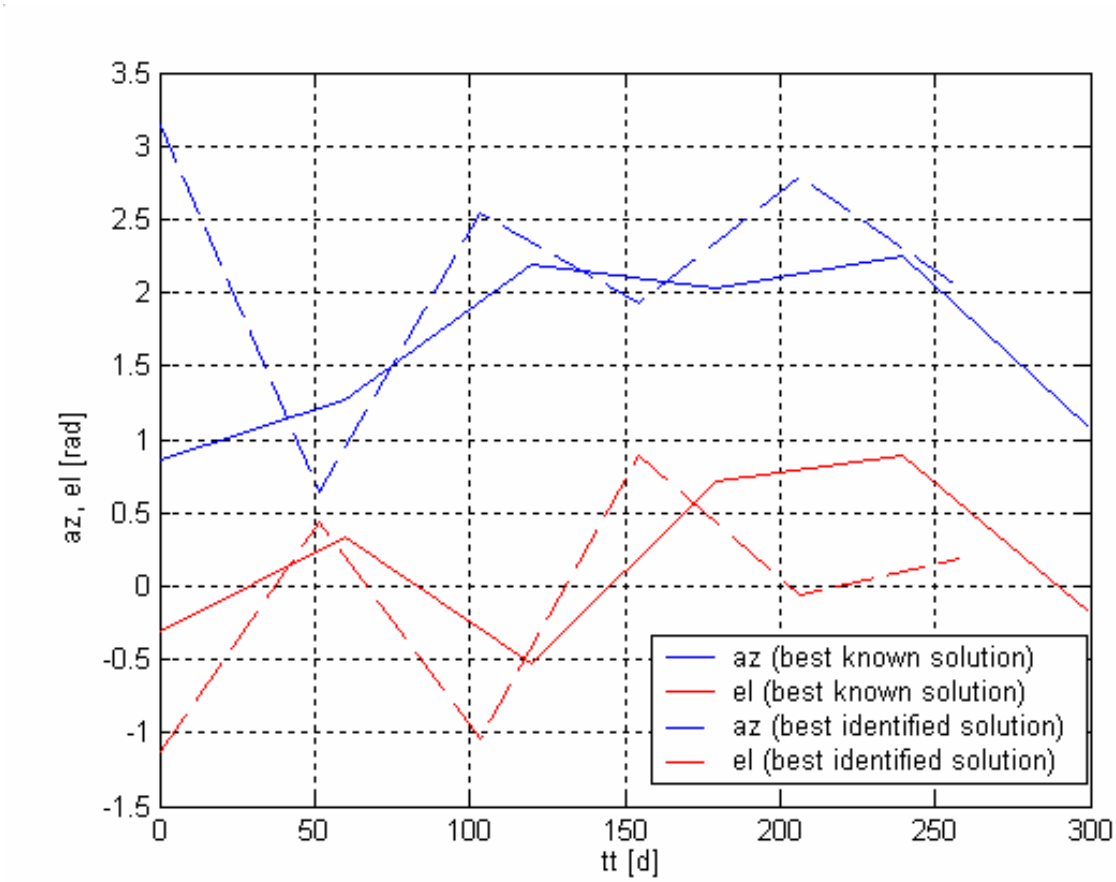

Figure 199: Comparison between the best identified solution and the best known solution: thrust azimuth and elevation over the transfer trajectory.

Objective function space		
Term	**Best identified solution**	**Best know solution**
$ObjFun$:	154.274	5.750
$R_F / R_{SoI,Mars}$:	0.104	0.002
v_F [*m/s*]:	1468.719	0.086
m_{prop} [*kg*]:	127.192	114.433

Table 122:Comparison between the best identified solution and the best known solution: objective function space.

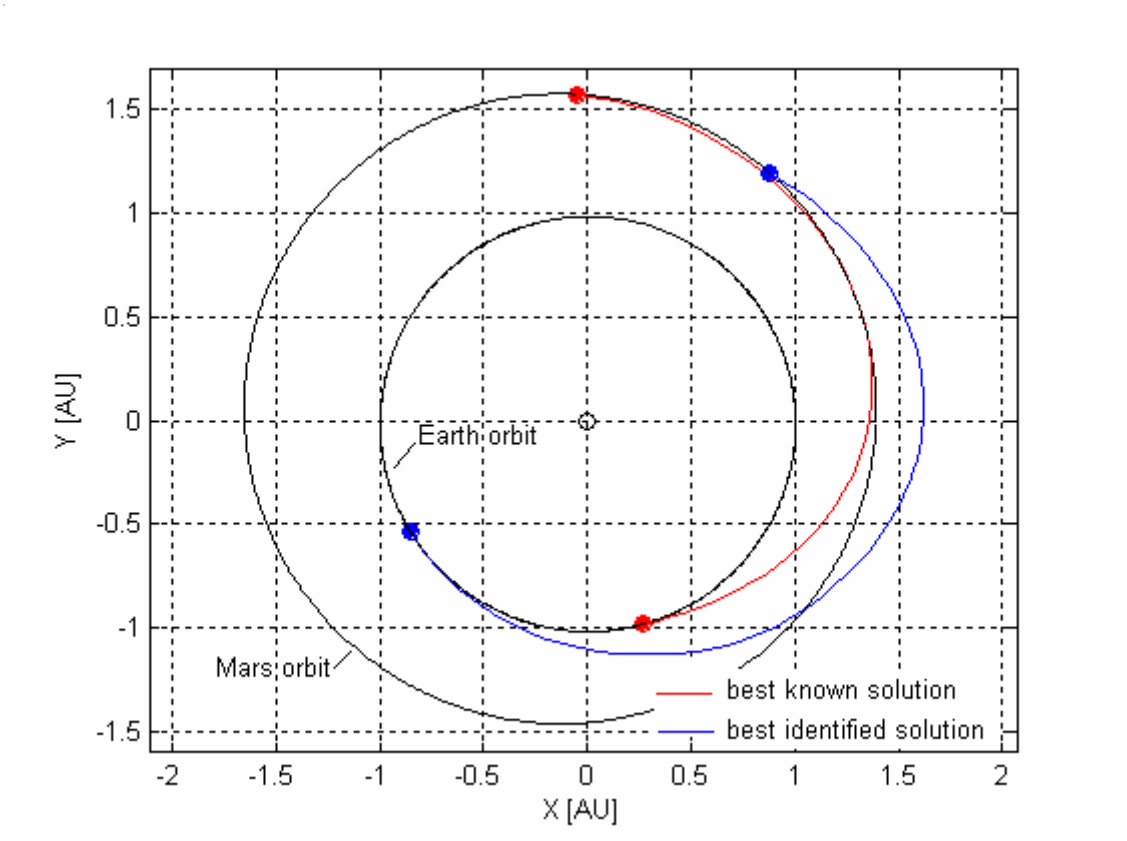

Figure 200: Comparison between the trajectories corresponding to the best identified solution and the best known solution.

Figure 201 shows the distribution of the solutions resulting from each optimization run over the plane of the objective function, ΔV , and the number of function evaluations, *nFunc.*, while Table 123 reports the statistical characteristics, which will be used for comparisons with the other optimization

algorithms, as well as the performances corresponding to the best identified solution.

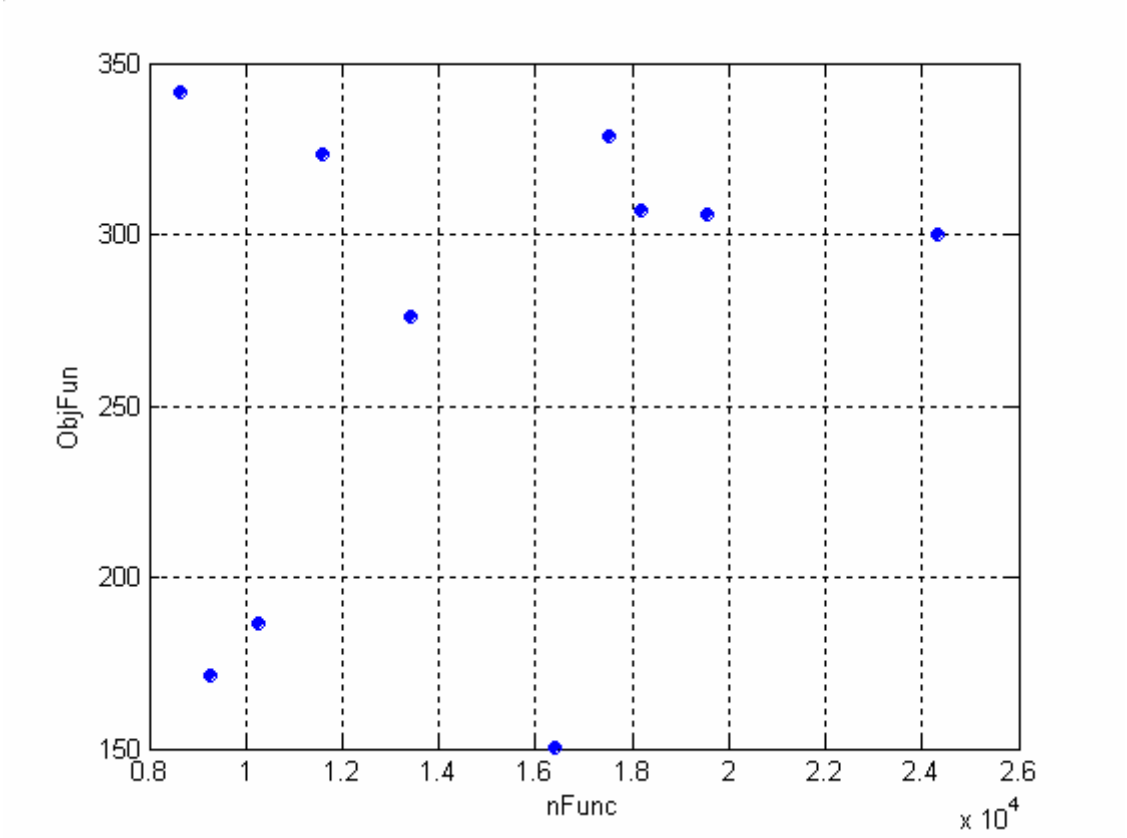

Figure 201: Distribution of the solutions resulting from each GAOT optimization run over the $nFunc - \Delta V$ plane.

Evaluation criterion	Mean value	Standard deviation	Best identified solution
ObjFun:	269.198	71.416	154.274
nFunc:	14919.300	5121.398	16410
Runtime [STU]:	3.564	1.564	4.238

Table 123: Statistical characteristics of the identified solutions.

By proceeding in analogy with the previously investigated mission analysis classes, the estimation of the number and features of the distinct local minima reached by means of the ten runs is performed; such an analysis will allow the estimation of the number of runs which have been able to reach the basin of attraction of the global optimum, which in fact can be considered as a success

index in performing the optimization process. To attain such a task, the optimal solutions corresponding to all ten runs have been used as starting solutions for ten local optimization processes in order to accurately estimate the local minimum corresponding to the basin of attraction each optimal solution belong to. The consequences of the local optimization processes in the *nFunc* - ΔV plane are shown in Figure 202, where each improved solution is linked to the corresponding starting one by means of a straight line.

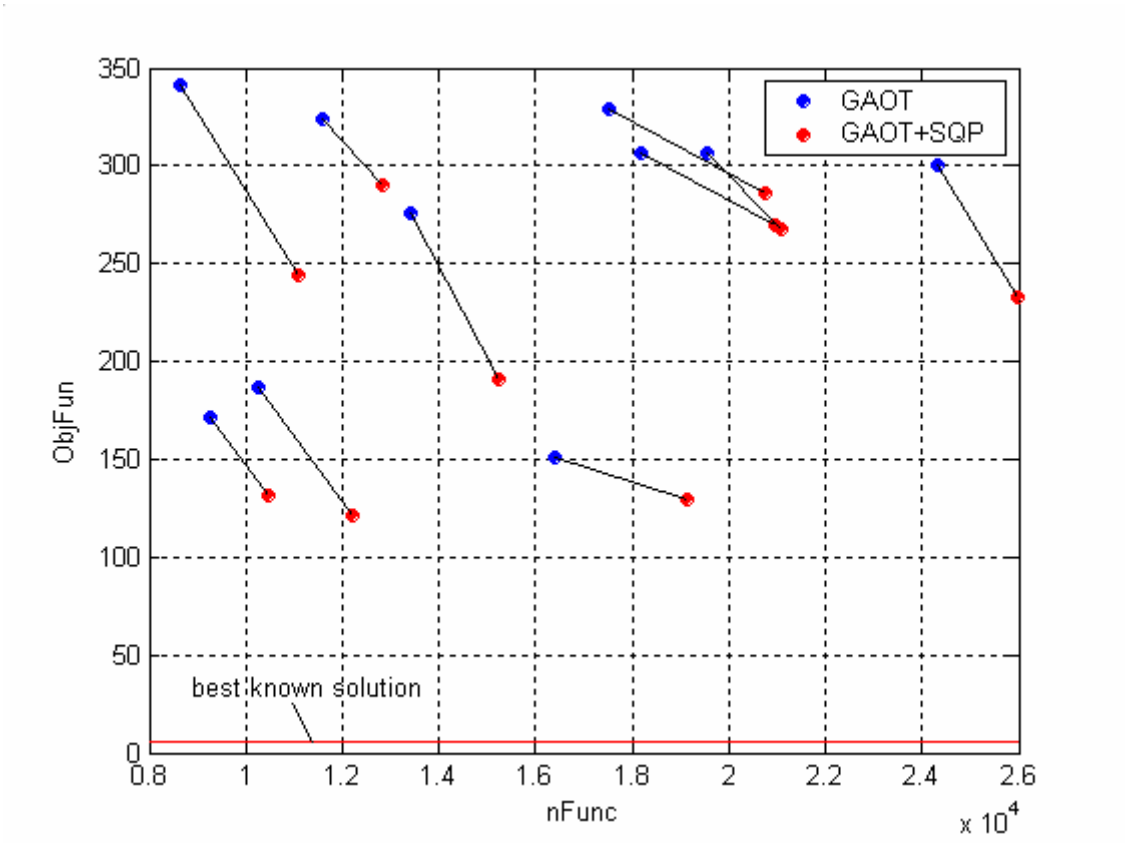

Figure 202: Comparison between solutions resulting from GAOT runs and their improvements by means of a further local optimization process via SQP algorithm over the $nFunc - \Delta V$ plane.

Figure 202 shows that different local minima corresponds to GAOT runs. By considering the objective function values reached at the end of the optimization processes, no solution seems to correspond to the best known one. In fact, let investigate the solutions in the normalized search space. Table 124 reports, corresponding to each GAOT+SQP run, the reached objective function value and the distance (in Euclidean metric) with respect to the best known solution.

	ObjFun	Distance
run 1	121.376	1.2268
run 2	289.680	1.8419
run 3	190.407	1.0597
run 4	129.321	0.92134
run 5	285.754	1.523
run 6	269.552	1.4895
run 7	267.177	1.6412
run 8	131.933	1.0891
run 9	243.598	1.3223
run 10	233.039	1.2251

Table 124: GAOT+SQP optimization runs: objective function values and Euclidean distance in the normalized search space with respect to the best known solution.

An empirical analysis suggest to define two solutions as identical when the Euclidean distance is less than 1% of the hyper diagonal of the normalized search space, that is 0.040 in a 16-dimensional space. The consequence of such definition is that no run has been able to get the best known solution, that is 0/10 GAOT runs successfully identified the basin of attraction of the best known solution.

GAOT-shared

As GAOT-shared implements a genetic algorithm including a niching technique, we report again the statistical characteristics. Ten runs have been processed in order to solve the previously defined problem. Default options suggested by the providers of the code have been used in all the runs. The threshold of dissimilarity, σ_S, for the sharing method and the shape parameter of the sharing function, α, have been set respectively to:

$\sigma_S = 0.1$ and $\alpha = 1$

We used again a population of 100 individuals, evolving for a maximum number of generations equal to 10000.

Algorithm parameters	
Number of individuals:	100
Maximum number of generations:	10000

Table 125, Table 126 and Figure 203 report the best identified solution compared with the best known solution in terms of the values of the design variables and of the objective function terms, while Figure 204 plots the resulting interplanetary transfer trajectories.

Search space		
Design variable	**Best identified solution**	**Best know solution**
Date of departure [*d*]:	1225.439	553.253
Transfer time [*d*]:	226.995	299.462
Thrust level [*N*]:	0.162	0.130
Escape velocity from Earth [*m/s*]:	1661.833	2676.327

Table 125: Comparison between the best identified solution and the best known solution: search space.

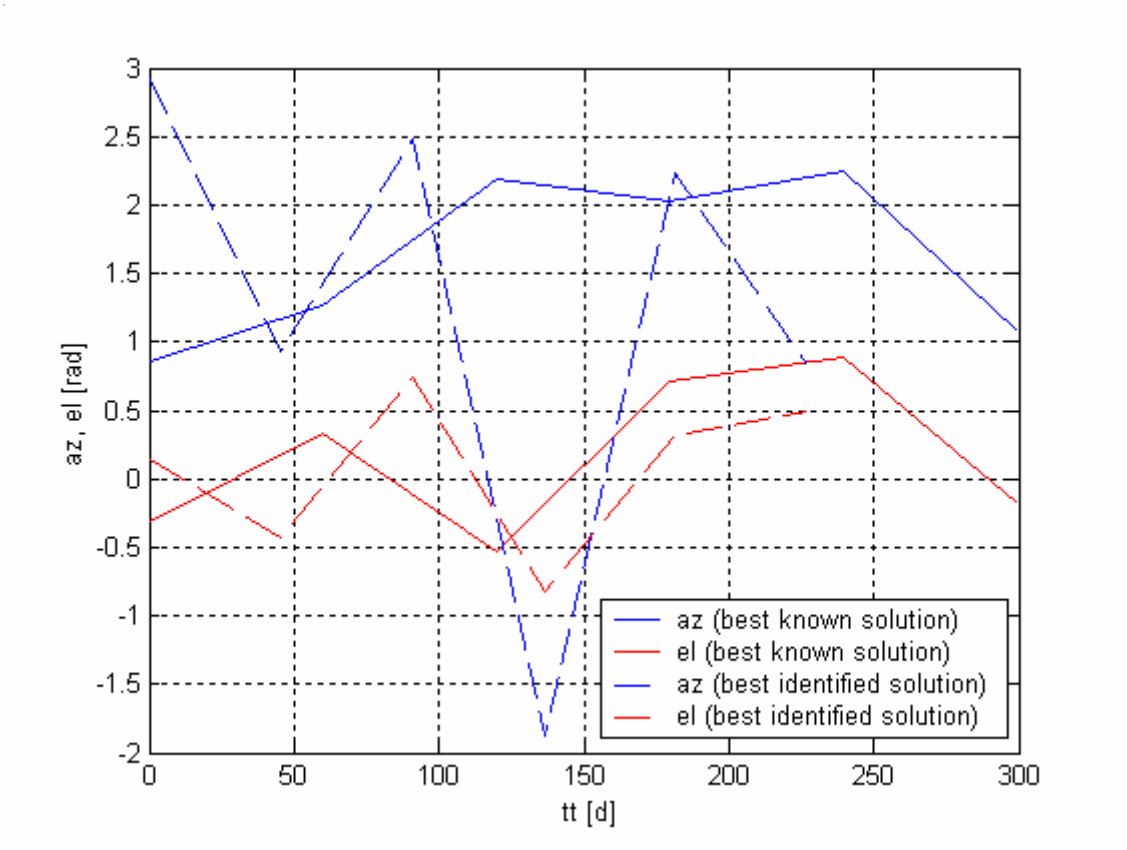

Figure 203: Comparison between the best identified solution and the best known solution: thrust azimuth and elevation over the transfer trajectory.

Objective function space		
Term	**Best identified solution**	**Best know solution**
$ObjFun$:	257.807	5.750
$R_F / R_{SoI,Mars}$:	8.296	0.002
v_F [*m/s*]:	1694.607	0.086
m_{prop} [*kg*]:	107.713	114.433

Table 126: Comparison between the best identified solution and the best known solution: objective function space.

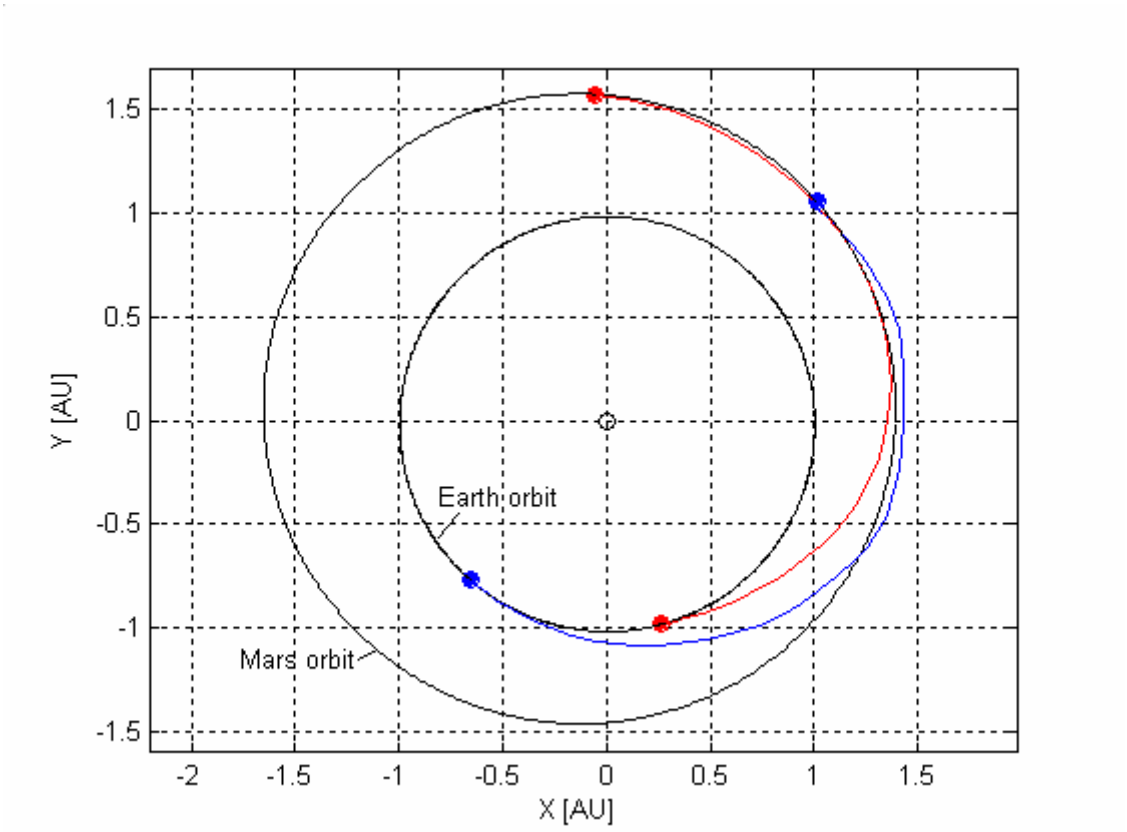

Figure 204: Comparison between the trajectories corresponding to the best identified solution and the best known solution.

Figure 205 shows the distribution of the solutions resulting from each optimization run over the plane of the objective function, ΔV, and the number of function evaluations, *nFunc*, while Table 126 reports the statistical characteristics, which will be used for comparisons with the other optimization algorithms, as well as the performances corresponding to the best identified solution. Note that, as one can expect, the low accuracy of GAOT-shared corresponds to a low number of function evaluations required for that the stopping condition becomes active.

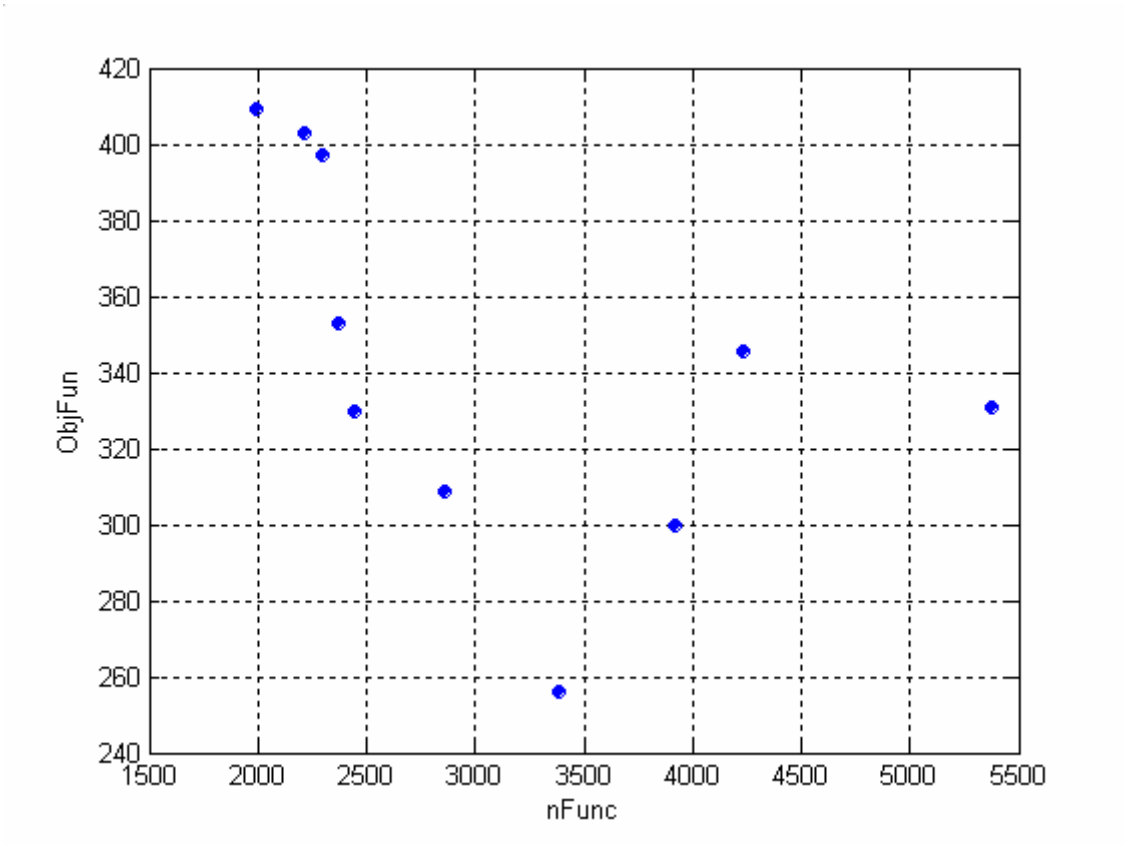

Figure 205: Distribution of the solutions resulting from each GAOT-shared optimization run over the $nFunc - \Delta V$ plane.

Evaluation criterion	Mean value	Standard deviation	Best identified solution
Objective function:	343.238	49.457	257.807
nFunc.:	3109.500	1099.448	3384
Runtime [STU]:	0.621	0.217	0.870

Table 126: Statistical characteristics of the identified solutions.

By proceeding in analogy with the GAOT case, the optimal solutions corresponding to all ten runs have been used as starting solutions for ten local optimization processes in order to accurately estimate the local minimum corresponding to the basin of attraction each optimal solution belong to. Figure 206 illustrates the consequences of the local optimization processes in the *nFunc* - ΔV plane.

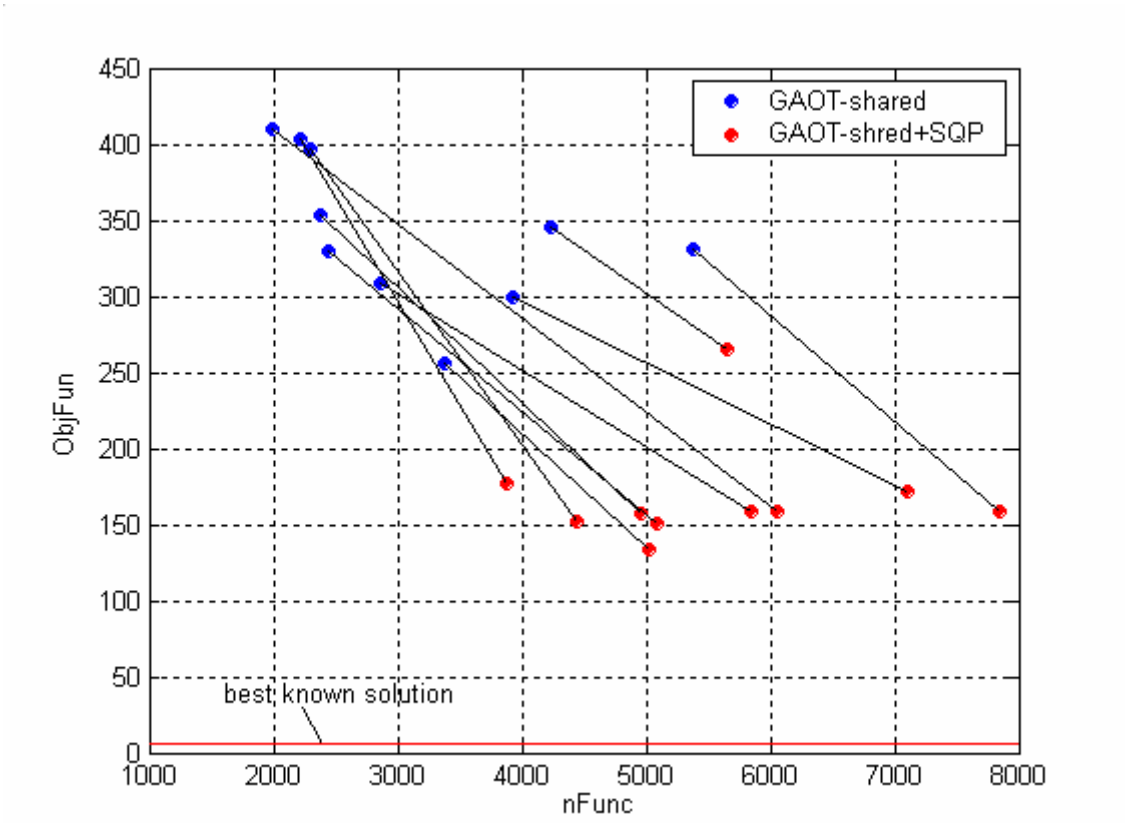

Figure 206: Comparison between solutions resulting from GAOT-shared runs and their improvements by means of a further local optimization process via SQP algorithm over the $nFunc - \Delta V$ plane.

Figure 206 shows again that different local minima corresponds to GAOT-shared runs. In order to estimate the number of identified solutions which lie in the basin of attraction of the best known solutions, solutions are now investigated in the normalized search space. Table 127 reports, corresponding to each GAOT-shared+SQP run, the reached objective function value and the distance (in Euclidean metric) with respect to the best known solution.

	ObjFun	Distance
run 1	158.217	1.007
run 2	157.833	0.981
run 3	158.935	1.007
run 4	172.207	1.167
run 5	152.208	1.151
run 6	150.717	1.251
run 7	177.606	1.181
run 8	159.181	1.026
run 9	264.712	1.469
run 10	132.966	0.982

Table 127: GAOT-shared+SQP optimization runs: objective function values and Euclidean distance in the normalized search space with respect to the best known solution.

As stated above, two solutions are considered as identical when the Euclidean distance is less than 0.040. As a consequence no run has been able to get the best known solution, that is only 0/10 GAOT-shared runs successfully identified the basin of attraction of the best known solution.

GATBX

As GATBX implements a genetic algorithm, we report the statistical characteristics. Ten runs have been processed in order to solve the previously defined problem. Default options suggested by the providers of the code have been used in all the runs. A population of 100 individuals evolving for a maximum number of generations equal to 10000 has been processed again.

Algorithm parameters	
Number of individuals:	100
Maximum number of generations:	10000

Table 128, Table 129 and Figure 207 reports the best identified solution compared with the best known solution in terms of the values of the design variables and of the objective function terms, while Figure 208 plots the resulting interplanetary transfer trajectories.

Search space		
Design variable	**Best identified solution**	**Best know solution**
Date of departure [*d*]:	522.649	553.253
Transfer time [*d*]:	276.645	299.462
Thrust level [*N*]:	0.161	0.130
Escape velocity from Earth [*m/s*]:	2531.142	2676.327

Table 128: Comparison between the best identified solution and the best known solution: search space.

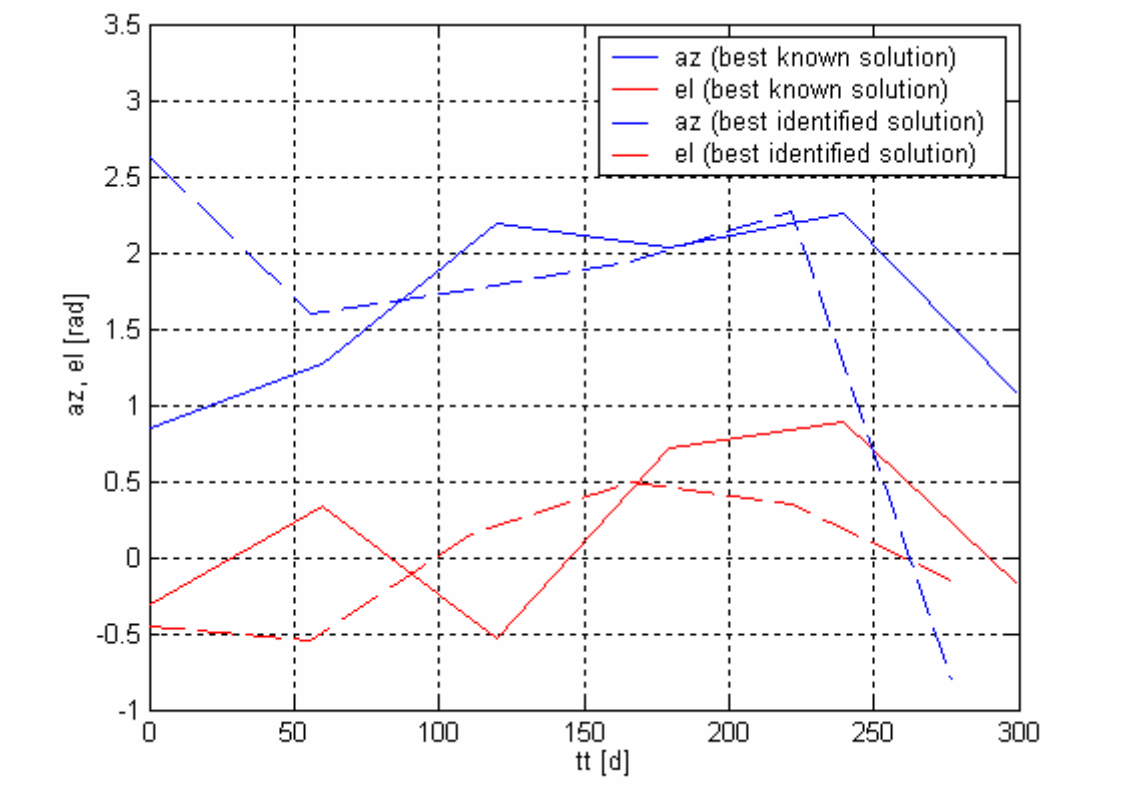

Figure 207: Comparison between the best identified solution and the best known solution: thrust azimuth and elevation over the transfer trajectory.

Objective function space		
Term	**Best identified solution**	**Best know solution**
$ObjFun$:	7.603	5.750
$R_F / R_{SoI,Mars}$:	0.086	0.002
v_F [*m/s*]:	2.099	0.086
m_{prop} [*kg*]:	130.617	114.433

Table 129: Comparison between the best identified solution and the best known solution: objective function space.

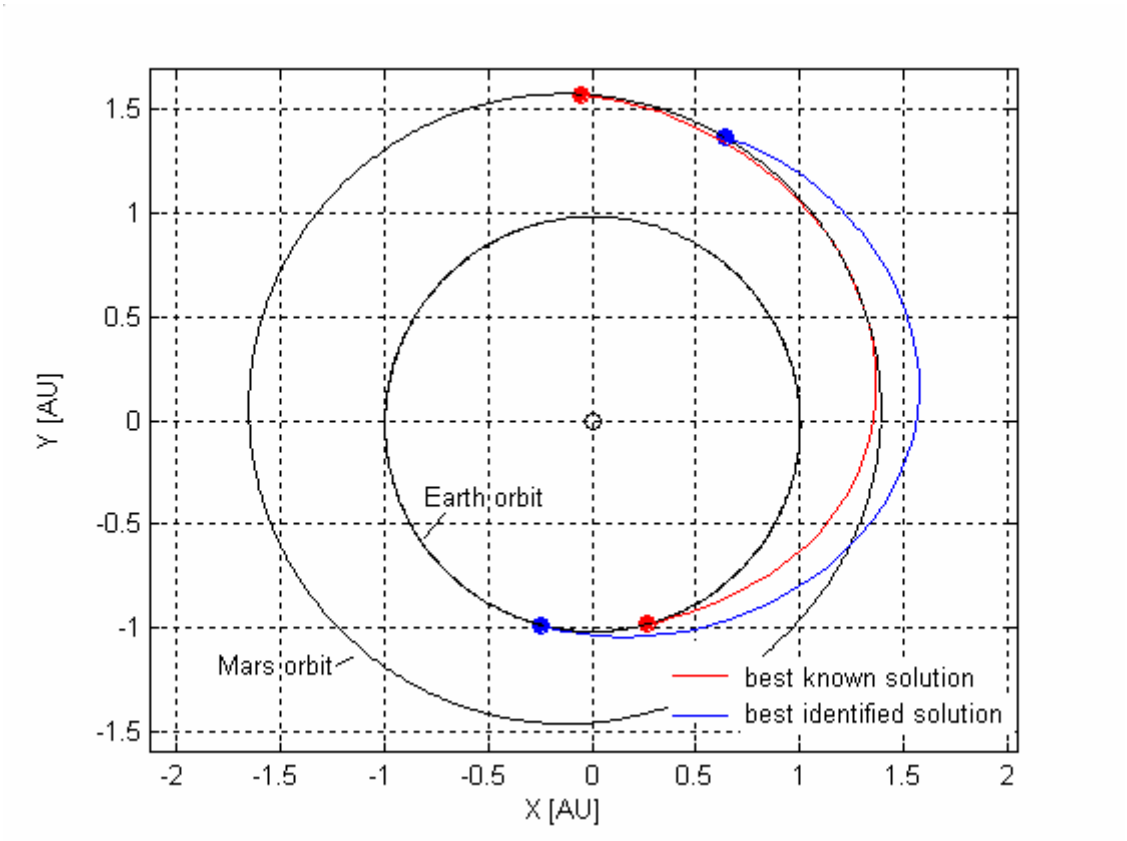

Figure 208: Comparison between the trajectories corresponding to the best identified solution and the best known solution.

Figure 209 shows the distribution of the solutions resulting from each optimization run over the plane of the objective function, ΔV , and the number of function evaluations, *nFunc*, while Table 130 reports the statistical characteristics, which will be used for comparisons with the other optimization

algorithms, as well as the performances corresponding to the best identified solution.

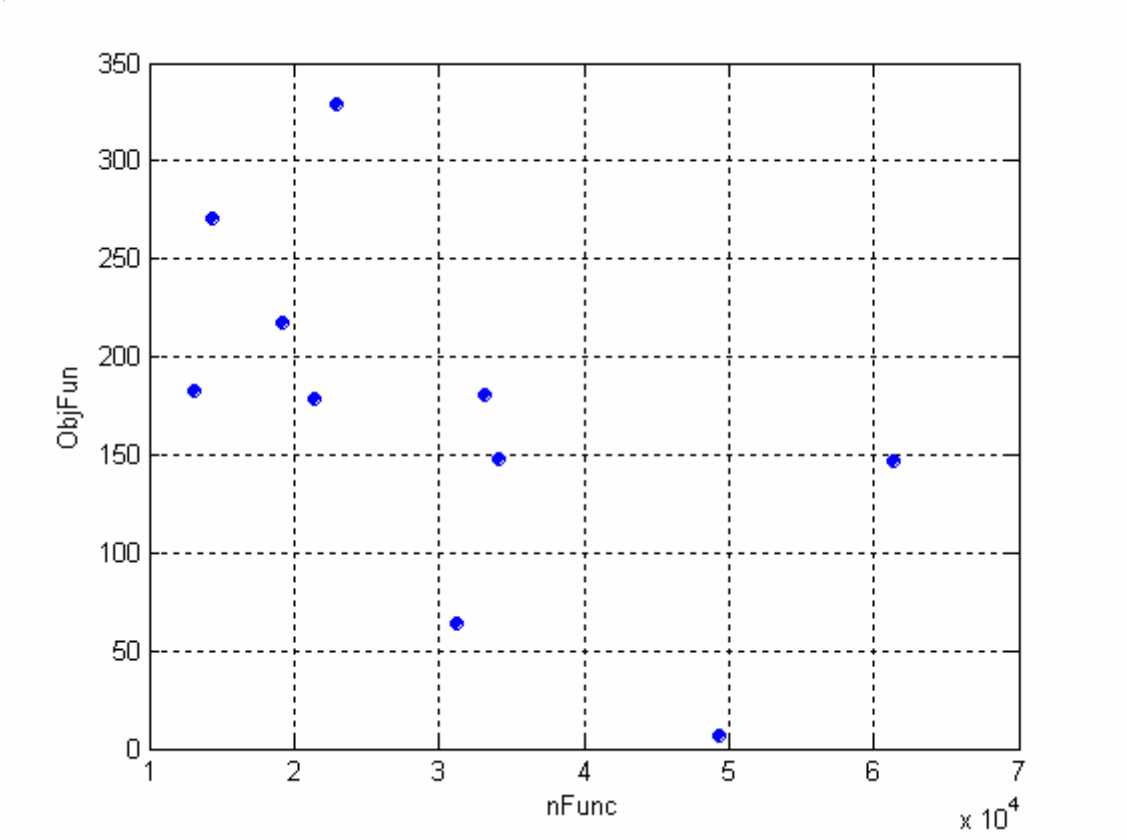

Figure 209:Distribution of the solutions resulting from each GATBX optimization run over the $nFunc - \Delta V$ plane.

Evaluation criterion	Mean value	Standard deviation	Best identified solution
Objective function:	172.559	92.517	7.603
nFunc.:	30036	15485.451	49380
Runtime [STU]:	7.105	4.068	15.146

Table 130: Statistical characteristics of the identified solutions.

The optimal solutions corresponding to all ten runs are now used again as starting solutions for ten local optimization processes in order to accurately estimate the local minimum corresponding to the basin of attraction each optimal solution belong to and to evaluate the number of GATBX successful

runs. Figure 210 illustrates the consequences of the local optimization processes in the *nFunc* - ΔV plane.

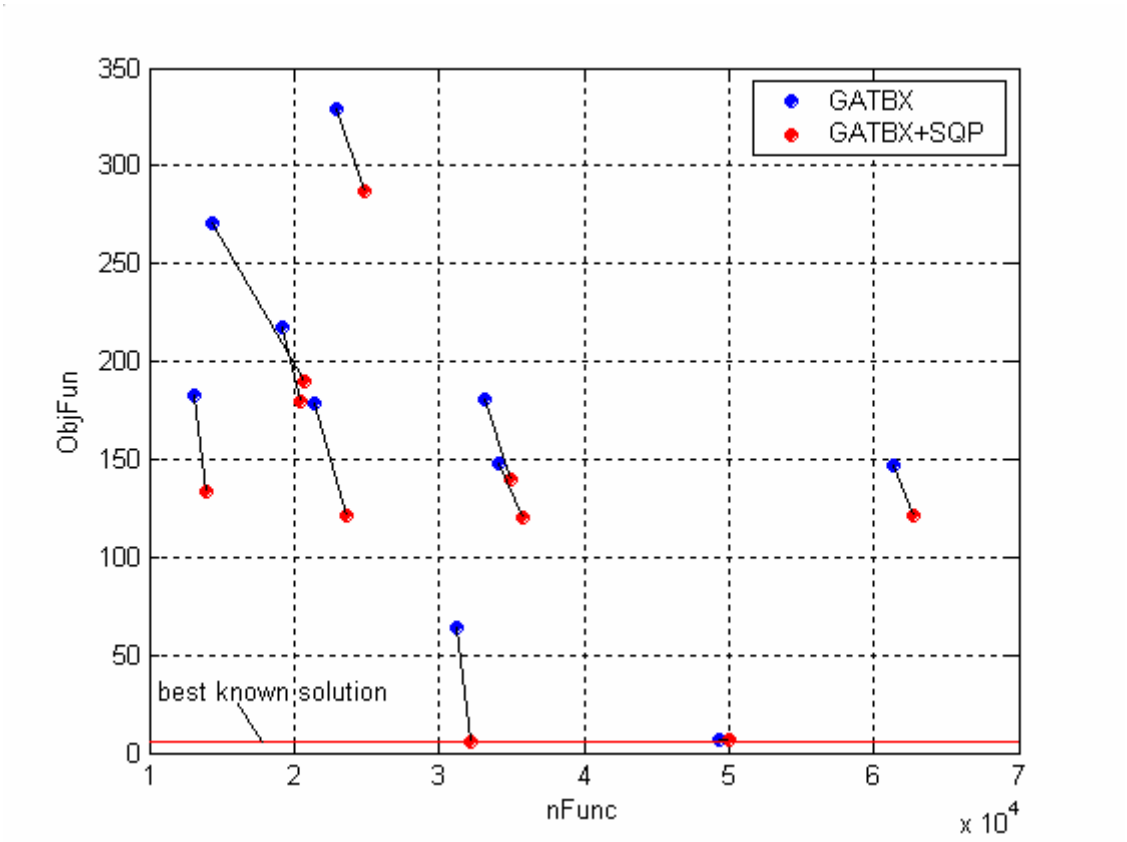

Figure 210: Comparison between solutions resulting from GATBX runs and their improvements by means of a further local optimization process via SQP algorithm over the $nFunc - \Delta V$ plane.

Different local minima corresponds to GATBX runs. In order to estimate the number of identified solutions which lie in the basin of attraction of the best known solutions, solutions are now investigated in the normalized search space. Table 131 reports, corresponding to each GATBX+SQP run, the reached objective function value and the distance (in Euclidean metric) with respect to the best known solution.

	ObjFun	Distance
run 1	189.994	1.141
run 2	287.531	1.568
run 3	121.513	1.056
run 4	121.762	1.117
run 5	179.497	1.116
run 6	139.253	1.134
run 7	120.167	1.181
run 8	5.870	0.776
run 9	133.503	1.381
run 10	6.461	0.723

Table 131: GATBX+SQP optimization runs: objective function values and Euclidean distance in the normalized search space with respect to the best known solution.

By considering two solutions as identical when the Euclidean distance is less than 0.040, no runs were able to get the best known solution, that is only 0/10 GATBX runs successfully identified the basin of attraction of the best known solution. It is worth noting that, although GATBX was not able to reach the basin of attraction of the best known solution (according to the definition of identical solutions given above), it could achieve the basin of attraction of two solutions which are in fact quite comparable with the best known one in terms of objective function values (see runs 8 and 10). Figure 211 shows the trajectories corresponding to such solutions compared with the best known one.

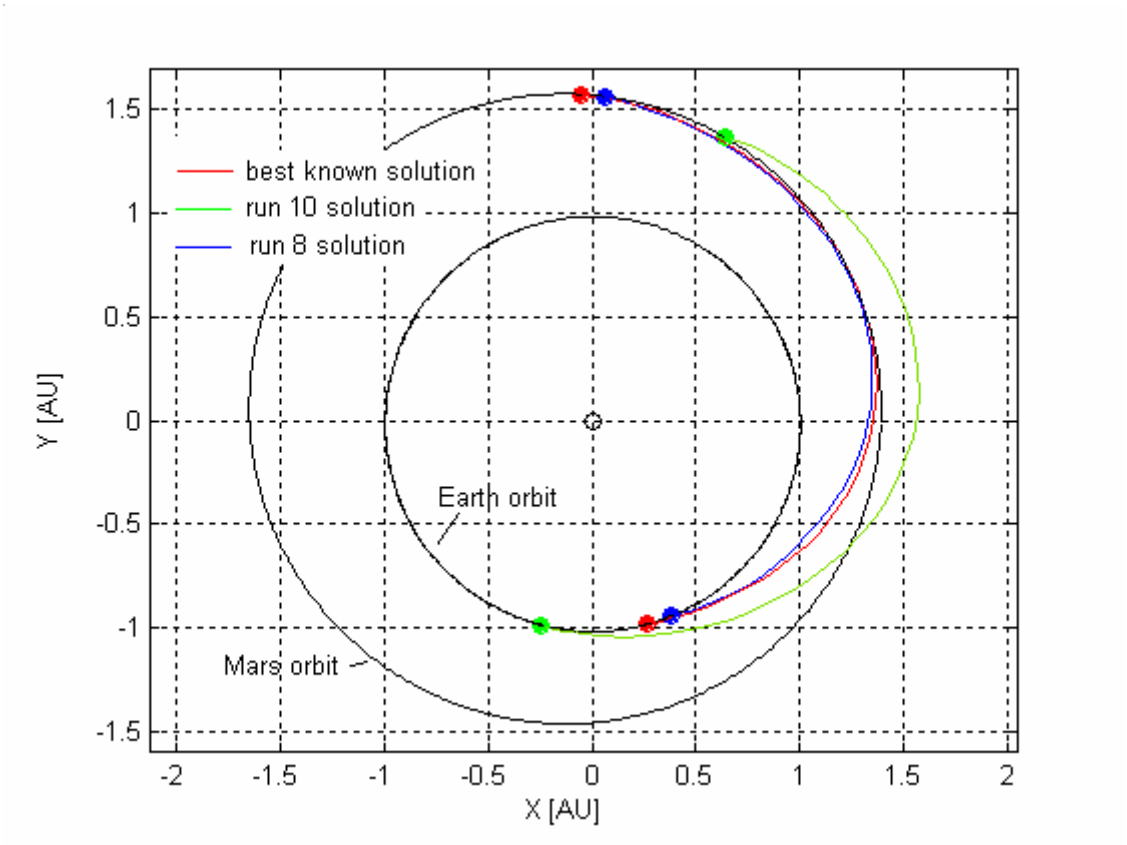

Figure 211: Comparison between the best known solution and solutions corresponding to run 8 and run 10.

It is worth noting that, although the objective function values are comparable, the identified local minima are different, paticularly in the date of departure, whose values in case of the three analysed solutions are reported in Table 132.

	Best identified solution	**run 8**	**run 10**
Date of departure [d]:	553.253	560.291	522.644

Table 132: Date of departure corresponding to the best known solution and solutions run 8 and run 10.

Note that differences in the date of departure are quite little but significant. However the comparable objective function values let us suppose that all the three analysed local minima belong to a big valley structure, that is a “corridor” or a line in the search space along which objective function values are comparable, confirming the results gained in the objective function structure

analysis. Such results are supported by the relative closeness of the three solutions in the search space (see Figure 212, where solutions are reported in the normalized search space corresponding to the date of departure-transfer time plane).

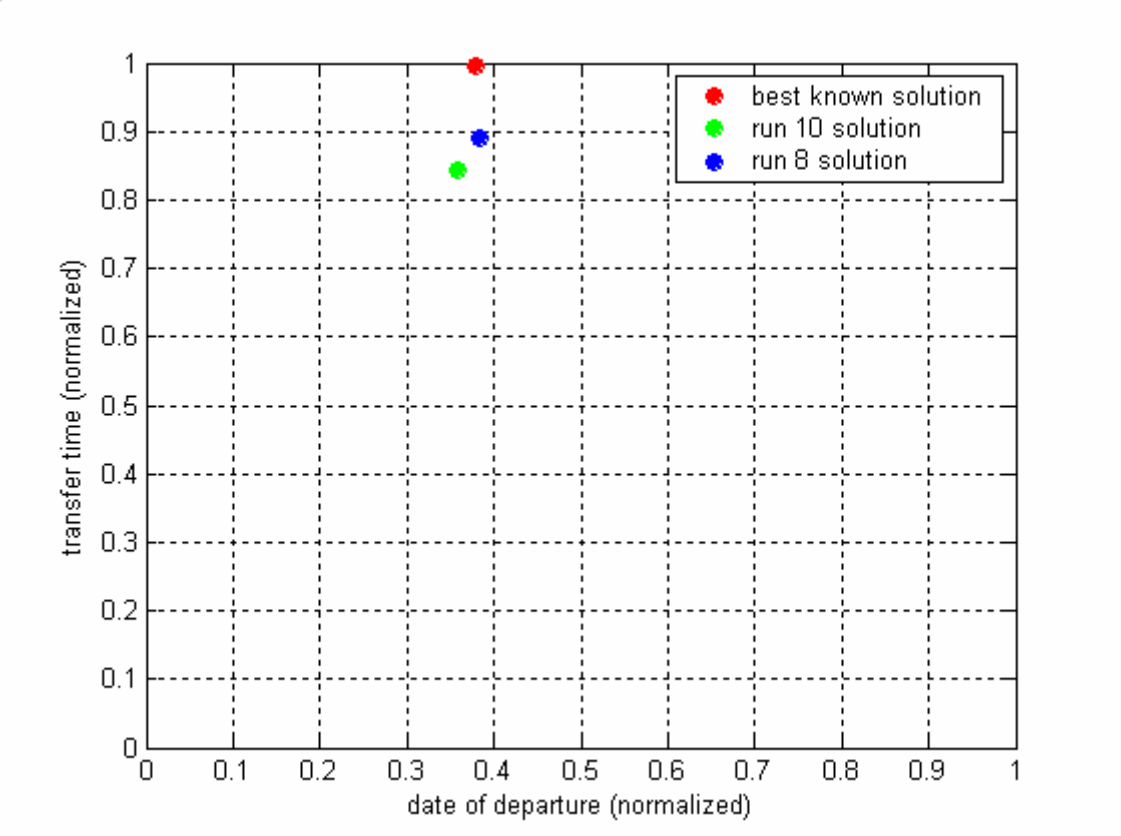

Figure 212: Best known solution, run 8 solution and run 10 solution in the in the normalized search space corresponding to the date of departure-transfer time plane.

It is important noting that the identification of such big valley structures in the search space is quite advantageous in designing transfer trajectories: in fact such structures give us a continuous set of comparable optimal solutions distributed over the date of departure design variable, which is fundamental in identifying the width of the optimal launch windows. The development of tools facing such task should be promoted in future works.

GATBX-migr

As GATBX-migr implements a genetic algorithm including a migration operator applied among a predefined set of subpopulations, we report the statistical characteristics. Ten runs have been processed in order to solve the previously defined problem. Default options suggested by the providers of the code have been used in all the runs. A population of 100 individuals evolving for a maximum number of generations equal to 10000 has been processed. The population has been divided in 5 subpopulations, each one including 20 individuals.

Algorithm parameters	
Number of individuals:	100
Maximum number of generations:	10000
Number of subpopulations:	5
Number of individuals per subpopulation:	20

Table 133, Table 134 and Figure 213 reports the best identified solution compared with the best known solution in terms of the values of the design variables and of the objective function terms, while Figure 214 plots the resulting interplanetary transfer trajectories.

Search space		
Design variable	**Best identified solution**	**Best know solution**
Date of departure [*d*]:	526.149	553.253
Transfer time [*d*]:	266.741	299.462
Thrust level [*N*]:	0.168	0.130
Escape velocity from Earth [*m/s*]:	2416.231	2676.327

Table 133: Comparison between the best identified solution and the best known solution: search space.

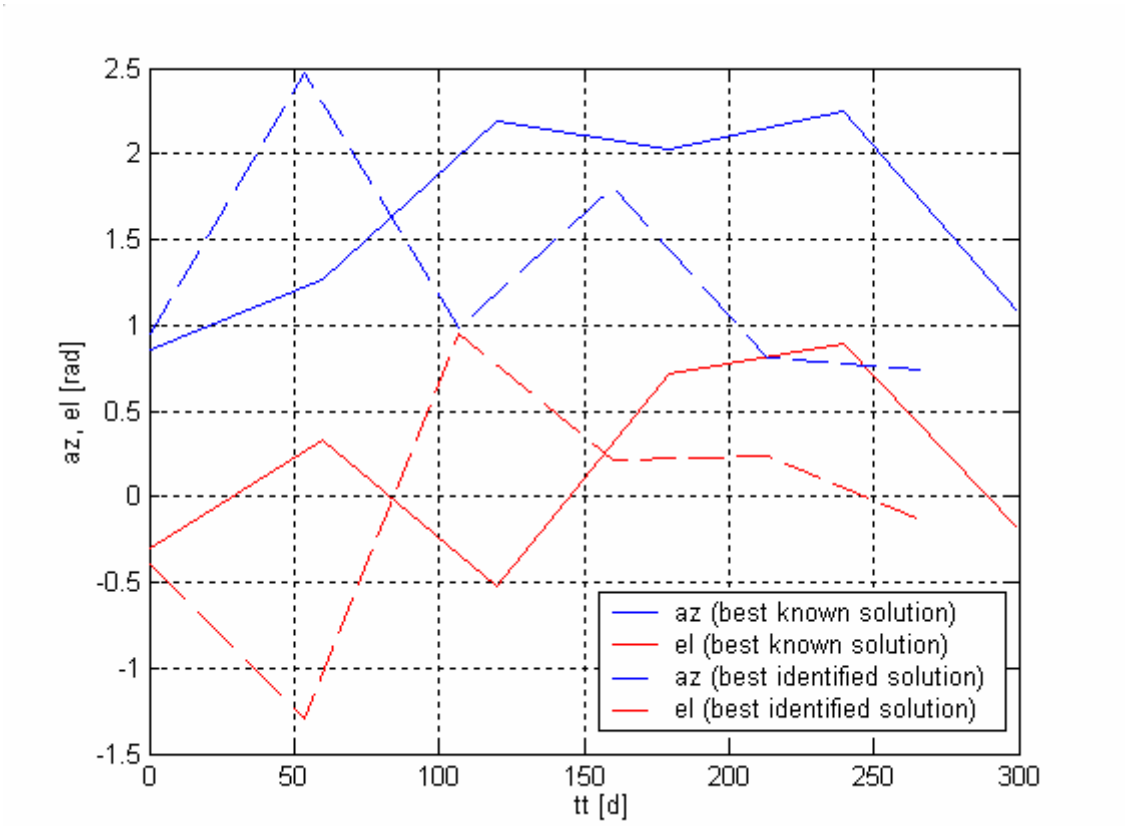

Figure 213: Comparison between the best identified solution and the best known solution: thrust azimuth and elevation over the transfer trajectory.

Objective function space		
Term	**Best identified solution**	**Best know solution**
$ObjFun$:	10.279	5.750
$R_F / R_{SoI,Mars}$:	0.074	0.002
v_F [*m/s*]:	29.609	0.086
m_{prop} [*kg*]:	131.560	114.433

Table 134: Comparison between the best identified solution and the best known solution: objective function space.

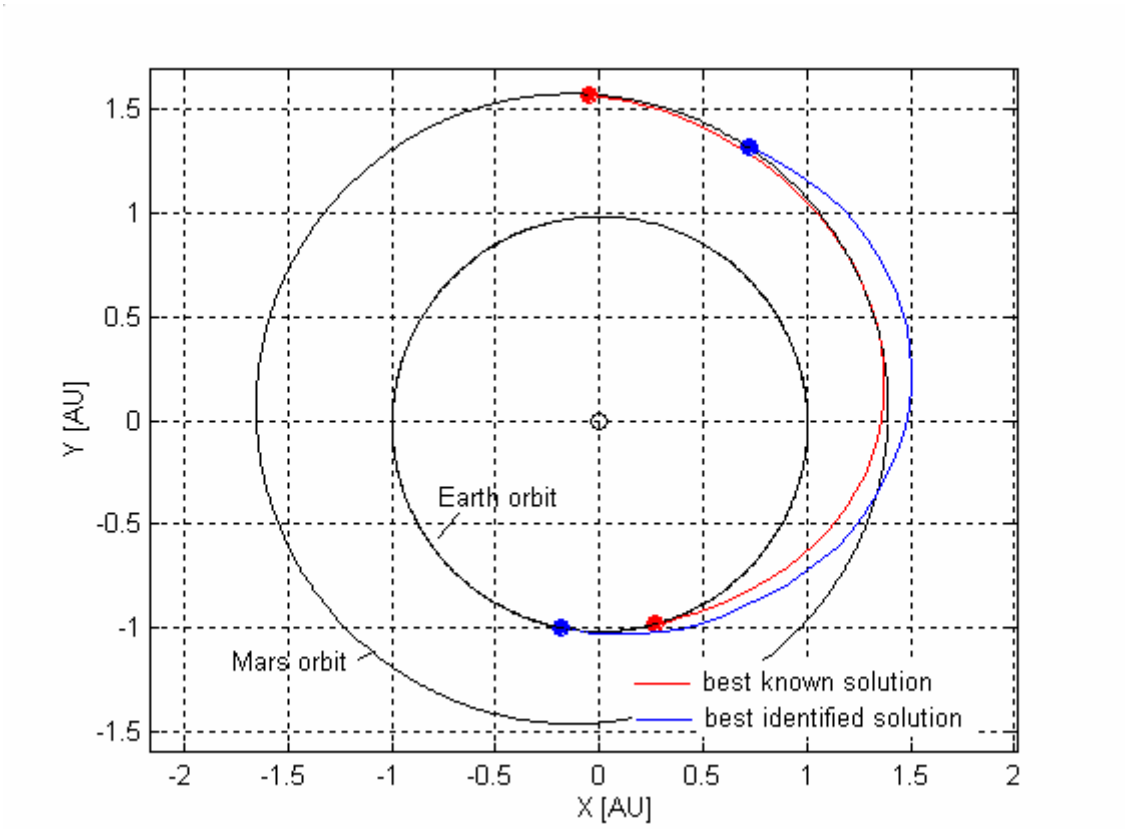

Figure 214: Comparison between the trajectories corresponding to the best identified solution and the best known solution.

Figure 215 shows the distribution of the solutions resulting from each optimization run over the plane of the objective function, ΔV, and the number of function evaluations, *nFunc*, while Table 135 reports the statistical characteristics, which will be used for comparisons with the other optimization algorithms, as well as the performances corresponding to the best identified solution.

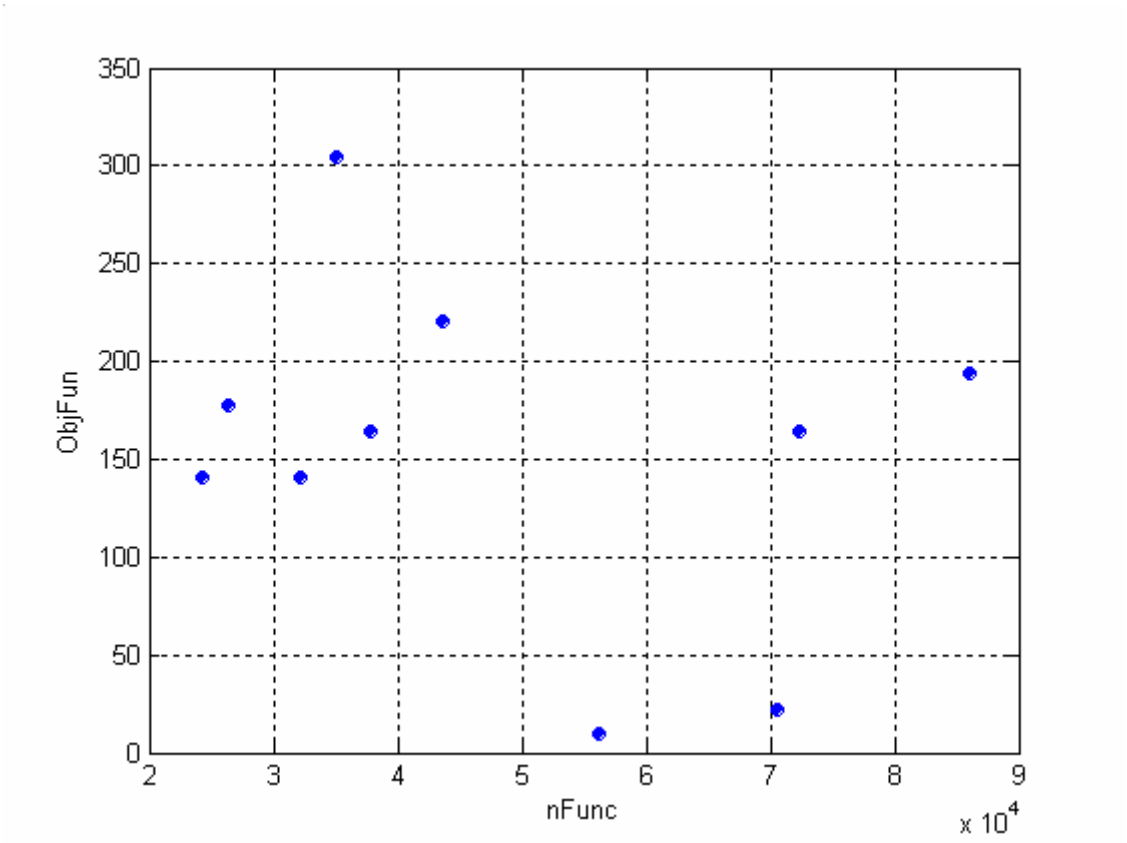

Figure 215: Distribution of the solutions resulting from each GATBX-migr optimization run over the $nFunc - \Delta V$ plane.

Evaluation criterion	Mean value	Standard deviation	Best identified solution
Objective function:	153.807	87.043	10.279
nFunc.:	48436	21584.383	56260
Runtime [STU]:	9.511	4.140	8.495

Table 135: Statistical characteristics of the identified solutions.

By proceeding in analogy with the previous algorithm performance analyses, the optimal solutions corresponding to all ten runs have been used as starting solutions for ten local optimization processes in order to accurately estimate the local minimum corresponding to the basin of attraction each optimal solution belong to.

Figure 216 illustrates the consequences of the local optimization processes in the *nFunc* - ΔV plane.

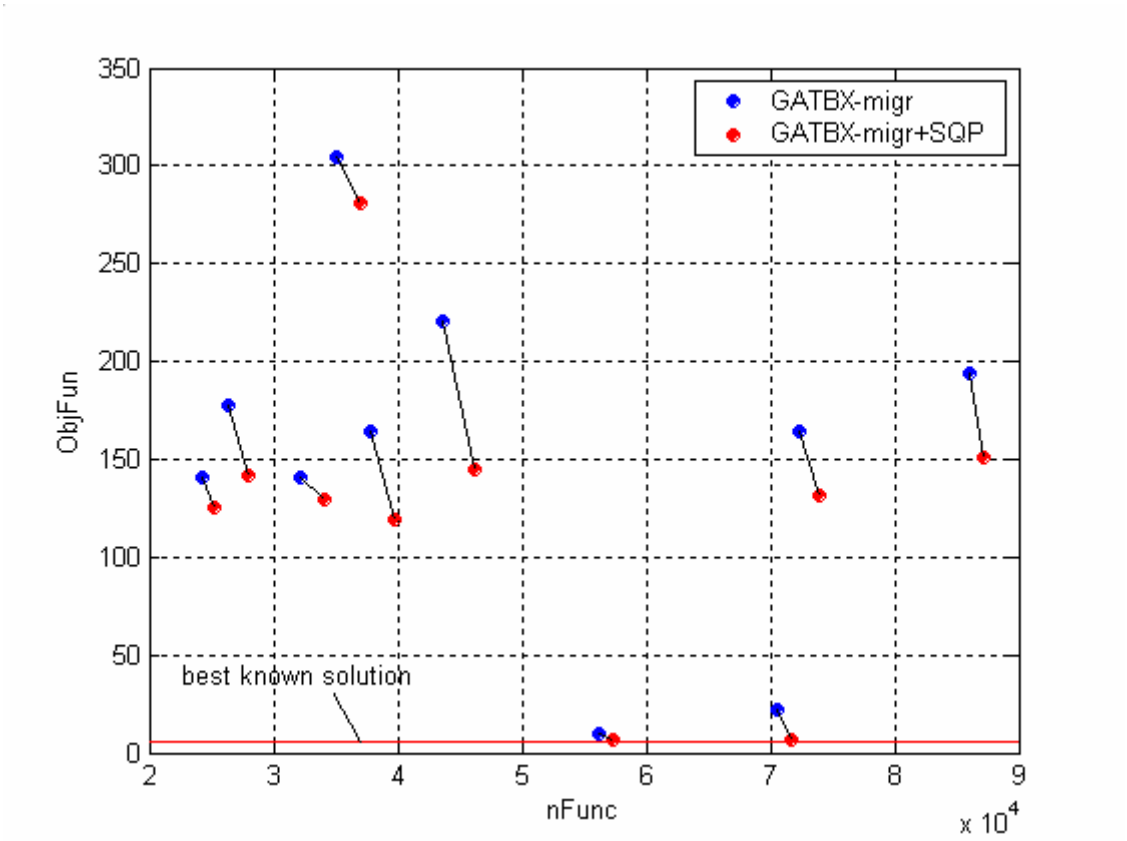

Figure 216: Comparison between solutions resulting from GATBX-migr runs and their improvements by means of a further local optimization process via SQP algorithm over the $nFunc - \Delta V$ plane.

Figure 216 shows again that different local minima corresponds to GATBX-migr runs. In order to estimate the number of identified solutions which lie in the basin of attraction of the best known solutions, solutions are now investigated in the normalized search space. Table 136 reports, corresponding to each GATBX-migr+SQP run, the reached objective function value and the distance (in Euclidean metric) with respect to the best known solution.

	ObjFun	Distance
run 1	141.757	0.917
run 2	125.117	1.350
run 3	6.451	0.739
run 4	280.545	1.377
run 5	144.582	1.118
run 6	131.604	0.925
run 7	119.263	1.079
run 8	151.281	1.088
run 9	6.325	0.913
run 10	128.991	1.170

Table 136: GATBX-migr+SQP optimization runs: objective function values and Euclidean distance in the normalized search space with respect to the best known solution.

As stated above, two solutions are considered as identical when the Euclidean distance is less than 0.040. As a consequence no GATBX-run has been able to get the best known solution, that is only 0/10 GATBX-migr runs successfully identified the basin of attraction of the best known solution. However, as already noted in case of GATBX-migr algorithm, two solutions have been reached which have objective function values comparable with that achieved by the best known solution, that is runs 3 and 9. Such solutions are reported in Figure 217.

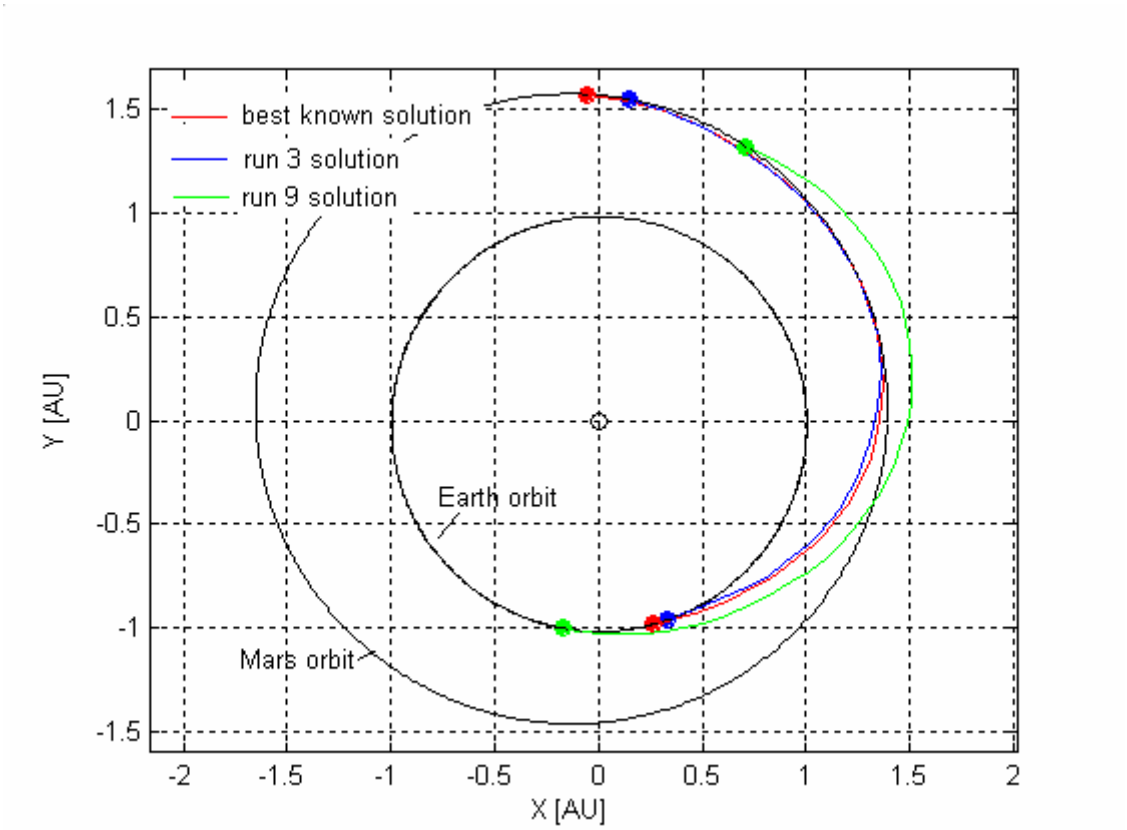

Figure 217: Comparison between the best known solution and solutions corresponding to run 3 and run 9.

The identified local minima are different, as the consideration of the date of departure values can show (see Table 137).

	Best identified solution	run 3	run 9
Date of departure [d]:	553.253	557.451	527.145

Table 137: Date of departure corresponding to the best known solution and solutions run 3 and run 9.

FEP

As FEP implements an evolutionary programming algorithm, we report, as already done for genetic algorithms, the statistical characteristics. Ten runs have been processed in order to solve the previously defined problem. Default options suggested by the providers of the code have been used in all the runs.

We used again a population of 100 individuals evolving for a maximum number of generations equal to 10000.

Algorithm parameters	
Number of individuals:	100
Maximum number of generations:	10000

Table 138, Table 139 and Figure 218 report the best identified solution compared with the best known solution in terms of the values of the design variables and of the objective function terms, while Figure 219 plots the resulting interplanetary transfer trajectories.

Search space		
Design variable	**Best identified solution**	**Best know solution**
Date of departure [*d*]:	553.354	553.253
Transfer time [*d*]:	299.394	299.462
Thrust level [*N*]:	0.131	0.130
Escape velocity from Earth [*m/s*]:	2663.050	2676.327

Table 138: Comparison between the best identified solution and the best known solution: search space.

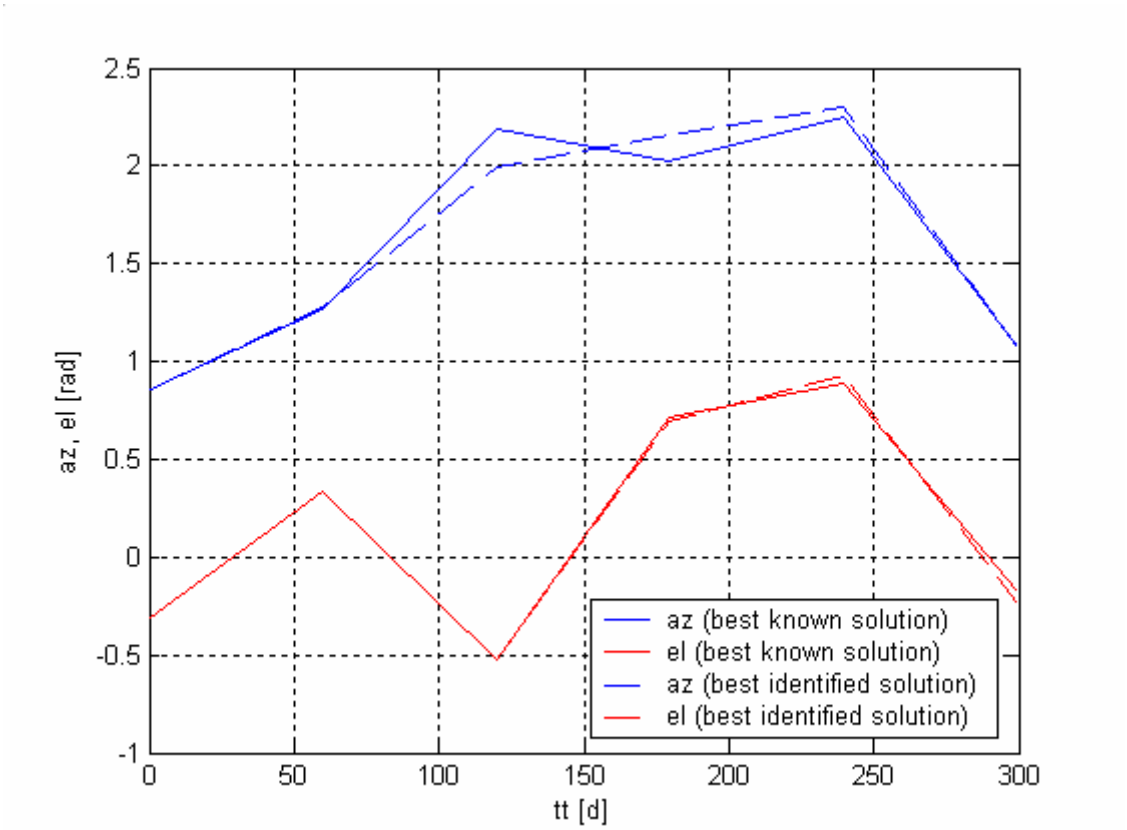

Figure 218: Comparison between the best identified solution and the best known solution: thrust azimuth and elevation over the transfer trajectory.

Objective function space		
Term	**Best identified solution**	**Best know solution**
$ObjFun$:	14.169	5.750
$R_F / R_{SoI,Mars}$:	0.009	0.002
v_F [*m/s*]:	83.297	0.086
m_{prop} [*kg*]:	115.060	114.433

Table 139: Comparison between the best identified solution and the best known solution: objective function space.

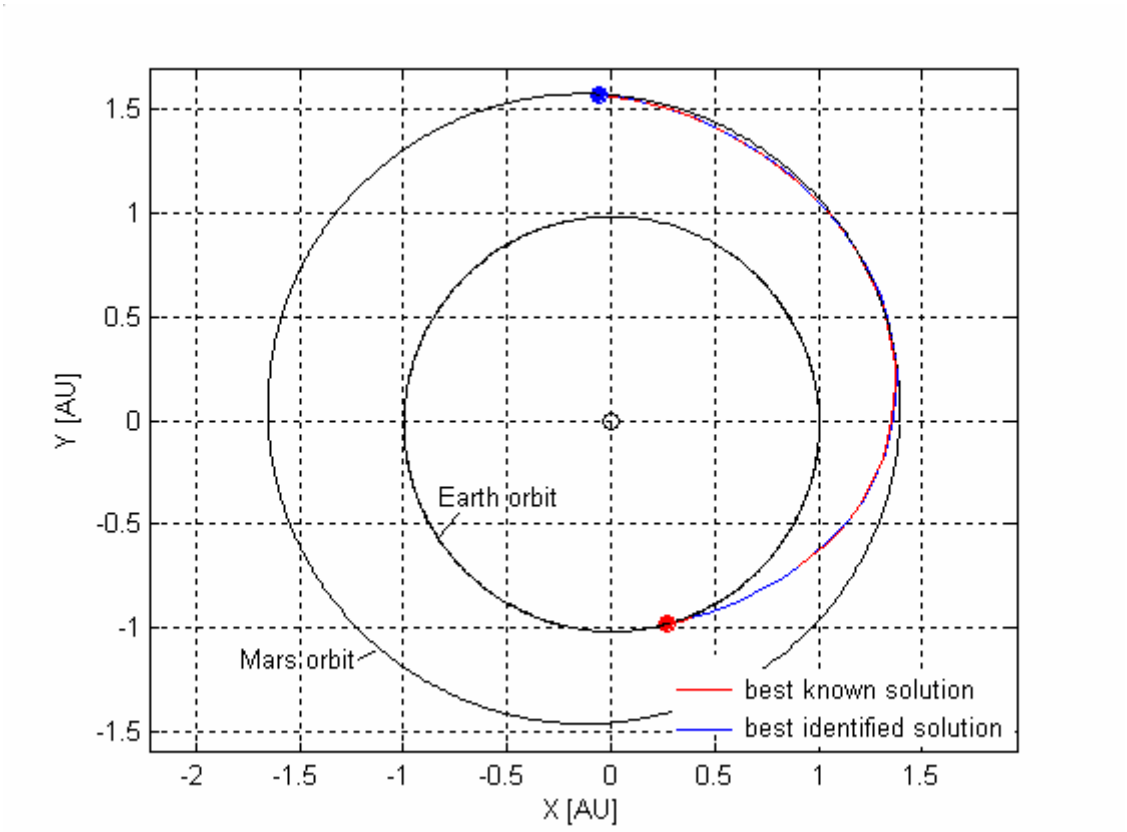

Figure 219: Comparison between the trajectories corresponding to the best identified solution and the best known solution.

Figure 220 shows the distribution of the solutions resulting from each optimization run over the plane of the objective function, ΔV, and the number of function evaluations, *nFunc.*, while Table 140 reports the statistical characteristics, which will be used for comparisons with the other optimization algorithms, as well as the performances corresponding to the best identified solution.

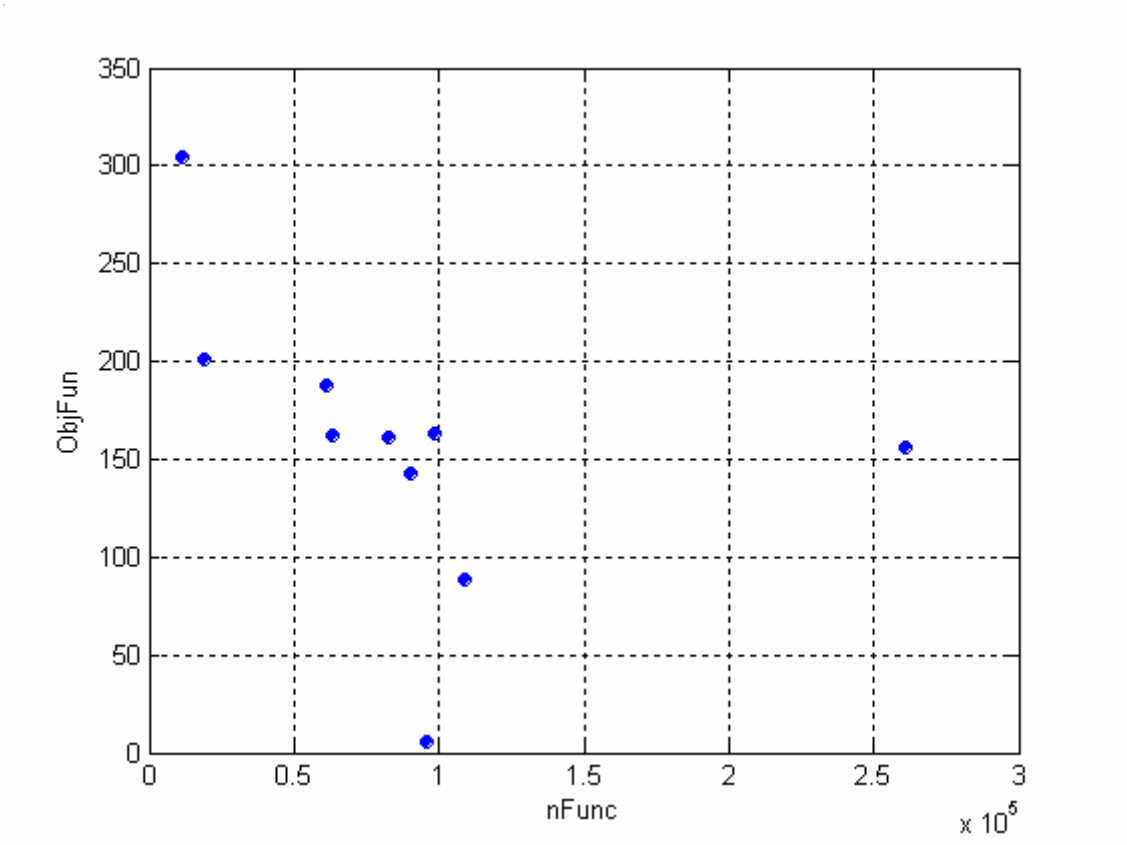

Figure 220: Distribution of the solutions resulting from each FEP optimization run over the $nFunc - \Delta V$ plane.

Evaluation criterion	Mean value	Standard deviation	Best identified solution
Objective function:	157.191	76.266	14.169
nFunc.:	89013.900	68704.199	95585
Runtime [STU]:	14.996	9.551	16.487

Table 140: Statistical characteristics of the identified solutions.

The estimation of the number and features of the distinct local minima reached by means of the ten runs is performed. The optimal solutions corresponding to all ten runs have been used as starting solutions for ten local optimization processes in order to accurately estimate the local minimum corresponding to the basin of attraction each optimal solution belong to. The consequences of the local optimization processes in the *nFunc* - ΔV plane are shown in Figure 221,

where each improved solution is linked to the corresponding starting one by means of a straight line.

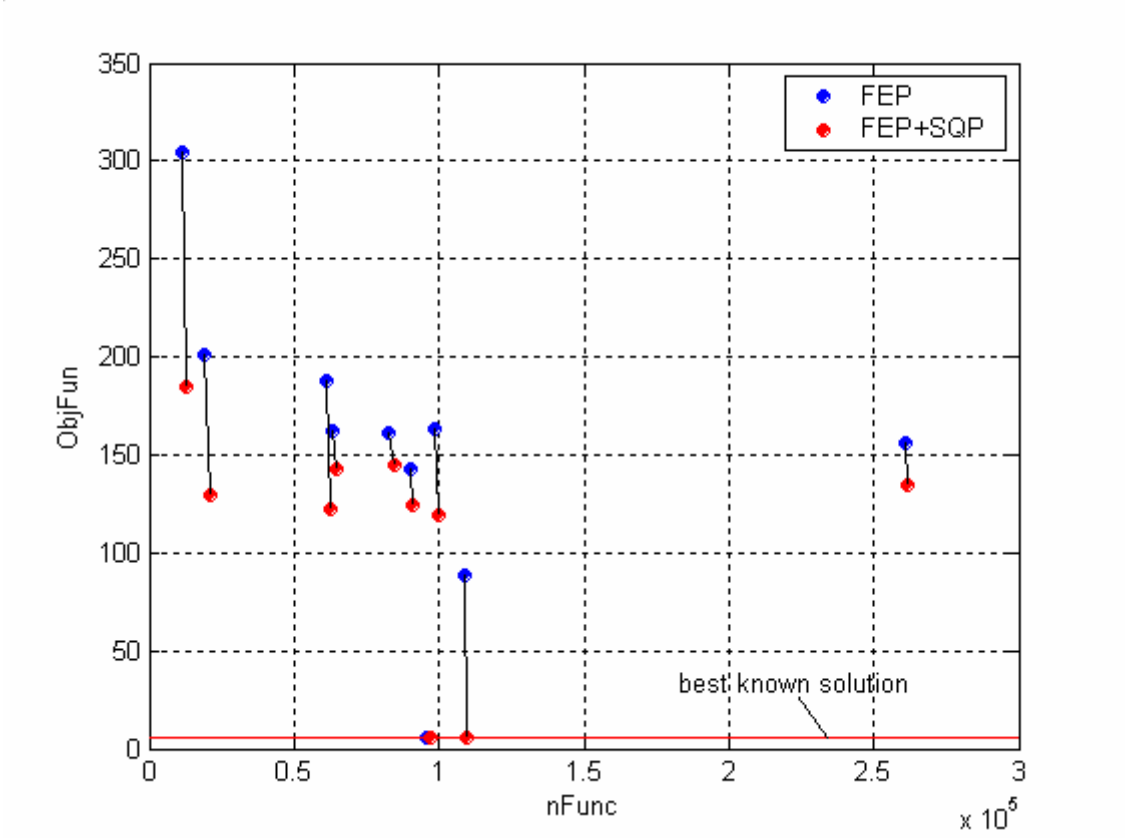

Figure 221: Comparison between solutions resulting from FEP runs and their improvements by means of a further local optimization process via SQP algorithm over the $nFunc - \Delta V$ plane.

Figure 221 shows that different local minima corresponds to FEP runs. By considering the objective function values reached at the end of the optimization processes, two solutions seem to correspond to the best known one. Let us investigate the solutions in the normalized search space. Table 141 reports, corresponding to each FEP+SQP run, the reached objective function value and the distance (in Euclidean metric) with respect to the best known solution.

	ObjFun	Distance
run 1	144.831	1.014
run 2	129.172	0.954
run 3	5.656	0.513
run 4	118.967	1.238
run 5	184.309	1.128
run 6	124.500	1.193
run 7	134.372	1.012
run 8	143.076	1.276
run 9	5.705	0.011
run 10	121.917	1.291

Table 141: FEP+SQP optimization runs: objective function values and Euclidean distance in the normalized search space with respect to the best known solution.

By considering two solutions as identical when the Euclidean distance is less than 1% of the hyper diagonal of the normalized search space, that is 0.040 in a 16-dimensional space, one run has been able to get the best known solution, that is 1/10 FEP runs successfully identified the basin of attraction of the best known solution. Moreover, FEP identified an alternative solution which is in fact comparable with the best known solution in terms of the objective function value, that is run 3 solution. Figure 222 compares the trajectory corresponding to such solution with the best known one.

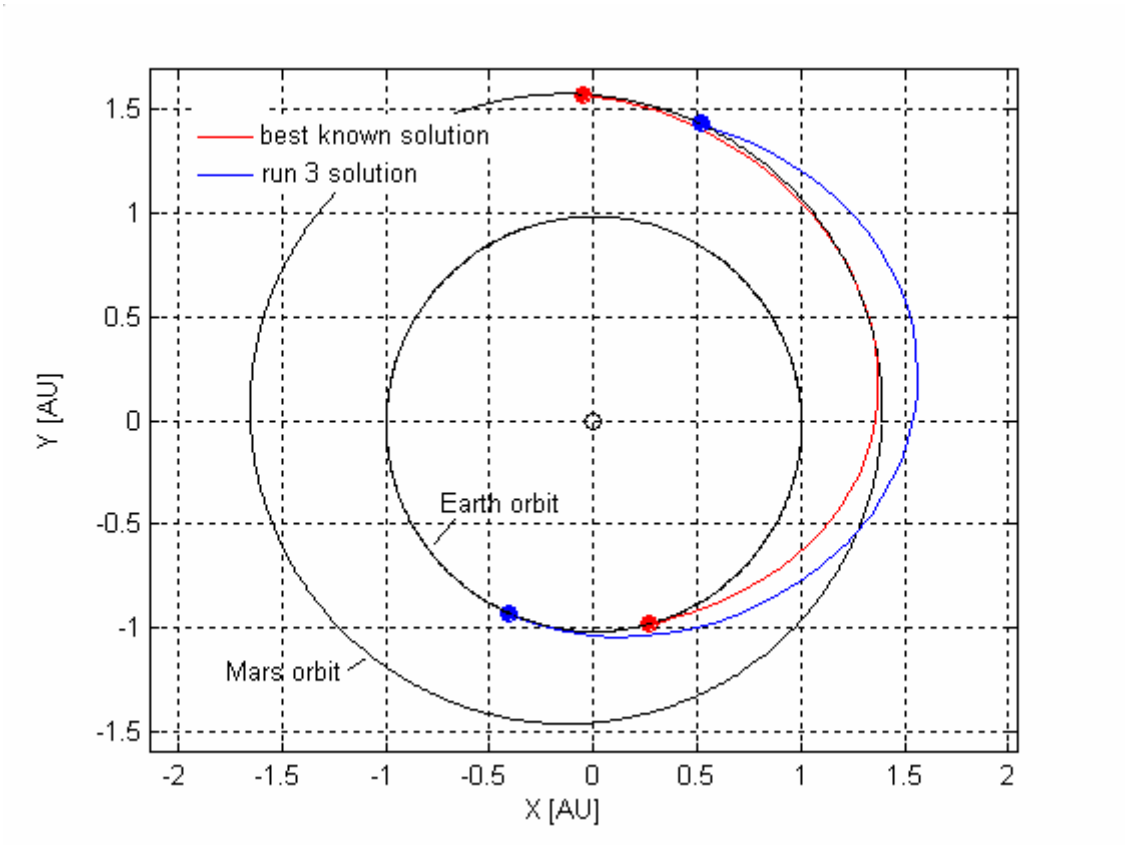

Figure 222:Comparison between the best known solution and solutions corresponding to run 3.

Table 142 reports the date of departure corresponding to the two analysed solutions.

	Best identified solution	**run 3 solution**
Date of departure [d]:	553.253	512.841

Table 142: Date of departure corresponding to the best known solution and run 3 solution.

DE

As DE implements a Differential Evolution algorithm, we report the statistical characteristics. Ten runs have been processed in order to solve the previously defined problem. Default options suggested by the providers of the code have been used in all the runs. Again, due to the high complexity of low thrust direct planet-to-planet interplanetary transfer problem and the high number of design

variables, we used 100 individuals evolving for a maximum number of iterations equal to 10000.

Algorithm parameters	
Number of individuals:	100
Maximum number of generations:	10000

Table 143, Table 144 and Figure 223 report the best identified solution compared with the best known solution in terms of the values of the design variables and of the objective function terms, while Figure 224 plots the resulting interplanetary transfer trajectories.

Search space		
Design variable	**Best identified solution**	**Best know solution**
Date of departure [*d*]:	528.585	553.253
Transfer time [*d*]:	293.142	299.462
Thrust level [*N*]:	0.162	0.130
Escape velocity from Earth [*m/s*]:	2331.437	2676.327

Table 143: Comparison between the best identified solution and the best known solution: search space.

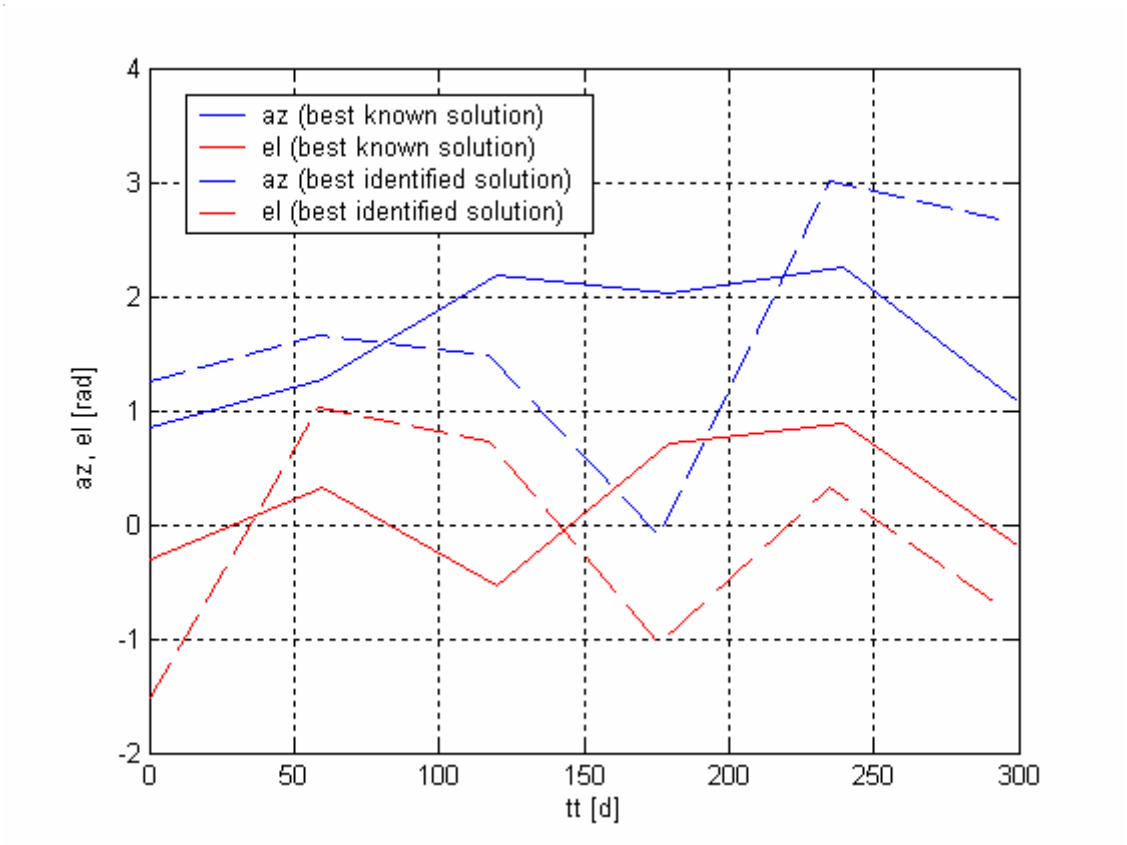

Figure 223: Comparison between the best identified solution and the best known solution: thrust azimuth and elevation over the transfer trajectory.

Objective function space		
Term	**Best identified solution**	**Best know solution**
$ObjFun$:	224.672	5.750
$R_F / R_{SoI,Mars}$:	6.561	0.002
v_F [*m/s*]:	1520.989	0.086
m_{prop} [*kg*]:	139.320	114.433

Table 144: Comparison between the best identified solution and the best known solution: objective function space.

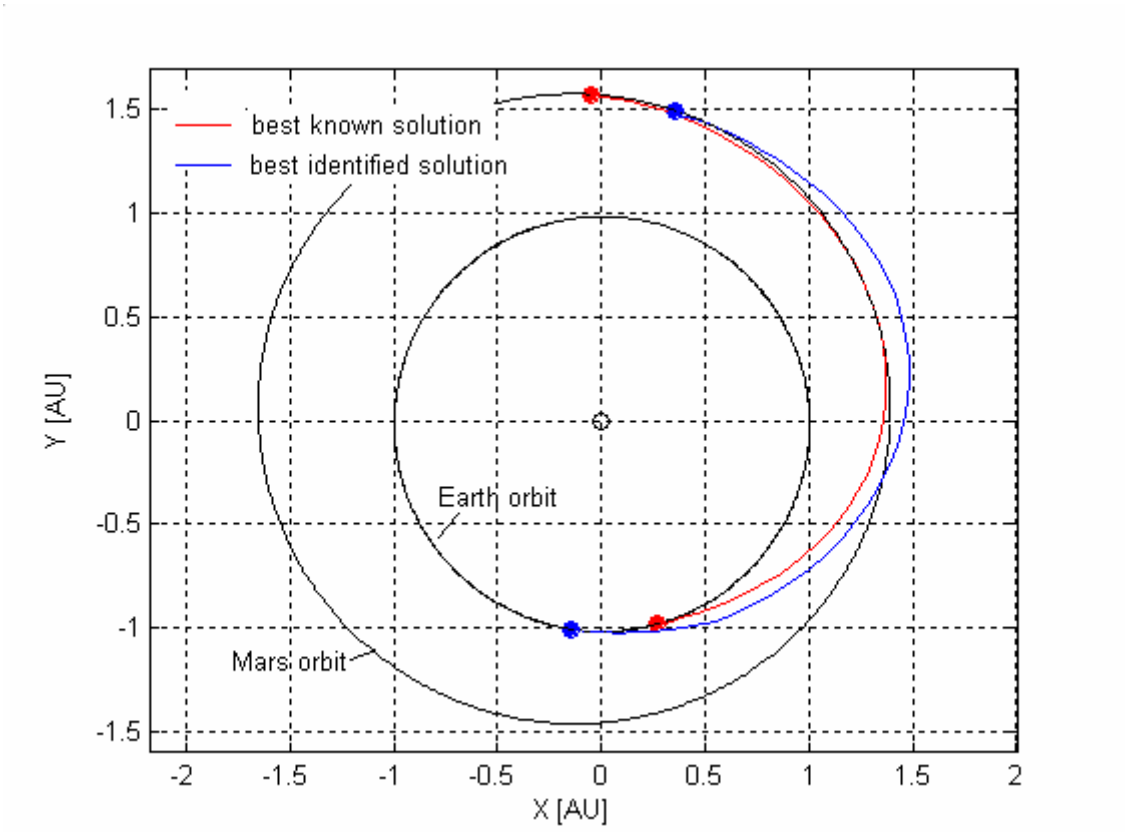

Figure 224: Comparison between the trajectories corresponding to the best identified solution and the best known solution.

Figure 225 shows the distribution of the solutions resulting from each optimization run over the plane of the objective function, ΔV, and the number of function evaluations, *nFunc.*, while Table 145 reports the statistical characteristics, which will be used for comparisons with the other optimization algorithms, as well as the performances corresponding to the best identified solution.

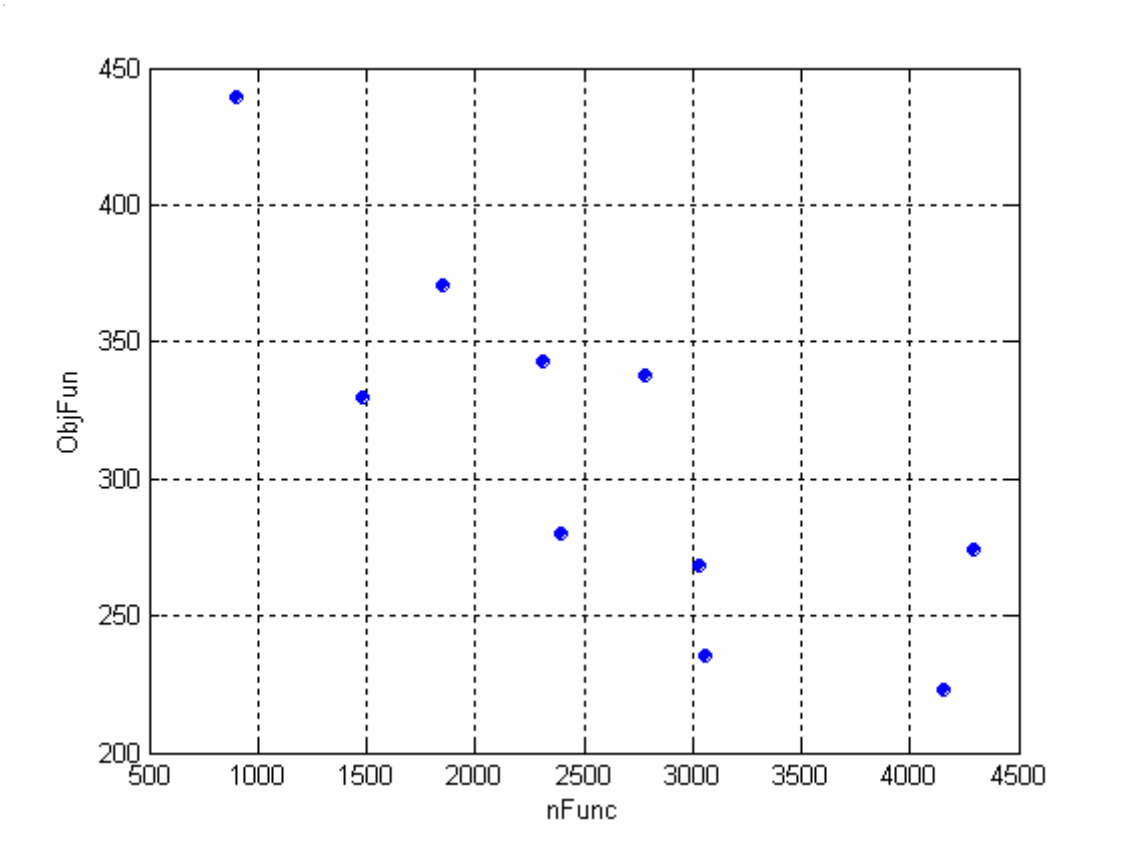

Figure 225: Distribution of the solutions resulting from each DE optimization run over the $nFunc - \Delta V$ plane.

Evaluation criterion	Mean value	Standard deviation	Best identified solution
Objective function:	310.233	66.478	224.672
nFunc.:	2625.000	1081.359	4151
Runtime [STU]:	0.437	0.177	0.689

Table 145: Statistical characteristics of the identified solutions.

The estimation of the number and features of the distinct local minima reached by means of the ten runs is now performed. To attain such a task, the optimal solutions corresponding to all ten runs have been used as starting solutions for ten local optimization processes in order to accurately estimate the local minimum corresponding to the basin of attraction each optimal solution belong to. The consequences of the local optimization processes in the *nFunc* - ΔV

plane are shown in Figure 226, where each improved solution is linked to the corresponding starting one by means of a straight line.

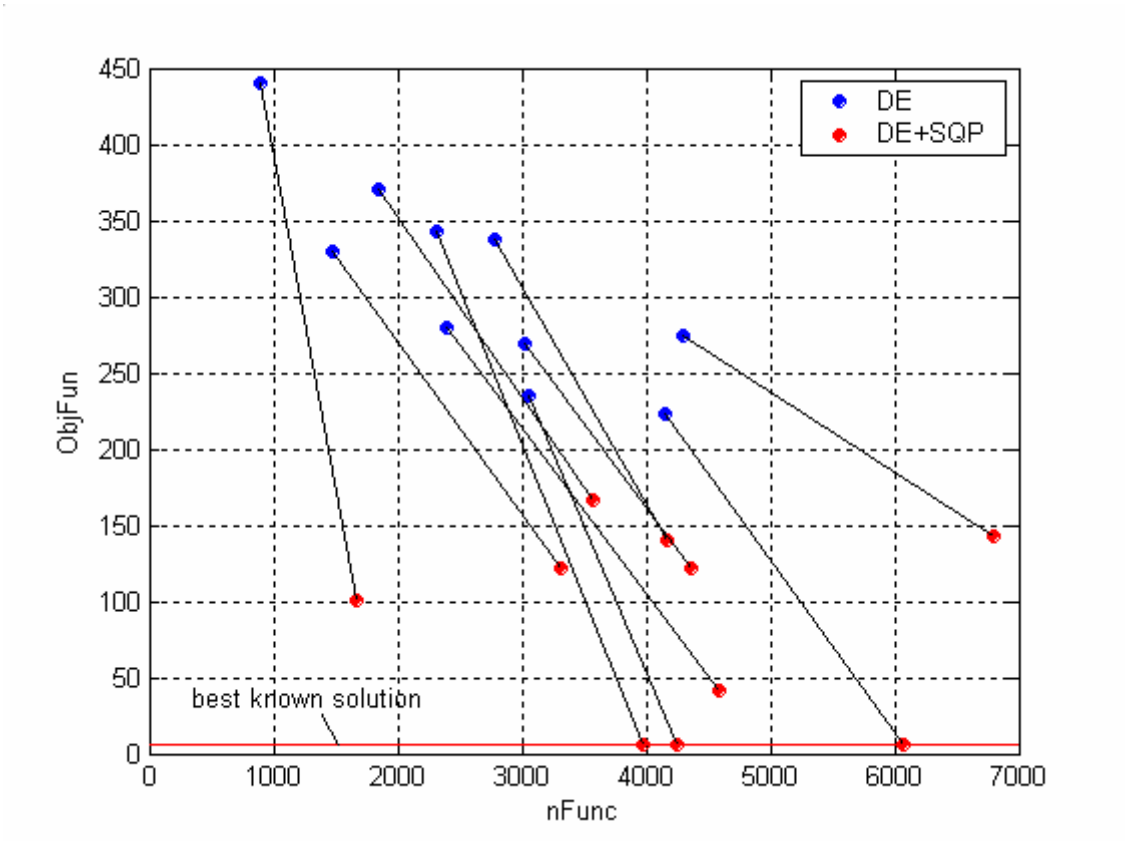

Figure 226: Comparison between solutions resulting from DE runs and their improvements by means of a further local optimization process via SQP algorithm over the $nFunc - \Delta V$ plane.

Figure 226 shows that different local minima corresponds to DE runs. Let us investigate the solutions in the normalized search space. Table 146 reports, corresponding to each DE+SQP run, the reached objective function value and the distance (in Euclidean metric) with respect to the best known solution.

	ObjFun	Distance
run 1	121.389	1.198
run 2	166.862	1.124
run 3	6.076	0.666
run 4	101.114	1.645
run 5	6.060	0.767
run 6	140.131	1.388
run 7	41.376	1.394
run 8	6.097	0.673
run 9	142.843	1.108
run 10	121.596	1.286

Table 146: DE+SQP optimization runs: objective function values and Euclidean distance in the normalized search space with respect to the best known solution.

An empirical analysis suggest to define two solutions as identical when the Euclidean distance is less than 1% of the hyper diagonal of the normalized search space, that is 0.040 in a 16-dimensional space. The consequence of such definition is that no run has been able to get the best known solution, that is 0/10 DE runs successfully identified the basin of attraction of the best known solution. However, three solutions have been reached which have objective function values comparable with that achieved by the best known solution, that is runs 3, 5 and 8. Such solutions are reported in Figure 227.

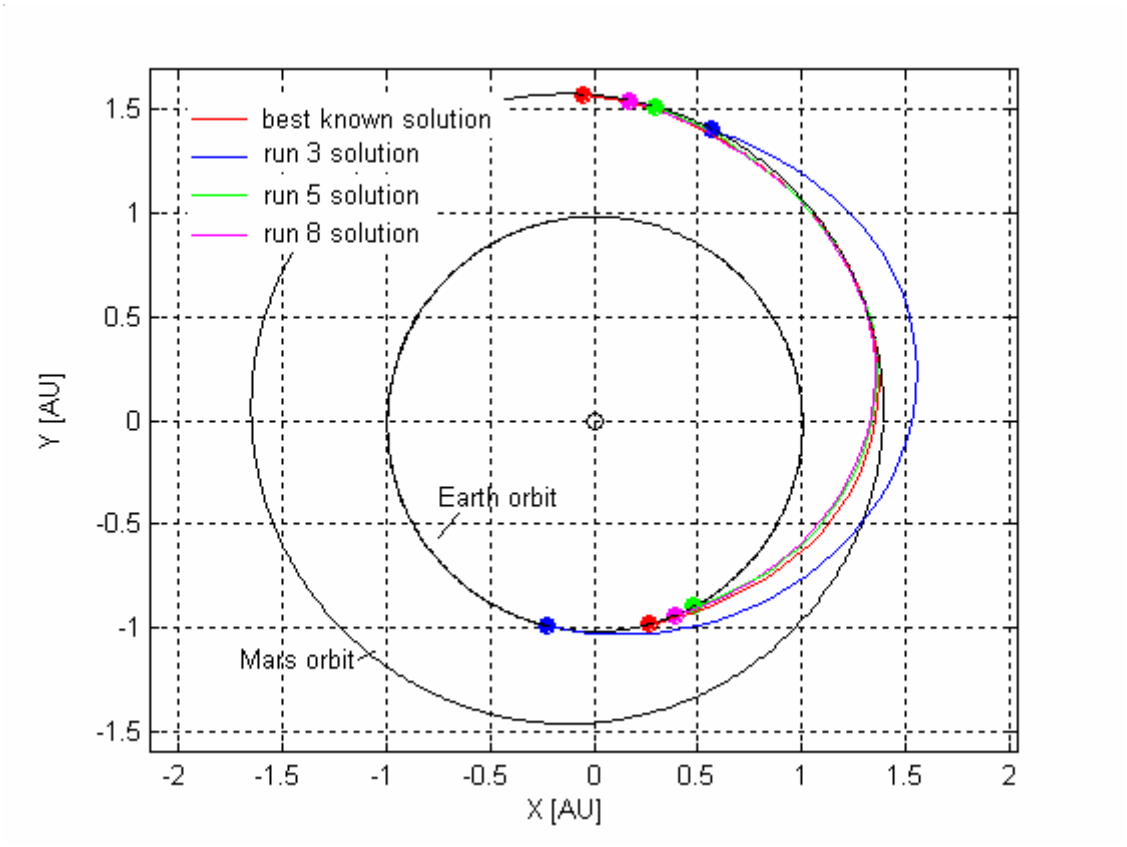

Figure 227: Comparison between the best known solution and solutions corresponding to run 3 and run 9.

The identified local minima are different, as the consideration of the date of departure values can show (see Table 147).

	Best identified solution	run 3	run 5	run 8
Date of departure [d]:	553.253	523.430	566.859	560.769

Table 147: Date of departure corresponding to the best known solution and run 3, run 5 and run 9 solutions.

ASA

As ASA implements an Adaptive Simulated Annealing algorithm, we report the statistical performance characteristics. Ten runs have been processed in order to solve the previously defined problem. Default options suggested by the providers of the code have been used in all the runs. Note that, unlike the previous cases, the adaptive simulated annealing needs a starting solution,

which strongly affects the optimal solution reached. Due to the comparative purposes of this work, we decided to use ten different random starting solutions, uniformly distributed in the search box. Table 148, Table 149 and Figure 228 report the best identified solution compared with the best known solution in terms of the values of the design variables and of the objective function terms, while Figure 229 plots the resulting interplanetary transfer trajectories.

Search space		
Design variable	**Best identified solution**	**Best know solution**
Date of departure [*d*]:	516.549	553.253
Transfer time [*d*]:	291.885	299.462
Thrust level [*N*]:	0.141	0.130
Escape velocity from Earth [*m/s*]:	2545.910	2676.327

Table 148: Comparison between the best identified solution and the best known solution: search space.

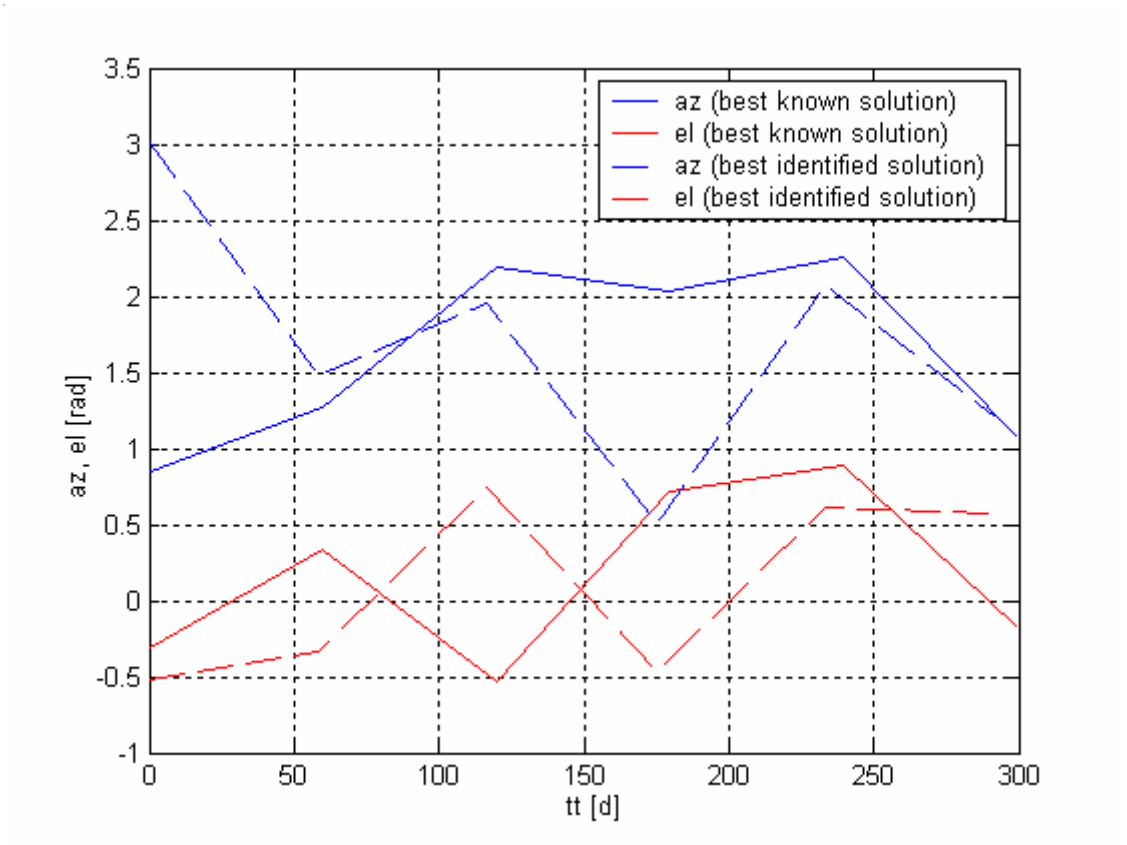

Figure 228: Comparison between the best identified solution and the best known solution: thrust azimuth and elevation over the transfer trajectory.

Objective function space		
Term	**Best identified solution**	**Best know solution**
$ObjFun$:	10.272	5.750
$R_F / R_{SoI,Mars}$:	0.234	0.002
v_F [*m/s*]:	18.842	0.086
m_{prop} [*kg*]:	120.992	114.433

Table 149: Comparison between the best identified solution and the best known solution: objective function space.

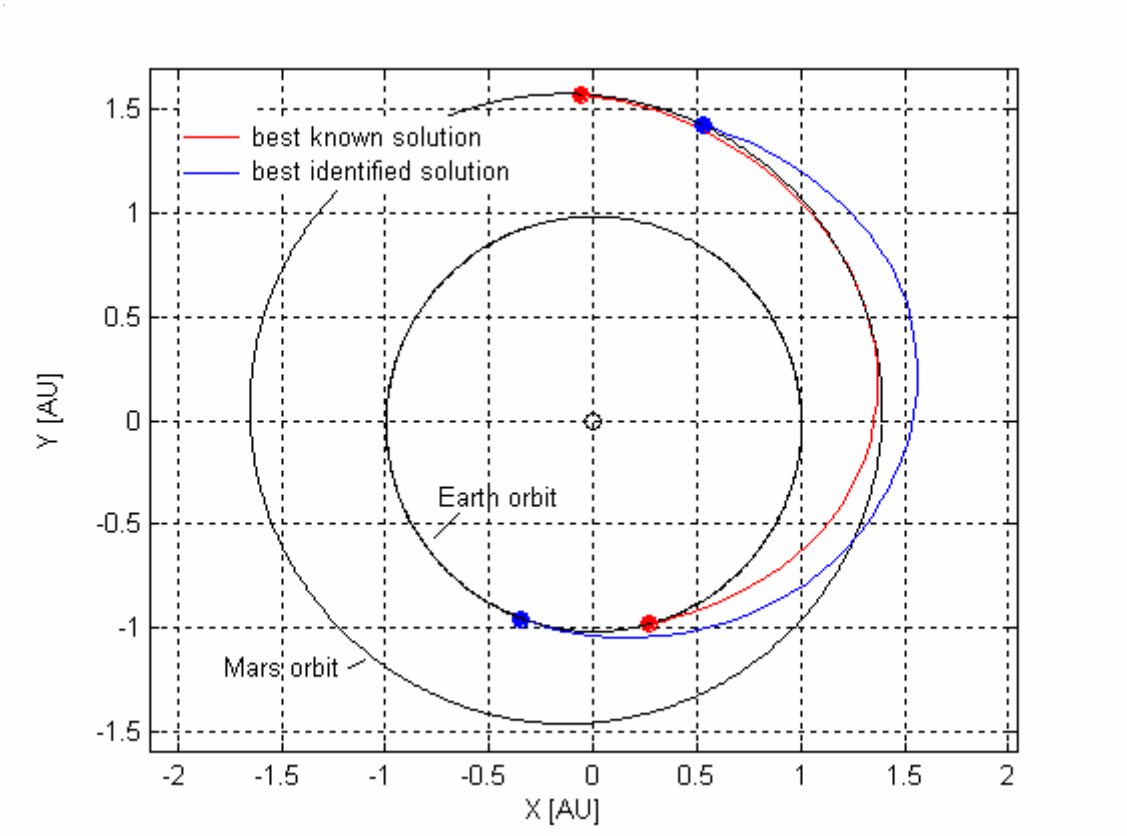

Figure 229: Comparison between the trajectories corresponding to the best identified solution and the best known solution.

Figure 230 shows the distribution of the solutions resulting from each optimization run over the plane of the objective function, ΔV, and the number of function evaluations, *nFunc*, while Table 150 reports the statistical characteristics, which will be used for comparisons with the other optimization algorithms, as well as the performances corresponding to the best identified solution.

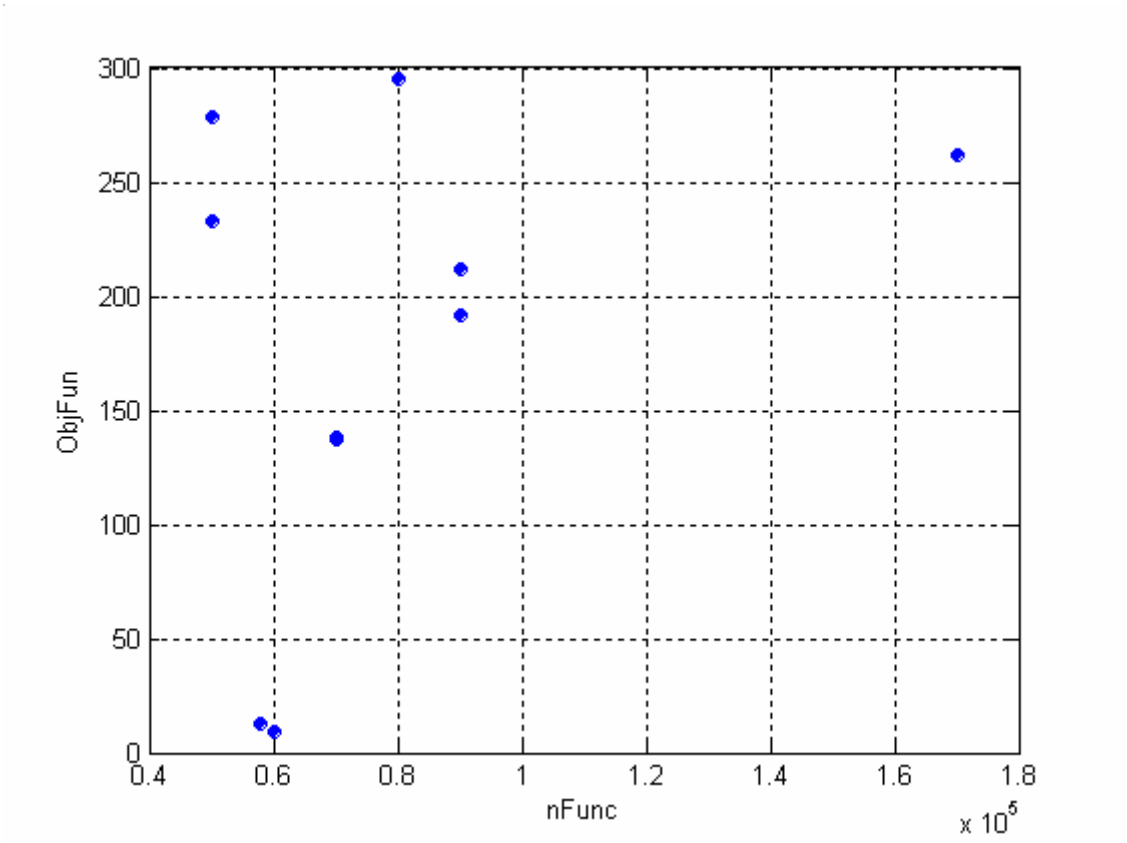

Figure 230: Distribution of the solutions resulting from each ASA optimization run over the $nFunc - \Delta V$ plane.

Evaluation criterion	Mean value	Standard deviation	Best identified solution
Objective function:	176.977	102.314	10.272
nFunc.:	78783.8	35239.439	60000
Runtime [STU]:	12.985	5.856	10.533

Table 150: Statistical characteristics of the identified solutions.

The optimal solutions corresponding to all ten runs are now used again as starting solutions for ten local optimization processes in order to accurately estimate the local minimum corresponding to the basin of attraction each optimal solution belong to and to evaluate the number of ASA successful runs. Figure 231 illustrates the consequences of the local optimization processes in the *nFunc* - ΔV plane.

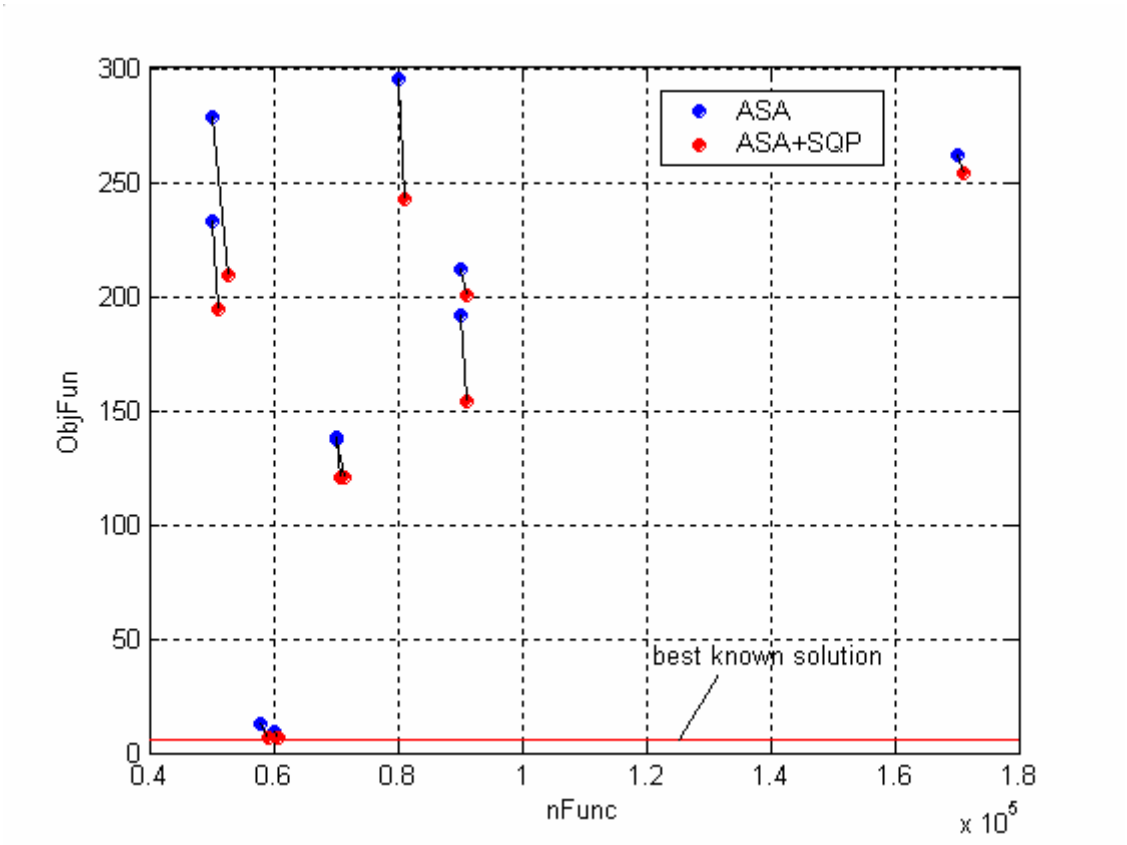

Figure 231: Comparison between solutions resulting from ASA runs and their improvements by means of a further local optimization process via SQP algorithm over the $nFunc - \Delta V$ plane.

Different local minima corresponds to ASA runs. In order to estimate the number of identified solutions which lie in the basin of attraction of the best known solutions, solutions are now investigated in the normalized search space. Tale 151 reports, corresponding to each ASA+SQP run, the reached objective function value and the distance (in Euclidean metric) with respect to the best known solution.

	ObjFun	Distance
run 1	242.950	1.093
run 2	120.547	1.086
run 3	253.604	1.596
run 4	208.814	1.129
run 5	153.765	0.974
run 6	6.487	0.786
run 7	200.014	1.422
run 8	6.273	0.761
run 9	120.364	1.013
run 10	194.330	1.222

Table 151: ASA+SQP optimization runs: objective function values and Euclidean distance in the normalized search space with respect to the best known solution.

By considering two solutions as identical when the Euclidean distance is less than 0.040, no runs were able to get the best known solution, that is 0/10 ASA runs successfully identified the basin of attraction of the best known solution. It is worth noting that, although ASA wasn't able to reach the basin of attraction of the best known solution (according to the definition of identical solutions given above), it could achieve the basin of attraction of two solutions which are in fact quite comparable with the best known one in terms of objective function values (see runs 6 and 8). Figure 232 shows the trajectories corresponding to such solutions compared with the best known one.

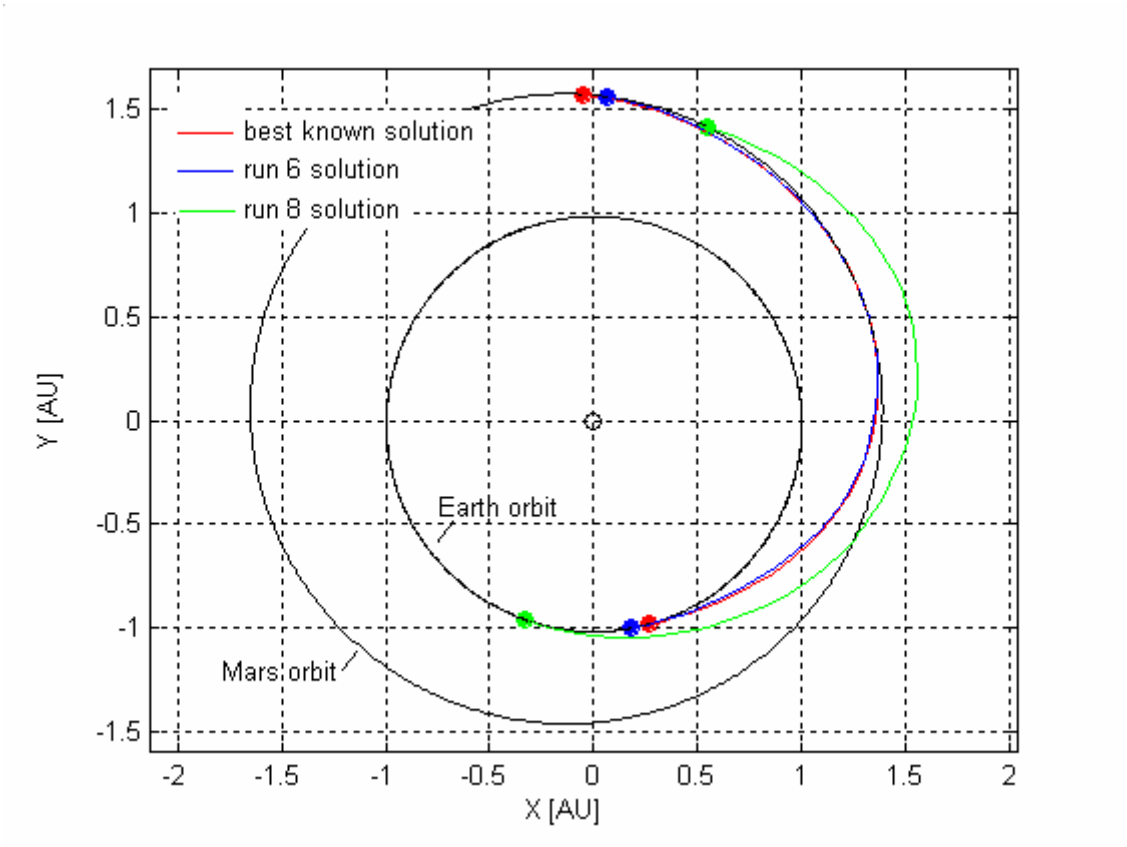

Figure 232: Comparison between the best known solution and solutions corresponding to run 6 and run 8.

It is worth noting that, although the objective function values are comparable, the identified local minima are different, as the analysis of the date of departure values shows, whose values in case of the three analysed solutions are reported in Table 152.

	Best identified solution	**run 6**	**run 8**
Date of departure [d]:	553.253	547.964	517.339

Table 152: Date of departure corresponding to the best known solution and solutions run 6 and run 8.

glbSolve

As glbSolve algorithm implements a deterministic optimization approach, statistical characteristics are not needed in this case. Only one run has been processed in order to solve the previously defined problem. Default options suggested by the providers of the code have been used. As the low thrust direct planet-to-planet interplanetary transfer problem has high complexity features and a high number of design variables, we used a maximum number of iterations equal to 10000.

Algorithm parameters	
Maximum number of generations:	10000

Table 153, Table 154 and Figure 233 report the identified solution compared with the best known solution in terms of the values of the design variables and of the objective function terms, while Figure 234 plots the resulting interplanetary transfer trajectories.

Search space		
Design variable	**Best identified solution**	**Best know solution**
Date of departure [*d*]:	1217.500	553.253
Transfer time [*d*]:	225.000	299.462
Thrust level [*N*]:	0.165	0.130
Escape velocity from Earth [*m/s*]:	2500	2676.327

Table 153: Comparison between the best identified solution and the best known solution: search space.

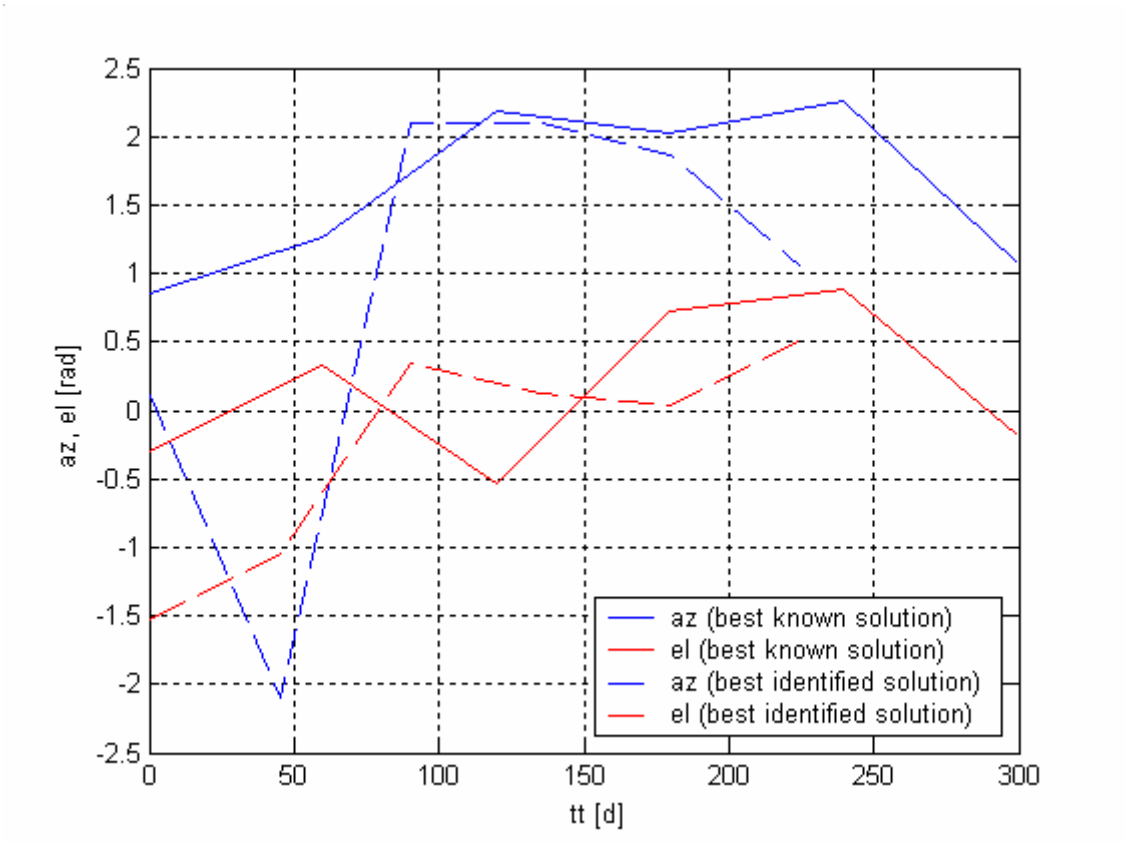

Figure 233: Comparison between the best identified solution and the best known solution: thrust azimuth and elevation over the transfer trajectory.

Objective function space		
Term	**Best identified solution**	**Best know solution**
$ObjFun$:	158.571	5.750
$R_F / R_{SoI,Mars}$:	0.152	0.002
v_F [*m/s*]:	1515.863	0.086
m_{prop} [*kg*]:	109.305	114.433

Table 154: Comparison between the best identified solution and the best known solution: objective function space.

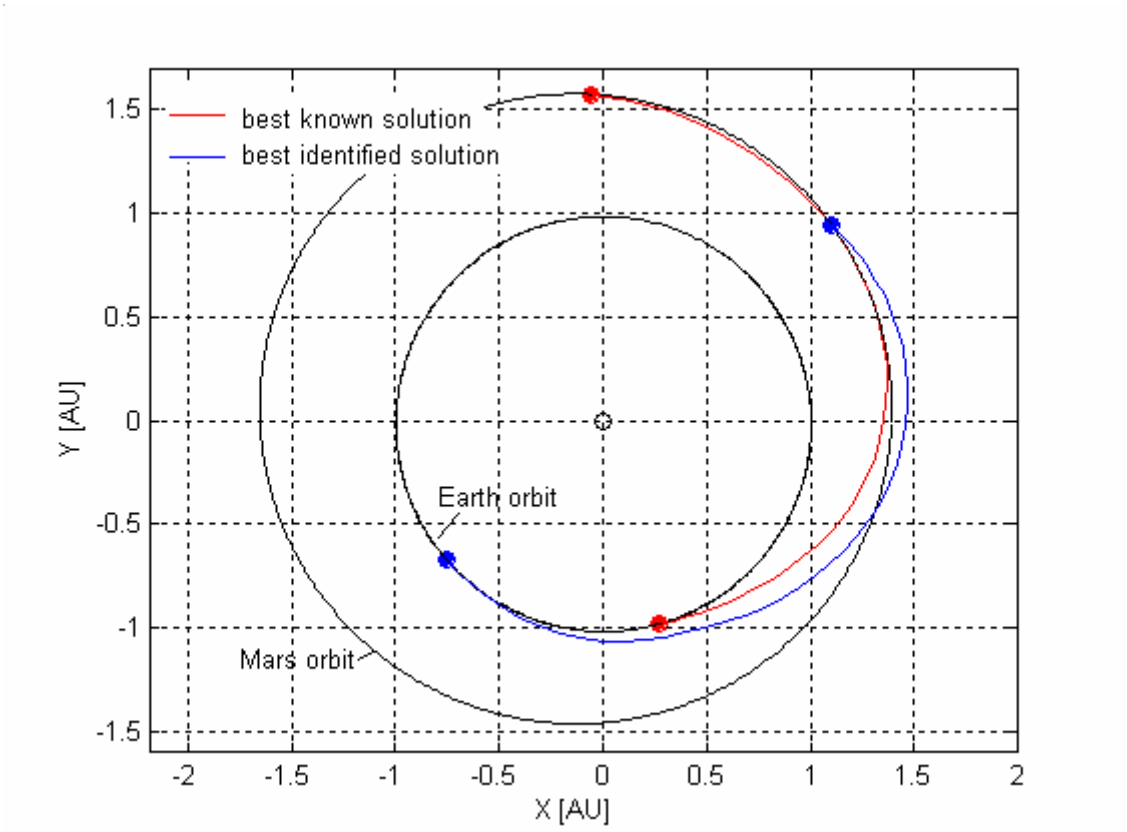

Figure 234: Comparison between the trajectories corresponding to the best identified solution and the best known solution.

Table 155 reports the characteristics of the identified solution, which will be used for comparisons with the other optimization algorithms.

Evaluation criterion	Identified solution
ObjFun:	158.571
nFunc.:	29003
Runtime [STU]:	5.477

Table 155: Characteristics of the identified solutions.

In order to accurately identify the local minimum reached by *glbSolve* algorithm, a local optimization process by means of a SQP algorithm is now performed, where the solution identified by *glbSolve* is considered as the starting point for the local search process. The starting solution and the improved one are

reported in Figure 235 on the *nFunc-ObjFun* plane, while Figure 236 compares the improved solution with the best known one in terms of transfer trajectory.

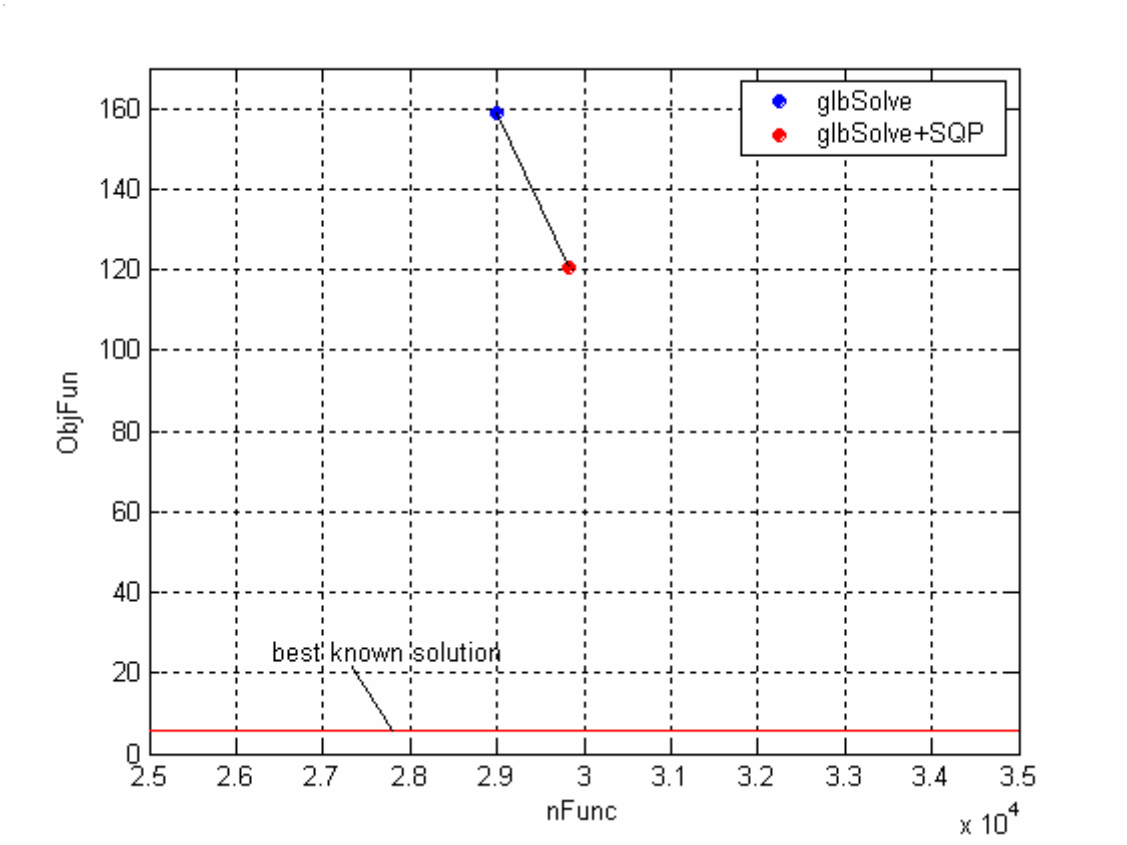

Figure 235: Comparison between solution resulting from glbSolve run and its improvement by means of a further local optimization process via SQP algorithm over the $nFunc - \Delta V$ plane.

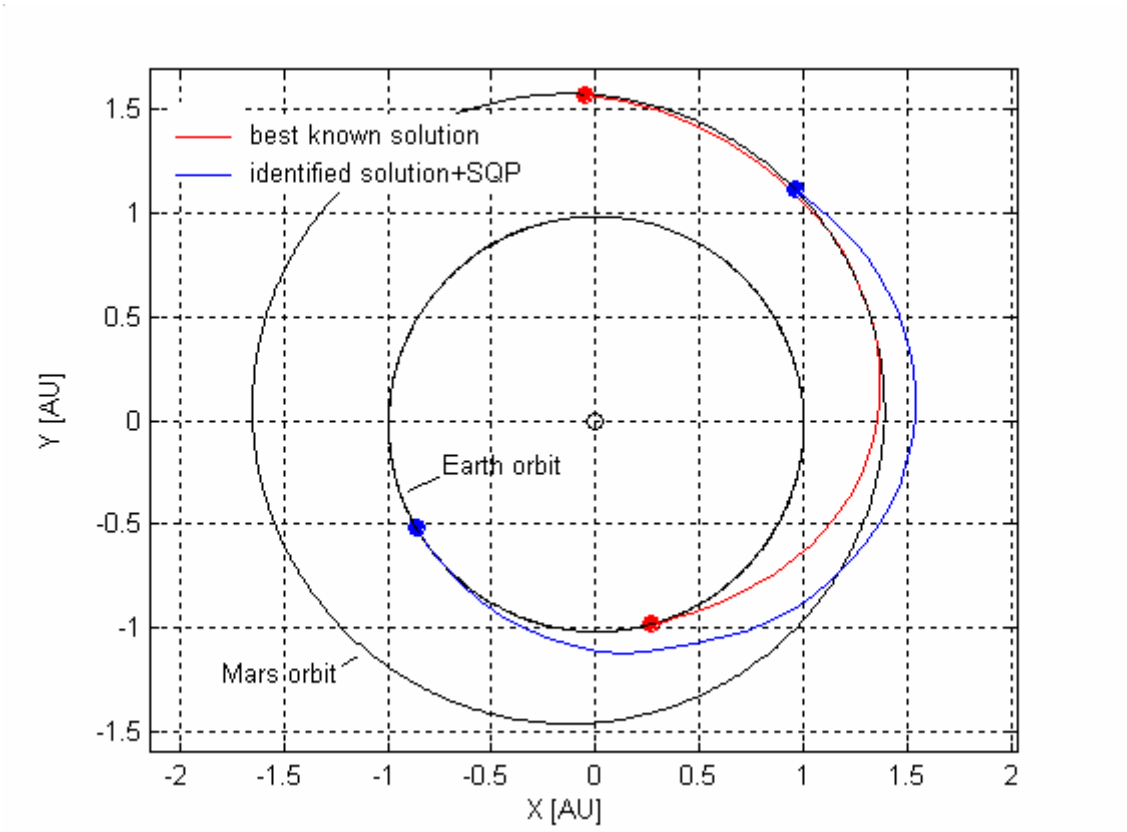

Figure 236:Comparison between solution resulting from glbSolve+SQP run and thebest known solution in terms of transfer trajectory.

The solution is now investigated in the normalized search space. Table 156 reports, corresponding to the glbSolve+SQP run, the reached objective function value and the distance (in Euclidean metric) with respect to the best known solution.

	ObjFun	**Distance**
glbSolve+SQP run	120.713	1.314

Table 156: glbSolve+SQP optimization runs: objective function values and Euclidean distance in the normalized search space with respect to the best known solution.

By considering two solutions as identical when the Euclidean distance is less than 0.040, the run wasn't able to get the best known solution, that is glbSolve run failed in identifying the basin of attraction of the best known solution.

MCS

As MCS algorithm implements a deterministic optimization approach, only one run has been processed in order to solve the previously defined problem. Default options suggested by the providers of the code have been used.Table 157, Table 158 and Figure 236 report the identified solution compared with the best known solution in terms of the values of the design variables and of the objective function terms, while Figure 237 plots the resulting interplanetary transfer trajectories.

Search space		
Design variable	**Best identified solution**	**Best know solution**
Date of departure [*d*]:	1195.711	553.253
Transfer time [*d*]:	193.957	299.462
Thrust level [*N*]:	0.168	0.130
Escape velocity from Earth [*m/s*]:	2160.898	2676.327

Table 156: Comparison between the best identified solution and the best known solution: search space.

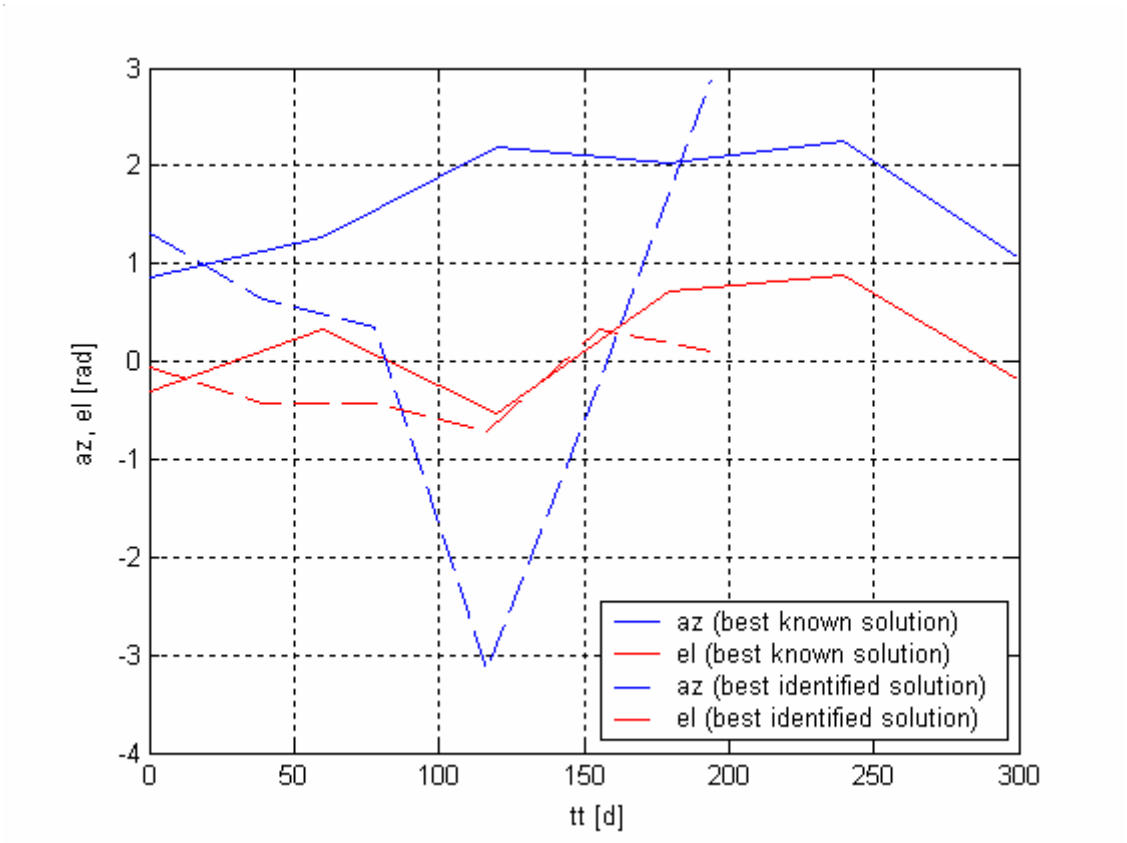

Figure 236: Comparison between the best identified solution and the best known solution: thrust azimuth and elevation over the transfer trajectory.

Objective function space		
Term	**Best identified solution**	**Best know solution**
$ObjFun$:	319.497	5.750
$R_F / R_{SoI,Mars}$:	0.029	0.002
v_F [*m/s*]:	3144.205	0.086
m_{prop} [*kg*]:	95.662	114.433

Table 157: Comparison between the best identified solution and the best known solution: objective function space.

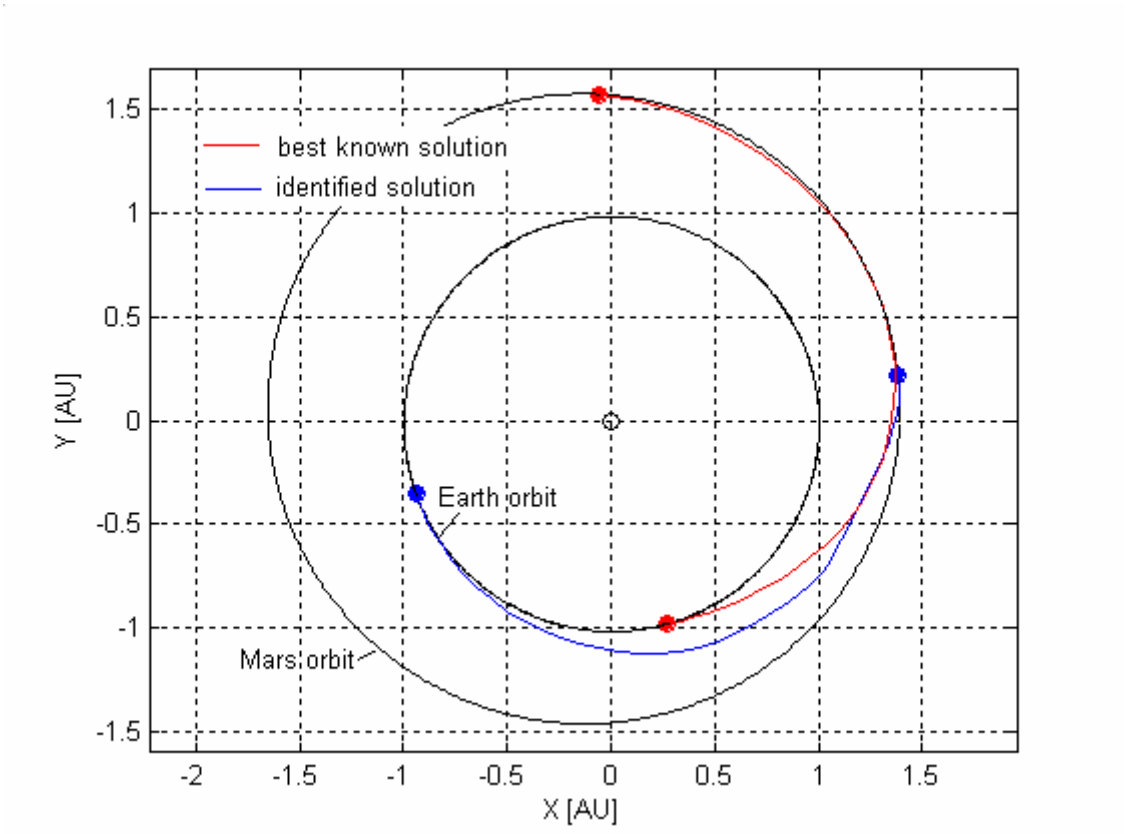

Figure 237: Comparison between the trajectories corresponding to the best identified solution and the best known solution.

Table 158 reports the characteristics of the identified solution, which will be used for comparisons with the other optimization algorithms.

Evaluation criterion	Identified solution
ObjFun:	319.497
nFunc.:	19183
Runtime [STU]:	2.960

Table 158: Characteristics of the identified solutions.

A local optimization process by means of a SQP algorithm is now performed, where the solution identified by MCS is considered as the starting point for the local search process. The starting solution and the improved one are reported in

Figure 238 on the *nFunc-ObjFun* plane, while Figure 239 compares the improved solution with the best known one in terms of transfer trajectory.

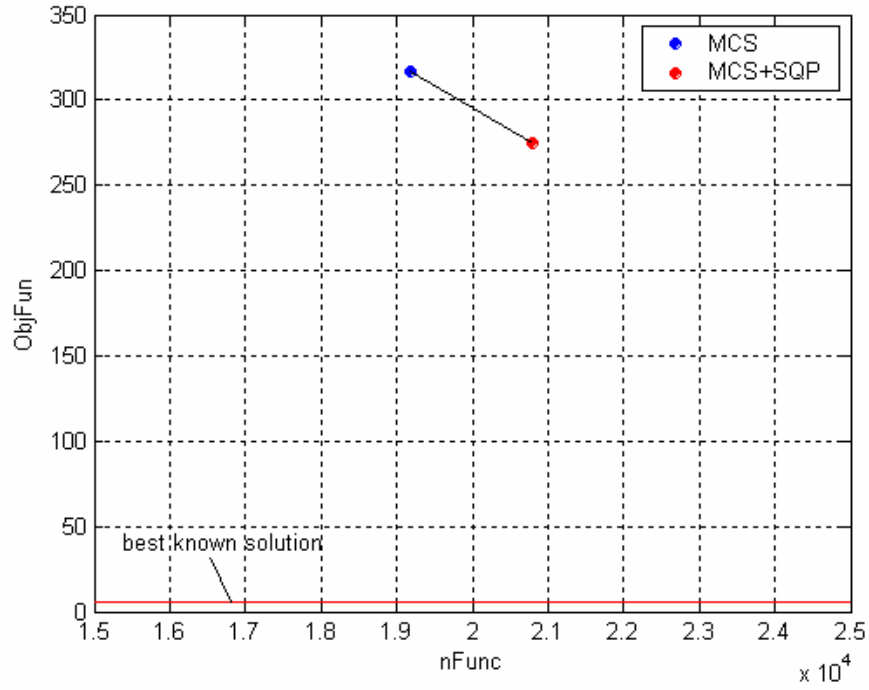

Figure 238: Comparison between solution resulting from MCS run and its improvement by means of a further local optimization process via SQP algorithm over the $nFunc - \Delta V$ plane.

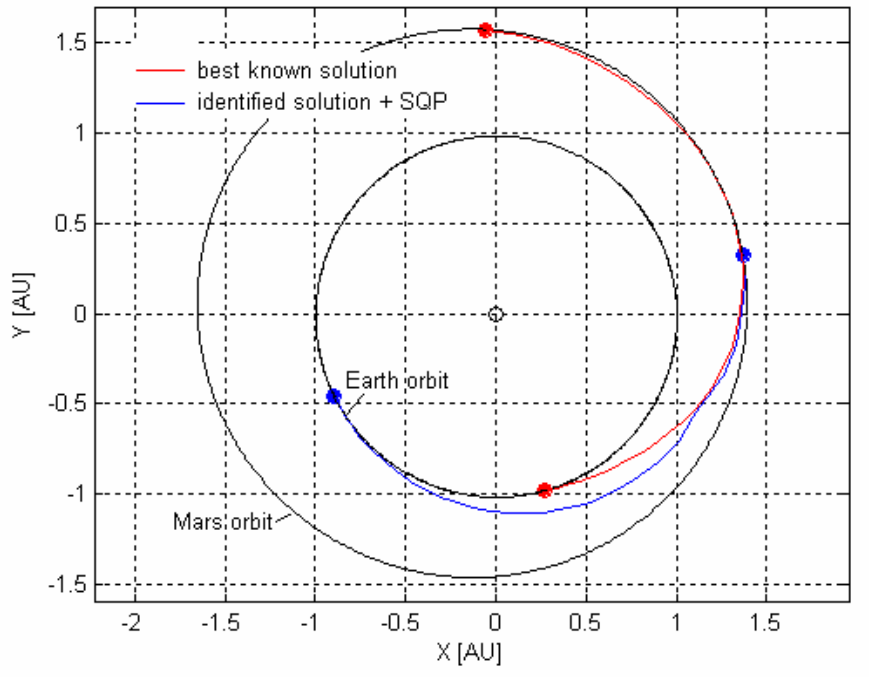

Figure 239: Comparison between solution resulting from MCS+SQP run and the best known solution in terms of transfer trajectory.

The solution is now investigated in the normalized search space. Table 159 reports, corresponding to the MCS+SQP run, the reached objective function value and the distance (in Euclidean metric) with respect to the best known solution.

	ObjFun	Distance
MCS+SQP run	319.497	1.512

Table 159: MCS+SQP optimization run: objective function values and Euclidean distance in the normalized search space with respect to the best known solution.

By considering two solutions as identical when the Euclidean distance is less than 0.040, the run wasn't able to get the best known solution, that is MCS run failed in identifying the basin of attraction of the best known solution.

rbfSolve

As rbfSolve algorithm implements a deterministic optimization approach, based on objective function response surface assessment and analysis suitable for costly objective function problems, statistical features analysis don't hold here. Only one run have been processed in order to solve the previously defined problem. Default options suggested by the providers of the code have been used. As already stated in the other mission analysis test problems, the termination conditions available in TOMLAB version of rbfSolve tool (which is not freely available) do not include suitable rules for practical problems with not a priori information about the global optimum solution. As a consequence, a maximum number of objective function evaluations has been fixed for terminating the optimization process. By revising the previous analysis, in case of low thrust direct planet-to-planet transfer, the number of objective function evaluations was quite high: FEP required about 10^5 objective function evaluations. However, as already noted in Multiple Gravity Assist analysis, rbfSolve is tailored for costly optimization processes and can not dealing with so high number of objective function evaluations due to the high required memory for handling the interpolation process. As a consequence, such limitations

forced us to fix a maximum number of objective function evaluations of the order of 10^3. As it concerns the validity of the achieved results, considerations similar to those highlighted in case of Multiple Gravity Assist hold in this case also: in particular, if the response surface algorithm is not able to identify and accurately approximate the basin of attraction of the global optimum in a low number of objective function evaluations, it is likely the case the response surface based algorithm has not converged to the global optimum solution. Hence, the fixed number of objective function evaluations has been set to 1000.

Algorithm parameters	
Maximum number of objective function evaluations:	1000

Table 160, table 161 and Figure 240 report the identified solution compared with the best known solution in terms of the values of the design variables and of the objective function terms, while Figure 241 plots the resulting interplanetary transfer trajectories.

Search space		
Design variable	**Identified solution**	**Best know solution**
Date of departure [*d*]:	526.526	553.253
Transfer time [*d*]:	235.040	299.462
Thrust level [*N*]:	0.122	0.130
Escape velocity from Earth [*m/s*]:	2639.289	2676.327

Table 160: Comparison between the identified solution and the best known solution: search space.

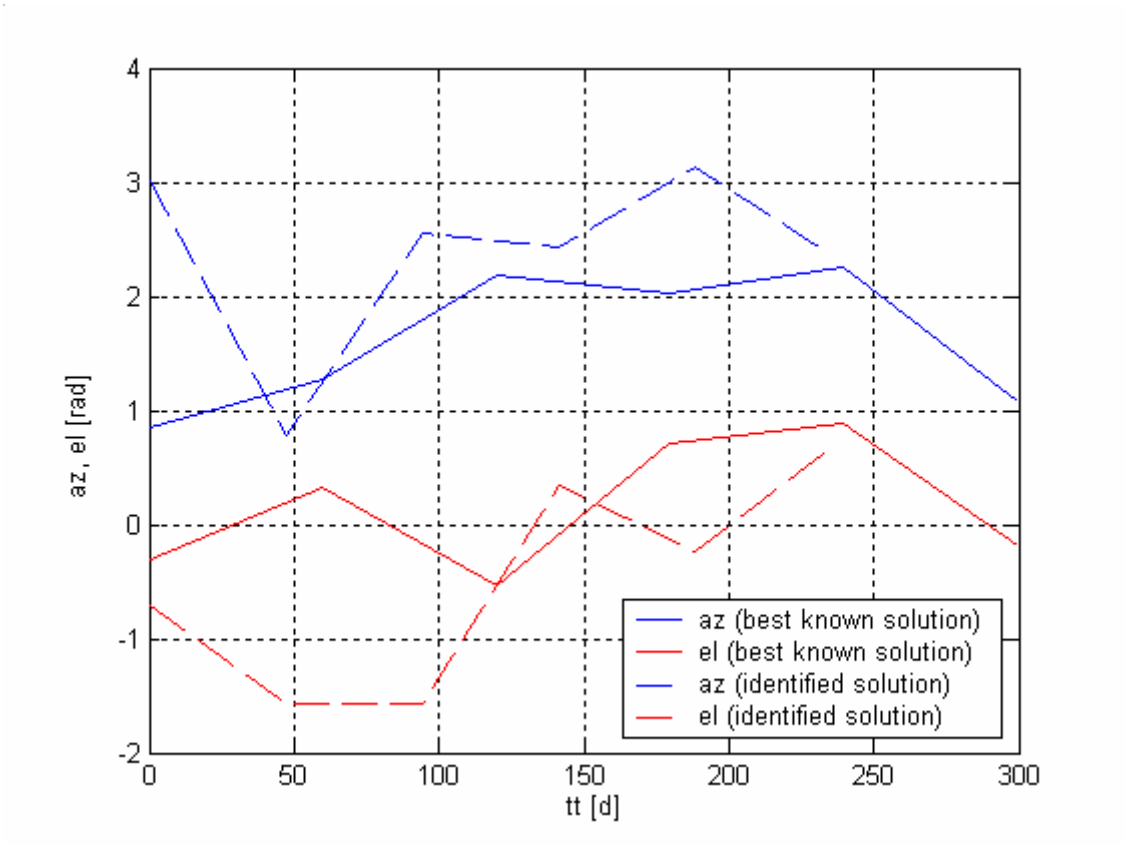

Figure 240: Comparison between the identified solution and the best known solution: thrust azimuth and elevation over the transfer trajectory.

Objective function space		
Term	**Identified solution**	**Best know solution**
$ObjFun$:	352.787	5.750
$R_F / R_{SoI,Mars}$:	23.191	0.002
v_F [*m/s*]:	1166.648	0.086
m_{prop} [*kg*]:	84.241	114.433

Table 161: Comparison between the identified solution and the best known solution: objective function space.

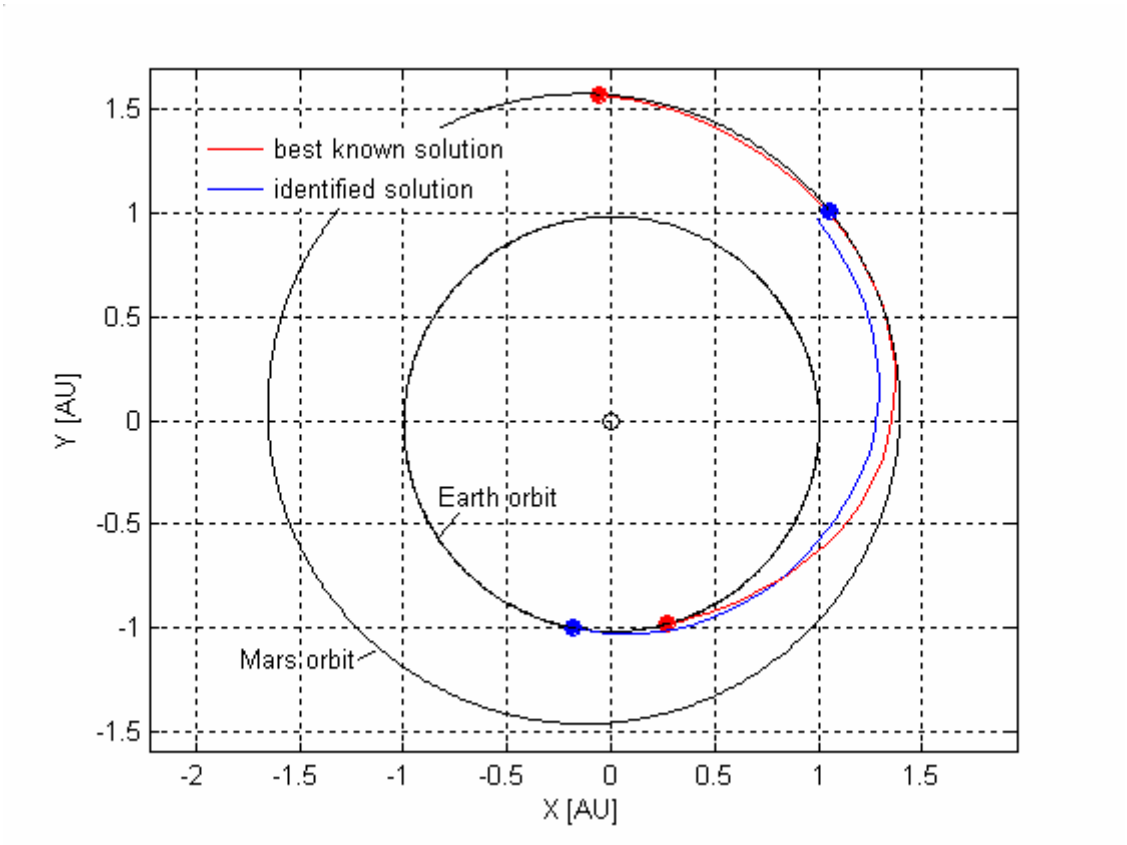

Figure 241: Comparison between the trajectories corresponding to the identified solution and the best known solution.

Table 162 reports the characteristics of the identified solution, which will be used for comparisons with the other optimization algorithms.

Evaluation criterion	Identified solution
ObjFun:	352.787
nFunc.:	1000
Runtime [STU]:	77.754

Table 162: Characteristics of the identified solutions.

A local optimization process by means of a SQP algorithm is now performed, where the solution identified by rbfSolve is considered as the starting point for the local search process. The starting solution and the improved one are

reported in Figure 242 on the *nFunc-ObjFun* plane, while Figure 243 compares the improved solution with the best known one in terms of transfer trajectory.

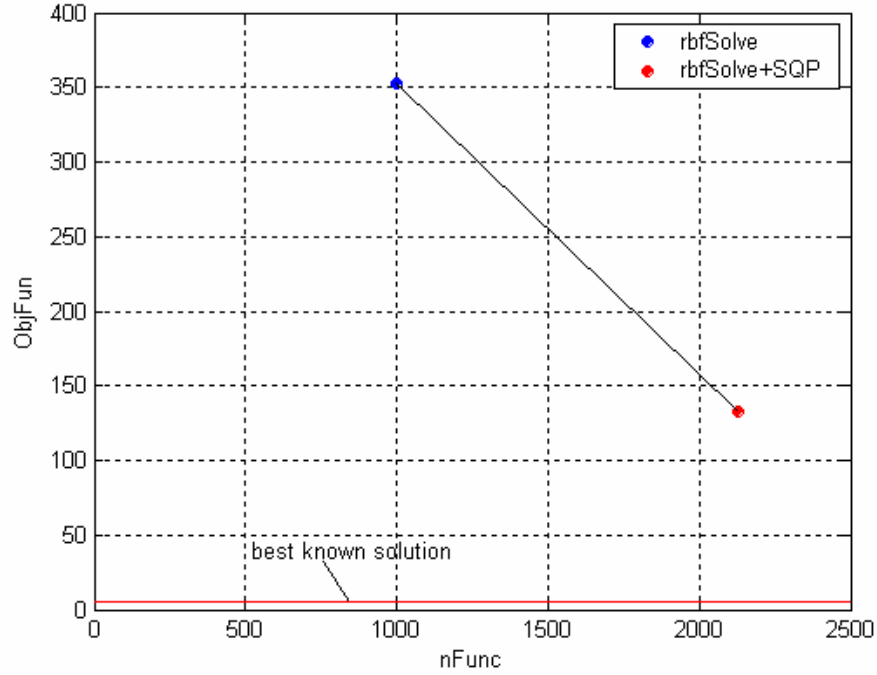

Figure 242: Comparison between solution resulting from *rbfSolve* run and its improvement by means of a further local optimization process via SQP algorithm over the $nFunc - \Delta V$ plane.

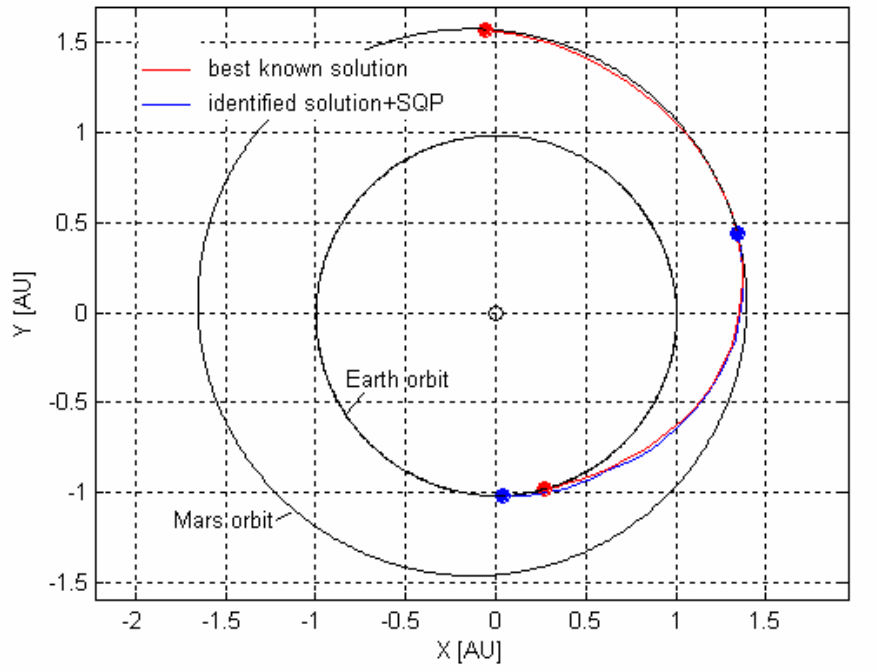

Figure 243: Comparison between solution resulting from rbfSolve+SQP run and the best known solution in terms of transfer trajectory.

The solution is now investigated in the normalized search space. Table 163 reports, corresponding to the rbfSolve+SQP run, the reached objective function value and the distance (in Euclidean metric) with respect to the best known solution.

	ObjFun	Distance
rbfSolve+SQP run	133.213	1.261

Table 163: rbfSolve+SQP optimization run: objective function values and Euclidean distance in the normalized search space with respect to the best known solution.

By considering two solutions as identical when the Euclidean distance is less than 0.040, the run wasn't able to get the best known solution, that is rbfSolve run failed in identifying the basin of attraction of the best known solution. Anyway, it is interesting to analyse the feature of the identified solution, which is in fact quite different from the previously reported ones. Table 164, Table 165 and Figure 244 report the identified solution compared with the best known solution in terms of the values of the design variables and of the objective function terms.

Search space		
Design variable	**Identified solution + SQP**	**Best know solution**
Date of departure [*d*]:	539.724	553.253
Transfer time [*d*]:	178.174	299.462
Thrust level [*N*]:	0.168	0.130
Escape velocity from Earth [*m/s*]:	2637.871	2676.327

Table 164: Comparison between the solution resulting from rbfSolve+SQP run and the best known solution: search space.

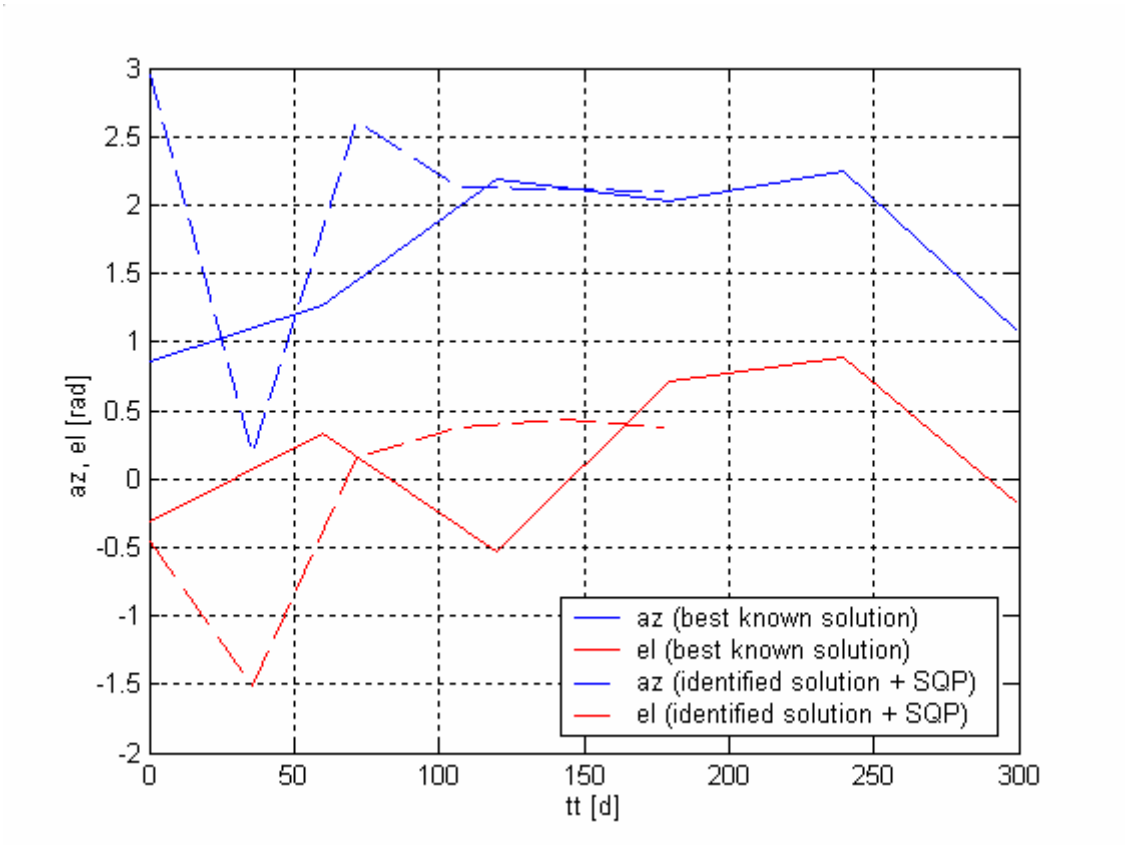

Figure 244: Comparison between the solution resulting from rbfSolve+SQP run and the best known solution: thrust azimuth and elevation over the transfer trajectory.

Objective function space		
Term	**Identified solution + SQP**	**Best know solution**
$ObjFun$:	133.212	5.750
$R_F / R_{SoI,Mars}$:	0.014	0.002
v_F [*m/s*]:	1286.746	0.086
m_{prop} [*kg*]:	87.878	114.433

Table 165: Comparison between the solution resulting from rbfSolve+SQP run and the best known solution: objective function space.

The local minimum corresponding to the basin of attraction identified by rbfSolve corresponds to an interplanetary transfer with considerable lower transfer time and propellant consumption for the electric engine. However, a final relative velocity of 1286.746 *m/s* characterizes the arrival at Mars, which

might force the further use of chemical propulsion system, making hybrid the resulting propulsion system.

Summary of results:

Table 166 reports the summary of results for the low-thrust direct planet-to-planet transfer problem in a tabular form.

Algorithm	Objective function	Fun. evaluations	Runtime [STU]
GAOT	269.198 (σ = 71.416)	14919.3 (σ = 5121.398)	3.564 (σ = 1.564)
GAOT-shared	343.238 (σ = 49.457)	3109.5 (σ = 1099.448)	0.621 (σ = 0.217)
GATBX	172.559 (σ = 92.517)	30036 (σ = 15485)	7.105 (σ = 4.068)
GATBX-migr	153.807 (σ = 87.043)	48436 (σ = 21584)	9.511 (σ = 4.140)
FEP	157.191 (σ = 76.266)	89013.9 (σ = 68704.199)	14.996 (σ = 9.551)
DE	310.233 (σ = 66.478)	2625 (σ = 1081.359)	0.437 (σ = 0.177)
ASA	176.977 (σ = 102.31)	78783.8 (σ = 35239)	12.985 (σ = 5.856)
glbSolve	158.571	29003	5.477
MCS	319.497	19183	2.960
RbfSolve	352.787	1000	77.754
EPIC*	10.24 (σ = 11.33)	80799 (σ = 16952)	-

Table 166: Summary of results for the low-thrust direct planet-to-planet transfer problem transfer problem (* courtesy of Dr. Massimilano Vasile).

Note that Table 166 also reports the performances of EPIC algorithm, which have been supplied by Dr. Massimiliano Vasile. Unfortunately, the analysis of EPIC results on the search space couldn't be accomplished and the runtime performances were not available. Due to the partially conflicting performance

criteria considered in this work and by proceeding in analogy with the 2-impulse direct planet-to-planet and multiple gravity assist transfer problem analysis, concepts and techniques typically adopted in multiobjective optimization problems (such as the concept of the Pareto dominance) are here used in order to assess the optimization algorithms performances. Due to the presence of not optimized codes among the tested ones and to the necessity of creating a MEX file for ASA algorithm, the main evaluation criteria to be considered have been taken as the objective function value reached, *objFun*, and the number of model function evaluations needed, *nFunc*. Figure 245 reports such performances in a *objFun* - *nFunc* plane in order to identify the Pareto optimal solutions.

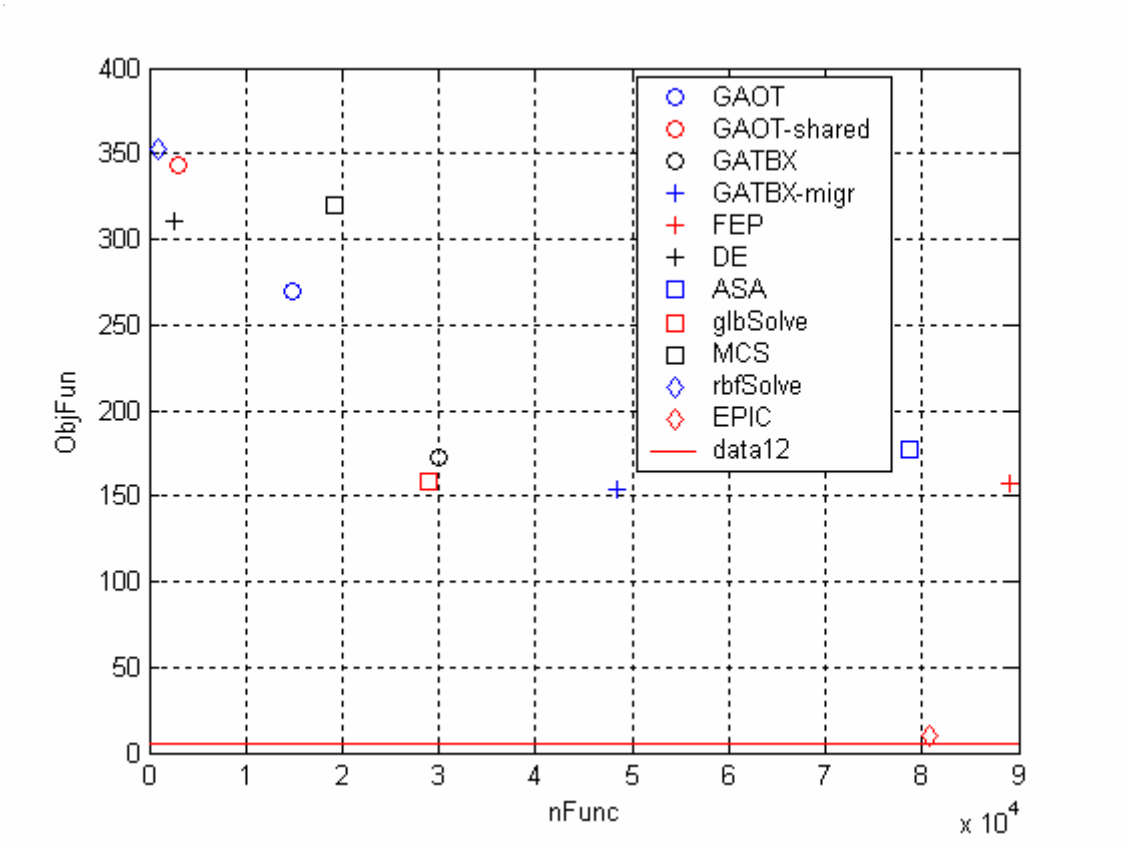

Figure 245: Algorithms performances in the *objFun- nFunc* plane.

Note that Figure 245 reports the performances listed in Table 166, which contains statistical performances in case of randomized optimization algorithms. By applying the concepts of Pareto dominance, Table 167 reports for each algorithm, the number of algorithms which dominated, and then outperformed it.

Algorithm	# of dominating algorithms
GAOT	0
GAOT-shared	1
GATBX	1
GATBX-migr	0
FEP	2
DE	0
ASA	3
GlbSolve	0
MCS	2
RbfSolve	0
EPIC	0

Table 167: Number of dominating algorithms.

Table 167 shows that the set of Pareto optimal solutions includes six solutions: the algorithms which best solved the low-thrust direct planet-to-planet transfer problem in a Pareto optimal sense are GAOT, GATBX-migr, DE, glbSolve, rbfSolve and EPIC. Their performances are shown in Figure 246

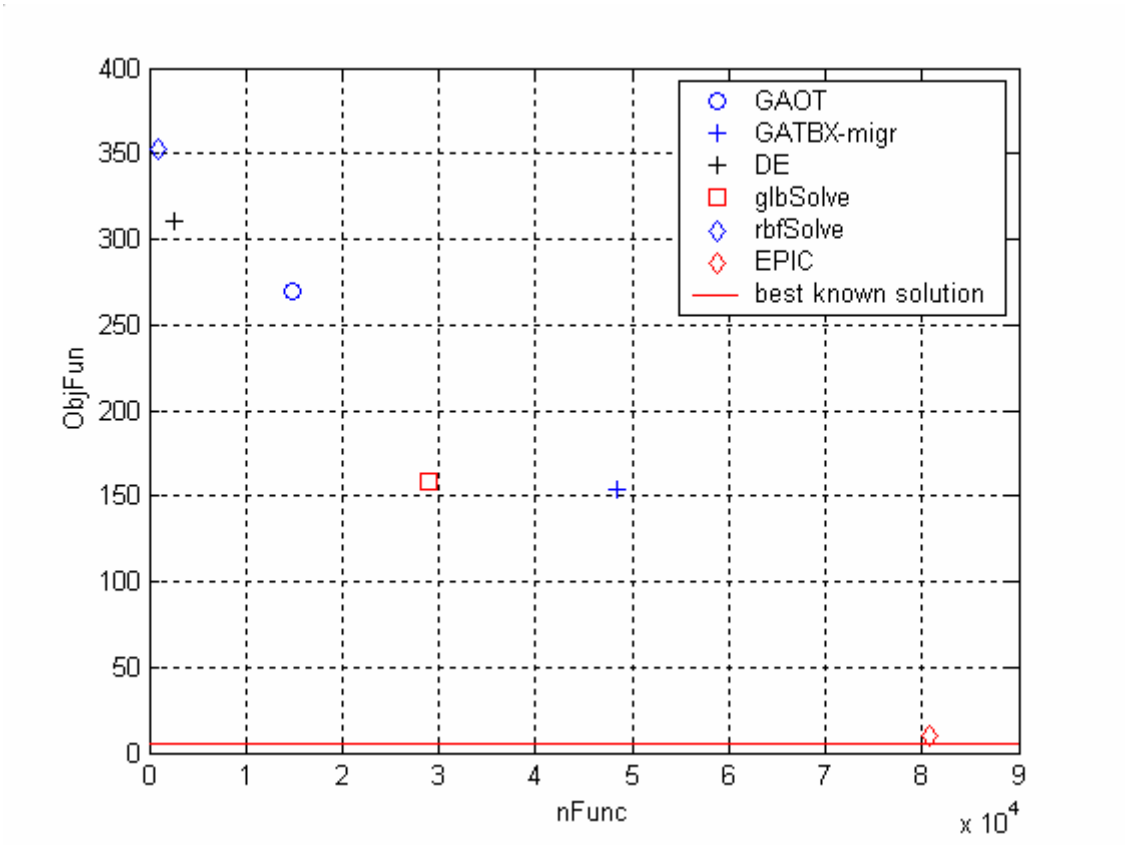

Figure 246: Pareto optimal algorithms.

For the sake of completeness, let consider now the runtime performances. We have now three performance criteria. Figure 247 and Figure 248 report the algorithms performances in the *objFun* **-** *nFunc* plane and in the *nFunc* **-** *runtime* plane respectively, which have not been considered so far. Note that EPIC performances couldn't be reported in the following analysis, due to the lack on required runtime information.

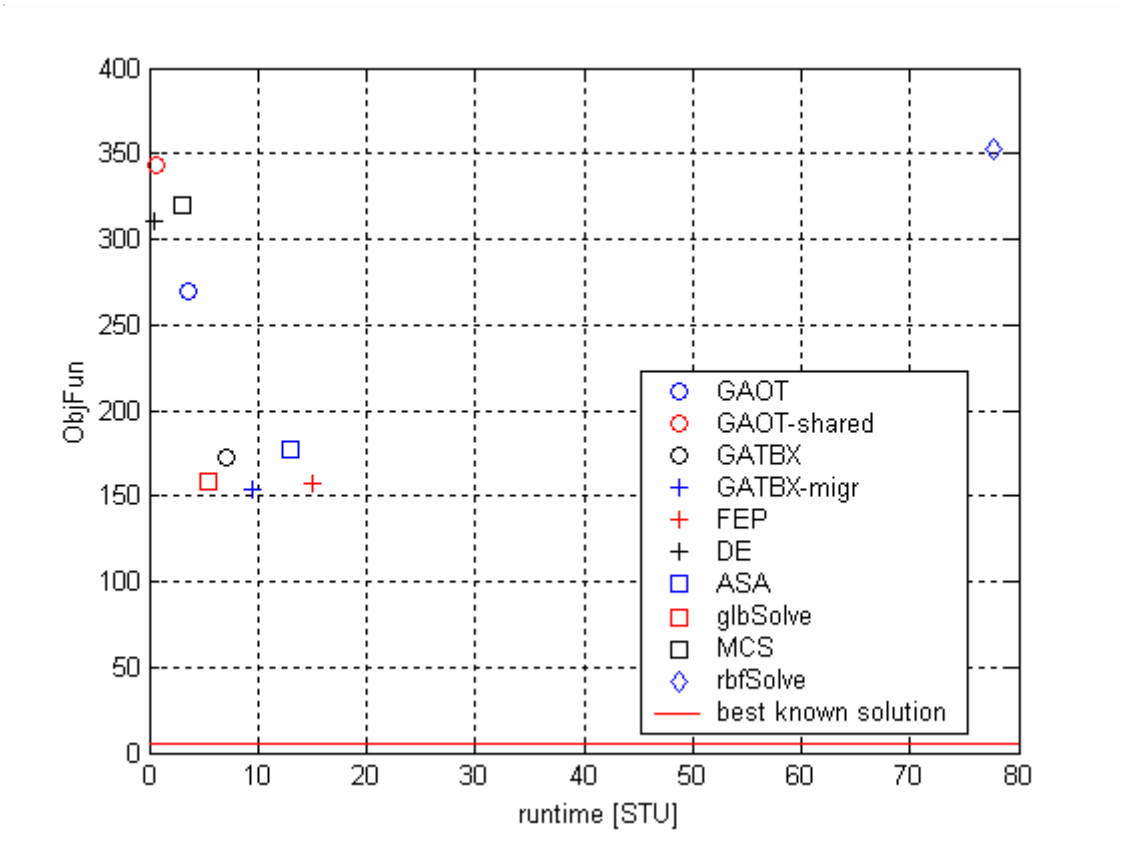

Figure 247: Algorithms performances in the *objFun* - *runtime* plane.

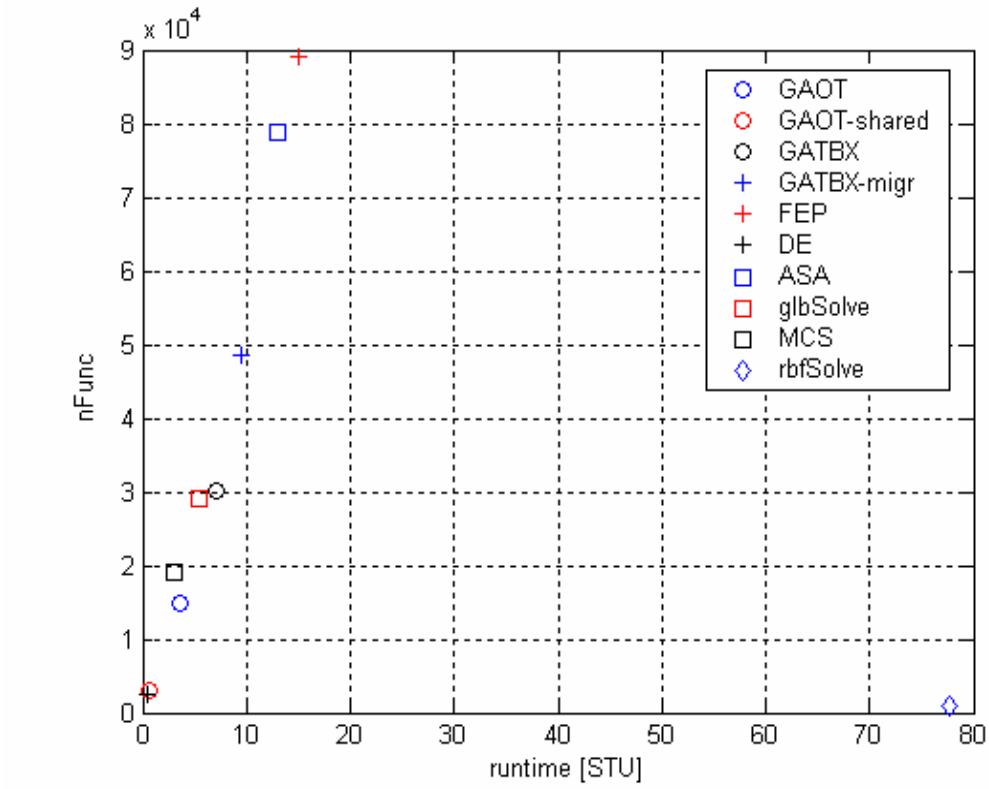

Figure 248: Algorithms performances in the *nFunc* - *runtime* plane.

By applying again the concepts of Pareto dominance in this three-criteria case, Table 168 reports for each algorithm, the number of algorithms which dominated it.

Algorithm	# of dominating algorithms
GAOT	0
GAOT-shared	1
GATBX	1
GATBX-migr	0
FEP	1
DE	0
ASA	3
glbSolve	0
MCS	1
rbfSolve	0

Table 168: Number of dominating algorithms in the three criteria case.

Table 168 shows that no changes in the Pareto optimal set members occurred in analysing the three criteria case. Finally the performance of all algorithms in identifying the basin of attraction of good solution are analysed, as resulting from the local optimization processes performed at the end of each algorithm run. Indeed, as stated above, only FEP algorithm were able to get the basin of attraction of the best known solution; however other algorithms succeeded in reaching basin of attraction of good solutions, which are in fact comparable with the best known one in terms of objective function values. As a consequence, such successful runs are considered as representative of good algorithm performances and are included in Table 169 (note that for randomized algorithms the number of successful runs over the total number of performed runs is reported).

Algorithm	Success
GAOT	0/10
GAOT-shared	0/10
GATBX	2/10
GATBX-migr	2/10
FEP	2/10
DE	3/10
ASA	2/10
glbSolve	No
MCS	No
rbfSolve	No

Table 169: Algorithms performance in identifying the basin of attraction of good solutions.

Table 169 shows that DE algorithms turned out to have the highest rate of success at reaching the basin of attraction of good solutions in case of low-thrust direct planet-to-planet interplanetary transfers problem. This is a quite interesting result: as shown in Figure 245, DE resulted in quite high mean objective function values; however, the global search performed by means of differential evolution seemed to be effective at finding good basin of attraction. Anyway, it is worth noting that little differences in rate of success with respect to GATBX, GATBX-migr, FEP and ASA exist. Moreover, an impressive consideration can be highlighted: all algorithms resulted in very low rate of success. Actually, we must consider that information about the success rate of EPIC couldn't be included in the previous table, because of not availability to the authors. Nevertheless, by looking at the mean objective function value obtained by EPIC (10.24) and by considering the objective function value corresponding to the best known solution (5.75), it is likely the case that most EPIC runs could reach the basin of attraction of good solutions, which are comparable in fact with the best known one. As a consequence, in order to identify the best performing algorithm in case of low-thrust direct planet-to-

planet transfer problem, by combining information coming up from Pareto optimality analysis carried out on the *obj – nFunc* two criteria case and rate of success investigation, whose results are reported inTable 169, we can state that:

- GAOT and GAOT-shared tools, as well as the non randomized algorithms glbSolve, MCS and rbfSolve are not suitable for global optimization of low-thrust direct planet-to-planet transfer problems using the mathematical models here employed.

- Among the remaining tools, DE, GATBX-migr and EPIC showed good performances in a Pareto optimal sense: in particular, DE and GATBX-migr resulted in similar, even if low, rate of success; however, by considering that the rate of success is evaluated by performing local optimization processes requiring similar further objective function evaluations and by noting that DE meanly required considerable fewer objective function evaluations for performing the global search, DE tool seems to be preferable with respect to GATBX-migr; as a consequence DE and EPIC seem to be the most promising tools.

- As stated above, no information are available about the rate of success of EPIC. However the impressive results of the global search in terms of mean objective function value reached seem to be indicative of performances particularly high even in this sense, especially if compared with the scarce results of the other tools. As a consequence, in spite of a higher mean number of objective function evaluations required to perform the global search, the authors believe that EPIC should be considered as the best performing algorithm for solving the low-thrust direct planet-to-planet transfer problem using the mathematical models here applied.

10. LUNAR WEAK STABILITY BOUNDARY TRANSFER

Problem class statement:

Objective function assessment	
Objective function:	$\Delta V = \Delta V_1 + \Delta V_2$ where: • ΔV_1 is the impulsive manoeuvre required to put the spacecraft in the Lambert's three-body arc starting from the initial circular orbit around the Earth • ΔV_2 is the impulsive manoeuvre necessary to inject the spacecraft on the capture trajectory W_{L1}^{S}
Mathematical models:	• Restricted three-body dynamical model • Two dimensional motion (synodic dimensionless reference frame) • Combination of invariant manifolds and Lambert's three-body arcs • Impulsive manoeuvres (i.e. instantaneous variations in velocity) for linking the three-body arcs

Search space characterization	
Number of design variables:	3
Design Variables:	• Angle identifying the starting point

	over the initial circular orbit (θ) • Time of the backward propagation of the stable manifold W_{L1}^{S} from the libration point *L1*, whose final point identify the target of the Lambert's three-body arc (t_W) • Transfer time corresponding to the Lambert's three-body arc from the initial circular orbit to the target point on the stable manifold W_{L1}^{S} previously identified (t_L)
Topology:	Continuous variables
Constraints	
Constraints typology:	Box constraints
Box intervals:	• $\left[\theta^{LB},\theta^{UB}\right]=\left[0,360\right]deg$ • $\left[t_L^{LB},t_L^{UB}\right]=\left[0.1,3\right]$ *d* • $\left[t_W^{LB},t_W^{UB}\right]=\left[5,150\right]$ *d*
General considerations	
Objective function analysis:	Discontinuous on the boundaries of a finite set of regions over the search space; C^2 in the remaining points.
Problem complexity:	High

Number of global optima: A priori unknown.

A systematic analysis of the objective function over the search space, followed by local optimization processes starting from 100 random first guess solutions uniformly distributed over the search space (each local search requiring a number of objective function evaluations of the order of $0.5 \cdot 10^2$) led to the following best known solution, that seems to be the global one over the considered search space (although no rigorous mathematical demonstration has been provided).

Search space	
θ :	70.835 *deg*
t_L :	1.273 *d*
t_W :	107.670 *d*
Objective space	
ΔV :	3080.767 *m/s*
ΔV_1 :	3080.756 *m/s*
ΔV_2 :	0.011 *m/s*

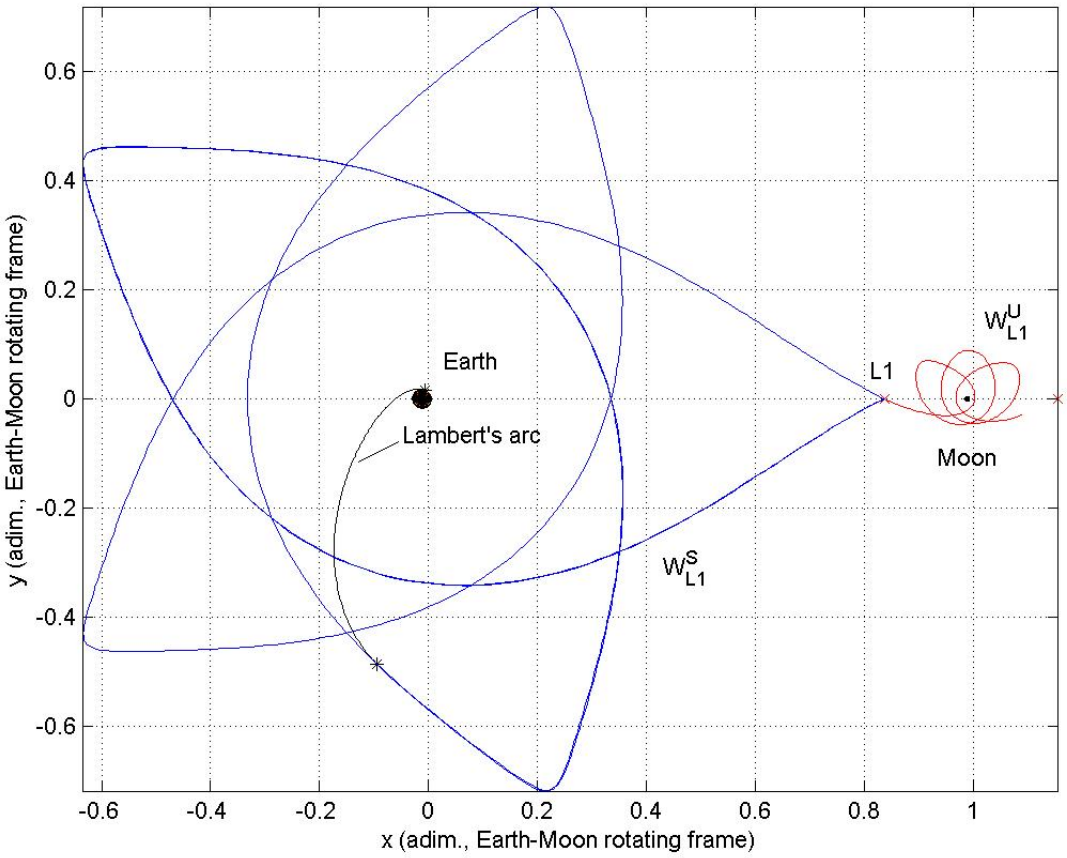

Figure 249: Best known solution: trajectory representation in the dimensionless Earth-Moon rotating frame.

Number of local optima: A priori unknown.

Hardware platform:

Two platforms have been used, whose main hardware features are reported in the following table.

Platform number	Hardware features
Platform 1:	Intel Pentium 4 – 3.06GHz laptop
Platform 2:	AMD Athlon™ XP 2600 desktop

Operating system:

Two different operating systems correspond to the two used platforms, whose main data are reported in the following table.

Platform number	Hardware features
Platform 1:	Microsoft Windows XP Home edition Version 2002 Service Pack 1
Platform 2:	Microsoft Windows 2000 Professional edition 5.00.2195 Service Pack 4

Timings:

The Standard Unit Time (see Dixon & Szegö, 1978) has been measured.

Performances:

In the following, the performances of each global optimization tool in solving the problem of Lunar transfers using libration points are reported. The evaluation criteria will be mainly based on the analysis of the optimal solution reached and the number of the required model function evaluations. Due to the presence of not optimized codes among the tested ones, timing will not be considered as a main evaluation criterion.

GAOT

As GAOT implements a genetic algorithm, we report the statistical characteristic, typically considered in case of randomized solution methods. Ten run have been processed in order to solve the previously defined problem. Default options suggested by the providers of the code have been used in all the runs: note that by tuning the algorithm parameters one may improve the performance of the solvers, but, due to the comparative purposes of this work,

the tuning effects have not been considered. As the model used for designing Lunar transfers using libration points has high complexity features and a low number of design variables, we used 50 individuals evolving for a maximum number of generations equal to 1000.

Algorithm parameters	
Number of individuals:	50
Maximum number of generations:	1000

Table 170 and Table 171 report the best identified solution compared with the best known solution (note that the best solution is here measured by considering the minimum objective function value reached and is different from the Pareto optimal solution described below).

Search space		
Design variable	**Best identified solution**	**Best known solution**
θ [*deg*]:	286.417	70.835
t_L [*d*]:	1.275	1.273
t_W [*d*]:	26.226	107.670

Table 170: Comparison between the best identified solution and the best known solution: search space.

Objective function space		
Term	**Best identified solution**	**Best known solution**
ΔV [*m/s*]:	3082.940	3080.767
ΔV_I [*m/s*]:	3080.914	3080.756
ΔV_F [*m/s*]:	2.026	0.011

Table 171:Comparison between the best identified solution and the best known solution: objective function space.

The previous tables show that the, although the two solutions are in fact comparable in terms of the objective function value, they seem to identify quite different solutions in the search space. Such a consideration is confirmed by the trajectory representation (see Figure): the best solution identified by GAOT belong to a different family of solutions which is comparable to the best known one in terms of objective function value, but are characterized by a considerable lower transfer time to L1 (27.501 *d* instead of 108.943 *d* corresponding to the best known solution).

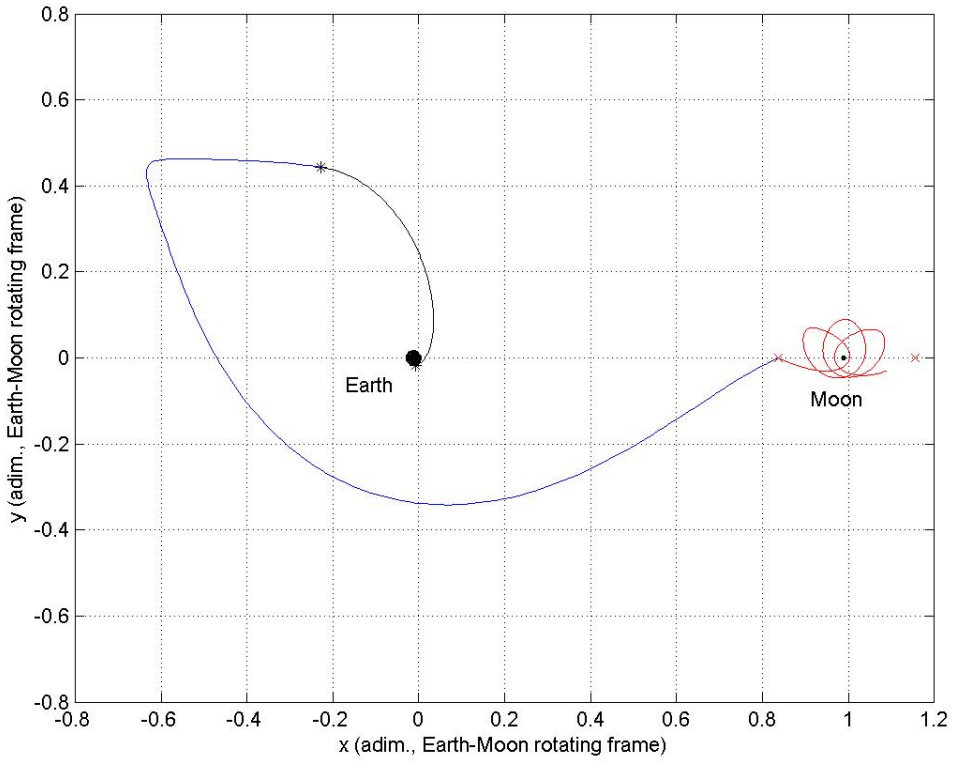

Figure 250: Best identified solution: trajectory representation.

By revising the objective function structure analysis of the problem of lunar transfer using libration points, the best solution identified by GAOT can be clearly related to the family of solutions corresponding to subgroup 2, which is not the best identified one (subgroup 8). Let us now consider the statistical characteristics of the identified solution set. Table 12 reports the mean value and the standard deviation of the performances which will be used for comparisons with the other optimization algorithms.

Evaluation criterion	Mean value	Standard deviation
ΔV [*m/s*]:	3292.300	194.112
Model function evaluations:	2089.3	1592.775
Runtime [STU]:	8.327	6.252

Table 172: Statistical characteristics of the identified solutions.

Table 172 shows that the mean value of the optimal objective function values reached at the end of each optimization process is quite different from the best identified one and is characterized by a high standard deviation. Such a result let us suppose that no all the performed optimization processes have been able to identify the basin of attraction of the same solution. Figure 251 reports the final solutions corresponding to each optimization run in the *nFunc-ΔV* plane (where *nFunc* is the number of objective function evaluations), while Figure 252 illustrates their distribution over the search space (the best identified solution is highlighted by a green dot) compared with the best known solution (red dot).

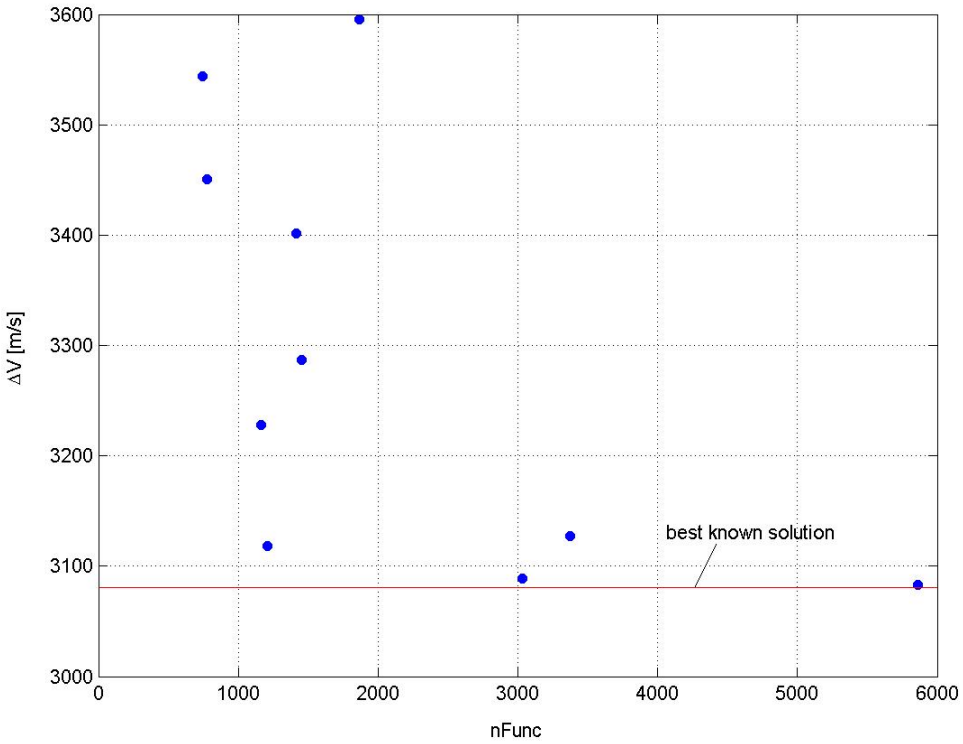

Figure 251: Distribution of the final solutions corresponding to each optimization run on the *nFunc-ΔV* plane.

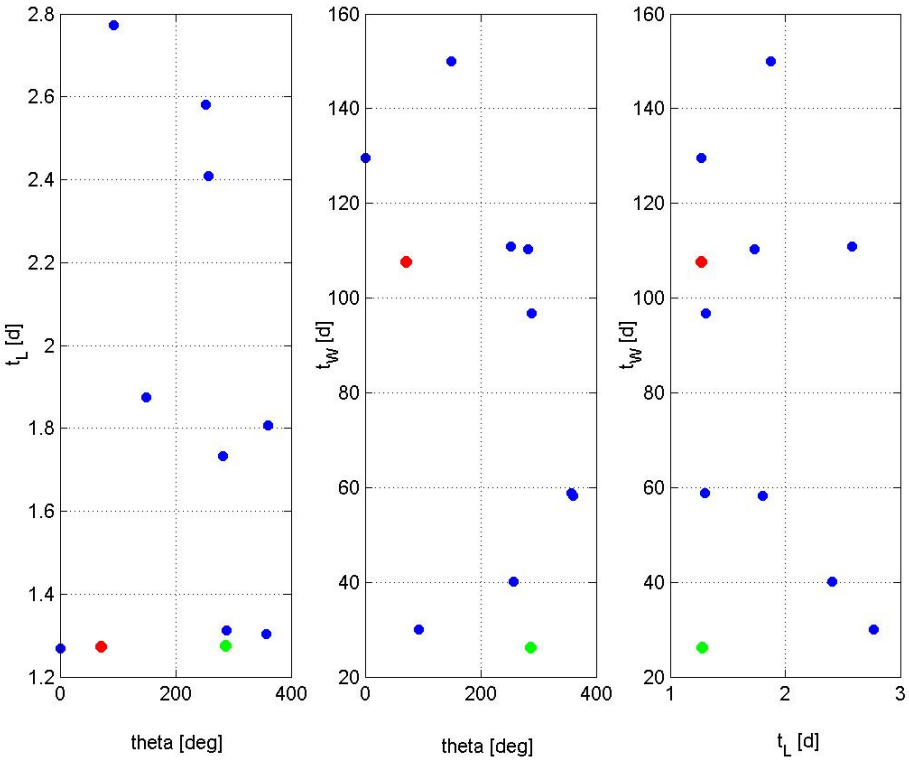

Figure 252: Distribution of the final solutions corresponding to each optimization run on the search space.

Figure 251 and Figure 252 fairly illustrates that the presence of comparable local minima which has been highlighted in the analysis of the objective function structure, hindered the effectiveness of GAOT algorithm at reaching the basin of attraction of the best known solution. In particular, the figures seem to confirm that no GAOT solution was able to get the basin of attraction of the best known solution. In order to better analyse such a matter, the ten identified solutions have been used as starting points for ten local optimization processes performed by means of a SQP algorithm. Figure 253 reports the improved solutions over the *nFunc-ΔV* plane.

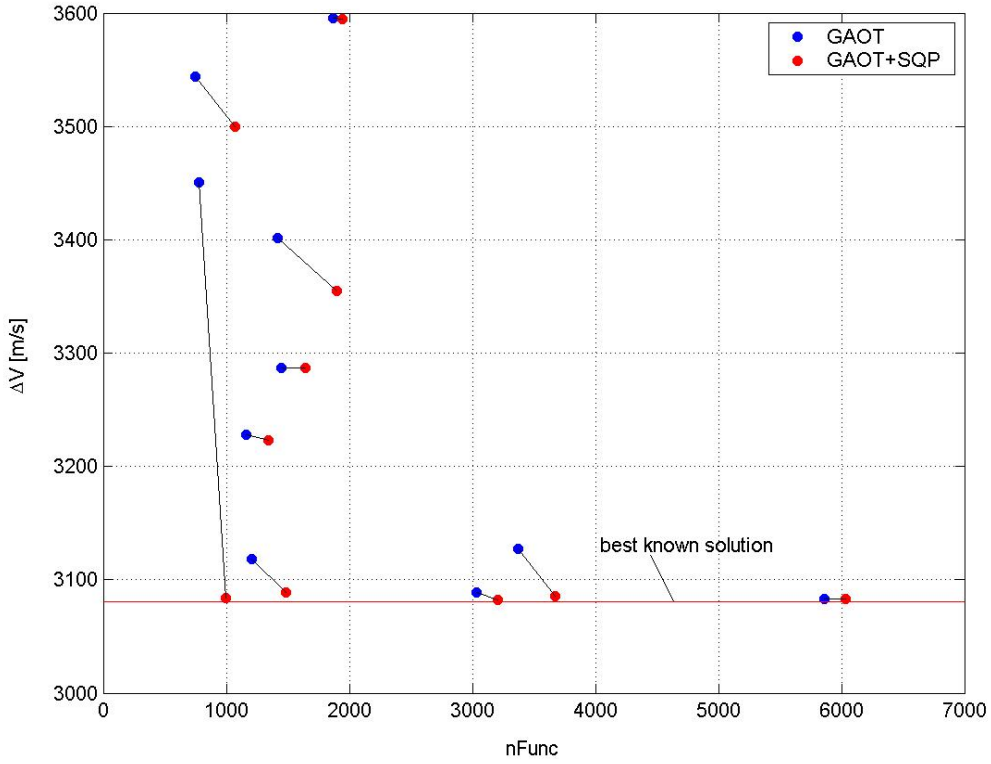

Figure 253: Distribution of the improved solutions at the end of a local optimization process on the *nFunc-ΔV* plane.

By investigating the improved solutions in the normalized search space, Table 173 reports, corresponding to each GAOT+SQP run, the reached objective function value and the distance (in Euclidean metric) with respect to the best known solution.

	ΔV [*m/s*]	Distance
run 1	3286.695	0.799
run 2	3355.121	0.770
run 3	3499.922	0.618
run 4	3088.938	0.248
run 5	3223.252	0.676
run 6	3083.992	0.869
run 7	3082.174	0.865
run 8	3085.618	0.607
run 9	3082.795	0.821
run 10	3595.060	0.418

Table 173: GAOT+SQP optimization runs: objective function values and Euclidean distance in the normalized search space with respect to the best known solution.

An empirical analysis suggest to define two solutions as identical when the Euclidean distance is less than 1% of the hyper diagonal of the normalized search space, that is 0.017 in a 3-dimensional space. As a consequence, the previous analysis confirms that 0/10 GAOT runs were able to identify the basin of attraction of the best known solution. However, it should be noted that the 5/10 runs could reach the basin of attraction of local minima comparable to the best known one. A careful analysis showed that such comparable local minima are in fact related to a subset of the ten transfer families identified in the objective function structure analysis; in particular, no one corresponds in fact to the best identified one (subgroup 8). Let us now analyse the main features of the final population: to do that, the final population corresponding to the best identified solution is investigated. Figure 254 shows the distribution of the population over the search space at the end of the optimization process.

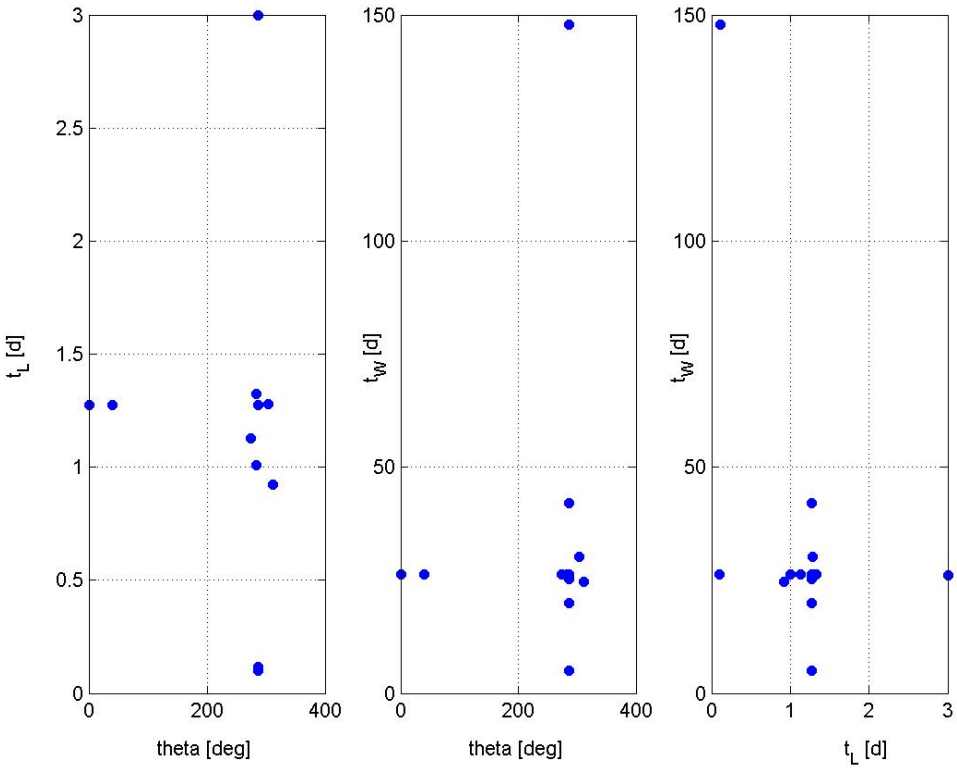

Figure 254: Distribution of the population over the search space at the end of the optimization process corresponding to the best identified solution.

The previous figures show that the individuals in the final population are widely distributed over the search space. Figure 255 reports the objective function values corresponding to each individual.

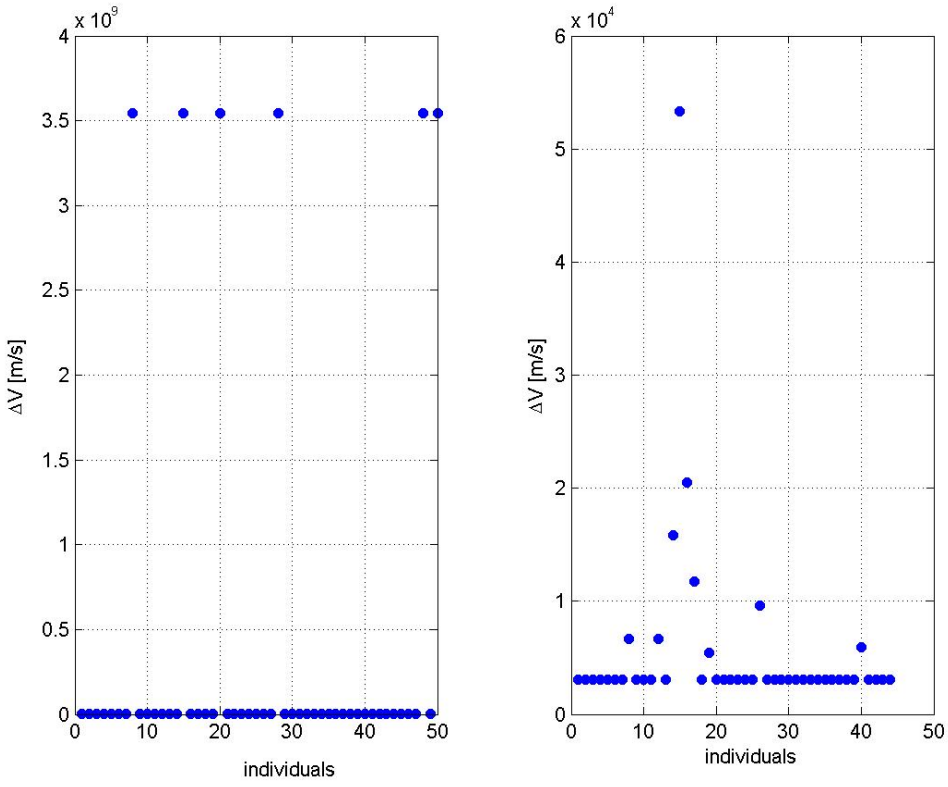

Figure 255: Objective function values of individuals in the final population corresponding to the best identified solution.

Figure 255 shows that some individuals in the final population corresponds to region of the search space where the algorithm for Lambert's three-body problem solution couldn't converge to an admissible solution. A careful analysis of the search space shows that other individuals are quite concentrated around the best identified solution: indeed, the final population of GAOT algorithm concentrates around a unique optimum solution, without keeping information of other local optima solutions; the wide distribution of the highlighted in Figure 255 corresponds in fact to the effects of the crossover and mutation operators.

GAOT-shared

As GAOT-shared implements a genetic algorithm including a niching technique, we report again the statistical characteristics. Ten runs have been processed in order to solve the previously defined problem. Default options suggested by the providers of the code have been used in all the runs. The threshold of

dissimilarity, σ_S, for the sharing method and the shape parameter of the sharing function, α, have been set respectively to:

$$\sigma_S = 0.1 \qquad \text{and} \qquad \alpha = 1$$

We used again a population of 50 individuals, evolving for a maximum number of generations equal to 100.

Algorithm parameters	
Number of individuals:	50
Maximum number of generations:	100

Table 174 and Table 175 report the best identified solution compared with the best known solution.

Search space		
Design variable	**Best identified solution**	**Best known solution**
θ [*deg*]:	355.901	70.835
t_L [*d*]:	1.313	1.273
t_W [*d*]:	129.706	107.670

Table 174: Comparison between the best identified solution and the best known solution: search space.

Objective function space		
Term	**Best identified solution**	**Best known solution**
ΔV [*m/s*]:	3337.437	3080.767
ΔV_I [*m/s*]:	3102.607	3080.756
ΔV_F [*m/s*]:	234.830	0.011

Table 175: Comparison between the best identified solution and the best known solution: objective function space.

The previous tables show that the two solutions identify in fact quite different Lunar transfer in the search space. Such a consideration is confirmed by the trajectory representation (see Figure 256): the best solution identified by GAOT-shared belong to a different family of solutions.

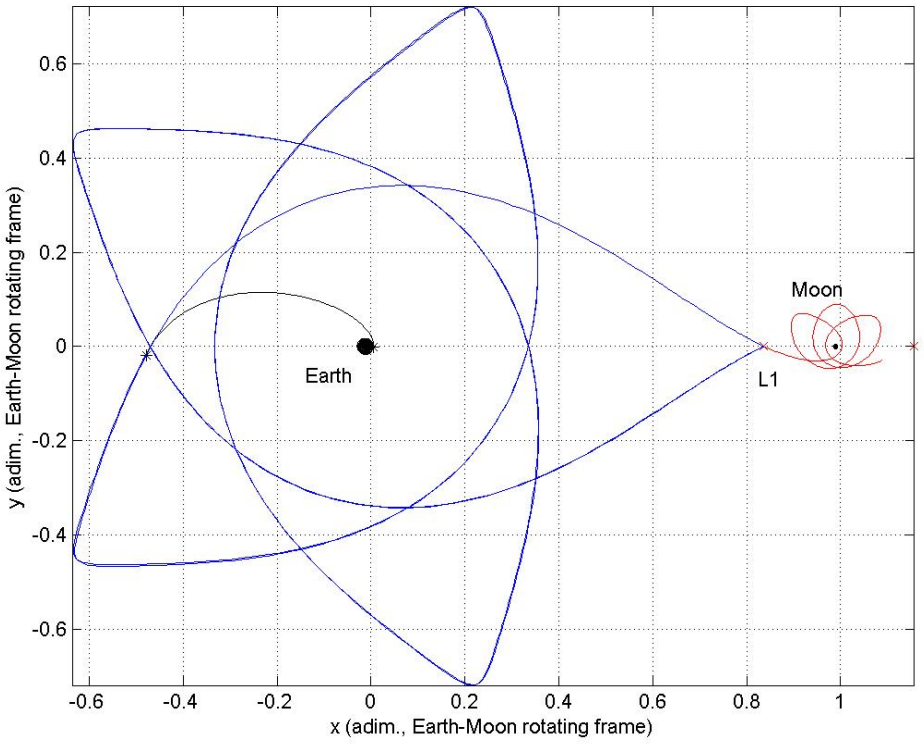

Figure 256: Best identified solution: trajectory representation.

By revising again the objective function structure analysis of the problem of lunar transfer using libration points, the best solution identified by GAOT-shared can be related to the family of solutions corresponding to subgroup 10, which is different from the best identified one (subgroup 8). Let now consider the statistical characteristics of the identified solution set. Table 176 reports the mean value and the standard deviation of the performances which will be used for comparisons with the other optimization algorithms.

Evaluation criterion	Mean value	Standard deviation
ΔV [*m/s*]:	3597.104	216.418
Model function evaluations:	606.2	151.610
Runtime [STU]:	1.836	0.545

Table 176: Statistical characteristics of the identified solutions.

Table 176 shows that the mean value of the optimal objective function values reached at the end of each optimization process is quite different from the best identified. Such a result let us suppose that no all the performed optimization processes have been able to identify the basin of attraction of the same solution. Figure 257 reports the final solutions corresponding to each optimization run in the *nFunc-ΔV* plane, while Figure 258 illustrates their distribution over the search space (the best identified solution is highlighted by a green dot) compared with the best known solution (red dot).

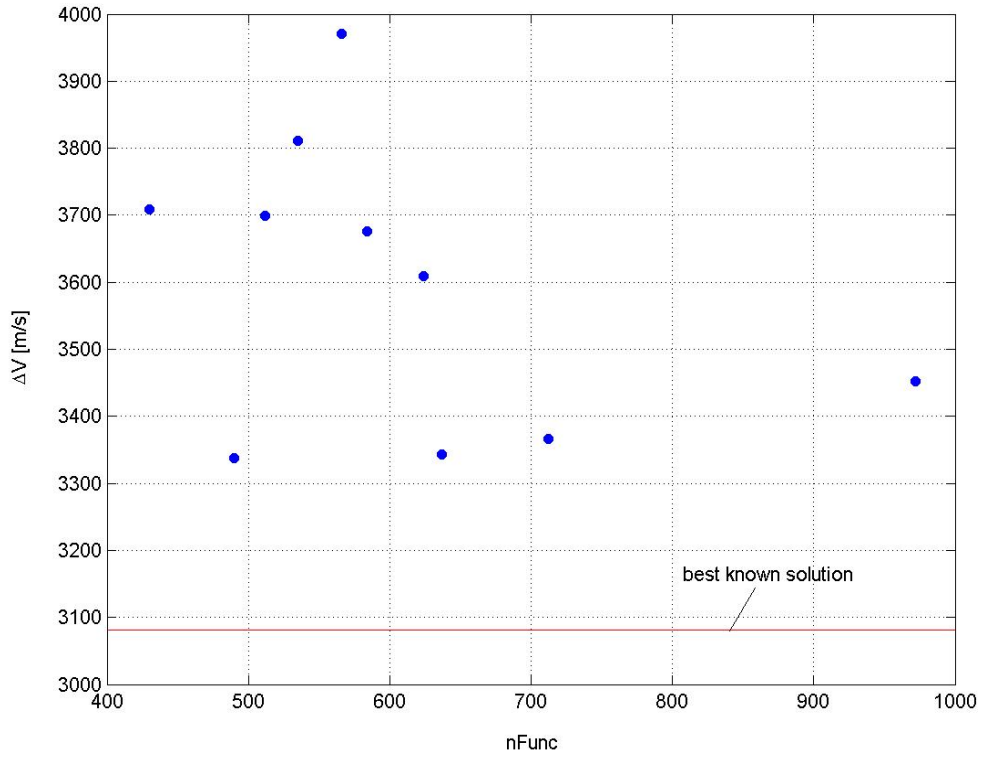

Figure 257: Distribution of the final solutions corresponding to each optimization run on the *nFunc-ΔV* plane.

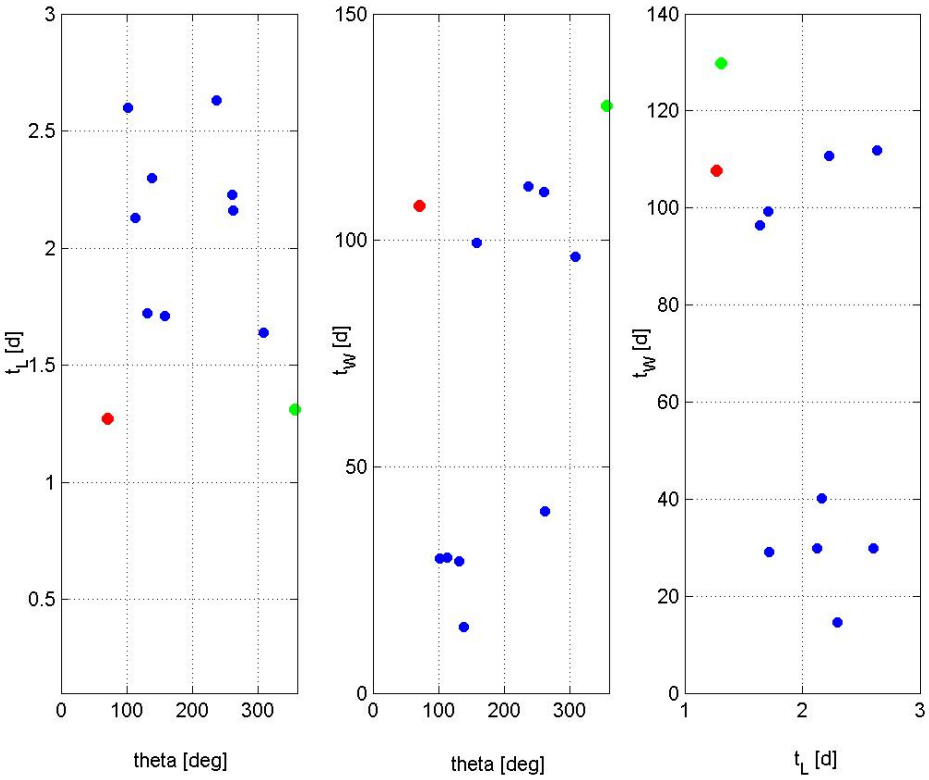

Figure 258: Distribution of the final solutions corresponding to each optimization run on the search space.

Figure 257 and Figure 258 show that no GAOT-shared runs were able to reach the best known solution. Then, ten local optimization processes have been performed by means of a SQP algorithm, using the identified solutions as starting points in order to confirm this result. Figure 259 reports the improved solutions over the *nFunc-ΔV* plane.

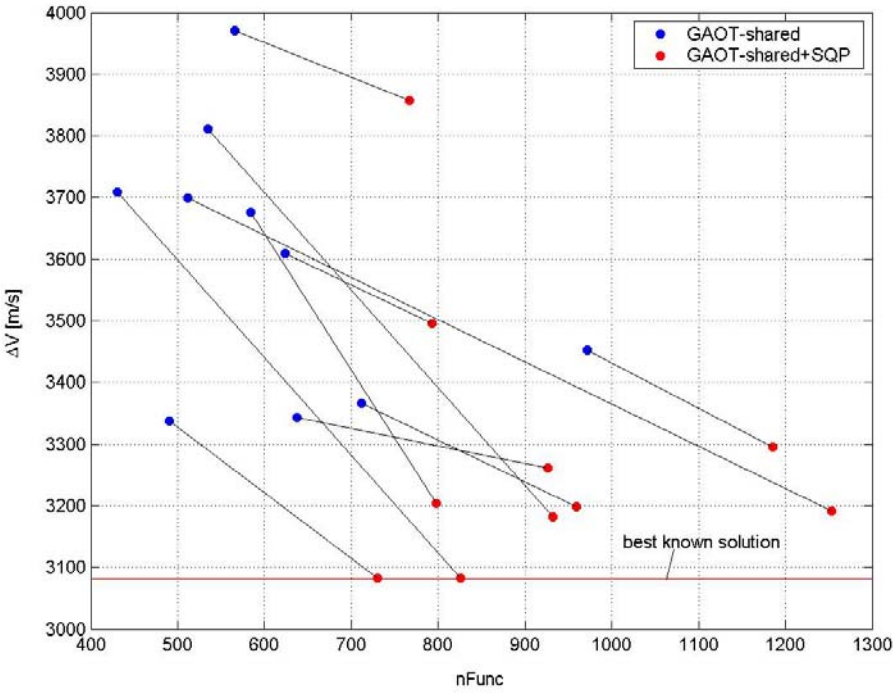

Figure 259: Distribution of the improved solutions at the end of a local optimization process on the *nFunc-ΔV* plane.

By investigating the improved solutions in the normalized search space. Table 177 reports, corresponding to each GAOT-shared+SQP run, the reached objective function value and the distance (in Euclidean metric) with respect to the best known solution.

	ΔV [*m/s*]	Distance
Run 1	3083.167	0.811
Run 2	3182.232	0.665
Run 3	3191.104	0.723
Run 4	3496.193	0.589
Run 5	3857.829	0.290
Run 6	3204.485	0.674
Run 7	3261.598	0.655
Run 8	3083.079	0.606
Run 9	3294.944	0.789
run 10	3198.760	0.726

Table 177: GAOT-shared+SQP optimization runs: objective function values and Euclidean distance in the normalized search space with respect to the best known solution.

By considering two solutions as identical when the Euclidean distance is less than 1% of the hyper diagonal of the normalized search space, that is 0.017 in a 3-dimensional space, the previous analysis confirms that 0/10 GAOT-shared runs were able to identify the basin of attraction of the best known solution. Anyway, 2/10 runs could reach the basin of attraction of local minima comparable to the best known one (runs 1 and 8). Such comparable local minima are in fact both related to the transfer family identified in the objective function structure analysis corresponding to subgroup 10, which is not the best identified one. Let us now analyse the main features of the final population: to do that, the final population corresponding to the best identified solution is investigated. Figure 260 shows the distribution of the population over the search space at the end of the optimization process.

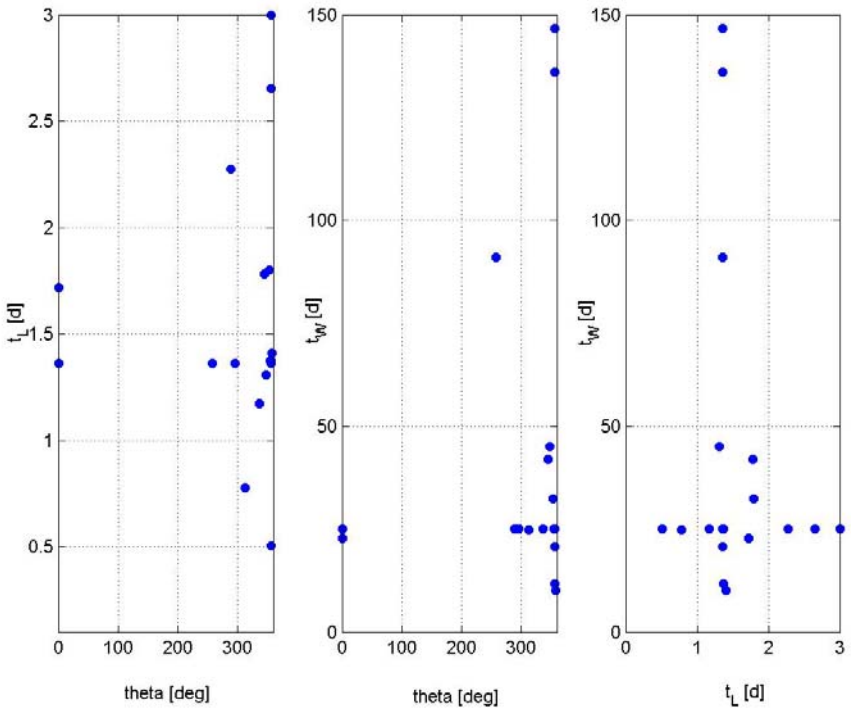

Figure 260: Distribution of the population over the search space at the end of the optimization process corresponding to the best identified solution.

The previous figures show that the individuals in the final population are widely distributed over the search space; the effects of the sharing operator can be highlighted again: concentration of individuals and then accurate identification of the local optimum are voided. Figure 261 reports the objective function values corresponding to each individual.

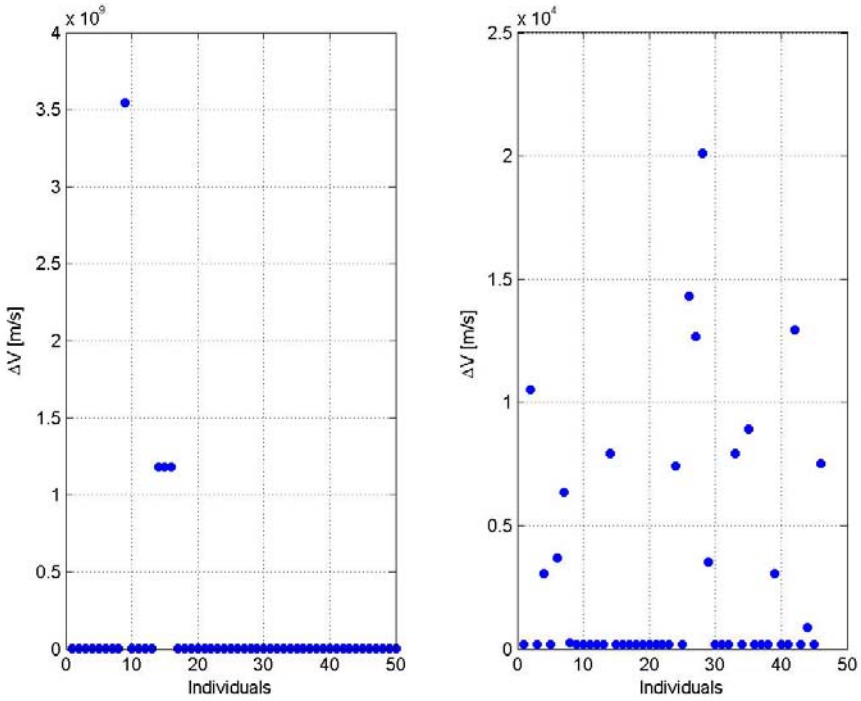

Figure 261: Objective function values of individuals in the final population corresponding to the best identified solution.

Figure 261 shows again that some individuals in the final population corresponds to region of the search space where the algorithm for Lambert's three-body problem solution couldn't converge to an admissible solution. By analysing the search space we can see that the all remaining individuals identify in fact the best identified solution: indeed, the final population of GAOT-shared algorithm concentrates around a unique optimum solution, without keeping information of other local optima solutions.

GATBX

As GATBX implements a genetic algorithm, we report the statistical characteristics. Ten runs have been processed in order to solve the previously defined problem. Default options suggested by the providers of the code have been used in all the runs. In analogy with the previous genetic algorithms, we used again a population of 50 individuals evolving for a maximum number of generations equal to 1000.

Algorithm parameters	
Number of individuals:	50
Maximum number of generations:	1000

Table 178 and Table 179 report the best identified solution compared with the best known solution.

Search space		
Design variable	**Best identified solution**	**Best known solution**
θ [*deg*]:	70.434	70.835
t_L [*d*]:	1.273	1.273
t_W [*d*]:	36.976	107.670

Table 178: Comparison between the best identified solution and the best known solution: search space.

Objective function space		
Term	**Best identified solution**	**Best known solution**
ΔV [*m/s*]:	3082.470	3080.767
ΔV_I [*m/s*]:	3080.774	3080.756
ΔV_F [*m/s*]:	1.696	0.011

Table 179: Comparison between the best identified solution and the best known solution: objective function space.

The two solutions are comparable in terms of the objective function value, letting us suppose that GATBX best identified solution belong to one of the transfer families identified in the objective function structure analysis. However, differences in the search space, particularly referring to t_W values, indicate that the two solutions belong to two different families. Such a consideration is confirmed by the trajectory representation (see Figure 262).

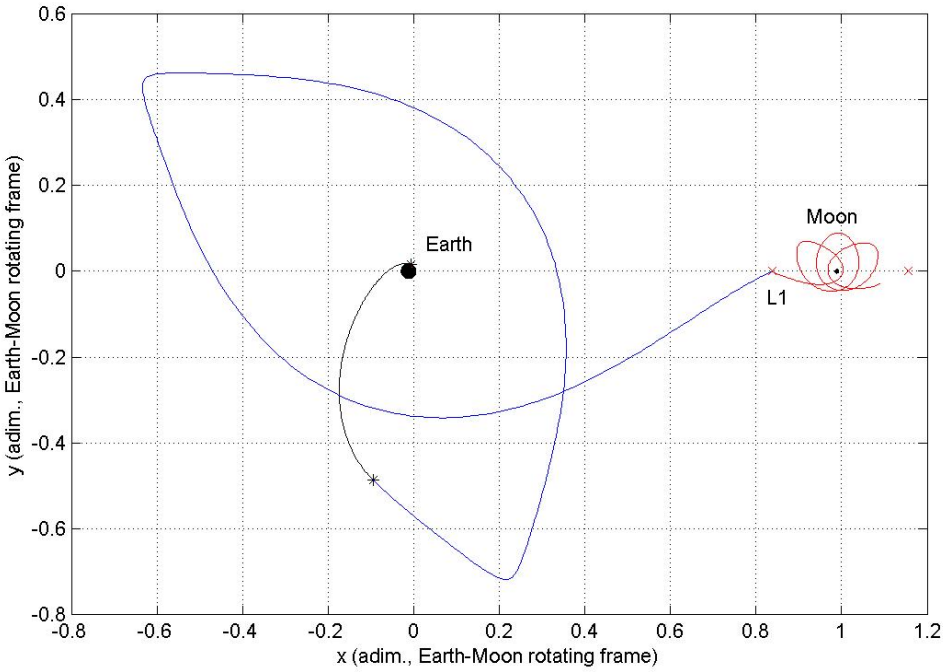

Figure 262: Best identified solution: trajectory representation.

By revising the objective function structure analysis, the best solution identified by GATBX can be clearly related to the family of solutions corresponding to subgroup 3, which is not the best identified one. Let now consider the statistical characteristics of the identified solution set. Table 180 reports the mean value and the standard deviation of the performances which will be used for comparisons with the other optimization algorithms.

Evaluation criterion	Mean value	Standard deviation
ΔV [*m/s*]:	3208.216	162.882
Model function evaluations:	5710	2999.096
Runtime [STU]:	38.668	19.305

Table 180: Statistical characteristics of the identified solutions.

As reported in Table 180, the mean value of the optimal objective function values reached at the end of each optimization process is quite different from the best identified one and is characterized by a high standard deviation, letting us suppose that no all the performed optimization processes have been able to identify the basin of attraction of the same solution. Figure 263 reports the final solutions corresponding to each optimization run in the *nFunc-ΔV* plane, while Figure 264 illustrates their distribution over the search space (the best identified solution is highlighted by a green dot) compared with the best known solution (red dot).

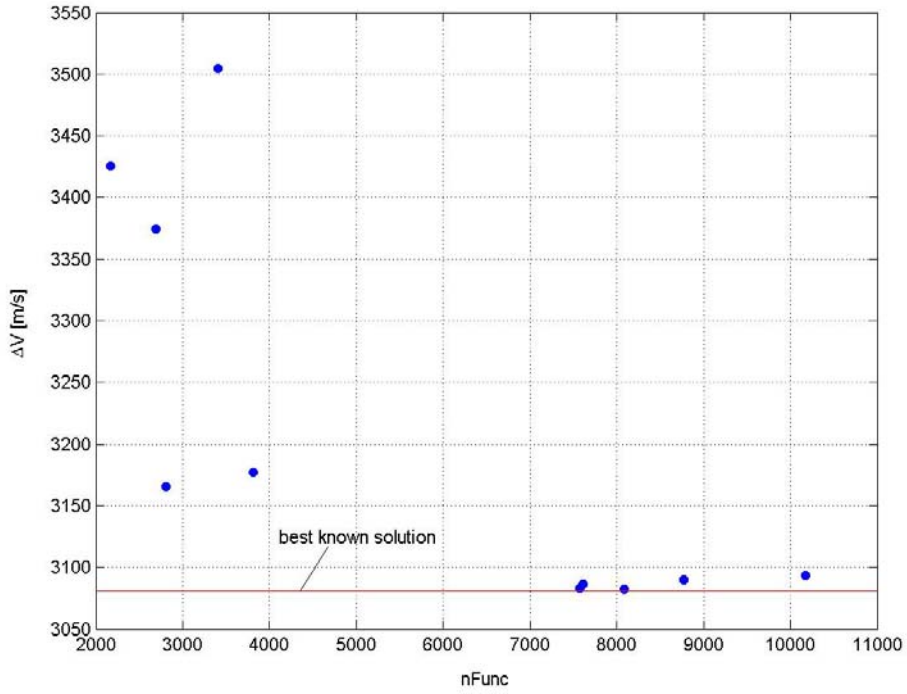

Figure 263: Distribution of the final solutions corresponding to each optimization run on the *nFunc-ΔV* plane.

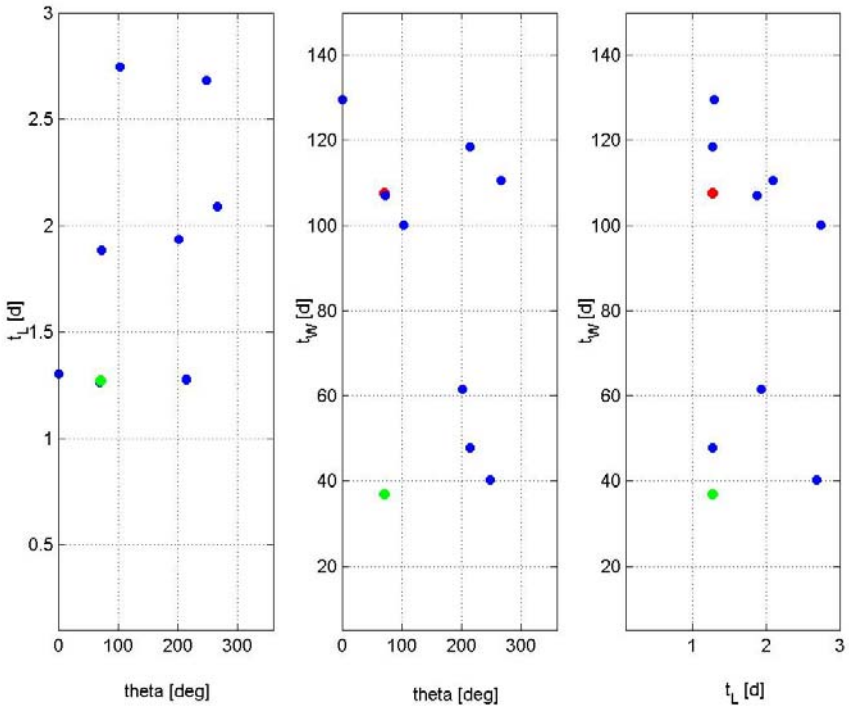

Figure 264: Distribution of the final solutions corresponding to each optimization run on the search space.

Figure 263 and Figure 264 illustrate that, although the coincidence of the best identified solution with the best known one in the θ - t_L subspace, no one solution could reach the best known one; this confirms the important effects of the presence of several comparable local minima on the effectiveness of the global search. In order to better identify the reached basins of attraction, the ten identified solutions have been used as starting points for ten local optimization processes performed by means of a SQP algorithm. Figure 265 reports the improved solutions over the *nFunc-ΔV* plane.

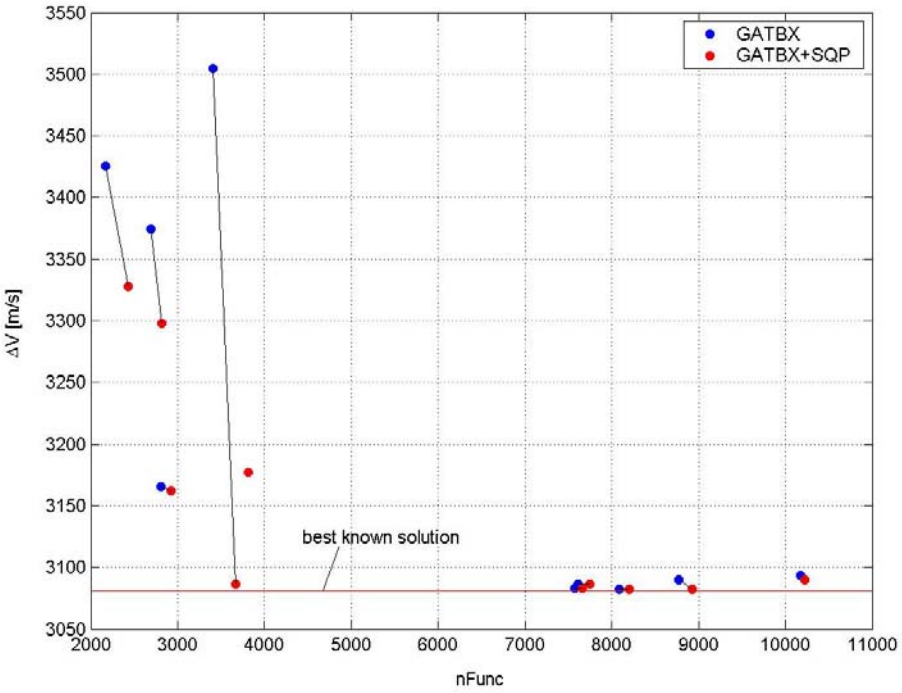

Figure 265: Distribution of the improved solutions at the end of a local optimization process on the *nFunc-ΔV* plane.

The improved solutions are now analysed in the normalized search space. Table 181 reports, corresponding to each GATBX+SQP run, the reached objective function value and the distance (in Euclidean metric) with respect to the best known solution.

	ΔV [*m/s*]	Distance
run 1	3082.309	0.488
run 2	3083.238	0.406
run 3	3177.197	0.833
run 4	3297.694	0.620
run 5	3327.673	0.569
run 6	3086.674	0.487
run 7	3090.202	0.248
run 8	3162.470	0.517
run 9	3086.758	0.006
run 10	3082.102	0.576

Table 181: GATBX+SQP optimization runs: objective function values and Euclidean distance in the normalized search space with respect to the best known solution.

Table 181 shows that, by defining two solutions as identical when the Euclidean distance is less than 1% of the hyper diagonal of the normalized search space, that is 0.017 in a 3-dimensional space, 1/10 GATBX runs were able to identify the basin of attraction of the best known solution, as Figure 266 confirms. Note that, due to the accuracy of the local optimization algorithms and to the sensitivity of the objective function, the objective function values corresponding to run 9 is slightly higher than the best identified one.

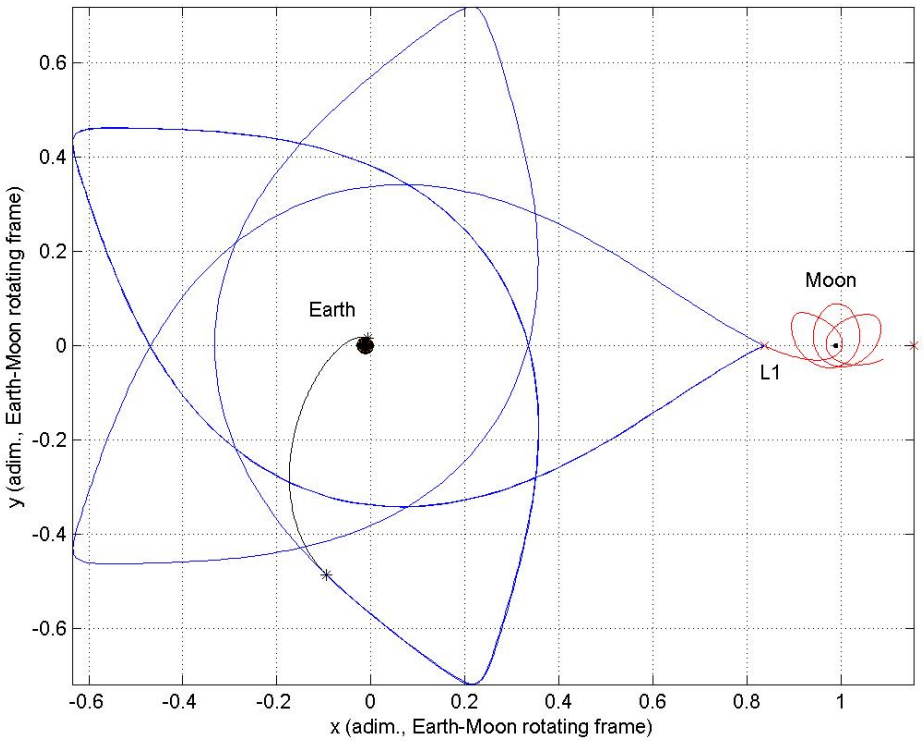

Figure 266: Transfer trajectory corresponding to run 9.

Moreover, it is worth noting that further 5/10 runs could reach the basin of attraction of local minima comparable to the best known one (runs 1, 2, 6, 7 and 10). A careful analysis showed that such comparable local minima are in fact related to a subset of the ten transfer families identified in the objective function structure analysis; in particular, again no one corresponds in fact to the best identified one (subgroup 8). The main features of the final population are now investigate: to do that, the final population corresponding to the best identified solution is studied. Figure 267 shows the distribution of the population over the search space at the end of the optimization process. Figure 268 reports the objective function values corresponding to each individual.

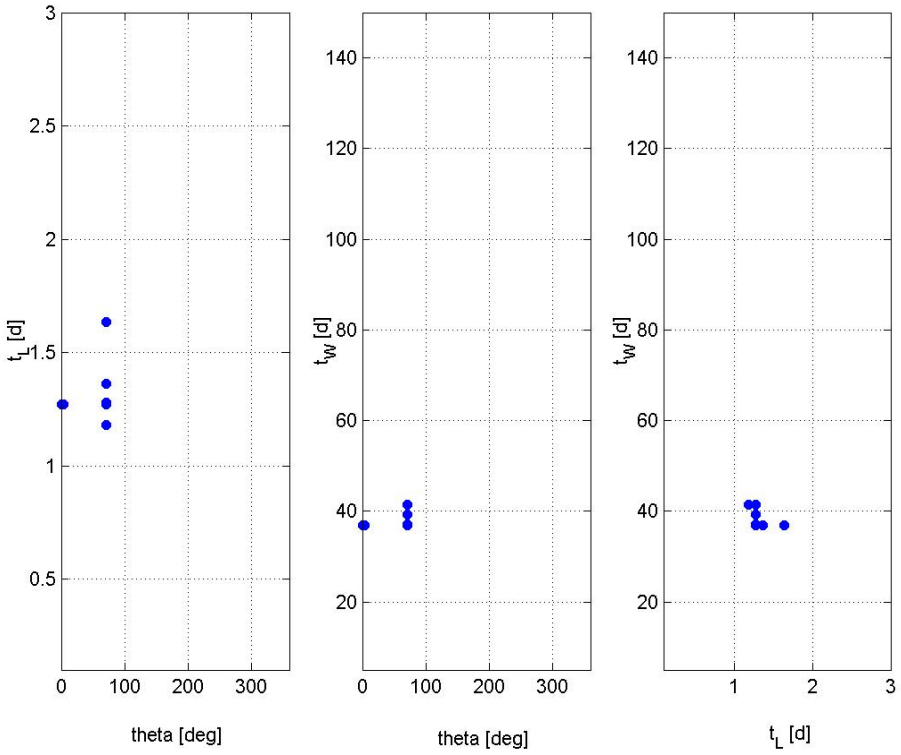

Figure 267: Distribution of the population over the search space at the end of the optimization process corresponding to the best identified solution.

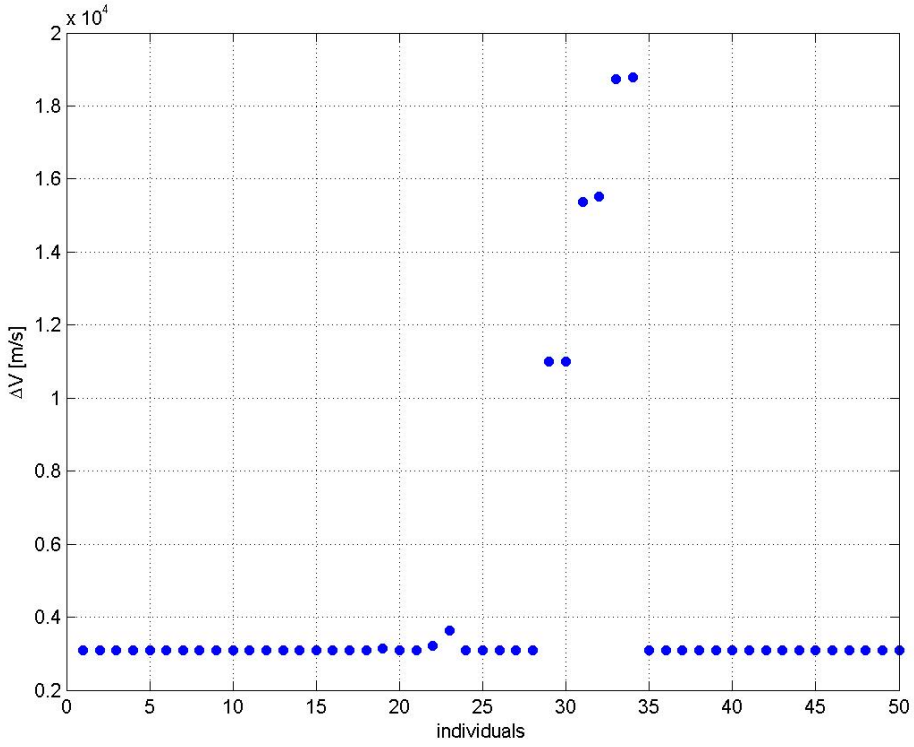

Figure 268: Objective function values of individuals in the final population corresponding to the best identified solution.

Figure 268 shows that individuals are quite concentrated around the best identified solution: indeed, the final population of GATBX algorithm concentrates around a unique optimum solution, without keeping information of other local optima solutions.

GATBX - migr

As GATBX-migr implements a genetic algorithm including a migration operator applied among a predefined set of subpopulations, we report the statistical characteristics. Ten runs have been processed in order to solve the previously defined problem. Default options suggested by the providers of the code have been used in all the runs. A population of 50 individuals evolving for a maximum number of generations equal to 1000 has been processed. The population has been divided in 5 subpopulations, each one including 10 individuals.

Algorithm parameters	
Number of individuals:	50
Maximum number of generations:	1000
Number of subpopulations:	5
Number of individuals per subpopulation:	10

Table 182 and Table 183 report the best identified solution compared with the best known solution.

Search space		
Design variable	**Best identified solution**	**Best known solution**
θ [*deg*]:	139.544	70.835
t_L [*d*]:	1.307	1.273
t_W [*d*]:	85.825	107.670

Table 182: Comparison between the best identified solution and the best known solution: search space.

Objective function space		
Term	**Best identified solution**	**Best known solution**
ΔV [*m/s*]:	3088.672	3080.767
ΔV_I [*m/s*]:	3081.123	3080.756
ΔV_F [*m/s*]:	7.549	0.011

Table 183: Comparison between the best identified solution and the best known solution: objective function space.

The two solutions are comparable in terms of the objective function value, thus indicating the possible belonging of the best identified solution to one of the transfer families identified in the objective function structure analysis. However, the design variables show evident differences, letting us suppose that they identify different local minima. Such a consideration is confirmed by the trajectory representation; see Figure 269.

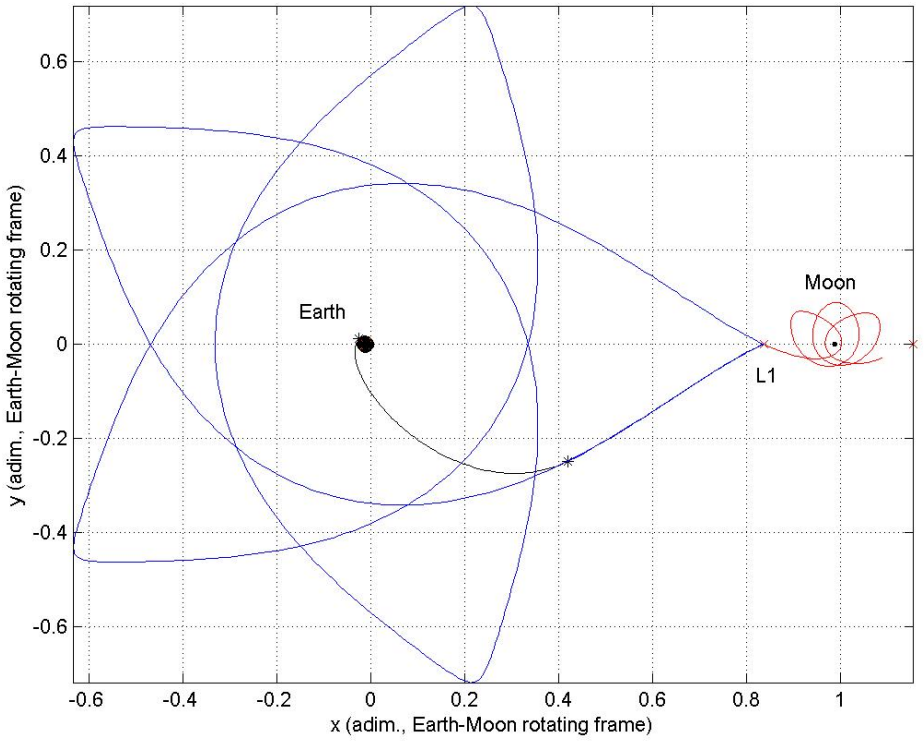

Figure 269: Best identified solution: trajectory representation.

The best solution identified by GATBX-migr can be related in fact to the family of solutions identified in the objective function structure analysis corresponding to subgroup 6, which is not the best identified one. As it concerns the statistical characteristics of the identified solution set, Table 184 reports the mean value and the standard deviation of the performances which will be used for comparisons with the other optimization algorithms.

Evaluation criterion	Mean value	Standard deviation
ΔV [*m/s*]:	3203.474	111.245
Model function evaluations:	7050	2144.968
Runtime [STU]:	53.471	14.408

Table 184: Statistical characteristics of the identified solutions.

The mean value of the optimal objective function values reached at the end of each optimization process reported in Table 184 is quite different from the best identified one and is characterized by a high standard deviation. This lets us suppose that no all the performed optimization processes identified the basin of attraction of the same solution. To better analyse this point, Figure 270 reports the final solutions corresponding to each optimization run in the *nFunc-ΔV* plane, while Figure 271 illustrates their distribution over the search space (the best identified solution is highlighted by a green dot) compared with the best known solution (red dot).

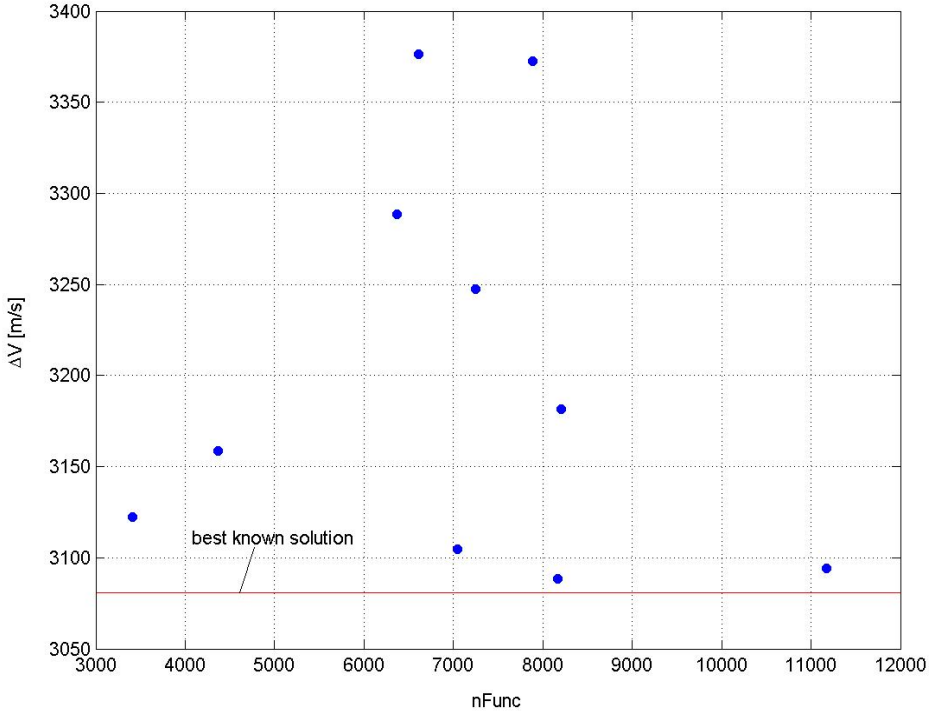

Figure 270: Distribution of the final solutions corresponding to each optimization run on the *nFunc-ΔV* plane.

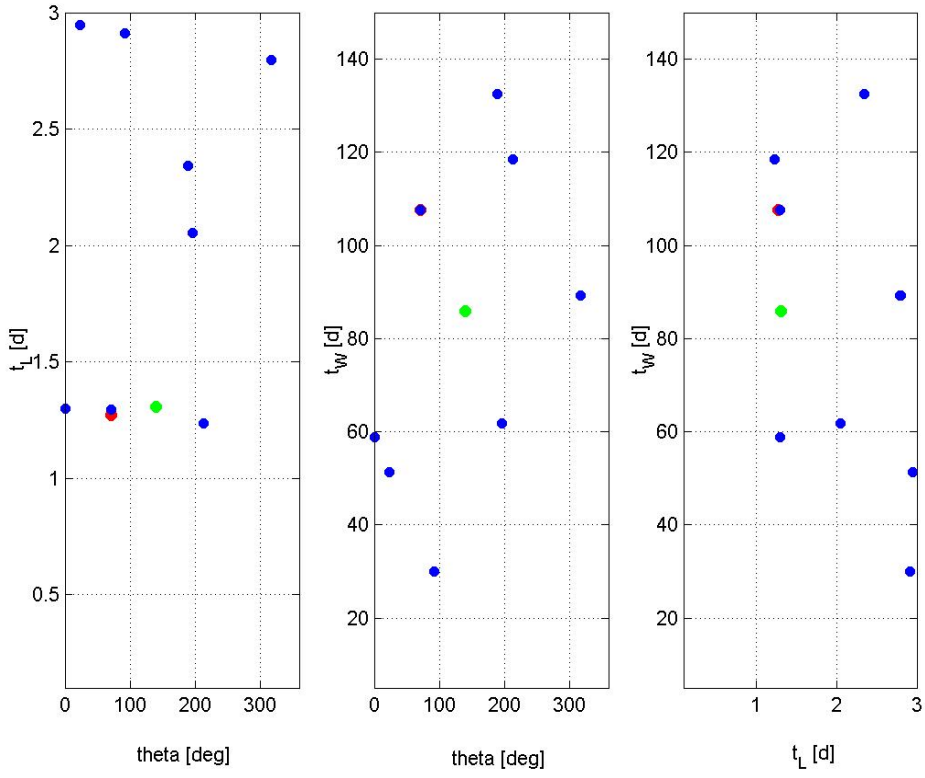

Figure 271: Distribution of the final solutions corresponding to each optimization run on the search space.

Figure 270 and Figure 271 show that, although the best identified solution is different from the best known one, one of the remaining local minima seems to lie in the neighbourhood of it. Actually, by investigating the remaining identified solutions, one solution could be recognized as belonging to the transfer family of subgroup 8 (see Table 185, Table 186 and Figure 272, where this solution has been indicated as “alternative solution”).

Search space		
Design variable	**Alternative solution**	**Best known solution**
θ [*deg*]:	71.695	70.835
t_L [*d*]:	1.295	1.273
t_W [*d*]:	107.630	107.670

Table 185: Comparison between the alternative identified solution and the best known solution: search space.

Objective function space		
Term	**Alternative solution**	**Best known solution**
ΔV [*m/s*]:	3104.864	3080.767
ΔV_I [*m/s*]:	3082.724	3080.756
ΔV_F [*m/s*]:	22.141	0.011

Table 186: Comparison between the alternative identified solution and the best known solution: objective function space.

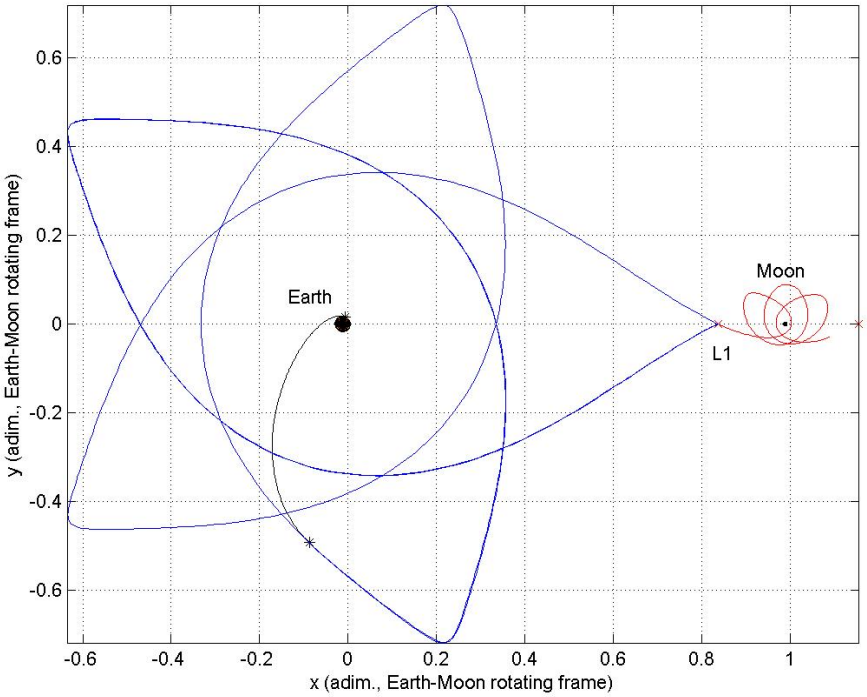

Figure 272: Alternative identified solution: trajectory representation.

As can be seen from Table 185, Table 186 and Figure 272, GATBX-migr identified the basin of attraction of the best known solution in at least one run; however, the accuracy in finding such solution, although quite good (the Euclidean distance in the normalized search space being $7.926 \cdot 10^{-3}$), is not good enough to detect the very small differences in the objective function values corresponding to the compared local minima. Again, this confirms the important effects of the presence of several comparable local minima on the effectiveness of the global search. In order to better identify the reached basins of attraction corresponding to each run, the ten identified solutions have been used as starting points for ten local optimization processes performed by means of a SQP algorithm. Figure 273 reports the improved solutions over the *nFunc-ΔV* plane.

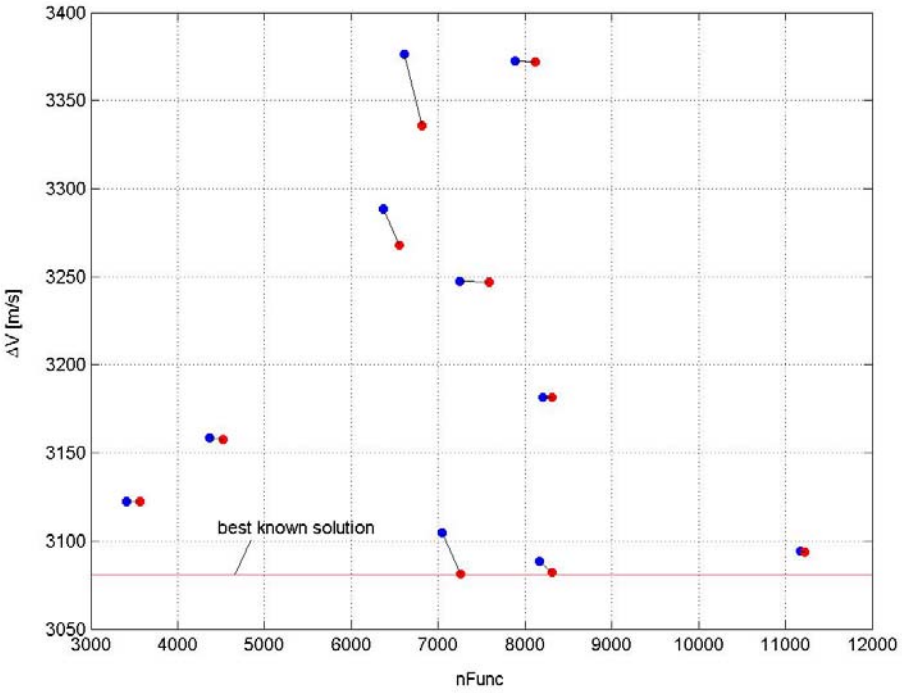

Figure 273: Distribution of the improved solutions at the end of a local optimization process on the *nFunc-ΔV* plane.

In analogy with the previous cases, the improved solutions are now studied in the normalized search space. Table 187 reports, corresponding to each GATBX-migr+SQP run, the reached objective function value and the distance (in Euclidean metric) with respect to the best known solution.

	ΔV [*m/s*]	Distance
run 1	3181.315	0.8709
run 2	3082.343	0.243
run 3	3335.858	0.577
run 4	3247.075	0.709
run 5	3157.891	0.872
run 6	3372.239	0.780
run 7	3267.985	0.524
run 8	3122.526	0.403
run 9	3081.312	0.001
run 10	3093.880	0.391

Table 187: GATBX-migr+SQP optimization runs: objective function values and Euclidean distance in the normalized search space with respect to the best known solution.

By defining two solutions as identical when the Euclidean distance is less than 1% of the hyper diagonal of the normalized search space, that is 0.017 in a 3-dimensional space, we can conclude that 1/10 GATBX-migr runs were able to identify the basin of attraction of the best known solution. However, as already highlighted in the previous cases, it is interesting to identify the number of runs which could identify local optima comparable to the best known one, which can be related to transfer families identified in the objective function structure analysis: in particular, a careful analysis of the solutions showed that 3/10 further runs could reach the basin of attraction of comparable local minima (runs 2, 8, and 10). Such comparable local minima, which are related in fact to a subset of the ten transfer families identified in the objective function structure analysis, do not correspond to the best identified solution (subgroup 8). Let us now investigate the main features of the final population: to do that, the final population corresponding to the best identified solution is again studied. Figure 274 shows the distribution of the population over the search space at the end of

the optimization process, while Figure 275 reports the objective function values corresponding to each individual.

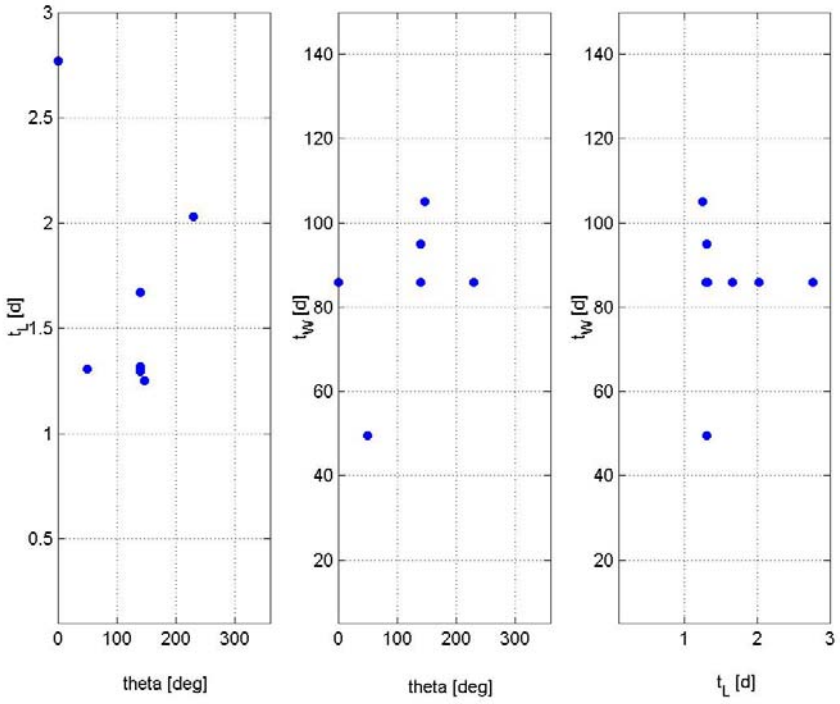

Figure 274: Distribution of the population over the search space at the end of the optimization process corresponding to the best identified solution.

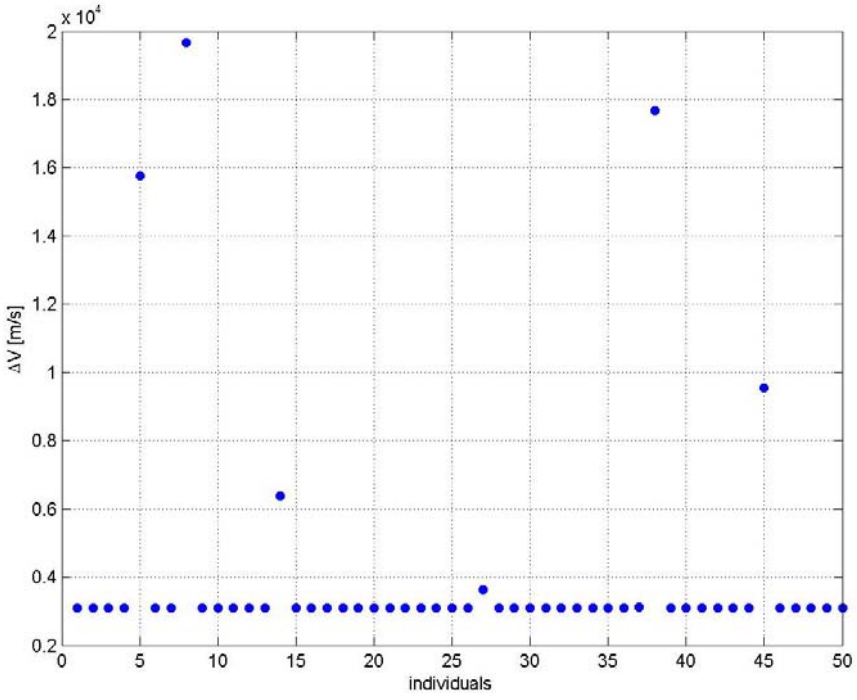

Figure 275: Objective function values of individuals in the final population corresponding to the best identified solution.

Although Figure 275 shows that the final population includes individuals not concentrated around the identified local minimum, a careful analysis showed that no local minima correspond to them, which should be related to the effects of the genetic operators on the members of each subpopulation.

FEP

As FEP implements an evolutionary programming algorithm, we report, as already done for genetic algorithms, the statistical characteristics. Ten runs have been processed in order to solve the previously defined problem. Default options suggested by the providers of the code have been used in all the runs. We used again a population of 50 individuals, evolving for a maximum number of generations equal to 100.

Algorithm parameters	
Number of individuals:	50
Maximum number of generations:	100

Table 188 and Table 189 report the best identified solution compared with the best known solution.

Search space		
Design variable	**Best identified solution**	**Best known solution**
θ [*deg*]:	71.318	70.835
t_L [*d*]:	1.273	1.273
t_W [*d*]:	107.670	107.670

Table 188: Comparison between the best identified solution and the best known solution: search space.

Objective function space		
Term	**Best identified solution**	**Best known solution**
ΔV [*m/s*]:	3083.427	3080.767
ΔV_I [*m/s*]:	3083.091	3080.756
ΔV_F [*m/s*]:	0.336	0.011

Table 189: Comparison between the best identified solution and the best known solution: objective function space.

The previous tables show that the best identified solution coincides in fact with the best known solution, as confirmed by the trajectory representation, Figure 276.

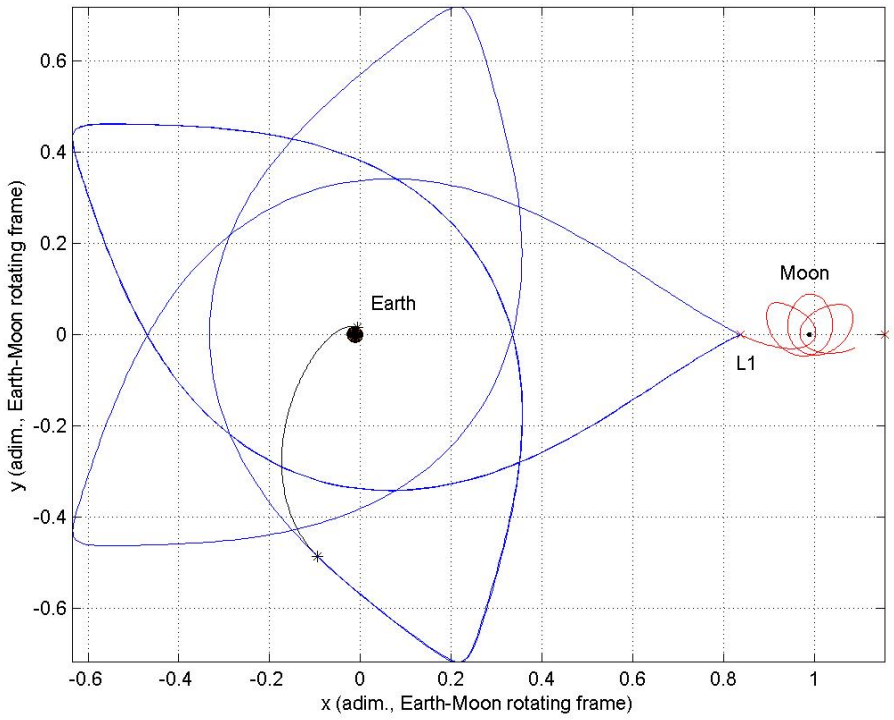

Figure 276: Best identified solution: trajectory representation.

From the objective function structure analysis of the problem of lunar transfer using libration points, the best solution identified by FEP can be recognized as related to the family of solutions corresponding to subgroup 8, which coincides

with the best identified one. Let now consider the statistical characteristics of the identified solution set. Table 190 reports the mean value and the standard deviation of the performances which will be used for comparisons with the other optimization algorithms.

Evaluation criterion	Mean value	Standard deviation
ΔV [*m/s*]:	3274.490	154.361
Model function evaluations:	2369.5	1575.070
Runtime [STU]:	14.089	15.007

Table 190: Statistical characteristics of the identified solutions.

Table 190 shows that the mean value of the optimal objective function values reached at the end of each optimization process is quite different from the best known one with a high standard deviation. Such a result let us suppose that no all the performed optimization processes have been able to identify the basin of attraction of the same solution. Figure 277 reports the final solutions corresponding to each optimization run in the *nFunc-ΔV* plane, while Figure 278 illustrates their distribution over the search space (the best identified solution is highlighted by a green dot) compared with the best known solution (red dot).

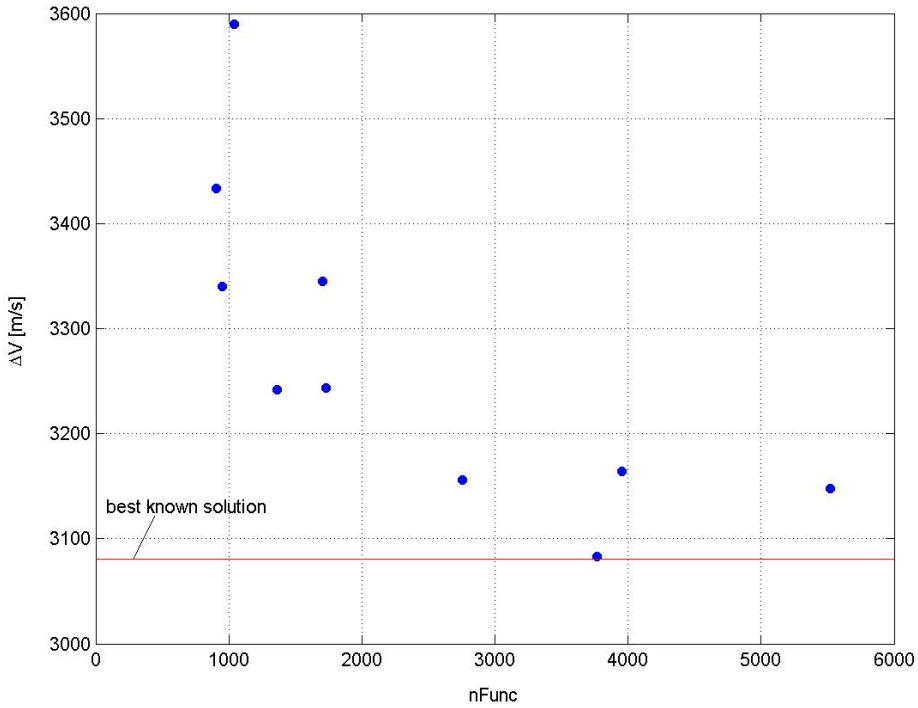

Figure 277: Distribution of the final solutions corresponding to each optimization run on the *nFunc-ΔV* plane.

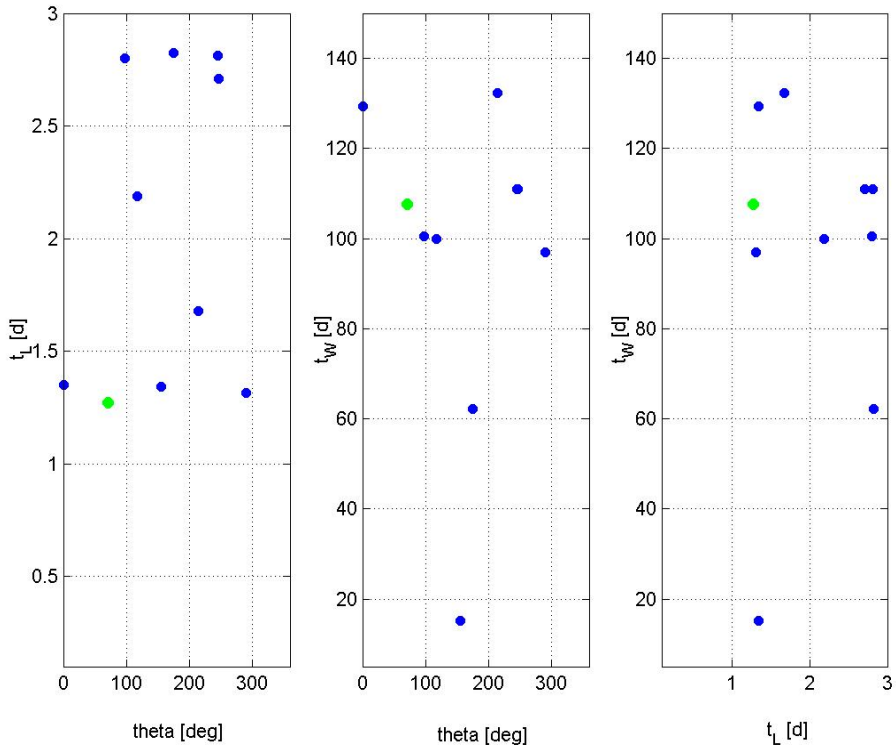

Figure 278: Distribution of the final solutions corresponding to each optimization run on the search space.

Figure 277 and Figure 278 show that, although the best identified solution coincides with the best known one, no further FEP runs could directly reach it. Anyway, in order to accurately characterize the basins of attraction corresponding to each identified solution, ten local optimization processes have been performed by means of a SQP algorithm, using the identified solutions as starting points. Figure 279 reports the improved solutions over the *nFunc-ΔV* plane.

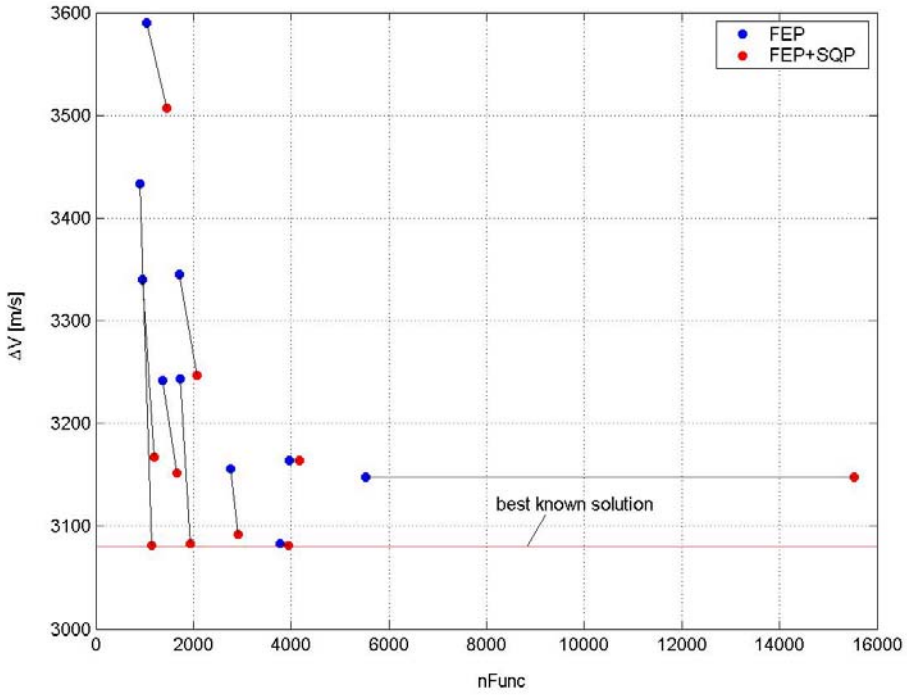

Figure 279: Distribution of the improved solutions at the end of a local optimization process on the *nFunc-ΔV* plane.

By investigating the improved solutions in the normalized search space, Table 191 reports, corresponding to each FEP+SQP run, the reached objective function value and the distance (in Euclidean metric) with respect to the best known solution.

	ΔV [*m/s*]	Distance
run 1	3147.936	0.718
run 2	3081.820	0.001
run 3	3164.208	0.697
run 4	3082.932	0.604
run 5	3152.141	0.682
run 6	3092.418	0.246
run 7	3081.053	0.666
run 8	3247.172	0.414
run 9	3167.237	0.546
run 10	3507.449	0.458

Table 191: FEP+SQP optimization runs: objective function values and Euclidean distance in the normalized search space with respect to the best known solution.

By considering two solutions as identical when the Euclidean distance is less than 1% of the hyper diagonal of the normalized search space, that is 0.017 in a 3-dimensional space, the previous analysis confirms that 1/10 FEP runs were able to identify the basin of attraction of the best known solution. Anyway, a careful analysis of the improved solutions showed that 3/10 runs could reach the basin of attraction of local minima comparable to the best known one (runs 4, 6 and 7), which can be related to transfer families identified in the objective function structure analysis. Let us now analyse the main features of the final population: to do that, the final population corresponding to the best identified solution is investigated. Figure 280 shows the distribution of the population over the search space at the end of the optimization process, while Figure 281 reports the objective function values corresponding to each individual.

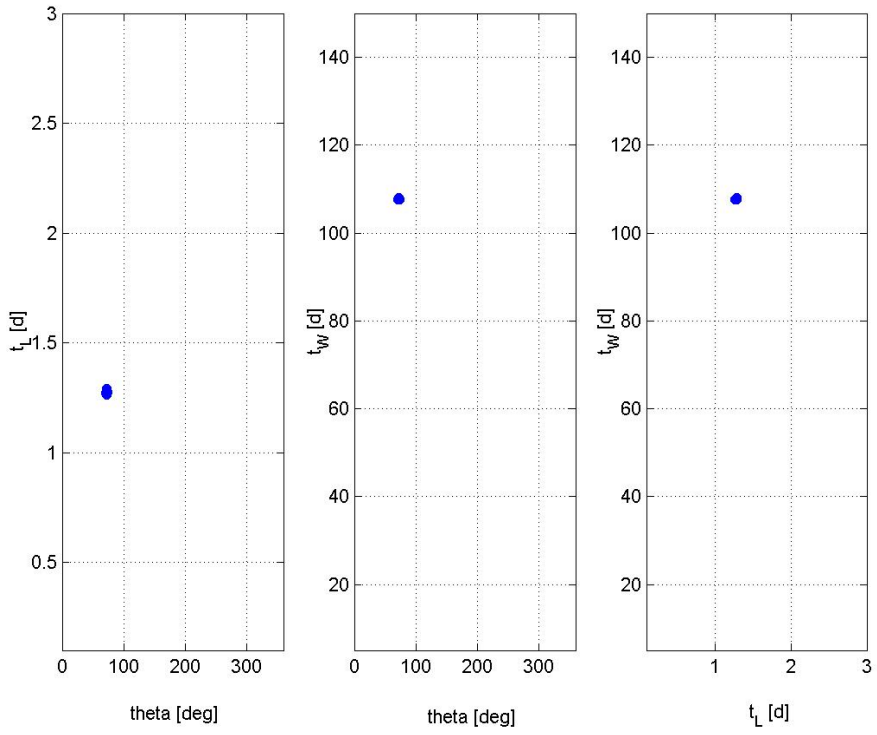

Figure 280 - Distribution of the population over the search space at the end of the optimization process corresponding to the best identified solution.

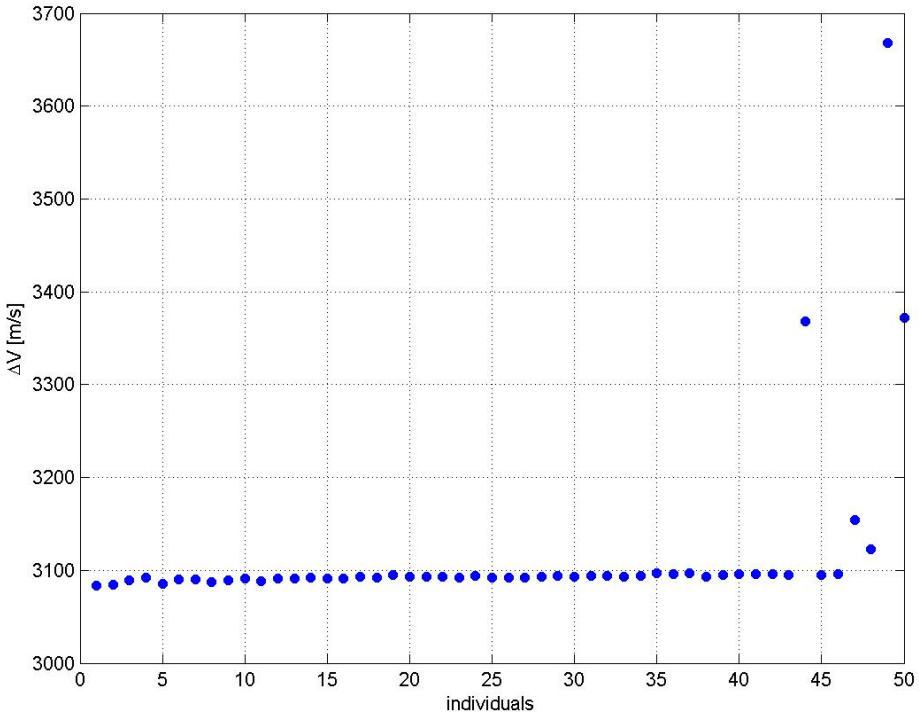

Figure 281: Objective function values of individuals in the final population corresponding to the best identified solution.

Figure 280 and Figure 281 show that the individuals in the final population are concentrated over the search space in a narrow neighbourhood of the best identified solution; however, relatively low accuracy and sensitivity of the objective function lead to relatively higher objective function values corresponding to some individuals. Anyway, the final population of FEP algorithm concentrates around a unique optimum solution, without keeping information of other local optima solutions.

DE

As DE implements a Differential Evolution algorithm, we report the statistical characteristics. Ten runs have been processed in order to solve the previously defined problem. Default options suggested by the providers of the code have been used in all the runs. In analogy with the previous genetic algorithms, we used again a population of 50 individuals evolving for a maximum number of generations equal to 1000.

Algorithm parameters	
Number of individuals:	50
Maximum number of generations:	1000

Table 192 and Table 193 report the best identified solution compared with the best known solution.

Search space		
Design variable	**Best identified solution**	**Best known solution**
θ [*deg*]:	32.101	70.835
t_L [*d*]:	2.764	1.273
t_W [*d*]:	121.690	107.670

Table 192: Comparison between the best identified solution and the best known solution: search space.

Objective function space		
Term	**Best identified solution**	**Best known solution**
ΔV [*m/s*]:	3193.673	3080.767
ΔV_I [*m/s*]:	3162.143	3080.756
ΔV_F [*m/s*]:	31.530	0.011

Table 193: Comparison between the best identified solution and the best known solution: objective function space.

The two solutions are in fact quite different in terms of objective function values, letting us suppose that DE best identified solution does not belong to one of the transfer families identified in the objective function structure analysis. Such a consideration is confirmed by the trajectory representation, see Figure 182.

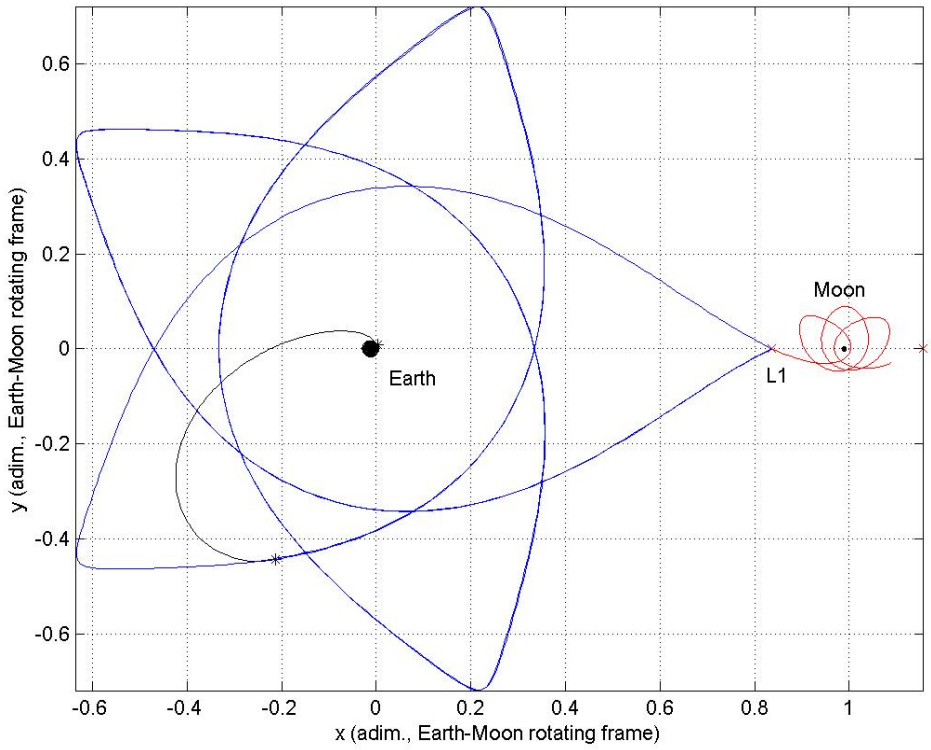

Figure 282: Best identified solution: trajectory representation.

The best solution identified by DE is not related to any family of solutions identified in the objective function structure analysis. Actually, it is typically related to a new set of families of lunar transfers, which differ from the previous identified one only for the Lambert's three-body arc: the conic-like orbit in the Earth-centred reference frame corresponding to the stable manifold is the same as in the previous case, but the Lambert's arc inject the spacecraft in this manifold corresponding to points near the apogee on the line coming out from it. A systematic analysis showed that similar transfers are identifiable, which are related to the insertion in the stable manifold in similar points, corresponding to the each revolution around the Earth. Let us now consider the statistical characteristics of the identified solution set. Table 194 reports the mean value and the standard deviation of the performances which will be used for comparisons with the other optimization algorithms.

Evaluation criterion	Mean value	Standard deviation
ΔV [*m/s*]:	3432.502	184.870
Model function evaluations:	1096.2	322.346
Runtime [STU]:	2.945	1.029

Table 194: Statistical characteristics of the identified solutions.

As reported in Table 194, the mean value of the optimal objective function values reached at the end of each optimization process is quite different from the best identified one and is characterized by a high standard deviation, letting us suppose that no all the performed optimization processes have been able to identify the basin of attraction of the same solution. Figure 283 reports the final solutions corresponding to each optimization run in the *nFunc-ΔV* plane, while igure 284 illustrates their distribution over the search space (the best identified solution is highlighted by a green dot) compared with the best known solution (red dot).

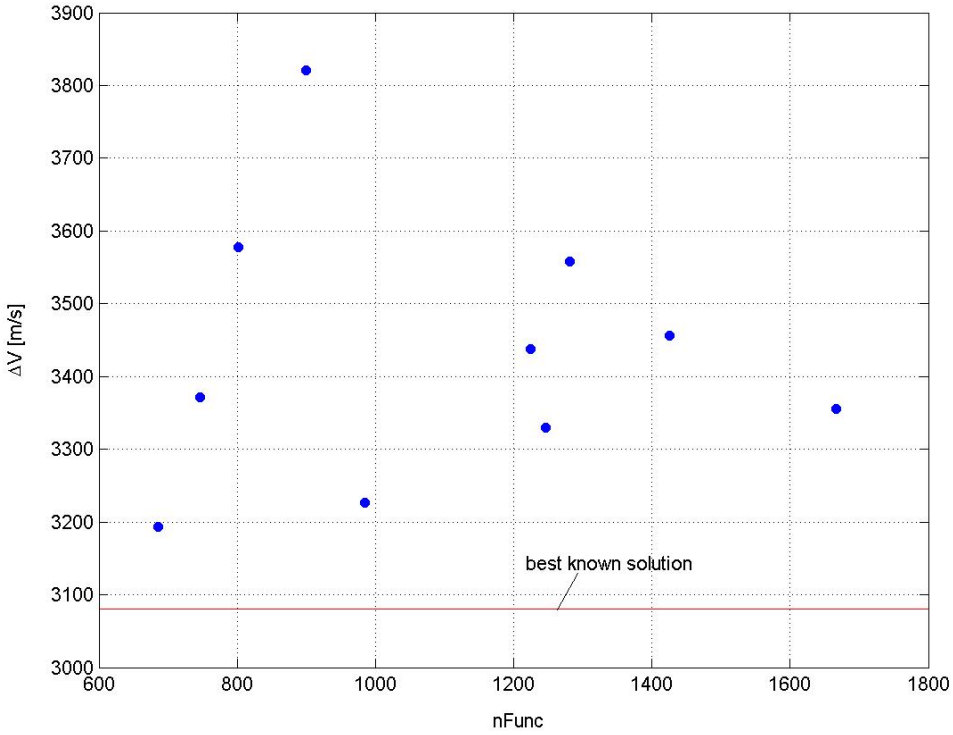

Figure 283: Distribution of the final solutions corresponding to each optimization run on the *nFunc-ΔV* plane.

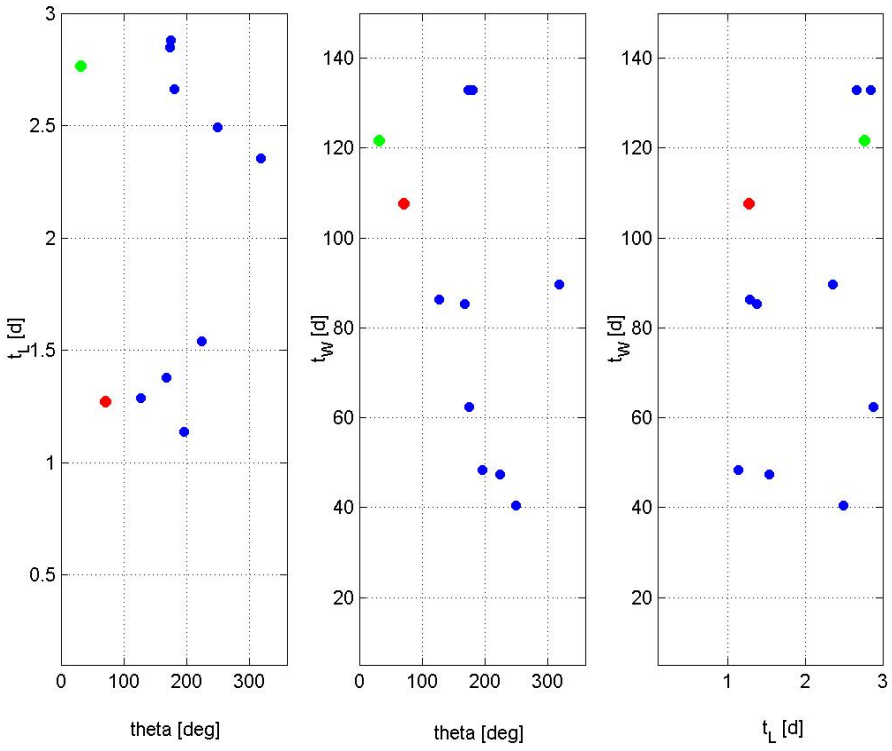

Figure 284: Distribution of the final solutions corresponding to each optimization run on the search space.

Figure 283 and Figure 284 show that no solutions could reach the best known one. In order to better identify the reached basins of attraction, similarly to the previous cases, the ten identified solutions have been used as starting points for ten local optimization processes performed by means of a SQP algorithm. Figure 285 reports the improved solutions over the *nFunc-ΔV* plane.

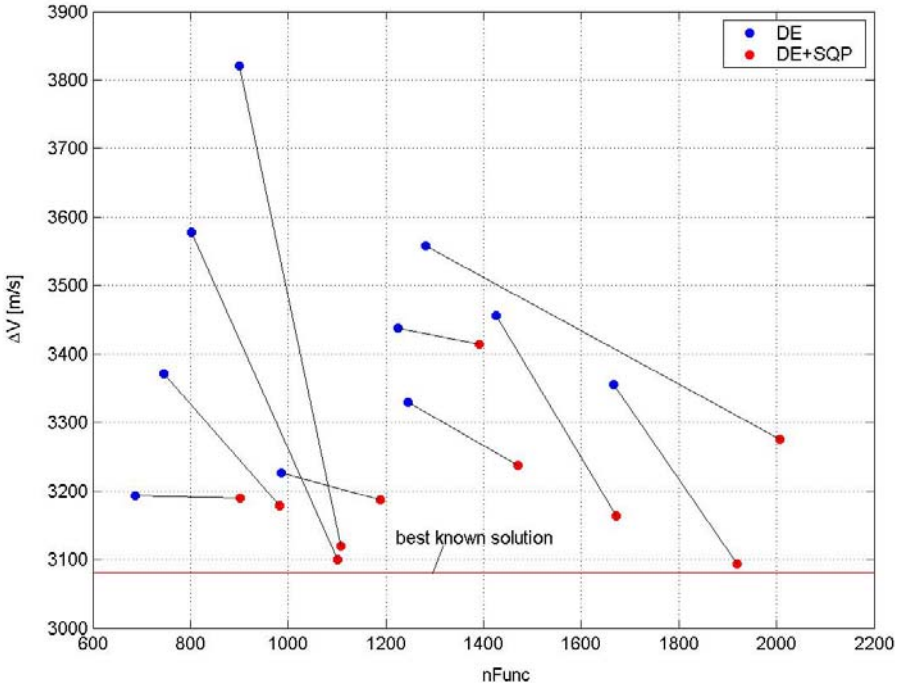

Figure 285: Distribution of the improved solutions at the end of a local optimization process on the *nFunc-ΔV* plane.

The improved solutions are now analysed in the normalized search space. Table 195 reports, corresponding to each DE+SQP run, the reached objective function value and the distance (in Euclidean metric) with respect to the best known solution.

	ΔV [*m/s*]	Distance
run 1	3189.665	0.534
run 2	3276.178	0.848
run 3	3099.697	0.578
run 4	3414.689	0.215
run 5	3187.481	0.638
run 6	3163.848	0.676
run 7	3237.658	0.810
run 8	3094.371	0.578
run 9	3119.811	0.244
run 10	3178.252	0.645

Table 195: DE+SQP optimization runs: objective function values and Euclidean distance in the normalized search space with respect to the best known solution.

Figiure 285 and Table 195 let us determine that no runs were able to get the basin of attraction of the best known solution and, moreover, no runs identified basin attraction of local minima belonging to the set of transfer families characterized in the objective function structure analysis. Such considerations are confirmed by a systematic analysis of the resulting lunar transfer as well as by the fact that, by considering two solutions as identical when the Euclidean distance is less than 1% of the hyper diagonal of the normalized search space (that is 0.017 in a 3-dimensional space) 0/10 DE runs were able to identify the basin of attraction of the best known solution. The main features of the final population are now investigate: to do that, the final population corresponding to the best identified solution is studied. Figure 286 shows the distribution of the population over the search space at the end of the optimization process, while Figure 287 reports the objective function values corresponding to each individual.

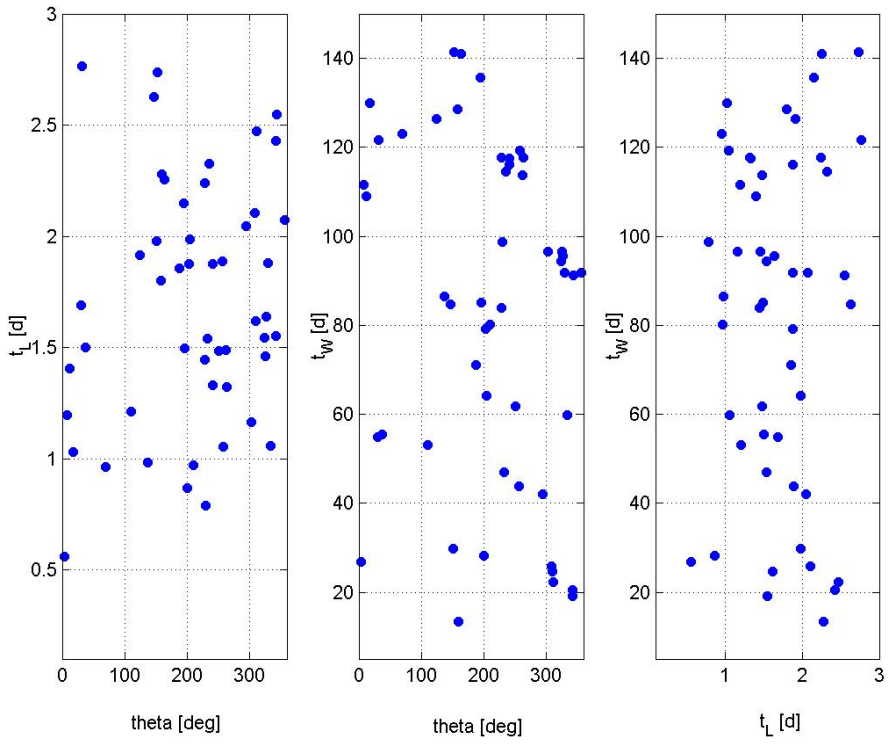

Figure 286: Distribution of the population over the search space at the end of the optimization process corresponding to the best identified solution.

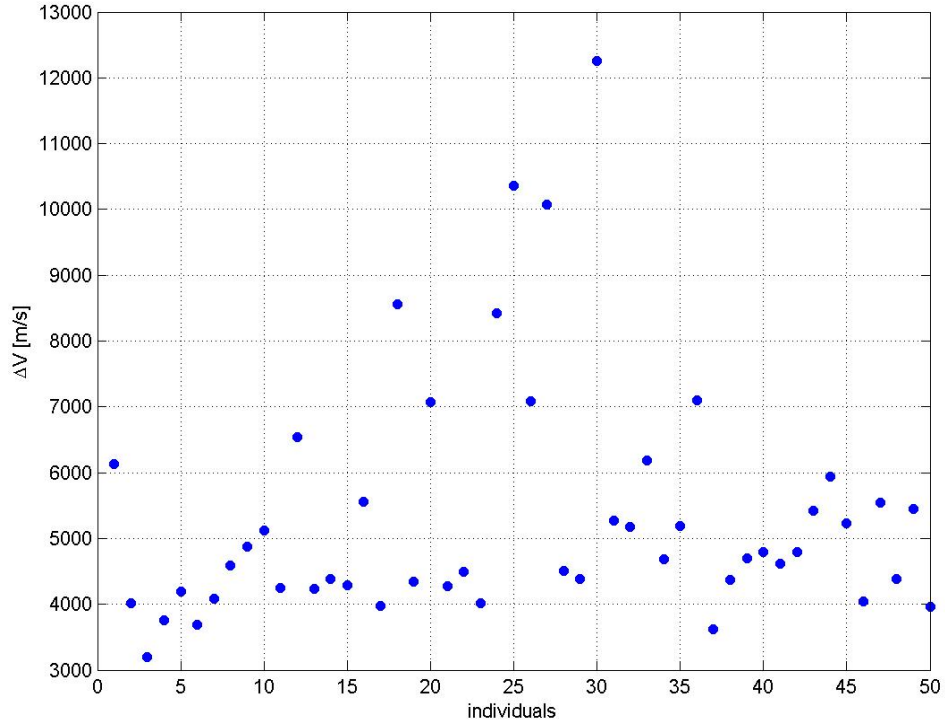

Figure 287: Objective function values of individuals in the final population corresponding to the best identified solution.

An impressive wide distribution of the final population over the search space can be recognized in Figure 286. However, Figure 287 seems to highlight that no niches on the objective function value are present, which indicates that the wide distribution of individuals over the search space does not necessarily corresponds to the detection of several local minima over the search space, as a systematic analysis of the resulting transfer trajectories confirmed. Actually, the wide distribution of individuals should be related to the effects of the differential operators used by DE for the global search.

ASA

As ASA implements an Adaptive Simulated Annealing algorithm, we report the statistical performance characteristics. Ten runs have been processed in order to solve the previously defined problem. Default options suggested by the providers of the code have been used in all the runs. Note that, unlike the previous cases, the adaptive simulated annealing needs a starting solution, which strongly affects the optimal solution reached. Due to the comparative purposes of this work, we decided to use ten different random starting solutions, uniformly distributed in the search box. Table 196 and Table 197 report the best identified solution compared with the best known solution.

Search space		
Design variable	**Best identified solution**	**Best known solution**
θ [*deg*]:	139.282	70.835
t_L [*d*]:	1.29642	1.273
t_W [*d*]:	15.137	107.670

Table 196: Comparison between the best identified solution and the best known solution: search space.

Objective function space		
Term	**Best identified solution**	**Best known solution**
ΔV [*m/s*]:	3080.823	3080.767
ΔV_I [*m/s*]:	3080.623	3080.756
ΔV_F [*m/s*]:	0.200	0.011

Table 197: Comparison between the best identified solution and the best known solution: objective function space.

The two solutions are comparable in terms of the objective function value, thus indicating that the best identified solution belongs in fact to one of the transfer families identified in the objective function structure analysis. However, the design variables show evident differences, letting us suppose that they identify different local minima. Such a consideration is confirmed by the trajectory representation, see Figure 288.

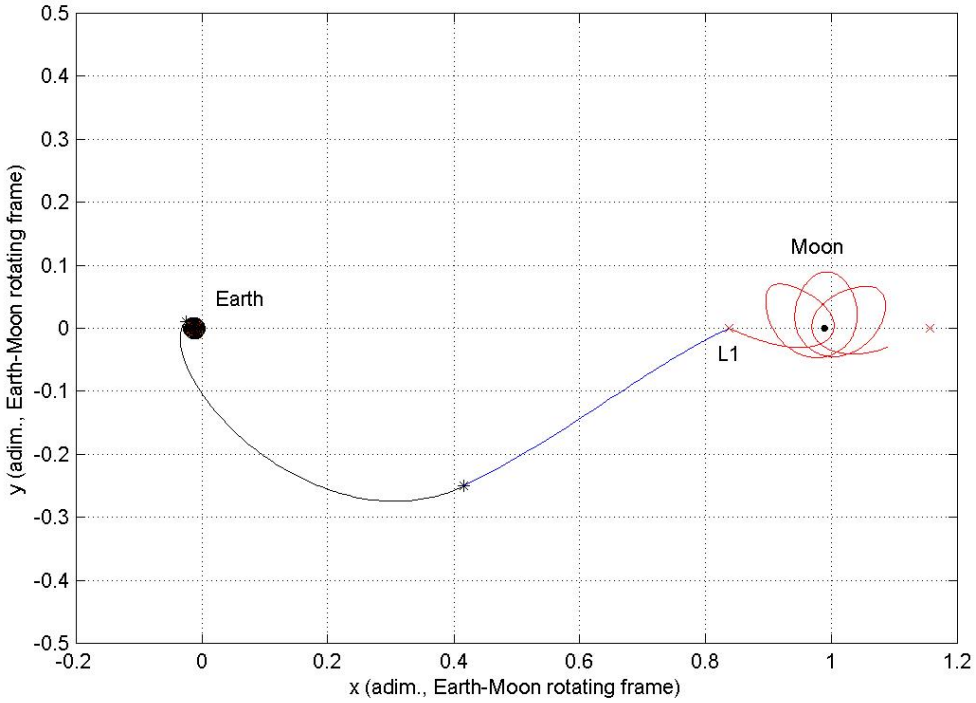

Figure 288: Best identified solution: trajectory representation.

The best solution identified by ASA can be related in fact to the family of solutions identified in the objective function structure analysis corresponding to subgroup 1, which is not the best identified one. As it concerns the statistical characteristics of the identified solution set, Table 198 reports the mean value and the standard deviation of the performances which will be used for comparisons with the other optimization algorithms.

Evaluation criterion	Mean value	Standard deviation
ΔV [*m/s*]:	3162.392	131.859
Model function evaluations:	4825.1	82.108
Runtime [STU]:	31.361	3.894

Table 198: Statistical characteristics of the identified solutions.

The mean value of the optimal objective function values reached at the end of each optimization process reported in Table 198 is different from the best identified one and is characterized by a high standard deviation. This lets us suppose again that no all the performed optimization processes identified the basin of attraction of the same solution. To better analyse this point, Figure 289 reports the final solutions corresponding to each optimization run in the *nFunc-ΔV* plane, while Figure 290 illustrates their distribution over the search space (the best identified solution is highlighted by a green dot) compared with the best known solution (red dot).

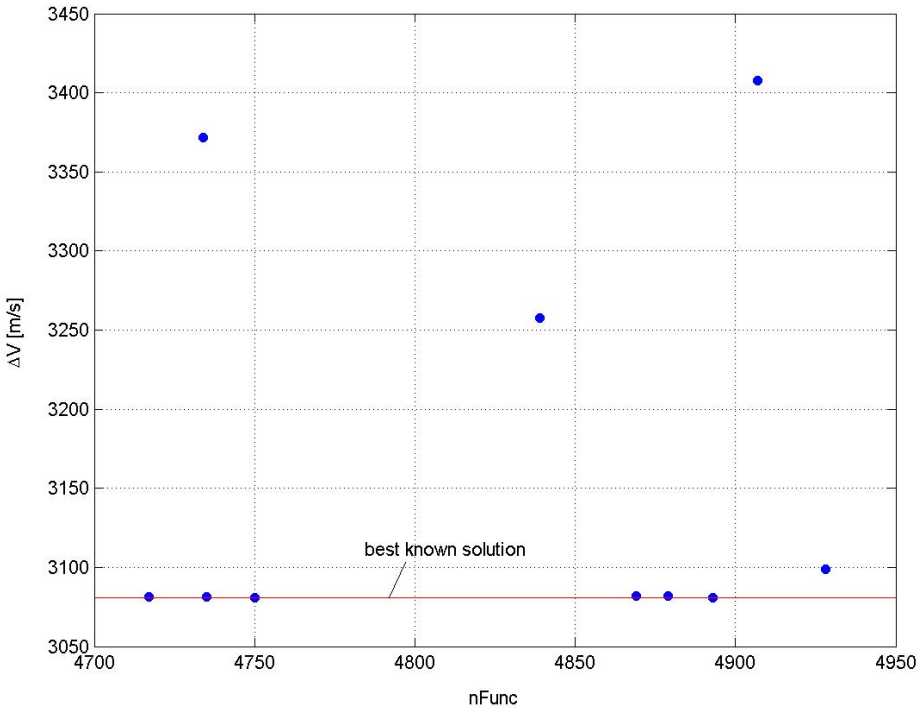

Figure 289: Distribution of the final solutions corresponding to each optimization run on the *nFunc-ΔV* plane.

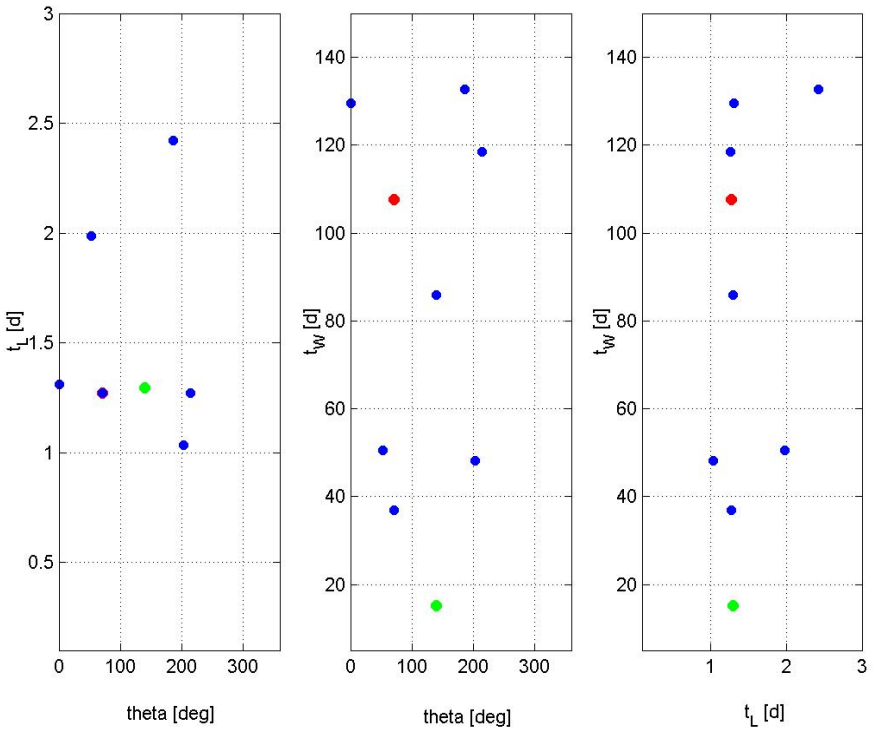

Figure 290: Distribution of the final solutions corresponding to each optimization run on the search space.

Figure 289 and Figure 290 show that, although ASA seems to have identified several local minima comparable with the best known one, no run was able to identify its basin of attraction. Such result should be related again to the important effects of the presence of several comparable local minima on the effectiveness of the global search. In order to better identify the reached basins of attraction corresponding to each run, the ten identified solutions have been used as starting points for ten local optimization processes performed by means of a SQP algorithm. Figure 291 reports the improved solutions over the *nFunc-ΔV* plane.

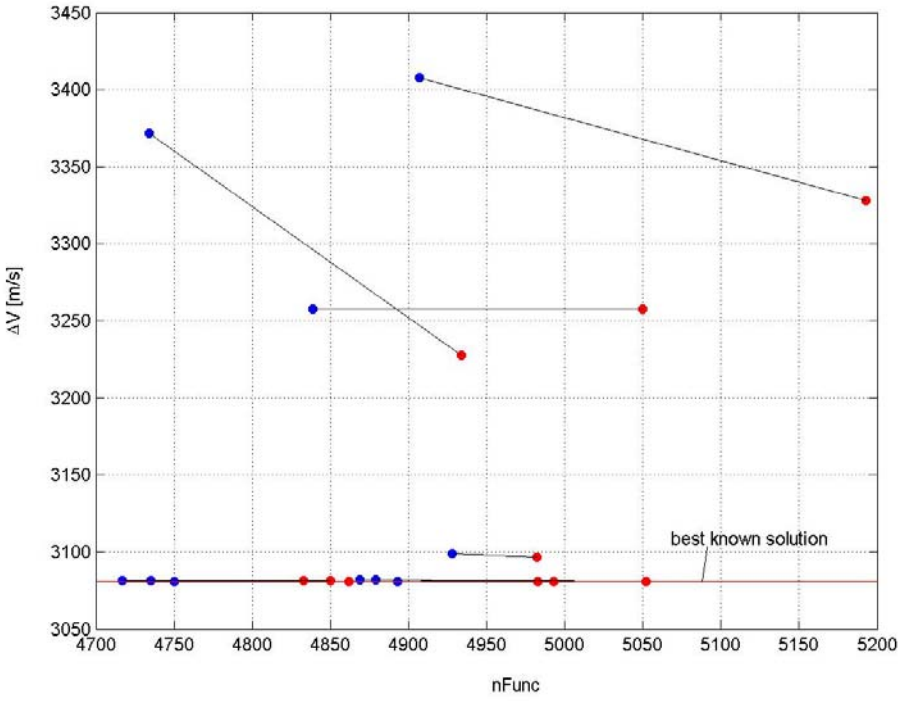

Figure 291: Distribution of the improved solutions at the end of a local optimization process on the *nFunc-ΔV* plane.

Figure 291 shows that low improvements have been gained by means of the SQP search, which highlights the effectiveness of the local component of the ASA search at accurately identifying the local minimum corresponding to the detected basin of attraction. In analogy with the previous cases, the improved solutions are now studied in the normalized search space. Table 189 reports, corresponding to each ASA+SQP run, the reached objective function value and the distance (in Euclidean metric) with respect to the best known solution.

	ΔV [*m/s*]	Distance
run 1	3080.815	0.406
run 2	3081.170	0.488
run 3	3080.766	0.666
run 4	3328.015	0.521
run 5	3227.446	0.599
run 6	3080.703	0.243
run 7	3096.411	0.248
run 8	3080.708	0.666
run 9	3081.245	0.666
run 10	3257.415	0.538

Table 189: ASA+SQP optimization runs: objective function values and Euclidean distance in the normalized search space with respect to the best known solution.

By defining two solutions as identical when the Euclidean distance is less than 1% of the hyper diagonal of the normalized search space, that is 0.017 in a 3-dimensional space, we can conclude in fact that 0/10 ASA runs were able to identify the basin of attraction of the best known solution. However, as already highlighted in the previous cases, it is interesting to identify the number of runs corresponding to local optima comparable to the best known one, related to transfer families identified in the objective function structure analysis: in particular, a careful analysis of the solutions via a systematic study of the corresponding lunar transfers showed that 7/10 runs could reach the basin of attraction of comparable local minima (runs 1, 2, 3, 6, 7, 8, and 9). Such comparable local minima, which are related in fact to a subset of the ten transfer families identified in the objective function structure analysis, do not correspond to the best identified solution (subgroup 8).

glbSolve

As glbSolve algorithm implements a deterministic optimization approach, statistical characteristics are not needed in this case. Only one run has been processed in order to solve the previously defined problem. Default options suggested by the providers of the code have been used. We used a maximum number of iterations equal to 1000.

Algorithm parameters	
Maximum number of iterations:	1000

Table 190 and Table 191 report the identified solution compared with the best known solution.

Search space		
Design variable	**Identified solution**	**Best known solution**
θ [*deg*]:	120.082	70.835
t_L [*d*]:	2.147	1.273
t_W [*d*]:	29.167	107.670

Table 190: Comparison between the identified solution and the best known solution: search space.

Objective function space		
Term	**Identified solution**	**Best known solution**
ΔV [*m/s*]:	3359.190	3080.767
ΔV_I [*m/s*]:	3109.076	3080.756
ΔV_F [*m/s*]:	250.114	0.011

Table 191: Comparison between the identified solution and the best known solution: objective function space.

The previous tables show that the identified solution does not coincide in fact with the best known solution, as confirmed by the trajectory representation, see Figure 292.

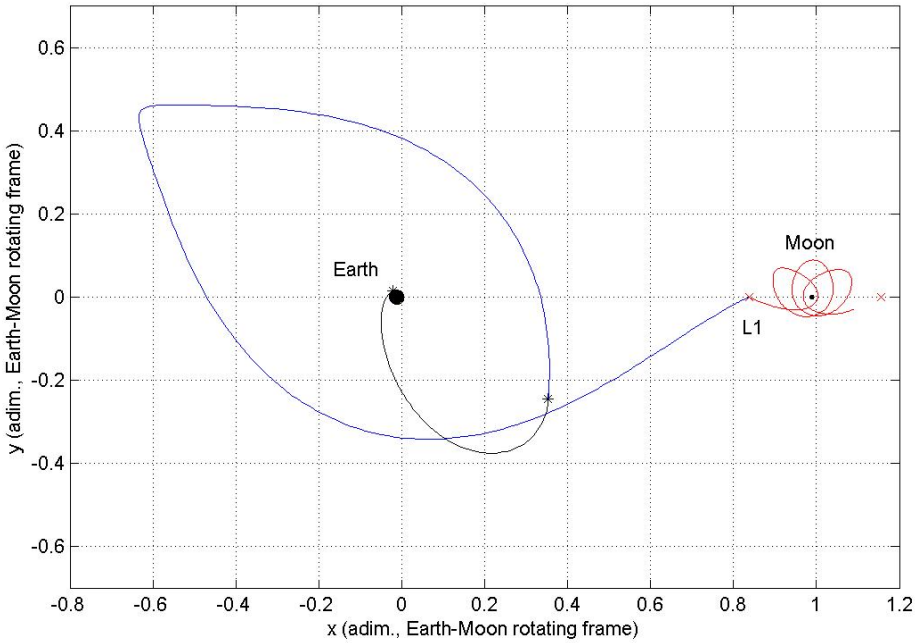

Figure 292: Identified solution: trajectory representation.

Similarly to the results gained in case of DE tool application to the problem of lunar transfer using libration points, the best solution identified by glbSolve is not related to any family of solutions identified in the objective function structure analysis. Actually, as the DE best identified solution, it is typically related to the set of families of lunar transfers characterized by a Lambert's three-body arc injecting the spacecraft in the stable manifold corresponding to points near the apogee of the conic-like orbit in the Earth-centred inertial frame on the line coming out from it. Table 192 reports the characteristics of the identified solution, which will be used for performance comparisons with the other optimization algorithms.

Evaluation criterion	Identified solution
ΔV [*m/s*]:	3359.190
Model function evaluations:	1311
Runtime [STU]:	5.240

Table 192: Characteristics of the identified solution.

In order to accurately identify the local minimum reached by *glbSolve* algorithm, a SQP based algorithm is now used to perform a local optimization process, where the solution identified by *glbSolve* is considered as the starting point for the local search process. The starting solution and the improved one are reported in Figure 293 on the *nFunc-ΔV* plane, while Figure 294 plots the transfer trajectory corresponding to the improved solution.

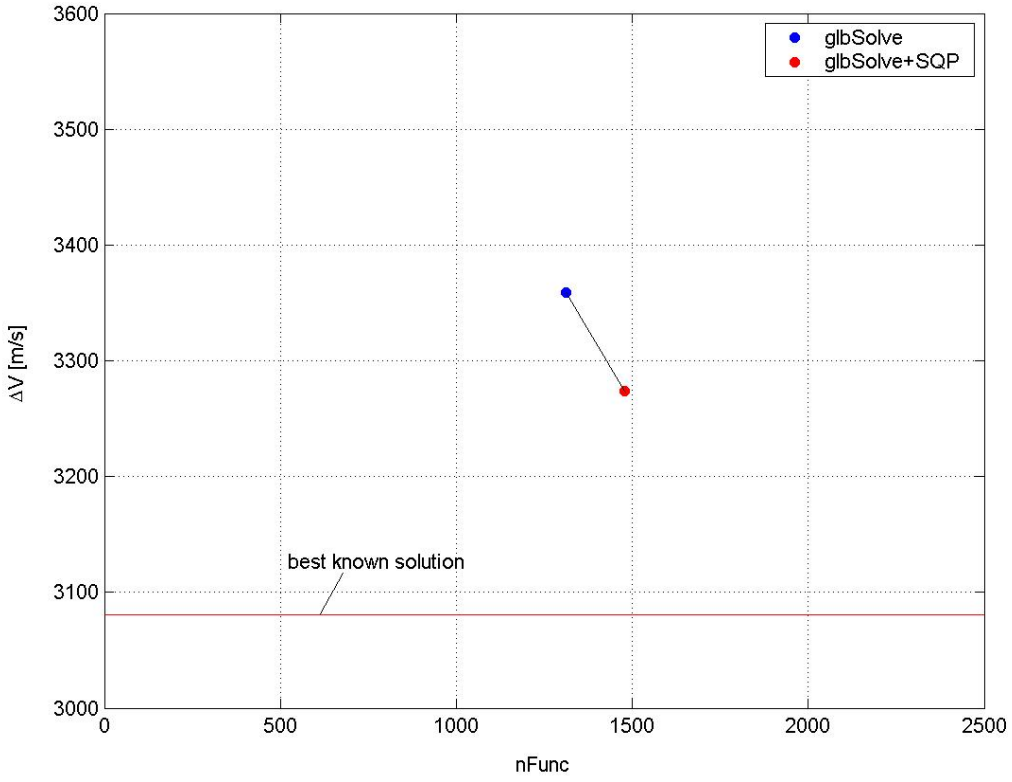

Figure 293: Distribution of the improved solution at the end of a local optimization process on the *nFunc-ΔV* plane.

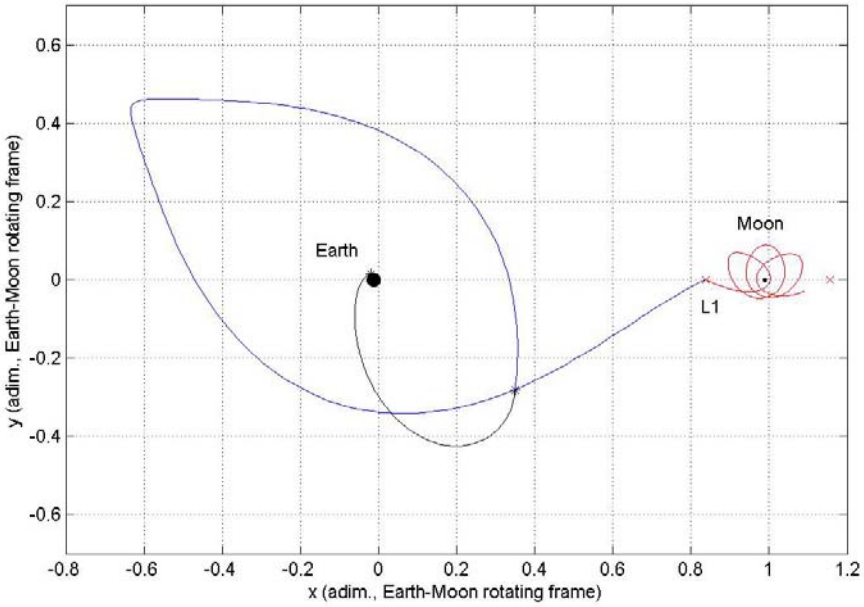

Figure 294: Improved solution via local optimization process: transfer trajectory.

The local optimization process confirms that the solution identified by glbSolve does not lie in the basin of attraction of the best known one and does not belong to any of the families of lunar transfers characterized in the objective function structure analysis, as confirmed by Table 193, which reports, corresponding to the glbSolve+SQP run, the reached objective function value and the distance (in Euclidean metric) with respect to the best known solution.

	ΔV [*m/s*]	Distance
glbSolve+SQP run	3273.594	0.678

Table 193: glbSolve+SQP optimization run: objective function value and Euclidean distance in the normalized search space with respect to the best known solution.

By considering two solutions as identical when the Euclidean distance is less than 1% of the hyper diagonal of the normalized search space, that is 0.017 in a 3-dimensional space, glbSolve run was not able to identify the basin of

attraction of the best known solution. As already noted in previous analyses, one of the output of glbSolve is the matrix of all rectangle center points sampled during the whole optimization run. By means of this matrix one can analyse the ability of glbSolve in exploring the whole search space: Figure 295 shows the distribution of the sampled points over the search space (the identified solution is highlighted by a green dot) compared with the best known solution (red dot).

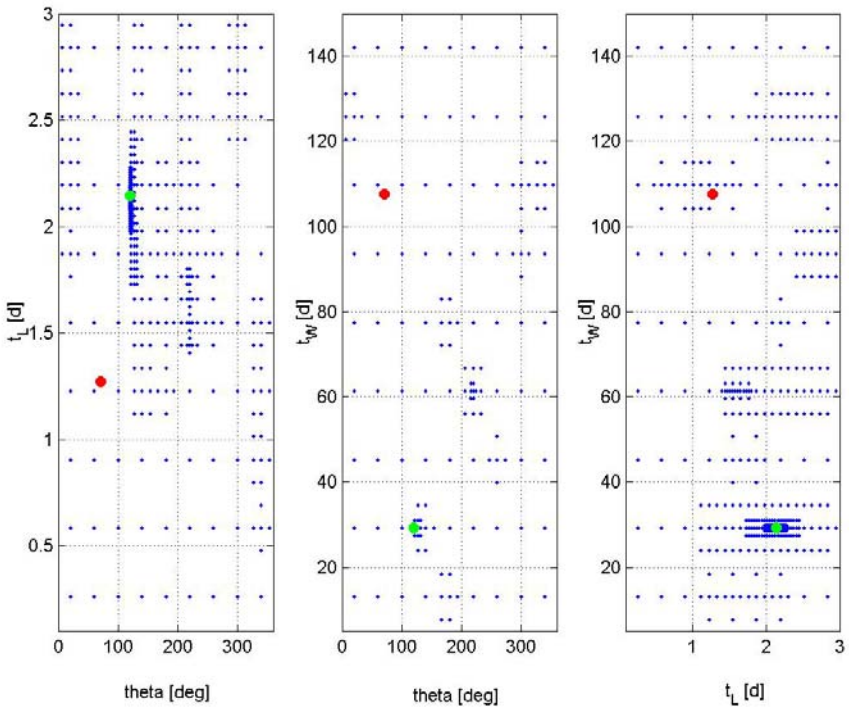

Figure 295: Distribution of the population over the search space at the end of the optimization process corresponding to the best identified solution.

Figure 295 shows that, after exploring different promising regions of the search space, glbSolve finally converges to the identified local minimum. The detection of several promising regions before convergence is highlighted in Figure 296 and Figure 297, which plots the objective function values corresponding to each rectangle center point: the 1311 sampled points are ordered along the x-axis from the first rectangle center point sampled during the optimization process to the final one.

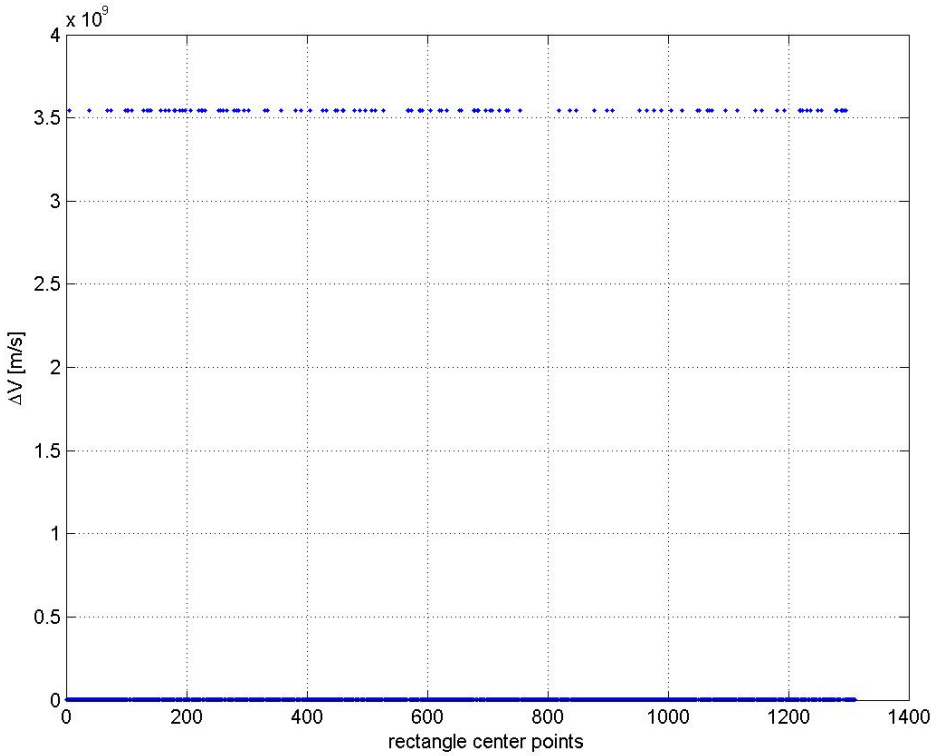

Figure 296: Objective function values corresponding to each rectangle center point.

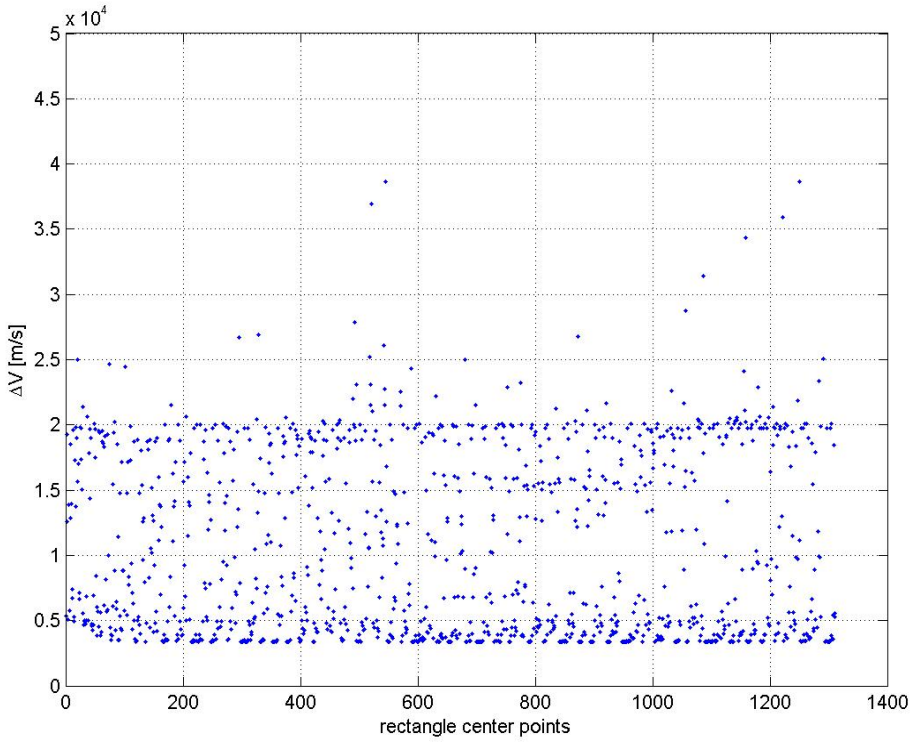

Figure 297: Objective function values corresponding to each rectangle center point (close up of Figure 296).

The center points corresponding to the highest objective function values in Figure 296 corresponds to regions where the algorithm for the solution of the Lambert's three-body problem couldn't converge. By omitting such solutions, Figure 297 shows that, after analysing worse solutions at the beginning of the optimization process, glbSolve algorithm finally got the identified local optimum solution.

MCS

As MCS algorithm implements a deterministic optimization approach, only one run has been processed in order to solve the previously defined problem. Default options suggested by the providers of the code have been used. We used a maximum number of objective function evaluation equal to 10000.

Algorithm parameters	
Maximum number of iterations:	10000

Table 194 and Table 195 report the identified solution compared with the best known solution.

Search space		
Design variable	**Identified solution**	**Best known solution**
θ [*deg*]:	148.121	70.835
t_L [*d*]:	1.882	1.273
t_W [*d*]:	150	107.670

Table 194: Comparison between the identified solution and the best known solution: search space.

Objective function space		
Term	**Identified solution**	**Best known solution**
ΔV [*m/s*]:	3594.321	3080.767
ΔV_I [*m/s*]:	3112.293	3080.756
ΔV_F [*m/s*]:	482.028	0.011

Table 195: Comparison between the identified solution and the best known solution: objective function space.

The previous tables show that the identified solution does not coincide in fact with the best known solution, as confirmed by the trajectory representation, Figure 298.

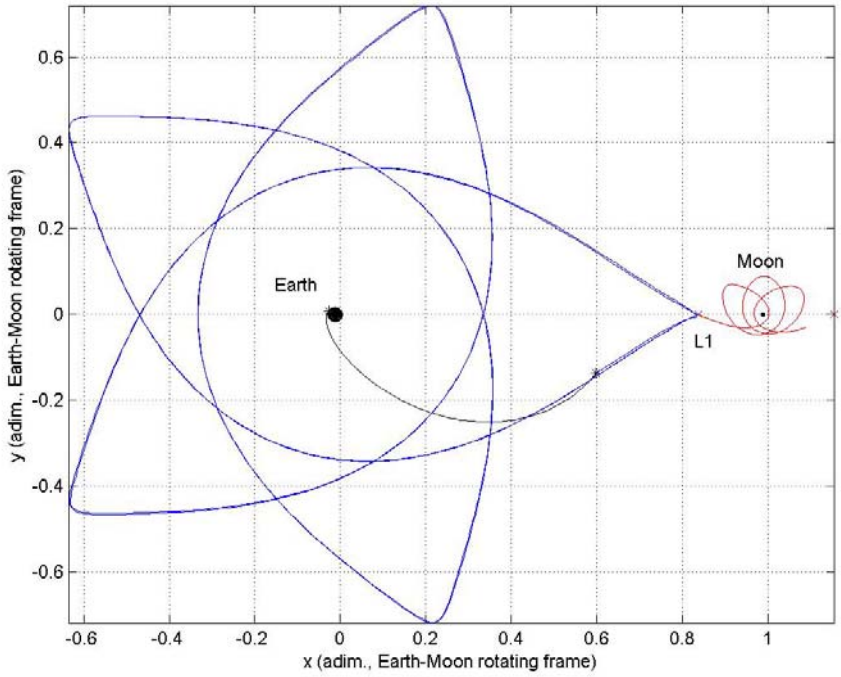

Figure 298: Identified solution: trajectory representation.

It is interesting to note that the transfer trajectory corresponding to the solution identified by MCS seems to belong to the family of solutions indicated in the objective function structure analysis as subgroup 6. However, the time spent on the stable manifold is higher than in subgroup 6: subgroup 6 corresponds to

values of t_W of about 85 *d*, while the solution identified by MCS has a value of t_W equal to 150 *d*, that is the upper limit for such variable. This observation let us understand that the identified solution corresponds to a transfer configuration similar to that of subgroup 6, but occurring in a different revolution of the spacecraft around the Earth on the conic-like orbit in the Earth-centred inertial frame. The characteristics of the identified solution, which will be used for performance comparisons with the other optimization algorithms, are reported in Table 196.

Evaluation criterion	Identified solution
ΔV [*m/s*]:	3594.321
Model function evaluations:	585
Runtime [STU]:	3.719

Table 196: Characteristics of the identified solution.

In order to better analyse the previous consideration about the identified solution, a local optimization process is now performed by means of a SQP based algorithm to accurately identify the local minimum corresponding to the reached basin of attraction. The solution identified by MCS is considered as the starting point for the local search process. The starting solution and the improved one are reported in Figure 299 on the *nFunc-ΔV* plane, while Figure 300 plots the transfer trajectory corresponding to the improved solution.

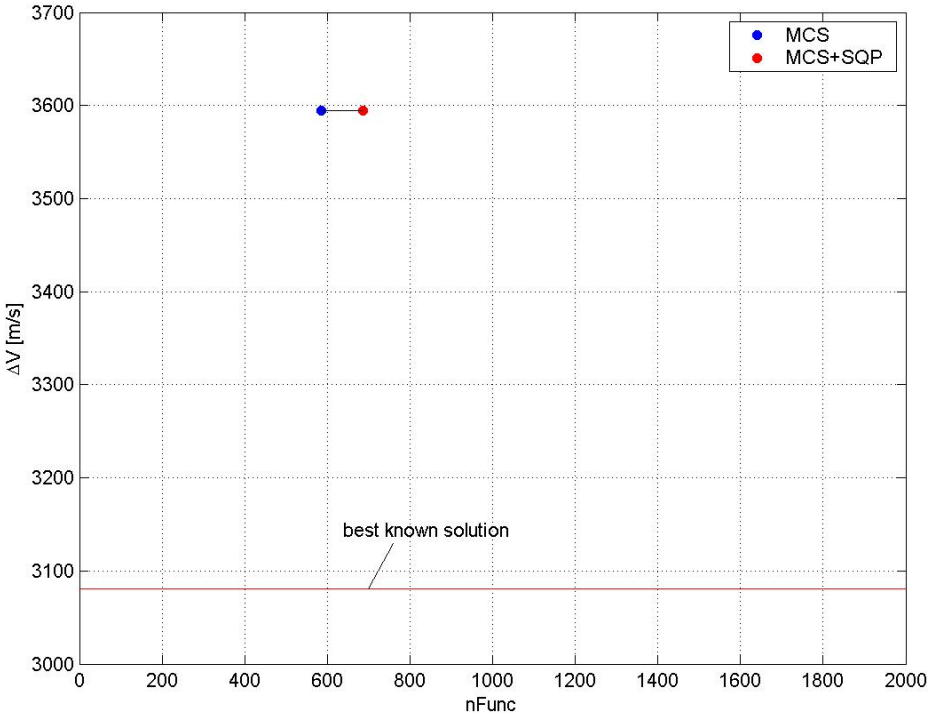

Figure 299: Distribution of the improved solution at the end of a local optimization process on the *nFunc-ΔV* plane.

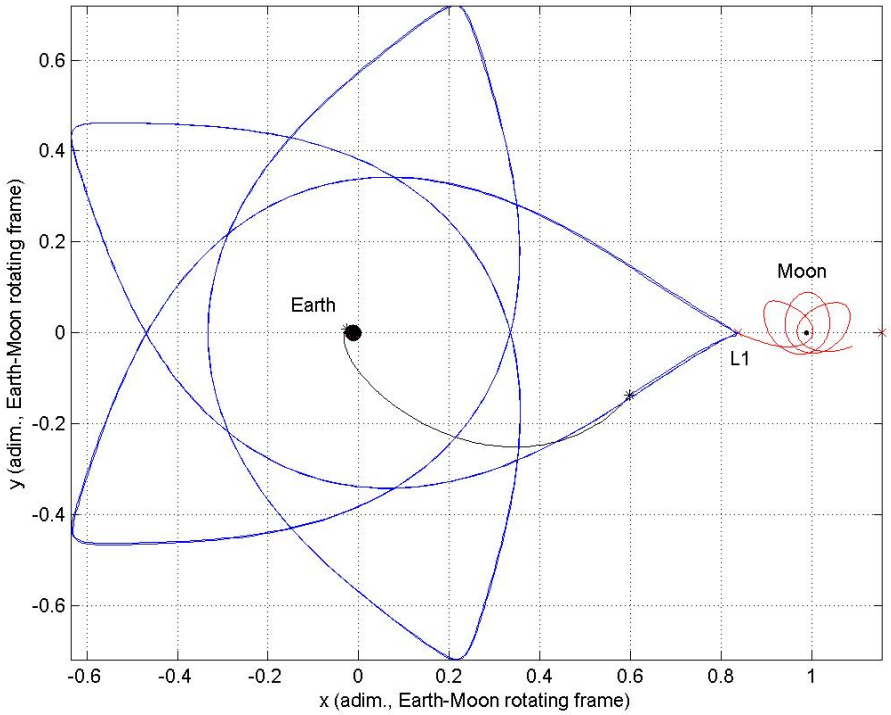

Figure 300: Improved solution via local optimization process: transfer trajectory.

Figure 299 and Figure 300 show that the local optimization process only slightly improves the solution identified by MCS. This is due to the fact that such solution lies on the upper limit admissible value of the time spent on the stable manifold to *L1*: a further improvement could be allowed by increasing this limit. Anyway, the local optimization process confirms that the solution identified by MCS does not lie in the basin of attraction of the best known one and does not belong to any of the families of lunar transfers characterized in the objective function structure analysis. Similarly to the previous cases, such result is evident by analysing Table 197, which reports, corresponding to the MCS+SQP run, the reached objective function value and the distance (in Euclidean metric) with respect to the best known solution.

	ΔV **[*m/s*]**	**Distance**
MCS+SQP run	3594.315	0.419

Table 197: MCS+SQP optimization run: objective function value and Euclidean distance in the normalized search space with respect to the best known solution.

By considering two solutions as identical when the Euclidean distance is less than 1% of the hyper diagonal of the normalized search space, that is 0.017 in a 3-dimensional space, MCS run was not able to identify the basin of attraction of the best known solution. As already stated for previous analyses, although MCS algorithm is a global optimization algorithm, it has the important feature of keeping, in a so called “shopping basket”, good points reached during the optimization process. Figure 301 illustrates the whole shopping basket kept by MCS during the performed optimization process.

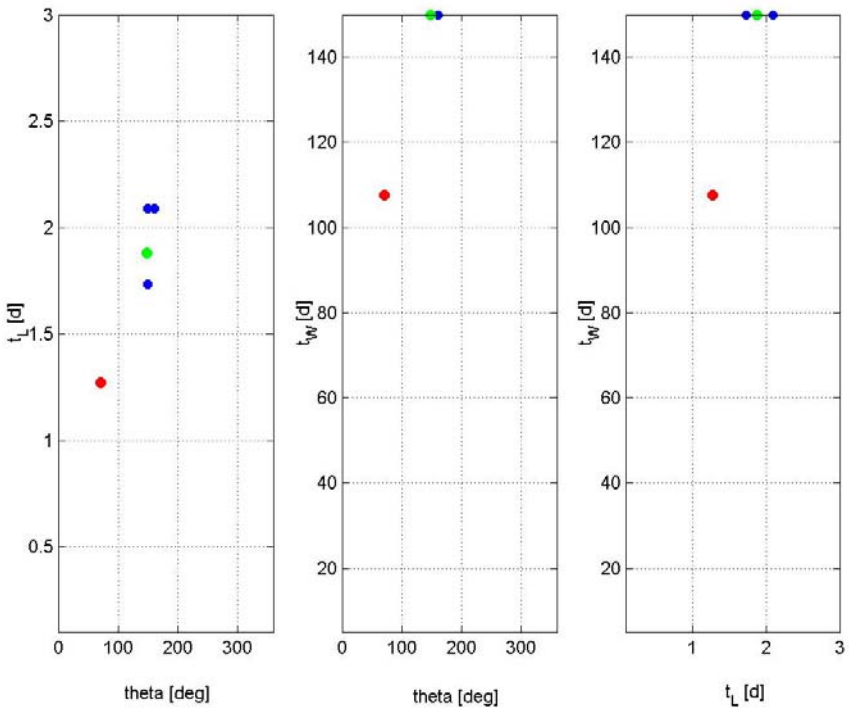

Figure 301: Shopping basket at the end of the optimization process.

Figure 301 shows that MCS shopping basket got trapped in the boundary region of the search space lying on the upper limit of the time spent on the stable manifold, without keeping information of other promising regions of the search space.

rbfSolve

As rbfSolve algorithm implements a deterministic optimization approach, based on objective function response surface assessment and analysis suitable for costly objective function problems, statistical features analysis don't hold here. Only one run have been processed in order to solve the previously defined problem. Default options suggested by the providers of the code have been used. As already stated in the other mission analysis test problems, the termination conditions available in TOMLAB version of rbfSolve tool (which is not freely available) do not include suitable rules for practical problems with not a priori information about the global optimum solution. As a consequence, a maximum number of objective function evaluations has been fixed for terminating the optimization process. The previous analysis showed that, in

case of the problem of lunar transfers using libration points, the number of objective function evaluations was high: GATBX-migr required about 7000 objective function evaluations. However, as already noted in Multiple Gravity Assist and Low Thrust direct planet-to-planet transfers analyses, rbfSolve is tailored for costly optimization processes and can not dealing with a high number of objective function evaluations due to the high required memory for handling the interpolation process. As a consequence, a maximum number of objective function evaluations of the order of 10^3 had to be fixed. As it concerns the validity of the achieved results, considerations similar to those highlighted in case of Multiple Gravity Assist hold in this case also: in particular, if the response surface algorithm is not able to identify and accurately approximate the basin of attraction of the global optimum in a low number of objective function evaluations, it is likely the case the response surface based algorithm has not converged to the global optimum solution. Hence, the fixed number of objective function evaluations has been set again to 1000.

Algorithm parameters	
Maximum number of objective function evaluations:	1000

However, as already occurred in the 2-impulse direct planet-to-planet transfer problem, a particular exit condition terminated the optimization process, which typically happens when the approximating surface generated by the algorithm can not improve due to the generation of successive identical solutions for improving the interpolation surface; the maximum number of successive identical solutions is automatically set by rbfSolve algorithm once used the default options. Table 198 and Table 199 report the identified solution compared with the best known solution.

Search space		
Design variable	**Identified solution**	**Best known solution**
θ [*deg*]:	128.096	70.835
t_L [*d*]:	2.094	1.273
t_W [*d*]:	99.959	107.670

Table 198: Comparison between the identified solution and the best known solution: search space.

Objective function space		
Term	**Identified solution**	**Best known solution**
ΔV [*m/s*]:	3579.249	3080.767
ΔV_I [*m/s*]:	3320.974	3080.756
ΔV_F [*m/s*]:	258.274	0.011

Table 199: Comparison between the identified solution and the best known solution: objective function space.

The previous tables show that the solution identified by rbfSolve does not coincide in fact with the best known solution, as confirmed by the trajectory representation; this can be see in Figure 302.

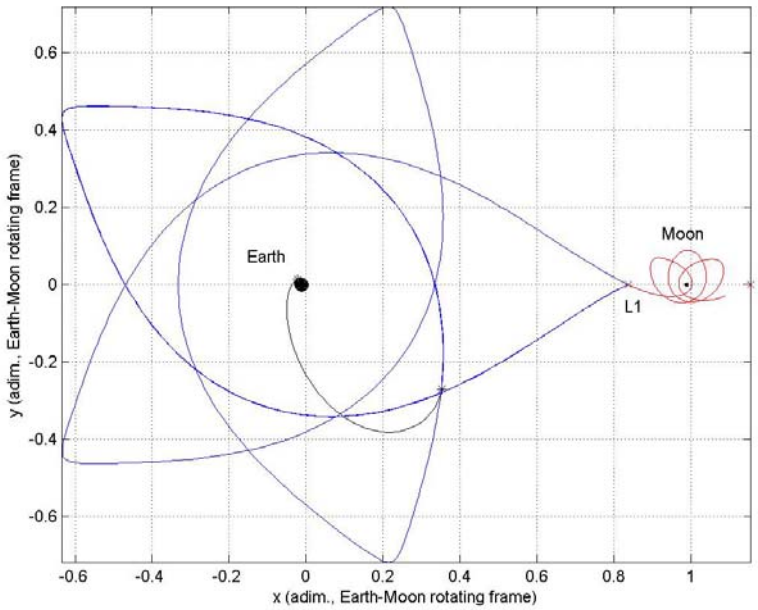

Figure 302: Identified solution: trajectory representation.

Similarly to the results gained in case of DE and glbSolve tools application to the problem of lunar transfer using libration points, the best solution identified by rbfSolve is not related to any family of solutions identified in the objective function structure analysis. Actually, it seems to be related to the previously identified set of families of lunar transfers characterized by a Lambert's three-body arc injecting the spacecraft in the stable manifold corresponding to points near the apogee of the conic-like orbit in the Earth-centred inertial frame on the line coming out from it. Table 200 reports the characteristics of the identified solution, which will be used for performance comparisons with the other optimization algorithms.

Evaluation criterion	Identified solution
ΔV [*m/s*]:	3579.249
Model function evaluations:	474
Runtime [STU]:	6.128

Table 200: Characteristics of the identified solution.

In order to accurately identify the local minimum reached by *rbfSolve* algorithm, a SQP based algorithm is now used to perform a local optimization process, where the solution identified by *rbfSolve* is considered as the starting point for the local search process. The starting solution and the improved one are reported in Figire 303 on the *nFunc-ΔV* plane, while Figure 304 plots the transfer trajectory corresponding to the improved solution.

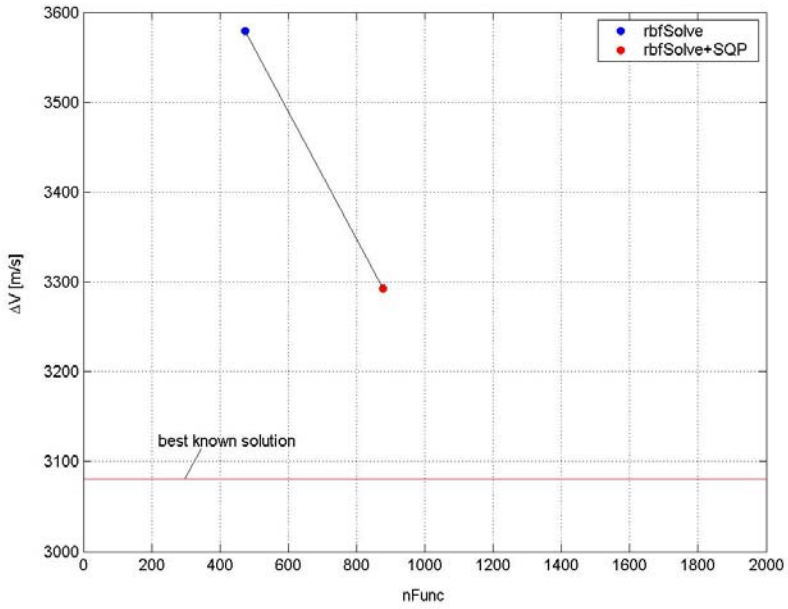

Figure 303: Distribution of the improved solution at the end of a local optimization process on the *nFunc-ΔV* plane.

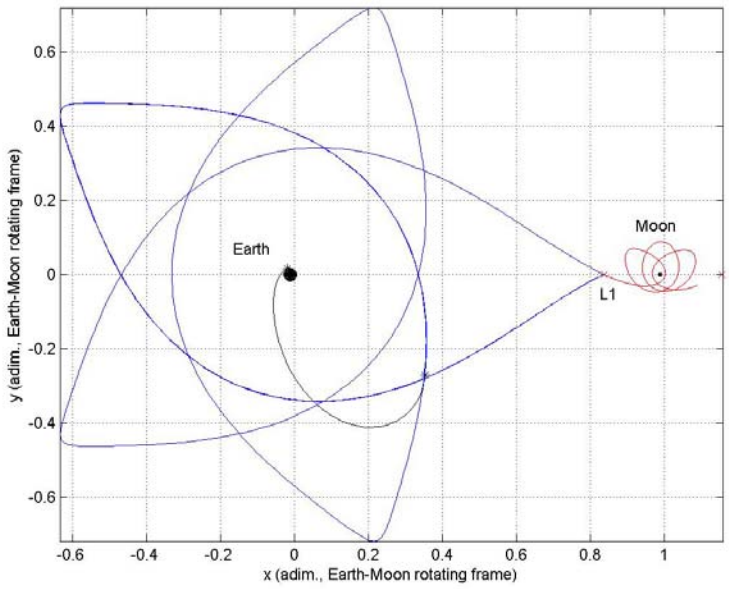

Figure 304: Improved solution via local optimization process: transfer trajectory.

The local optimization process does not change the feature of the transfer trajectory, which confirms to not belong to any of the families of lunar transfers characterized in the objective function structure analysis. Such a result is showed Table 201, which reports, corresponding to the rbfSolve+SQP run, the reached objective function value and the distance (in Euclidean metric) with respect to the best known solution.

	ΔV [*m/s*]	Distance
rbfSolve+SQP run	3292.968	0.394

Table 201: rbfSolve+SQP optimization run: objective function value and Euclidean distance in the normalized search space with respect to the best known solution.

By considering two solutions as identical when the Euclidean distance is less than 1% of the hyper diagonal of the normalized search space, that is 0.017 in a 3-dimensional space, rbfSolve run was not able to identify the basin of attraction of the best known solution. One of the output of the optimization process is the matrix of all sampled points in the search space, which are shown in Figure 305 (the identified solution is highlighted by a green dot, compared with the best known one which is indicated by a red dot).

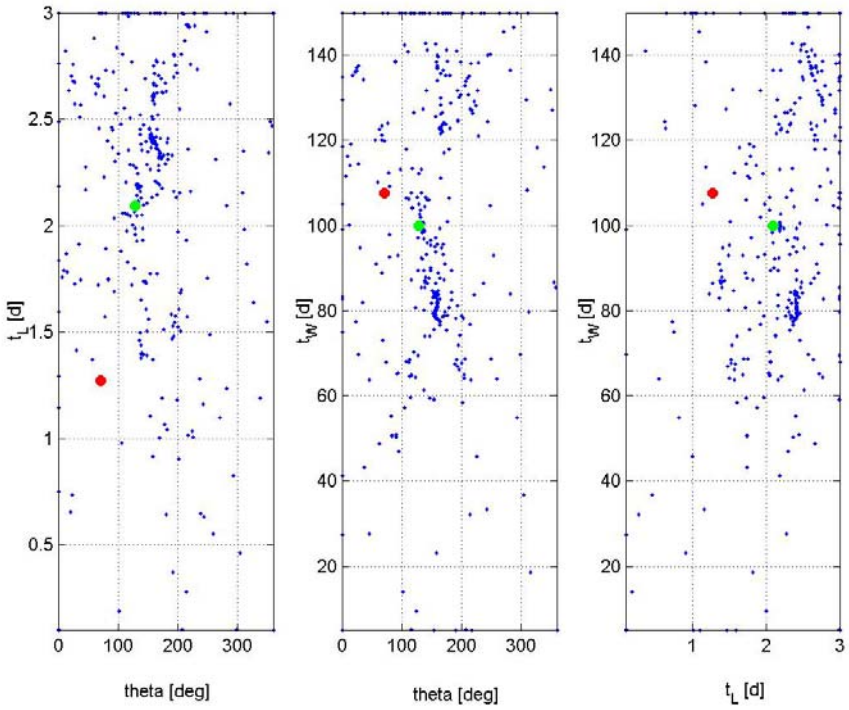

Figure 305: Distribution of all sampled points during the optimization process.

Figure 305 shows that the algorithm do not accurately sampled the region of the search space near the global optimum solution. Note that the objective function model has discontinuities in the search space and, as stated in previous analyses, global optimization algorithms based on response surface methodologies have well-known difficulties in handling such objective function structure.

Summary of results:

Table 202 reports the summary of results for the problem of lunar transfer using libration points in a tabular form.

Algorithm	ΔV [*m/s*]	Fun. evaluations	Runtime [STU]
GAOT	3292.3 (σ = 194.112)	2089.3 (σ = 1592.775)	8.327 (σ = 6.252)
GAOT-shared	3597.104 (σ = 216.418)	606.2 (σ = 151.610)	1.836 (σ = 0.545)
GATBX	3208.216 (σ = 162.882)	5710 (σ = 2999.096)	38.668 (σ = 19.305)
GATBX-migr	3203.474 (σ = 111.245)	7050 (σ = 2144.968)	53.471 (σ = 14.408)
FEP	3274.49 (σ = 154.361)	2369.5 (σ = 1575.07)	14.089 (σ = 15.007)
DE	3432.502 (σ = 184.87)	1096.2 (σ = 322.346)	2.945 (σ = 1.029)
ASA	3162.392 (σ = 131.859)	4825.1 (σ = 82.108)	31.361 (σ = 3.894)
glbSolve	3359.19	1311	5.24
MCS	3594.321	585	3.719
rbfSolve	3579.249	474	6.128

Table 202: Summary of results for the problem of lunar transfers using libration points.

By proceeding in analogy with the previous mission analysis classes, due to the partially conflicting performance criteria considered in this work, concepts and techniques typically adopted in multiobjective optimization problems (such as the concept of the Pareto dominance) are here used in order to assess the optimization algorithms performances. As already stated, due to the presence of not optimized codes among the tested ones and to the necessity of creating a MEX file for ASA algorithm (which slightly affects the runtime performances), the main evaluation criteria to be considered have been taken as the best objective function value reached, ΔV, and the number of model function evaluations needed, *nFunc*. Figure 306 reports such performances in a ΔV - *nFunc* plane in order to identify the Pareto optimal solution (the red line in figure representing the best known solution).

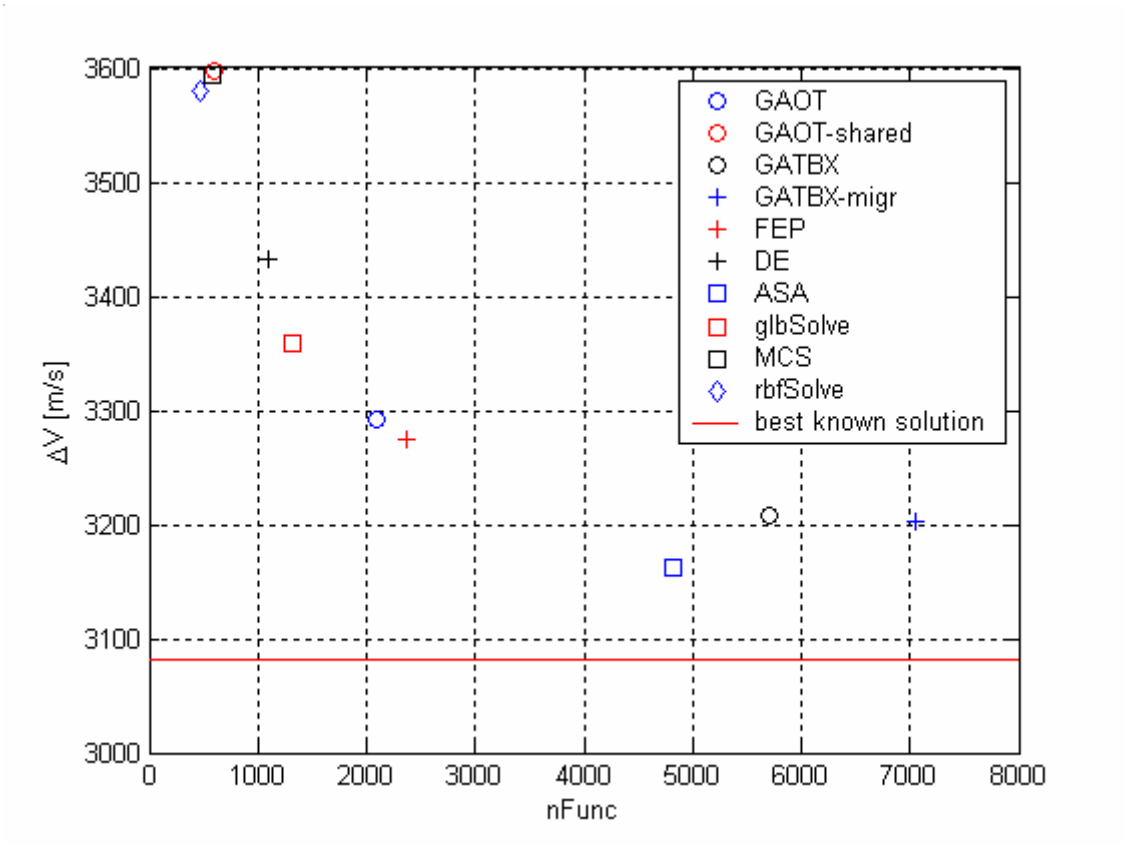

Figure 306: Algorithms performances in the ΔV - *nFunc* plane.

Note that Figure 306 reports the performances listed in Table 202, which contains statistical performances in case of randomized optimization algorithms. By applying the concepts of Pareto dominance, Table 203 reports for each algorithm, the number of algorithms which dominated, and then outperformed it.

Algorithm	# of dominating algorithms
GAOT	0
GAOT-shared	2
GATBX	1
GATBX-migr	1
FEP	0
DE	0
ASA	0
glbSolve	0
MCS	1
rbfSolve	0

Table 203: Number of dominating algorithms.

Table 203 shows that a wide set of Pareto optimal solutions can be identified: the algorithms which best solved the problem of lunar transfer using libration points (in a Pareto optimal sense) are GAOT, FEP, DE, ASA, glbSolve, and rbfSolve, whose performances are highlighted in Figure 307.

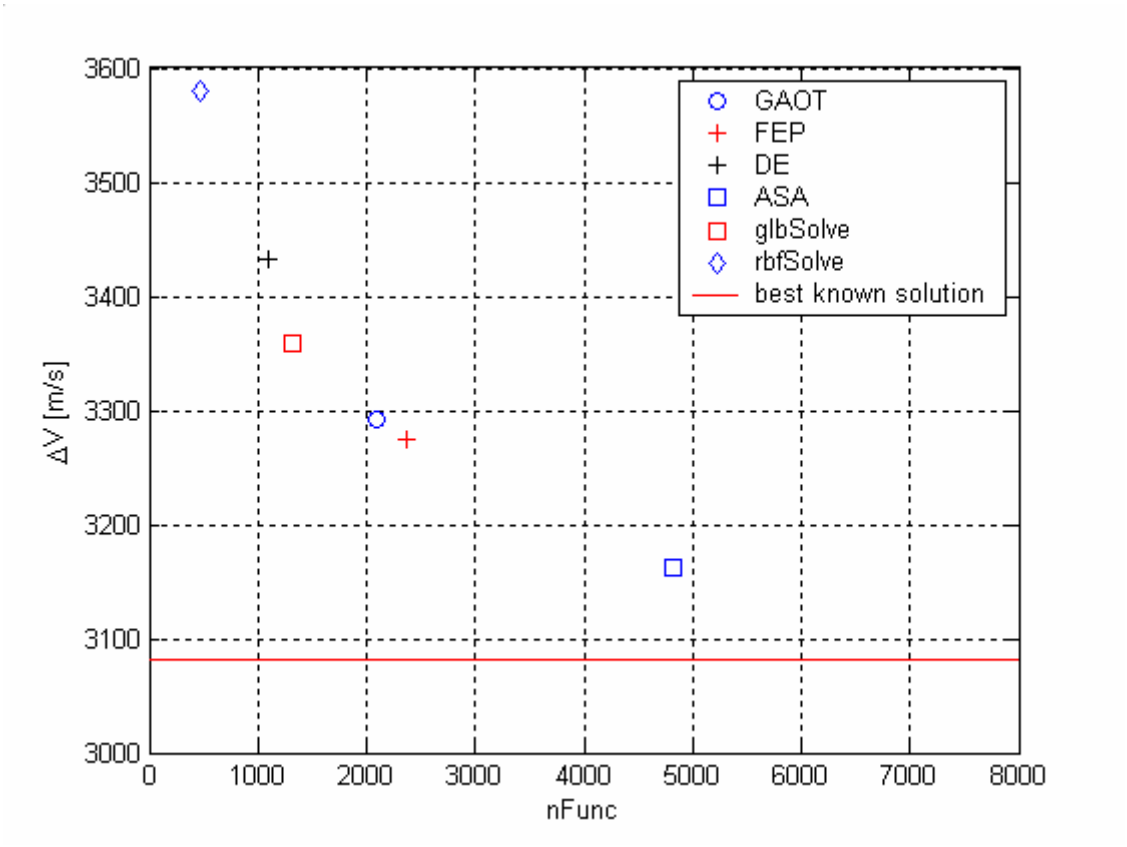

Figure 307: Pareto optimal algorithms.

In particular, it is worth noting that GATBX and GATBX-migr algorithms, which in fact are based on the same genetic operators (although the migration operator is involved in GATBX-migr), where completely dominated by ASA algorithm, which could reach a better objective function value in a lower number of objective function evaluations. This is not the case if compared with the remaining optimization tools, where a Pareto equivalence holds. However, we must take care of the results gained: as noted in the previous analysis and as will be reported later, most optimization tool couldn't identify the basin of attraction of the best known solution and only few optimization runs could reach local optima solutions comparable with the best known one. As a consequence, the results presented in Table 202, Table 203 and Figure 306 should be simply related to the use of the algorithms as black box tools for solving mission analysis related optimization problems and they indicate the mean performances of the tools in case of the randomized algorithms or the right performance in case of the deterministic ones. For the sake of completeness, in

analogy with the previous mission analysis classes, consider now the runtime performances and let analyze the consequences of including the runtime performance on the identification of the Pareto optimal algorithm. We have now three performance criteria. Figure 308 and Figure 309 report the algorithms performances in the ΔV - *runtime* plane and in the *nFunc* - *runtime* plane respectively, which have not been considered so far.

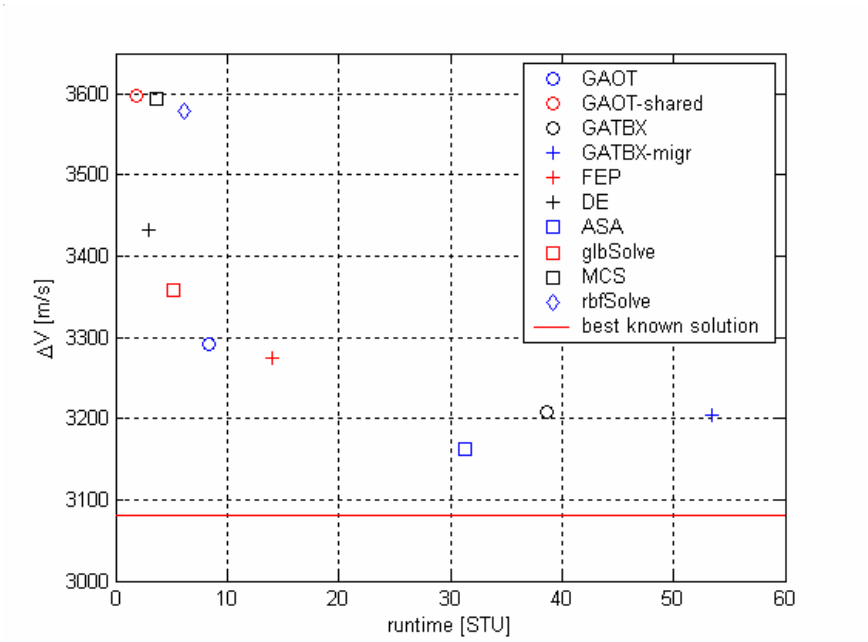

Figure 308: Algorithms performances in the *nFunc* - *runtime* plane.

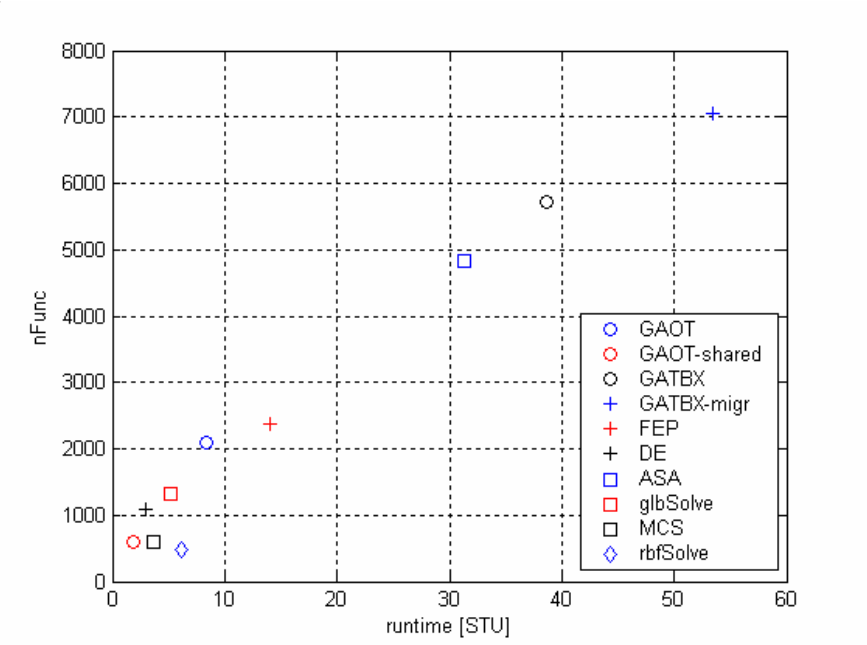

Figure 309: Algorithms performances in the *nFunc* - *runtime* plane.

By applying again the concepts of Pareto dominance in this three-criteria case, Table 204 reports for each algorithm, the number of algorithms which dominated it.

Algorithm	# of dominating algorithms
GAOT	0
GAOT-shared	0
GATBX	1
GATBX-migr	1
FEP	0
DE	0
ASA	0
glbSolve	0
MCS	0
EGO	0

Table 204: Number of dominating algorithms in the three criteria case.

Table 204 shows that the set of Pareto optimal algorithms now includes also GAOT-shared and MCS algorithms. Finally the goodness of the basin of attraction identified by the various algorithms is analysed, as resulting from the local optimization processes performed at the end of each algorithm run. First of all, Table 205 reports the successful runs corresponding to the optimization algorithms which were able to identify the basin of attraction of the best known solution (note that for randomized algorithms the number of successful runs over the total number of performed runs is reported).

Algorithm	Success
GAOT	0/10
GAOT-shared	0/10
GATBX	1/10
GATBX-migr	1/10
FEP	1/10
DE	0/10
ASA	0/10
glbSolve	No
MCS	No
EGO	No

Table 205: Algorithms performance in identifying the basin of attraction of the best known solution.

Table 205 shows that the rate of success of all algorithms was really low: this is mainly related to the stiffness of the analysed optimization problem which is associated to the presence of several comparable local minima. However, by revising the achieved results and by referring to the objective function structure analysis, it is worth noting that most algorithms could have more success in the identification of local minima belonging to the identified set of lunar transfer families comparable to the best known one in terms of objective function values. This led to the decision of reporting such successful runs together with those which identified the basin of attraction of the best known solution (see Table 205), by considering them as representative of good algorithm performances and included in Table 206.

Algorithm	Success
GAOT	5/10
GAOT-shared	2/10
GATBX	6/10
GATBX-migr	4/10
FEP	4/10
DE	0/10
ASA	7/10
glbSolve	No
MCS	No
rbfSolve	No

Table 206: Algorithms performance in identifying the basin of attraction of the best known solution.

Table 206 shows that ASA algorithm turned out to have the highest rate of success in reaching the basin of attraction of good solutions. As a consequence, in order to identify the best performing algorithm in case of the problem of lunar transfer using libration points, by combining information coming up from Pareto optimality analysis, carried out on the ΔV – *nFunc* two criteria case, and rate of success investigation, whose results are reported in Table 206, we can state that:

- The non randomized codes glbSolve, MCS and rbfSolve, due to their inability to identify basin of attractions corresponding to neither the best known solution nor the comparable ones characterized in the objective function structure analysis, can not be considered as suitable for solving the previously identified problem.

- GATBX and GATBX-migr algorithms have been outperformed by ASA tool in both Pareto optimality and effectiveness at identifying the basin of attraction

of good solutions. In fact, one can observe that they were the only ones which were able to identify the basin of attraction of the best known solution; however, such a result was reached only corresponding to 1/10 runs, which seems to the authors a too low percentage for justifying the use of this success for preferring them to remaining algorithms.

- Due to the relatively low rate of success at identifying basin of attractions of good solutions in comparison with the remaining algorithms, DE and GAOT-shared are not included in the set of well performing optimization tools for the problem here analysed.

As a consequence, GAOT, FEP and ASA turned out to be the best performing tools for the problem of lunar transfer using libration points. Their performances are highlighted in Figure 310, which reports the corresponding results in the ΔV – *nFunc* plane, and Table 207, which reports their rate of success at identifying the basin of attraction of good solutions.

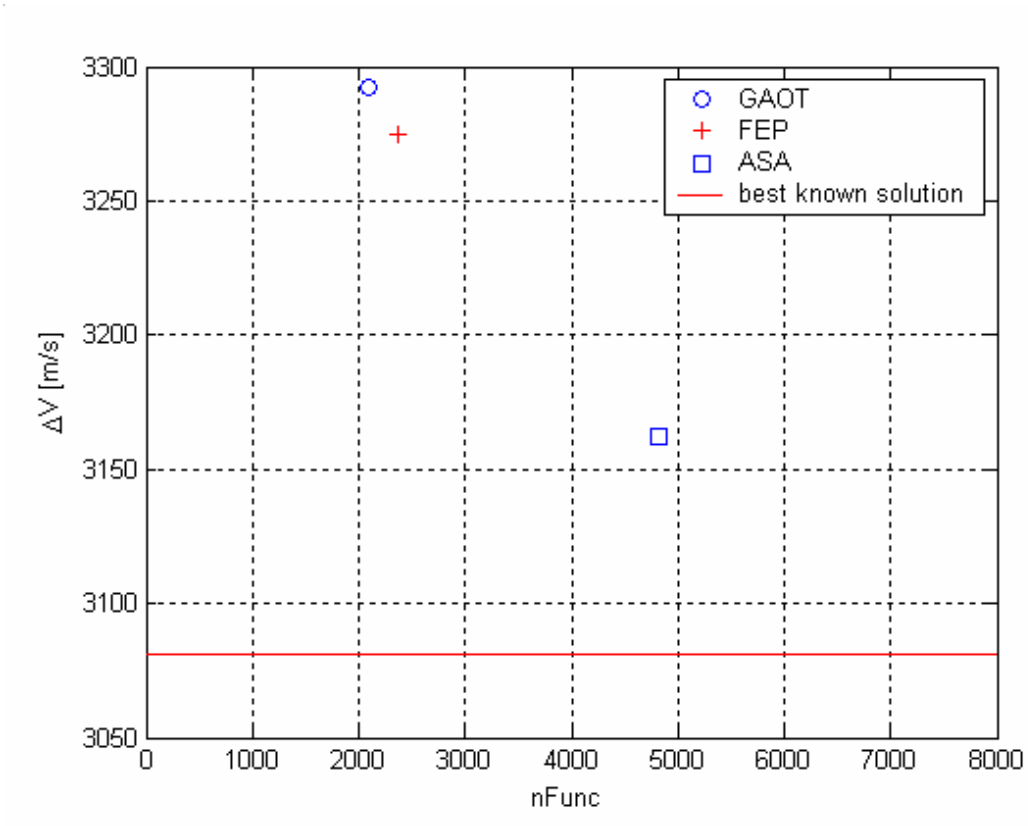

Figure 310: GAOT, FEP and ASA performances in the ΔV - *nFunc* plane.

Algorithm	Success
GAOT	5/10
FEP	4/10
ASA	7/10

Table 207: GAOT, FEP and ASA performances in identifying the basin of attraction of the best known solution.

Figire 310 and Table 207 show that ASA could reach a better mean objective function value with more effectiveness at identifying the basin of attraction of solutions comparable to the best known one (which belong to the set of lunar transfer families identified in the objective function structure analysis); however, it meanly required a number of objective function evaluations which is about twice the number necessary to GAOT and FEP, which anyway turned out to have good values of the rate of success (see Table 207).

11. CONCLUSIONS AND RECOMMENDATIONS

This work has been carried out under an European Space Agency contract in the context of the Ariadna program during the six months period April-October 2004. The aim of this study was an investigation of the effectiveness of some global optimisation techniques at solving practical problems related to space trajectory design. Four mission analysis classes have been investigated: the two impulse direct planet-to-planet transfer problem (referring to an Earth-Mars transfer), the Multiple Gravity Assist interplanetary transfer problem (referring to an Earth-Saturn transfer), the low thrust direct planet-to-planet transfer problem (referring again to an Earth-Mars transfer) and the problem of lunar transfer using the interior libration point *L1* in a Restricted Three Body Problem environment. In the framework of each corresponding optimisation problem, a suitable objective function has been defined for performing single objective optimisation processes. Hence, proper mathematical models have been used for the evaluation of relevant quantities for the objective function assessment and, consequently, appropriate design variables have been selected, defining the search space. Box-constrained optimisation problems have been taken into account by defining proper upper and lower bounds for each design variable, while possible inequality constraints have been treated using the classical approach of defining the objective function as a suitable weighted sum of several terms, including the constraints violation. Once the optimisation problem has been fully defined, an exhaustive and systematic analysis of the resulting objective function structure has been performed in order to identify typical features which would mostly affect the global search; discontinuity as well as non-differentiability regions have been identified over the search space and particular care has been taken to characterize the objective function in the neighbourhood of the best known solution, as this constitutes a remarkable feature strongly affecting the effectiveness of some global optimisation algorithms at identifying it. The use of a multi-start search using local optimisation processes starting from initial guesses randomly distributed over the search space assisted the systematic analysis and allowed the identification of big valley structures. Such structures

turned out to be mainly related to the periodicity of all the investigated objective functions with respect to particular design variables, as the time spent on the stable manifold to L1 in case of lunar transfer using the interior libration point *L1* and the date of departure from Earth in the remaining test cases.

Following this complete and comprehensive objective function structure analyses have been carried out, and a set of global optimisation tools has been selected for testing purposes. The set embraced classical genetic algorithms including different genetic operators for performing the global search (GAOT and GATBX), genetic algorithms with sharing and migration operators (GAOT-shared and GATBX-migr respectively), evolutionary programming (Fast Evolutionary Programming, FEP), differential evolution (DE), an improved simulated annealing (Adaptive Simulated Annealing, ASA), branching methods (glbSolve and MCS), response surface based optimisation algorithms (rbfSolve) and, in some cases, an innovative hybrid systematic-heuristic method combing branching techniques and evolutionary programming (EPIC). The previously described optimisation problems corresponding to the four different mission analysis classes have been submitted to the whole set of global optimisation tools and an extensive study has been carried out in order to recognize suitable problem-method relation corresponding to the identification of the best performing algorithms for each mission analysis problem. By considering the objective function value reached at the end of the optimisation process, the number of objective function evaluations performed required and the effectiveness at identifying the basin of attraction of the best known solution as well as of good solutions comparable to the best known one, results of the test phase can be resumed as follows:

- *Two impulse direct planet-to-planet transfer problem*: due to its deterministic features, the success at reaching the best known solution and the corresponding relatively low number of required objective function evaluations, Multilevel Coordinate Search (MCS) turned out to outperform all the remaining algorithms, thus resulting as the best performing one.

- *Multiple Gravity Assist interplanetary transfer problem*: in case of interest on the only mean objective function value reached and mean number of objective function evaluations required as main evaluation criteria, EPIC turned out to be the most advisable one for practical use in space trajectory design optimization; however, due to lack of information about the effectiveness of EPIC at identifying the basin of attraction of the best known solution (not necessarily related to better mean objective function values, because of the presence of several comparable local optima), GAOT resulted to have the highest rate of success in solving the global search problem;

- *Low thrust direct planet-to-planet transfer problem*: low rate of success characterized all the tested algorithms at identifying the basins of attraction of both the best known solution and solutions comparable to it. In such an environment Differential Evolution (DE) and EPIC turned out to constitute the best compromises based on the previously described performance criteria. Anyway, it should be noted that no information is available about the EPIC rate of success; however, the impressive results of its global search in terms of mean objective function value seem to be indicative of particularly good performances even in this sense, especially if compared with the scarce results of the other tools. As a consequence the authors think that more comprehensive analyses should be performed on EPIC, which seems to represent the most promising global optimization tool for solving the low thrust direct planet to planet transfer problem;

- *Problem of Lunar transfer using the interior libration point L1*: GAOT, FEP and ASA turned out to be the best performing ones. In particular, ASA could reach a better mean objective function value with more effectiveness at identifying the basin of attraction of solutions comparable to the best known one if compared with GAOT and FEP, which performed in a similar way in fact; however, it meanly required a number of objective function evaluations which is about twice the

number necessary to GAOT and FEP, which anyway turned out to have good rates of success.

Moreover, general considerations can be stated about the test results for some global optimisation tools. The effects of the sharing operator on the GAOT scheme can be highlighted: by promoting the diversity of the individuals in the population, the sharing operator hinders the concentration of the individuals around the optimal solutions; this led to low accuracy at describing the optimum solutions and to a premature optimisation process arrest because the stopping criteria easily became active. It is worth noting that, as stated above, no tuning procedures have been performed on the available tools and so GAOT default options have used even using the sharing operator. However, as reported in [Sareni, and Krähenbuhl, 1998], sharing should use low recombination operators to promote stability of generated subpopulation and to avoid the formation of poor individuals. As a consequence, future works must address such a matter, by deeply investigating the effects of tuning processes on GAOT-shared scheme to enhance the global search and to promote the preservation of subpopulations, even allowing the simultaneous identification of distinct optimal niches over the search space. Moreover, it is interesting to note how the migration operator always led to improvements on the mean value of objective function reached at the end of the optimisation processes: as a consequence, it can be stated that the migration operator allowed evident improvements in the effectiveness of the global search. However, it should be noted that such improvements always resulted in corresponding higher values of number of objective function evaluations performed. Moreover, interesting analyses could be performed in future works for comparing performances gained by sharing and migration operators: indeed, such techniques aim to promote both a broad global search over the search space and the maintenance of subpopulations for identifying several local optima corresponding to each algorithm run. Then, comparative studies should be performed for recognizing the most suitable technique for this purpose; however, as stated above, a tuning procedure on recombination operators should be carried out first in case of using sharing operators. Furthermore, it is quite impressive to note how the deterministic

glbSolve and, in particular MCS, tools lost their good performances in passing from the two impulse direct planet-to-planet transfer problem to the remaining ones: the high multimodality and the fragmentation of the big valley structures associated to Multiple Gravity Assist interplanetary transfers with a high number of gravity assist manoeuvres could be investigated as the main reason of such behaviour in this problem; as it concerns the problem of lunar transfer using the interior libration point L1, because of the highlighted important difficulties of glbSolve and MCS, the presence of discontinuities in the neighbourhood of the best known solution identified in the objective function structure analysis certainly affected the performances of such tools in this second mission analysis problem; however, no clear explanations could be identified of the scarce performances showed by these deterministic tools in solving the low thrust direct planet-to-planet transfer problem. Finally, performances showed by rbfSolve, which could not identify the basin of attraction of good solutions in none of the performed tests, seem to be associable to the well known difficulties of response surface based global optimisation algorithm at handling optimisation processes on discontinuous and non-differentiable objective functions. However, it should be noted again that no clear insights have been identified on the scarce performances in case of the low thrust direct planet-to-planet transfer problem.

It is worth noting that, off course, limitations affects the achieved results. First of all, each mission analysis class has been investigated by selecting a particular transfer problem and by facing it with proper, but anyway particular, mathematical models. The authors believe that the decisions taken about such a matter in this work can be considered as representative of practical interesting problems in space trajectory design. However, further analyses should be performed, including additional transfer problems, alternative mathematical models and search space definitions for getting a more complete insight in the broad field of mission analysis. Secondly, it is widely known in the global optimisation community that optimisation algorithms can be suitably tuned to enhance their performances. However, as already occurred in remarkable existing comparative studies (Neumaier et al., 2004), due to the comparative

purposes of this work, the large scale of comparisons performed, the available devices and the high time required by some optimisation case, it was impossible to do such tuning. Finally, regarding the termination condition, note that, as stated by Huyer and Neumaier [Huyer and Neumaier, 1999] and already described in previous chapters, in practical global optimisation problems such as those analysed in this work, one does not know the solution in advance and needs a criterion that tells the program when to stop searching for a better local optimum. For those algorithms where such a criterion was not included, a common stopping rule has been developed and implemented, which appeared to be suitable and robust. However, the achieved results are necessarily strictly affected by the employed stopping criterion. Nevertheless, the effects of the stopping criteria on the algorithm performances were not addressed here, where most algorithms have been used as black-box tools.

As a final remark, the authors would like to recommend future extensive works on assessing the sure benefits of a better management of the mathematical techniques used for the objective function evaluation in the problem of lunar transfer using the interior libration point L1, particularly referring to the penalty terms employed in case of non convergence of the shooting algorithm for the solution of the Lambert's three-body problem. Moreover, a better investigation of EPIC performances should be accomplished: thanks to its combination of systematic and evolutionary techniques, EPIC tool seemed to handle the global search in a more effective way. Finally, this work could be considered as a contribution to the complex identification of the most promising global optimisation techniques for solving practical problems in space trajectory design optimisation; further extensive studies are necessary to address such a matter and the development of tailored global optimisation tools for mission analysis should be promoted, as they certainly will lead to better results if compared to those achieved by the classical black-box tools here investigated.

APPENDIX 1: NOTES ON NP-COMPLEXITY

It has been stated that convex quadratic programming is solvable in polynomial time with the ellipsoid method or an interior point method [Vavassis, 1995]. However a quadratic function:

$$f(\ ) = \frac{1}{2}\ \ ^{T} H\ \ + c^{T} \qquad [37]$$

is convex if *H* is positive semidefinite, i.e., if all the eigenvalues of *H* are nonnegative. Even if only one eigenvalue is negative, the problem turns out to be NP-hard [Pardalos and Vavasis, 1991].

The mission analysis problems analysed in this report are not quadratic, but they can be locally approximated with a quadratic function. This suggest the following question: if it is possible to show that the objective function is locally non-convex, meaning that at least one of the eigenvalues of the locally defined *H* is negative, could one state that the global search is then NP-hard? The answer to this important question will constitute an important subject for future developments.

REFERENCES

Betts, J.T., Orb, S.O.: 'Optimal Low Thrust Trajectories to the Moon', *SIAM Journal of Applied Dynamical Systems*, Vol. 2, No. 2, pp. 144-170, 2003.

Dachwald, B.: 'Optimisation of Solar Sail Interplanetary Trajectories Using Evolutionary Neurocontrol', *Journal of Guidance Control and Dynamics*, Vol. 27, No. 1, pp. 66-72, 2004

Dixon, L.C.W., and Szegö, G.P.: The global Optimization Problem: an introduction. In *Towards Global Optimisation 2*, North-Holland, Amsterdam (L.C.W. Dixon and G.P. Szegö eds.), pp. 1-15. 1978.

Gurfil, P., Kasdin, N.J.: 'Niching Genetic Algorithms-based Characterization of Geocentric Orbits in the 3D Elliptic Restricted Three-body Problem', *Computer Methods in Applied Mechanics and Engineering*, Vol. 191, pp. 5683-5706, 2002.

Hughes, G., and McInnes, C.R.: 'Solar Sail Hybrid Trajectory Optimisation', *Advances in the Astronautical Sciences*, Vol. 109, pp. 2369-2380, 2001.

Jones, D.R., Perttunen, C.D. and Stuckman, B.E.: 'Lipschitzian Optimization without the Lipschitz Constant'. *Journal of Optimization Theory and Applications*, Vol. 79, pp. 157-181, 1993

Pardalos, P. M., Vavasis, S. A.: 'Quadratic Programming with one Negative Eigenvalue is NP-hard', Journal of Global Optimisation, Vol. 1, pp. 15-22, 1991.

Pintér, J.D.: 'Global Optimization: software, test problems, and applications', In, *Handbook of Global Optimization* (Horst, R. and Pardalos, P.M., eds.), Kluwer Academic Publishers, Dordrecht Boston London, 1995.

Reeves, C.R., Yamada, T.: 'Genetic Algorithms, Path Re-linking and the Flowshop Sequencing Problem', *Evolutionary Computation*, Vol. 6, pp. 45-60, 1998.

Shcherbina, O, Neumaier, A., Sam-Haroud, D., Vu, X.H., Nguyen, T.V.: Benchmarking Global Optimization and Constraint Satisfaction Codes. *COCOS 2002*, pp: 211-222, 2002.

Vavasis, S. A.: 'Complexity Issues in Global Optimisation: A Survey', In *Handbook of Global Optimisation*, Horst, R. and Pardalos, P. M. (eds.), Kluwer, Dordrecht, pp. 27-41, 1995.

Wirthman, D.J., Park, S.Y., Vadali, S.R.: 'Trajectory Optimisation Using Parallel Shooting Method on Parallel Computer', *Journal of Guidance, Control and Dynamics*, Vol. 18, No. 2, pp. 377-379, 1995.

References on used global optimization tools:

GAOT:

Houck, C., Joines, J., and Kay, M., 1995. A Genetic Algorithm for Function Optimization: A Matlab Implementation, NCSU-IE TR 95-09.

Michalewicz, Z., 1994. *Genetic Algorithms + Data Structures = Evolution Programs*. AI Series, Springer-Verlag, New York.

Reference web site: http://www.ie.ncsu.edu/mirage/GAToolBox/gaot/

GAOT-shared:

Sareni, B., Krähenbuhl, L., 1998. Fitness sharing and niching methods revisited. *IEEE Trans. Evolutionary Computation*, 2(3): 97-106.

GATBX and GATBX-migr:

Chipperfield, A.J., and Fleming, P.J., 1995. The MATLAB Genetic Algorithm Toolbox. *IEE Colloquium on Applied Control Techniques Using MATLAB*, Digest No. 1995/014.

Chipperfield, A.J., Fleming, P.J., and Fonseca, C.M., 1994. Genetic Algorithm Tools for Control Systems Engineering, presented at *Adaptive Computing in Engineering Design and Control*, Plymouth, UK.

Reference web site: http://www.shef.ac.uk/cgi-bin/cgiwrap/~gaipp/gatbx-download

FEP:

Yao, X., 1997. Global Optimization by Evolutionary Algorithms, *Proc. Of the Second Aizu International Symposium on Parallel Algorithm\Architecture Synthesis* (pAs-97), Aizu-Wakamatsu, Japan, IEEE Computer Society Press, pp. 282-291.

YAO, X., LIU, Y., and LIN, G., 1999. Evolutionary programming made faster, *IEEE Transactions on Evolutionary Computation*.

Di Lizia, P., Lavagna, M., and Finzi, E.A., 2004. Global multiobjective optimization of space mission design using evolutionary methods and interval analysis, *55th International Astronautical congress*, Vancouver, Canada.

Zitzler, E., 2002. Evolutionary Algorithms for Multiobjective Optimization, *Evolutionary methods for Design, Optimization and Control*, CIMNE, Barcelona, Spain, pp. 19-26.

Deb, K., 2000. An Efficient Constraint Handling Method for Genetic Algorithms. *Computer Methods in Applied Mechanics and Engineering*.

DE:

Storn, R., and Price, K., 1995. Differential Evolution - a Simple and Efficient Adaptive Scheme for Global Optimization over Continuous Spaces. *Technical Report* TR-95-012, ICSI.

Reference web site: http://www.icsi.berkeley.edu/~storn/code.html

SIMULATED ANNEALING:

Kirkpatrick, S., Gelatt, C.D., Jr., and Vecchi, M.P., 1983. *Optimization by simulated annealing*, Science 220, 4598, 671-680.

Metropolis, N., Rosenbluth, A.W., Rosenbluth, M.N., Teller, A.H., and Teller, E., 1953. Equation of state calculations by fast computing machines, J. Chem. Phys. 21, 6, 1087-1092.

Ingberg, L., 1993, *Simulated Annealing: Practice versus theory*, Mathl. Comput. Modelling 18, 11, 29-57.

Ingber, L., 2000. Adaptive simulated annealing (ASA): Lessons learned. CoRR cs.MS/0001018.

Reference web site: http://www.ingber.com/#ASA-CODE

GLBSOLVE:

Jones, D.R., Perttunen, C.D., and Stuckman, B.E., 1993. Lipschitzian Optimization Without the Lipschitz Constant, JOTA Vol. 79, No. 1.

Reference web site: http://www.tomlab.biz/

MCS:

Huyer, W., and Neumaier, A., 1999. Global optimization by multilevel coordinate search. *J. Global Optimization* 14, 331-355.

Reference web site: http://www.mat.univie.ac.at/~neum/software/mcs/

rbfSolve:

Jones, D.R., 2001. A Taxonomy of Global optimization Methods Based on Response Surfaces. *Journal of Global Optimization* 21 (4), 345:383.

Reference web site: http://www.tomlab.biz/